A New Transiting Planet Search Applied to *Kepler* and K2: Discovery of Hundreds of Planet Candidates, Eclipsing Binary Stars, and a Self-lensing Binary System

Ethan Kruse

A dissertation
submitted in partial fulfillment of the
requirements for the degree of

Doctor of Philosophy

University of Washington

2018

Reading Committee:

Eric Agol, Chair

Suzanne Hawley

Rory Barnes

Program Authorized to Offer Degree:
Astronomy

University of Washington

Abstract

A New Transiting Planet Search Applied to *Kepler* and K2: Discovery of Hundreds of Planet Candidates, Eclipsing Binary Stars, and a Self-lensing Binary System

Ethan Kruse

Chair of the Supervisory Committee:
Professor Eric Agol
Department of Astronomy

Since the launch of the *Kepler* telescope in 2009, the transit method has become the most common way to discover exoplanets. Several groups have created planet search pipelines for both the original *Kepler* mission and its successor K2. While well designed to find the majority of exoplanets, certain classes of exoplanets are more likely to be overlooked by most planet searches: notably systems displaying three or fewer transits or those with transit timing variations. I have developed a comprehensive planet search technique that is capable of detecting most transiting exoplanets, including the ones commonly missed by other searches.

In this thesis I present my transiting planet search, `QATS`, and I apply it to the first nine campaigns of K2. I have found over 700 planet candidates, including high multiplicity systems with five or six planets. I compare my results to those of other groups and show I am sensitive to planets at all orbital periods, including single transits. I put my results into the context of the wider exoplanet sample, and I show how planets from K2 can answer some questions created by the *Kepler* planets.

Finally, I demonstrate the flexibility of my planet search technique by presenting a fortuitous discovery: the first self-lensing binary star system. What at first appeared to be a reverse transit — the star getting brighter when a planet passed in front — is instead a white

dwarf in a binary star system whose light gravitationally lenses its companion every orbit.

The methods developed in this thesis will be useful for any future transit searches as well, most notably the new *TESS* mission. With observation sectors of just 27 days, `QATS`'s ability to detect single transits can dramatically extend *TESS*'s sensitivity to planets in more distant orbits; on the other end, `QATS`'s transit timing variation detection will help find planets in the continuous viewing zone, or perhaps planets in an extended mission.

TABLE OF CONTENTS

LIST OF FIGURES

LIST OF TABLES

ACKNOWLEDGMENTS

This document presents the culmination of six years of work, and I would not have made it to this point without the help and support of dozens of people. I am deeply grateful to all of them.

My advisor, Eric Agol, has been involved in my work since before day one. He played a large role in recruiting me to the University of Washington and has helped guide me onto my current path ever since. Thank you for the patience, kindness, and attention you've given me all these years.

Our research group has sparked many ideas, supported my work, made suggestions and improvements, and helped when I was stuck. I'd especially like to thank Dan Foreman-Mackey, Sarah Ballard, and Rodrigo Luger for their contributions to the work and ideas in this thesis.

The astronomy department as a whole has been a great combination of nurturing and challenging through the years. Thank you to Suzanne Hawley for inviting me to her group meetings, providing career and life advice, and talking sports with me. Julianne Dalcanton has similarly been a supportive advisor in times of need and is always willing to lend an ear.

The best part of the department, however, is without a doubt the graduate students. Thank you to each and every one for hours of talking, laughing, foosing, and whining. John L., Kolby, Grace, and Jim have been especially valuable for my well-being, and I'd like to thank them for the long talks and fun times.

Beyond the department, thank you to my family and friends for their love and support through the good, but especially the bad, times. On the days it felt like I couldn't keep going, I always had someone to turn to.

Adam and Katie have always been there to encourage me and remind me how far I've come. Thank you to Anya and Emily for their consistent friendship. From the meals made together, study parties, and too-frequent hospital visits, you've really made Seattle feel like home.

Finally, and most of all, thank you to my parents and brother and sister for the innumerable games, jokes, adventures, and distractions along the way. I always look forward to times when we're all together.

DEDICATION

To my parents, for their unwavering
and abounding love and support.

Chapter 1

INTRODUCTION

The study of exoplanets — planets orbiting stars other than our Sun — is fundamentally an exploration of our place in the universe. How did our Solar System form and evolve into how we see it today? Are we alone, or can we find evidence of life on other planets? Does every star have planets? Are planets like Earth common or is the Earth unique? The answers to these questions have been a matter of scientific and philosophical debate for centuries, but evidence to support those answers has been slow to arrive. Only in the past couple decades have we made headway by discovering the first planets beyond the currently known eight in our own Solar System. At first a slow trickle, the rate of exoplanet discovery quickened as telescopes grew, instrumentation technology improved, and the search for exoplanets went to space.

In this thesis I present my contributions to the field by developing and demonstrating the utility of a new transiting planet discovery pipeline. My method is more robust than previous efforts, and I have found hundreds of new planet candidates.

This first chapter provides an introduction to the topics discussed throughout the thesis. I begin by reviewing the history of exoplanet searches and methods of discovery, with emphasis on the transit method and transiting planet search techniques. I then introduce the *Kepler* spacecraft — whose data this thesis relies upon. I discuss how large samples of planets are used to test and refine a cohesive planet formation and evolution theory, highlighting recent developments, open questions, and ways forward. Finally, I outline my contributions and the structure of the subsequent chapters.

1.1 Methods to Find Exoplanets

In the sixteenth century, Giordano Bruno was the first to extend the Sun-centered Copernican model of our solar system by suggesting that every star is another sun capable of hosting its own planets (Bruno, 1584). Fifty years later, Johannes Kepler predicted the Solar System planets of Mercury and Venus would occasionally pass in front of the Sun as seen from Earth (Kepler & Bartsch, 1630). These 'transits' were observed in 1631 (Mercury) and 1639 (Venus), confirming Kepler's laws of orbital motion; Venus's transits a century later also allowed for the first estimate of the physical scale of the Solar System (Smith, 1769).

By the middle of the nineteenth century, the transit of a planet blocking some light from its star was considered a possible explanation for variable stars — stars whose brightness measurably changed over time. As Dionysius Lardner (1853) explains in his Hand-books of Natural Philosophy and Astronomy:

> It has been suggested that the periodical obscuration or total disappearance of the star may arise from transits of the star by its attendant planets. The transits of Venus and Mercury are the basis of this conjecture.

However, Lardner also noted that all the planets in the Solar System were too small to cause the magnitude of variability observed at the time; observations simply weren't sensitive enough to detect the 0.01% change in brightness due to a transit of Earth or Venus, or even the 1% change from a theoretical transit of a Jupiter-sized planet around a Sun-sized star. Any potential transit explanation for variable stars at the time would require planets very near the size of their host star.

Aside from transits, other ideas to detect exoplanets were developed in the early half of the twentieth century. Perhaps the most obvious would be direct detection (also known as direct imaging): point a telescope at a star and resolve its planets as other nearby but distinct points of (reflected or emitted) light. Aitken (1938) showed that such direct detection of planets was beyond the capabilities of observatories at the time; stars are so distant and

bright that any planets would be too close and too dim to distinguish from the much brighter stellar source.

As opposed to directly seeing light from a planet, two other indirect methods were considered: as with transits, these methods indirectly infer the existence of planets based on the effect they have on their host star's light. Both rely on the reciprocal force of gravity — planets do not orbit stationary stars; instead, both star and planet orbit their mutual center of mass. Thus even if we cannot see a planet's light directly, we may be able to watch the star wobble due to a planet's gravitational influence.

The two indirect stellar motion methods — astrometry and radial velocity — are complementary. Astrometry aims to precisely measure the position of the star and watch it move in the two dimensions on the sky. Radial velocity instead measures the third dimension: motion of the star toward and away from us.

In the following sections I describe each of these four methods of planet detection: astrometry, radial velocity, direct imaging, and finally transits. Each is sensitive to different types of planets and allows us to infer different properties about those planets, helping complete our understanding of planet formation and evolution.

1.1.1 Astrometry

Astrometry is the accurate measure of the position of a star on the sky. If a star is isolated, with no companion stars or planets, its astrometric position on the sky will change due to only two factors: the slow movement of the star through the galaxy relative to the Sun (proper motion), and its annual apparent change in position due to the Earth's orbit around the Sun (parallax).

If a star has a companion star or planet, its orbital motion around their joint center of mass will be added to its measured astrometric signal. The angle on the sky θ we see a star's orbit make due to a companion is equal to

$$\theta = \left(\frac{m_c}{M_*}\right)\left(\frac{a}{D}\right)$$

where the star of note has mass M_* and its companion mass m_c, and the two are separated by a semi-major axis a and at a distance from Earth D. Perhaps intuitively then, the more massive a companion, the more distant the companion's orbit, and the closer the system to the Earth, the larger and more easily detected the astrometric signal for a given star will be. Observing how long such an orbit takes along with its shape allows one to measure the system's orbital period as well as other orbital parameters like the eccentricity.

Astrometry succeeded at finding hidden stellar companions as early as the mid-nineteenth century. Bessel (1844) observed astrometric variations for Procyon and Sirius, the brightest star in the night sky. He concluded, "if we were to regard Sirius and Procyon as double stars, the change of their motions would not surprise us." Twenty years later, a companion was found to Sirius, Sirius B, whose location and motion matched the predictions perfectly, but was observed to be "only feebly self-luminous" — the first discovery of a white dwarf (Bond, 1862a,b).

Other astrometric discoveries from the same time period were more speculative. Jacob (1855) claimed that deviations in the binary orbit of the two stars in 70 Ophiuchi were "highly probable" to be caused by an unseen planet. A planet at a different period in the same system was proposed by See (1896), though this was shown to be unstable by Moulton (1899). Neither of these claims of astrometric planet detection have held up to modern scrutiny.

More claims of an astrometric detection of a planet started in 1943 around one of the stars in the binary 61 Cygni. The signal was supposedly due to a planet with a mass 16 times that of Jupiter on a five year orbit and Strand (1943) claimed therefore that "planetary motion has been found outside the solar system." Eight years later, a substellar companion was announced around the star Lalande 21185 (van de Kamp & Lippincott, 1951), followed by the announcement of a planet near the mass of Jupiter around Barnard's star (van de Kamp, 1963).

Notably, however, all of these claims came from the same Sproul Observatory telescope, and later analyses identified systematic effects that could be the cause of the signals (Black,

1980; Hershey, 1973); furthermore, none of them could be confirmed with independent data from other observatories (e.g. Gatewood & Eichhorn, 1973). Current data refutes all of these 'planets', and they instead serve as a cautionary tale of the difficulties of planetary-precision astrometry (Kürster et al., 2003).

Only recently has astrometry begun to meaningfully contribute to exoplanet science. The first use was to constrain the orbit and mass of a planet discovered via radial velocity (Benedict et al., 2002). Differential astrometry has been able to identify planet-mass companions disturbing binary star orbits, but cannot distinguish which star the planets orbit (Muterspaugh et al., 2010). Finally, a companion planet or brown dwarf has been found around a nearby brown dwarf (Sahlmann et al., 2013).

These sparse achievements reinforce the difficulty of the precise astrometry required to detect exoplanet orbits. Yet the age of astrometry may have finally arrived with the launch of the *Gaia* spacecraft in 2013 (Gaia Collaboration et al., 2016). The most precise astrometry mission ever created, *Gaia* is expected to discover some 20,000 planets by the end of its baseline five year mission — most approximately the mass of Jupiter on distant orbits around nearby stars (the exact combination to produce the largest signal) (Perryman et al., 2014).

1.1.2 Radial Velocity

Where astrometry measures the motion of a star due to its planets on the plane of the sky, radial velocity measures the star's motion toward and away from the Earth. This is accomplished through spectroscopy (the splitting of light into its respective colors like a prism) and carefully measuring the wavelength of a star's dark spectral lines caused by atomic absorption removing specific wavelengths of light. Because of the Doppler effect, as a star moves toward and away from us, all of its light — and therefore also its spectral lines — get blue- and red-shifted respectively; the wavelengths at which we observe the absorption lines shift back and forth.

The amplitude of this effect K for a star of mass M_* depends on the gravitational constant G, the mass of the planet m_p, and the planet's orbital period P, eccentricity e, and inclination

i via the relationship

$$K = \left(\frac{2\pi G}{P}\right)^{\frac{1}{3}} \frac{m_p \sin i}{(M_* + m_p)^{\frac{2}{3}}} \frac{1}{\sqrt{1-e^2}}$$

For a full derivation, see Lovis & Fischer (2010).

Therefore, unlike astrometry, the more distant a planet from its host star, the smaller the radial velocity effect and the more difficult the planet is to detect. In addition, while the period and eccentricity can be measured from the observations, the inclination cannot be separated from the planet mass. Radial velocity observations always have a degeneracy between m_p and $\sin i$; with radial velocity observations alone, one can never measure the true mass of a planet, only its minimum mass (if the plane of the orbit points directly toward Earth and $\sin i = 1$; see e.g. Marcy & Butler, 1998).

The size of this radial velocity effect is small for planets: the Sun's radial velocity variation is dominated by the 12.5 m/s effect of Jupiter — Earth contributes just 10 cm/s. Massive planets like Jupiter on very short orbits (e.g. a few days) would cause the largest radial velocity amplitude (50-100 m/s), and their short periods would require less time to sample a full orbit; if such planets exist, therefore, they would be easiest and likely the first to be discovered.

The idea of using radial velocity variations to search for planets had been developed by the mid-twentieth century (Struve, 1952), but it took another 40 years for the technology to reach the requisite precision. In 1989, a sample of 70 stars at a precision of 230 m/s found some binary star systems, but no substellar companions (Marcy & Benitz, 1989). By the mid-1990s, several groups had achieved precision of about 10 m/s and had surveyed hundreds of stars for a few years (see e.g. review by Marcy & Butler, 1998), and the planets began to roll in.

The first planet around a main sequence star, 51 Peg b, was discovered via radial velocity in 1995 by Mayor & Queloz (1995), and it was indeed a 'hot Jupiter' — half a Jupiter mass with an orbital period of just 4 days. By convention, planets are named after their host star with a lowercase letter suffix starting with b for the first planet; additional planets

would be e.g. 51 Peg c, 51 Peg d, etc (Hartkopf & Mason, 2004). Within three years, seven other approximately Jupiter-mass planets had been discovered from radial velocity surveys (4 with periods shorter than the Solar System's Mercury), and the era of exoplanets had begun (Marcy & Butler, 1998).

In the two decades since, radial velocities surveys have achieved velocity precision at the m/s level and discovered hundreds of planets (Lovis & Fischer, 2010). Compounding technical limitations, today stellar magnetic variability is often the limiting factor in survey precision. Stellar spots, oscillations, granulation, and other dynamic effects all distort the spectral lines and thus mask the small amplitude shifts caused by orbiting planets (reviewed by Wright, 2017).

Nonetheless, radial velocity campaigns have continued to march toward smaller masses and multi-planet systems. In 2004, Neptune-mass planets were announced in systems with at least two planets already known (Santos et al., 2004; McArthur et al., 2004). The technique is also being used to measure masses or upper limit mass constraints for Earth-size planets discovered via the transit method (Marcy et al., 2014).

1.1.3 Direct Imaging

Perhaps the most challenging method of exoplanet detection is direct imaging. Rather than inferring a planet's existence based on its effect on its host star, direct imaging aims to separate the light from a planet into its own point source in an image — distinct from the light collected from its star. This strategy has two main challenges: contrast and resolution.

Planets do not generate their own light via nuclear fusion as stars do. Any light emitted from a planet comes from either reflection or emission: reflection of the star's light off the planet or (generally thermal) emission from the planet's internal energy — supplied by both stellar absorption and contraction from formation.

The fraction of a star's light that reflects off a planet ($F_{\rm ref}$) is proportional to its radius and distance from the star, with the planet's Bond albedo (reflectiveness, A_B) determining

what fraction of the light hitting it is reflected:

$$F_{\text{ref}} = A_B \frac{\pi r_p^2}{4\pi a^2} = \frac{A_B}{4}\left(\frac{r_p}{a}\right)^2$$

For nearly all planets, this ratio is exceptionally small: all planets in our solar system have values around $10^{-9} - 10^{-10}$ — for every approximately billion photons we would receive from a Solar System twin viewed from afar, we would receive one photon reflected off one of the planets.

Fortunately, planets do generate their own light through thermal emission. All planets are heated by their star (with the radiation that is not reflected), and planets can supply additional internal energy via radioactive decay or contraction. Planets have temperatures of hundreds of Kelvin with thermal peaks in the infrared part of the spectrum (wavelengths of 10-100 µm). Looking in the infrared can therefore reduce the contrast by several orders of magnitude — Jupiter appears about 10^{-4} times as bright as the Sun in thermal infrared wavelengths (Marcy & Butler, 1998). A summary of the contrast of some Solar System planets to the Sun is shown in Figure 1.1.

Planets that form with significant gaseous atmospheres will slowly release energy as the atmosphere contracts and cools over time, providing a significant boost to the planet's temperature and therefore its luminosity: one third of Jupiter's radiative output today, five billion years after formation, is still due to its steady contraction (Erickson et al., 1978).

A planet cooling over time naturally means that it is brighter when it is younger. Derivations show that a planet's luminosity L depends on its mass and its age t with a functional form

$$L \propto t^{-\frac{5}{4}} m_p^{\frac{5}{2}}$$

(Bowler, 2016). The rapid decline in brightness with age means directly imaging the youngest planets should be easiest, and searches have subsequently focused on young stars.

Beyond their faint luminosities, the second hurdle to directly imaging exoplanets is the resolution required to distinguish them from their host stars. The angular resolution of two

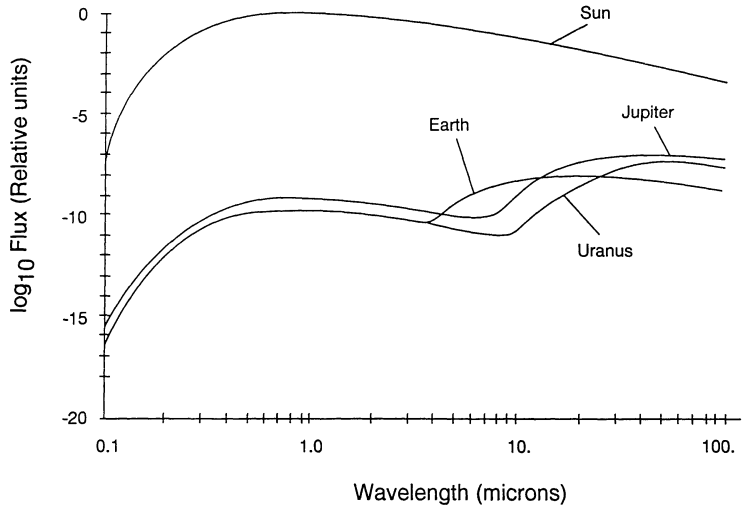

Figure 1.1: Relative spectral energy distributions of three representative planets in our Solar System, scaled to the Sun. At wavelengths less than a few microns, the planet's light is dominated by reflection of the Sun. At longer wavelengths the planet's thermal emission dominates, bringing the planet's flux several orders of magnitude closer to the Sun's. Figure from Black (1995).

point sources for a telescope is given by its diameter d, and the wavelength at which it observes λ — which translates into a physical separation a when multiplied by an object's distance D:

$$a = 1.22\frac{\lambda D}{d}$$

With a modern telescope of 10 m diameter at infrared wavelengths (5 µm), the diffraction limited resolution of a star at 10 pc would be about 2 AU — good enough to detect our Solar System's outer gas giants.

However, this is only the theoretical (diffraction) limit; in reality, the atmosphere distorts starlight beyond pure point sources. To directly image planets very near to their stars, these atmospheric effects need to be removed. The technological development of 'adaptive optics' to correct the distorting effects of the atmosphere in real time was what allowed direct imaging to become a reality (reviewed by Oppenheimer & Hinkley, 2009). The first directly imaged planets around stars came with one planet around Beta Pictoris (Lagrange et al.,

2009) and three planets around HR 8799 (Marois et al., 2008). Dozens more have followed in the years since.

By watching the planet orbit, its period and other orbital parameters can be derived, but direct imaging cannot directly determine either the mass or the radius of a planet — all one has is the luminosity of the planet, which can be influenced by other factors like temperature (Bowler, 2016). This limitation can make it difficult to differentiate between planets and brown dwarfs in direct imaging searches.

The major benefits to direct imaging searches for planets are the complementary planets it can find as well as the detailed information about those planets. Like astrometry, direct imaging is most effective at finding massive planets on long orbits (in this case preferentially around young stars) — in contrast to radial velocity and transits which are best at shorter periods. Furthermore, because direct imaging can detect light directly from the planet, the planet's atmosphere can be studied via spectroscopy (Lagrange, 2014).

1.1.4 Transits

While Lardner (1853) proposed transits of planets as an explanation for the observed variability of some stars, the transit method was exclusively used as a means to study binary stars until the onset of the twenty-first century. The first discovery of a binary star system in which one star transits (eclipses) the other was the star Algol (Goodricke, 1783). By the twentieth century, eclipsing binaries had become common, and a comprehensive model was developed, through which one could derive the parameters of the stars and their orbit based on the timing and shape of each star eclipsing the other (Russell, 1912a,b).

These eclipsing binary stars have orbital periods as short as a day or two, and in the context of the (now refuted) astrometric planet announced by Strand (1943), Struve (1952) suggested planets may well exist at such short distances from their stars, despite the lack of any such planets in our own Solar System. He further suggested that such planets, if they existed and were as large as Jupiter, would transit and block as much as 2% of the light from their star: a depth nearly detectable with the tools available at the time.

The theory for planetary transits is much the same as for two stars eclipsing one another in the limiting case of one star emitting no light of its own. In the simplest approximation, a planet with radius r_p in front of a star of size R_* blocks as much light (a change in observed flux from the star ΔF) as the ratio of their areas on the sky

$$\Delta F = \frac{\pi r_p^2}{\pi R_*^2} = \left(\frac{r_p}{R_*}\right)^2$$

Therefore, in observing repeated transits, one can measure the orbital period of the planet and its size relative to its host star. Additional information (e.g. from spectroscopy) is needed about the physical size of the star to convert this transit depth into a physical planet size. A more complete derivation can be found in Winn (2010).

A Jupiter-sized planet will block around 1% of the light from a Sun-like star during transit, and such precision was available by the 1980s (Borucki & Summers, 1984). However, two other properties of transiting planets make such searches more difficult: their likelihood and their duration. Unlike all other planet discovery methods, transits are only detectable for a narrow range of orientations. The probability p of a randomly positioned distant observer having a planet's orbit with semi-major axis a aligned such that transits can be seen is approximately

$$p \approx \frac{R_*}{a}$$

(Winn, 2010). For the Earth around the Sun, this works out to just 1 in 200, and for Jupiter 1 in 1000. While radial velocity signals slowly decline in magnitude with more face-on inclinations, the complete absence of any transit signal at most orientations means the number of stars surveyed needs to be large in order to ensure detections.

Even if a planet is favorably aligned for transits to be seen from Earth, however, the odds of one occurring at any given time are again low. A transit of the Earth as seen from afar would last just 12 hours, or 0.15% of its orbital period of a year (1 in 700). Very short period planets can spend closer to 3% of their orbital period in transit. Nevertheless, unlike radial

velocities or astrometry, where observations can always add information toward a planet detection by sampling different phases of the orbit, for well over 90% of the time observing a star for transits, no signal will be detected. These lack of transit detections can be used to constrain the period of an already known planet (e.g. Luger et al., 2017b), but not to definitively find and confirm one.

In summary, a star would need to be nearly continuously monitored for transits to ensure the detection of these infrequent transit events, and because of the low geometric probability, hundreds of stars would have to be monitored to guarantee the detection of a single transiting planet, even if every star hosted one. While photometric precision at about 1% existed in 1984, it was not available for the wide fields of view capable of measuring hundreds of stars at once, and so transit searches were considered infeasible for the time being (Rosenblatt, 1971; Borucki & Summers, 1984).

With the discovery of hot Jupiters from radial velocity in 1995, however, the calculus changed. With a period of just a few days, the odds of transit assuming a random alignment are around 10%, and with knowledge of the radial velocity orbit, the time of transit can be estimated, allowing for targeted observations only around potential transit times. Just such a targeted campaign was launched for the newly discovered radial velocity planet of HD 209458 b (Mazeh et al., 2000). The transit was detected, and transits were added to the list of successful exoplanet detection techniques (Charbonneau et al., 2000; Henry et al., 2000).

The first decade of the 2000s saw numerous ground-based transit searches launched in HD 209458 b's wake. CCD camera technology developed enough to allow for wide field monitoring of thousands of stars at high enough precision to detect Jupiter-sized transits (Borucki et al., 2001). The first planet discovered through transits was OGLE-TR-56 b in 2003 (Konacki et al., 2003). The most prolific of these various transit surveys have been WASP (Pollacco et al., 2006) and HATNet (Bakos et al., 2004) which have discovered over 150 and 60 planets to date, respectively.

Nearly all ground-based transit searches use wide field cameras with modern CCDs to survey as many stars as precisely as possible. Yet atmospheric effects make accurate photom-

etry at a precision less than 1% difficult, and daylight and weather make constant monitoring of stars impossible from the ground. To push the transit method to Earth-size planets with depths of just 0.01% or lower, one needs to get out of the Earth's atmosphere and go to space.

1.2 The Kepler and K2 Missions

Planet discoveries started slowly after the first planet around a main sequence star (Mayor & Queloz, 1995), but they began to accelerate into the early 2000s. By 2009, a couple hundred exoplanets had been found, most via the radial velocity method, and most about the size or mass of our Solar System's gas giants. Then in 2009, the *Kepler* telescope launched. *Kepler* is a space telescope designed explicitly to find Earth-sized planets via the transit method, and it changed much of what we know about exoplanets. Today we have over 3500 confirmed exoplanet discoveries[1], and more than two thirds were found with data from the *Kepler* telescope — and the majority of those planets are smaller than Neptune.

1.2.1 The Kepler Mission

Mission Conception

In 1992, NASA introduced the Discovery Program — a series of principal-investigator proposed and led, but cost-capped, missions. Unlike traditional NASA flagship missions with predetermined targets and requirements, Discovery missions can propose any scientific objectives.

In every call for proposals, Bill Borucki and his collaborators submitted a space-based transiting planet telescope — despite 51 Peg b not being discovered until 1995. The 1992 and 1994 missions were titled FRESIP (FRequency of Earth-Sized Inner Planets) (Borucki et al., 1996), and were rejected because of doubts about the stability of CCD detectors at the time (Borucki, 2016). The 1996 proposal was rebranded as the *Kepler* mission, but

[1] as listed on NASA's Exoplanet Archive.

it was also rejected because automated precision photometry of thousands of stars was an untested technology. To prove the technology from the ground, the Vulcan Photometer was installed at Lick Observatory and successfully observed 6000 stars simultaneously — including eventually the first transiting planet of HD 209458 b (Borucki et al., 2001).

The 1998 *Kepler* mission proposal was again rejected due to concerns about the mission's sensitivity and reliability. An end-to-end test of all the fundamental capabilities of the telescope in simulated conditions was carried out over 14 months with positive results (Koch et al., 2000). Finally, the fifth proposal of the *Kepler* mission was accepted in 2000 and it was launched in 2009 (Borucki, 2016).

Kepler Instrument and Mission Design

Everything about the *Kepler* mission's design is oriented toward observing a large number of Sun-like stars at high photometric precision for a number of years to discover Earth-sized transiting planets. The *Kepler* spacecraft consists of a 1.4 m mirror focusing a 105 $\deg^2$ field of view onto 42 tiled CCDs. The spacecraft was launched into an Earth-trailing orbit which allows it to complete its goal of studying the same stars for the duration of the mission without interruption by the Earth or Sun in the field of view (FOV) — so long as the FOV is more than 55° above the ecliptic.

The FOV was chosen near the constellation Cygnus to meet the 55° above the ecliptic requirement, maximize the number of spectral type FGK dwarf stars similar to the Sun, and minimize the number of contaminating background giant stars (Koch et al., 2010). A full image of the final field of view is shown in Figure 1.2.

To maximize signal, the telescope needs to collect as wide a spectrum of light as possible. However, stars are especially active and variable in the UV (especially in the 393 and 397 nm Ca II H & K lines), which would increase noise and make transit signals more difficult to detect; meanwhile, silicon CCDs as used on *Kepler* become transparent in the near IR, causing fringing and reflection noise (Borucki, 2016). To minimize the noise while maximizing flux, *Kepler*'s bandpass filter was designed to collect as much light as possible between 423

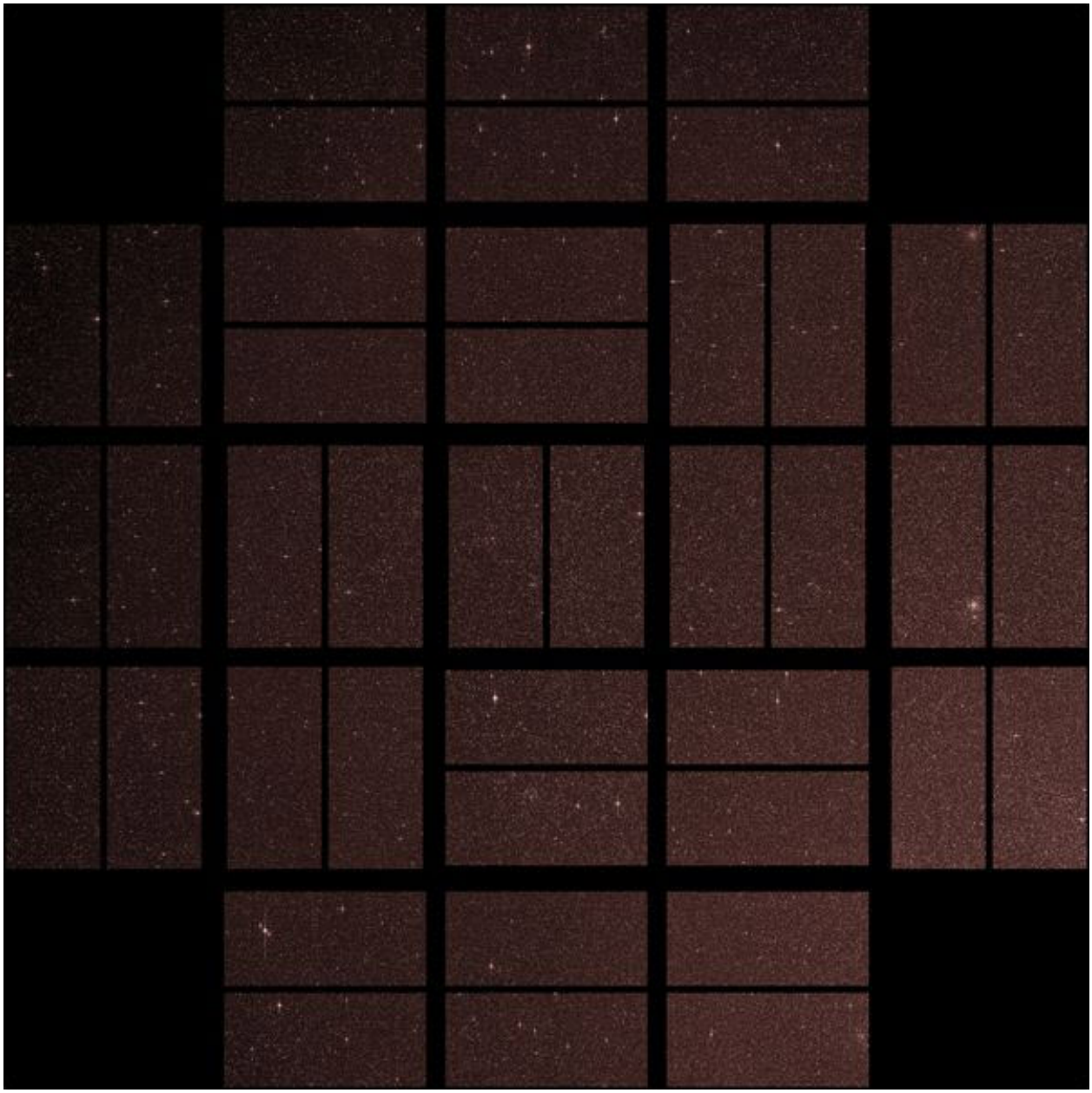

Figure 1.2: NASA image of the full *Kepler* field of view with all 42 CCDs.

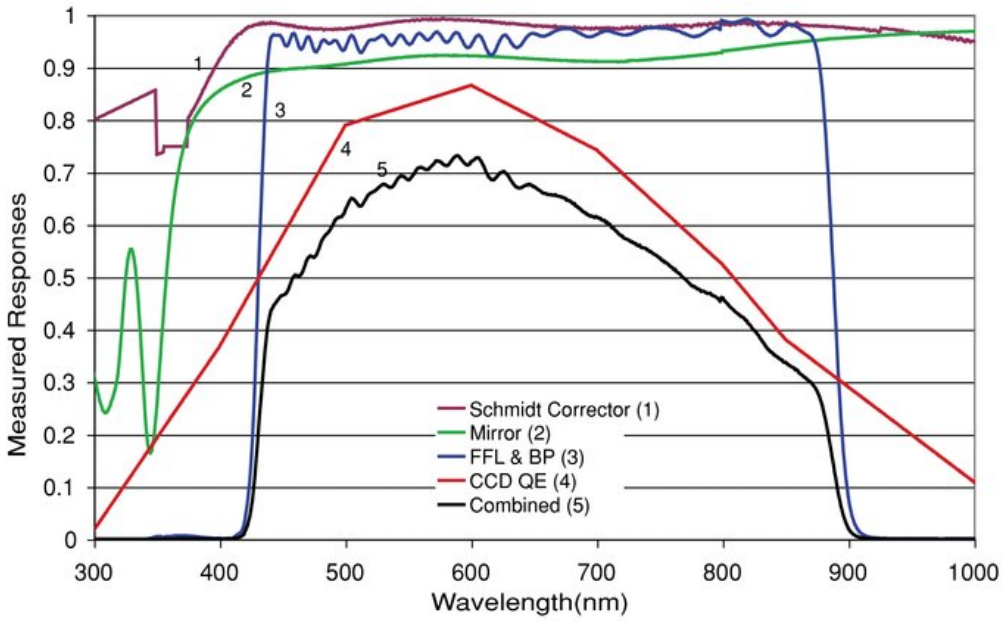

Figure 1.3: The overall *Kepler* response function (black) and its corresponding components: Schmidt corrector lens (purple), telescope mirror (green), bandpass filter coating (blue), and the CCD efficiency (red). Figure from Koch et al. (2010).

and 897 nm (Figure 1.3).

Because of the poor data transfer rate in deep space and limited onboard storage, it was impossible to design the mission to return a full image of the FOV frequently enough for a transit search. Instead, only 6% of the pixels are saved: small 'postage stamps' of pixels around 170,000 preselected stars (Borucki, 2016).

To keep its solar panels toward the Sun, the spacecraft has to rotate every 90 days; these interruptions in data collection are used to downlink stored data and change targets if desired; thus the *Kepler* mission is divided into 'quarters' of data, with stars falling on different pixels every quarter. Data downlinks are performed every month due to limited storage space onboard, causing shorter data gaps (Haas et al., 2010).

With only 170,000 of the 4 million stars in the FOV able to be observed every quarter, extensive observations were done before launch to select the most suitable targets. All stars were observed in seven filters which were then used to estimate stellar parameters. This

catalog (the *Kepler* Input Catalog [KIC]), was used to select targets with an emphasis on main sequence stars small and bright enough to detect transits of Earth-sized planets (Brown et al., 2011).

Data collection with *Kepler* is done in a series of 6.02 s exposures. The default science mode is to stack 270 of these exposures (30 minutes total) into one observation that is stored and sent back to the ground. This 30 minute observation is the 'long cadence' mode and is returned for all 170,000 target stars' pixels (Koch et al., 2010). For most stars then, *Kepler* measures their brightness every 30 minutes continuously (the only planned gaps being the quarterly rotation and monthly data downlink). For a preselected 512 stars every quarter, there is enough storage space for an additional 'short cadence' mode: sets of 9 exposures (every 1 minute). These stars have both a long cadence and short cadence light curve available for study (Haas et al., 2010).

All raw long and short cadence pixels are downloaded to Earth for calibration and analysis. The *Kepler* reduction pipeline has several modular steps to produce science-quality light curves. `CAL` (Quintana et al., 2010) calibrates the pixels similar to most telescope data reduction (e.g. correcting for gain, cosmic rays, flat fields, bias levels), then passes the pixels to `PA` which fits and removes sky background levels; these calibrated pixels are combined into simple aperture photometry (SAP) light curves (Twicken et al., 2010b; Jenkins et al., 2010a). The `PDC` module then attempts to remove systematic errors and correct for background flux from nearby stars in the aperture and produces corrected PDC light curves (Twicken et al., 2010a).

All told, *Kepler* produced light curves of 170,000 stars for four years at a nearly continuous cadence of 30 minutes at a precision of about 100 ppm (Christiansen et al., 2012) — exactly the recipe required to find small transiting planets.

Methods to Find Transiting Planets

With a measure of a star's brightness every 30 minutes for several years, the question then becomes: how does one use that to find transiting planets? Unlike the first transiting planet

found (Charbonneau et al., 2000), we don't know the period and phase of potential planets in advance to search for a transit in a narrow window of time.

The search for periodic signals in data is by no means a new problem in astronomy or science in general. One of the more ubiquitous methods to identify periodic signals is some variation on a Fourier transform, which relies on decomposing the signal into sines and cosines of varying periods (Deeming, 1975). For signals like a transit, however, where the signal is not a slowly varying function distributed across the entire period, but instead a sharp dip concentrated in less than 5% of phase, Fourier analyses prove ineffective (Kovács et al., 2002). Instead, transit searches have been designed explicitly around finding a short duration periodic signal.

Over the years, numerous transit searches have been written, but all share some similar characteristics. The basic principle is to compute a 'single event statistic' (SES) that defines how well a transit of a given duration fits the data at every point in the light curve. These SES values are then folded over a range of periods and phases to find the maximum 'multiple event statistic' (MES). The search is thus divided into a three-dimensional grid of possible transit durations, phases, and periods.

One of the earliest and most frequently used examples of a dedicated transit search method is Box Least Squares (`BLS`; Kovács et al., 2002). `BLS` operates by assuming the light curve can be described by just two numbers: the constant baseline flux of a star, and its flux when a planet is transiting it. To form the grid search, at every period one wants to consider the data get folded and uniformly binned. Then, for every possible phase and transit duration under consideration, the least squares model is used to calculate the optimal depth of a box at that phase and duration to fit the binned data. How well this box model fits at every combination of phase, duration, and period (the MES) can be used to determine if any of the grid points overall favor a transit with those parameters.

By binning, `BLS` can work around unevenly sampled data, which is a necessity for the ground-based transit searches it was designed for. However, the simplicity of its model requires the data to be uniformly cleaned. Data from many different epochs are combined

together at one phase and compared to a model that assumes any variation in stellar flux must be caused by a box-shaped transit. Any other astrophysical variability (flares, spot modulation, etc) must be completely removed before applying `BLS`. It can be exceptionally difficult to accomplish this without removing or modifying actual transits.

With *Kepler*'s exquisite photometry, the simplified `BLS` model no longer works. Stellar variability in the form of oscillations and rotation can be considerably larger in amplitude than both planet transits and the noise of an individual observation. The Transiting Planet Search (`TPS`) is the official *Kepler* pipeline to find planets in its data (Jenkins et al., 2010b), while the Transiting Exoearth Robust Reduction Algorithm (`TERRA`) is an independent technique (Petigura & Marcy, 2012), and both are designed to remove astrophysical variability before searching for planets. In the end, they operate the same as `BLS` however, by searching for planets on a three-dimensional grid of transit duration, period, and phase.

Highlights of Kepler's Exoplanet Results

The *Kepler* mission and its data analysis pipelines were an immediate success. From just the first 33 days of data, the team found over 700 planet candidates, and the majority were smaller than Neptune (Borucki et al., 2011a). Those 700 candidates in 33 days of data already represented more planets (not to mention much smaller) than had been discovered through the combined efforts of all searches over the previous 15 years.

As new quarters of data came down, the team released updated catalogs of all planet candidates found through their pipeline (Borucki et al., 2011b; Batalha et al., 2013; Burke et al., 2014; Rowe et al., 2015; Mullally et al., 2015; Coughlin et al., 2016; Thompson et al., 2018). By the end, the team found over 4000 planet candidates on periods reaching out to several hundred days, and over 80% were smaller than Neptune (Thompson et al., 2018). A concise summary of the contribution *Kepler* has made to the known exoplanet population is shown in Figure 1.4.

With thousands of planet candidates, many groups began the followup work required to confirm the planets, measure their masses, better understand their stars, and calculate the

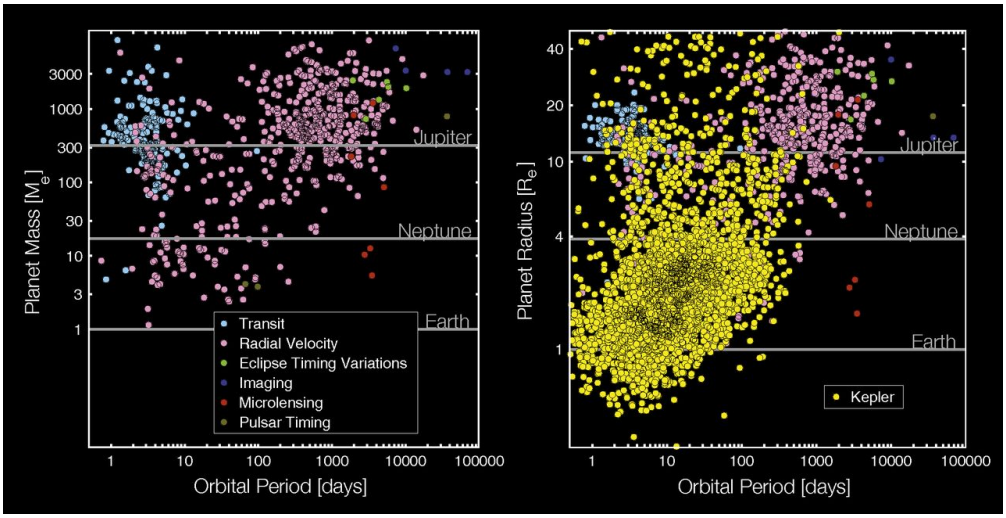

Figure 1.4: *Kepler*'s contribution to the exoplanet population. Left: all planets as of 2014 discovered without *Kepler*. Right: Same as left, but with the *Kepler* planet candidates added. An estimated mass-radius relation has been applied to convert between the two when one parameter is unknown. Figure from Batalha (2014).

occurrence rates of planets of various sizes in different environments.

While some tests can be done on the light curve data alone to test whether a seemingly planetary transit signal is in fact due to an eclipsing binary or other type of false positive, additional observations are usually required to confirm a planet candidate as a bona fide planet.

The best way to confirm a transiting signal is due to a planet is to detect it through another planet discovery method and measure its mass, in practice almost exclusively done using radial velocity. If a radial velocity detection matches a transit detection, then not only do they help validate each other's signals, but they provide complementary information about the planet.

The transit signal (with an estimate of the star's radius) gives the planet's radius, and it also ensures the planet's orbit is edge on to the Earth; the radial velocity signal measures the planet's minimum mass, and because we know its inclination from the transit to good precision, the degeneracy with inclination is broken to yield the planet's true mass. Consequently,

if we know a planet's mass and radius, those combine to produce the planet's bulk (average) density. This density measurement can be used to determine a planet's composition: rocky planets like Earth without significant atmospheres can't have densities lower than about 4 g/cm^3; conversely, ice and gas giants like Neptune to Jupiter have densities around 1-2 g/cm^3 (Seager et al., 2007).

Many short period planets were detected via radial velocity (Marcy et al., 2014), which was used to determine for the first time that for planets above about 1.6 $R_\oplus$, densities begin to decline, indicating a critical radius below which planets tend to be rocky and above which planets tend to have significant gaseous envelopes (Weiss & Marcy, 2014; Rogers, 2015).

Unfortunately, most planets cannot be detected and confirmed via radial velocity: they are on too distant orbits, have too low masses, or orbit stars too faint to accurately measure the signal with today's technology. For planets in multi-planet systems, planets can gravitationally interact, slightly altering their orbits away from purely Keplerian ellipses. This manifests as transits occurring not perfectly periodically: they show transit timing variations (TTVs) (Agol et al., 2005). Modeling these TTVs can measure the masses of planets in multi-planet systems and confirm them as real planets (e.g. Lissauer et al., 2011a; Carter et al., 2012) or detect non-transiting planets through their TTV influence (Ballard et al., 2011), even when they are too faint or distant to detect via radial velocity.

The majority of *Kepler*'s discoveries have not had their masses measured or planetary status confirmed through any means, so they remain planet candidates. However, by modeling false positives, planets in multi-planet systems have found to be reliably real (Morton, 2012; Fressin et al., 2013). Through carefully calculating the odds of any form of false positive for each individual signal, thousands of *Kepler*'s candidates have been 'validated' as statistically very likely to be real planets (Lissauer et al., 2014; Rowe et al., 2014).

Another part of followup work is to know the host stars better. Because transits only constrain the relative size of a planet to its host star, precision of the planet's radius cannot be better than that of the star's radius. Extensive campaigns were set up to take high resolution adaptive optics images of exoplanet host stars to detect any binary companions

or unrelated nearby stars that might be contaminating the stellar parameter measurements (Adams et al., 2012; Ziegler et al., 2016; Furlan et al., 2017).

In addition, many groups took spectra of the candidates' host stars to constrain their masses, radii, and temperatures better than the estimates made from the seven filters that went into the KIC (Johnson et al., 2017; Furlan et al., 2018). With these improved stellar radii measurements, Fulton et al. (2017) found a gap in *Kepler*'s short period planet radius distribution: planets are commonly found with radii $R < 1.5\mathrm{R}_\oplus$ and $R > 2\mathrm{R}_\oplus$, but there are relatively few in between — again indicative of a split between rocky and gaseous planets.

Another benefit to better stellar parameters is a better estimate of how much flux a planet receives from its host star — and therefore what its 'equilibrium temperature' is in its orbit. If a planet receives approximately the same energy from its star as the Earth does, it is deemed in its star's 'habitable zone': the zone where liquid water might be stable on the surface of a planet (Kasting et al., 1993).

The exact boundaries and definitions of the habitable zone are a matter of debate and depend on assumptions about the planet's atmosphere, orbit, and evolution (Kopparapu et al., 2013; Barnes et al., 2015), but one of *Kepler*'s stated mission goals was to find and estimate the occurrence rate of Earth-sized planets near the habitable zone. In the final *Kepler* sample, 47 planet candidates fall within their habitable zone definition (Thompson et al., 2018).

With a full sample of planet candidates, the final challenge is to calculate the underlying frequency of planets as a function of their radius, distance from their host star, mass of their host star, etc.

Many different efforts have been made to calculate planet occurrence rates, and each reaches slightly different conclusions. Generally though, planets on orbits shorter than our Solar System's innermost planet Mercury (88 days) appear common. Something like 30% of Sun-like stars host planets between the sizes of Earth and Neptune on periods shorter than 100 days (Petigura et al., 2013a; Burke et al., 2015; Fulton et al., 2017; Zhu et al., 2018). These small planets have high multiplicities: adjusting for odds of detection, the planetary

systems have on average three such planets per system (Zhu et al., 2018). While *Kepler* focused on Sun-like stars, small planets appear even more common around M dwarfs. Also found at high multiplicity, M dwarfs seem to host double the number of planets Neptune-size or smaller (Dressing & Charbonneau, 2015; Mulders et al., 2015). Larger gas giants are rarer at short orbital periods around all types of stars. Only about 1-2% of stars host a gas giant planet at periods less than 100 days (Petigura et al., 2013a).

End of the Kepler Mission

In order to maintain the required sensitivity to meet the mission goals, the *Kepler* telescope must keep the FOV steady on the detector to remarkable precision. This stability is accomplished through four fine guidance sensors at the corners of the CCD that carefully monitor the positions of a number of stars 10 times per second. Any small drifts in pointing are then passed to *Kepler*'s four reaction wheels that continuously finely adjust the spacecraft's positioning (Borucki, 2016).

Three reaction wheels are required to keep the spacecraft pointed accurately in all three dimensions; *Kepler* was launched with a fourth as a spare. However, three years into the mission the first reaction wheel failed. A year later a second failed, bringing an end to *Kepler*'s precision pointing and thus its main mission.

1.2.2 The K2 Mission

With the failure of the second of four reaction wheels in 2013, the *Kepler* spacecraft lost the ability to finely point in all three dimensions. As this fine pointing was necessary for the goals of the primary mission, data collection for stars in its original FOV ceased.

One of the main forces torquing the spacecraft that must be corrected with the reaction wheels is the photon pressure from the Sun. Engineers found that by orienting the spacecraft such that the solar photon flux was nearly balanced, it could stay relatively stable for up to twelve hours, and a crude thruster fire could be used to bring its pointing back nearly to where it started (Howell et al., 2014).

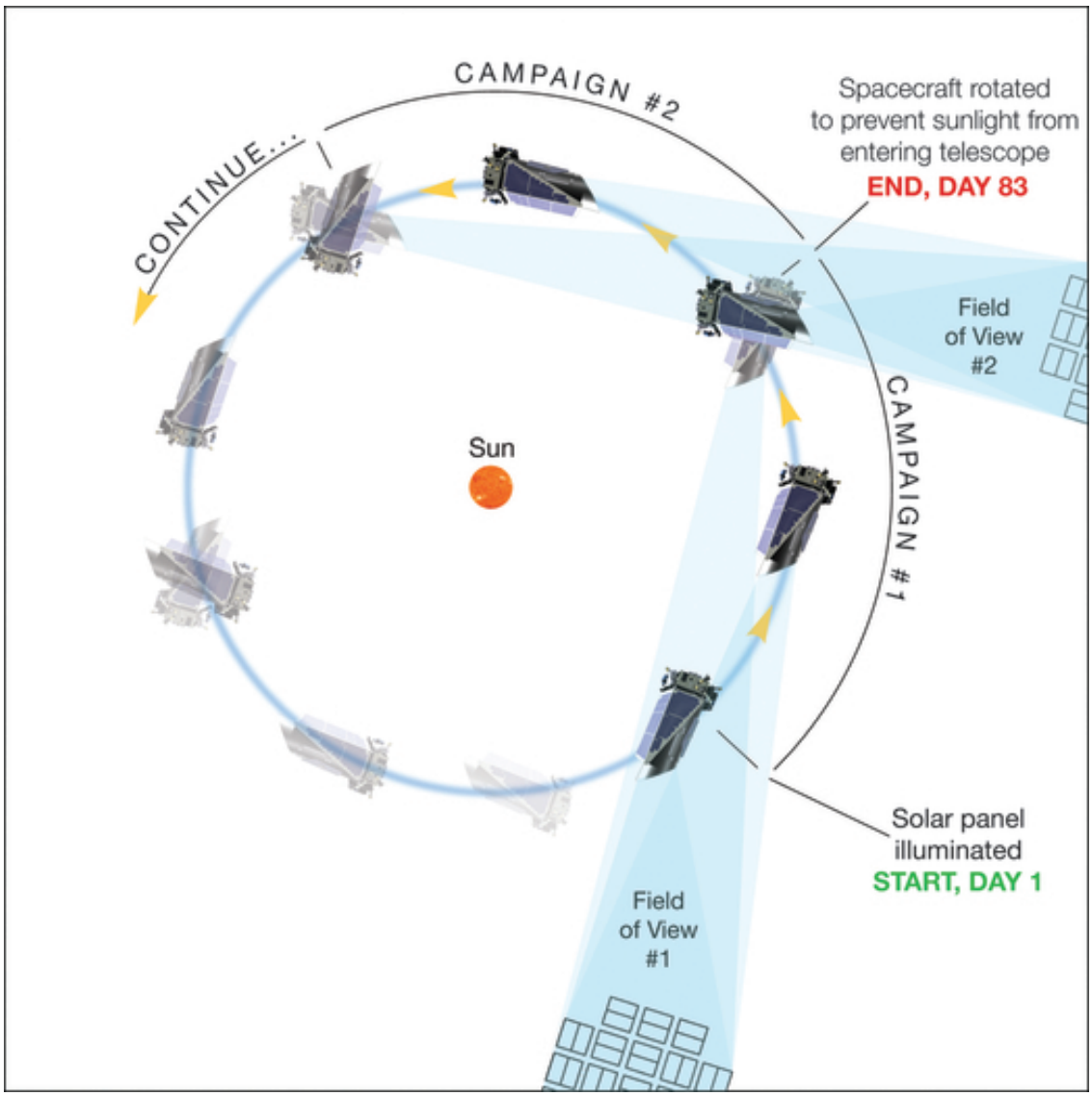

Figure 1.5: Schematic of the K2 Mission. As the spacecraft orbits the Sun, it points at a FOV such that the incident solar photon pressure is balanced. After a quarter of an orbit, it rotates to avoid sunlight drifting into the aperture. Figure from Howell et al. (2014).

This orientation requires pointing along the ecliptic, which means the Sun will drift into the FOV after about 80 days, necessitating a rotation and pointing to a new FOV. Thus, to continue observing, the telescope can no longer point at the same stars continuously, but must switch fields periodically. This new observing mode of 80 day 'campaigns' (Figure 1.5) makes up the new K2 mission (Howell et al., 2014).

The additional drift means more pixels are required per star, so only about 20,000 stars can be observed per K2 campaign instead of the 170,000 from the original mission. However, the targets are selected via community proposals this time, so a wider variety of stars can be targeted; moreover, because the FOVs are scattered around the ecliptic, young clusters and different stellar populations can be observed for the first time.

Although K2 can recover some stability in pointing by balancing the photon pressure, the telescope's drift is still significantly larger than in the original mission: noise levels increased by a factor of about 4, and the constant thruster fires create discontinuities in the light curves every 6-12 hours (Howell et al., 2014). With this reduced data quality, the *Kepler* team still calibrates the light curves, but does not run its own planet search for each campaign. To maximize the science output from K2 then, the community needs to develop tools to better remove the increased systematics of K2 light curves and then run their own planet searches on every campaign. I present one such effort in this thesis.

1.3 Current Understanding of Planet Formation and Evolution

The goal of exoplanet discovery missions like *Kepler* is more than just 'stamp collecting' and increasing the tally of known planets. We ultimately want to use those planets as empirical constraints on our theories of planet formation and evolution. With a large sample of planets around stars of different masses and ages, we can statistically compare the known planets against predictions from various planet formation theories.

In this section I briefly review our current understanding of planet formation, how it has been shaped by the recent flood of new *Kepler* planets, and where some of the outstanding questions lie.

1.3.1 Basics of Planet Formation

Our theory of planet formation ties directly into star formation. Stars form from a collapsing molecular cloud of gas and dust composed of approximately 99% H and He and 1% all other elements (Lissauer, 1995). When collapsing from a scale of light years down to about 100 AU, even the smallest random net rotation in the cloud gets amplified by the conservation of angular momentum, resulting in a rotating, flattened disk (Shu et al., 1994). Most mass accretes into the center forming the protostar, but the majority of the angular momentum remains in the rotating disk with a mass of around 0.02 $M_{\odot}$, where small solid dust and ice particles progressively consolidate into planets (Hayashi, 1981). This rotating disk formation model gives a natural explanation for the Solar System planets' joint orbital planes and why their orbital directions match the rotation of the Sun. In addition to losing material to the central star, the gas in the disk is heated and escapes through photo-evaporation, eventually resulting in complete disk dissipation; observations limit typical disk lifetimes to just 10 Myr (Mamajek, 2009).

Growth of Solids

Planets are thought to form from this gaseous, star-forming disk in that brief ten million year window. Of the 1% of the disk composed of heavier elements, some of those can be solids in the form of dust grains if the local temperature is below that material's condensation or sublimation point. Because the temperature of the disk increases toward the central protostar, the cooler outer reaches allow for more solid materials, creating various 'lines' beyond which certain solids exist (Grossman & Larimer, 1974); the most notable of these is the water ice 'snow line'. The rarer irons and silicates dominate the inner, hotter regions of disks (inside of an AU or so) as the only solids, but farther out more volatile yet common materials like water, ammonia, and methane form the majority of the solids (Lodders, 2003).

These grains slowly collide and clump together forming progressively larger solids in the disk, up to about a mm or cm size. Above this scale, barriers seemingly prevent further

growth. First, collisions may become energetic enough that the particles bounce off one another instead of sticking (Wada et al., 2009; Testi et al., 2014). Even if grains can stick and grow, all solids feel a gas drag in the disk that tends to decay their orbits. At the meter size, this drag is maximized and particles' orbits decay into the star in as few as 100 years, leaving very little time to merge into much larger objects more resistant to orbital decay (Weidenschilling, 1977; Morbidelli & Raymond, 2016).

One of the leading theories to overcome this 'meter barrier' problem is known as the streaming instability (Youdin & Goodman, 2005). Many different mechanisms have been proposed to seed local overdensities of particles in a dynamic disk (turbulence, local pressure bumps, vertical shear instability, baroclinic instability; for a review see Izidoro & Raymond, 2018). Regardless, a local overdensity of small particles speeds up the surrounding gas through the reciprocal force of the drag-inducing collisions, thereby reducing the drag and rate of orbital decay. This allows faster inspiraling isolated particles to catch up (Johansen & Youdin, 2007), accentuating the overdensity, and further slowing the group's inspiral rate, creating a runaway collection of small particles. If the concentration of solid particles to gas reaches a high enough level, a gravitational collapse becomes possible, directly forming an object on the kilometer size or larger (Johansen et al., 2007; Schäfer et al., 2017).

Planetesimals to Planets

Regardless of the mechanism, once the solids start reaching kilometer size scales (called planetesimals), their gravity and mutual interactions play larger roles as they begin disturbing the material in the disk and one another. These planetesimals first enter a 'runaway growth' phase where the largest bodies grow most rapidly by gravitationally focusing material to boost their effective radii, creating a small number of large objects (approximately moon-sized, called planetary embryos) that accrete everything in their path (Safronov, 1972; Lissauer, 1995).

As these embryos grow, they begin to dynamically stir the surrounding planetesimals, which slows their growth. This mode is 'oligarchic' growth, in which the embryos are growing

faster than the smaller planetesimals, but smaller embryos catch up in size to the largest ones (Wetherill & Stewart, 1989; Izidoro & Raymond, 2018). If embryos get too close, they scatter or merge, and the disk gas then damps their orbits back to circularity. This creates a series of embryos isolated from one another and separated by a few mutual Hill radii (Kokubo & Ida, 1995; Ormel et al., 2010).

These planetesimals and embryos can continue to grow by attracting the small mm to cm-size grains, known as pebble accretion (Johansen & Lacerda, 2010; Johansen & Lambrechts, 2017). The small pebbles continue to form and spiral inwards while planetesimals and embryos are growing throughout the disk. As the pebbles pass planetesimals, gas drag can slow them enough to be captured and accreted by the planetesimals (Lambrechts & Johansen, 2012). This can grow planets quickly and could be the dominant growth mechanism of embryos bigger than the Moon as they filter as much as 10% of the pebbles passing through their orbit (Morbidelli & Nesvorny, 2012; Johansen & Lambrechts, 2017). As the gas in the disk clears and embryos clear most pebbles and planetesimals from their orbits, the eccentricity and inclination damping disappears, and instabilities can grow, causing a chaotic cascade of large collisions and consolidation into fully formed planetary systems (Kenyon & Bromley, 2006; Cresswell et al., 2007; Bitsch & Kley, 2010).

This process is enough to form terrestrial planets, but the ice and gas giants need to collect their gas before it dissipates. If cores grow large enough (10 $M_{\oplus}$) while gas in the disk is still around, the core can accrete and retain the gas in the disk, forming a H and He atmosphere as seen in our outer ice giants (Bodenheimer & Pollack, 1986). This gaseous atmosphere can only grow as fast as it is able to cool, creating a phase of relatively slow gas accretion (Pollack et al., 1996). If the gaseous atmosphere reaches a critical mass of order the core mass, however, a hydrostatic equilibrium is impossible, and the atmosphere collapses, allowing for accelerated accretion rates, and planets grow to gas giants the size of Saturn or Jupiter (Stevenson, 1982; Wuchterl, 1993).

Planet Migration and Evolution

A final process likely to play a crucial role in planetary system formation and evolution is disk migration. While the disk dictates the movement of grains and small planetesimals, often decaying their orbits via gas drag, planet embryos can affect the gas disk itself.

Once embryos reach masses about a tenth that of Earth, they start to create density waves in the gaseous disk (Goldreich & Tremaine, 1979). These waves create both inward and outward torques which vary in magnitude based on different properties of the disk (Armitage, 2018). The net effect can be positive or negative, leading to either inward or outward migration (termed type I) of the planet (Bitsch et al., 2014).

Massive planets ($\gtrsim 10$ $M_\oplus$) can create wakes large enough that they clear gaps in the disk of all gas (Crida et al., 2006). This creates a new form of inward planetary migration (type II), causing the largest planets to drift inward, though at slower rates than type I (Dürmann & Kley, 2015).

One consequence of this migration of planets away from their formation location is the possible creation of resonances. Planets will initially migrate inwards at different rates due to their different masses and local disk properties. Pairs of planets can then fall into mean motion resonances — when the orbital periods are perfect integer ratios of one another (e.g. 2:3, 3:4); these resonances are difficult to break, and instead the planets begin to migrate together while staying in resonance (Cresswell & Nelson, 2006). This process creates inwardly migrating resonant chains of planets, some of which survive today in the *Kepler* sample (Fabrycky et al., 2014).

1.4 The Boundary Between Rocky and Gaseous Exoplanets

One of the most sought answers in exoplanet science is the boundary between rocky and gaseous exoplanets. Is there a mass or radius limit below which most planets tend to be rocky, while those above the limit have a hydrogen and helium gaseous envelope? The answer puts constraints on planet formation and migration models, but it also helps prioritize followup of

individual systems. In the coming years, large telescopes like James Webb will have limited time to study small planets, and a community priority is to use that time to study rocky planets that may be similar to the Earth.

To turn a rocky planet into a gaseous one requires a very small amount of gas. Rocky cores have bulk densities of 4-10 g/cm^3, and they are limited in size to about 3 $R_\oplus$; adding more mass to cores of that size doesn't increase the radius because of electron degeneracy pressure (Seager et al., 2007). On the other hand, taking a rocky core of 1.2 $R_\oplus$ and adding a hydrogen and helium envelope just 0.1% of the core's mass inflates the radius to 1.5 $R_\oplus$ (Lopez & Fortney, 2014). A 1% by mass envelope brings the radius to 2 $R_\oplus$. A 0.1% mass fraction atmosphere also creates a surface pressure of hundreds of atmospheres — a planet very unlike the Earth (Lopez & Fortney, 2014). The small change in mass with a simultaneously large increase in radius causes a noticeable decrease in bulk density, creating two methods to detect the transition between rocky and gaseous planets: a size above which planet densities begin to decrease, or a gap in the radius distribution since any gaseous atmosphere quickly inflates a rocky planet's radius.

The first data containing masses and radii of small exoplanets arrived with *Kepler*. Radial velocity followup of small *Kepler* planets indicated that bulk densities started to decrease at a planet radius of about 1.5 $R_\oplus$, hinting that planets above that size begin hosting gaseous hydrogen and helium envelopes (Weiss & Marcy, 2014; Rogers, 2015).

Initially, the uncertainty in the radii of *Kepler*'s target stars was 25% on average, limiting knowledge of a transiting planet's radius to at least that (Huber et al., 2014). Any radius gap caused by a sudden transition between rocky planets and those with significant gaseous envelopes would be washed out with uncertainties so large that planets of size 1.5 and 2 $R_\oplus$ cannot be reliably distinguished. Petigura et al. (2017) set out to get high resolution spectroscopy of the *Kepler* host stars and better characterize them. With the better data, Johnson et al. (2017) reduced the uncertainties in the stellar radius to just 11%. With the higher star and planet radii precision, Fulton et al. (2017) found a gap in the planet radius distribution for *Kepler* planets with periods less than 100 days: there are relatively fewer

planets with radii between 1.5-2.0 $R_\oplus$ than there are on either side — further evidence of the size boundary between rocky and gaseous exoplanets.

What makes some short period planets rocky and others gaseous remains an open puzzle. One potential explanation is a difference in formation time: rocky planets finished forming after the gas disk has dissipated, depriving them of any chance to accrete an atmosphere (Lee et al., 2014). This model is believed to be true for the inner rocky planets of our own Solar System (Lissauer, 1987). Another explanation is one of evolution and atmospheric evaporation: nearly all short period planets form quickly and with gaseous atmospheres, but thinner atmospheres are evaporated via energy from the host star over time (Owen & Wu, 2013; Jin & Mordasini, 2018).

Lopez & Rice (2016) showed that if atmospheric evaporation were the dominant mechanism, the location of the radius gap would shrink farther from the star. The critical metric is the incident flux of the star; the more energy a planet receives from its star, the more atmosphere can be evaporated, and more massive cores can be evaporated, creating large exposed rocky cores and a radius gap at relatively high radii. Far from the star, only small cores with a tenuous gravitational hold on a thin atmosphere will be evaporated, leading to only small rocky cores and a radius gap occurring at a smaller planet radius.

If the difference between rocky and gaseous planets is predominantly due to a late formation history, then the radius gap will trend the other way. The final size of a rocky planet is thought to roughly correspond to how much material is in the disk at its formation location (Chiang & Laughlin, 2013). Migration and scattering make this a noisy measure, but in general there is more disk material farther from the star, and so rocky planets are expected to be larger farther away (Hansen & Murray, 2013). This formation mechanism therefore predicts the location of the radius gap will increase farther from the host star, contrasting the photo-evaporation prediction (Lopez & Fortney, 2013; Lopez & Rice, 2016).

Fulton et al. (2017) did not have a large enough sample or good enough planetary parameters to distinguish a slope in the radius gap as a function of incident flux from the host star. Van Eylen et al. (2017) used asteroseismology to get stellar radii at a precision of 3%, with

a tradeoff of a much smaller sample of planets. Still, they found the radius gap decreasing at larger separations, providing support for the photo-evaporation theory.

The location and shape of the radius gap will be an active area of research in the coming years, and a larger sample of planets near it can only help. In addition to constraining formation and evaporation models by its shape, how many planets are found within the gap can help constrain the amount of ices that make up rocky planets. Planets with a large amount of volatile ices will have larger cores that would act to fill in the gap (Jin & Mordasini, 2018). Meanwhile, if the photo-evaporation model is accurate, many planets that seem rocky today would have actually had a very different history from the Earth, with a thick atmosphere earlier in their life that may affect how we view their habitability (Luger et al., 2015).

One further set of planets that may help us distinguish the limiting size for rocky compositions are the ultra-short-period (USP) planets. USPs have periods less than a day and are roasted by their host stars. At such high incident fluxes, all atmosphere is thought to be stripped away, leaving a pure sample of rocky cores (Owen & Wu, 2013). Sanchis-Ojeda et al. (2014) found that all USPs in the *Kepler* sample are consistent with radii below 2 $R_\oplus$; a larger sample of USPs may help constrain the rocky core size distribution.

1.5 Thesis Outline

In this thesis I present my own contributions to the field of exoplanet discovery. I begin in Chapter 2 by describing the pipeline I developed to find planets from the K2 mission. I also motivate its design to be a general purpose method to find transiting planets often overlooked by other searches: planets with transit timing variations or displaying only one or two transits.

Chapter 3 puts this pipeline to action, searching the first nine K2 campaigns for planets. I present my sample of astrophysical candidates and describe how I separate the planet candidates from eclipsing binaries and probable false positives. I also highlight the individual characteristics of the most interesting candidates and binaries.

Chapter 4 puts my discoveries into context. I compare my pipeline to previous efforts to find planets in K2. I show how K2's more diverse stellar sample contributes to our samples of planets in different environments and how K2's generally brighter host stars spread across the sky allows for easier followup.

Chapter 5 emphasizes the versatility of my methods. In a search of the original *Kepler* planet candidates for additional candidates, I came across a unique system. I show here how it can be modeled as the first self-lensing binary star system — where a white dwarf in an eclipsing binary gravitationally lenses its companion causing a periodic brightening of the system.

Finally, in Chapter 6 I summarize my work and discuss future improvements. I will use lessons learned from the work of this thesis to further improve my pipeline's sensitivity to planets, and I will apply that work to the newest K2 campaigns. I discuss what followup can be done on my planet candidates to better characterize the stars and planets and how that will help address some of the open questions in planet formation introduced in this chapter. Finally, I show how this work will apply to the newest space-based transit search, the *TESS* mission.

Chapter 2

AN UPDATED QUASIPERIODIC AUTOMATED TRANSIT SEARCH PIPELINE

In this chapter I develop the methodology of a planet search pipeline. I introduce our work to return the degraded data quality of the K2 mission back to near that of the original *Kepler* mission. I then explain, using examples from a well known 3-planet system (K2-3) found in an early campaign, how I have modified the original `QATS` planet search to make it more robust and enable it to find planets in the K2 data. I discuss how we separate astrophysical signals from false positives returned by `QATS`, how we repeatedly search a star for multi-planet systems, and how we model the planet candidates we do find.

2.1 Introduction

The *Kepler* mission (Borucki et al., 2010) produced an abundance of transiting planet candidates within the 400 square degrees and four years (2009-2013) of its survey of $\approx 2\times10^5$ stars (Borucki, 2016; Coughlin et al., 2016; Thompson et al., 2018). The failure of the spacecraft's second of four reaction wheels in 2013 halted the prime mission due to pointing degradation; three wheels are required to stabilize the pitch, yaw, and roll of the spacecraft. Symmetric irradiation by the Sun on the solar panels has been used to balance the telescope along a third axis, allowing continued operation with only two reaction wheels (Howell et al., 2014). However, such a balance is only achieved by pointing the telescope along the ecliptic — away from the original *Kepler* mission field of view.

To avoid sunlight in the aperture, the telescope is reoriented to a new field of view along the ecliptic every ∼80 days (a 'campaign'). These campaigns along the ecliptic comprise a new mission entitled K2 (Howell et al., 2014). Because the K2 campaigns cover more

varied portions of the galaxy and the target list is driven by community proposals, the K2 targets are more diverse than the mostly solar-like stars of the *Kepler* mission. Late-type M dwarf stars have been favored as targets because these give the best chance within the limited campaign duration to find small, temperate planets which may be rocky and lie in the surface liquid water 'habitable zone' (Kasting et al., 1993; Kopparapu et al., 2013). Stellar clusters of varying ages have also been targeted, including Praesepe (also called Beehive) (Mann et al., 2017; Libralato et al., 2016; Obermeier et al., 2016), M67 (Nardiello et al., 2016), Pleiades (David et al., 2016a), and Hyades (Mann et al., 2016) to uniformly study many stars at the same age.

While the photon pressure is approximately balanced and keeps the spacecraft relatively stable, the pointing of K2 does drift over a timescale of six hours, followed by a thruster fire which brings the pointing back near the initial position. The pointing typically drifts by ≈3-4 arcseconds (corresponding to ≈1 pixel) in early campaigns and by slightly smaller angles in the later campaigns. These pointing drifts lead to gradual systematic changes in the measured flux of target stars due to variations in sub-pixel sensitivity that cause a different number of photoelectrons to be detected depending on the location of a star on the detector. The gradual systematic change in flux is followed by an abrupt discontinuity caused by the thruster fire changing the pointing more dramatically between cadences. These effects combine to create light curves dominated by saw-tooth shaped systematics on timescales of 6-12 hours; the changes in flux due to these systematic effects are about an order of magnitude larger than the white noise level of most targets.

The official *Kepler* pipeline used for the prime mission is not designed to handle these pointing drift systematics. The team processes the pixels and produces calibrated pixel files using the same methods as the original mission, but the derived light curves retain the systematic saw-tooth shaped effects (Howell et al., 2014). Altogether, the raw photometric precision of an average 12th magnitude star in K2 is ≈400 ppm (compared to 100 ppm in the original *Kepler* mission), which is too noisy to detect small transits (Howell et al., 2014).

Many groups have modeled the additional K2 systematics with custom pipelines to gen-

erate light curves with reduced instrumental noise and artifacts. Since the measured flux correlates strongly with the position of stars on the detector, Vanderburg & Johnson (2014) developed a K2 detrending algorithm, `K2SFF`, that decorrelates the raw K2 flux against the centroid position of each star versus time with a non-linear function. Vanderburg & Johnson (2014) have demonstrated a precision within a factor of two or better of the original *Kepler* mission, depending on the magnitude of the target star.

Other approaches to the detrending utilize common-mode variations amongst stars (Montet et al., 2015; Foreman-Mackey et al., 2015), a Gaussian Process approach to decorrelating the flux against time and stellar centroid (`K2SC`; Aigrain et al., 2016; Pope et al., 2016), and PSF-fitting to derive light curves for multiple stars in each postage stamp (Lund et al., 2015).

In this and subsequent chapters we present a new search for planets in the K2 dataset utilizing an approach to detrending that further improves the photometric noise to within 20% of the original *Kepler* mission for stars in the magnitude range $11 < Kp < 13$, where Kp is the magnitude defined in the *Kepler* bandpass. The new approach, EPIC Variability Extraction and Removal for Exoplanet Science Targets (`EVEREST`), solely utilizes information from pixels within the aperture containing each star and sidesteps estimating the stellar centroids (Luger et al., 2016). This new approach can provide improved light curves for K2 target stars, which enables a more sensitive search for planetary transits.

In section 2.2 we summarize the `EVEREST` detrending pipeline, and then discuss our planet search pipeline; we also detail the vetting of candidates, the search for multiple candidates, the flagging of eclipsing binaries, and the Markov chain analysis procedure used for each candidate. In chapter 3 we summarize the results of our search and the properties of the candidates. In chapter 4 we discuss the implications of those results.

2.2 Methods

2.2.1 Pipeline Overview

Before diving into details, this section sketches the general outline of our pipeline — from raw pixels to planet candidates — and points the reader to the relevant sections discussing each piece in more depth.

To address the systematic variations in the K2 photometry, we have developed a new pipeline for decorrelation of the raw K2 light curves, `EVEREST` (Luger et al., 2016, 2017a) which we briefly review in §2.2.2. Our approach makes use of the pixel level decorrelation (`PLD`) technique, which bypasses the centroid and instead decorrelates the light curve against the normalized flux in each pixel within the aperture (Deming et al., 2015). Once `EVEREST` has removed the most significant systematics, we apply some further filtering to the data to remove spurious outliers (§2.2.3).

We then use a modified version of the Carter & Agol (2013) quasi-periodic automated transit search (`QATS`) technique to search for planet candidates. Although designed specifically to find planets exhibiting transit timing variations (TTVs), `QATS` can also be used as a general purpose planet detection method, which we apply to the K2 dataset. `QATS` relaxes the strictly periodic constraint assumed in most planet search techniques, such as Boxed Least Squares (`BLS`; Kovács et al., 2002). Instead, consecutive transits must only fall within a tunable time window — the wider the window, the larger the TTVs that can be captured. However, wider time windows come at the cost of raising the noise floor, making the detection of the smallest planets more difficult. We compromise by searching over three different windows, from perfectly periodic to a very large TTV signal.

The original `QATS` technique worked directly with the light curve fluxes, but we instead calculate the log likelihood ratio ($\frac{1}{2}\Delta\chi^2$) between a transit of a fixed depth and duration and a simple polynomial continuum centered at every cadence in the light curve (§2.2.4). We repeat this search for a grid of possible transit depths and durations. By searching over a range of transit depths, we force the algorithm to only look for features that have the same

depth for every transit event, in contrast to the original version of QATS as well as other techniques like BLS.

For each depth, duration, period, and QATS transit window tuple, we input to QATS the log likelihood ratio versus time to find the maximum likelihood times satisfying these constraints (§2.2.5). Over the entire range of duration, depth, period, and transit window combinations the largest log likelihood ratio solution is selected as the best planet candidate for that star.

QATS will return a 'maximum likelihood candidate' for every single star regardless of its actual likelihood of being a planet candidate, so we perform some automated cuts to select only the most likely candidates (§2.2.6). Systems that pass the automated cuts are then manually vetted (§2.2.7) for astrophysical significance (i.e. planet transits or eclipsing binaries). All stars that have one candidate are passed back through the entire process after masking out the known candidate to search for further signals; we repeat until nothing passes and we have a final list of vetted candidates (§2.2.8).

This final list of astrophysical candidates is modeled through a Markov chain Monte Carlo (MCMC) analysis to determine the system's parameters (§2.2.9). We also run an MCMC for each candidate's odd and even events separately to help identify eclipsing binaries (§3.1.1) and to check for period and ephemeris matches between candidates indicating likely false positives (§3.1.2). All systems that are not flagged by these cuts as false positives or eclipsing binaries compose our final list of planet candidates.

2.2.2 Data Selection and Light Curve Detrending

We used the EVEREST 1.0 detrended light curves for K2 campaigns 0-8 (Luger et al., 2016) as the starting point for our planet search. These were derived from MAST Data Releases 1-11[1] of the calibrated pixel-level light curves and a version of the EVEREST code that is permanently archived on Zenodo[2]. We selected all long cadence targets with object type star or null, yielding a sample of 152,865 stars in C0-8 (we do not search any short cadence

[1] https://keplerscience.arc.nasa.gov/k2-pipeline-release-notes.html

[2] http://doi.org/10.5281/zenodo.56577

light curves). The EVEREST light curves were generated using aperture number 15 of the K2SFF pipeline (Vanderburg & Johnson, 2014; Vanderburg, 2014).

The details of the detrending process are described in Luger et al. (2016). Briefly, the PLD technique in EVEREST uses the normalized flux in each pixel in the aperture as inputs, similar to how a centroid calculation works. The normalization removes the astrophysical signal within the aperture (assuming that the flux is due in total to the target star), leaving only instrumental signals in the pixel time series. EVEREST uses pixel fluxes and products of powers of pixel fluxes as inputs to a linear model that is subtracted from the data to yield a systematics-free light curve. Cross-validation is performed to optimize the number of regressors and prevent overfitting, and a gaussian process (GP) is employed to capture correlated stellar variability. We find that the EVEREST light curves recover *Kepler*-like precision for stars brighter than $Kp \sim 13$.

2.2.3 Further Light Curve Preparation

Prior to searching the publicly available EVEREST light curves for planets, we cleaned up any regions that could interfere with detecting transits. The two main obstacles in the K2 data are: 1) bad data points occurring at the same cadence across multiple light curves (primarily due to poorly modeled thruster fire events) and 2) outliers unique to one particular light curve (e.g. stellar flares or cosmic rays).

A straightforward, albeit time-consuming, way to find bad cadences impacting many light curves is to run an initial planet search and make a histogram of the cadences identified as the centers of transits. As transit times should not correlate between stars, the distribution of transit times across all stars should be uniform; an obvious preference for 'transits' occurring at a particular cadence across multiple stars is highly indicative of some systematic effect. In our first search we found such pileups, as shown for a subset of Campaign 1 in Figure 2.1.

For each campaign, we removed the most troublesome cadences, as well as the ones just before and after, in every light curve; we also manually inspected a handful of the events to see if a longer duration segment needed to be removed to eliminate the problem. To identify

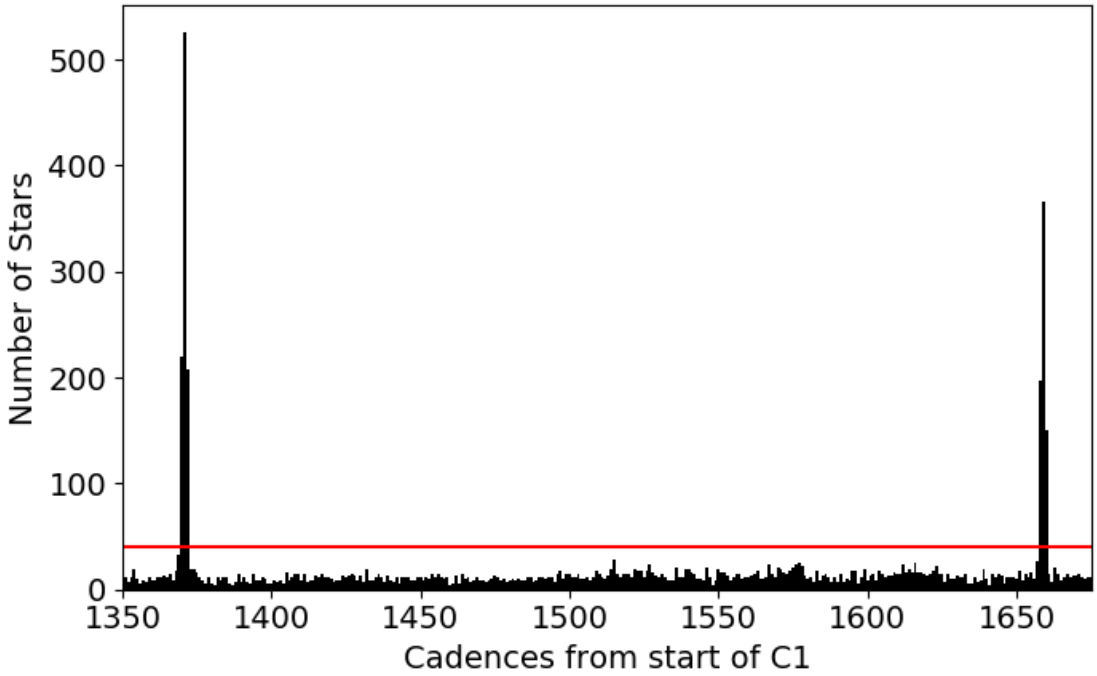

Figure 2.1: Zoom in on a segment of Campaign 1 (about 1 week of long cadence data). Number of stars whose top 'candidate' has a period longer 9 days and a 'transit' time at a particular cadence. If there were not correlated systematics between stars, each cadence should have approximately the same number of events. The spikes represent uncorrected systematics, and we remove from our search any cadences above the red line (40 different stars; see Table 2.1), as well as the cadences before and after the problematic ones.

Table 2.1: Identification of bad cadences. For each campaign, we list the minimum number of stars showing a 'transit' at a cadence required for us to remove that cadence (and what percentage of possible stars that limit is). We also list how many total cadences are removed per campaign. See Table 2.2 for the complete list of removed cadences.

Campaign	Min Number Affected for Removal	Removal % of Possible Stars	Number of Cads Removed	Percent of Campaign Removed
0	20	0.43%	34	2.10%
1	40	0.29%	115	2.93%
2	30	0.26%	108	2.84%
3	30	0.27%	123	3.63%
4	30	0.26%	86	2.48%
5	50	0.28%	116	3.17%
6	50	0.22%	221	5.72%
7	30	0.27%	89	2.24%
8	50	0.31%	100	2.60%

the problem cadences, we used all stars which have a top candidate with a period of 9 days or longer — including those later removed by our automated vetting procedures. Nine days was chosen as a cutoff because shorter period candidates are likely less affected by single bad cadences and only add noise to this measure. A histogram of the number of stars for which a potential transit event is identified at every cadence is shown in Figure 2.1. The threshold for the number of affected stars to require a cadence's removal (listed in Table 2.1) changes with each campaign and with the total number of stars with longer period top candidates, but in general cadences which affect more than about 0.2% of such eligible stars were removed. Altogether, we removed around 3% of cadences per campaign at this stage; the list of excluded cadences in each campaign can be found in Table 2.2.

Next we removed outliers within each individual light curve. Single point outliers are especially common in K2 light curves, frequently cannot be removed by `EVEREST` detrending, and need to be mitigated. To identify the outliers, we ran a median filter through the light curve (kernel size of 5 cadences) and compared the flux at any given cadence to its median filter value. The residuals between the observed flux and the median filter were treated as

Table 2.2: Kepler cadence numbers removed from all light curves before searching for planets.

C0	C1	C2	C3	C4
89616-89618	91495-91499	95552-95558	99621-99624	103773-103779
89630-89632	91809-91811	95971-95973	99636-99670	103783-103790
89659-89661	91940-91942	96021-96023	99762-99765	103804-103806
89665-89669	92000-92004	96332-96334	99858-99862	103808-103814
89725-89728	92071-92075	96378-96471	100050-100053	104004-104006
89794-89797	92083-92086	96546-96550	100243-100245	104016-104018
90288-90290	92336-92338	97208-97212	100445-100449	104052-104054
90365-90393	92371-92375	97353-97355	100459-100461	104088-104090
	92504-92507	97625-97627	100902-100904	104316-104318
	92528-92531	98265-98267	101105-101108	104965-104967
	92803-92807	98313-98315	101131-101134	105071-105074
	93091-93095	98373-98376	101411-101413	105179-105181
	93464-93466	98960-98964	101489-101494	105359-105363
	93798-93801		101947-101949	105443-105445
	94075-94079		102066-102069	106032-106034
	94460-94462		102078-102081	106127-106131
	94471-94473		102343-102345	106617-106621
	94490-94492		102404-102407	106635-106637
	94640-94642		102476-102478	106702-106707
	94762-94765		102559-102561	106800-106802
	94771-94775		102769-102771	
	94844-94847		102857-102860	
	94868-94871		102864-102866	
	95036-95038		102875-102877	
	95072-95074			
	95120-95123			
	95144-95148			
	95155-95159			

Table 2.2: Kepler cadence numbers removed from all light curves before searching for planets. (continued)

C5	C6	C7	C8
107579-107590	111362-111554	115890-115893	119938-119947
107592-107629	112003-112007	116753-116755	119950-119953
107823-107825	112126-112129	117401-117404	119956-119958
107918-107922	112161-112165	117415-117417	119985-119989
108124-108126	112197-112200	117437-117440	120046-120048
108182-108185	112303-112306	117737-117739	120149-120160
108291-108294	112473-112477	117978-117980	120274-120276
108687-108689	112508-112512	117984-117986	120671-120674
109071-109073	112653-112657	118000-118003	120763-120771
109551-109553	112702-112705	118017-118020	120945-120948
109815-109819	112736-112740	118025-118029	121030-121034
109924-109926	112779-112781	118073-118076	121426-121430
110020-110022	112795-112799	118083-118087	121470-121489
110045-110047	112813-112816	118096-118099	121632-121634
110211-110214	112880-112884	118113-118116	122278-122282
110234-110237	112941-112945	118169-118172	122374-122378
110415-110418	113180-113182	118288-118291	122566-122568
110932-110934	113266-113268	118306-118308	122586-122595
111041-111044	113686-113689	118361-118364	122673-122678
	113878-113882	118672-118675	122686-122688
	113925-113929	118864-118867	122758-122761
	113937-113940	119022-119024	123010-123014
	114225-114228	119238-119240	123526-123528
	114415-114421		123622-123626
	114428-114432		
	114434-114436		
	114669-114672		
	114789-114792		
	115089-115095		

a normal distribution centered on the median whose width we fit with the median absolute deviation (MAD) — scaling appropriately with

$$\sigma = \frac{1}{\Phi^{-1}\left(\frac{3}{4}\right)}\text{MAD} \approx 1.4826 \cdot \text{MAD}$$

where Φ^{-1} is the quantile function of the normal distribution.

Any cadence whose flux deviates more than 10 standard deviations (positive or negative) from the median filter prediction was labeled as an outlier candidate, as were any adjacent cadences that were more than 3 standard deviations from the median filter value (this captures, e.g., the exponential decay of flares). Any single cadence or set of two consecutive cadences identified in this manner was immediately removed as an outlier. However, short duration transits also get classified as large flux deviations from the median baseline value. We made use of a transit's symmetry to retain any potential transit signals: if a group of 3 or more cadences had its most extreme outlier at the central cadence(s) we did not remove the group. Removing all one- and two-point outliers may bias the search against deep short duration (one hour or less) transits, and we discuss this limitation in §4.1.3.

Quiet stars usually had fewer than 10 cadences removed as outliers at this stage; active stars with flares had a higher fraction of cadences removed. Stars where `EVEREST` performed poorly (due to, e.g., saturation or crowding from nearby bright stars) also had an increased number of outliers removed in this process.

2.2.4 Calculating Likelihoods

With potential outliers removed, we began the transit search using `QATS`. The original `QATS` algorithm makes the assumption that the input data have a zero-mean 'continuum' and white noise, which requires perfect instrumental and astrophysical detrending and in practice is not achievable for all K2 stars. We have modified the input to the `QATS` algorithm by replacing the observed flux at each cadence in the light curve with the log likelihood ratio $\left(\frac{1}{2}\Delta\chi^2\right)$ between a local polynomial fit to the data with and without an added transit (of

fixed depth and duration) centered there. Positive log likelihoods indicate that the local light curve is better fit by adding the transit, centered on that cadence, to the modeled polynomial continuum. In this section we describe how we choose our grid of transit depths and durations and then calculate the likelihood ratio between a transit of that fixed scale and a polynomial continuum. In §2.2.5 we describe how each of those series of likelihoods are input to `QATS` to search for planets.

To calculate the likelihood ratio between a transit and polynomial continuum, we first need to choose an appropriate polynomial order and continuum width (nearby out-of-transit cadences on either side of a putative transit at the cadence of interest). These values need to be chosen independently for each light curve to account for the different timescales of variability present in each star.

For a given light curve, we tested several possible combinations of continuum widths, from 0.2 - 0.6 days with a spacing of 0.1 days, and polynomial order, from 2-5. For each combination, we calculated the $\frac{1}{2}\Delta\chi^2$ as described below for 500 randomly chosen points in the light curve. We fit these 500 $\frac{1}{2}\Delta\chi^2$ values for their median μ_w and standard deviation σ_w (calculated robustly using $\sigma_w = 1.4826 \cdot \mathrm{MAD}$) and chose as the optimal continuum width w and polynomial order M the combination that minimized the coefficient of variation $\frac{\sigma_w}{\mu_w}$. This criterion is intended to give the most uniform likelihood ratio throughout the light curve so that the transit events are easier to identify.

In all of our χ^2 calculations, the uncertainties on each data point were taken to be uniform throughout the light curve and set to our estimate of the white noise level in the light curve. We calculated the white noise level by determining the MAD of the residuals of a linear fit through 1000 random 4-hour segments of the light curve. The median value of these 1000 residual MADs was taken to be the white noise level σ, after scaling by the normal factor of 1.4826.

Having chosen the polynomial continuum parameters, we can calculate the likelihood of a transit at every cadence in the light curve: we model a potential transit with a polynomial continuum plus a transit centered on that cadence (t_0). This model can be approximated

as a linear model if the transit duration T is fixed rather than a free parameter. The modeled flux m at cadence t_i (using all cadences within the transit and continuum region $t_i \in \left[t_0 - w - \frac{T}{2}, t_0 + w + \frac{T}{2}\right]$) is determined by the sum of a polynomial continuum and the transit model

$$m(t_i) = \sum_{j=0}^{M} a_j (t_i - t_0)^j + \frac{\delta}{\delta_0}\Big(\mathcal{F}\left(t_i, t_0, T, b, u_1, u_2, \delta_0\right) - 1\Big) \tag{2.1}$$

where the continuum polynomial has order M with coefficients $(a_0, ..., a_M)$, and $\mathcal{F}$ is a Mandel-Agol transit model integrated over the cadence duration with mid-transit time t_0, duration T (first to fourth contact), impact parameter b, limb darkening parameters (u_1, u_2) (linear and quadratic), and maximum depth of transit δ_0.

In all cases we used a transit shape with fixed parameters $(b, u_1, u_2, \delta_0) = (0.3, 0.4, 0.25, 0.02)$. The maximum depth of transit can be well approximated by the following function of limb darkening parameters, impact parameter, and planet to star radius ratio $\frac{R_p}{R_*}$

$$\delta_0 = \left(\frac{R_p}{R_*}\right)^2 \frac{1 - u_1(1 - \sqrt{1 - b^2}) - u_2(1 - \sqrt{1 - b^2})^2}{1 - u_1/3 - u_2/6}. \tag{2.2}$$

Inverting this equation gives $\frac{R_p}{R_*} \approx 0.13$ in our chosen transit model, appropriate for a Jupiter-sized planet transiting the Sun or an Earth-sized planet transiting an M dwarf — roughly what one would expect to find in the 80 day duration K2 campaigns. To maintain linearity (and therefore greatly reduce computation time), this fixed transit shape is scaled to the appropriate depth δ, rather than adjusting e.g. the $\frac{R_p}{R_*}$, which would slightly change the shape of the transit as the depth changes and break the linearity with depth. Our method is robust to the precise shape of the transit model, however, and even a simple box model would work nearly as well.

With the transit shape and duration fixed, the model is linear in the remaining free parameters: the transit depth and polynomial coefficients $(\delta, a_0, ..., a_M)$. Although the transit shape is not critical to the search and thus held at one set of fixed values, we do need to

search over a variety of transit durations. Because the model $m(t_i)$ is a nonlinear function of the transit duration, T, we repeat the search over a grid of 16 fixed transit durations from 2 to 17 hours, with each duration 15% wider than the previous one.

We solved for the linear coefficients $(\delta, a_0, .., a_M)$ at every duration in our grid and with the transit model midpoint t_0 at every cadence for which there was at least one valid cadence both in transit as well as on each side of the continuum. The solution to this linear equation produces the optimal transit depth, $\delta_{\rm opt}$, at that t_0 and T combination (as well as the optimal polynomial continuum parameters). Further, because of the nature of linear equations, the χ^2 at any other depth δ is a quadratic function and can be computed later after solving the linear equation just once.

We used these optimal depths, $\delta_{\rm opt}$, to decide at which transit depths to search the light curve: we should only search for planets at depths where at least some cadences suggest there might be such a transit. As an example, the distribution of the optimal depths at all cadences for one particular duration of the Campaign 1 star EPIC 201367065 (the confirmed 3-planet system K2-3) is shown in Figure 2.2. Because in-transit cadences are rare, even for stars with planets, the majority of the light curve has optimal transit depths near 0, with a roughly Gaussian spread (different for each duration). We searched every light curve at every duration for small transits at depths corresponding to 2, 2.5, and 3 standard deviations. Above 3σ, the optimal depths were binned with a width of 2σ, and any bins containing a local maximum (a cadence where the $\delta_{\rm opt}$ is larger than those immediately preceding and following; identified in the bottom panel of Figure 2.3) were also searched. This procedure allowed us to adapt the grid of depths to the individual noise properties of each star, and avoided spending time searching for transit depths that would be undetectably small or transit depths larger than the data suggest exists. On average, this method produced around 8 depths to search for each duration, or about 100-150 combinations of depth and duration per star.

Having chosen the depths to search for planets at each transit duration, we finally need to calculate at every cadence the log likelihood ratio between pure continuum ($\delta = 0$) and a transit at that chosen depth. Because of the simplicity of the linear model, these χ^2

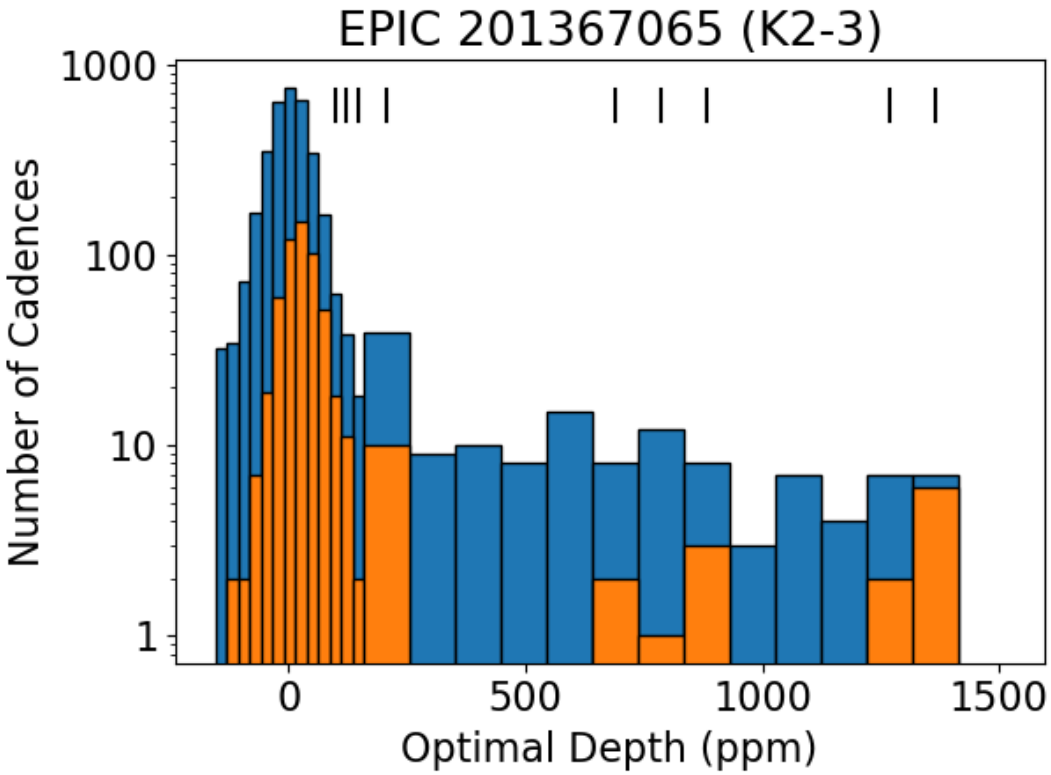

Figure 2.2: Optimal depth distribution of all cadences (blue) and cadences at local maxima (orange; see Figure 2.3) for the search of K2-3 with fixed transit duration $T = 3.04$ hours. Bin width is 0.5σ between $[-3\sigma, 3\sigma]$ and 2 sigma beyond that. Tick marks indicate those depths chosen for the `QATS` planet search, as described in the text. Note that the three planets in this system have depths of 1416, 822, and 782 ppm, falling nicely within our chosen search depths.

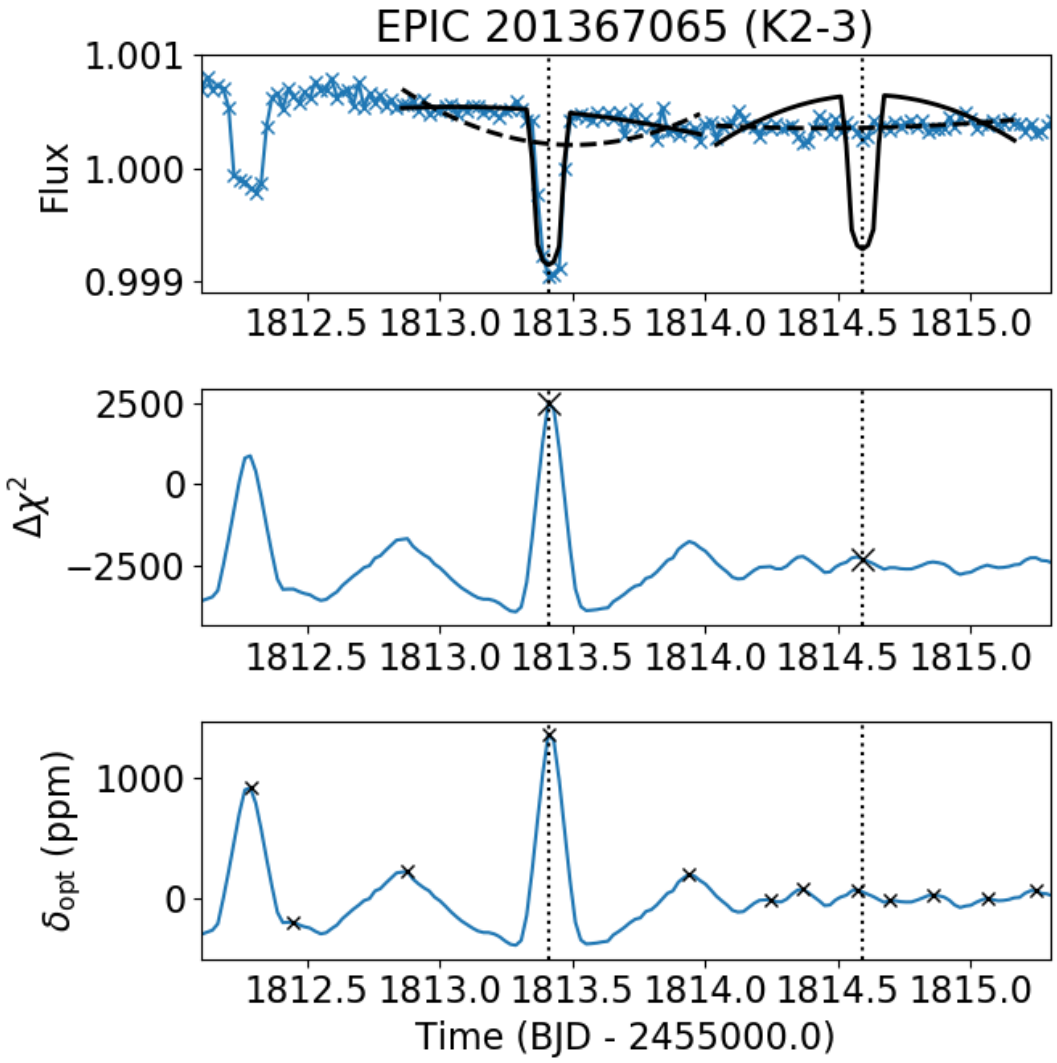

Figure 2.3: Example $\Delta\chi^2$ calculation at a transit of the planet K2-3b and an arbitrary continuum region. The top panel depicts a region of the light curve around a specific transit time and a time with no transits (dotted lines). The dashed line is the polynomial continuum fit to the region ($\delta = 0$) while the solid curve is the polynomial continuum fit plus an assumed transit at the particular cadence (of fixed duration $T = 3.04$ hours and depth $\delta = 1365$ ppm). The difference in χ^2 between these models is plotted as an '$\times$' in the middle panel, which also shows how this $\Delta\chi^2$ varies with the transit model's t_0 at every cadence. The bottom panel depicts the depth at which the $\Delta\chi^2$ is maximized when the transit model (still at fixed duration $T = 3.04$ hours) is centered there. Local maxima used for determining which depths to search for planets are marked with an '$\times$'. Note one of the transits of K2-3c is visible on the left.

calculations are straightforward and we generated the $\Delta\chi^2$ for every cadence, duration, and depth combination.

An example of this process is demonstrated in Figure 2.3 with K2-3 for a fixed duration and depth combination. The top panel shows the polynomial fit compared to a polynomial plus transit fit (of the fixed depth and duration) for a t_0 centered on one of the transits of the 10-day period K2-3b as well as for an arbitrary continuum region. The middle panel shows how the $\Delta\chi^2$ between the two models changes depending on which cadence the fixed-scale transit is centered. Finally, the bottom panel depicts the $\delta_{\rm opt}$ — showing at every cadence what transit depth (still with the fixed transit duration) maximizes the $\Delta\chi^2$. Cadences centered on real transit events will have optimal depths comparable to the true transit depth, while continuum regions will have optimal depths near 0, indicating the region is best fit without a transit at all.

One final step is required since `QATS` requires evenly spaced data: we need to handle data gaps and locations in the light curve where the $\Delta\chi^2$ were not computed. Because of the correlated structure of the log likelihoods, simply filling in gaps with randomly chosen likelihoods biases the planet search. To do a better job at capturing this correlation, we used an autoregressive technique to interpolate from surrounding regions.

We first clipped from the $\Delta\chi^2$ series any points more than $\pm5\sigma$ from the median value to avoid predicting anomalous values (such as transits) in gaps without any data. On each side of a data gap, we fit an autoregressive model using the `statsmodels` Python package's `statsmodels.tsa.ar_model.AR` and a maximum lag length of 30 cadences to predict $\Delta\chi^2$ values within the data gap (Seabold & Perktold, 2010). The two models were then combined using inverse linear weights: the model based on data before the gap had weights linearly declining from 1 to 0, while the model from data after the gap contributed weights increasing from 0 at the beginning of the gap to 1 at the end. Cadences within the gap were assigned simulated $\Delta\chi^2$ values based on the appropriate weighted average of the two autoregressive models. The results for the data gap in the K2-3 system are shown in Figure 2.4.

To summarize our procedure: we calculated the log likelihood ratio ($\frac{1}{2}\Delta\chi^2$) between a

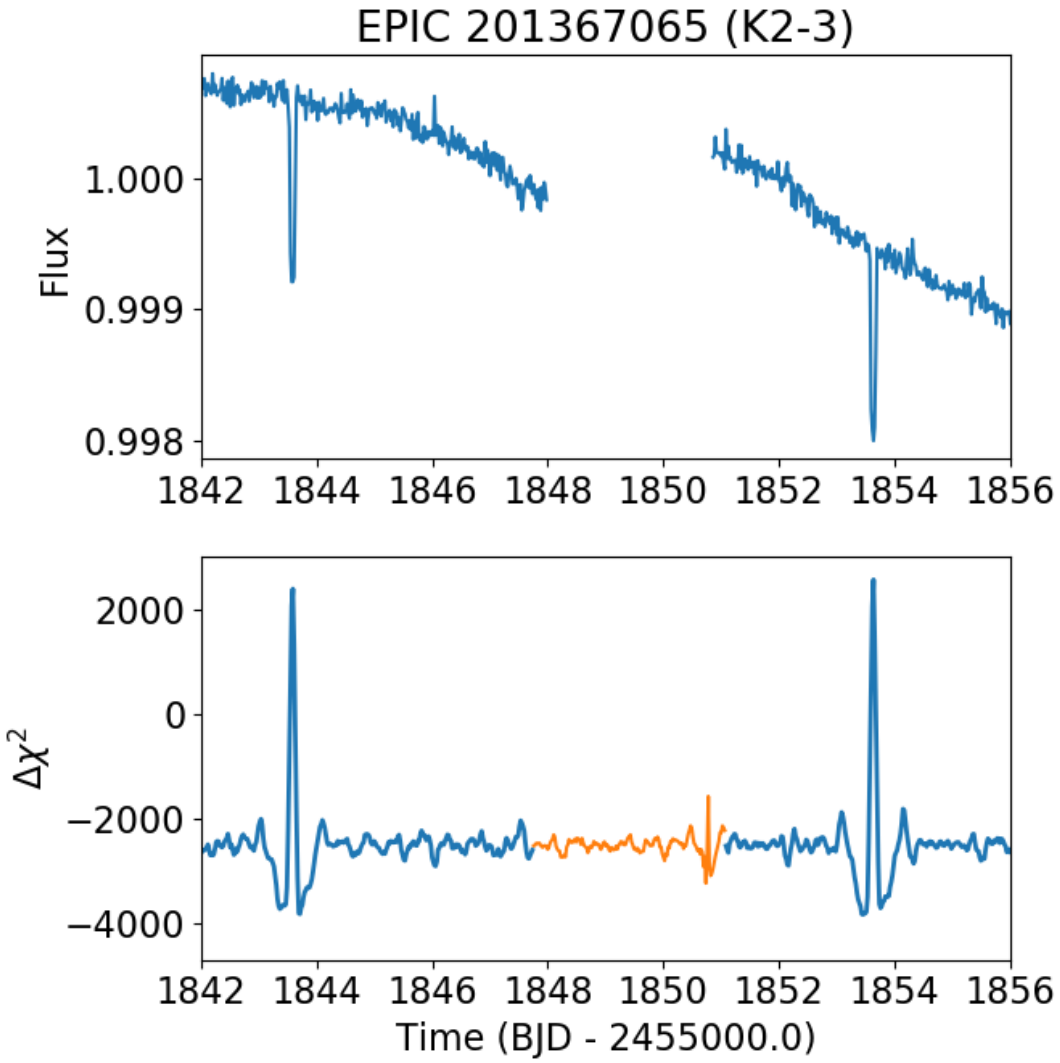

Figure 2.4: Filling data gaps with simulated $\Delta\chi^2$ values using an autoregressive model. Top: Flux of the K2-3 system near the data gap in the middle of C1. Transits of K2-3b can be seen on either side. Bottom: The calculated $\Delta\chi^2$ at every cadence (blue) between the continuum model and a continuum model plus transit of fixed duration $T = 3.04$ hours and depth $\delta = 1365$ ppm. The orange line filling in the data gap is the simulated $\Delta\chi^2$ values. Overall it does a reasonable job reproducing the correlated structures seen in the real values. A slight artifact from the transit can be seen near the end of the gap, but a large spike is prevented due to the clipping of inputs to the model.

local polynomial and a polynomial plus a transit of fixed duration and depth at every cadence in the light curve. This likelihood ratio is what was fed into the `QATS` algorithm instead of raw fluxes. The likelihood ratio calculation was repeated over a grid of transit durations (always the same between 2-17 hours) and transit depths (varying values with each duration depending on the $\delta_{\rm opt}$ distribution). On average, this method produced 100-150 different duration and depth combinations per star, each of which was fed to `QATS` to search for a planet with a transit of that scale.

2.2.5 QATS

With a complete, evenly spaced measure of the log likelihood of a transit of a certain depth and duration at every cadence in the light curve, we can run `QATS`. As a brief summary of how it works, given a chosen minimum and maximum allowable time span between transits, T_{min} and T_{max}, `QATS` returns the maximum total likelihood, and the set of cadences that maximize it, from the input series of likelihoods. The parameters T_{min} and T_{max} are integer multiples of the *Kepler*/K2 long cadence. We refer to the 'period' as $P = (T_{min} + T_{max})/2$, and the number of cadences between them, $W = T_{max}$ - T_{min}, as the transit window — indicating the allowable range of TTVs. For a periodic search we set $W = T_{max}$ - $T_{min} = 1$; we cannot set $T_{max} = T_{min}$ as this would require the period of the planet to be an exact integer multiple of the number of cadences. The original version of `QATS` contains a transit duration parameter in units of the number of cadences; we set this to unity as the log likelihood already accounts for an assumed transit duration.

Because we don't know the period of any potential planets in advance, we searched over possible periods ranging from a minimum of 0.3 days ($T_{min} = 14$ cadences) up to the entire duration of each campaign. Any candidate with a period between 0.3-0.6 days was rerun with a minimum period of 0.1 days (2.4 hours) to ensure we found the correct period and were not biased by the lower limit. We also searched for periodic planets ($T_{max} = T_{min}+1$) as well as two quasiperiodic allowances $\big(T_{max} = \text{ceil}\big[1.0033T_{min}\big]$ and $T_{max} = \text{ceil}\big[1.0066T_{min}\big]\big)$. The more we relax the periodic constraint by widening W, the larger TTVs `QATS` can find,

but at the cost of extra noise because QATS is also more easily able to string together random positive deviations. Under the widest 0.66% quasiperiodic window, the first case in which $T_{max} = T_{min} + 2$ occurs at $154 = 152 + 2$ cadences, or a period of 3.1 days.

For every unique combination of T_{min} and T_{max} ($\sim$7000 total), QATS returned the maximum total likelihood improvement possible for a transiting planet at the specified depth and duration. We don't need to discuss the phase, because for a given period QATS implicitly searches over all phases. For a given depth and duration combination, we plot the QATS total likelihoods over all periods (and thus also phases) and transit windows to create a QATS 'spectrum', as in the top panel of Figure 2.5. We have a similar spectrum for each of the $\sim$150 depth and duration combinations per star. For most cases, the maximum log-likelihood improvement is negative (a transiting planet is less likely than a pure stellar continuum), but the combinations where the maximum likelihood is positive could be a planet. For every star we saved the depth, duration, period, and transit window combination that produced the maximum likelihood improvement (greater than 0) across all possible combinations as the best planet candidate in the system.

2.2.6 Selection of the Most Significant Candidates

The maximum likelihood and period for every star in C1 is shown in the top panel of Figure 2.6. Each K2 target with a maximum likelihood above 0 is shown at its period with the color corresponding to the best fit transit duration. The blue cloud (short transit durations) at lower total likelihood improvements and intermediate periods shows the baseline level for stars without planets. It is almost always possible to stitch together a handful of regions where the stellar continuum is randomly lower than average for a few cadences, so a shallow-depth, short-duration transit can marginally improve the fit. The sudden onset of candidates at 3.1 days is the result of the widened QATS window, making it easier for random noise to add up.

The larger likelihoods at long periods and longer transit durations tend to be caused by 'transits' being fit to local stellar activity. In some cases a 'transit' is fit to a local minimum

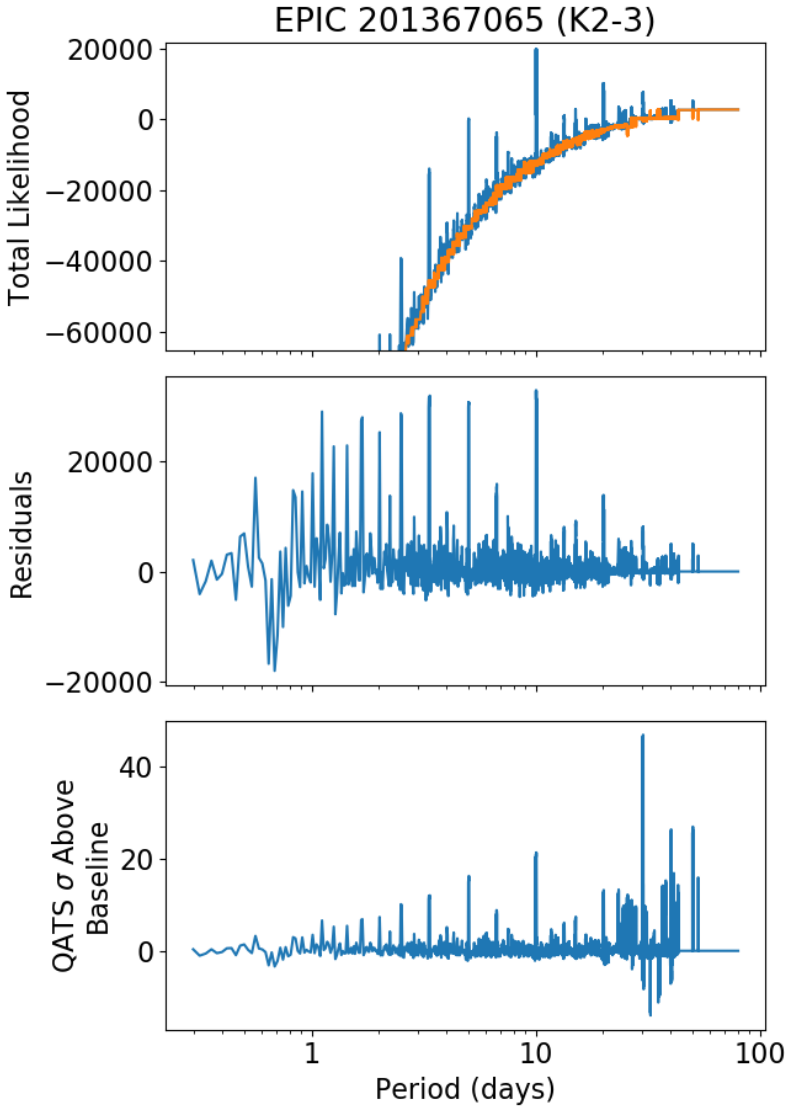

Figure 2.5: Top: Total `QATS` likelihoods (blue) in the search of K2-3 with a transit of fixed duration $T = 3.04$ hours and depth $\delta = 1365$ ppm. The highest likelihood period is at 10.03 days – the period of the largest and shortest period planet in the system. Other spikes of high likelihood occur at aliases of the true period (e.g. 1:N). The orange line is our estimate of the baseline level, ignoring the spikes at significant periods (see text for details). Note the search continued to a minimum period of 0.3 days, but we trim for clarity of the longer periods. Middle: The residuals after subtracting the `QATS` spectrum from the robust baseline estimate. The baseline residuals decrease in magnitude at longer periods. Bottom: The `QATS` total likelihood above the baseline, in standard deviations. Periods beyond about 20 days have three or fewer events contributing to the total likelihood and this measure loses its effectiveness.

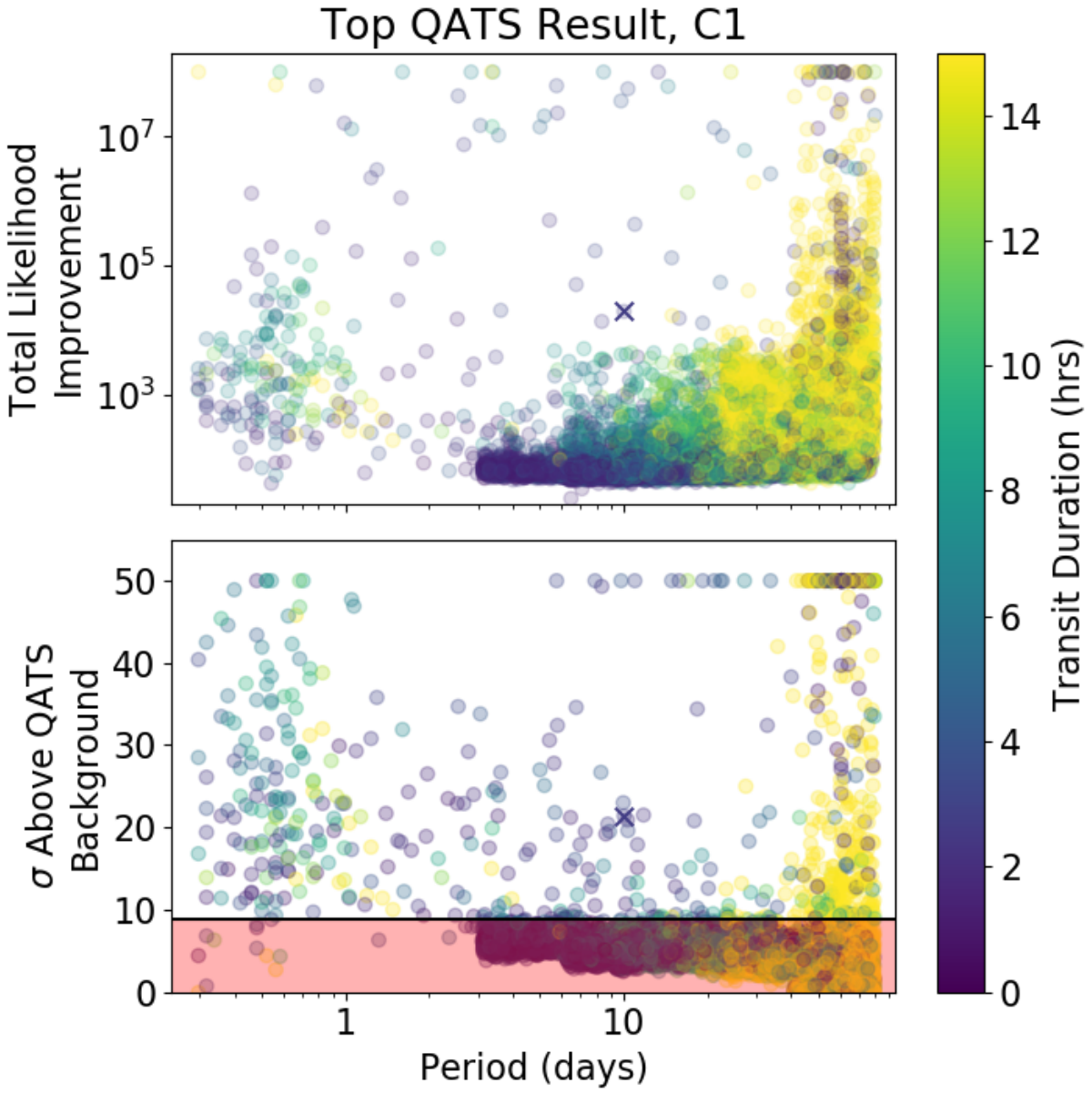

Figure 2.6: Top: The period and maximum likelihood result for every star in C1, color-coded by the transit duration used. The sudden density of results at 3.1 days is due to the first allowed increase of the `QATS` window, and the long duration cloud at periods longer than 40 days is due to the limited effectiveness of one- and two-transit candidates (see text). Any values above 10^8 are clipped down to 10^8 for clarity. The $\times$ marks the first planet in the K2-3 system which we have used as an example. Bottom: The results from the top panel after normalizing the peak event to standard deviations above the `QATS` spectrum background level. The line and shaded region at 8.86 indicate our cutoff: any points below that are rejected from manual examination. Any values above 50 are clipped down to 50 for clarity.

due to stellar rotation, while in other cases the fits are skewed by flares or cosmic rays that were missed in our outlier rejection step.

To narrow the results from the top candidate in every star to only the ones most likely to have a real transiting planet, we made several automated cuts, which we describe next.

QATS Peaks

An indicator of a transiting planet candidate is that the QATS spectrum should show much improved likelihoods at the planet's period and its aliases compared to other periods. As seen in the top panel of Figure 2.5 for the 10-day planet in K2-3, the total likelihood smoothly increases with increasing period, but overlaid on that smooth background is a series of sharp likelihood increases at the 10 day period and its aliases (1:N, 3:2, etc).

Since nearly every star will produce a total likelihood above zero at some small depth, short transit duration, and long period, we need a way to distinguish planets from noise. Our first automated cut focused on the fact that planets will have these spikes in their QATS spectrum at the planet's period and aliases thereof, while other stars show only the smoother spectrum. To distinguish between the two, we measured how high above the surrounding 'baseline' level the maximum likelihood in a QATS spectrum is.

Unfortunately, there is no theoretical means to predict the baseline for a QATS spectrum, so we must make an empirical estimate. To do so, we robustly fit a second order polynomial to a local region of the QATS spectrum, while including a linear step parameter for changes in the QATS window size as well as the number of transits detected. The robust estimate (an iterative fit where points 3 standard deviations away from the fit are down weighted) was crucial to avoid biasing the baseline estimate due to the spikes in likelihood from planets.

The robust baseline estimate is shown in the top panel of Figure 2.5 as the orange line, and the residuals after subtracting this baseline in the middle panel. Aside from the spikes from the planet's period and its aliases, the residuals decrease with period with a power law of $\alpha \approx -0.5$, which we accounted for by measuring the MAD of the residuals as a function of period. Using those MAD estimates, we normalized the QATS spectrum against

the baseline level and calculated the z-score (standard deviations above the baseline) for each total likelihood, as shown in the bottom panel of Figure 2.5. Because real planets have spikes rising high above the surrounding regions, we expect this z-score measure to separate planets with high values from the remainder of the stars without significant transit signals.

The distribution of z-scores for the maximum likelihood candidate signal for every star in C1 is shown in the bottom panel of Figure 2.6; indeed most of the stars show relatively low values, while the high z-scores often contain astrophysical events — either EBs or transiting planets.

Marginalizing over the period, the distribution of each star's maximum likelihood event in standard deviations above the `QATS` spectrum baseline level (this time for all C0-8) is shown in the top panel of Figure 2.7. Most stars form a Gaussian distribution at the core with z-scores of 3-8, with long tails in both directions. The upper tail contains the planets and eclipsing binaries, which exhibit the sharp spikes in the `QATS` spectrum and should be further followed up.

We pause to note however, as seen in the bottom panels of Figures 2.5 and 2.6, the z-score measure begins to break down at the longest periods ($\gtrsim 40$ days). When the period becomes large enough for only one or two cadences to contribute to the total likelihood, many `QATS` quasiperiodic period windows (with a choice of, e.g., two cadences near the ends of a campaign or a single cadence near the middle) will end up with the same total likelihood — choosing only the single cadence in the light curve with the highest likelihood. This clumping of many periods with the same total likelihood affects our `QATS` spectrum baseline estimate and the standard deviation estimate of the residuals, causing many periods to have either a z-score near 0 or an artificially high value (and is thus the cause for the excess of candidates at the low end of the Gaussian tail in Figure 2.7).

More careful handling of one- and two-transit events will be addressed in updated versions of our search pipeline; for now we accept these z-score estimates and the increased likelihood of false positives and false negatives at the longest periods in this stage of automated vetting. The main effects are a) an increased likelihood that one- and two-transit planets have a higher

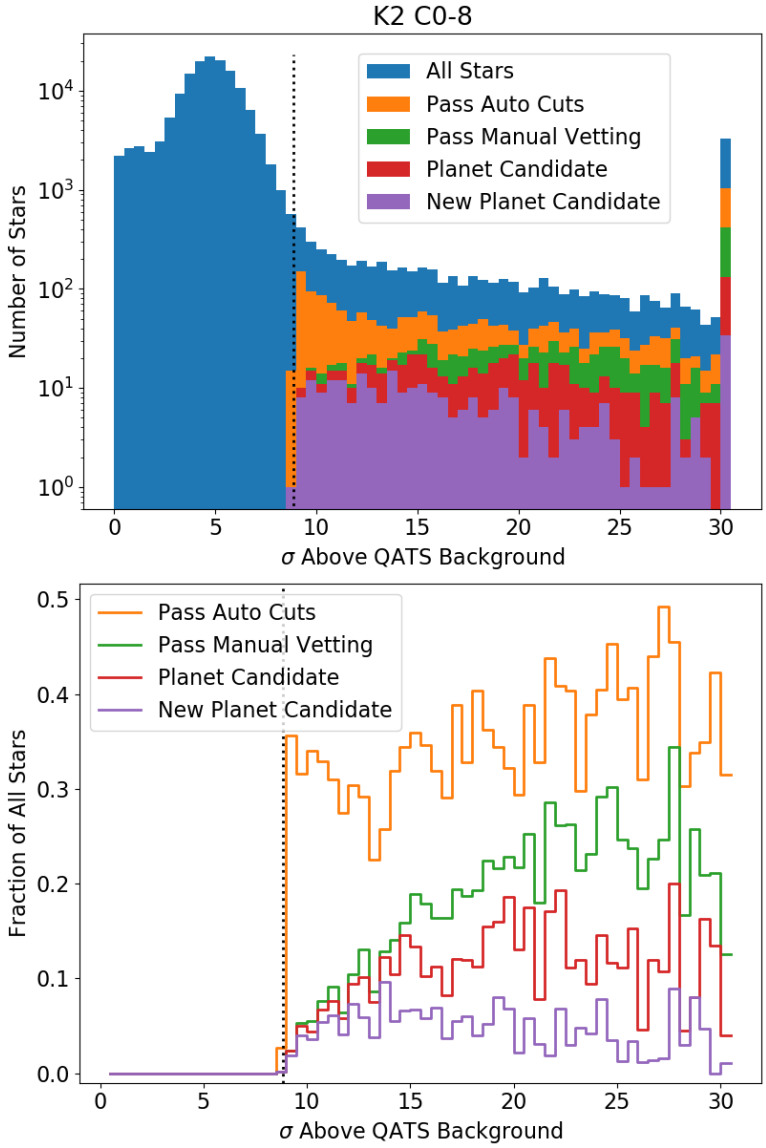

Figure 2.7: Top: For all stars (C0-8, blue), the distribution of heights above the `QATS` spectrum baseline value of the maximum likelihood candidate, in standard deviations (the z-score; see Figure 2.5). The vertical dotted line indicates our cutoff in C1 (see Table 2.3 for other campaigns), below which candidates are removed from our search; this cutoff corresponds to 3.5 standard deviations away from the Gaussian core of the distribution. The orange bars show stars that pass all further automated cuts; green are those that pass the manual vetting as well; red are the planet candidates (after removing EBs); purple shows only our new planet candidates (those not found by any previous groups). All candidates above the maximum value (30) are grouped together in the last bin. Bottom: same as top panel, but showing the fraction of stars in the bin that pass each respective level of cuts.

Table 2.3: Minimum z-score cutoff for each campaign. Any star with a maximum likelihood candidate below this threshold (Figure 2.7) is removed from our search.

Campaign	Min z-score
0	8.71
1	8.86
2	9.61
3	8.93
4	8.93
5	8.87
6	8.99
7	9.54
8	8.99

chance of being missed in this search (having z-scores of ~ 0); and b) the inflated z-scores at long periods also means an increased number of false positives passing our automated threshold — however, these are subsequently culled in the manual vetting and ultimately have minimal impact on the validity of the final candidate list.

To select a minimum z-score threshold for candidates, we looked at the distribution (top panel of Figure 2.7) for each campaign individually. We fit for the median and standard deviation of the z-score distribution (using the MAD) for each campaign; however, to avoid biasing the fit with the long tails, we only used candidates with periods less than 10 days and z-scores between 1.5 and 10. We then selected as our minimum z-score threshold a value of 3.5 standard deviations above this fit — the exact value is listed for each campaign in Table 2.3, but is near a z-score of 9.

We chose 3.5 standard deviations to balance eliminating nearly all stars from the core distribution indicative of no planets, while not eliminating potentially real planet candidates from the long tail too early. As this is just the first of several rounds of automated and manual cuts, we wanted to be lenient at this first stage. In Figure 2.7 we also show how many stars pass all our automated cuts (described below), then those that also pass the manual vetting, those that become planet candidates (not EBs), and finally the new planet

candidates that have not been found by any other groups. The bottom panel shows the same, except as a fraction of stars in the bin.

Above z-scores of $\sim$ 20, our results stay consistent: about 35% of all stars will end up passing all the automated cuts, and about half of those will go on to pass the manual vetting as well. As the z-score drops from 20 to our lower limit near 9, the rate of systems passing the automated cuts remains consistent, but fewer systems pass our manual vetting (§2.2.7), indicating more contamination by false positives. We discuss the lowest signal to noise candidates further in §4.1.

In total, we identified 8086 candidates across all campaigns above our z-score cutoffs (5.3% of all stars searched). However, the majority of these are spurious due to the `QATS` algorithm picking up on stellar variability (which is also quasiperiodic and will produce a similar `QATS` spectrum as periodic transits) or other sources of false positives. To separate planets from quasiperiodic stellar variability, we made a cut based upon the candidate transit morphology, which we describe next.

Morphology Cut: Sine Fit Vs. Transit Model

As seen in Figure 2.6 the fraction of systems passing the z-score cut is exceptionally high at periods less than a couple days. The majority of these systems are variable stars where a 'transit' can be well fit at the local minimum of stellar oscillations or variability. Although stars display a wide diversity of variability, in general stellar variability is roughly sinusoidal while transits are more localized in time and phase. To automatically eliminate the most obvious cases of stellar variability, we compared a folded transit fit to a folded sinusoidal fit and eliminated systems where the sinusoidal fit is better.

We selected each transit and a continuum region twice the transit duration on either side (or 0.2 days, whichever is larger for especially short transits). We fit a transit model plus local polynomial to each transit and found the optimal global transit parameters. We then repeated the procedure, but fit a local polynomial continuum plus a sine wave, optimizing for the amplitude, phase, and period of the sine curve. The sine curve fit was initialized

with a semi-amplitude of negative the transit depth and a phase such that the sine curve's minimum is at the center of transit. We tested three different initial sine curve periods to start the optimization (0.5, 1, and 2 times the transit duration) and used the best result.

A comparison between the transit and sine fit for a real transiting planet (K2-3b) is shown in Figure 2.8, while a false positive due to stellar variability is demonstrated in Figure 2.9. Any candidates in which the sine fit had a smaller χ^2, and thus higher likelihood, than the transit fit was rejected as being caused by stellar variability. This cut eliminated 5029 of the 8086 systems passing the z-score test (62%), leaving 3057 systems to continue to the next stage.

Duration Limits

After the z-score and sine-vs-transit fit comparisons, the final automated cut we made is on the transit duration. The motivation behind this cut was a subset of obvious false positives that were difficult to differentiate via our other cuts but had poor fits and exceptionally long durations.

We chose an empirical cut to eliminate events of long durations by comparing the period versus duration relation of the KOIs (Thompson et al., 2018) and ensuring the cut was well above them. Our chosen relation for the maximum allowed duration T_{max} to pass the automated cut was (in hours) $T_{max} = 0.017 \cdot P + 7$. Thus, anything under 7 hours will pass no matter its period, while at a 10 day period, the candidate must have a duration less than 11 hours.

This ad hoc decision will be revisited in future searches, but in this case the cut removed 110 stars that would otherwise have passed on to manual vetting. The most likely real astrophysical victims of this cut are short period, near contact binaries rather than a large population of genuine planet candidates.

After all three automatic cuts (z-score, sine-vs-transit fit comparisons, and transit duration), we were left with 2,947 candidates. These were then subjected to diagnostic plots and manual inspection. The distribution of these candidates after the automated cuts are shown

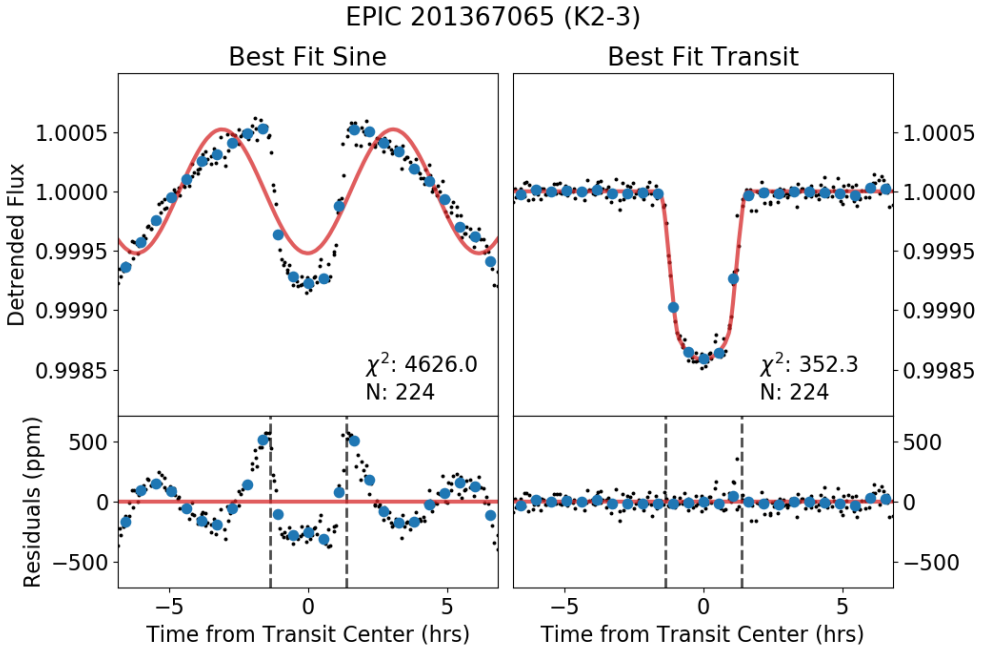

Figure 2.8: Comparison between a local polynomial plus sine curve fit (left) and a local polynomial plus transit fit (right) to a real planet (K2-3b). In both cases the local polynomial has been divided out of each transit before plotting the folded fit of all transits together. The individual cadences are shown in the background in black points, while the binned median is displayed by larger blue points. The best fit model is the red line. The χ^2 of the fit and number of cadences contributing are displayed in the lower right corner. Bottom: residuals of each fit on the same scale, emphasizing how much better the transit fit is in this case. The vertical dashed line shows the beginning and end of the best fit transit.

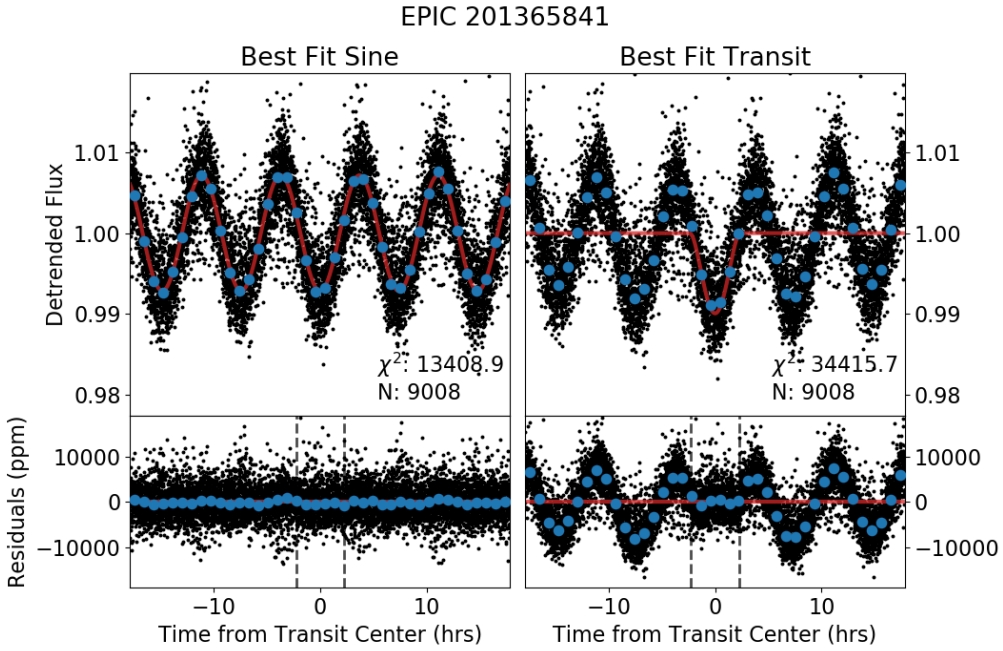

Figure 2.9: Same as Figure 2.8, but for a star in which the sinusoidal fit was better than the transit model fit. This candidate was discarded as likely being due to stellar variability.

in Figure 2.10 and after both the automated and manual vetting in Figure 2.11.

2.2.7 Manual Vetting of the Most Significant Candidates

To date, only two transit searches have been fully automated: (1) the Foreman-Mackey et al. (2016) search of quiet, bright *Kepler* stars for single transit events; and (2) the Thompson et al. (2018) final official *Kepler* planet list that uses a Robovetter (Coughlin et al., 2016) to automatically test for completeness and reliability. Both those searches were only able to accomplish full automation by building upon years of efforts to understand and quantify the instrumental systematics of *Kepler* and using the results of manual vetting and sorting of candidates by previous groups to help train and verify the automated pipelines.

K2, while using the same telescope as *Kepler*, has dramatically different and more extreme instrumental artifacts due to the thruster fires and pointing drift. Further, each K2 reduction

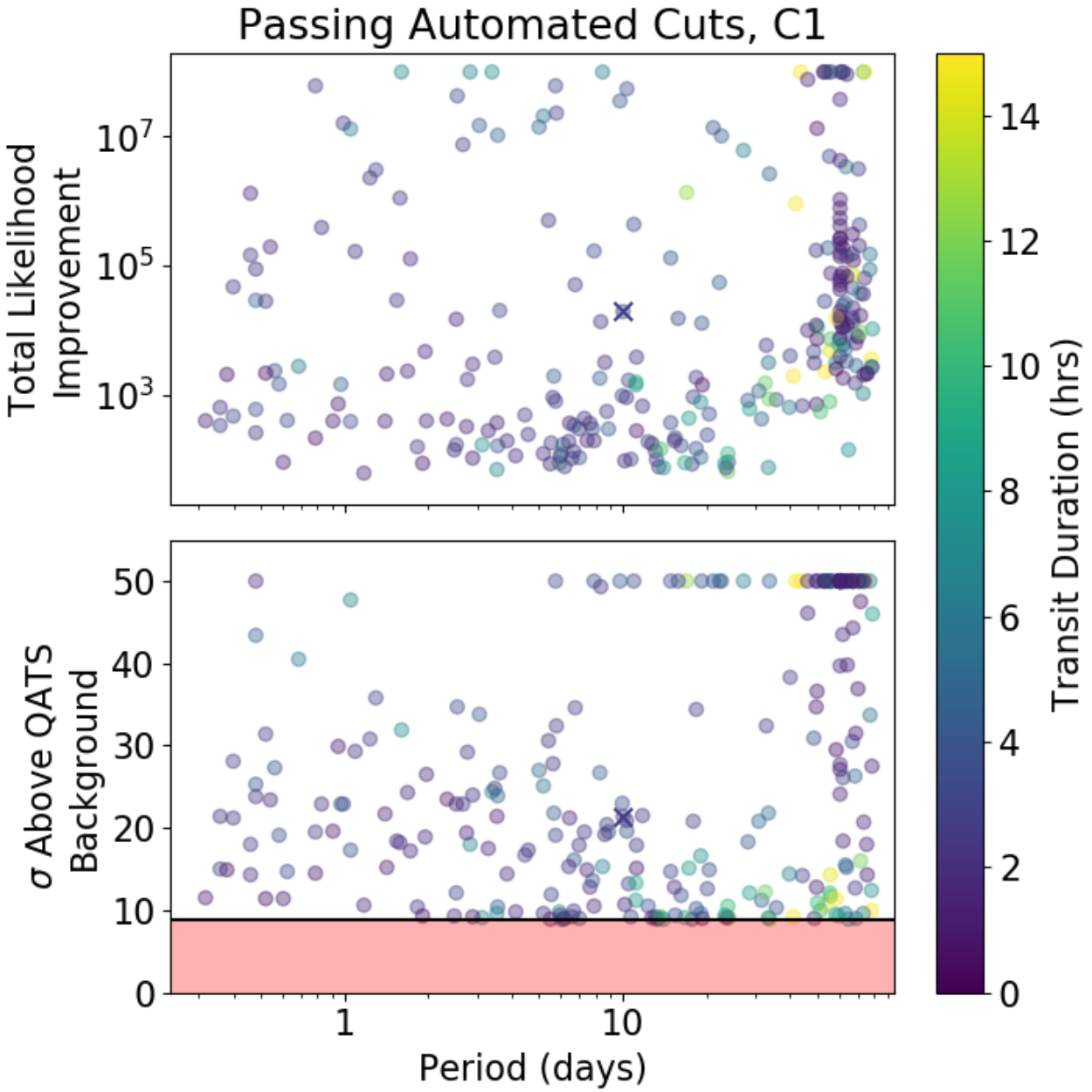

Figure 2.10: Same as Figure 2.6 but only for those systems that passed the automated cuts and were passed onto the manual vetting stage. The × marks the first planet in the K2-3 system we have used as an example. One remaining artifact is the vertical line of candidates around 60 days. This is a result of a bad cadence affecting a small number of stars that was not identified and left uncorrected by our outlier removal in §2.2.3. These systems were all removed in the manual vetting stage however (see Figure 2.11).

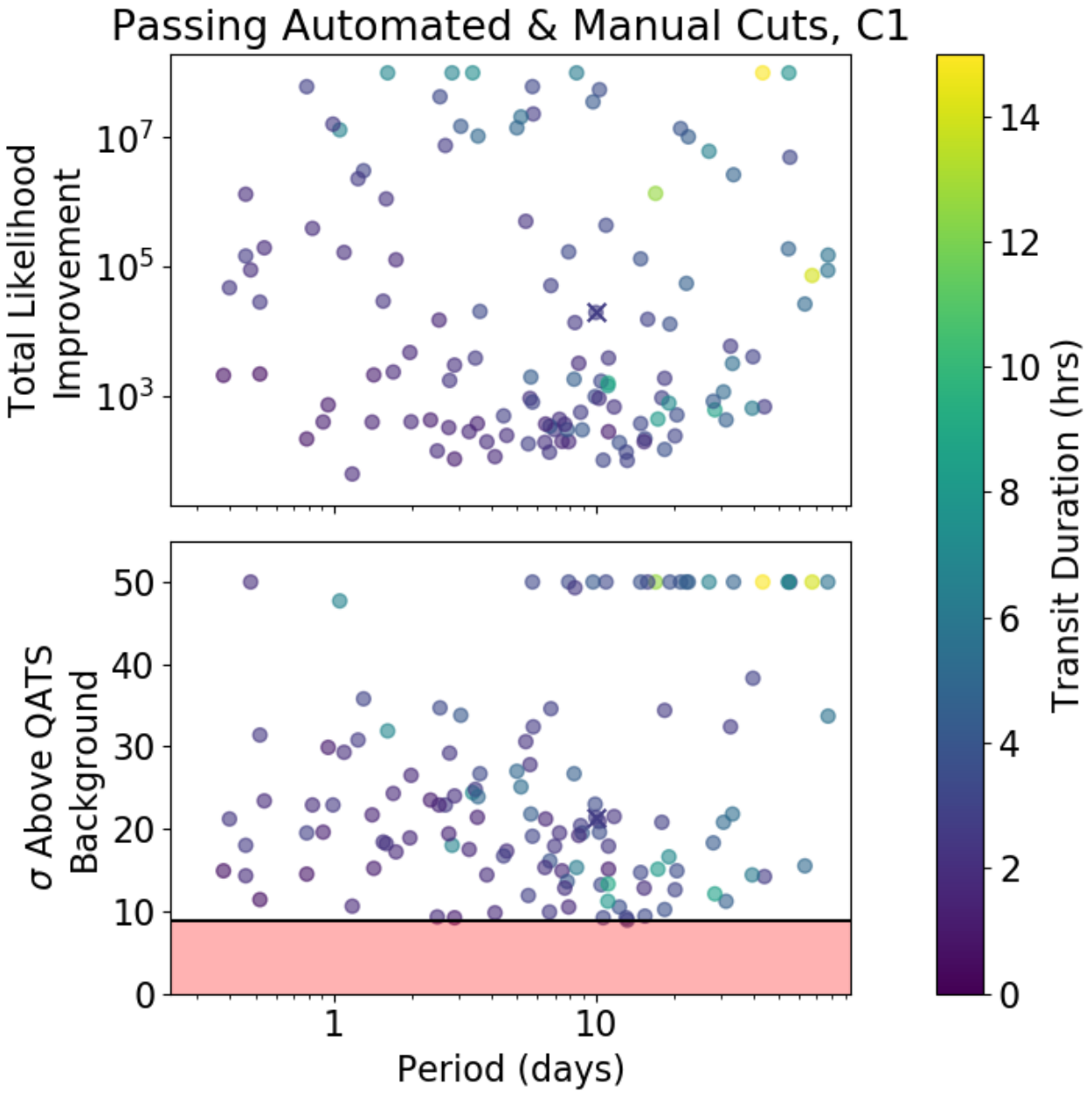

Figure 2.11: Same as Figures 2.6 and 2.10 but only for those systems that passed both the automated and manual vetting stages. The × marks the first planet in the K2-3 system we have used as an example.

pipeline introduces its own biases. Thus, as with nearly every other planet search to date, we visually inspected all 2,947 candidates that passed our automated cuts and removed systems manually judged to be unlikely to be due to a transiting planet or eclipsing binary star. This process is inevitably subjective, but in this section we describe our manual vetting tools and diagnostic plots used to discriminate false positives.

The `QATS` algorithm returns an array of transit time estimates for a particular planet candidate, but only to the nearest cadence; it also returns the transit depth and duration grid points that generated that maximum likelihood candidate. We first refined the transit times as well as solved for the best transit parameters, including refining the impact and limb darkening parameters, which were fixed to the 'default transit shape' in the `QATS` search.

We used an iterative procedure to find the best times and transit parameter values. We started with the input `QATS` transit shape and let each transit time float individually to allow for sub-cadence precision. We made no assumptions about periodicity, and thus can account for TTVs. We then fixed those transit times and optimized the five transit parameters (δ, T, b, u_1, u_2). We iteratively continued this approach until we reached 'convergence,' which we defined as neither the depth nor duration changing by more than 0.1% between iterations. We found this to be sufficiently accurate for visual inspection and use in further diagnostics; however, we note that we use a more rigorous (but much more computationally intensive) MCMC approach for all reported parameter measurements (see §2.2.9). In most cases we achieved convergence within a few iterations, although we capped it at 40 to prevent infinite loops (most common in false positives not actually well fit by a transit shape or planets with very shallow transits whose individual times cannot be well determined).

With better transit parameters and transit time estimates, we created diagnostic plots for vetting planet candidates. First, we generated a 'river plot' for each candidate (Figure 2.12). We fit our measured transit times with a periodic ephemeris $t_N = t_0 + NP$. We then plot each detrended transit (the best fit polynomial continuum divided out) as a row in the figure, with time 0 the best fit periodic ephemeris.

Perfectly periodic planets will show a vertical river of blue transits centered at 0 offset

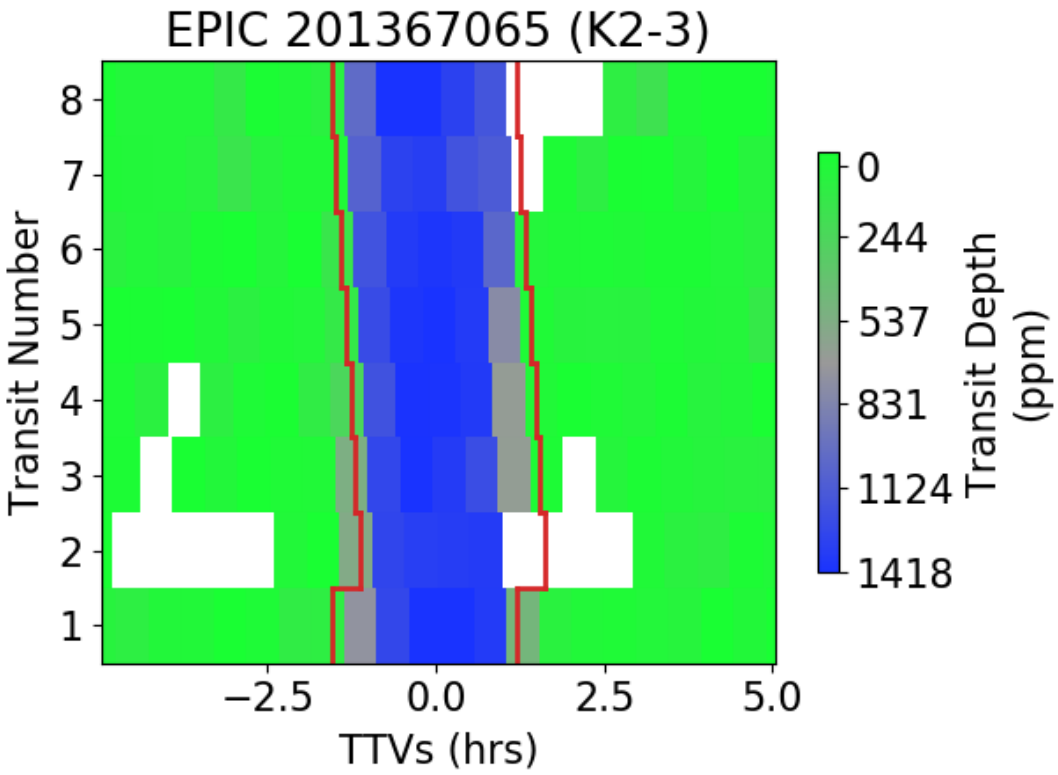

Figure 2.12: The 'river plot' diagnostic for the first planet in the K2-3 system. Each detrended transit is plotted along a row with time 0 at the mean period. Green points are cadences near the continuum level while blue are those with fluxes near the best fit transit depth. White cadences are missing or outlier cadences that were removed before the search. The red line shows ingress and egress for a transit centered on the cadence `QATS` identified.

in the river plot. Planets with TTVs cannot be fit by a linear ephemeris, so some transits will arrive early or late, creating a more meandering river. Regardless, real planets will have correlated transit timing, with subsequent transits not occurring too much earlier or later than the one immediately previous. In contrast, essentially random individual transit timing relative to the periodic ephemeris indicates `QATS` picked up on noise and the candidate is unlikely to be real.

Our next diagnostic plot is a transit stack of all transits (or the first 20 for extremely short period planets) as in Figure 2.13. The left column shows the raw fluxes of each transit (vertically offset for clarity), while the right column shows the detrended fluxes (polynomial continuum removed). This figure allows us to individually analyze every transit, and the color scheme allows us to compare the even and odd transits to the overall best fit model. From this information we can visually determine if all the transits appear consistent or if perhaps one or two false positives are dominating the detection; we can also check for likely binary star false positives if the even and odd transits have different depths or durations. This plot allows us to discard false positives where the individual 'transits' have wildly different and non-transit-shaped events, often due to outliers or systematic or stellar variability.

We also plot a snapshot of the entire light curve (Figure 2.14) with the times of transit identified by vertical dashed lines. This allows us to easily identify broader trends in the light curve and to quickly see if the identified 'transits' happen to occur in a bad region of data or if the entire light curve may have problems which put the validity of the candidate in doubt (e.g. due to `EVEREST` having problems with blended sources and saturated stars).

Finally, we calculated a simple autocorrelation of the entire light curve and identified the period of the first local maximum as in Figure 2.15. The autocorrelation function helps to identify likely periods of stellar variability and provokes extra skepticism if a candidate is at the same period as the autocorrelation period.

Taking all of these diagnostic plots into consideration along with the `QATS` spectrum, we vetted each candidate that passed the automated cuts. In this manual vetting stage, only one decision was made: is the candidate astrophysically real or is it a false positive.

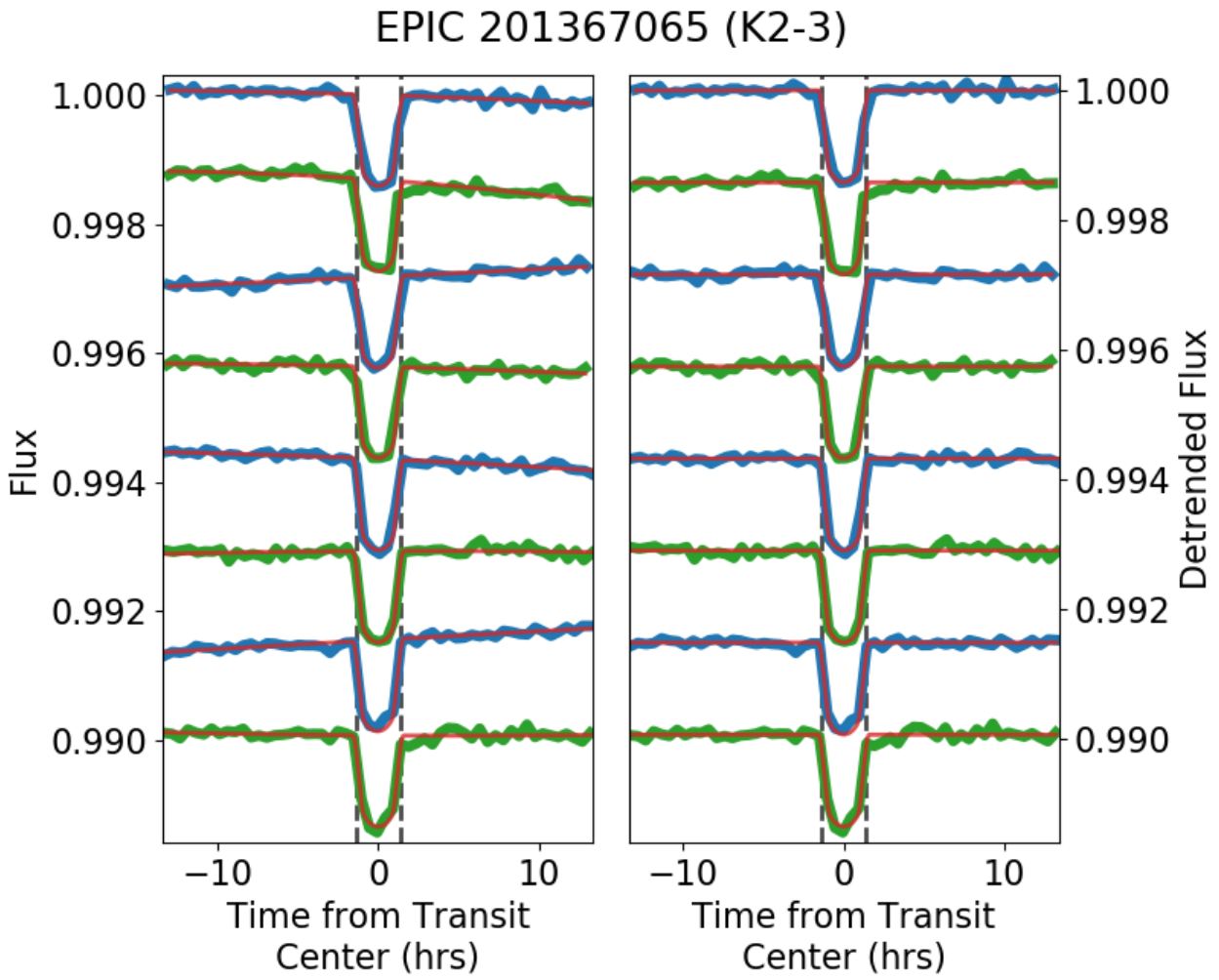

Figure 2.13: Transit stack for the first planet in K2-3. The left panel is the raw fluxes with the transit plus polynomial model (red line), and the right panel is only the transit model (red line; polynomial stellar continuum model divided out). Odd transits are in blue while even transits are in green. The dashed lines behind depict ingress and egress of the transit model. Each transit is vertically offset for clarity.

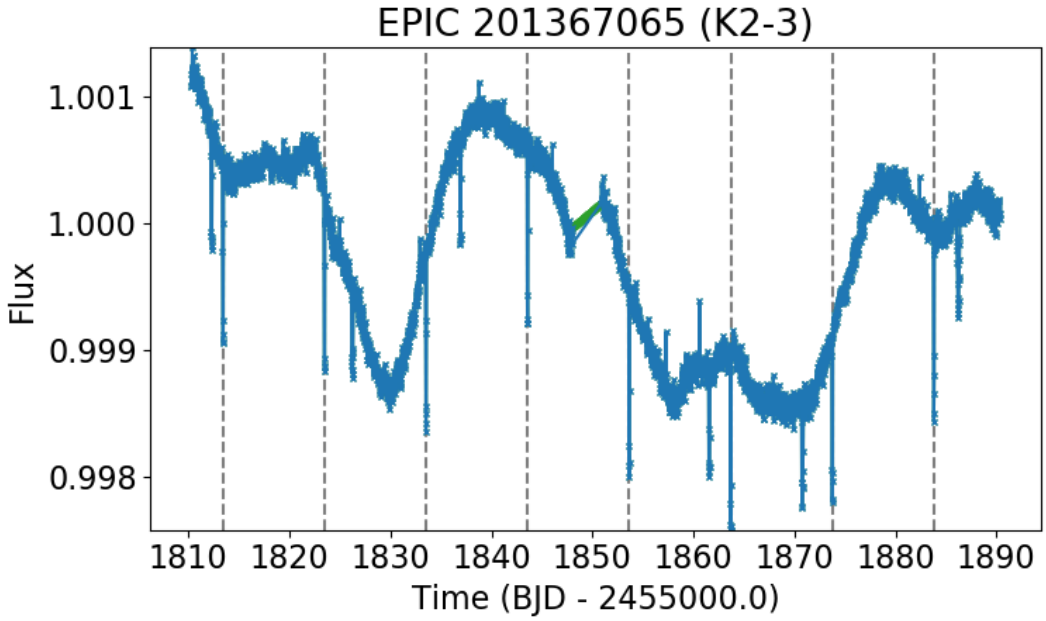

Figure 2.14: The full `EVEREST` light curve of the K2-3 system with the first planet's transits marked by the dashed lines.

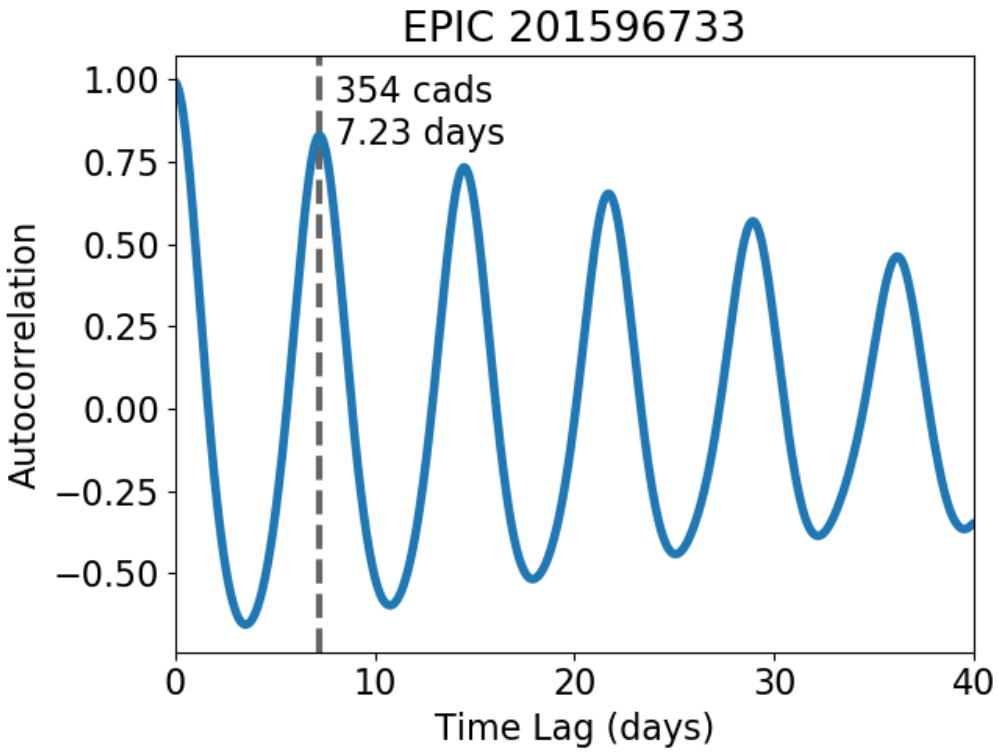

Figure 2.15: Autocorrelation function of the light curve of the planet candidate host EPIC 201596733. Our identified local maximum indicating the star's rotation period is marked by the dashed line and annotated in both days and *Kepler* cadences. (Note this is not the K2-3 system as that one does not have an identifiable rotation period.)

In other words, planet candidates and eclipsing binaries are grouped together and separated from stellar variability, systematic errors, and other false alarms. The eclipsing binary versus planet candidate decision is made later through automated cuts (§3.1).

While no quantitative limitations can be placed on what passes and what does not (or else manual vetting wouldn't be necessary), some examples of systems that did not pass the manual cut are as follows. On the short period end, the dominant false positive cases were a result of stellar rotation and/or oscillations which are asymmetric or otherwise able to have the transit model fit marginally better than a simple sine curve; these often have the same autocorrelation period as the candidate event period.

At long periods, the biggest problem was outliers failing to be completely removed in our light curve cleaning. Many of these appear to be systems where `EVEREST` was unable to properly model a large number of cadences. A quick examination of the full light curve diagnostic plot showed a large number of outliers throughout the light curve, not just at the 'periodic' events picked up by `QATS`, and the individual transits are only one or two cadences and have varied depths. These false alarms are often due to crowding or saturation, which version 1 of `EVEREST` often handles poorly; version 2 of `EVEREST` does better with these stars and a future planet search of the `EVEREST 2.0` light curves may turn up additional planet candidates.

Most of these long period (one to three transits) and short duration (one to three cadences per transit) candidate decisions were easy to reject, but some were less clearly false positives. Still, we erred on the side of caution and rejected them because of the preponderance of outliers in K2 light curves. In the end, none of the candidates with durations shorter than 2 hours and periods longer than 30 days passed through our manual vetting (31 of *Kepler*'s 4500 candidates meet those criteria), although this was not an intentional rule. Those longer period systems that did pass were deep enough and long enough to show distinct shaping due to limb darkening, as opposed to a three cadence dip with no nuanced shape.

While most vetting decisions were relatively easy, the most common borderline cases were low signal to noise systems: candidates with a shallow transit depth near the edge of our

sensitivity. These are the most subjective, and we again erred on the side of caution, as evidenced by the declining fraction of systems passing our manual vetting in Figure 2.7. If anything seemed suspicious, the system was rejected. The most common causes for rejection were stellar variability at a period near that of the candidate, small flares near individual events that skewed the fits and likely caused the spikes in $\Delta\chi^2$ that `QATS` picked up on, and transits showing significant transit timing variations.

We only accepted systems with TTVs if the individual transits were easily identifiable. Over long baselines with many transits, small transits below the noise with TTVs is exactly what `QATS` is designed for; however, over the short baseline of K2 (which itself doesn't allow enough time for most real TTVs to develop), and with only a dozen or fewer transits, `QATS`'s flexibility more often allows it to string together noise than find actual planets with TTVs. In fact that is mostly what the top 'candidate' looks like in the thousands of systems that didn't pass our `QATS` z-score cut.

Manually reviewing 2,947 candidates is a time intensive process (24 hours of work if given just 30 seconds per star), and I was the only one to vet every single one. Of these, I passed 1280 as being astrophysically real (planets or EBs). Eric Agol reviewed those 1280 candidates and agreed with my assessment for all but 6 — a sign of the conservative approach I took to the vetting. Those 6 systems were removed, leaving 1274 stars with at least one candidate.

2.2.8 Multi-Planet Searching

For all systems that passed the first stage of manual vetting (1,274 of the 2,947), we iteratively searched the light curve again for further planets until the newest candidate no longer passed the automatic and manual vetting stages. The only change we made to the process was lowering the z-score threshold for subsequent events to 8; this change was made because of the significantly smaller number of systems required to analyze and a desire to pass as many potentially interesting candidates onto the manual vetting process as feasible.

To avoid rediscovering candidates, we masked all of them out before searching the light curve again. This was accomplished by fitting the continuum region around the transit as

above, except this time ignoring all the cadences within the duration of the event. We filled in those in-transit fluxes with the polynomial interpolation and added white noise to match the rest of the light curve.

2.2.9 Modeling Candidates

In all, 1662 candidates around 1274 stars passed both the automated and manual vetting stages. Many of these are eclipsing binaries, however, and we used MCMC results to help separate the true planet candidates from likely eclipsing binaries and false positives (due to e.g. ephemeris matching indicating the same source is contaminating multiple targets).

We modeled each transiting planet and obtain the optimal physical parameters and associated uncertainties with an affine-invariant Markov chain (`emcee`; Foreman-Mackey et al., 2013). Before running the MCMC, we recalculated the light curve with `EVEREST`, this time masking out all transiting signals to prevent their partial removal by the detrending process, and thus to obtain accurate transit depths.

In the case of multi-planet systems, any transits by other planets in the continuum regions were masked and removed before we started the following detrending and fitting. However, for cadences where other planets' transits overlap with the one being fit, no attempt was made to disentangle them: that transit will be deeper. Any candidates with a significant fraction of transits overlapping those of other planets may have biased parameters.

We modeled the local variability around each transit (centered on the original cadence `QATS` predicted) with a 3rd order polynomial and a continuum region on each side with a width given by the larger of 0.2 days or two transit durations. Each transit was detrended using the fixed best transit model while the surrounding polynomial continuum is optimized. In some cases third order is not enough to capture the stellar variability, so we continued to increment the polynomial order up to a maximum of sixth order while the model's reduced chi square was above 1.5. We then fed each of these detrended transits into MCMC to find the optimal transit model parameters.

Although our search allowed for TTVs, in this stage we modeled all candidates as peri-

odic and used only a period and initial time of transit as parameters due to computational constraints. The other parameters in our MCMC model are the transit duration T (uniform prior between 0 and the width of the detrended window, W), planet to star radius ratio R_p/R_* (log uniform prior with a maximum of 10), two quadratic limb darkening parameters using the transformed Kipping (2013) q_1, q_2 formalism (uniform prior between 0 and 1), and impact parameter b. The initial transit time and period have priors such that the center of every transit must fall within the detrended transit window W.

As with many prior analyses, we found that low signal-to-noise transits produced almost no constraints on the transit shape. This simply means the limb darkening parameters default to the distribution of the prior, but the impact parameter can cause extra complications. Without a signal-to-noise large enough to distinguish between "U"-shaped planet transits, and "V"-shaped grazing eclipsing binaries, finely-tuned planet-to-star radius ratios and impact parameters can match the transit depth for any impact parameter. As this study is focused on planet candidates, and to help the MCMC converge, we limited the impact parameter to a uniform prior between $[0, 1 + 2\sqrt{\delta}]$.

We added five additional parameters to account for further uncertainty in the light curves. A systematic error parameter (log uniform prior between 10^{-7} and 10^{-1}) allows for inflating the white noise on each data point. A flux dilution parameter accounts for the fraction of flux in the light curve due to additional light from another star (a binary companion, background star, or extra light spilling into the aperture) diluting the transit depth (log uniform prior between 10^{-6} and 1). By adopting a maximum flux dilution value of 1 we implicitly assume the planet candidate transits the brightest star in the aperture; if additional observations suggest this is not true, the MCMC should be rerun with a more informative and accurate prior. Further, this prior, by definition, will not hold when modeling an eclipsing binary when the brighter star eclipses the dimmer star, and the radius ratio in such cases can exceed our limit of 10. We therefore urge caution in using the fit parameters for the eclipsing binary systems. Complete and accurate modeling of all K2 EBs is beyond the scope of this thesis.

The final three parameters in our MCMC fits are for an outlier mixture model (Foreman-

Table 2.4: The parameters and ranges for the transit model fitting. The ephemeris parameters, t_0 and P, are allowed to vary such that every transit time falls within the detrended window W centered on the original `QATS` predicted time.

parameter	description	range
t_0	initial time of transit	
P	orbital period	
T	transit duration	$\mathcal{U}(0, W)$
$\log(R_p/R_*)$	log radius ratio	$\mathcal{U}(-8, 1)$
q_1, q_2	quadratic limb-darkening	$\mathcal{U}(0, 1)$
b	impact parameter	$\mathcal{U}[0, 1 + 2\sqrt{\delta}]$
$\log(\sigma_{sys})$	log systematic error	$\mathcal{U}(-7, -1)$
$f_{dilution}$	log flux dilution	$\mathcal{U}(-6, 0)$
Q	fraction of normal data	$\mathcal{U}(0, 1)$
$\mu_{outlier}$	median of outliers	$\mathcal{U}[1 - \delta, 1 + \delta]$
$\log(\sigma_{outlier})$	log standard deviation outliers	$\mathcal{U}(-7, 0)$

Mackey, 2014). Because thruster fires, flares, etc, cause numerous outlier events in K2 data, we needed a way to prevent the outliers from skewing the transit model. We accomplished this with a mixture model, for which the three parameters are: the fraction of data points in the normal transit model (uniform prior between 0 and 1), the outlier points' median (uniform prior between $[1 - \delta, 1 + \delta]$) and the standard deviation (log uniform between 10^{-7} and 1).

All of the parameters describing the model used for transit fitting, along with their priors, are summarized in Table 2.4. A total of twelve parameters are allowed to vary within the range of priors. Other parameters, such as the `EVEREST` detrending parameters, the continuum windows, and the coefficients of the polynomials used in detrending each transit, are held fixed during the fitting.

We ran the MCMC (using 60 walkers) initially for a burn in phase of 10,000 steps. Every

10,000 steps thereafter, if any chains got stuck in regions of lower probability (the chain's maximum likelihood was smaller than a factor of half of overall maximum likelihood), we stopped and reset the sampler near the previous maximum likelihood solution to bring all chains into similar parameter space. All iterations up to this point were also discarded as part of the burn in. We terminated the MCMC chains once we achieved 2000 independent samples of each parameter (measured using the number of steps times the number of walkers divided by the longest autocorrelation length) or one million iterations if convergence seemed unlikely. Lack of convergence can occur when the `EVEREST` light curves are not well detrended and each transit or eclipse has varying and inaccurate depths. This is most common for deep EBs and is noted below.

Finally, in addition to calculating full chains for the parameters of the model, we calculated three derived parameters at every step for each walker. We measured the transit depth (Mandel & Agol (2002) value at the step's impact parameter, adjusted for the quadratic limb darkening parameters and extra light flux dilution), semi-major axis to stellar radius ratio (a/R_*, calculated assuming a circular orbit and edge-on inclination, Eq. 14 of Winn (2010)), and the subsequent stellar density (Eq. 30 of Winn (2010)).

Chapter 3

RESULTS OF QATS SEARCH OF K2 CAMPAIGNS 0 THROUGH 8

From the initial sample of 152,865 stars in K2 C0-8, 1662 candidates around 1274 stars passed our automated and manual vetting for astrophysical significance. Table 3.1 summarizes the results of our cuts for astrophysical significance, showing how many stars were cut and remain in the pipeline after each stage of the automatic and then manual vetting. Also, the iterative search for additional candidates around the 1274 that passed the first stage of manual vetting turned up a further 388 astrophysical candidates, as indicated in the table. However, many of these objects are actually eclipsing binaries or other false positives. With our full list of candidates set, we turn toward discriminating between the likely eclipsing binaries and planet candidates.

3.1 Identifying Eclipsing Binaries and False Positives

In doubly eclipsing binaries where the primary and secondary eclipses have significantly different depths, QATS will find the deeper eclipse first and then the shallow secondary in our followup search for additional signals. In this case, we have two distinct candidates at the same period with different depths, and we can confidently label the system as an eclipsing binary.

When the primary and secondary eclipses approach the same depth, however, QATS will often combine them together into a single candidate at half the true binary orbital period. Careful modeling of the odd and even events independently can determine that the two sets do indeed have different depths or ephemerides (i.e. the secondary eclipse is not precisely at phase 0.5), which then allows us to once again label the system as an eclipsing binary

Table 3.1: Summary of the search and how many candidates pass each stage in the first search of every star. The final line gives the number of candidates found after masking the 1274 candidates, and subsequently searching for additional transit signals.

Stage	Change at This Step	Number After This Step
All C0-8 stars (§2.2.2)	—	152,865
`QATS` signal $> 9\sigma$ above baseline (§2.2.6)	-144,766	8086
Transit fit better than sine fit (§2.2.6)	-5029	3057
Duration not too long for period (§2.2.6)	-110	2947
Manually vetted as astrophysical (§2.2.7)	-1673	1274
Additional candidates passing all vetting found in multi-planet search (§2.2.8)	+388	1662

instead of a planet candidate.

Another confounding factor in the search for planet candidates is the source of false positives due to the same binary signal appearing in many different targets at varying depths. This contamination can be caused by internal reflections within the telescope, by electronic crosstalk between readout channels, and/or by sources affecting the signal of other sources on the same CCD column; these false positives were identified in the original *Kepler* mission and found to be the cause of $\sim$10% of the KOIs (Coughlin et al., 2014). These false positives thus need to be seriously considered, and can be found by looking for multiple candidates that have the same period and ephemeris — indicating they are ultimately caused by the same source.

Taking all of these contaminants into consideration, we ran three different tests to discriminate and remove the obvious EB cases and false positives from our planet candidate sample:

1. Odd–even tests to check for consistent parameters between odd and even candidate transit events;

2. A period and ephemeris collision match to test for the same signal appearing in multiple targets;

3. A maximum depth cut to remove singly eclipsing EBs.

We describe each of these in the following subsections.

3.1.1 Odd–Even Tests

For every candidate, in addition to a full fit with all transits, we carried out the MCMC fit (§2.2.9) to the odd and even transits separately and then compared the posterior distributions. Any depth variations or ephemeris offsets are indicative of the candidate actually consisting of both the primary and secondary eclipses of an EB.

Figure 3.1 compares every candidate's odd and even transits, showing how many standard deviations apart the period and depth are. We separate the candidates into four classes: 1) systems `QATS` identified as two different signals at the same period (we treat the first as the 'odd' and second as the 'even' here); 2) systems manually noted to have possible depth or ephemeris variations during the manual vetting (before the MCMC was run, §2.2.7); 3) candidates in multi-planet systems (multiple candidates at different periods, each showing more than one transit); 4) all other candidates.

The `QATS` and manually identified EBs should show significant depth and/or ephemeris differences between their odd and even fits, indicating they are caused by two different eclipse events. The multi-planet systems — which in the original *Kepler* sample were found to be much more likely to be real planets (Rowe et al., 2014) — should show no differences between the odd and even depths and ephemerides since they will predominantly be equivalent subsets of the same planetary transit. Indeed, that is what we find in Figure 3.1, further motivating this cut. Because `EVEREST 1.0` can sometimes get transit depths wrong, even after masking

them out before running the pipeline, we were conservative in our cuts; we set our limits at 10σ for both depth and transit ephemeris. If the odd and even depths or ephemerides deviated from one another above this value, we automatically categorized the system as an eclipsing binary. This cut eliminated 210 candidates and thus created 210 doubly eclipsing EBs.

We also made the same tests when multiple candidates around a star have nearly the same period. This accounts for instances where `QATS` found primary and secondary eclipses individually (usually because the depths are wildly different or the secondary eclipse phase is far from 0.5). When two or more candidates were found around the same star, we checked to see whether the periods were the same within 5% tolerance. We identified 256 target stars which showed two transiting candidates each (512 candidates in total) for which the periods were consistent within this tolerance (the `QATS` binaries in Figure 3.1). In only two pairs of the 512 objects (two of the 256 targets) were the depths and ephemerides consistent within our cuts. Those two pairs (EPICs 211942779, 214984368) were combined together and reclassified as single planet candidates; however, we note they both appear to be EBs with depths slightly too shallow to discriminate the differences, due to our high thresholds with a single campaign of data. All others were removed from the planet candidates list and labeled EBs.

3.1.2 Period and Ephemeris Matching

Nearby targets whose point spread functions overlap can cause one EB to be detected at varying depths in nearby sources. Similarly, bright stars can have their light reflect across to widely separated areas of the detector, again causing the same signal to appear at different depths in many stars (Coughlin et al., 2014).

Within each campaign, we compared the period and time of first transit for every pair of candidates (Figure 3.2). Any pair where both the periods and first transit times were consistent within 5 standard deviations were flagged as false positives. It is beyond the scope of this thesis to track down which (if any) of the targets is the true source — sometimes the

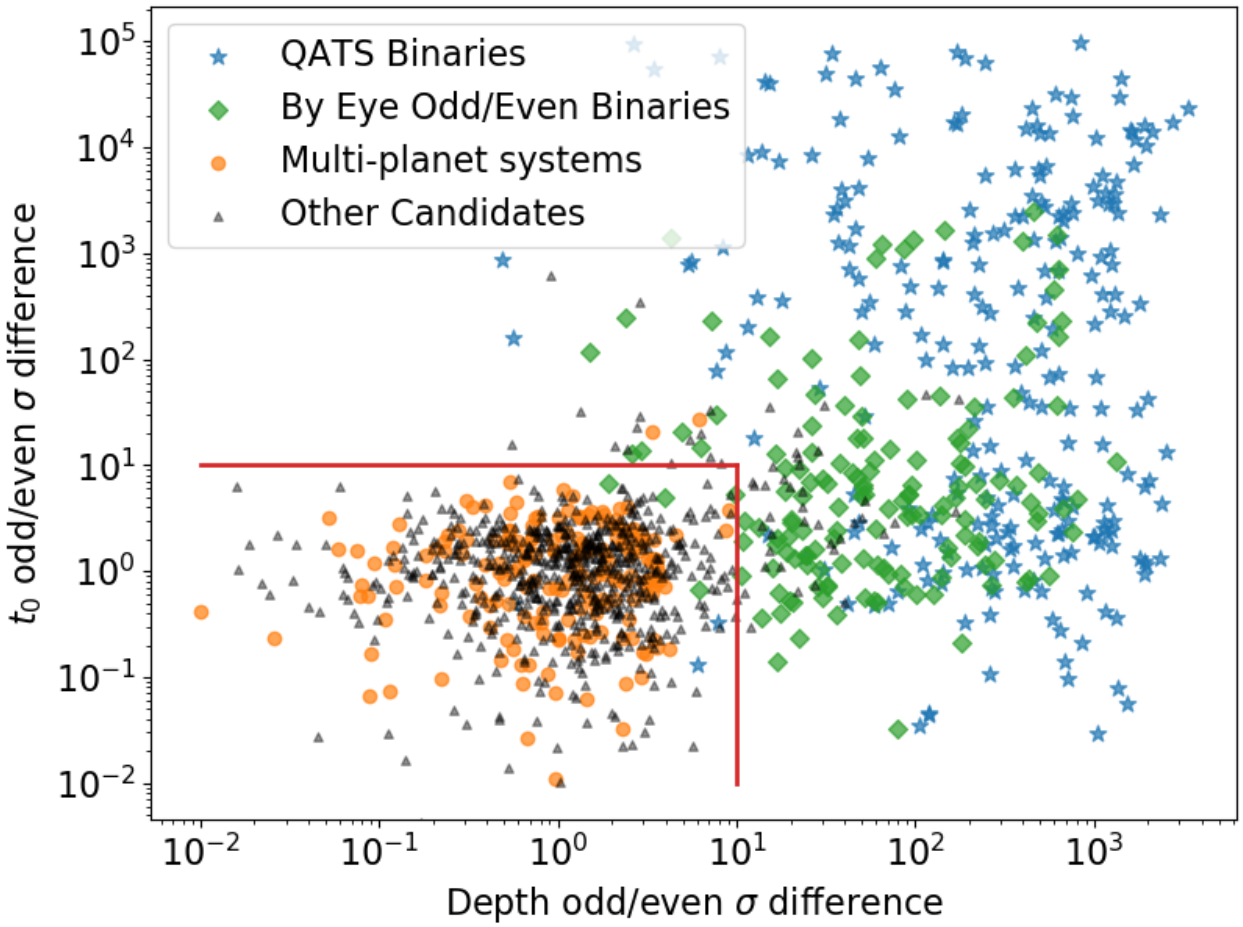

Figure 3.1: Odd–even test for eclipsing binaries. All of our candidates are shown, sorted into categories (see text for details). The red lines indicate our cut between EB and planet candidates — only systems in the lower left pass and are labeled planet candidates at this stage.

Table 3.2: EPICs identified as hosting false positives (the same signal appearing in multiple targets). These systems are removed from both our candidates and EB lists.

False Positives EPICs			
201467358	201467521	202627452	202627721
203728604	203730072	204676803	204676841
205916737	205916793	210386880	210386883
210512752	210512842	211078690	211079188
212409658	212497267	212516916	212516935
212563850	212563954	212844216	212844260
220222029	220222060	220391408	220391520

actual EB is a bright star whose light is not downloaded in the postage stamps. Through this method we identified 32 candidates or EBs (around 28 distinct EPICs) with matching periods and transit times and labeled them as false positives. They are listed in Table 3.2.

3.1.3 Depth Cut

After eliminating the obvious false positives and doubly eclipsing EBs, we were left with 922 candidates around 797 stars. However, none of our previous cuts account for singly eclipsing EBs. Rather than make any judgments about transit shape, we imposed a simple depth cut of 4%, which comfortably encompasses all confirmed *Kepler* planets to date[1]. Only 11 of the 2297 confirmed *Kepler* planets have depths above 2%, and just 2 are above 3%. Any candidate with a transit deeper than 4% was labeled as a likely eclipsing binary for our purposes. This cut eliminated 116 candidates.

[1] As listed on the NASA Exoplanet Archive

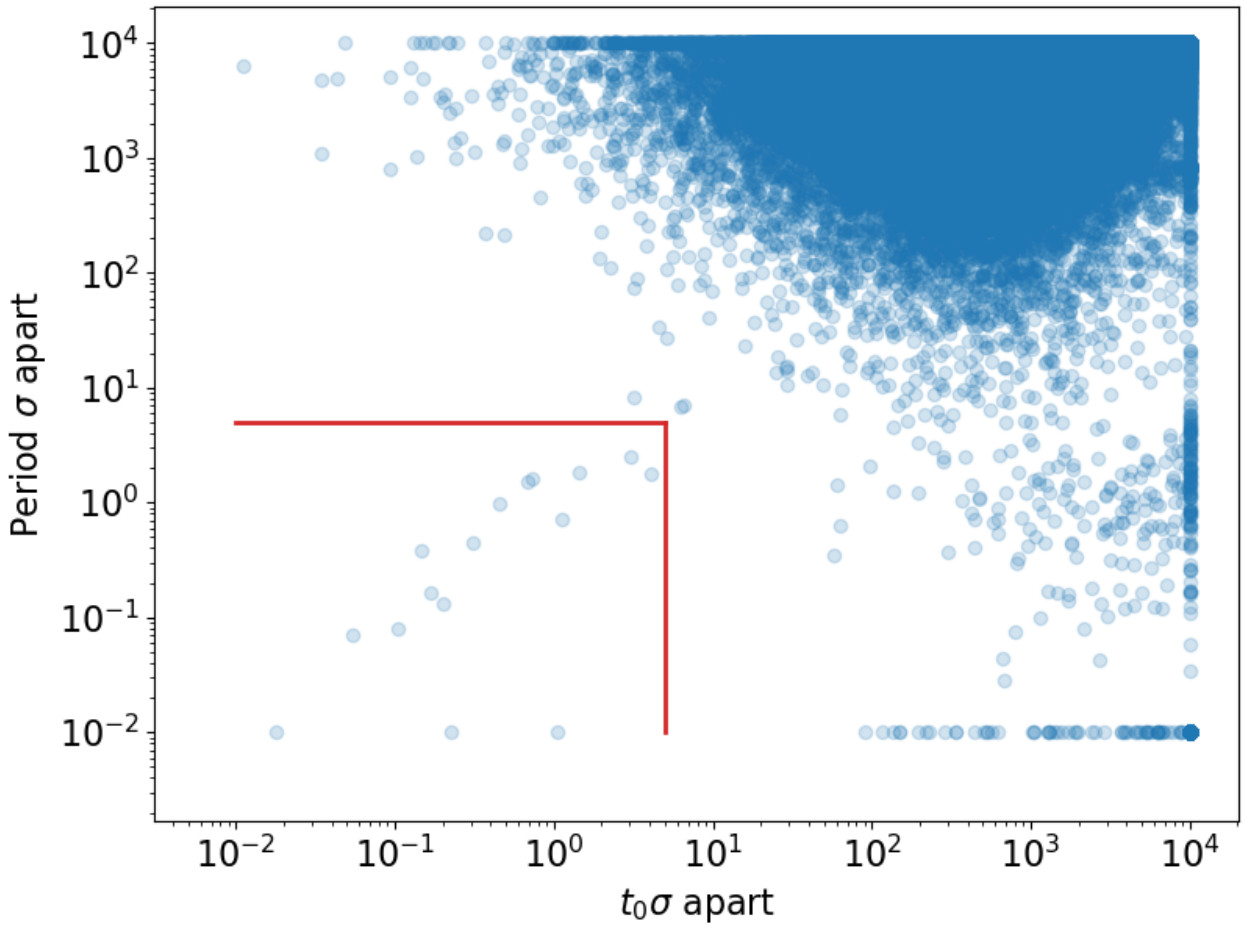

Figure 3.2: Difference in period and t_0 between all pairs of candidates in the same campaigns (clipped between $[10^{-2}, 10^{4}]$ for clarity). Any pairs with both parameters within 5σ (lower left of red lines) are labeled false positives.

3.2 Stellar Parameters

To convert the observationally measured planet-to-star radius ratio to a physical planetary radius, we require parameters of the host star. While the target stars in the K2 fields have not been studied as extensively as the original *Kepler* field, some work has been done to characterize all of the K2 stars.

Most recently, the *Gaia* second data release (DR2) has provided stellar parameters (radius, temperature, and luminosity) for over 70 million sources, though notably excluding all stars with radii less than 0.5 $R_\odot$ (Gaia Collaboration et al., 2016, 2018; Andrae et al., 2018). For stars they do constrain, they have stellar radius errors of about 10%.

For our stellar parameters, we adopt the *Gaia* DR2 radii, luminosities, and effective temperatures when available. As recommended by Andrae et al. (2018), we only trust the *Gaia* parameters when the parallax uncertainty is less than 20% and the Priam flag values suggest the effective temperature can be trusted. We also only use the *Gaia* values if the *Gaia* source is within 3″ of the EPIC listed coordinates. Altogether, *Gaia* provides parameters for 643 of our 806 planet candidates.

For stars not in the clean *Gaia* sample, our secondary source of stellar parameters comes from Huber et al. (2016), who classified 88% of the stars targeted in C1-8. They provide stellar radii to an uncertainty of about 40%. They do not directly give a luminosity estimate (needed for the incident flux calculations), so we derive one from the effective temperature and radius. The Huber et al. (2016) values fill in stellar parameters for all but 17 candidates, of which 14 are in C0 and not covered by their work. For those 17 candidates, we simply leave blank any field relying on stellar parameters and report only those deduced directly from the light curve.

The median error in stellar radius for our *Gaia* stars (most of those above 0.5 $R_\odot$) is 5.7%, although see Andrae et al. (2018) for reasons this may be an underestimate. For the Huber et al. (2016) stars, the stellar radius uncertainty has a median of 17.9%.

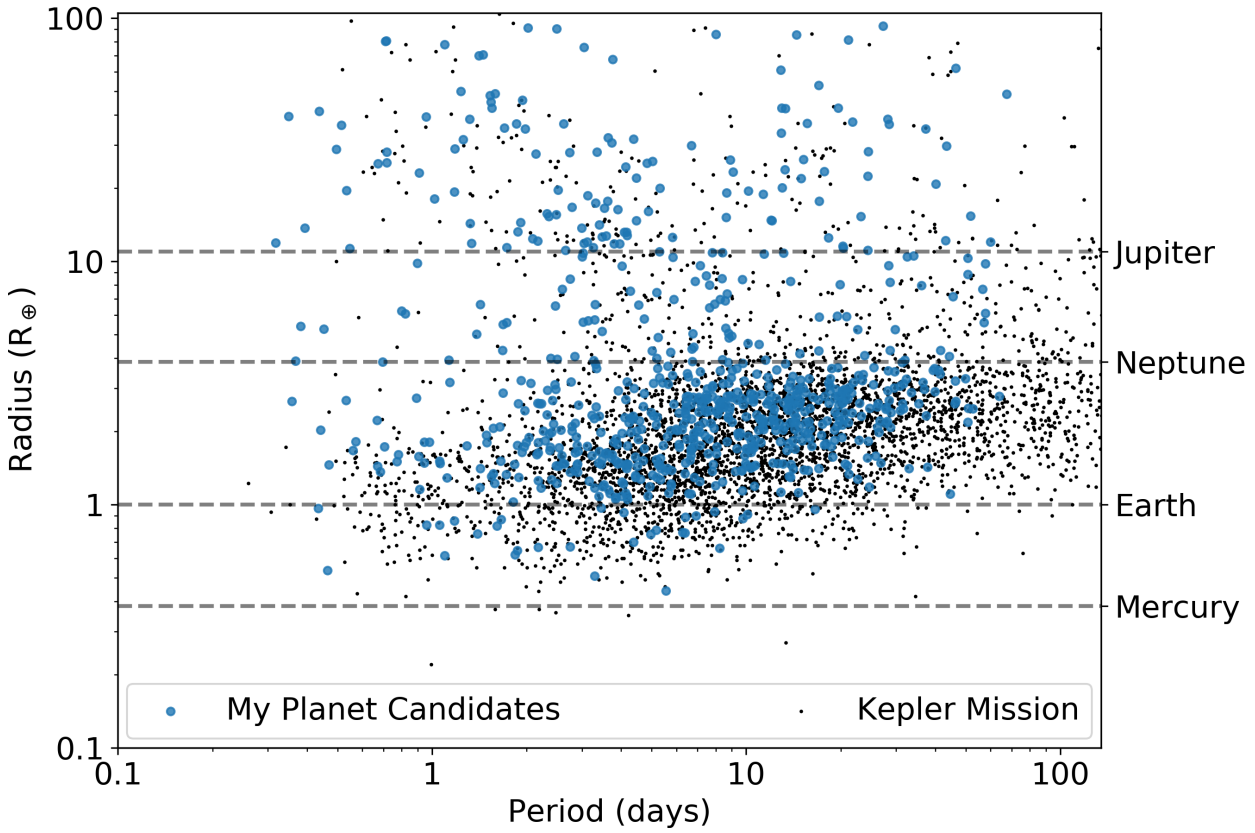

Figure 3.3: Our planet candidates (larger blue points) as a function of period and radius compared to the *Kepler* planet candidates (smaller black points). The right hand scale shows the size of some Solar System planets for references.

3.3 General Properties of the Planet Candidates

After applying our selection cuts to eliminate EBs and false positives, we are left with 806 planet candidates around 693 stars, listed in Table A.1. Our recovered multiplicity rate is tabulated in Table 3.3; most notably we have four 4-planet systems (EPICs 205071984, 206135682, 212157262, & 220221272), two 5-planet systems (EPICs 211413752 & 211428897), and a 6-planet system (EPIC 210965800), discussed below.

Our planet radius and incident flux ranges are calculated using the $-\sigma$, median, and $+\sigma$ values from our MCMC analysis, combined with the respective stellar uncertainties. In other

Table 3.3: Summary of our planetary system multiplicity — the number of systems we found with a given number of planet candidates.

Multiplicity	# of Systems
1	601
2	71
3	14
4	4
5	2
6	1

words, the lower and upper errors are each treated as one-sided normal distributions and propagated independently.

All of our planet candidates are shown as a function of period and radius in Figure 3.3 and compared to the *Kepler* candidates. As with *Kepler*, the majority (69%) of our candidates are smaller than Neptune, and the period and radius distribution is qualitatively similar between the two samples. The notable difference is that our candidates cut off at periods of about 50 days due to K2's limited campaign duration; similarly, we are not as efficient at finding small, long period planets without the benefit of several years to build up enough small signal to noise transits for detection.

We compare our multiplicity to that from the *Kepler* planet candidate sample in Figure 3.4. To make a more uniform comparison, we only consider KOI multiplicity at periods less than 50 days — KOIs with periods beyond 50 days are not counted in the systems. Still, the KOIs have relatively fewer singles and more multi-planet systems: 87% of our systems are single, compared to 79% of the KOI sample with periods less than 50 days. This could be another result of *Kepler*'s longer baseline, allowing the detection of smaller planets inside periods of 50 days. It could also indicate our sample contains slightly more false positives in the single candidate systems, and/or that the stellar target selection results in different planet populations being compared.

We also show how the period ratios of neighboring planets in our multi-planet systems

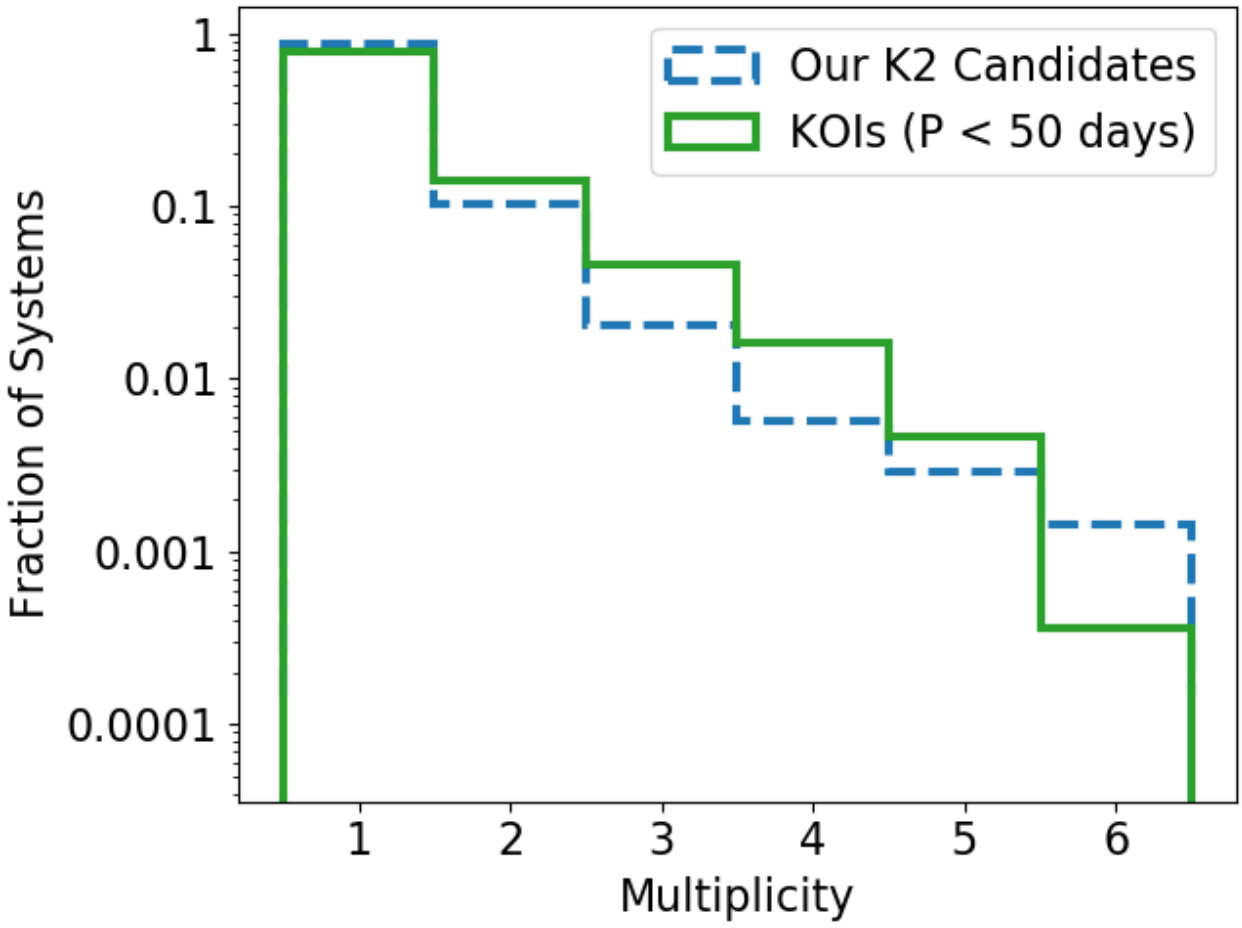

Figure 3.4: The multiplicity of our planet candidate systems compared to the *Kepler* planet candidates (restricted to periods less than 50 days).

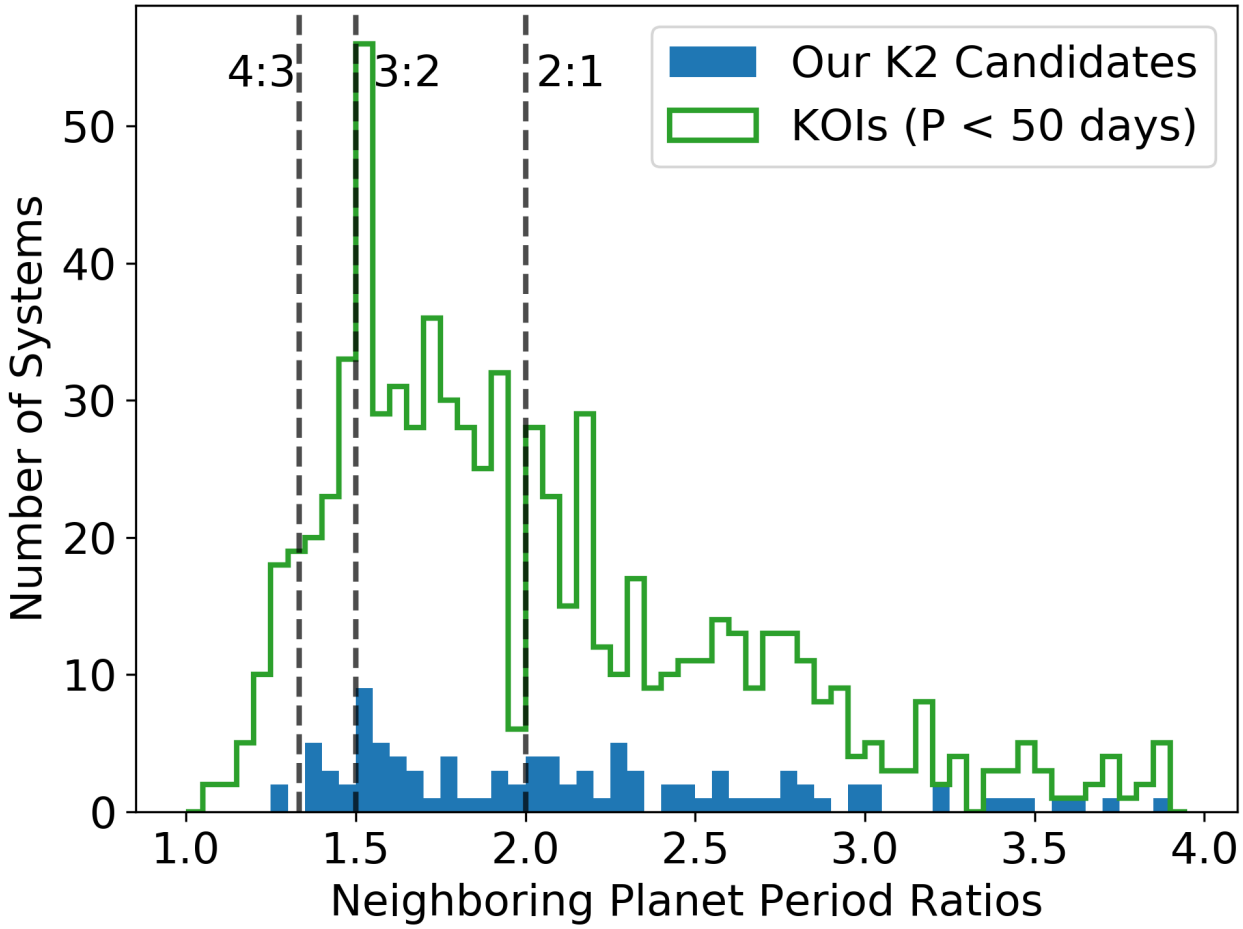

Figure 3.5: The period ratios neighboring planets in our multi-planet systems compared to those of the *Kepler* planet candidates with periods less than 50 days.

compare to the *Kepler* sample (Figure 3.5). While we have many fewer systems, we find the same pileup of planet pairs just outside of a 3:2 period ratio that was uncovered from *Kepler* (Lissauer et al., 2011b; Fabrycky et al., 2014).

3.4 Comments on Individual Systems

We pause briefly to discuss and call attention to some individual systems uncovered in our search that show unusual or especially interesting properties.

3.4.1 Transit Timing Variations

The main reason `QATS` was developed was to detect planets with TTVs. However, TTVs will not be nearly as evident in the brief 80 days of a K2 campaign as they were in the 4 years of *Kepler*. In *Kepler*, a TTV planet's transit times would vary on timescales of many hundreds of days (Mazeh et al., 2013). In an 80 day window, those variations often would not show their full amplitude, and the planet would be difficult to distinguish from one without TTVs. Still, we use the full power of `QATS` and allow for it to pick up large TTV systems (§2.2.5).

A quantitative search separating small amplitude TTVs from periodic systems is beyond the scope of this thesis, but we did make note of any candidates with TTV amplitudes visible by eye in the manual vetting stage. Because our MCMC model does not account for TTVs, the parameters of these candidates will not be completely accurate. In total, four single planet systems were noted as showing signs of TTVs: EPICs 201561956, 212639319, 220639177, and 211924657, the last of which is the most notable and we discuss further.

The C5 star EPIC 211924657 hosts a single 2.64 day candidate that shows considerable TTVs (TTV amplitude on par with the transit duration, shown in Figure 3.6). This star is considered an M dwarf and thus does not have *Gaia* parameters, but with the Huber et al. (2016) stellar radius, the planet is 1.5 $R_\oplus$. No additional transit signals have been detected, but TTV modeling may be able to constrain the properties of the perturbing planet, especially because this target has also been observed in C16 and C18 — providing a 3 year baseline for the TTVs.

3.4.2 Single Transit Candidates

As discussed at the end of §2.2.6, our chosen metric to separate planet candidates from noise based on the `QATS` spectrum peaks above the baseline breaks down at the longest periods, resulting in a reduced sensitivity to one- and two-transit candidates. Furthermore, we only search for events with durations up to 17 hours, and systems with periods of 50 up to hundreds of days that would only produce one or two transits in a campaign might have

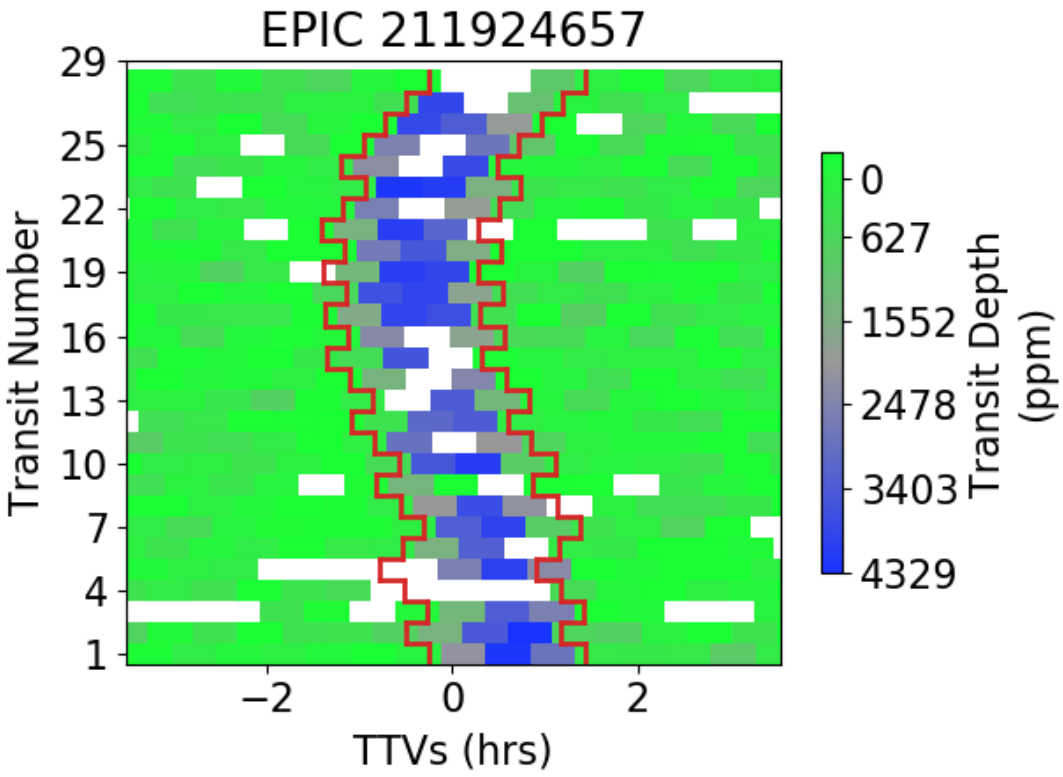

Figure 3.6: Same as Figure 2.12, a 'river plot' showing the large transit timing variations of the planet candidate EPIC 211924657.1 (period 2.64 days).

durations longer than that limit, causing us to miss them.

Nevertheless, we detected 72 astrophysical single 'transit' events in total. Of those, the majority are exceptionally deep and labeled as EBs via our depth cut (§3.1.3) or likely secondary eclipses for a deep EB that eclipsed twice. Just 11 are labeled planet candidates, and most of those are v-shaped and likely to be shallow secondary eclipses of long period EBs.

However, one of our single transit events (211087003.1) also hosts an inner candidate with three transits (period 28 days), which provides strong evidence the single transit is from an outer planet in the system.

3.4.3 High Multiplicity Systems

Perhaps the most exciting aspect of `EVEREST`'s detrending is the capability to find systems with several planets. To date, one 5-planet system has been announced from K2's C0-8, but it contained 3 single-transit events which makes the periods hard to constrain (and also caused our search to miss them) (Vanderburg et al., 2016a). Recently, another 5-planet system has been announced from C12, and all five planets have well determined periods (Christiansen et al., 2018). Here we add two more 5-planet systems as well as a new 6-planet system.

EPIC 211413752 hosts five planets, of which only the deepest (9.33 day period) had been previously reported. The planets have periods of 2.15, 4.53, 6.13, 9.33, and 26.27 days; the middle three are very near to 3:4:6 period ratios, a common trait of short period multi-planet systems (Fabrycky et al., 2014). The host star is uncertainly labeled a giant by Huber et al. (2016), but *Gaia* classifies it as a K dwarf, which is more consistent with the stellar densities of ≈ 1 g/cm^3 derived from each of the planet candidates. With the *Gaia* value, the planets range between 1.6-3.6 $R_\oplus$.

Similarly, we report EPIC 211428897 hosts 5 planets, of which the first, second, and fourth had been previously found (Dressing et al., 2017b). This star has been characterized by both Dressing et al. (2017b) and Huber et al. (2016) as an M dwarf, and it astoundingly

hosts five planets all with periods less than 7 days: 1.61, 2.18, 3.29, 4.97, and 6.27 days. These planets also appear to be near a resonant chain of periods, with corresponding ratios near 3:4, 2:3, 2:3, and 4:5 respectively and are all smaller than the Earth (between 0.5-0.8 $R_\oplus$). Both of these 5-planet systems are in C5 and have been observed again in C16 or C18.

Finally, the C4 star EPIC 210965800 is host to K2's first 6-planet system. Only the deepest planet (8.75 days) had been previously found, but we add five additional planets bracketing it at periods of 1.83, 4.28, 13.16, 21.09, and 30.29 days. The second through fourth planets form a chain near 1:2:3 period ratios, but the innermost and outer two planets are relatively far from first order resonances. The host star is slightly sub-solar, and the planets range from 1.5-3.8 $R_\oplus$.

3.5 Eclipsing Binaries

In our search for planets, we inevitably uncovered EBs as well, which we have done our best to separate out (§3.1). Compared to our 806 planet candidates around 693 stars, we found 573 EB systems (462 of which we found both the primary and secondary eclipses). Our ratio of 1.21 transiting planet host stars per EB compares very favorably to the original *Kepler* mission which has a ratio of 1.19 (3456 planet host stars[2] to 2909 EBs[3] (Kirk et al., 2016) listed in the online catalogs).

While not the focus of this thesis, we list all of our EBs in Table A.2 and briefly discuss some of the highlights and caveats. We compare the EB sample to the planet candidates in Figure 3.7. The two have similar period distributions, but of course the EBs have considerably deeper eclipses than planet transits.

Despite EBs typically having deeper eclipses, we do not expect our list to be complete. First, our search only extends out to a maximum duration of 17 hours. Secondly, we impose an upper duration limit as a function of period for any astrophysical candidates (§2.2.6), imposed to reduce false positives. Those restrictions are both loose enough not to eliminate

[2] `https://exoplanetarchive.ipac.caltech.edu/`

[3] `http://keplerebs.villanova.edu/`

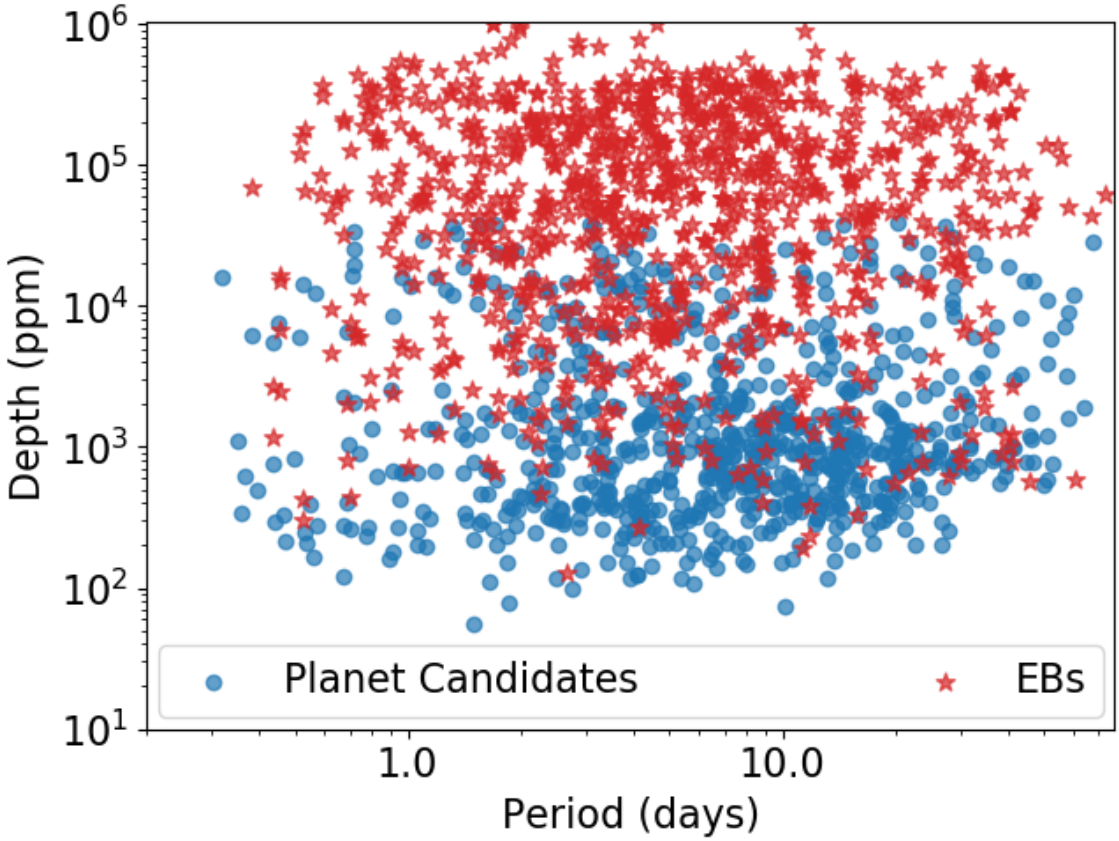

Figure 3.7: Distribution of our planet candidates and eclipsing binaries as a function of period and transit or eclipse depth. By our definition, anything above 4% transit depth (4×10^4ppm) is labeled as an EB, forcing that upper limit for planets (§3.1.3).

the vast majority of planets, but may more substantially reduce EB yields. Any evolved or very large stars will have much longer transit and eclipse durations, but planetary transit depths are so small around such large stars that we would not expect to find them anyway. However, EB depths can still be substantial around large stars, but we would either not find or prematurely eliminate any eclipse signals because of their long durations. Finally, `EVEREST` can have trouble with deep eclipses; while it tries to mask them out before detrending, some eclipses can slip by and cause the pipeline to overfit them, changing their depths. `QATS` may then have trouble recovering the system when the depths are not consistent.

We also emphasize that the parameters listed in Table A.2 may not be fully accurate for the EBs. In our MCMC analysis which calculates the values in the table (§2.2.9), we include a 'second light' parameter that allows for contaminating flux in the aperture, but we limit that ratio of additional to host star light to 1 — the majority of flux is assumed to be from the star being transited/eclipsed. By definition, however, one star in an EB is brighter than the other (except in rare cases of perfectly equal stars), and when it eclipses the other our assumption is broken. Similarly, our prior on R_p/R_* only allows for values up to 10; some EBs may have stars more than $10\times$ bigger than the other, which would prevent it from being modeled accurately. Our limits on impact parameter may also prevent EBs from being modeled accurately, and in some cases quadratic limb darkening is not precise enough to fully model the eclipses.

All of these poor assumptions for EB modeling combine to cause the EB fits to not be fully accurate. The periods and ephemerides can usually be trusted, but the depths and durations should only be used as guides to select various systems for followup and analysis.

3.5.1 Eclipsing Binaries of Note

In this section, we briefly mention some EBs that stood out during the manual vetting stage and may warrant individual followup.

- EPIC 212096658 is a 2.93 day binary which shows eclipse timing variations in both

the primary and secondary eclipses (Figure 3.8). By the end of C5, both show a full sinusoidal cycle of ETVs from a perturbing third body in the system.

- EPIC 203878683 is a 13.75 day binary that also shows signs of ETVs (amplitude ≈ 10 minutes). In this case, the ETV signal is only parabolic, and the ETVs of the primary and secondary eclipses are anti-correlated.

- EPIC 201740472 is a short period EB candidate with a period of just 0.96 days. Despite the short orbital period, the system's orbit is far from circular, and the secondary eclipse occurs at phase 0.72.

- EPIC 216814711 is a 4.5 day binary and a classic example of a 'heartbeat' star — eccentric, short period binaries where periastron passages induce tidal pulsations in the stars and cause them to brighten (Thompson et al., 2012).

- EPIC 212432524 is a 4.95 day whose secondary eclipse is noticeably asymmetric. The ingress of the 10% deep secondary eclipse is about 1% shallower than the egress, and this shape is consistent throughout the campaign.

- EPIC 210766835 is a 24.78 day EB that show large eclipse depth variations. The three primary eclipses in the campaign have depths of around 7%, 10%, and 11%, while the secondary depths change by about 0.2%. The star appears isolated in the aperture, and the depth variations are evident in other reductions of the light curve, so they appear to be astrophysical and not an artifact of `EVEREST`.

- EPIC 220374480 presents a single 40% deep eclipse, but it is obviously asymmetric. The eclipse appears as if it were an inner binary with both stars nearly simultaneously eclipsing a third companion.

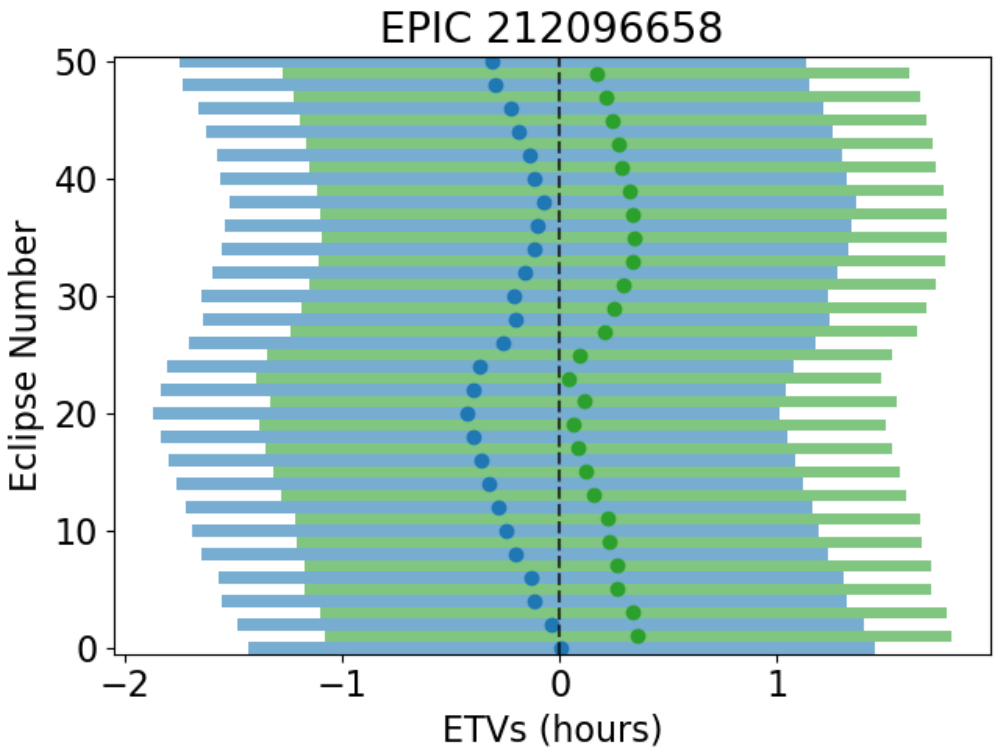

Figure 3.8: Eclipse timing variations evident in the 2.93 day binary EPIC 212096658. The best fit times of the individual primary (blue, left) and secondary (green, right) eclipses are shown as points, with the shading indicating the duration of the eclipses. The ETVs are calculated based on the combined average eclipse period of 1.47 days, with the approximately 20 minute horizontal timing offset between primary and secondary caused by the secondary eclipse's slight phase offset from 0.5.

Chapter 4

SCIENCE APPLICATIONS OF OUR PLANET CANDIDATES AND K2'S DIVERSE STELLAR SAMPLE

In the previous chapters, I introduced my `QATS` pipeline and used it to search K2 C0-8 for planets. I showed that I can find several hundred planet candidates and eclipsing binaries and explained the tests I used to discriminate between the two.

In this chapter, I compare my search to previous efforts by other groups and provide some supporting evidence for the validity of our multi-planet systems. I also demonstrate that K2 is sampling stars of different masses and magnitudes and in different environments than the original *Kepler* sample. I show how the K2 planet candidates will add to our understanding of planet formation and evolution by providing data points in previously poorly sampled regions of parameter space.

4.1 Comparison to Previous Searches

The K2 mission began with a trial campaign (C0) from March to May 2014. However, the spacecraft didn't enter fine guidance pointing until the latter half, so only the final 35 days of the campaign produced higher quality data. The data was released publicly in September 2014, and several groups began developing ways to correct for the pointing drift due to the loss of the two reaction wheels (Vanderburg, 2014; Lund et al., 2015). Individual planets began to be published (e.g. Petigura et al., 2015), and Foreman-Mackey et al. (2015) published the first candidates from a systematic search of C1.

Since then, there have been hundreds of planet candidates announced, but we choose to compare our `QATS` pipeline to those with more than one campaign of overlap and at least 100 candidates on their list. The list of other searches and the detailed comparison of the

Table 4.1: Comparison of our results to previous groups with at least two campaigns of overlap and more than 100 candidates. The columns indicate how many planet candidates are on one list and in parentheses how many overlap between their search and ours. The final row indicates our search compared to every published K2 candidate in C0-8, including smaller searches not included individually in this table.

Candidate List	Campaigns Searched	Number They Found (We Also Found)	Number We found (They Also Found)
Barros et al. (2016)	1-6	177 (134)	554 (105)
Crossfield et al. (2016)	0-4	190 (147)	347 (120)
Vanderburg et al. (2016b)	0-3	234 (184)	275 (144)
Pope et al. (2016)	5-6	168 (125)	231 (113)
Petigura et al. (2018)	5-8	147 (128)	420 (101)
Mayo et al. (2018)	0-8	227 (191)	767 (188)
All previous searches[1]	0-8	743 (516)	806 (438)

overlap between our lists of planet candidates can be found in Table 4.1. In general, we find approximately 75-90% of the candidates found by other groups; however, they tend to find just 20-50% of our candidates. Compared to every published K2 C0-8 planet candidate to date from all searches (even those not individually listed in the table), we also find 69% of them, while 46% of our candidates are new and unlisted in every other search.

Our new candidates (those missed by other groups) are unlikely to be dominated by false positives or EBs that we include in our lists but other groups found and discarded. Figure 4.1 highlights how our new planet candidates differ from the candidates shared between our search and previous efforts. Our planet candidates tend to be found at lower total transit signal to noise values, indicative of our better sensitivity to small planets. We calculate the total signal to noise as $\frac{\delta}{\sigma}\sqrt{NT}$ with δ the transit depth, σ the light curve noise level, N the number of transits and T the transit duration (in cadences). Our new planet candidates have a median total transit signal to noise of 37, and 67% of our new planet candidates have a median total transit signal to noise below the median value of 62 for planet candidates at least one other group also found.

[1] As listed on NASA Exoplanet Archive, including others not individually listed above.

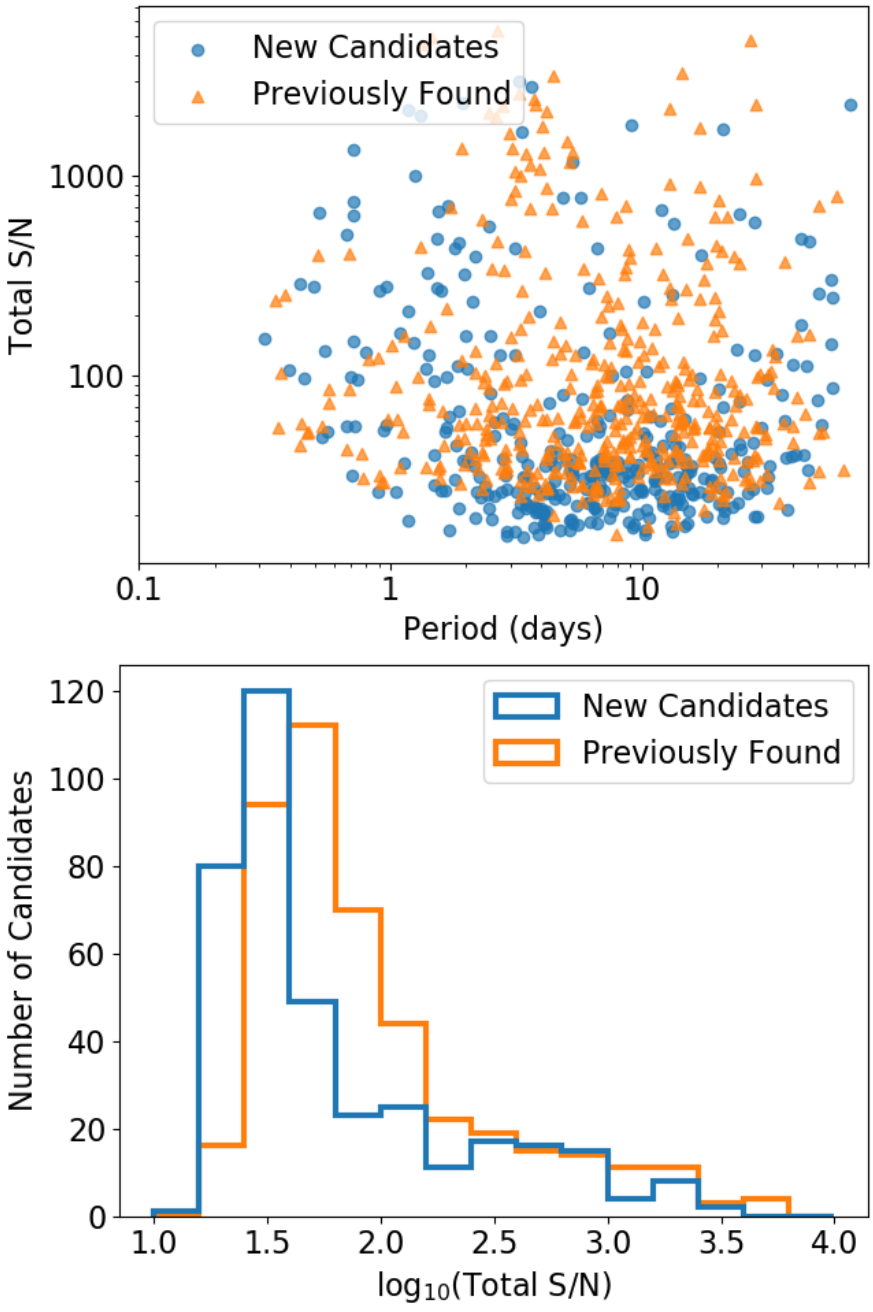

Figure 4.1: Our candidate sample compared to those found by other groups. Top: Our new planet candidates (circles) compared to those any other group has found as well (triangles) as a function of period and total transit signal to noise. Bottom: Same, but marginalized over period to highlight the lower signal to noise transits of our new planet candidates.

Our new candidates are also unlikely to be false positives found by digging into noise due to the similarity between our new candidates and previously found ones. For one, we find 46 new candidates in systems that already had at least one planet previously found (e.g. five new planets in the previously single EPIC 210965800 and two new planets in the previously three-planet system 211428897). In total, 25% (92/368) of our new planet candidates are found in multi-planet systems, consistent with the overall 25% rate (205/806) for all our planet candidates.

Instead, we believe the vast majority of our newly discovered planet candidates are in fact real planets that went undetected by other groups for any of several reasons. First, `EVEREST` produces higher precision light curves than other groups. A full comparison between `EVEREST` and other groups can be found in Luger et al. (2016), but in general `EVEREST 1.0` (as used in this thesis) produced light curves of 20-50% higher precision than `K2SFF` (Vanderburg & Johnson, 2014) and `K2SC` (Aigrain et al., 2016). Our better results could also be due to differences in the planet search methods themselves. One possible difference is the approach used to reject outliers before searching. Our version of `QATS` also includes a grid search in depth, helping enforce similar transit depths between events; this differs from most other searches that only use a three-dimensional grid of period, phase, and transit duration. Our inclusion of depth may help boost low signal to noise candidates over the threshold of detection.

4.1.1 Planets We Missed

If indeed our planet search is more sensitive to the smallest planets, and we're finding almost twice as many planets as had been found by all previous searches combined, then it merits pausing to discuss why there were any planets found by other groups that we missed. In this section we explore those cases and discuss the different ways they fell out of our search.

The 227 planets found by other groups that were missed in our search (bottom row of Table 4.1), orbit 183 unique stars. Of those 183 stars where others find planets that we missed, the simplest explanation is one of differing target lists: we didn't search 8 of those

stars, leaving 175 systems to explain. Another 10 systems are not actually problems; we found the same candidates, but we disagree on the period (almost always by a factor of 2). For example, EPIC 201577112 has a candidate with two transits separated by 44 days, which we call the planet's period. However, if the planet's period were 22 days a potential third transit would have fallen in the C1 data gap, and Vanderburg et al. (2016b) used 22 days as the period (they were the only other group to find this candidate).

Missed Planets as Top `QATS` Result

Of the 165 remaining systems with planets we 'missed', one third of them (58) were in fact found by `QATS` as the top candidate, but they were dropped somewhere along the way. 34 of those 58 were dropped at the very first of our automated cuts, the `QATS` spectrum peak above the baseline level (§2.2.6). The most common reason (20) was that the candidate only had one or two transits in the campaign, which we have a documented difficulty detecting. Six of the candidates were dropped because the transit duration is shorter than an hour, and many of the transits were removed as outliers, making the overall signal much weaker. These systems may be recovered in future versions of `QATS` as we improve the pipeline, especially for the one and two transit systems (see §6.3.1).

Six more systems were discarded in the other two stages of automated vetting. Two were discarded for having the sine curve fit better than a transit. EPIC 203533312 is a 0.18 day likely eclipsing binary, and EPIC 206152015 is a 0.81 day eclipsing binary with out of eclipse variability at a larger amplitude than the eclipses (Barros et al. (2016) only found the primary eclipse and called it a planet candidate). We might revisit the sine curve test in future versions, but recovering short period binaries with large amplitude variability is not a present priority.

The other four systems (EPICs 206247743, 206439513, 206439513, 210609658) were removed by our duration limit: they all have exceptionally long transit durations for their orbital periods, most likely indicating they are orbiting evolved stars and could be EBs (and two of the four have v-shaped transits, also indicative of EBs). Removing the duration cut

would allow these systems to be detected, but it will place extra burden on the manual vetting stage (an extra 110 systems to vet to find these 4 candidates) unless we are able to better remove results due to stellar variability without the duration limit.

Finally, 17 planet candidates found by other groups were removed by us at the manual vetting stage (without any prior knowledge of the candidacy status from other groups). One reason they were removed was because the planet candidate has a very similar period to the obvious stellar rotation period, and we weren't confident enough that the transits were distinct from stellar variability (EPICs 204346718, 210843708, 210857328, 211834065). Most of the candidates were removed in manual vetting though because they were on the low signal to noise end, and we weren't confident enough to pass them.

Our manual rejection of 17 systems approved by other groups highlights the subjectivity of manual vetting at the lowest signal to noise limit. On the other hand, it bolsters the idea that our new candidates are not due to laxer vetting standard on our part by allowing through lower signal to noise false positives than others.

Missed Planets Overlooked by `QATS`

Of the remaining 107 systems where our search does not find a planet claimed by other groups, in 2 of them (EPICs 203823381 and 212737443) the top result from `QATS` was instead a long period candidate (1 or 2 transits) that appears to be an outer companion to the inner planet others found; because that outer companion didn't pass our automated cuts (as with other one and two transit systems), we never masked it out and searched for the inner planet.

Four more systems (EPICs 201488365, 202072965, 204489514, 212579424) are clear, deep EBs, but `EVEREST` had trouble detrending them. `EVEREST 2.0` handles deep EBs better, and these would be found in a search of the newer light curves. On the other hand, these systems are definitively not planet candidates, despite their label as such by other groups.

Finally, we have the 101 systems in which others claim there to be planet candidates, but our search comes up with nothing. In roughly a third of these cases, the `EVEREST` light curve shows excessive amounts of outliers indicative of poor detrending; most of these stars show

evidence of crowded apertures, saturated pixels, or stellar light drifting out of the aperture during the campaign — all of which are known to cause degraded quality in our v1.0 light curves. Inspection of v2.0 light curves show better quality and often the transits visible by eye, indicating that we will be able to recover a number of these 'missing' candidates using the newest detrending.

Even in cases where there is nothing obviously wrong with the light curve, using the updated `EVEREST` 2.0 light curves can help. For example, EPIC 211784767 is an isolated, 12th magnitude star which looks fine in v1.0, but `QATS` finds no evidence of a 3.58 day planet as claimed by Barros et al. (2016). However, running an identical version of `QATS` on the `EVEREST` 2.0 light curve turns up the planet exactly where expected, at the same depth and duration claimed.

We cannot find every 'missing' planet simply by upgrading `EVEREST`, however. Around 50 candidates found by other groups elude detection in our search, even with v2.0. We note, though, that all of those candidates are planets only found by one group, even though every campaign (C0-8) has been searched by at least three different groups.

Consistency of planet yields between groups has been a recurring problem for K2 searches (see e.g. Petigura et al. (2018)'s comparison to Pope et al. (2016) and Barros et al. (2016) where catalogs overlap on about 60% of each other's candidates). Our recovery rate of 75-90% of planets found by other groups is better than these previous overlaps, and improving our pipeline and updating `EVEREST` will only bolster that result.

4.1.2 Evidence Supporting the Validity of Our Multi-Planet Systems

In this section we'll provide two lines of evidence that the planets in our multi-planet systems in particular are indeed real and orbit the same star, even if they were missed by other searches. Both methods rely on the Keplerian orbits of planets and the fact that real planets orbiting the same star are expected to follow those laws. On the other hand, if the candidates were not real, but false positives resulting from digging into noise, the resulting orbits have no reason to obey the Keplerian relationships.

First, we derive the relevant quantities needed in this discussion. Kepler's third law says that (assuming the planet mass is insignificant, $M_p \ll M_*$)

$$a^3 = \frac{GM_*}{4\pi^2} P^2$$

For a planet on a circular orbit ($e = 0$), the orbital velocity v is the orbit's circumference divided by its period

$$v = \frac{2\pi a}{P}$$

and the transit duration T (for an impact parameter of $b = 0$) is the diameter of the planet plus star divided by that velocity

$$T = \frac{2}{v} (R_* + R_p)$$

$$T = \frac{P}{\pi a} (R_* + R_p)$$

Using Kepler's third law to substitute P for a,

$$T = P^{\frac{1}{3}} \left(\frac{4}{\pi G M_*} \right)^{\frac{1}{3}} (R_* + R_p)$$

Finally, if the planet's radius is much less than that of the star, such that $R_* + R_p \approx R_*$, this relation can be simplified further to

$$T = \left(\frac{3}{\pi^2 G} \right)^{\frac{1}{3}} \rho_*^{-\frac{1}{3}} P^{\frac{1}{3}}$$

where ρ_* is the average stellar density.

Normalized Duration Ratios

For planets orbiting the same star, so ρ_* is the same, the ratio between the transit duration and third root of the orbital period, which we call the normalized transit duration, must be

the same constant value:

$$\frac{T}{P^{\frac{1}{3}}} = \left(\frac{3}{\pi^2 G}\right)^{\frac{1}{3}} \rho_*^{-\frac{1}{3}} \tag{4.1}$$

We can define the normalized duration ratio ξ as the ratio of the normalized transit durations between two planets:

$$\xi \equiv \frac{T_1 P_2^{\frac{1}{3}}}{T_2 P_1^{\frac{1}{3}}}$$

For two planets, 1 and 2, orbiting the same star, the normalized durations must be the same and $\xi = 1$. However, this is only strictly true under the assumptions made in this derivation: namely that $e = 0$, $b = 0$, $M_p \ll M_*$, and $R_p \ll R_*$. These assumptions are of course not always true, but ξ should be close to 1 for all planet pairs in multi-planet systems. Significant deviations from $\xi = 1$ hint that planets are not orbiting the same star, or that at least one of the candidates may not be real but a false positive due to instrument systematics or digging too deep into noise. This normalized duration ratio has been used in the past to provide evidence that multi-planet systems are real planets orbiting the same star (Steffen et al., 2010; Fabrycky et al., 2014).

We compare our normalized duration ratio distribution for all our K2 multi-planet pairs to those of the *Kepler* KOIs with periods less than 50 days in Figure 4.2. Because our sample size is much smaller than the KOIs (154 to 1186 planet pairs), our metric is noisier. However, both distributions show a similar pattern: a peak in the normalized duration ratio at 1, indicative of most multi-planet pairs being real candidates that orbit the same star.

However, another trend appears in both our K2 and the *Kepler* sample: an asymmetry favoring normalized duration ratios slightly above 1. In Figure 4.2 we plot both ξ and ξ^{-1}; if the true distribution were values of $\xi = 1$ with random scatter, the two would be symmetric, but instead we see ξ slightly favoring values above 1.

This asymmetric distribution has been used by Fabrycky et al. (2014) as evidence of multi-planet systems having small mutual inclinations — orbiting in nearly the same planes. If planets are perfectly coplanar, then any inclination of that mutual plane as viewed from Earth

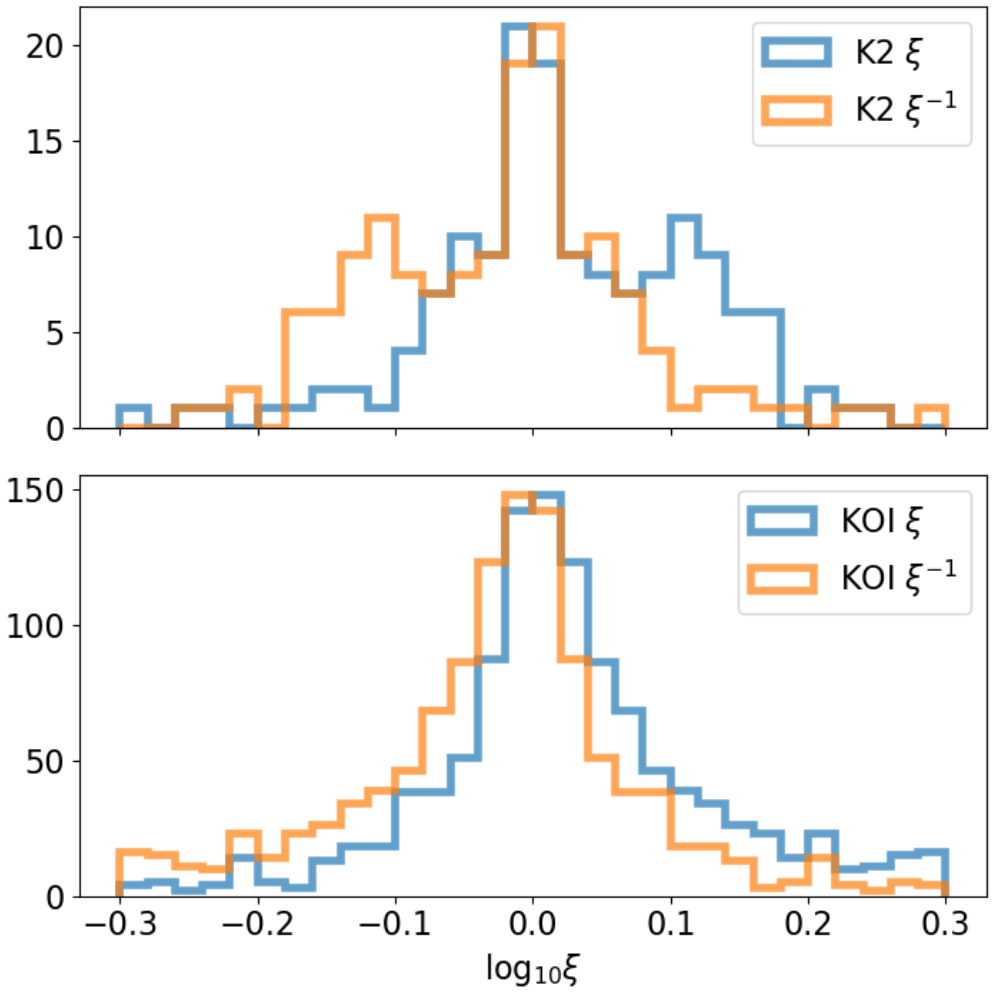

Figure 4.2: Top: Our candidate normalized duration ratios (ξ) and its inverse for all pairs of planets in multi-planet systems. The ratio is always the inner planet divided by the outer planet. Bottom: Same, but for the KOIs with periods less than 50 days. The asymmetry in the ratio and its inverse indicates a small inclination dispersion between planets (see text for discussion).

will cause the outer planets in a system to have higher impact parameters than the inner planets; therefore the outer planets will have slightly shorter normalized durations, causing ξ to be slightly above 1. Allowing for a small eccentricity and mutual inclination distribution can create the smaller tail of ξ ratios below 1 while the majority are still distributed above 1.

After searching all 19 K2 campaigns, we'll roughly double our sample of multi-planet pairs and may be able to quantitatively measure if the K2 ξ distribution differs from the *Kepler* one, which will tell us about the mutual inclination distribution of planets in different environments.

Stellar Density Comparisons in Multi-Planet Systems

As demonstrated in Equation 4.1.2, a measure of a transit's duration and period can provide insight about the average density of the host star. Once again, these measures should provide identical stellar densities under the stated assumptions, but eccentricity, inclination, and non-negligible planet masses or radii will cause the stellar density estimates to deviate slightly from one planet to another. Nonetheless, when comparing multiple planets in a system, we should get similar stellar densities; vast deviations suggest our candidates are not real or not orbiting the same star.

As described in §2.2.9, we generate the derived stellar density for every step in our MCMC chains for every planet candidate, using equations from Winn (2010) and Seager & Mallén-Ornelas (2003). This allows us to get full posterior distributions for the stellar density estimates and compare the results for pairs of planets in our multi-planet systems.

The difference in density between each pair of planets is shown in Figure 4.3. Like the normalized duration ratios, the derived stellar densities for most pairs of planets are consistent, indicating the planets in the multi-planet systems are real and orbiting the same star.

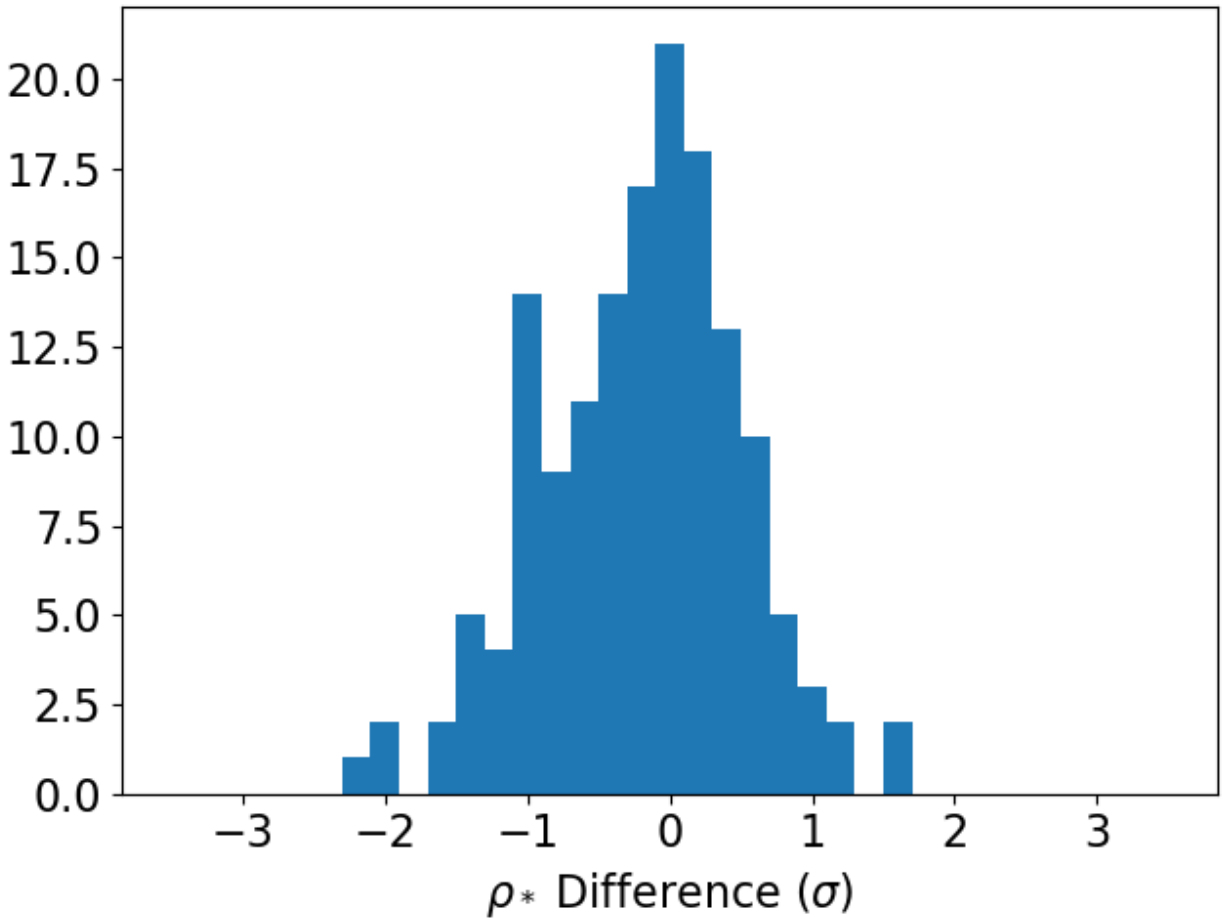

Figure 4.3: Difference in stellar density estimates between pairs of planets in our multi-planet systems (in standard deviations apart).

4.1.3 Ultra-Short-Period Planets

One goal of `QATS` is to detect all planets, even those edge cases that cause the most trouble for most methods. In this section and the following we look at `QATS`'s performance in the two period limits of a transit search: ultra-short-period (USP) planets and single transit events.

USP planets, usually defined as those with periods less than a day, are a unique class of planet predominantly found with *Kepler* (Sanchis-Ojeda et al., 2014). Many pipelines set a minimum period to start their planet searches above one day, making USP detections challenging. Furthermore, USP transit durations are also very short, less than an hour in many cases, which means they span just one or two *Kepler* cadences, and can be difficult to find even if the pipeline searches for such short duration events. The official *Kepler* search (TPS; Jenkins et al., 2010b), for example, sets a minimum transit duration of 1 hour and a minimum period of 1 day, so many USP planets were missed before a dedicated search for them (Sanchis-Ojeda et al., 2014).

In our search of C0-8, we used a minimum transit duration of 2 hours and a minimum period of 0.3 days, so the especially short duration events will be harder to detect. Because we also removed one and two cadence outliers, very deep USP candidates may also have had many transits removed and thus been overlooked. Nevertheless, we compare our search to the dedicated USP search of Adams et al. (2016), who found 19 USP candidates in C0-5.

Of their 19 candidates, we found 12. However, we also found 6 new planet candidates in C0-5 not in their catalog (or in their list of likely EBs). Two of these candidates (EPICs 202092559 and 210801536) have depths less than 200 ppm. We also find 15 previously unreported USP candidates in C6-8. Of these 21 combined new USP candidates, after applying our stellar parameters, 7 have radii less than 4 $R_\oplus$, indicative of small planets worth following up.

4.1.4 Single Transit Events

One of the benefits to our version of `QATS` is that it can be used to identify both periodic and single transit events simultaneously. As discussed in §2.2.6, this first search has a reduced sensitivity to single transit events, often labeling them as having no signal above the `QATS` spectrum baseline and prematurely cutting them from the pipeline. This will be adjusted in future versions (see §6.3.1), but even so, we have detected 72 single transit events in our C0-8 search. The other reason our `QATS` search will have difficulty with some single transit events is our duration limit. We only search for events up to a maximum of 17 hours, and planets or EBs that only eclipse once in a K2 campaign may be on orbital periods of hundreds of days with event durations much longer than 17 hours. For example, the longest duration transiting planet so far was found in C14 and lasts for 54 hours (Giles et al., 2018) — longer than our longest complete search window that includes the transit and 0.6 days of continuum on either side.

Single transit searches have historically been done independently of periodic searches, and the most common approach is not systematic but rather scanning all light curve by eye for potential transit events. Wang et al. (2015b) found 41 long period systems in the original *Kepler* by eye with citizen scientists from the Planet Hunters initiative; Uehara et al. (2016) similarly found 28 single transits manually. Foreman-Mackey et al. (2016) performed the most comprehensive systematic single transit search in *Kepler*, creating an automated search and validation procedure and finding 16 candidates.

The only systematic search for single transit events in K2 has been Osborn et al. (2016) who searched C1-3 and found 7 candidates, of which we found 2 (EPICs 203311200 and 201635132). Two of the Osborn et al. (2016) candidates have durations significantly longer than a day, explaining our lack of detection, one is very shallow and does not appear in the `EVEREST` light curve, and the other two were found but rejected by `QATS` in its automated vetting stage as described above. We also find 20 additional single transit candidates in C1-3 not mentioned by Osborn et al. (2016); however, these are much deeper and it's not clear if

they filtered likely EBs out from their sample.

The most comprehensive single transit search of K2 to date is another manual one. LaCourse & Jacobs (2018) searched C0-14 by eye and found 164 single transit events, 101 of which are in C0-8 around 100 different stars. Of those 101 events, we find just 34 — a sign that we can improve our detection of single transit events significantly. Most are identified by `QATS` but eliminated in the automatic cuts stage, while about a dozen have durations longer than a day and are missed altogether. On the other hand, we find 34 systems in C0-8 with a single transit event that is not listed in the LaCourse & Jacobs (2018) catalog.

Altogether, our 72 single transit events represent the largest such catalog to date in either *Kepler* or K2 found via systematic search (i.e. not by eye). `QATS` is also the only transit search that is able to find both single transits and periodic planets simultaneously — not to mention those with TTVs. This capability has proven useful in the short 70-80 day K2 campaigns, but it about to take on even more significance for the upcoming *TESS* mission data where the majority of stars will only be observed for just 27 days. *TESS* is discussed in more detail in §6.3.3.

4.2 K2's Brighter and Smaller Stellar Sample

The *Kepler* mission was designed for a very specific task: finding Earth-sized planets around stars like the Sun. To accomplish its goal, *Kepler*'s stellar sample was carefully crafted to include as many FGK-type main sequence stars as possible that were bright enough to detect small transits. By stellar type, only about 4000 of *Kepler*'s 200,000 targets were M dwarfs, and they yielded just 150 of the mission's over 4000 planet candidates (Dressing & Charbonneau, 2013, 2015). On the magnitude side, 60% of *Kepler*'s observed targets and 65% of its planet candidates' host stars were fainter than 14th magnitude, making followup difficult. Radial velocity followup of small planets is typically only possible for stars brighter than 12-13th magnitude (Marcy et al., 2014).

On the other hand, the K2 targets are chosen via community proposal, and a much more diverse set of stars have been selected around typically brighter stars. 50% of K2's targets

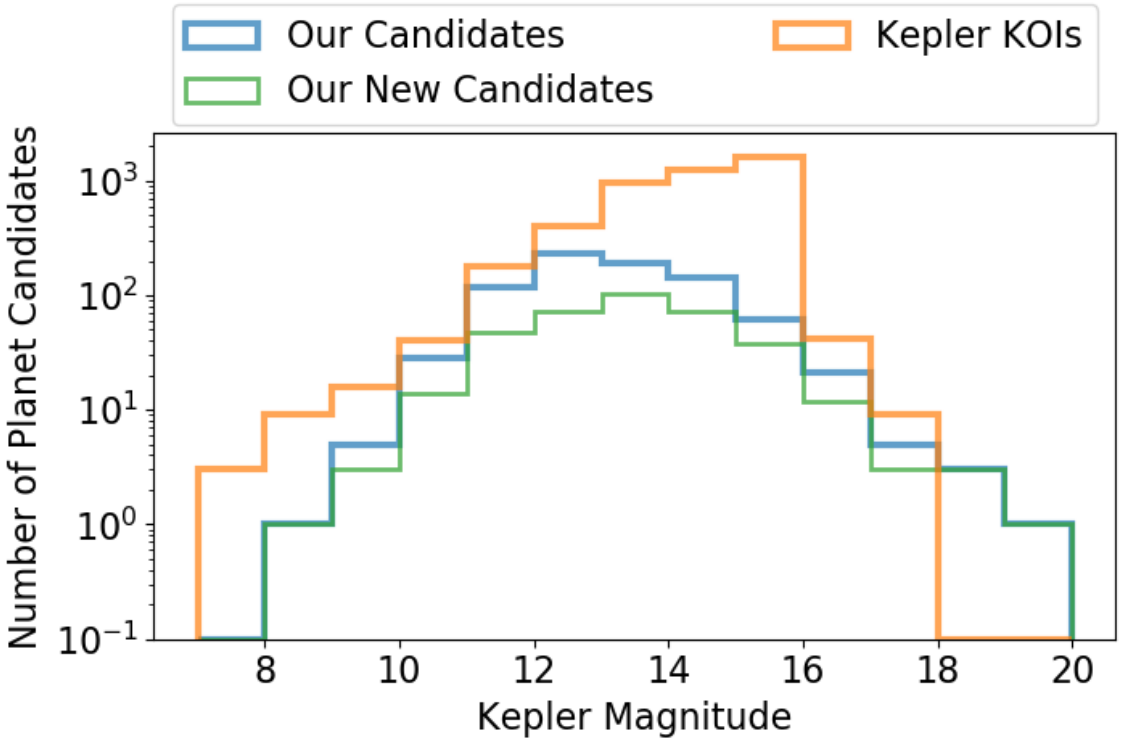

Figure 4.4: *Kepler* magnitudes of our K2 candidates compared to original *Kepler* candidates. At magnitudes brighter than 14, C0-8 is within a factor of 2 of *Kepler*. The lower green line shows only our new candidates, previously undetected by all other groups.

are brighter than 14th magnitude, and 30% are listed in the EPIC as M dwarfs (radii below 0.6 $R_\odot$) by Huber et al. (2016).

Figure 4.4 shows how the K2 planet candidates skew brighter: while 85% of *Kepler* candidates are fainter than 13th magnitude, 47% of our K2 planet candidates are brighter than 13th magnitude. At all magnitudes brighter than 13, our K2 candidate count from C0-8 is within a factor of 2 of the original *Kepler*; after a complete search through all K2 campaigns (C18 is the latest), K2 will have found more planets around stars brighter than 13th magnitude and amenable to followup than *Kepler* did. In addition, K2's planets are on average shorter period than *Kepler* because of the limited K2 campaign duration, so the RV signal will be larger for the average K2 planet.

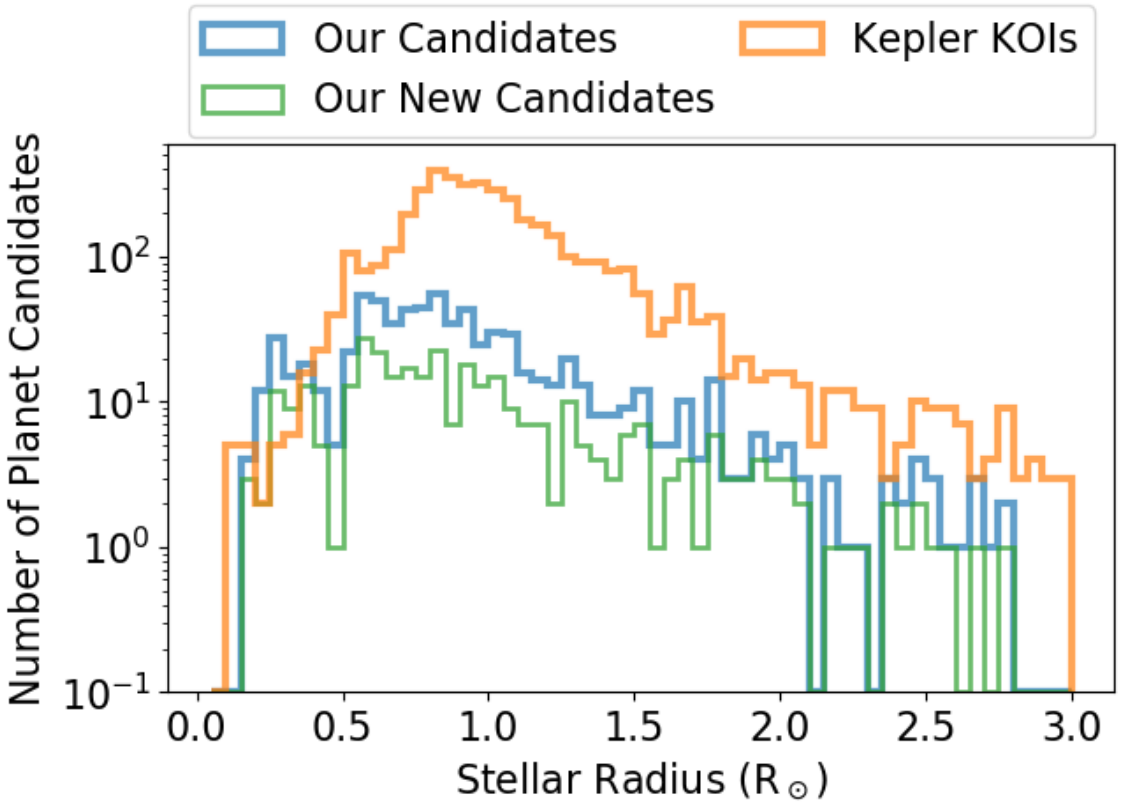

Figure 4.5: Stellar host star radius distribution for the KOIs compared to our K2 planet candidates. *Kepler* focused on stars like the Sun, while K2 has surveyed more M dwarfs. K2 has already found more planet candidates around M dwarfs than *Kepler* did. The dip in the K2 distribution near 0.5 $R_\odot$ is likely a systematic artifact of the transition from *Gaia* stellar parameters above that radius to EPIC parameters below. The lower green line shows only our new candidates, previously undetected by all other groups.

As a function of host star radius, K2 has focused on M dwarfs considerably more than *Kepler* did. Figure 4.5 shows the *stellar* radius distribution for the planet candidates' host stars. Above 0.7 $R_\odot$, *Kepler* has found 5-10× as many candidates as our K2 C0-8 sample. Yet around small M dwarfs, K2's planet candidate count already outnumbers that from *Kepler*. K2 has already matched *Kepler*'s total planet candidate count for stars less than 0.5 $R_\odot$, and will more than double it after all 19 campaigns are thoroughly searched.

These measures are combined in Figure 4.6 to show how much K2 is helping find planets around M dwarfs bright enough for followup. K2 has already more than doubled the number of planets transiting stars brighter than 13th magnitude and smaller than the Sun (184 in K2 versus 127 from *Kepler*).

4.3 Future Research Enabled by This Work

To date, over 1000 refereed papers have been published about the original *Kepler* planet sample[2], and only around a dozen of those are actual exoplanet discovery announcements, dominated by those from the core *Kepler* team itself (from Borucki et al. (2011a) to Thompson et al. (2018)). All the other hundreds of publications and years of analysis by groups around the globe were made possible by the few who were able to develop a successful planet search and provide the thousands of planets for others to work with.

In this thesis, I join the small number of people who have successfully developed a planet search pipeline from scratch, implementing on my own all the checks, tests, and diagnostics needed to find planets while being flexible enough to gracefully handle the innumerable forms of stellar and systematic variability. This work has successfully expanded the scope of K2, nearly doubling the number of planet candidates. The major goal of this thesis is to enable with K2 the same breadth of study as the handful of *Kepler* new planet catalog announcements. While impossible to single-handedly reproduce all of that followup and analysis myself, in this section I lay out a sampling of the avenues available now that my

[2]Based on the Kepler Science Center count.

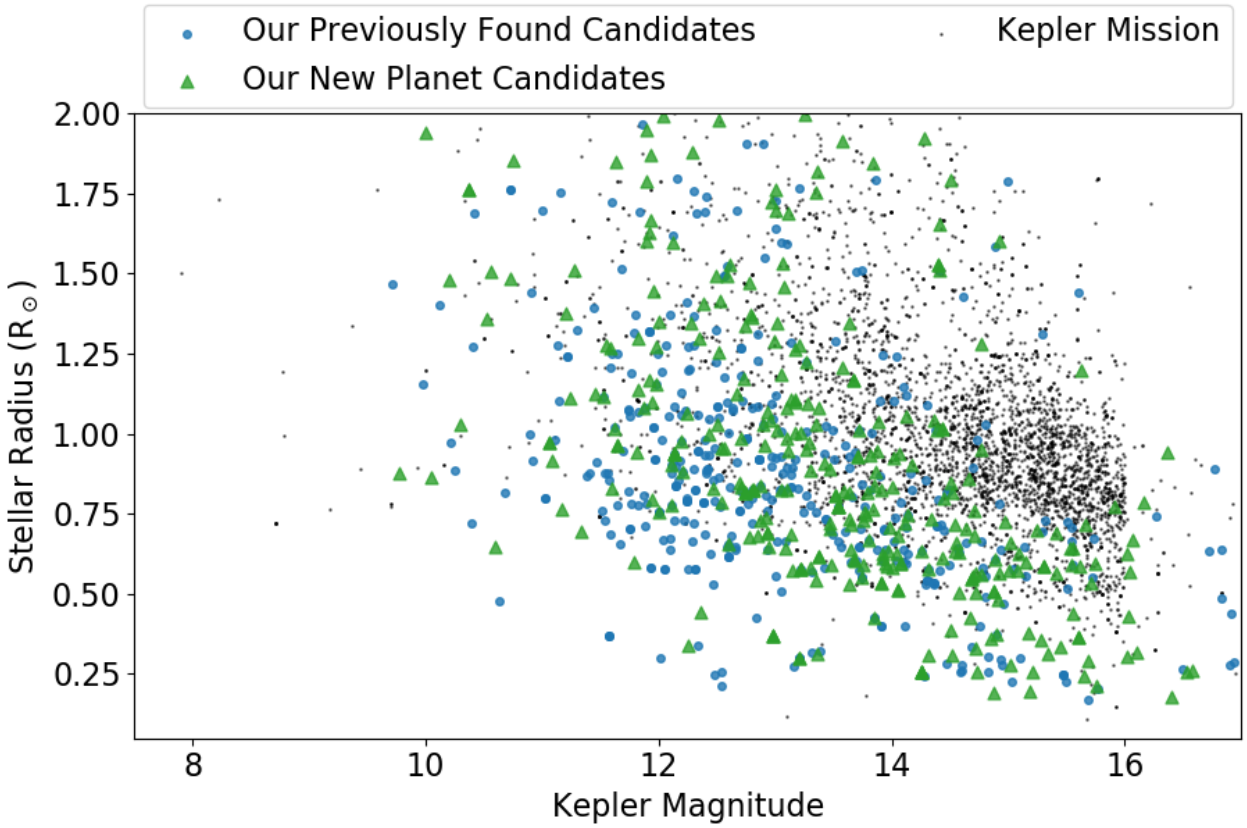

Figure 4.6: *Kepler* magnitude versus host star radius for our K2 planet candidates (circles, previously found by other groups; triangles, newly found in our search) and the *Kepler* KOIs. K2 is dramatically expanding the number of planets around bright M dwarfs. The sharp cutoff at 16th magnitude is an artifact of *Kepler*'s target selection process.

candidates have been found; I show any preliminary results available with the limited data in hand, and I discuss what other followup work would be needed for a thorough analysis.

4.3.1 Better Stellar Parameters

One theme throughout this section is a need to better understand the host stars. Because transits only provide the radius ratio between a planet and star, a precise host star radius is required to get a precise physical planet size. Nearly all future work with our K2 planet sample can therefore be improved by more precise host star characterization, especially their radii.

As discussed in §3.2, we've utilized the stellar characterization of Gaia Collaboration et al. (2016) and Huber et al. (2016). However, the *Gaia* results rely exclusively on data from that mission, while Huber et al. (2016) did not have access to the *Gaia* distances. A better approach would be to combine the two, as has been done for the original *Kepler* field by Berger et al. (2018). They're able to improve stellar radii estimates by a factor of 4-5 over broadband photometry alone (down to radii errors of $\sim$ 8%, allowing for similarly better constraints on planet radii).

Spectroscopic followup of the host stars can also provide better stellar constraints, and yield extra information like the star's metallicity and more precise measure of the star's effective temperature. Johnson et al. (2017) used spectroscopy to measure stellar radii to 11%, and they likely can do even better by combining with *Gaia* data.

4.3.2 Exploring the Radius Gap

As introduced in §1.4, the possible boundary between rocky and gaseous exoplanets is one of the most intriguing results to come from the *Kepler* population. Fulton et al. (2017) found a gap in the radius distribution of small exoplanets at periods less than 100 days, indicating planets with radii of 1.5-2.0 $R_\oplus$ are relatively rare. Lopez & Rice (2016) and Van Eylen et al. (2017) provide tentative evidence that this gap is due to photo-evaporation of the atmospheres because the gap appears to move to smaller planet radii at lower stellar

fluxes incident on the planets. These short period rocky planets therefore may have started off with gaseous atmospheres, and only later come to have their rocky cores exposed after intense stellar radiation blew off the entire gaseous envelope.

Introduced in §3.2, the nominal errors for our *Gaia* stellar radii (most of the stars above 0.5 $R_\odot$) are just 6% (better than the Fulton et al., 2017, 11%), while the M dwarf sample with parameters from Huber et al. (2016) have larger uncertainties of 18%. This translates into a median planet radius error of 14% and 29% respectively. The disparity is larger for luminosity. Because the K2 stars are brighter than average for *Gaia*, and *Gaia* was designed specifically to measure the distance and brightness of stars, *Gaia* uncertainties on stellar luminosities average just 2.5%. However, Huber et al. (2016) does not estimate luminosity for the EPIC stars at all, so our luminosity values are derived from the temperature and radius and have a median uncertainty of 37%. This makes our incident flux estimates for M dwarfs extremely uncertain compared to the larger stars in the *Gaia* sample (90% and 50% respectively).

Using the stellar luminosity and radius, combined with the derived a/R_* from the transit fits, we estimate the flux received for each candidate, assuming a circular orbit; the results are shown in Figure 4.7. We also show the plot from Fulton et al. (2017) using *Kepler* planets for comparison. In both of our samples, the radius gap appears strongest at incident fluxes near 300 $S_\oplus$ and occurs at a radius of about 2 $R_\oplus$. Our radius and incident flux errors are slightly too large to make out a significant gap with our limited planet sample, but we show the radius distribution for our full sample as well as the planets with nominal incident fluxes between 200 and 1000 $S_\oplus$ in Figure 4.8. Again, there's tentative evidence of a stronger radius gap in our planet candidates at the same incident flux region found by Fulton et al. (2017).

Because of K2's larger focus on M dwarfs, we have an opportunity to explore how the radius gap might change as a function of host star mass. Wu (2018) claims a dependence of the radius gap on the host of the primary star such that larger stars host larger planets and the gap moves to larger radii. However, they also note that M dwarfs provide a key anchor to that relation and there are not enough known planets around M dwarfs near the radius

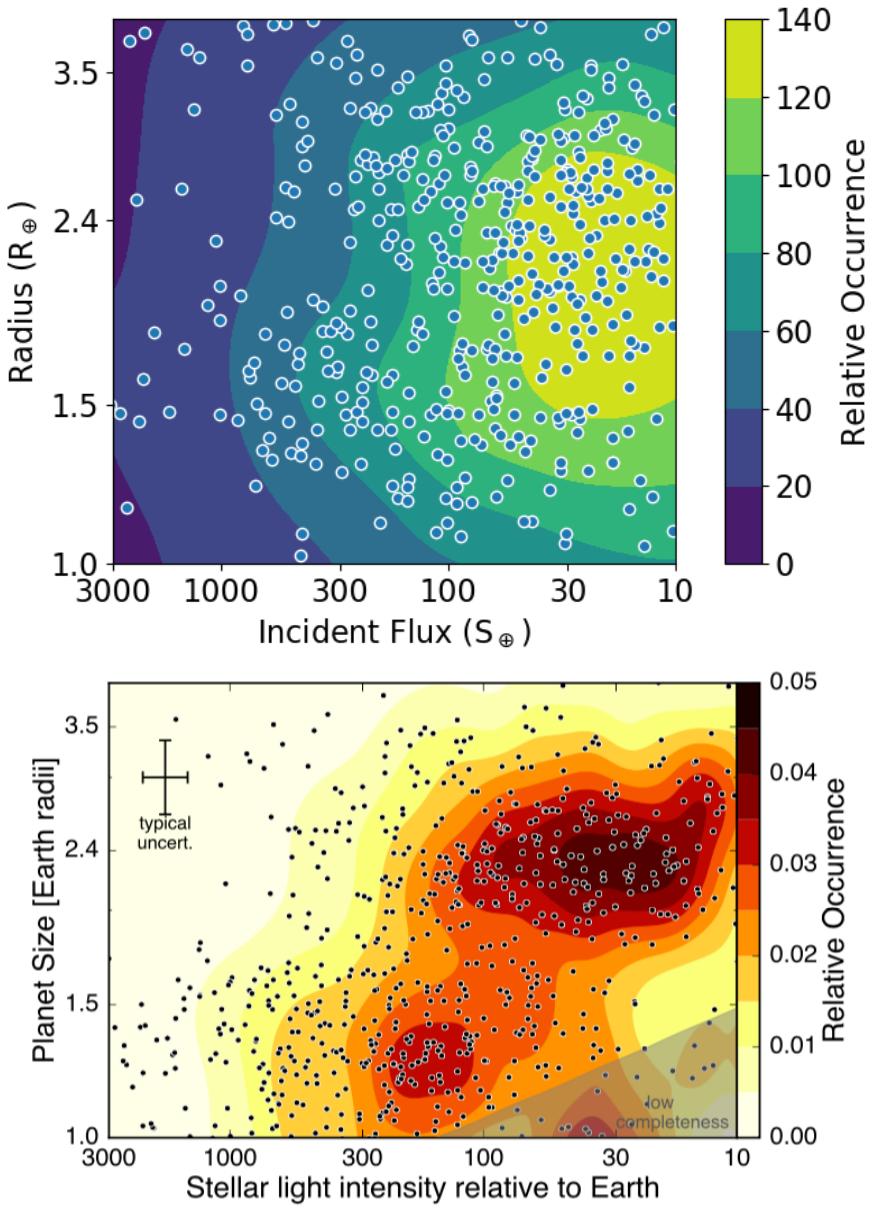

Figure 4.7: Top: Incident flux versus planet radius for our K2 planet candidates. Each point shows one of our planet candidates, while the underlying contours show the distribution while accounting for uncertainties (typical errors are 50% in incident flux and 20% in planet radius). We do not correct for pipeline completeness. Bottom: Same, but for Fulton et al. (2017), who shows a completeness-corrected contour underneath the individual *Kepler* planet candidates. The radius gap is identified by the 'pinching' of the contour plots between the small and large radius groups of planets.

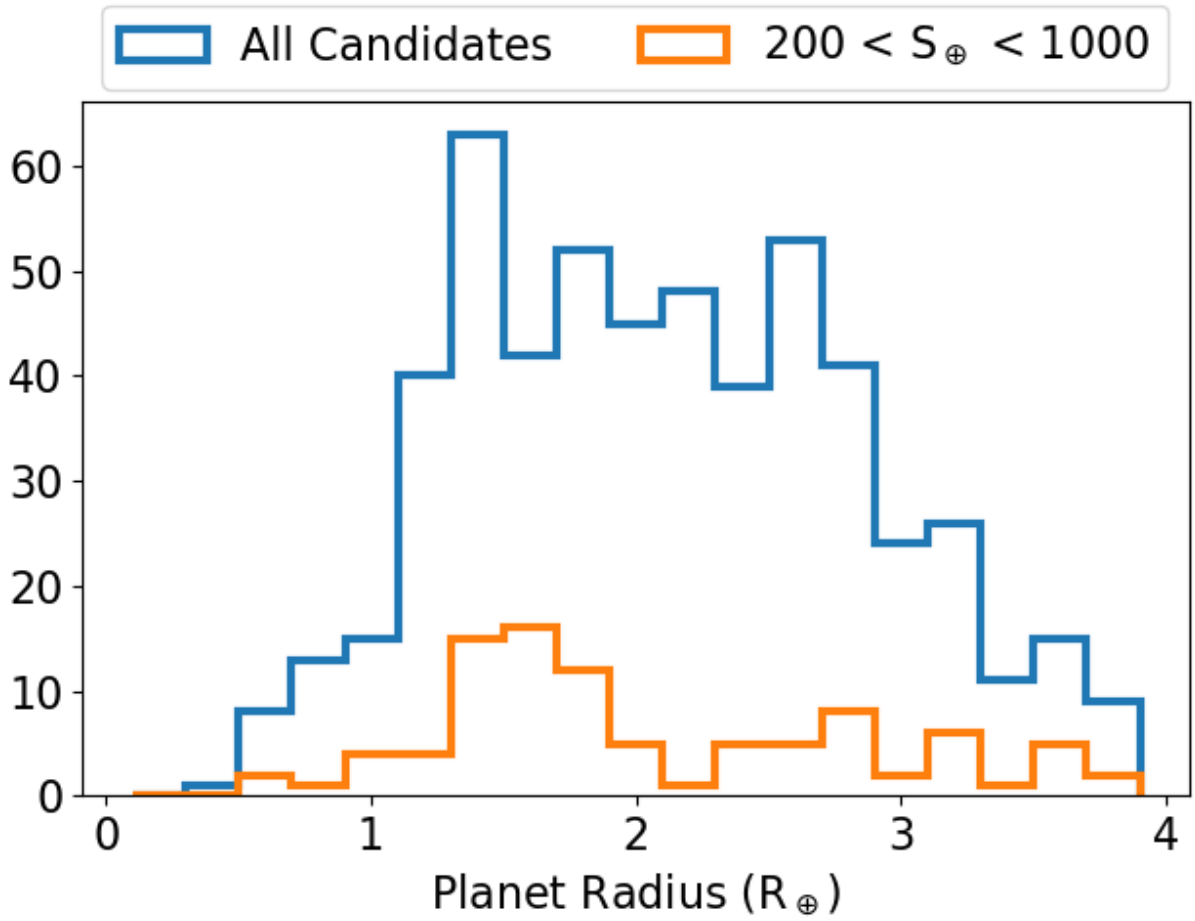

Figure 4.8: Radius distribution of all our candidates and those with incident fluxes near the most distinct section of the Fulton et al. (2017) gap. There is tentative evidence of a dearth of our K2 planets near 2 $R_\oplus$ at incident fluxes coincident with the gap found by Fulton et al. (2017).

gap yet.

Our work provides the first step: finding the planets at all. As our survey of the K2 campaigns doubles the number of planet candidates around M dwarfs, followup characterization with *Gaia* and ground-based spectra can better constrain the incident fluxes and planet radii to measure how the shape and location of the radius gap might depend on various stellar and environmental properties.

4.3.3 The Habitable Zone

Due to the nature of the short K2 campaign durations, most of our planet candidates are found at very short periods and correspondingly high instellations. However, a handful of planet candidates around smaller stars may lie within their star's liquid water 'habitable zone'. Unfortunately, because the more precise *Gaia* parameters only consider stars above 0.5 $R_\odot$, most of the possible habitable zone planets only have the EPIC parameters with poor luminosity estimates.

We plot the incident fluxes near the habitable zone in Figure 4.9, limited only to those systems where our measure of the incident flux is more than 1 standard deviation above 0 (80% of our candidates). The majority of planets are well interior to the habitable zone, although the uncertain incident fluxes allow many to cover the entire region within one standard deviation.

Many candidates have such uncertain stellar luminosities that their parameters more than span the entire habitable zone. A better characterization of our new M dwarf hosts will be necessary to pin down potential habitable zone planets, as was done by Dressing et al. (2017a).

Even so, there are 5 planet candidates in or near the habitable zone with planet radii small than 2 $R_\oplus$. Of those five, four have been previously found by other groups (201367065.3 [K2-3d], 205489894.1, 201912552.1 [K2-18b], 211579112.1), while one is new: 210508766.3.

Our new small planet candidate near the habitable zone, EPIC 210508766.3 (if confirmed would be K2-83d), is an outer companion to a previously confirmed two-planet system (Cross-

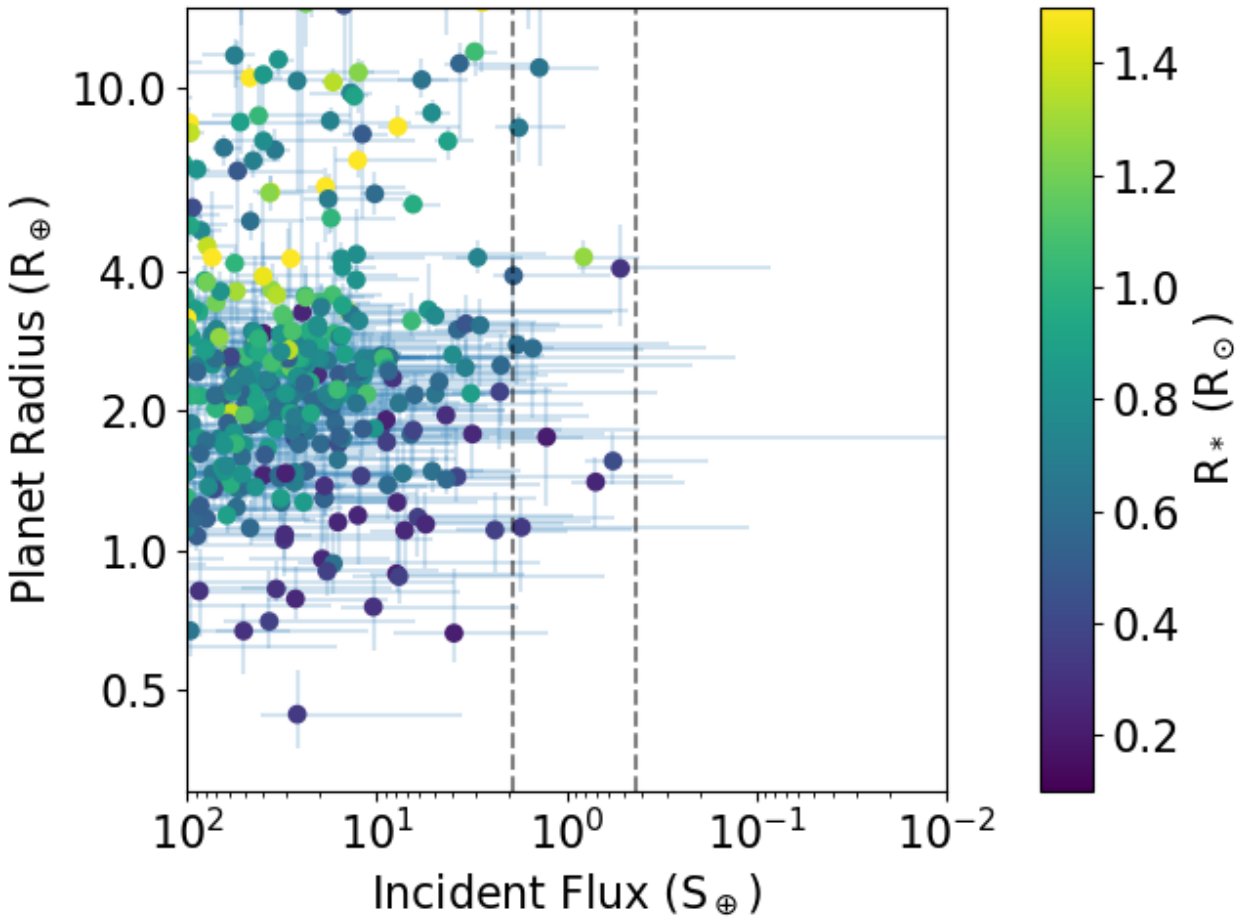

Figure 4.9: View of our K2 candidates near the habitable zone, limited to those with an incident flux more than one standard deviation above 0. The candidates are colored by the host star's radius. Because of the imprecise luminosities available for the M dwarf host stars, the incident fluxes near the habitable zone are uncertain and many planets span the entire zone and beyond. Incident fluxes for Venus (left dashed) and Mars (right dashed) mark approximate boundaries of the habitable zone.

field et al., 2016; Dressing et al., 2017b). Dressing et al. (2017a) characterizes the star as an M1 dwarf, slightly larger and brighter than the values we use from the EPIC, but the planet remains habitable regardless. This planet highlights the usefulness of `EVEREST` and `QATS` by finding outer small, cool companions that other groups overlooked. Finding outer, cooler companions with a limited number of transits will become especially important with *TESS*, and `QATS` could be used to help expand *TESS*'s reach to more habitable zone planets.

4.3.4 Young Planets in Clusters of Known Ages

One of the benefits of K2's survey of new parts of the sky is the capability to target stars in clusters. Clusters have often been a testbed of astrophysics, since the member stars are expected to be roughly the same age and metallicity, allowing for more controlled tests of how various processes change with stellar mass. Comparing properties between clusters can also be used to see how they evolve over time.

As reviewed in §1.3.1, exoplanets are expected to form in the first 10-100 Myr of a star's life. The migration and dynamical interactions of planets form systems that are not always stable long-term, and instabilities and scattering events are expected to reduce planet occurrence rates over time (Izidoro et al., 2017). Measuring masses and radii of hot Jupiters of known ages could clarify the mechanism behind 'inflated' hot Jupiters that seem to be larger than models predict (Demory & Seager, 2011; Sestovic et al., 2018); it could also help determine the still unknown formation mechanism of hot Jupiters based on occurrence rates over time (Adams & Laughlin, 2003). The planet radius distribution of Earth and Neptune-sized planets over time could also help unpack whether the radius gap is due to photoevaporation, which predicts larger planets at young ages (Lopez et al., 2012; Lopez & Rice, 2016). Finding planets in the very youngest clusters could constrain how quickly planet formation occurs, and whether short period planets formed in situ or migrated to those locations.

However, examples of young planets are rare. *Kepler* did not have any clusters younger than 1 Gyr in its field of view, and young stars are more active, producing noisier light

curves and radial velocity signals, making detecting young planets from the ground much more challenging (Paulson et al., 2004). At the start of the K2 mission, only 4 planets had been found in open clusters, and they were all Jupiter-sized (Quinn et al., 2012).

Thousands of stars in clusters have been targeted by K2, and one notable result came from C2 with the discovery of a planet (K2-33) in the 5 Myr cluster Upper Scorpius, which we also found (David et al., 2016b). This was our only candidate amongst the 1788 stars targeted in C2 associated with the young clusters.

In C5, K2 targeted the 800 Myr old Beehive cluster, and Mann et al. (2017) found seven planet candidates. We confirm all of those except for EPIC 211901114, which we missed; its transit duration is just 0.5 hours, much shorter than our minimum search of 2 hours. A dedicated `QATS` search at the half hour duration does in fact recover the planet though, indicating we could improve our sensitivity to USP and short duration planets by lowering our minimum transit duration below 2 hours. Of the 2000 C5 targets that are members of known clusters, we do not find any new planet candidates.

The biggest impact our search has had on planets in known clusters occurs in the C7 search of the 3 Gyr open cluster Ruprecht 147. Prior to our search, only 1 planet had been found amongst the 1061 member stars targeted (EPIC 219388192, another hot Jupiter). We found seven new planet systems, including the potential two planet system EPIC 219747794 and two single planet systems hosting planets just twice the size of Earth: EPICs 219480273 and 219800881.

4.3.5 Planet Occurrence Rates

One of the main goals of the *Kepler* mission was not just to find exoplanets, but to measure how common they are. Such occurrence rates require a knowledge of not just the planets found, but an estimate of how many planets were missed. Geometric corrections accounting for the probability of a planet to transit is relatively straightforward, but one also has to account for the likelihood of a given planet to be detected by the pipeline even when it does transit.

These occurrence rates have been calculated many times for the *Kepler* field (e.g. Burke et al., 2015; Dressing & Charbonneau, 2013; Petigura et al., 2013a), but K2 now allows for the same to be done in different parts of the sky, albeit limited to shorter period planets. These measurements would provide hints about potential changes in planet occurrence across galactic environments, metallicity, or stellar age. Radial velocity surveys have already shown a potential disparity in the rate of hot Jupiters compared to the *Kepler* sample, which K2 may help address (Wang et al., 2015a).

For our planet sample to be used in K2 occurrence rate calculations, we would need to get a detailed model of our pipeline's sensitivity to planets of various sizes and periods. This is done via transit injection tests, where simulated planets are injected into the data, and the pipeline is run and checked to see if the planet was recovered (Christiansen et al., 2016; Petigura et al., 2013b). Done enough times, a model can be built predicting the odds of discovering a planet of given parameters.

In our case, `EVEREST` has already been designed with transit injection tests in mind, so we could start at the raw pixel level. We would inject transits into the pixels, detrend the light curve with `EVEREST`, and then run `QATS`. Planets would be labeled 'detected' if they passed all cuts up to the manual vetting stage; because these injections would be run tens of thousands of times, manual vetting is infeasible.

With a measure of our pipeline's detection efficiency as a function of period and transit depth and duration, we could correct our planet sample for these biases. Converting from raw planet counts to occurrence rates is a complicated problem, perhaps exacerbated by the complex and disjointed selection of K2's various target stars (Foreman-Mackey et al., 2014); however, it at least becomes tractable with a measure of `QATS`'s detection efficiency.

Chapter 5

KOI-3278: A SELF-LENSING BINARY STAR SYSTEM

My `QATS` pipeline has been written with enough modularity that it can be used to search light curves for any quasiperiodic signal, not just transits. In this chapter, I present a fortuitous discovery that highlights the flexibility and sensitivity of my planet search pipeline. This particular case 'only' required inverting my usual transit model, but I could nearly as easily search for any other analytically described shape. During an early search of known Kepler Objects of Interest for additional exoplanet candidates, I found what looked like an upside-down transit. By explicitly searching for a negative transit (the star gets brighter when an object passes in front of it), the signal jumped out. More careful analysis proved this object to be the first self-lensing binary star system. Since then, a few more such systems have been found, lending credence to this one and expanding our knowledge of binary stellar evolution (Kawahara et al., 2018).

A version of this chapter was previously published in collaboration with Eric Agol in the April 2014 edition of Science (Kruse & Agol, 2014).

5.1 Modeling KOI-3278 as a Self-Lensing Binary System

Over 40% of Sun-like stars are bound in binary or multistar systems. Stellar remnants in edge-on binary systems can gravitationally magnify their companions, as predicted 40 years ago. By using data from the *Kepler* spacecraft, we report the detection of such a "self-lensing" system, in which a 5-hour pulse of 0.1% amplitude occurs every orbital period. The white dwarf stellar remnant and its Sun-like companion orbit one another every 88.18 days, a long period for a white dwarf–eclipsing binary. By modeling the pulse as gravitational magnification (microlensing) along with Kepler's laws and stellar models, we constrain the

mass of the white dwarf to be ∼63% of the mass of our Sun. Further study of this system, and others like it, will help to constrain the physics of white dwarfs and binary star evolution.

Einstein's general theory of relativity predicts that gravity can bend light and, consequently, that massive objects can distort and magnify more distant sources (Einstein, 1936). This lensing effect provided one of the first confirmations of general relativity during a solar eclipse (Dyson et al., 1920). Gravitational lensing has since become a widely used tool in astronomy to study galactic dark matter, exoplanets, clusters, quasars, cosmology, and more (Wambsganss, 1998; Meylan et al., 2006). One application had yet to be realized: in 1973, André Maeder predicted that binary star systems in which one star is a degenerate, compact object — a white dwarf, neutron star, or black hole — could cause repeated magnification of its companion star (instead of the standard eclipses) if the orbit happened to be viewed edge-on (Maeder, 1973). The magnification of these self-lensing binary systems is small, typically a part in one thousand or less if the companion is Sun-like, and so it was not until high-precision stellar photometry was made possible with the *CoRoT* and *Kepler* spacecrafts that this could be detected (Agol, 2002; Sahu & Gilliland, 2003). Stellar evolution models predicted that about a dozen self-lensing binaries could be found by the *Kepler* spacecraft (Farmer & Agol, 2003). A self-lensing binary system allows the measurement of the mass of the compact object, which is not true for most galaxy-scale microlensing events in which there is a degeneracy between the velocity, distance, and mass of the lensing object (Paczynski, 1996). Microlensing does affect several known white dwarfs in binaries in which the depth of eclipse is made slightly shallower (Marsh, 2001; Steinfadt et al., 2010; Rowe et al., 2010; Muirhead et al., 2013; Kaplan et al., 2014) but does not result in brightening because occultation dominates over magnification at the short orbital periods of those systems.

Here, we report that Kepler Object of Interest 3278 (KOI-3278) (Burke et al., 2014; Tenenbaum et al., 2014), a term intended for planetary candidates, is instead a self-lensing binary composed of a white dwarf star orbiting a Sun-like star. The candidate planetary transit signal is actually the repeated occultation of the white dwarf as it passes behind its stellar companion. A search for other planets in this system with the Quasiperiodic

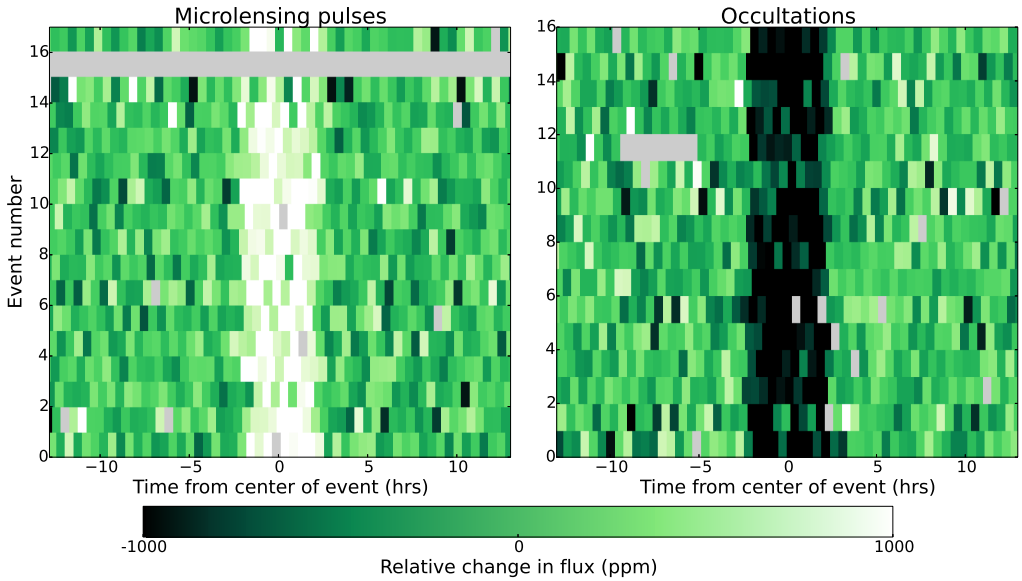

Figure 5.1: Detrended flux versus time for all 16 microlensing pulses and 16 occultations in KOI-3278. Each row depicts the relative fluxes in 29.3-min *Kepler* cadences around an event. The rows are separated by the orbital period, $P = 88.18$ days. White represents brighter flux and black dimmer, whereas gray represents missing data or outliers that have been removed. ppm, parts per million.

Automated Transit Search algorithm (Carter & Agol, 2013) turned up a series of symmetric pulses, brightenings rather than dimmings, with a near-identical period and duration as the transit candidate but occurring almost half an orbital period later. All these properties can be explained by magnification of the Sun-like star as the white dwarf passes in front; 16 microlensing pulses were found, in addition to 16 occultations. The pulses and occultations are periodic and uniform in magnitude and duration (Fig. 5.1), which is consistent with a nearly circular, Keplerian orbit. Because there is no other phenomenon (that we know of) that can cause such a brief, symmetric, periodic brightening, we constructed a model for KOI-3278 composed of an eclipsing white dwarf and G dwarf (Sun-like star) binary (§5.2).

Even without a full model, an estimate of the mass of the white dwarf, M_2, can be made directly from the light curve. The ratio of the fluence of the microlensing pulse, $F_{\rm pulse}$, to the stellar fluence over an orbital period, $F_{\rm tot}$, is given (Agol, 2003) by $F_{\rm pulse}/F_{\rm tot} = 5.4\times10^{-6}\sqrt{(1-b^2)}(M_2/M_\odot)(R_\odot/R_1)$, where R_1 is the radius of the G dwarf and b is the impact parameter [1]. Because the duration of the pulse is 5 hours, the period is 88.18 days, and the magnification is 10^{-3}, we calculated $F_{\rm pulse}/F_{\rm tot}[1-(b/0.7)^2]^{-1/2} \approx 3.3\times10^{-6}$ and $M_2 \approx 0.6M_\odot$, which is a typical mass for a white dwarf star (Kepler et al., 2007).

To jointly constrain the parameters of both stars, we fitted a full model simultaneously to the *Kepler* time-series photometry and the multiband photometry collected from other surveys (§5.2). We modeled the light curve by using a Keplerian orbit with the gravitational lensing approximated as an inverted transit light curve, which is appropriate when the Einstein radius is small (Agol, 2003). We compared the Padova stellar evolution models (Bressan et al., 2012) to the multiband photometry to constrain the properties of the G dwarf while accounting for extinction, $A_{\rm V}$. Last, we used cooling models to constrain the age of the white dwarf (Bergeron et al., 2011).

Our model provides an accurate description of the data (Fig. 5.2) with a reduced χ^2

[1]The impact parameter is the projected sky separation of the white dwarf and G dwarf at midpulse, in units of the radius of the G dwarf; we find a best-fit value of $b = 0.7$ based on the full model fit. This formula assumes a circular orbit, neglects limb-darkening, and neglects obscuration by the white dwarf; whereas these effects (although minor) are accounted for in our full model.

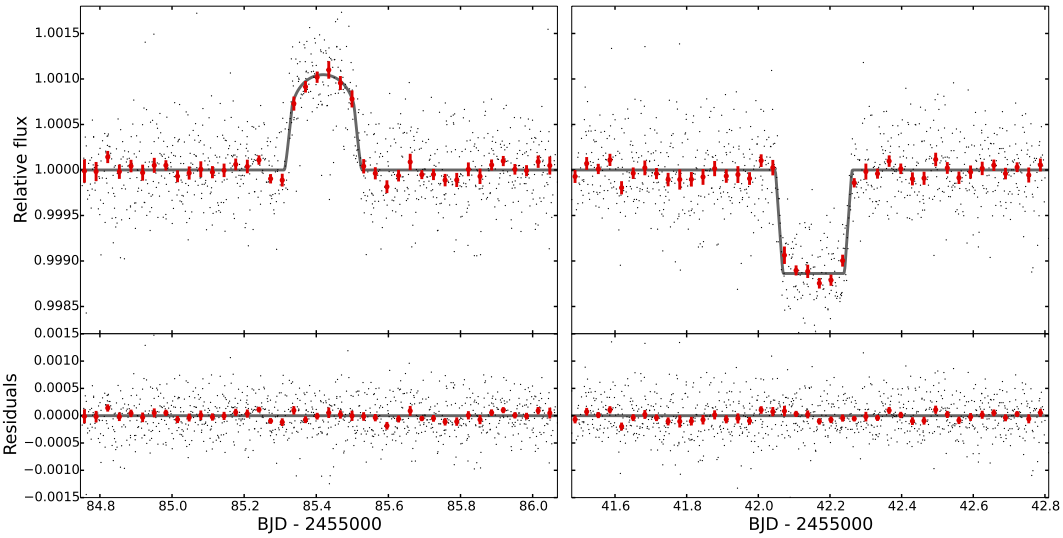

Figure 5.2: Model fit to the data. Detrended and folded *Kepler* photometry of KOI-3278 presented as black points (all pulses and occultations have been aligned), overplotted with the best-fit model (gray line) for the microlensing pulse (left) and occultation (right). Red error bars show the mean of the folded data over a 45-min time scale. Bottom graphs show the residuals of the data with the best-fit model subtracted. BJD, barycentric Julian date.

value of unity. From this model, we calculated the stellar parameters and the binary system's orbital properties (Table 5.1), with uncertainties derived from a Markov-chain Monte Carlo analysis (§5.3.3). The model produced a white dwarf mass of $M_2 = 0.63 M_\odot \pm 0.05 M_\odot$, with a G dwarf companion of $M_1 = 1.04^{+0.03}_{-0.06} M_\odot$, $R_1 = 0.96^{+0.03}_{-0.05} R_\odot$, and effective temperature $T_{\rm eff,1} = 5568 \pm 39$ K: a star very similar to our Sun. Because the white dwarf, with its small size, is much fainter than the G dwarf, we cannot yet measure its temperature directly. However, given the measured mass from gravitational lensing, we inferred its size to be $R_2 = 0.0117 R_\odot \pm 0.0006 R_\odot$ by using a mass-radius relation appropriate for carbon-oxygen white dwarfs. With a radius for the white dwarf, the measured occultation depth when it passes behind the G dwarf can be used to constrain the temperature of the white dwarf, which we found to be $T_{\rm eff,2} = 10,000 \pm 750$ K; this temperature would give the white dwarf the bluish hue of an A star. The Einstein radius, $R_{\rm E}$, is about twice the inferred size of the white dwarf, which allows lensing to dominate over occultation when the white dwarf passes in front. Gravitational lensing causes a distorted and magnified image of the G dwarf outside the Einstein ring in addition to a second inverted and reflected image of the G dwarf within the Einstein ring (Fig. 5.3); the inner image is partially occulted by the white dwarf's disk, reducing the observed magnification slightly.

Our model does not include the effect of star spots, but the *Kepler* G dwarf light curve displays their characteristic quasiperiodic fluctuations with a root mean square of 0.76%. We estimated that the spots would affect the derived stellar properties by less than a percent, smaller than the statistical errors in our model. Spot analysis revealed a G dwarf rotational period of $P_{\rm rot} = 12.5 \pm 0.1$ days. This short rotational period is expected for a G dwarf of only 0.89 ± 0.14 Gy (§5.4.1). The white dwarf cooling time is $t_{\rm cool} = 0.66 \pm 0.06$ Gy, which when added to the main sequence lifetime, t_2, of its progenitor with mass $M_{2,\rm init}$ gives a total age of the binary system of $t_1 = 1.6^{+0.9}_{-0.6}$ Gy; this age is marginally inconsistent (1.4σ) with the spin-down age of the G dwarf.

However, the G dwarf may have been spun up because of accretion of gas from the white dwarf progenitor. Because the white dwarf progenitor was previously a red giant, it should

Table 5.1: Parameters of the KOI-3278 binary star system. More information can be found in §5.3.2. The median and 68.3% bounds are given for each parameter. g_1, surface gravity in cm/s^2. L_{WD}, luminosity of the white dwarf. e, eccentricity. ω, argument of periastron. a, semi-major axis. i, inclination. F_2/F_1, flux ratio between the white dwarf and G dwarf in the *Kepler* band. D, distance. σ_{sys}, systematic errors in the multiband photometry.

G dwarf:	
$M_1(M_\odot)$	$1.042^{+0.028}_{-0.058}$
$R_1(R_\odot)$	$0.964^{+0.034}_{-0.054}$
$[Fe/H]_1$	$0.39^{+0.22}_{-0.22}$
t_1 (Gyr)	$1.62^{+0.93}_{-0.55}$
$T_{eff,1}$ (K)	5568^{+40}_{-38}
$\log(g_1)$	$4.485^{+0.026}_{-0.020}$
White dwarf:	
$M_{2,init}(M_\odot)$	$2.40^{+0.70}_{-0.53}$
$M_2(M_\odot)$	$0.634^{+0.047}_{-0.055}$
$T_{eff,2}$ (K)	9960^{+700}_{-760}
$R_2(R_\odot)$	$0.01166^{+0.00069}_{-0.00056}$
$R_E(R_\odot)$	$0.02305^{+0.00093}_{-0.00107}$
t_2 (Gyr)	$0.96^{+0.90}_{-0.53}$
t_{cool} (Gyr)	$0.663^{+0.065}_{-0.057}$
$L_{WD}(L_\odot)$	$0.00120^{+0.00024}_{-0.00023}$
Binary system:	
P (d)	$88.18052^{+0.00025}_{-0.00027}$
t_0 (-2,455,000 BJD)	$85.4190^{+0.0023}_{-0.0023}$
$e\cos\omega$	$0.014713^{+0.000047}_{-0.000061}$
$e\sin\omega$	$0.000^{+0.049}_{-0.054}$
a (AU)	$0.4605^{+0.0064}_{-0.0103}$
a/R_1	$102.8^{+3.7}_{-2.4}$
b_0	$0.706^{+0.020}_{-0.025}$
i (deg)	$89.607^{+0.026}_{-0.020}$
F_2/F_1	$0.001127^{+0.000039}_{-0.000039}$
D (pc)	808^{+36}_{-49}
σ_{sys}	$0.0246^{+0.0127}_{-0.0078}$
K_1 (km/s)	$21.53^{+0.96}_{-0.98}$
π (milli-arc sec)	$1.237^{+0.079}_{-0.053}$
α_1 (milli-arc sec)	$0.2169^{+0.0076}_{-0.0072}$
A_V (mags)	$0.206^{+0.017}_{-0.016}$

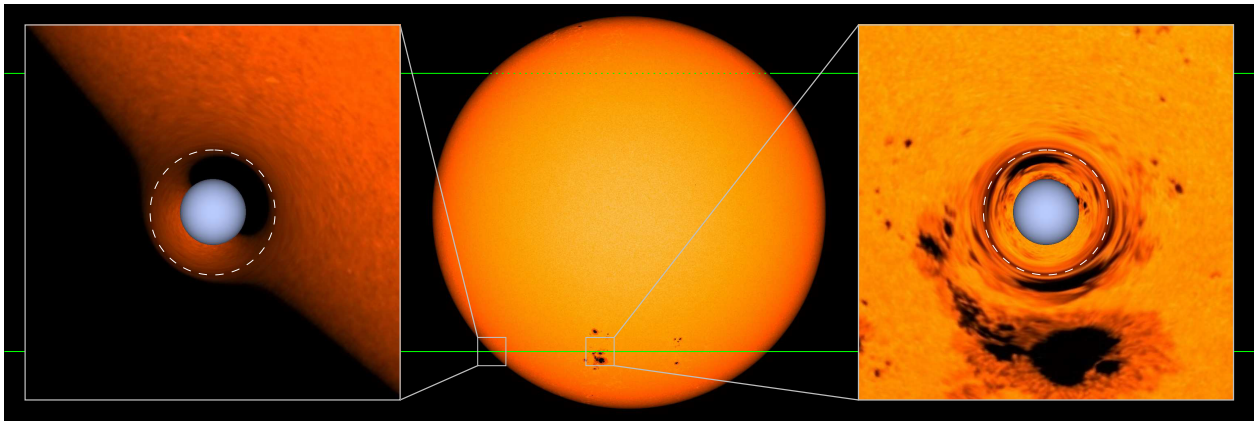

Figure 5.3: Illustration of lensing magnification. (Center) The false-color disk of a G dwarf (using an actual image of the Sun from NASA/SDO HMI), in which the green line shows the trajectory of the white dwarf, with the dotted portion indicating where it passes behind the G dwarf. (Left and right) Close-ups of areas boxed in center show the lensed image of the G dwarf at two different times during the microlensing pulse; the white dwarf is the blue sphere. The white dashed line shows the Einstein ring of the white dwarf. The model that we fit to the data does not contain spots; however, the spots and granulation make the lensing distortion more apparent.

have enveloped the G dwarf during a common envelope phase (Ivanova et al., 2013). The initial orbital period of the binary was likely several years long, and the period was likely shortened because of drag during the common envelope phase. During this phase, the G dwarf accreted some gas from the red giant, increasing its mass by 10^{-3} to $10^{-2} M_{\odot}$ and spinning the G dwarf up from the angular momentum contained in the accreted gas; this spin-up would have reset the age-spin relation, which could explain the slight age discrepancy.

KOI-3278 was the longest period eclipsing post–common envelope binary found at the time (Fig. 5.10), and it is also one of the only examples of an eclipsing Sirius-like system – a binary composed of a non-interacting white dwarf and a Sun-like (or hotter) main-sequence star (Rebassa-Mansergas et al., 2012; Zorotovic & Schreiber, 2013; Holberg et al., 2013). As such, it will help to provide constraints on the physics of formation and evolution of short and intermediate period evolved binary stars, thereby improving our knowledge of the formation of accreting binaries and sources of gravitational waves. We expect that a few

more self-lensing binaries could still be found in the *Kepler* data at shorter orbital periods than KOI-3278. The magnification decreases down to periods of ≈16 days, making them more difficult to find; at even shorter periods, occultation by the white dwarfs disk wins out over the lensing, causing a shallower eclipse as in KOI-256 (Muirhead et al., 2013). Systems like KOI-3278 should not be a substantial source of false-positives for exoplanets; only one was predicted to be found in the *Kepler* data with its magnification of ≈0.1% (Farmer & Agol, 2003).

Follow-up observations should better constrain the parameters of the white dwarf star in KOI-3278, allowing a test of the mass-radius relation for white dwarfs (Provencal et al., 1998; Parsons et al., 2012). Radial velocity observations should show a semi-amplitude of $K_1 = 21.5$ km/s and a line-broadening of 4 km/s. High-resolution spectroscopy will also better constrain the atmospheric properties of the G dwarf; in particular, spectral abundance anomalies caused by accretion of nuclear-processed material from the white dwarf progenitor should be sought. Measurements of the occultation of the white dwarf in the ultraviolet (with the Hubble Space Telescope) should appear much deeper, as much as 60% in depth as opposed to the 0.1% occultation depth in the *Kepler* band, and will yield constraints on the radius and temperature of the white dwarf. High angular resolution imaging would allow for better constraints to be placed on the presence of a third star in the system (§5.5). Last, parallax measurements, π, with the *Gaia* spacecraft (Perryman et al., 2001; Gaia Collaboration et al., 2016) will improve the precision of the properties of the G dwarf; *Gaia* can also detect the reflex motion, α_1, of the G dwarf as it orbits the center of mass with the white dwarf. This provides another means to detect systems like KOI-3278 with inclinations that do not show microlensing or occultation; there are likely 100 of these among the *Kepler* target stars alone, given the 1% geometric lensing probability of KOI-3278.

5.2 Photometric Time Series Model

5.2.1 Terminology

We use the term "self-lensing binary" to refer to a binary star system that is edge-on and in which one star causes a brightening of its companion — due to gravitational magnification, or "microlensing" — as it passes in front of the companion's disk (Gould, 1995; Sahu & Gilliland, 2003; Rahvar et al., 2011; Mao, 2012). Since a self-lensing binary had not previously been detected, we define some terminology for periodic microlensing in a binary star system. In particular, the brightening that occurs in KOI-3278 when the white dwarf magnifies the G dwarf is neither an eclipse nor a transit, which are associated with a decrease in the brightness of the system. Nor can this be described as a "microlensing event" since it repeats; it is not a single event. Maeder (1973) used the term "gravitational flash" to describe repeated microlensing in a binary; however, this term could also connote gravitational waves or explosive events. Others have used the term "anti-transit" (Di Stefano, 2011), but this has also been used to refer to a secondary eclipse that happens opposite in the orbit to the transit (Winn, 2010). Instead of these terms, we refer to the series of brightenings that occur as the white dwarf magnifies the G dwarf as a "microlensing pulse train", and to a single event as a "microlensing pulse" or "pulse" for short.

We refer to the G dwarf as the primary star and the white dwarf as the secondary, and we label their physical properties with 1 and 2; thus the masses and radii are M_1 and R_1 for the G dwarf and M_2 and R_2 for the white dwarf. We refer to the secondary eclipse, when the white dwarf passes behind the G dwarf, as the occultation.

5.2.2 Kepler Photometry

We used the simple-aperture-photometry flux (`SAP_FLUX`) from the *Kepler* pipeline for all available quarters (Q1-Q17). The times are the midpoint of each cadence, converted to Barycentric Julian Date (BJD). We rejected points that were flagged with cosmic ray contamination or single-point outliers (`SAP_QUALITY` flags 128 and 2048).

A plot of the pulses and occultations is shown in Figure 5.4.

5.2.3 Light Curve Model

We computed a light curve model for KOI-3278 (*Kepler* Input Catalog [KIC] 3342467) using transiting planet modeling software developed by Mandel & Agol (2002), but with the sign of the flux changes switched for the microlensing pulses. This inverted-transit approximation is justified because a lensing light curve shape is well approximated by that of a transit light curve (with small deviations at ingress and egress) when the Einstein radius is much smaller than the size of the lensed source, as is the case in this system; the only difference is a transit's loss of light becomes a corresponding addition for a lensing event with the pulse height governed by two ratios: the Einstein radius and the lensing star's radius to the radius of the lensed source (Heyrovský & Loeb, 1997; Agol, 2003). In this case the ingress and egress deviations ($\lesssim 1 \times 10^{-5}$, Figure 5.5) are undetectable at the level of precision of the *Kepler* data due to the 29.3 minute *Kepler* cadence. Consequently, we utilized this inverted transit approximation due to its much faster computation using analytic expression in terms of elliptic integrals (Mandel & Agol, 2002).

To an excellent approximation then, the pulse model is described by

$$F(t) = F_1(t)\left(1 + \frac{2R_E^2 - R_2^2}{R_1^2} \cdot \frac{I_1(t)}{\langle I_1 \rangle}\right) + F_2 \tag{5.1}$$

where $F(t)$ is the flux from the binary system, F_1 is the uneclipsed G dwarf flux, F_2 is the flux from the white dwarf (assumed to be constant), R_E is the Einstein radius of the white dwarf, $I_1(t)$ is the intensity of the G dwarf at the location behind the center of the white dwarf, and $\langle I_1 \rangle$ is the disk-averaged intensity of the G dwarf (this formula applies between ingress and egress).

The specific intensity of the G dwarf in the *Kepler* bandpass we modeled with a quadratic limb-darkening law; initial fits confirmed that the signal to noise of the pulses was not sufficient to fit for these coefficients independently, so we instead adopted them from a

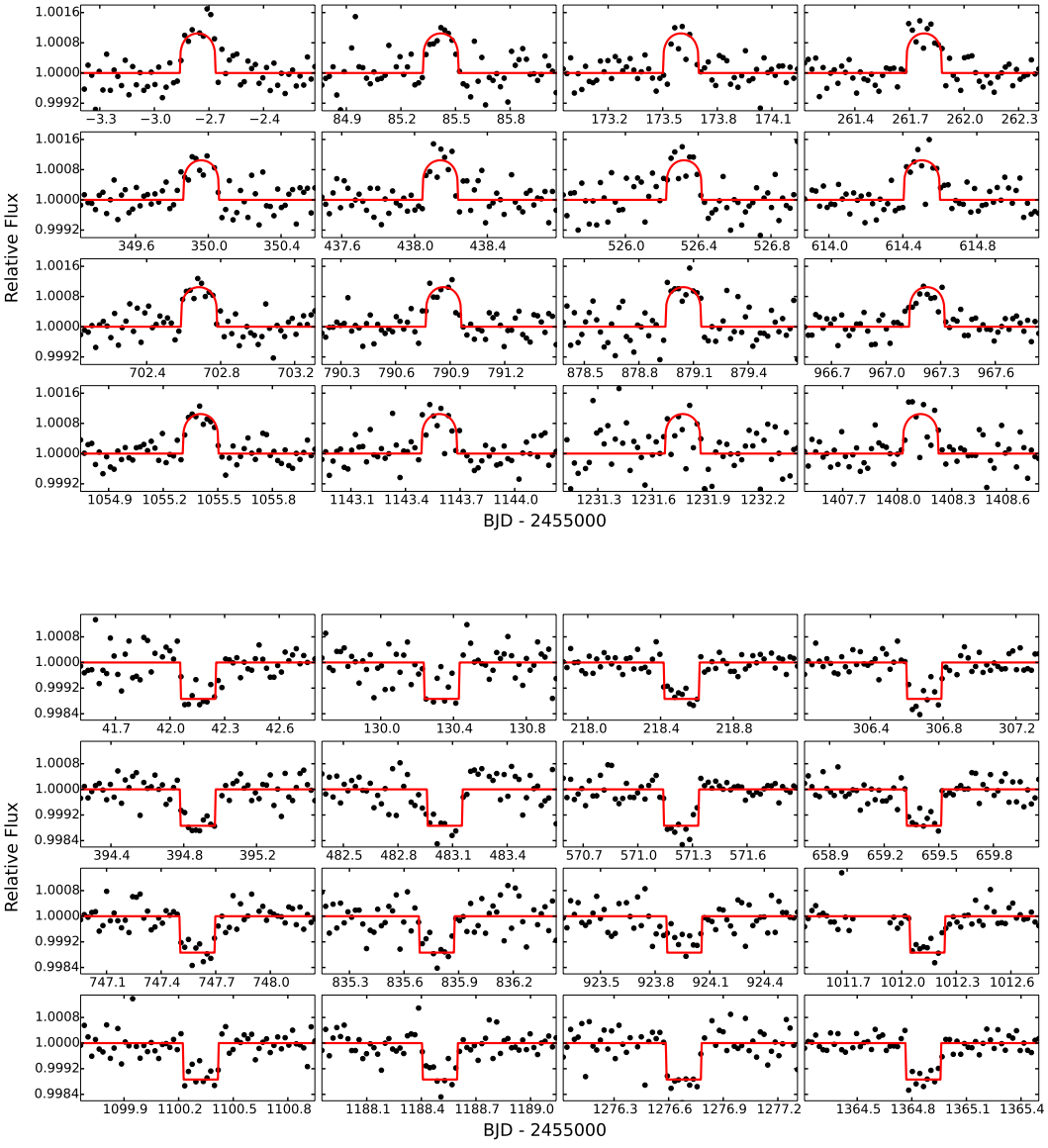

Figure 5.4: Detrended light curves encompassing the individual microlensing pulses (top) and occultations (bottom). The red lines show our best-fit model.

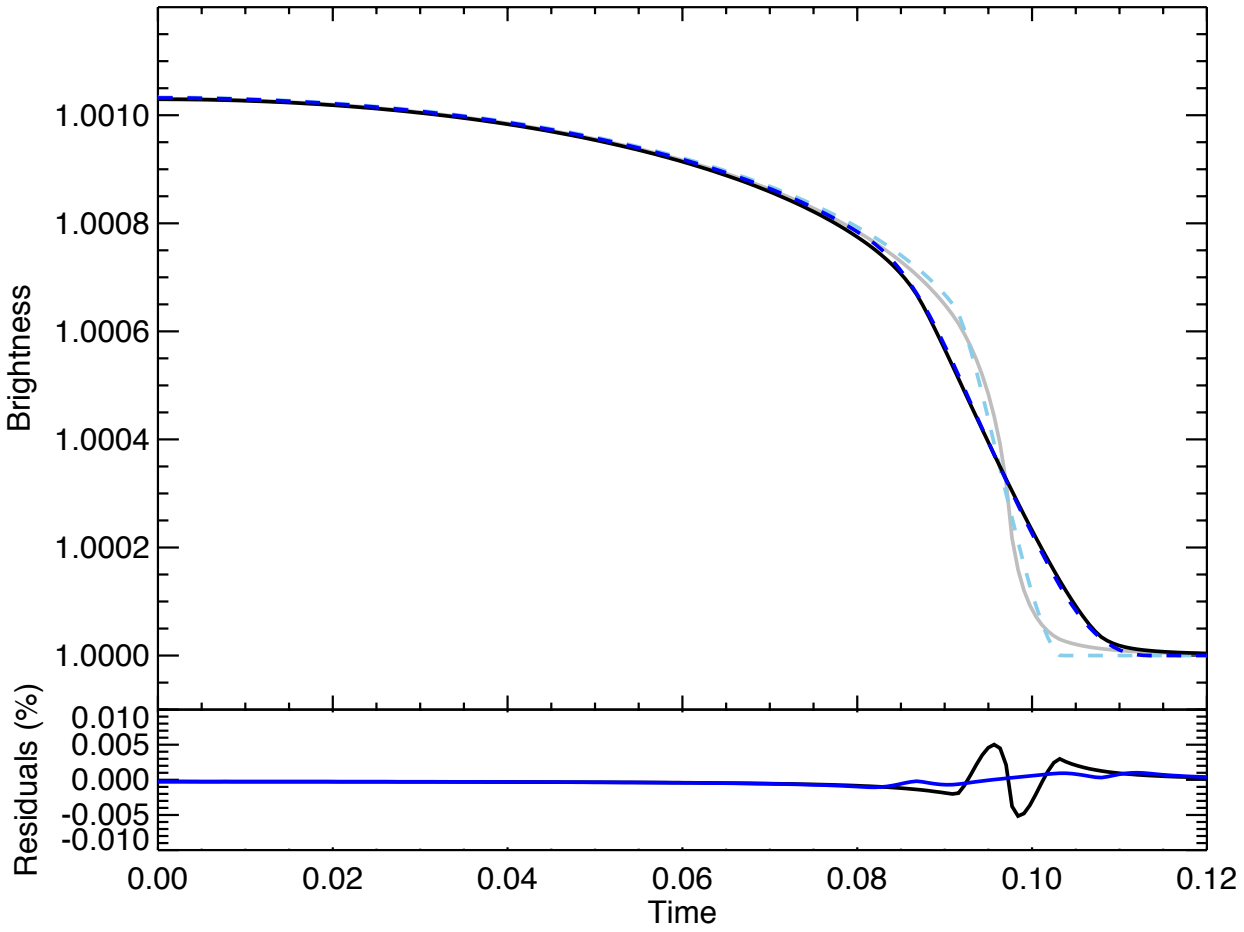

Figure 5.5: Comparison of the exact calculation of the microlensing pulse (Agol, 2002) with the inverted transit approximation (Agol, 2003) for the best-fit parameters of KOI-3278 (the pulse is symmetric, so we only plot the second half). Top panel: exact calculation (light grey, solid); inverted transit approximation (light blue, dashed); exact calculation convolved with *Kepler* long cadence (black, solid); inverted transit approximation convolved with *Kepler* long cadence (dark blue, dashed). Bottom panel: difference between the exact microlensing calculation and inverted transit approximation, without (black) and with (blue) convolution with the *Kepler* long cadence.

tabulation for the *Kepler* bandpass as a function of the effective temperature, metallicity, and surface gravity of the stellar atmosphere (Sing, 2010). We fitted the tabulated limb-darkening coefficients as a function of the atmospheric parameters, obtaining:

$$\begin{aligned} u_1 &= 0.4466 - 0.196\left(\frac{T_{eff,1}}{10^3} - 5.5\right) + 0.00692\log_{10}\left(\frac{g_1}{10^{4.5}}\right) + 0.0865[Fe/H]_1 \\ u_2 &= 0.2278 - 0.128\left(\frac{T_{eff,1}}{10^3} - 5.5\right) - 0.00458\log_{10}\left(\frac{g_1}{10^{4.5}}\right) - 0.0506[Fe/H]_1, \quad (5.2) \end{aligned}$$

where u_1, u_2 are the linear and quadratic limb-darkening coefficients, $T_{eff,1}$ is the effective temperature of the G dwarf in Kelvin, g_1 is the surface gravity of the G dwarf in cm sec^{-2}, and $[Fe/H]_1$ is the abundance ratio of iron to hydrogen, relative to the Sun, in units of dex (log base 10). This fit is valid in the range $5000 < T_{eff,1} < 6000$ K, $4 < \log_{10}(g_1) < 5$, and $-0.5 < [Fe/H]_1 < 0.5$, and is accurate to 0.005. These coefficients were used in conjunction with equation 5.1 to compute the light curve of the microlensing pulses, while the occultations were computed assuming a uniform flux for the white dwarf (Mandel & Agol, 2002).

Since the G dwarf is spotted and undergoes quasiperiodic fluctuations as the spots rotate in and out of view, we modeled the $F_1(t)$ near each pulse and occultation as a quadratic function of time and subsequently marginalized over these polynomial coefficients. To speed up the modeling, we carried out a linearized fit for the polynomial coefficients of $F_1(t_i) = \sum_{j=0}^{n} a_j(t_i - t_j)^j$ around each event, with $n = 2$. We first computed the light curve model $F(t)$ assuming $F_1(t) = 1$ and F_2/F_1 is a constant; we then divided this model into the light curve and solved the linear least-squares problem for the a_j that minimized χ^2, thus marginalizing over a_j. This procedure ignored the slight variation in the ratio $F_2/F_1(t)$, but since $F_2/F_1 \approx 10^{-3}$ and the variation in F_1 is a few percent at most, this error is of order 10^{-5}, which is substantially smaller than the observational uncertainties. In computing the model, we sub-sampled each data point by a factor of ten to properly resolve the ingress and egress of the microlensing pulses and occultations.

We neglected photometric Doppler shift (Loeb & Gaudi, 2003), ellipsoidal variability due

to tidal distortions, and reflected light from the companion star, which are only significant for binaries with short periods (Zucker et al., 2007), and are swamped by the stronger stellar variability in this system. Ellipsoidal brightening can be caused by transient tidal distortion near periastron passage for highly-eccentric binaries known informally as "heartbeat stars" (Welsh et al., 2011; Thompson et al., 2012); however, these brightenings are typically asymmetric and/or show nearby dips, i.e. they do not show the inverted-U shape of the pulse seen in KOI-3278. In addition, they typically occur near eclipse/occultation (if eclipsing) since the probability of eclipse is highest near periastron, while in KOI-3278 the brightening occurs opposite in phase to the occultation.

5.2.4 Orbital Model

We modeled the orbit of the stars as a Kepler ellipse. We used the sky plane as the reference plane, and we refer the orbital elements to the G dwarf, thereby defining the longitude of periastron ω as the angle from the point the G dwarf crosses the sky plane going away from the observer to the G dwarf's periastron. The separation between the stars, projected onto the sky, is given by:

$$r_{sky} = \frac{a(1-e^2)}{1+e\cos f}\sqrt{1-\sin^2 i \sin^2(\omega+f)}, \tag{5.3}$$

where a is the semi-major axis, e is the orbital eccentricity, i is the orbital inclination ($i = 90^\circ$ for edge-on orbit; $i = 0^\circ$ for a face-on orbit), and f is the true anomaly. Note that since we assume a Keplerian orbit with two bodies, the orbital elements of the two stars are the same, with the exception of the longitude of periastra which differ by 180 degrees.

The microlensing pulse occurs when the white dwarf passes in front of the G dwarf; at this point the G dwarf has a true anomaly which equals $f_0 = \pi/2 - \omega$. Instead of the time of periastron as a reference time, we use the midpoint of the first pulse, t_0, as the reference time of the orbit, which is related to the time of periastron, τ, by:

$$\tau = t_0 + \sqrt{1-e^2}\frac{P}{2\pi}\left[\frac{e\sin f_0}{(1+e\cos f_0)} - 2\sqrt{1-e^2}\arctan\left(\frac{\sqrt{1-e^2}\tan(f_0/2)}{(1+e)}\right)\right], \tag{5.4}$$

where P is the orbital period. To a good approximation, valid for small eccentricity, the time of occultation is given by $\delta t_{occ} \equiv t_{occ} - t_0 - \frac{P}{2} = \frac{2P}{\pi} e \cos\omega$.

5.3 Photometric Analysis

We carried out two independent analyses of the data: 1) separate fits to the microlensing pulse train and to the occultations; 2) joint fits to the pulse train and occultations using the orbital model above. Each fit made slightly different assumptions and used separate software; a comparison of these two analyses for consistency increased our confidence in each analysis and in our inference of the parameters of the system.

5.3.1 Separate Fits

The first set of fits used the Transit Analysis Package (TAP) (Gazak et al., 2012). The pulse and occultation light curves were each computed assuming a constant velocity and straight trajectory during each pulse/occultation event; this is a good approximation due to the large orbital radius and nearly edge-on configuration. The pulses/occultations were each fit with five physical parameters: initial time of pulse/occultation, t_0; period, P; impact parameter, b; transit duration, T; and the radius ratio, p. The impact parameter, b, is the sky-projected separation of the centers of the two stars at mid pulse/occultation, normalized to the radius of the G dwarf. The transit duration is defined to be: $T = 2R_1\sqrt{1-b^2}/v$, where v is the sky-velocity at mid-pulse/occultation. The radius ratio, p, is a parameter used in transit fitting, which is used to parameterize the limb-darkened microlensing pulse or occultation. In the case of the pulse, $p = -\sqrt{\frac{2R_E^2 - R_2^2}{R_1^2}}$, while in the case of the occultation, $p = \sqrt{F_2/(F_1+F_2)}$. Negative values of p are converted into a flux brightening rather than dimming, as is appropriate for the microlensing pulses.

In the TAP analysis, the limb-darkening of the G star was described by a quadratic limb-darkening law with parameters $u_1 = 0.4451$ (linear) and $u_2 = 0.2297$ (quadratic) which were taken from a stellar atmosphere model with $T_{eff} = 5500$ K, $log(g) = 4.5$, and $[Fe/H] = 0.0$ (Sing, 2010). The white dwarf was assumed to have no limb-darkening; this is a sufficient

Table 5.2: Light curve parameters

Pulses:	
Period (d)	88.18025 ± 0.00049
Duration (d)	0.1955 ± 0.0043
Pulse height D	0.00102 ± 0.00005
$t_0 + 7 \times P$ (JD-2,454,900)	702.68181 ± 0.00196
Occultations:	
Period (d)	88.18091 ± 0.00028
Duration (d)	0.1914 ± 0.0027
Occultation depth	0.00112 ± 0.00004
$t_0 + 7.5 \times P$ (JD - 2,454,900)	703.50886 ± 0.00124

approximation since only the ingress/egress of the occultation is sensitive to the white dwarf limb-darkening, while this portion of the light curve has very low signal-to-noise due to the long *Kepler* cadence. In addition to the quadratic variation of the G dwarf, a correlated-noise model assuming $1/f$ noise in addition to a white-noise component was solved for along with the model parameters (Carter & Winn, 2009). The red and white noise amplitudes were allowed to vary separately for each pulse and occultation.

Table 5.2 shows the results of the TAP fits; we fit the posterior of these parameters with a Gaussian, and report the mean and standard deviation of the Gaussian fits (each set of parameters was weakly correlated).

The ephemerides of the microlensing pulse train and the series of occultations were fit separately; we found that their periods were nearly identical, $P_{pulse} = 88.18025 \pm 0.00049$ d and $P_{occ} = 88.18091 \pm 0.00028$ d, for a difference of $P_{pulse} - P_{occ} = -0.9 \pm 0.8$ min. This indicates that both the microlensing pulse train and occultations can be described by a single, Keplerian orbital model, which justifies the joint fit in the next section. The occultation occurs $\Delta t_{occ} = t_{0,occ} - t_{0,pulse} - P/2 = 0.827 \pm 0.002$ days later than half of an orbital period after the pulse. This translates into $e \cos \omega = 0.01473 \pm 0.00004$.

We also found that the impact parameters of the pulse train and occultations were poorly constrained; only near-grazing configurations could be excluded. This is due, once again,

to the long-cadence data which place no constraint on the ingress/egress duration, approximately $6-9$ min, which is shorter than the 29.3-minute *Kepler* cadence. For the occultation, the TAP model was incorrect at ingress/egress in that it fixed the depth to equal the square root of the radius ratio; consequently we do not trust the impact parameter constraint on the occultation. For the pulse, the impact parameter likelihood showed a decline above an impact parameter of $b = 0.65$, which we fit with a linear decline down to $b = 1.06$.

We found that the durations of the pulses and the occultations were identical to within the errors, $T_{pulse} = 0.196 \pm 0.004$ d and $T_{occ} = 0.191 \pm 0.003$ d, for a difference of $T_{pulse} - T_{occ} = 6 \pm 7$ min and a ratio of $T_{pulse}/T_{occ} = 1.02 \pm 0.03$. A ratio near unity also indicates that both events can be described by a single Keplerian orbital model with (likely) small $x = e \sin \omega$. In theory the ratio of the durations can be used to constrain $e \sin \omega$; to lowest order in $x = e \sin \omega$: $\frac{T_{pulse}}{T_{occ}} = 1 + ax$, with $a = 2\frac{2b_0^2(1-y^2)-1}{1-b_0^2(1-y^2)^2}$, $y = e \cos \omega$ and $b_0 = a \cos i / R_1$ (the impact parameter if $e = 0$). In the limit $b_0 = 0$, $a = -2$, which yields $e \sin \omega = -0.0035 \pm -0.016$. However, at larger impact parameter the sign of a switches, and a goes to zero for $b_0 = 1/\sqrt{2}$; near this value the x^2 term which we have dropped in T_{pulse}/T_{occ} becomes important in constraining the value of $e \sin \omega$. The best-fit impact parameter from the joint model gives $b_0 = 0.706 \pm 0.022$; this translates to $a = -0.1 \pm 0.5$, which spans zero, so $e \sin \omega$ has a larger uncertainty than this linear expansion estimate; it is properly constrained by the full Markov chain solution.

To translate the separate constraints on the shape of the light curve into constraints on the system parameters, we next carried out an MCMC analysis using analytic formulas to describe the light curve parameters in terms of the masses, radii, and orbital parameters of the G dwarf and white dwarf (Winn, 2010). We found a strong correlation between T, p and b for the microlensing pulse fit, so we reparameterized p as $D(b) = p^2 \frac{1-u_1\mu-u_2\mu^2}{1-u_1/3-u_2/6}$ where $\mu = 1 - \sqrt{1-b^2}$. This parameter approximates the maximum height of the microlensing pulse, at its center, and is nearly uncorrelated with b and T. Although the TAP light curve fits held u_1 and u_2 fixed, we allowed these to vary during this second step of the analysis computing $D(b)$. We also transformed the zero-points of the ephemerides to points near the middle of the series of pulses/occultations so that they were uncorrelated with the

orbital periods. The results of these fits were used for rapid experimentation with various assumptions in our analysis and comparison with the joint fits described next; however, the joint fits have the advantage of self-consistently fitting all of the data simultaneously, so we use the joint fits for our final parameter constraints.

5.3.2 Joint Fits

The second model jointly simulated the pulses and occultations and compared to the observed *Kepler* fluxes near the events. Using the masses of the two bodies and their orbital elements as inputs ($M_1, M_2, P, t_0, i, e, \omega$), we calculated the two stars' projected sky separation (Equation 5.3) at all times of interest (i.e. *Kepler* cadences surrounding the pulses and occultations, subsampled by a factor of 10). We combined this sky separation with the radii of the two stars, their flux ratio, and the G dwarf's limb darkening coefficients ($R_1, R_2, \frac{F_2}{F_1}, u_1, u_2$) to predict the observed flux at each cadence using the method of §5.2.3; we then calculated the χ^2 of the model with these 12 parameters.

To further constrain the system parameters and break degeneracies between them, we utilized stellar evolution models and added photometric constraints from other surveys to our χ^2 calculation, which required adding additional input parameters (§5.3.2). The *Kepler* light curve does not have high enough signal to noise to constrain certain inputs (e.g. u_1, u_2, R_2), so we reparameterized them as a function of more accessible inputs (§5.3.2). We then used an MCMC analysis on our final set of 14 system parameters to determine the stellar and orbital properties and their posterior distributions.

Photometric Constraints on Stellar Parameters

Because we do not have spectroscopic data for this system, we relied on multiwavelength photometry and stellar evolution models for computing the stellar properties. A determination of the stellar characteristics based on multicolor photometry using the Dartmouth stellar evolution models (Dotter et al., 2008) has already been carried out by the *Kepler* team (Pinsonneault et al., 2012; Huber et al., 2014). However, these analyses have several

drawbacks: they assumed priors on the temperature, metallicity, and mass based upon the properties of stars in the Solar neighborhood; they assumed a simplistic model for the extinction/reddening correction; and the covariances between the resulting parameters were not reported. Instead, we carried out our own fits, using a simultaneous χ^2 minimization of the *Kepler* photometric light curve and multi-band photometry (Figure 5.6) from SDSS g, r, i, z (Abazajian et al., 2009), 2MASS J, H, K_s (Cutri et al., 2003), and WISE $W1, W2$ (Cutri & et al., 2012) in order to provide joint constraints on the properties of both stars and their orbital properties.

This method has the advantage of self-consistently accounting for all of the stellar properties simultaneously, as well as taking into account the covariances between stellar evolution model parameters. For example, the pulse/occultation duration is a function of the density of the G dwarf and the ratio of the total binary mass to the G dwarf mass; the G dwarf density strongly correlates with the effective temperature of the star in this temperature range. Also, the height of the microlensing pulse primarily constrains the mass of the white dwarf star, given the parameters for the G dwarf and orbit (Figure 5.7). By fitting the multi-color photometry and light curve simultaneously we obtained a self-consistent fit to all of these constraints on the G dwarf, white dwarf, and orbital elements.

The photometric fit in multiple bands required correction for reddening. The total extinction, $A_{\lambda,max}$, we estimated from reddening maps of the galaxy (Schlafly & Finkbeiner, 2011). We assumed $E(B-V)_{max}$ has a fractional uncertainty of 3.5% based on the scatter of nearby pixel elements in the extinction map, and fixed $R_V = 3.1$. We then corrected for the finite extent of the dust layer by adding a free scale height parameter with a prior of $h_{dust} = 119 \pm 15$ pc (Jones et al., 2011). The correction for the extinction column becomes: $A_\lambda = A_{\lambda,max}(1 - \exp[-D \sin 10.29^\circ / h_{dust}])$, where D is the distance to the binary in parsecs — another free parameter added to the model. Finally, we added a systematic uncertainty in the absolute calibration of the photometry, σ_{sys}, which we added in quadrature to the reported photometric errors of the measured magnitudes. We let σ_{sys} vary as a free parameter, and placed a prior on its value of $\prod_i^N (\sigma_i^2 + \sigma_{sys}^2)^{-N/2}$ where N=9 is the

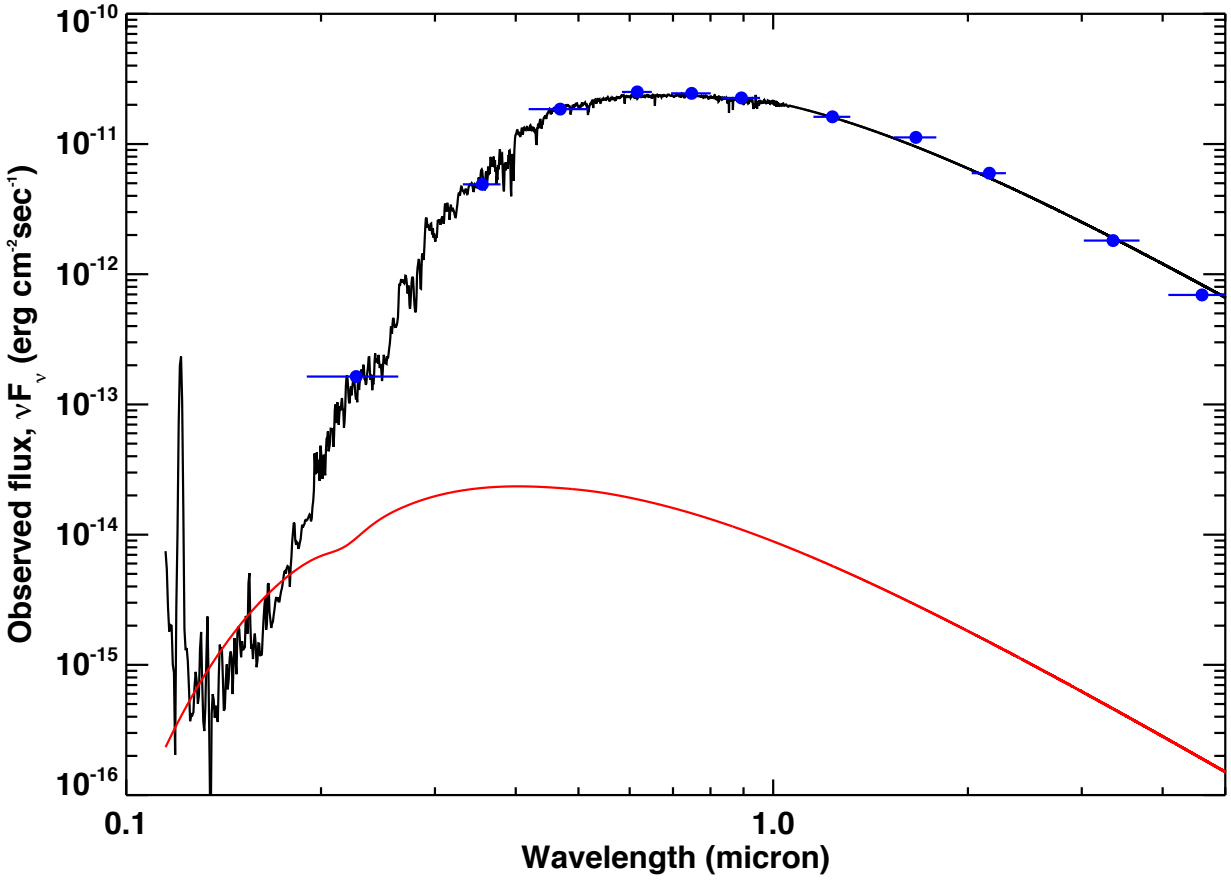

Figure 5.6: Spectral energy distribution of KOI-3278, computed from GALEX, SDSS, 2MASS, and WISE photometry (blue); the two shortest wavelength bands were not used in our fitting. Overplotted in black for illustration is a Pickles composite spectrum (Pickles, 1998) for a G5V star (T_{eff} = 5584 K), with extinction applied, as well as a blackbody at 9950 K with the best-fit size-ratio estimated for the white dwarf (red).

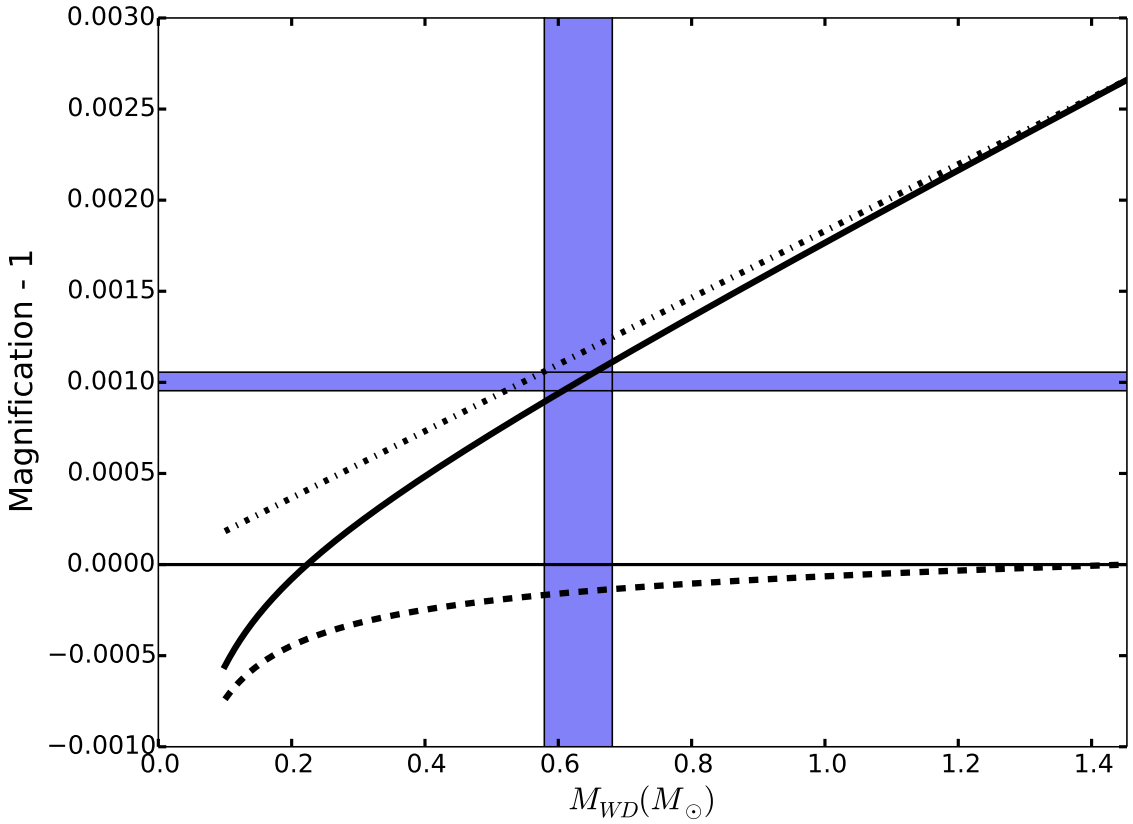

Figure 5.7: The "magnification" (minus one) versus mass of the white dwarf, neglecting limb-darkening of the G dwarf. The dashed-dotted curve shows the magnification versus white dwarf mass (i.e. assuming the white dwarf is transparent); the dashed curve shows the eclipse depth of the white dwarf (i.e. traditional eclipse ignoring lensing; remember more massive white dwarfs have smaller radii); and the black curve shows the predicted pulse height balancing the two effects. The blue regions show the 1σ uncertainties on the measured values.

number of photometric bands; this has the effect of giving a reduced χ^2 of order unity for the photometric fit. The median value of σ_{sys} was 2.5% in our fits.

Fitting the observed broadband magnitudes in addition to the *Kepler* light curve therefore required adding D, σ_{sys}, h_{dust}, and $E(B-V)_{max}$ as free parameters.

For modeling the SED of the G dwarf, we used the Padova PARSEC isochrones (Bressan et al., 2012), with scaled solar alpha abundances ($[\alpha/\mathrm{Fe}] = 0$). We used this publicly available grid of stellar models computed for ages from $0.004 < t_1 < 12.59$ Gyr (spaced by 0.05 dex), metallicities from $-1.8 < [Fe/H]_1 < 0.7$ (spaced by 0.1 dex), and masses from $0.1 < M_1 < 11.75 M_\odot$ (with spacings depending on age and metallicity, adaptively chosen by the isochrone model). By utilizing $M_1, [Fe/H]_1, t_1$ to parameterize our Markov chain fits, we place a uniform prior on these parameters. We carried out linear interpolations of these parameters in the grid of stellar models to compute the radius (R_1), effective temperature, $T_{eff,1}$, $\log(g_1)$, and absolute magnitudes of the G dwarf for comparison to the multi-band photometric data, and for computation of the light curve model (the age interpolation we carried out linearly in $\log_{10}(t_1)$, although we used t_1 as the Markov chain parameter in order to avoid favoring small ages).

We checked the robustness of our results by redoing the fits with Dartmouth isochrones (Dotter et al., 2008). Unfortunately the Dartmouth isochrones have coarse sampling (0.5 dex) in metallicity below Solar metallicity, so our interpolation fared poorly for sub-solar metallicity. Instead we reran our fits with only positive metallicity (using the separate fits described above), and we found that we obtained statistically identical results for both the Padova and Dartmouth isochrones with the constraint of super-solar metallicity. We conclude that our results are robust to the choice of isochrone; this is not surprising as the G dwarf star is near solar mass, where stellar evolution models are robustly constrained by comparison with our Sun. Note that the Dartmouth and Padova isochrones assume slightly different metallicities for the Sun ($Z = 0.019$ and $Z = 0.0147$, respectively), which we accounted for in our comparison.

Reparameterization

Some inputs to the light curve modeling are highly correlated (e.g. e, ω), while others are poorly constrained by the data due to the long *Kepler* cadence or low signal to noise (e.g. u_1, u_2). We therefore reparameterized our model inputs into more insightful and independent parameters.

As discussed in §5.2.3, the limb darkening coefficients of the G dwarf cannot be constrained by the data; u_1, u_2 are thus transformed into dependent functions of the G dwarf, which are in turn determined by the isochrones and input parameters $M_1, [Fe/H]_1, t_1$. The isochrones similarly determine R_1, and it is no longer treated as a free parameter.

We reparameterized the inclination angle in terms of the impact parameter of the white dwarf during the microlensing pulse if the orbit were circular, $b_0 \equiv (a/R_1)\cos i$.

We transformed the eccentricity and longitude of periastron to $e\sin\omega$ and $e\cos\omega$ since these are better characterized than e or ω alone; this change required placing a prior of $1/e$ (Eastman et al., 2013).

Since we could not constrain the white dwarf radius from these data, we assumed a mass-radius relation for the white dwarf given by

$$R_2(M_2) = 0.0108 R_\odot \sqrt{\left(\frac{M_2}{M_{ch}}\right)^{-2/3} - \left(\frac{M_2}{M_{ch}}\right)^{2/3}}, \tag{5.5}$$

where $M_{ch} = 1.454 M_\odot$ is the Chandrasekhar mass.

In our final fits, we constrained the age of the system to be the sum of the main-sequence lifetime of the white dwarf progenitor and white dwarf cooling time, which amounts to exchanging F_2/F_1 for the mass of the white dwarf progenitor, $M_{2,init}$ (see §5.4.2). Ultimately, the final set of parameters we fit for were:

$$\{P, t_0, e\sin\omega, e\cos\omega, b_0, M_2, M_{2,init}, M_1, t_1, [Fe/H]_1, \sigma_{sys}, D, h_{dust}, E(B-V)_{max}\} \tag{5.6}$$

for a total of 14 free parameters.

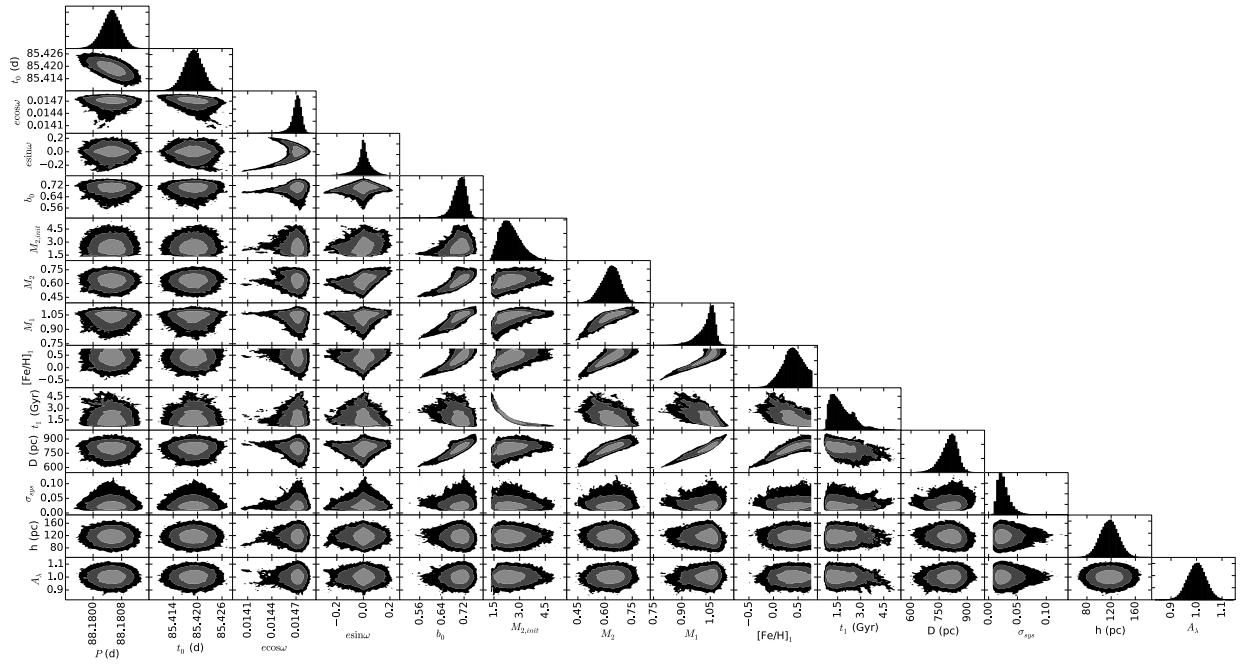

Figure 5.8: Contour plots showing the 1σ, 2σ, and 3σ constraints on pairs of parameters.

5.3.3 Results

Our initial joint fits gave a reduced chi-square slightly larger than unity, so we increased the *Kepler* photometric error bars by a factor of 1.13 in the joint fits to produce a reduced chi-square of unity in our fit to the *Kepler* time series photometry.

We ran a Markov Chain Monte Carlo simulation to constrain the fourteen model parameters using an ensemble sampler with affine-invariance (Goodman & Weare, 2010; Foreman-Mackey et al., 2013). We used a population of 50 chains and ran for a total of 100,000 generations, with maximum Gelman-Rubin statistic of 1.06.

Table 5.1 lists the resulting parameters derived from our simulations. Some parameters have extremely strong correlations; in particular, the measurement of the mass of the white dwarf is limited by our uncertainty in the model of the G dwarf star. Figure 5.8 shows the correlations between various model parameters.

5.4 Age Constraints

During our initial fits, we found a correlation between the age of the G dwarf and the mass of the white dwarf. This can be understood as follows: the multiband photometry constrains the effective temperature of the G dwarf. As stars evolve, they expand in size, but a larger radius for the G dwarf requires a larger mass of the white dwarf to reach the same microlensing pulse magnification (which scales as M_2/R_1^2). In addition, the larger radius of the G dwarf causes a longer transit duration; to fit the observed duration requires a higher impact parameter where the star is dimmer, which also works to increase the white dwarf mass needed to reach the same pulse height.

This leads to a problem with the age of the binary. To produce the observed flux ratio between the stars (derived from the occultation depth) requires a recently formed white dwarf. Yet older G dwarfs with larger radii require higher white dwarf masses to match the pulse heights; more massive white dwarfs are created by higher mass stars which have shorter main-sequence lifetimes. Hence older G dwarfs require both a short main-sequence lifetime for the white dwarf progenitor as well as a young white dwarf, producing a binary with contradictory stellar total ages.

We thus eliminated the high-mass WD and old G dwarf solutions by requiring our binary system to be coeval. We constrained the minimum age with the spin period of the G dwarf (§5.4.1), and constrained the maximum age with an initial-final mass relation for the white dwarf, which determines the nuclear-burning lifetime of the white dwarf progenitor (§5.4.2).

5.4.1 G Dwarf Rotation Period and Spin-Down Age

The light curve of KOI-3278 looks like a typical spotted star with star spots repeating every ≈12 days; a power spectrum that peaks strongly at 12.5 days (Figure 5.9). Using only Q3 data, the period of rotation was measured by Reinhold et al. (2013), in which they report a best-fit period of 12.36±0.05 days, consistent with our results from all 17 quarters.

The rotation period can be used to estimate the age of the G dwarf. We estimated the age

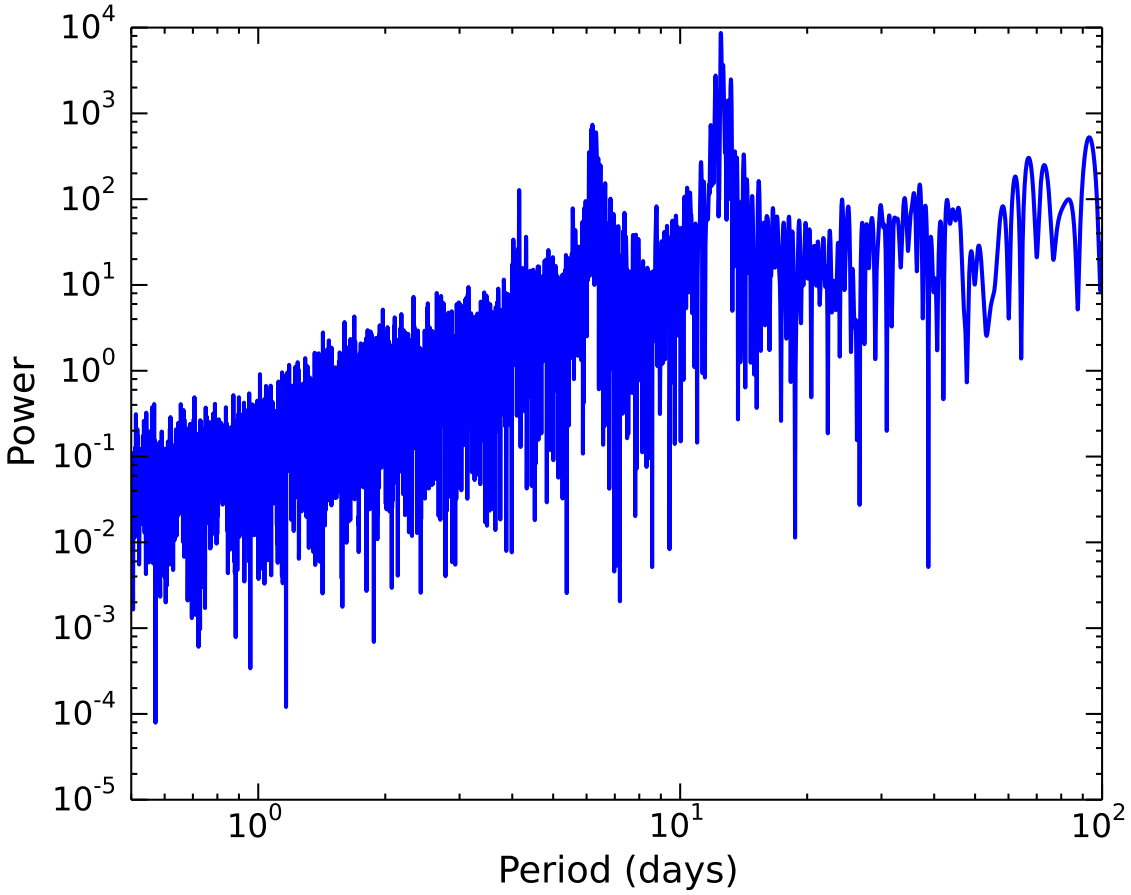

Figure 5.9: Frequency-power spectrum of KOI-3278, showing a strong peak at 12.5 days which we infer to be the rotational period of the G dwarf.

of the star based on the observed spin-down of stars as they age; so-called "gyrochronology." We used the calibrations of this relation by Mamajek & Hillenbrand (2008) to estimate the age of this star, which we found to be $t_{spin,1} = 0.89 \pm 0.15$ Gyr. We used this constraint only as the minimum age of the system, however, to allow for the possibility that the G dwarf was spun up via mass transfer during the white dwarf's formation.

5.4.2 Breaking the M_2–Age Degeneracy

To eliminate the models with contradictory ages, we placed a constraint on the age of the G dwarf by adding together the cooling age of the white dwarf and the nuclear-burning lifetime of its progenitor. However, the progenitor mass has some uncertainty due to uncertainties in the initial-final mass relation of white dwarfs, which is compounded by the fact that the common envelope evolution of this system would have modified the core mass of the white dwarf progenitor. After surveying the literature on the initial-final mass relation of white dwarfs (Weidemann, 2000; Kalirai et al., 2008; De Marco et al., 2011; Catalán et al., 2008; Zhao et al., 2012), and running a suite of binary stellar evolution models (described below), we found that most data and models lay within 10% of the final mass given by the initial-final mass relation found by Kalirai et al. (2008). Consequently, we allowed both the initial mass of the white dwarf, $M_{2,init}$, and the final mass, M_2, to vary, and placed a Gaussian prior on M_2 to lie within 10% of the Kalirai relation, which amounts to adding to the χ^2: $(M_2 - 0.109 M_{2,init} - 0.394)^2/(0.1 M_2)^2$.

We computed the nuclear-burning lifetime of the white dwarf progenitor, t_2, from the Padova models, and then set the cooling time of the white dwarf equal to $t_{cool} = t_1 - t_2$. The cooling time and mass of the white dwarf was then used to compute its *Kepler* magnitude (as described below), which was then used to fit the depth of the occultation. This procedure has the effect of requiring both stars to have the same age, but allowing for some uncertainty in the initial mass of the white dwarf progenitor. In doing so, we exchanged F_2/F_1 for $M_{2,init}$ as a free parameter in the model. This procedure eliminated the unphysical cases of large white dwarf masses in old systems.

WD Cooling

We can derive the absolute magnitude of the white dwarf star in the *Kepler* band from the flux lost as the white dwarf completely disappears behind the G dwarf during occultation; we can then use this to constrain the age and luminosity of the white dwarf based on white dwarf cooling models. We use the cooling models computed by Bergeron and collaborators (Holberg & Bergeron, 2006; Kowalski & Saumon, 2006; Tremblay et al., 2011; Bergeron et al., 2011), made available on their web site[2]. We performed a linear interpolation in the mass and log cooling age of the white dwarf to obtain the absolute magnitudes, luminosity, and effective temperature of the white dwarf. The absolute magnitude of the white dwarf in the *Kepler* band was computed by transforming the absolute magnitudes in the SDSS g, r and i bands: $Kp = 0.25g + 0.75r$ for $(g - r) \leq 0.3$ and $Kp = 0.3g + 0.7i$ for $(g - r) > 0.3$ (Brown et al., 2011).

We found a white dwarf age of $t_{cool} = 663 \pm 60$ Myr; equivalent ages were found for both Helium and Hydrogen atmosphere models. The effective temperature of the white dwarf is $T_{eff,2} = 9960 \pm 730$ K and its luminosity is $L_{WD} = (1.2 \pm 0.23) \times 10^{-3} L_{\odot}$; hence the small depth of the occultation in the *Kepler* band.

5.5 Blends

It is possible that the flux from another star (or stars) can be blended with the flux of the binary star, thus affecting our fit to the photometry and light curve. To test this, we added to our separate-fit model two components: 1) a bound blend star with the same metallicity and age as the G dwarf; 2) a blend star along the line of sight to the binary, contained within the *Kepler* photometry aperture.

For the first component, we added the flux of a second star to the multi-color photometry, drawing from the Padova isochrones as for the G dwarf, and we also included its effect on the pulse height and occultation depth.

---

[2] `http://www.astro.umontreal.ca/~bergeron/CoolingModels/`

For the second component, the contamination within the *Kepler* aperture can be estimated by combining the location of other stars in other photometric surveys with the *Kepler* point spread function to compute the flux contamination with the target aperture. The *Kepler* pipeline carries out this analysis, and finds that the contamination is between 4-8%, depending on the quarter of data that is used. We added the contamination flux to both our models to account for the slight reduction in the pulse height/occultation depth due to contamination that varies with quarter.

We reran the Markov chain fit including the mass of the third bound star, M_3, as an additional free parameter. We found that a bound star must be an M dwarf, $M_3 = 0.4 \pm 0.2 M_\odot$, to be consistent with the data, and would contribute only $1.4^{+3.7}_{-1.0}$% to the *Kepler* band flux. However, the M dwarf would contribute more significantly to the 2MASS/WISE bands and thus skew the effective temperature of the G dwarf to be somewhat hotter, and thus somewhat more massive, $M_1 = 1.07^{+0.04}_{-0.05} M_\odot$. This would imply a slightly higher white dwarf mass, $M_2 = 0.68^{+0.05}_{-0.06} M_\odot$, about 1σ different from the fit without a third star. The slightly higher mass for the white dwarf would produce a slightly higher mass for its progenitor, as well as a slightly smaller cooling age, and thus a slightly smaller overall age for the system. Higher contrast imaging and/or high resolution spectroscopy may be able to place stronger constraints on the presence of a third bound star in the system; however, the current constraints are strong enough that the mass derived for the white dwarf is not strongly affected by the third star.

5.6 Binary Stellar Evolution Models and Dynamical Constraints on the Presence a Bound Third Star

We carried out an initial exploration of the possible origin of this system using the BSE code (Tout et al., 1997; Hurley et al., 2000, 2002) to model the evolution of this system as a function of time. At the current orbital period, the G dwarf should have orbited within the surface of the red giant progenitor of the white dwarf, ejecting the outer envelope of the star; this is referred to as the "common envelope phase" (Paczynski, 1976; Iben & Livio, 1993).

We used the calibration of the common envelope evolution parameters derived empirically (De Marco et al., 2011), and carried out simulations with a range of initial masses and separations. As an example of these simulations, we found that the final conditions of this system could be achieved if the initial masses were $M_{2,init} \approx 2.5 M_\odot$, $M_1 \approx 1 M_\odot$ and the initial period was $P_0 \approx 1295$ days, corresponding to an initial semi-major axis of $a_0 \approx 3.5$ AU (we used $\alpha_{CE} = 0.3$ and $\lambda = 0.2$ in this simulation). The mass transferred during the Roche-lobe overflow and common envelope phase would be $\Delta M_1 = 0.008 M_\odot$, sufficient to spin up the G dwarf. The common envelope phase would start on the second asymptotic giant branch of the white dwarf progenitor, at an age of ≈ 0.8 Gyr, and result in a final mass of the white dwarf of $M_2 \approx 0.65 M_\odot$, consistent with the model constraints, and slightly less massive than the final mass of $0.69 M_\odot$ had the star evolved as a single star. As the common envelope phase causes rapid merging of the two stars before ejection of the evolved star's envelope, the final period is very sensitive to the initial period; the outer period thus has to be fine-tuned, and hence this sort of binary is expected to be rare (de Kool & Ritter, 1993; de Kool & Green, 1995; Green et al., 2000; Schreiber & Gänsicke, 2003; Willems & Kolb, 2004; Zorotovic et al., 2010; Davis et al., 2010; Toonen & Nelemans, 2013).

The possibility of a third body in the system is potentially constrained by the dynamical interactions of the 3 bodies due to the eccentric Kozai mechanism (Ford et al., 2000; Katz et al., 2011; Naoz et al., 2013). The observed eccentricity of the binary is small, $e_1 \approx 0.032$, which indicates that it was probably circularized during the common envelope phase, and avoided dynamical growth of its eccentricity with a third body, post-circularization. Since the timescale for growth of the eccentricity depends upon the quadrupole timescale, we estimate that the third body should satisfy $(a_2/AU)^3/(M_3/M_\odot) > 1.7 \times 10^8$ so that the Newtonian quadrupole timescale is less than the white dwarf cooling timescale. Thus, if the third body has a mass of $M_3 \approx 0.4 M_\odot$, the semi-major axis should be larger than $a_2 > 748$ AU, with an orbital period longer than 14,000 yr. This is at about a separation of $1''$ (at quadrature), and thus the presence of a third body could be constrained with future high-contrast imaging and dynamical simulations.

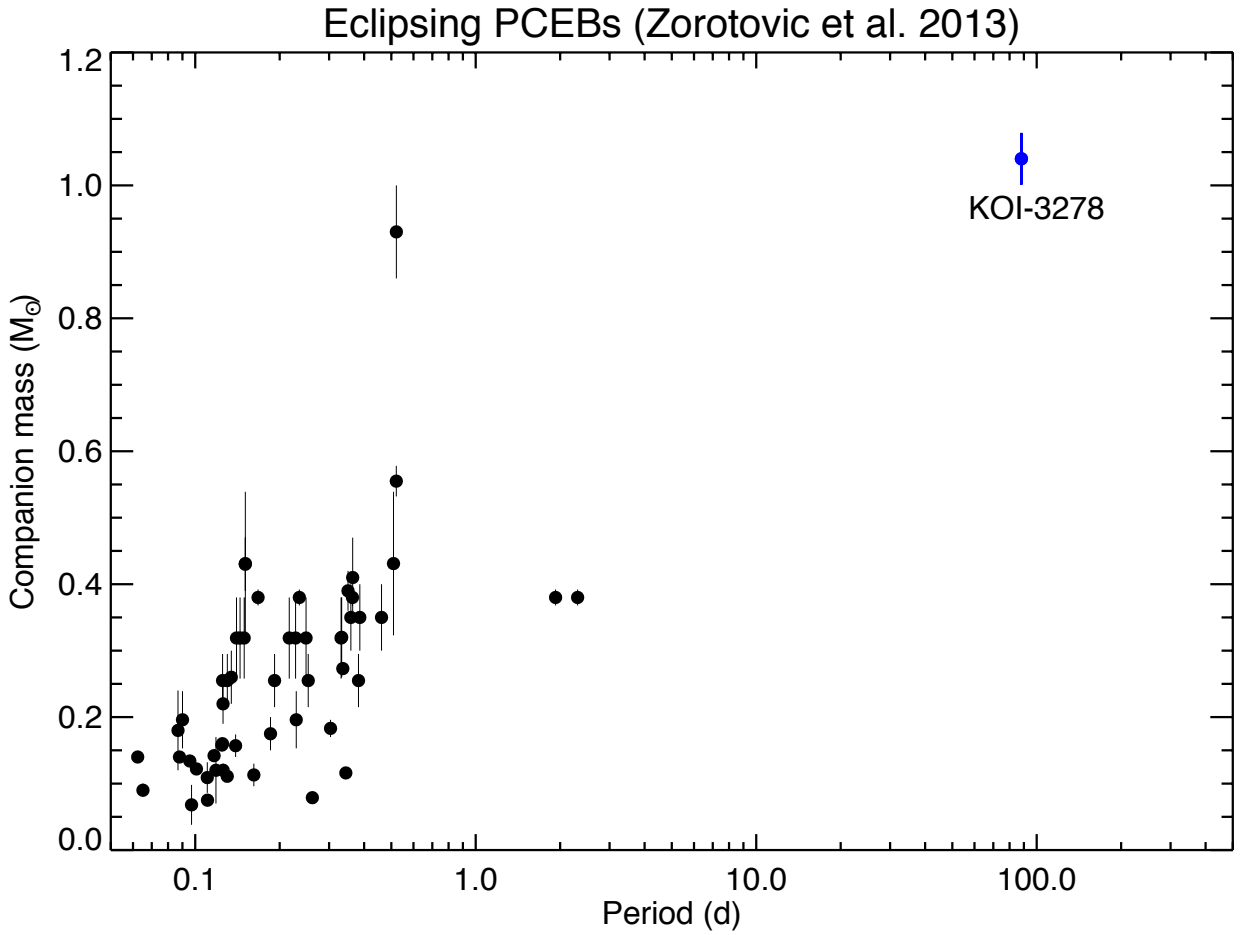

Figure 5.10: Mass-period distribution of known white dwarf–main sequence post common envelope eclipsing binaries.

The value of this system can be seen when comparing with prior white dwarf–main sequence eclipsing binaries found (Figure 5.10). KOI-3278 has the most massive companion star, as well as the longest period of all such systems. The longer period binaries are more difficult to find with ground-based surveys, and also have a lower probability of eclipse/occultation/microlensing. The cooler companion stars are easier to find due to their larger color difference to their companion white dwarf stars. KOI-3278 could only be found with continuous coverage and with high photometric sensitivity.

5.7 Predictions for Future Observations

Based on our Markov chain analysis, we found that the velocity semi-amplitude of the G dwarf should be $K_1 = 21.5 \pm 1$ km/s. The parallax of the system should be $\pi = 1.24^{+0.08}_{-0.05}$ milliarcseconds (mas) with a reflex motion of $\alpha = 0.22 \pm 0.08$ mas. The expected parallax measurement uncertainty for a $G = 15$ (*Gaia* magnitude) star is 0.02-0.03 mas (de Bruijne, 2012), so the parallax precision from *Gaia* should improve upon our analysis significantly, and enable another constraint on the mass of the white dwarf star.

We simulated the flux ratio of the white dwarf to the G dwarf as a function of wavelength, which we find reaches $\approx 5\%$ at 0.25 micron, increasing to 60% at 0.15 micron (although the absolute flux drops significantly towards shorter wavelength). We found that single occultation measurements in the ultraviolet could have similar signal-to-noise as the combined *Kepler* occultations, and allow a measurement of the temperature of the white dwarf, breaking the size-temperature degeneracy that required us to use a mass-radius relation for the white dwarf. For instance, we found that observations using the Hubble Space Telescope at 0.2-0.4 micron (with the G280 grating on the Wide Field Camera III) could achieve a S/N of ≈ 25 with observation of a single occultation (if it were photon-noise limited).

5.8 Acknowledgments

E.K. was funded by an NSF Graduate Student Research Fellowship. E.A. acknowledges funding by NSF Career grant AST 0645416; NASA Astrobiology Institutes Virtual Planetary Laboratory, supported by NASA under cooperative agreement NNH05ZDA001C; and NASA Origins of Solar Systems grant 12-OSS12-0011. Solar image courtesy of NASA/Solar Dynamics Observatory (SDO) and the Helioseismic and Magnetic Imager (HMI) science teams. The *Kepler* data presented in this thesis were obtained from the Mikulski Archive for Space Telescopes (MAST). The code used for analysis is provided in a repository at `http://www.github.com/ethankruse/koi3278`. The authors welcome requests for additional information regarding the material presented in this thesis.

We acknowledge the dedication and hard work of the *Kepler* team in obtaining and analyzing the data used in our analysis. This research has made use of the VizieR catalogue access tool, CDS, Strasbourg, France. This research has made use of NASA's Astrophysics Data System.

Chapter 6
CONCLUSIONS AND FUTURE WORK

The goal of this thesis was to introduce a new transiting planet detection pipeline: `QATS`. Chapter 2 introduced the methodology and described how I select and prepare light curves, search for planets, and select real astrophysical events from noise and false positives like stellar variability. I also described how we use a MCMC technique to measure the parameters of our planet and eclipsing binary candidates.

Chapter 3 applied `QATS` to the first nine campaigns of K2 mission data. I explained how I discriminate between eclipsing binary stars, false positives from other sources on the detector, and bona fide planet candidates. I also introduced our sources for stellar parameters. I then presented both my planet candidate and eclipsing binary lists, discussed some general properties of each, and highlighted some individually interesting systems.

Chapter 4 discussed the new population of planet candidates in more detail. I compared my results to searches done by other groups and demonstrated my improved sensitivity to weaker signals. I showed how K2's stellar sample differs from *Kepler*, producing more candidates around brighter and smaller stars. I also discussed evidence for a radius gap in the K2 sample, and introduced planets near their habitable zones.

Finally, Chapter 5 introduced a serendipitous discovery made possible by `QATS`'s flexibility. I presented the first self-lensing binary star system and discussed our modeling of the binary system using just the *Kepler* data and broadband photometric color constraints.

6.1 Summary of Main Results

Before looking to the future, I pause briefly to highlight some of the new methods and results introduced in this thesis.

6.1.1 Sensitivity of QATS

Most of the work in this thesis was enabled by the development and refinement of the QATS pipeline. Originally developed to find planets with TTVs (Carter et al., 2012; Carter & Agol, 2013), we have retained that sensitivity (e.g. our TTV planet candidate EPIC 211924657.1, Figure 3.6).

Yet the original version had trouble keeping up with other pipelines in detecting small, periodic planets. In this thesis, I improved QATS and am able to surpass other searches and detect planets with depths about a factor of two smaller in K2 (Figure 4.1).

My version of QATS is also the only systematic search that is able to simultaneously find periodic planets and single transit events (§4.1.4). This unique flexibility allows me to find long period planet candidates in K2 campaigns and will be even more beneficial for the shorter observing baselines of *TESS*, which I discuss more below (§6.3.3). Finding outer single transit events lends credence to the planetary nature of both the outer event and inner companions by nature of multi-planet systems being less likely to be false positives (Lissauer et al., 2014; Rowe et al., 2014). The single transit detection significantly lengthens the maximum period sensitivity of planet searches, strengthening the science return.

6.1.2 Planet Candidates

The main result of this thesis is the presentation of my planet candidate sample from K2 C0-8. I found 806 planet candidates, of which 368 are new and went undetected by all other groups searching the data, emphasizing the utility of EVEREST and QATS.

Before my search, all prior K2 searches had produced fewer than 80 total planets in multi-planet systems. From my search, 205 planet candidates are in multi-planet systems, of which 95 of those planets had been previously undetected (often finding second planets around what had previously been single systems). In total, I found 7 systems with 4 or more planets, including a 6-planet system.

Overall, our sample has nearly the same multiplicity distribution as *Kepler*, with a slight

preference for more single planet systems, likely due to K2's shorter baseline and decreased photometric performance preventing detection of some smaller companions (Figure 3.4). As with *Kepler*, the most common period ratio in our multi-planet systems is just outside the 3:2 resonance (Figure 3.5).

In addition to single transit events, `QATS` is sensitive to the ultra-short-period candidates. I introduced 21 new USP candidates, which would more than double K2's sample. More conservatively, looking only at those with derived radii indicating a rocky planet, I found 7 new USP candidates, increasing K2's sample size by 35%.

The power of *Gaia*'s precise stellar parameters allowed for a tentative K2 confirmation of the radius gap found in the short-period *Kepler* planets (Fulton et al., 2017). While Fulton et al. (2017) went through months of followup and stellar characterization, *Gaia* and K2 combined can produce a similar radius gap with no additional resources (Figure 4.7). This is only possible with a large enough planet sample, as done with the work in this thesis.

One of the main benefits of K2 is its different stellar sample from *Kepler*. The stars tend to be both brighter and smaller, creating a similar set of planet candidates. My C0-8 candidates produce about half as many planets as *Kepler* around stars brighter than 14th magnitude (Figure 4.4). After searching all K2 campaigns, I'll find as many or more bright candidates for potential followup as *Kepler*. I also was able to find new planet candidates in the open cluster Ruprecht 147. As K2 and *TESS* survey the entire sky, planet candidates around stars with known ages will be critical to testing how planet formation, migration, and evolution change with age.

In terms of host star size, K2 has already outdone *Kepler* around smaller stars. My planet candidate count already outnumbers *Kepler* around M dwarfs ($R < 0.5\ R_\odot$); only considering the new candidates only found by me, I have more planets than *Kepler* around late M dwarfs ($R < 0.3\ R_\odot$, Figure 4.5).

Finally, those planet candidates around the coolest M dwarfs may be temperate enough to lie in their star's 'habitable zone'. We found one new planet (EPIC 210508766.3) in a previously confirmed two-planet system in the habitable zone. With better parameters for

the M dwarfs, we may have more planets that will be deemed to lie in the habitable zone.

6.1.3 Eclipsing Binaries

While not the focus of this thesis, a byproduct of searching for planets is discovering a lot of eclipsing binaries. In this work I found 573 likely EBs, about 20% as many as found by *Kepler*. As with the planet candidates, many of these EBs are likely to be brighter and smaller than the *Kepler* sample by nature of the host star selection. I noted several EBs of interest as a starting point for future followup, including a case with obvious ETVs indicating a third body in the system (Figure 3.8).

Chapter 5 focuses on one EB in particular found in an early search of the *Kepler* planet candidates. Rather than an additional planet candidate, I found the first self-lensing binary star system, and the widest period EB containing a white dwarf at the time. This system, and others like it, can help constrain binary star evolution as one star evolves off the main sequence.

6.2 Future Science Enabled by Our Results

The work presented in this thesis will be a jumping off point for many other projects, enabling new science in a variety of fields. In this section I lay out some of the many possible ways the results presented here can be expanded upon and studied in more detail.

6.2.1 Long Baseline K2 Observations

Figure 6.1 shows the footprints of the K2 campaigns along the ecliptic. C2 and C15 have a one module (5% of the FOV) overlap, C6 and C17 overlap by about half the FOV, while C5, C16, and C18 overlap nearly entirely. These sets of campaigns are separated by about 3 years, allowing for observations of planets at nearly the same baseline as the original *Kepler* mission, except without the continuous coverage in between.

This overlap was advertised in advance, and we (along with many other groups) submitted

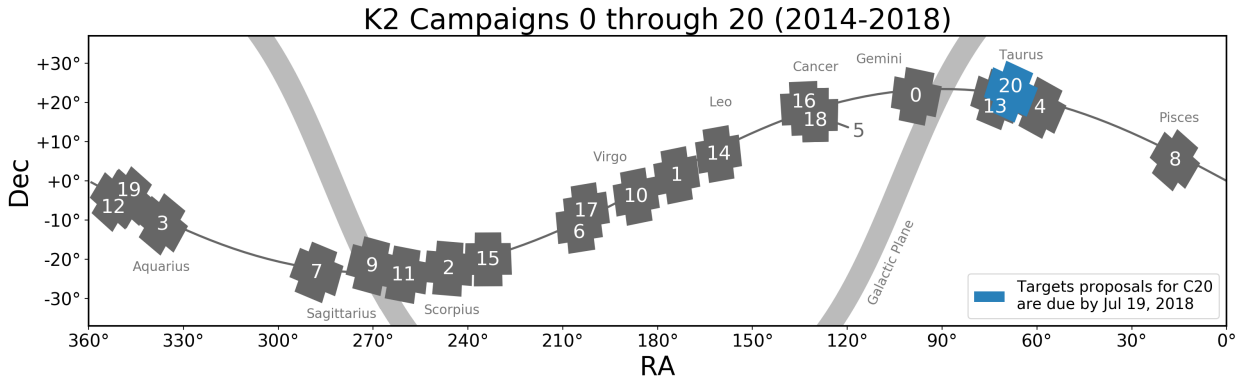

Figure 6.1: The footprint of all K2 campaigns along the ecliptic (solid line). C18 is currently being observed, C19 and C20 will be executed if the spacecraft still has fuel. Notably, there are overlapping campaigns, allowing stars to be observed multiple times over long baselines (C2/15, C6/17, C5/16/18).

all our known planet candidates and EBs in the overlap regions for reobservation. We had all 192 of our targets accepted, and they have all been observed again in C15-18.

This subset includes some high multiplicity systems like one of our five-planet systems (EPIC 211413752), as well as the one showing extreme TTVs. The 3 year baseline will allow for these TTVs to be tracked over long periods, or a lack of TTVs among the multis to be much better constrained, which in turn will yield higher precision constraints on the properties of the system (especially the planets' masses). Doubling the amount of data may allow us to find additional smaller planets in these systems and determine or better constrain orbital periods for those which only showed a single transit. A recent set of transits will also help keep errors in future transit times to a minimum, allowing for these systems to be followed up in the future without requiring wide windows to ensure catching the transits.

6.2.2 Planet Characterization

In this thesis, we did our best to characterize the stars and hence the planets with publicly available catalogs of parameters based largely on multiband photometry (Huber et al., 2016) and parallaxes (Gaia Collaboration et al., 2018; Andrae et al., 2018). Still, an individual stel-

lar spectrum remains a better way to measure a star's effective temperature and metallicity, which helps increase the precision on stellar and planetary radii.

Better stellar characterizations will allow for a more detailed study of the properties of our USP candidates to help constrain their formation and compositions; they will allow a better view of any radius gap in the K2 planet sample and to determine if there is a slope that confirms the shaping of that gap by photoevaporation. Better knowledge of the host stars will constrain their luminosities and thus the location of the habitable zones and help determine which small planets might lie within it.

Because the K2 sample will double the number of planets candidates around stars bright enough to be followed up with radial velocity (13th magnitude or so), many of our planets can have their masses measured. The resulting planet densities will help determine the boundary between rocky and gaseous planets; because of the relative lack of precision for the lowest mass planets, a larger sample size is incredibly beneficial. The planets orbiting the brightest stars are also prime candidates for atmospheric characterization. Earth-sized planets' atmospheres are extremely difficult to study today, but future missions like James Webb will make it easier; a large sample of bright transit hosts will help provide more options for atmospheric followup.

While a long baseline certainly helps measure TTVs, our full planet sample can be analyzed for TTVs or lack thereof more quantitatively than our simple by eye judgement. Especially for planets near a resonant period ratio where TTVs are strongest, a single campaign of data can be used to place upper limits on planet masses. For those systems in which there are TTVs, they can be modeled in combination with or independent of radial velocities to measure planet masses.

Finally, because of the diverse stars in the K2 sample, we can get a better handle on how planet populations change around different stars. Over the years, some trends are already evident; for example, more metal-rich stars tend to host more hot Jupiters (Fischer & Valenti, 2005), and Jupiter-sized planets are rarer around M dwarfs (Johnson et al., 2010).

The K2 host stars include lots of M dwarfs, stars in young clusters, and in general stars

spread across different galactic environments. Followup observations can sort the stars by age, metallicity, mass, or any other characteristic and look for differences in the planet population or occurrence rates. For example, it has been suggested that small planets form quite frequently in resonant chains, but those resonances are unstable over billion year timescales and thus *Kepler* observed only those that haven't yet hit an instability (Izidoro et al., 2017); looking at planet occurrences or multiplicity rates as a function of stellar age could help test that idea, made possible for the first time with K2.

6.2.3 Eclipsing Binaries

This thesis just briefly touched on the EB candidates found in K2, but binary stars are an entire field of study unto themselves. Among many other uses, EBs provide fundamental tests of stellar models and evolution.

As with the planet candidates, the eclipse times of the EBs can be analyzed more quantitatively to search for eclipse timing variations that indicate other stars (Conroy et al., 2014) or even circumbinary planets (Doyle et al., 2011). There are likely several more subtle cases of ETVs than the most obvious example spotted by eye in §3.5.1.

Close binary stars can tidally interact, changing their orbital properties (Mazeh, 2008). The EB eccentricity distribution as a function of period can be used to determine how effective tidal circularization is, and how stellar structure can affect the tidal dissipation rate (Van Eylen et al., 2016; Lurie et al., 2017).

With radial velocity followup of binary stars, both the masses and radii of both stars can be measured. These systems provide some of the most precise tests for stellar evolutionary models. Any discrepancies between observed masses and radii and the model predictions require more fine tuning or adjustments to the model's physics (Torres et al., 2010).

One of the outstanding problems in stellar modeling is with M dwarfs. Models tend to predict stellar radii that are consistently too small by about 3% (Spada et al., 2013). To date, there are only a couple dozen M dwarfs in EBs with precise parameters. Because K2 has targeted M dwarfs extensively, many of our EBs are likely to contain at least one, and

these systems will be bright enough for radial velocity followup, increasing the sample size substantially.

Finally, one system already has a radial velocity followup campaign underway: KOI-3278. The self-lensing binary has been confirmed via RV observation of the primary star, and the amplitude matches our predictions quite well.

6.3 Future Improvements and Applications for QATS

The methods and tools presented in this thesis have a much broader application than just the results presented here. The work is by no means done, and QATS can be used to search for planets around millions more stars in the coming few years. I will briefly lay out some plans to improve QATS in §6.3.1 and describe the datasets it can be applied to in §6.3.2.

6.3.1 Improvements to QATS

Each piece of the QATS pipeline could be independently analyzed and optimized for the stellar and instrumental qualities of a particular data set, but in this section I focus on two main areas holding the pipeline back, and one major feature that could dramatically increase QATS's impact.

The major roadblocks for the QATS pipeline in its present form do not come from actually detecting transit signals, but in separating those planets from the noise via the automated cuts. With only 1-3% of stars hosting detectable transiting planets, any cuts need to correctly identify and reject more than ∼98% of the stars without planets or else false positives will overwhelm true planets, even if all of the planets are correctly identified and pass. The more false positives that are allowed through, the higher the threshold has to be raised to prevent manual vetting from being swamped with false alarms, and the more real planets will be missed.

Both my proposed changes involve adjusting the automated vetting process to improve the true positive rate of passing planet candidates while decreasing the false positive rate.

The first focuses on planets that transit several times while the second looks to help detect the long period planets with three or fewer transits.

On the short period end, one of the automated cuts in our vetting process is the height of the dominant period peak in the QATS total likelihood 'spectrum' above baseline levels at other periods (§2.2.6). However, the shape and properties of the QATS spectrum are not analytical, can be difficult to estimate, and the baseline level becomes poorly sampled at both the shortest and longest periods.

One way to avoid this imprecise measure might be to eliminate the QATS spectrum from the automated cuts altogether. Instead, we can look at the period of the first and second highest peaks. For our real planet candidates, the large spikes in the total likelihood spectrum happen at predictable aliases of the planet's true period. For stars without any quasiperiodic activity, the period of the first and second highest QATS likelihoods should be much less likely to fall at e.g. a perfect 2:1 ratio.

The period ratio of the first and second highest QATS likelihoods will only work for candidates that have three or more transits; if the planet only transits once, all potential periods beyond half the campaign duration will register the same maximum total likelihood of the single transit.

A further test that might work for these single transits then is the actual value of the maximum likelihood. Because most of a light curve does not contain any transits, the vast majority of cadences have a negative likelihood of transit, but that value is equal in magnitude to the positive value that would be calculated if a transit were present. Therefore, each light curve creates a well sampled distribution of likelihoods to expect for a real transit. We might be able to compare the maximum QATS likelihood actually found to what might be expected based on the number of transits, and any candidates (whether single transit or short period) that have total likelihoods within range of the expected value calculated from the continuum regions would pass the cut.

Finally, an improvement to the pipeline that could improve the science results from the pipeline would be an end-to-end transit injection suite. As demonstrated in this thesis, QATS

is a successful and sensitive planet detection pipeline. However, we have no way at present of measuring exactly how sensitive.

One of the main goals of the *Kepler* mission was not just to find planets, but determine how frequent they are. Determining planet occurrence rates requires knowledge of how likely planets are to be detected by the pipeline in order to correct for that bias — typically a bias toward large, short period planets. The most common technique to determine occurrence rates from a planet search is to run injection tests: inject fake planets with known properties, run the search, and see how many of them are recovered (Petigura et al., 2013a; Christiansen et al., 2016).

`EVEREST` is currently designed to inject planets into the raw *Kepler* pixels, so the next step would be integrating that into a `QATS` search. By repeatedly searching the same star with different injected planets, we can calculate occurrence rates for all stars. This will allow us to compare occurrence rates across fields and see if anything changes in the K2 fields compared to the *Kepler* FOV. It will also allow for occurrence rates in known clusters to measure rates at specific ages.

6.3.2 Future Uses for `QATS`

In this thesis, we demonstrated the utility of `QATS` with its application to K2 C0-8, but as a general purpose transiting planet search method, it can be applied to light curves from any project. In this section we discuss plans to search for planets in existing and upcoming data sets.

More K2 and Kepler

In this thesis, we searched K2 C0-8 for planets. However, K2 has made it to C18, providing hundreds of thousands of new stars to search. While several groups have already searched C0-8 (§4.1), candidates from C10 onwards remain largely unpublished.

Meanwhile, `EVEREST` has been upgraded to a version 2 (Luger et al., 2017a). The new version better handles saturated targets, stars with contaminating light from other targets

in the aperture, and very faint stars. Overall, it provides 10-20% better precision with fewer outliers and problematic stars. Combining the improvements to `EVEREST` with my proposed improvements to `QATS`, we could also search C0-8 all over again to find small planets we previously missed, or planets with single transits or around saturated or faint stars that were poorly detrended before. As discussed in §4.1.1, with these improvements to both pipelines we can find some of the 227 candidates found by other groups in C0-8 but missed by our search.

Finally, as previously discussed, KOI-3278 was found in a search of *Kepler* planet candidates for additional planets with TTVs using an early iteration of `QATS`. In that search, we did in fact find a handful of TTV planet candidates that were missed by the periodic searches — exactly why `QATS` was originally designed. I plan on finishing that search with the updated version of the pipeline. There are likely a dozen or more large TTV planets still hiding in the *Kepler* data waiting to be found.

6.3.3 The Transiting Exoplanet Survey Satellite

In addition to searching already existing data sets provided by *Kepler*, I am also preparing for *TESS*, the Transiting Exoplanet Survey Satellite launched in April 2018 (Ricker et al., 2014).

While K2 did target different regions of the sky, *TESS* is going to cover near the whole sky, as shown in Figure 6.2. However, the expanded field of view comes with a tradeoff in observing baseline: each *TESS* sector will only be observed for 27 days. There will be some overlap zones, and the north and south ecliptic poles will be observed for nearly a year continuously, but 63% of the sky will only be covered for one 27 day sector.

Our work with `QATS` will therefore be useful at both ends: finding planets with TTVs in the ecliptic poles with the one year baseline, and finding one and two transit outer companions in the 27 day sectors.

Each *TESS* sector will have 200,000 stars selected that will be observed in short cadence (2 minutes) and only select 'postage stamps' of pixels around each source will be downloaded,

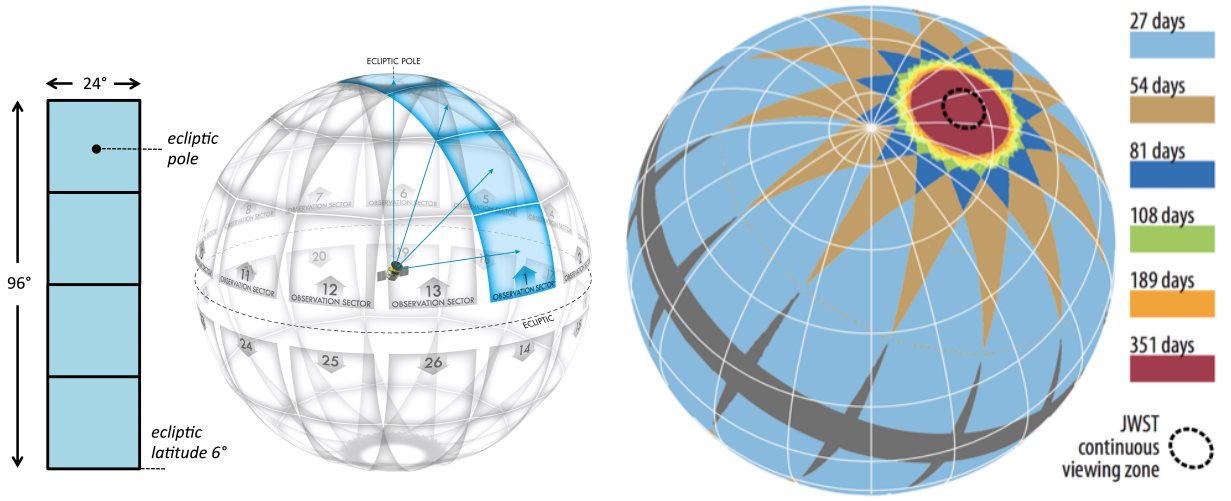

Figure 6.2: *TESS* field of view and observing strategy. Left: Field of view of each of *TESS*'s four cameras. Center: Observing strategy, showing the 13 different sectors in each hemisphere. Right: Total observing baseline for each part of the sky.

similar to what was done for both *Kepler* and K2. However, because of *TESS*'s proximity to Earth, there is enough bandwidth to download entire full frame images every 30 minutes. These long cadence images will therefore contain millions of sources in each sector.

All official *TESS* science team work has gone into pipelines for the short cadence postage stamps, leaving the full frame images for analysis by the community. Our work with `EVEREST` and `QATS` will allow us to search those full frame images for short period planets.

6.4 Closing Thoughts

The study of exoplanets was a largely theoretical and speculative field for the past several hundred years. Only in the last 25 years have we started to collect data points on the existence of planets beyond our own Solar System. The launch of *Kepler* took us into the era of Earth-sized exoplanets, and *TESS* is only going to accelerate those discoveries and help find planets around our closest stars.

These next 25 years will likely give us the ability to explore and characterize the atmo-

spheres of planets the size of Earth. We can finally begin to search for signs of life in those atmospheres or learn how unique Earth's water content and temperature may be.

I am excited to see how the field develops and how much more we can learn about how common exoplanets are and just how unique the Earth is. I hope to continue to stay involved in that process, and perhaps if I'm lucky my `QATS` pipeline first developed in this thesis will be used to find one of those Earth twins.

BIBLIOGRAPHY

Abazajian, K. N., Adelman-McCarthy, J. K., Agüeros, M. A., et al. 2009, ApJS, 182, 543, doi: 10.1088/0067-0049/182/2/543

Adams, E., Jackson, B., & Endl, M. 2016, in AAS/Division for Planetary Sciences Meeting Abstracts, Vol. 48, AAS/Division for Planetary Sciences Meeting Abstracts #48, 112.02

Adams, E. R., Ciardi, D. R., Dupree, A. K., et al. 2012, AJ, 144, 42, doi: 10.1088/0004-6256/144/2/42

Adams, F. C., & Laughlin, G. 2003, Icarus, 163, 290, doi: 10.1016/S0019-1035(03)00081-2

Agol, E. 2002, ApJ, 579, 430, doi: 10.1086/342880

—. 2003, ApJ, 594, 449, doi: 10.1086/376833

Agol, E., Steffen, J., Sari, R., & Clarkson, W. 2005, MNRAS, 359, 567, doi: 10.1111/j.1365-2966.2005.08922.x

Aigrain, S., Parviainen, H., & Pope, B. J. S. 2016, MNRAS, 459, 2408, doi: 10.1093/mnras/stw706

Aitken, R. G. 1938, Leaflet of the Astronomical Society of the Pacific, 3, 98

Andrae, R., Fouesneau, M., Creevey, O., et al. 2018, ArXiv e-prints. https://arxiv.org/abs/1804.09374

Armitage, P. J. 2018, ArXiv e-prints. https://arxiv.org/abs/1803.10526

Bakos, G., Noyes, R. W., Kovács, G., et al. 2004, PASP, 116, 266, doi: 10.1086/382735

Ballard, S., Fabrycky, D., Fressin, F., et al. 2011, ApJ, 743, 200, doi: 10.1088/0004-637X/743/2/200

Barnes, R., Meadows, V. S., & Evans, N. 2015, ApJ, 814, 91, doi: 10.1088/0004-637X/814/2/91

Barros, S. C. C., Demangeon, O., & Deleuil, M. 2016, A&A, 594, A100, doi: 10.1051/0004-6361/201628902

Batalha, N. M. 2014, Proceedings of the National Academy of Science, 111, 12647, doi: 10.1073/pnas.1304196111

Batalha, N. M., Rowe, J. F., Bryson, S. T., et al. 2013, ApJS, 204, 24, doi: 10.1088/0067-0049/204/2/24

Benedict, G. F., McArthur, B. E., Forveille, T., et al. 2002, ApJ, 581, L115, doi: 10.1086/346073

Berger, T. A., Huber, D., Gaidos, E., & van Saders, J. L. 2018, ArXiv e-prints. https://arxiv.org/abs/1805.00231

Bergeron, P., Wesemael, F., Dufour, P., et al. 2011, ApJ, 737, 28, doi: 10.1088/0004-637X/737/1/28

Bessel, F. W. 1844, MNRAS, 6, 136, doi: 10.1093/mnras/6.11.136

Bitsch, B., & Kley, W. 2010, A&A, 523, A30, doi: 10.1051/0004-6361/201014414

Bitsch, B., Morbidelli, A., Lega, E., Kretke, K., & Crida, A. 2014, A&A, 570, A75, doi: 10.1051/0004-6361/201424015

Black, D. C. 1980, Space Sci. Rev., 25, 35, doi: 10.1007/BF00200797

—. 1995, ARA&A, 33, 359, doi: 10.1146/annurev.aa.33.090195.002043

Bodenheimer, P., & Pollack, J. B. 1986, Icarus, 67, 391, doi: 10.1016/0019-1035(86)90122-3

Bond, G. 1862a, Astronomische Nachrichten, 57, 131

—. 1862b, American Journal of Science and Arts, 33, 286

Borucki, W. J. 2016, Reports on Progress in Physics, 79, 036901, doi: 10.1088/0034-4885/79/3/036901

Borucki, W. J., Caldwell, D., Koch, D. G., et al. 2001, PASP, 113, 439, doi: 10.1086/319537

Borucki, W. J., Dunham, E. W., Koch, D. G., et al. 1996, Ap&SS, 241, 111, doi: 10.1007/BF00644220

Borucki, W. J., & Summers, A. L. 1984, Icarus, 58, 121, doi: 10.1016/0019-1035(84)90102-7

Borucki, W. J., Koch, D., Basri, G., et al. 2010, Science, 327, 977, doi: 10.1126/science.1185402

Borucki, W. J., Koch, D. G., Basri, G., et al. 2011a, ApJ, 728, 117, doi: 10.1088/0004-637X/728/2/117

—. 2011b, ApJ, 736, 19, doi: 10.1088/0004-637X/736/1/19

Bowler, B. P. 2016, PASP, 128, 102001, doi: 10.1088/1538-3873/128/968/102001

Bressan, A., Marigo, P., Girardi, L., et al. 2012, MNRAS, 427, 127, doi: 10.1111/j.1365-2966.2012.21948.x

Brown, T. M., Latham, D. W., Everett, M. E., & Esquerdo, G. A. 2011, AJ, 142, 112, doi: 10.1088/0004-6256/142/4/112

Bruno, G. 1584, De l'infinito universo et mondi (London)

Burke, C. J., Bryson, S. T., Mullally, F., et al. 2014, ApJS, 210, 19, doi: 10.1088/0067-0049/210/2/19

Burke, C. J., Christiansen, J. L., Mullally, F., et al. 2015, ApJ, 809, 8, doi: 10.1088/0004-637X/809/1/8

Carter, J. A., & Agol, E. 2013, ApJ, 765, 132, doi: 10.1088/0004-637X/765/2/132

Carter, J. A., & Winn, J. N. 2009, ApJ, 704, 51, doi: 10.1088/0004-637X/704/1/51

Carter, J. A., Agol, E., Chaplin, W. J., et al. 2012, Science, 337, 556, doi: 10.1126/science.1223269

Catalán, S., Ribas, I., Isern, J., & García-Berro, E. 2008, A&A, 477, 901, doi: 10.1051/0004-6361:20078230

Charbonneau, D., Brown, T. M., Latham, D. W., & Mayor, M. 2000, ApJ, 529, L45, doi: 10.1086/312457

Chiang, E., & Laughlin, G. 2013, MNRAS, 431, 3444, doi: 10.1093/mnras/stt424

Christiansen, J. L., Jenkins, J. M., Caldwell, D. A., et al. 2012, PASP, 124, 1279, doi: 10.1086/668847

Christiansen, J. L., Clarke, B. D., Burke, C. J., et al. 2016, ApJ, 828, 99, doi: 10.3847/0004-637X/828/2/99

Christiansen, J. L., Crossfield, I. J. M., Barentsen, G., et al. 2018, AJ, 155, 57, doi: 10.3847/1538-3881/aa9be0

Conroy, K. E., Prša, A., Stassun, K. G., et al. 2014, AJ, 147, 45, doi: 10.1088/0004-6256/147/2/45

Coughlin, J. L., Thompson, S. E., Bryson, S. T., et al. 2014, AJ, 147, 119, doi: 10.1088/0004-6256/147/5/119

Coughlin, J. L., Mullally, F., Thompson, S. E., et al. 2016, ApJS, 224, 12, doi: 10.3847/0067-0049/224/1/12

Cresswell, P., Dirksen, G., Kley, W., & Nelson, R. P. 2007, A&A, 473, 329, doi: 10.1051/0004-6361:20077666

Cresswell, P., & Nelson, R. P. 2006, A&A, 450, 833, doi: 10.1051/0004-6361:20054551

Crida, A., Morbidelli, A., & Masset, F. 2006, Icarus, 181, 587, doi: 10.1016/j.icarus.2005.10.007

Crossfield, I. J. M., Ciardi, D. R., Petigura, E. A., et al. 2016, ApJS, 226, 7, doi: 10.3847/0067-0049/226/1/7

Cutri, R. M., & et al. 2012, VizieR Online Data Catalog, 2311

Cutri, R. M., Skrutskie, M. F., van Dyk, S., et al. 2003, VizieR Online Data Catalog, 2246

David, T. J., Conroy, K. E., Hillenbrand, L. A., et al. 2016a, AJ, 151, 112, doi: 10.3847/0004-6256/151/5/112

David, T. J., Hillenbrand, L. A., Petigura, E. A., et al. 2016b, Nature, 534, 658, doi: 10.1038/nature18293

Davis, P. J., Kolb, U., & Willems, B. 2010, MNRAS, 403, 179, doi: 10.1111/j.1365-2966.2009.16138.x

de Bruijne, J. H. J. 2012, Ap&SS, 341, 31, doi: 10.1007/s10509-012-1019-4

de Kool, M., & Green, P. J. 1995, ApJ, 449, 236, doi: 10.1086/176051

de Kool, M., & Ritter, H. 1993, A&A, 267, 397

De Marco, O., Passy, J.-C., Moe, M., et al. 2011, MNRAS, 411, 2277, doi: 10.1111/j.1365-2966.2010.17891.x

Deeming, T. J. 1975, Ap&SS, 36, 137, doi: 10.1007/BF00681947

Deming, D., Knutson, H., Kammer, J., et al. 2015, ApJ, 805, 132, doi: 10.1088/0004-637X/805/2/132

Demory, B.-O., & Seager, S. 2011, ApJS, 197, 12, doi: 10.1088/0067-0049/197/1/12

Di Stefano, R. 2011, AJ, 141, 142, doi: 10.1088/0004-6256/141/5/142

Dotter, A., Chaboyer, B., Jevremović, D., et al. 2008, ApJS, 178, 89, doi: 10.1086/589654

Doyle, L. R., Carter, J. A., Fabrycky, D. C., et al. 2011, Science, 333, 1602, doi: 10.1126/science.1210923

Dressing, C. D., & Charbonneau, D. 2013, ApJ, 767, 95, doi: 10.1088/0004-637X/767/1/95

—. 2015, ApJ, 807, 45, doi: 10.1088/0004-637X/807/1/45

Dressing, C. D., Newton, E. R., Schlieder, J. E., et al. 2017a, ApJ, 836, 167, doi: 10.3847/1538-4357/836/2/167

Dressing, C. D., Vanderburg, A., Schlieder, J. E., et al. 2017b, AJ, 154, 207, doi: 10.3847/1538-3881/aa89f2

Dürmann, C., & Kley, W. 2015, A&A, 574, A52, doi: 10.1051/0004-6361/201424837

Dyson, F. W., Eddington, A. S., & Davidson, C. 1920, Philosophical Transactions of the Royal Society of London Series A, 220, 291, doi: 10.1098/rsta.1920.0009

Eastman, J., Gaudi, B. S., & Agol, E. 2013, PASP, 125, 83, doi: 10.1086/669497

Einstein, A. 1936, Science, 84, 506, doi: 10.1126/science.84.2188.506

Erickson, E. F., Goorvitch, D., Simpson, J. P., & Strecker, D. W. 1978, Icarus, 35, 61, doi: 10.1016/0019-1035(78)90060-X

Fabrycky, D. C., Lissauer, J. J., Ragozzine, D., et al. 2014, ApJ, 790, 146, doi: 10.1088/0004-637X/790/2/146

Farmer, A. J., & Agol, E. 2003, ApJ, 592, 1151, doi: 10.1086/375806

Fischer, D. A., & Valenti, J. 2005, ApJ, 622, 1102, doi: 10.1086/428383

Ford, E. B., Kozinsky, B., & Rasio, F. A. 2000, ApJ, 535, 385, doi: 10.1086/308815

Foreman-Mackey, D. 2014, Blog Post: Mixture Models, doi: 10.5281/zenodo.15856. https://doi.org/10.5281/zenodo.15856

Foreman-Mackey, D., Hogg, D. W., Lang, D., & Goodman, J. 2013, PASP, 125, 306, doi: 10.1086/670067

Foreman-Mackey, D., Hogg, D. W., & Morton, T. D. 2014, ApJ, 795, 64, doi: 10.1088/0004-637X/795/1/64

Foreman-Mackey, D., Montet, B. T., Hogg, D. W., et al. 2015, ApJ, 806, 215, doi: 10.1088/0004-637X/806/2/215

Foreman-Mackey, D., Morton, T. D., Hogg, D. W., Agol, E., & Schölkopf, B. 2016, AJ, 152, 206, doi: 10.3847/0004-6256/152/6/206

Fressin, F., Torres, G., Charbonneau, D., et al. 2013, ApJ, 766, 81, doi: 10.1088/0004-637X/766/2/81

Fulton, B. J., Petigura, E. A., Howard, A. W., et al. 2017, AJ, 154, 109, doi: 10.3847/1538-3881/aa80eb

Furlan, E., Ciardi, D. R., Everett, M. E., et al. 2017, AJ, 153, 71, doi: 10.3847/1538-3881/153/2/71

Furlan, E., Ciardi, D. R., Cochran, W. D., et al. 2018, ArXiv e-prints. https://arxiv.org/abs/1805.12089

Gaia Collaboration, Brown, A. G. A., Vallenari, A., et al. 2018, ArXiv e-prints. https://arxiv.org/abs/1804.09365

Gaia Collaboration, Prusti, T., de Bruijne, J. H. J., et al. 2016, A&A, 595, A1, doi: 10.1051/0004-6361/201629272

Gatewood, G., & Eichhorn, H. 1973, AJ, 78, 769, doi: 10.1086/111480

Gazak, J. Z., Johnson, J. A., Tonry, J., et al. 2012, Advances in Astronomy, 2012, 697967, doi: 10.1155/2012/697967

Giles, H. A. C., Osborn, H. P., Blanco-Cuaresma, S., et al. 2018, ArXiv e-prints. https://arxiv.org/abs/1806.08757

Goldreich, P., & Tremaine, S. 1979, ApJ, 233, 857, doi: 10.1086/157448

Goodman, J., & Weare, J. 2010, Communications in Applied Mathematics and Computational Science, Vol. 5, No. 1, p. 65-80, 2010, 5, 65, doi: 10.2140/camcos.2010.5.65

Goodricke, J. 1783, Philosophical Transactions of the Royal Society of London Series I, 73, 474

Gould, A. 1995, ApJ, 446, 541, doi: 10.1086/175812

Green, P. J., Ali, B., & Napiwotzki, R. 2000, ApJ, 540, 992, doi: 10.1086/309379

Grossman, L., & Larimer, J. W. 1974, Reviews of Geophysics and Space Physics, 12, 71, doi: 10.1029/RG012i001p00071

Haas, M. R., Batalha, N. M., Bryson, S. T., et al. 2010, ApJ, 713, L115, doi: 10.1088/2041-8205/713/2/L115

Hansen, B. M. S., & Murray, N. 2013, ApJ, 775, 53, doi: 10.1088/0004-637X/775/1/53

Hartkopf, W. I., & Mason, B. D. 2004, in Revista Mexicana de Astronomia y Astrofisica, vol. 27, Vol. 21, Revista Mexicana de Astronomia y Astrofisica Conference Series, ed. C. Allen & C. Scarfe, 83–90

Hayashi, C. 1981, Progress of Theoretical Physics Supplement, 70, 35, doi: 10.1143/PTPS.70.35

Henry, G. W., Marcy, G. W., Butler, R. P., & Vogt, S. S. 2000, ApJ, 529, L41, doi: 10.1086/312458

Hershey, J. L. 1973, AJ, 78, 421, doi: 10.1086/111436

Heyrovský, D., & Loeb, A. 1997, ApJ, 490, 38, doi: 10.1086/304855

Holberg, J. B., & Bergeron, P. 2006, AJ, 132, 1221, doi: 10.1086/505938

Holberg, J. B., Oswalt, T. D., Sion, E. M., Barstow, M. A., & Burleigh, M. R. 2013, MNRAS, 435, 2077, doi: 10.1093/mnras/stt1433

Howell, S. B., Sobeck, C., Haas, M., et al. 2014, PASP, 126, 398, doi: 10.1086/676406

Huber, D., Silva Aguirre, V., Matthews, J. M., et al. 2014, ApJS, 211, 2, doi: 10.1088/0067-0049/211/1/2

Huber, D., Bryson, S. T., Haas, M. R., et al. 2016, ApJS, 224, 2, doi: 10.3847/0067-0049/224/1/2

Hurley, J. R., Pols, O. R., & Tout, C. A. 2000, MNRAS, 315, 543, doi: 10.1046/j.1365-8711.2000.03426.x

Hurley, J. R., Tout, C. A., & Pols, O. R. 2002, MNRAS, 329, 897, doi: 10.1046/j.1365-8711.2002.05038.x

Iben, Jr., I., & Livio, M. 1993, PASP, 105, 1373, doi: 10.1086/133321

Ivanova, N., Justham, S., Chen, X., et al. 2013, A&A Rev., 21, 59, doi: 10.1007/s00159-013-0059-2

Izidoro, A., Ogihara, M., Raymond, S. N., et al. 2017, MNRAS, 470, 1750, doi: 10.1093/mnras/stx1232

Izidoro, A., & Raymond, S. N. 2018, ArXiv e-prints. https://arxiv.org/abs/1803.08830

Jacob, W. S. 1855, MNRAS, 15, 228, doi: 10.1093/mnras/15.9.228

Jenkins, J. M., Caldwell, D. A., Chandrasekaran, H., et al. 2010a, ApJ, 713, L87, doi: 10.1088/2041-8205/713/2/L87

Jenkins, J. M., Chandrasekaran, H., McCauliff, S. D., et al. 2010b, in Society of Photo-Optical Instrumentation Engineers (SPIE) Conference Series, Vol. 7740, Society of Photo-Optical Instrumentation Engineers (SPIE) Conference Series

Jin, S., & Mordasini, C. 2018, ApJ, 853, 163, doi: 10.3847/1538-4357/aa9f1e

Johansen, A., & Lacerda, P. 2010, MNRAS, 404, 475, doi: 10.1111/j.1365-2966.2010.16309.x

Johansen, A., & Lambrechts, M. 2017, Annual Review of Earth and Planetary Sciences, 45, 359, doi: 10.1146/annurev-earth-063016-020226

Johansen, A., Oishi, J. S., Mac Low, M.-M., et al. 2007, Nature, 448, 1022, doi: 10.1038/nature06086

Johansen, A., & Youdin, A. 2007, ApJ, 662, 627, doi: 10.1086/516730

Johnson, J. A., Aller, K. M., Howard, A. W., & Crepp, J. R. 2010, PASP, 122, 905, doi: 10.1086/655775

Johnson, J. A., Petigura, E. A., Fulton, B. J., et al. 2017, AJ, 154, 108, doi: 10.3847/1538-3881/aa80e7

Jones, D. O., West, A. A., & Foster, J. B. 2011, AJ, 142, 44, doi: 10.1088/0004-6256/142/2/44

Kalirai, J. S., Hansen, B. M. S., Kelson, D. D., et al. 2008, ApJ, 676, 594, doi: 10.1086/527028

Kaplan, D. L., Marsh, T. R., Walker, A. N., et al. 2014, ApJ, 780, 167, doi: 10.1088/0004-637X/780/2/167

Kasting, J. F., Whitmire, D. P., & Reynolds, R. T. 1993, Icarus, 101, 108, doi: 10.1006/icar.1993.1010

Katz, B., Dong, S., & Malhotra, R. 2011, Physical Review Letters, 107, 181101, doi: 10.1103/PhysRevLett.107.181101

Kawahara, H., Masuda, K., MacLeod, M., et al. 2018, AJ, 155, 144, doi: 10.3847/1538-3881/aaaaaf

Kenyon, S. J., & Bromley, B. C. 2006, AJ, 131, 1837, doi: 10.1086/499807

Kepler, J., & Bartsch, J. 1630, Admonitio ad astronomos, rerumque coelestium studiosos, de raris mirisque anni 1631 phaenomenis, Veneris puta et Mercurii in Solem incursu (Godefrid Tampach)

Kepler, S. O., Kleinman, S. J., Nitta, A., et al. 2007, MNRAS, 375, 1315, doi: 10.1111/j.1365-2966.2006.11388.x

Kipping, D. M. 2013, MNRAS, 435, 2152, doi: 10.1093/mnras/stt1435

Kirk, B., Conroy, K., Prša, A., et al. 2016, AJ, 151, 68, doi: 10.3847/0004-6256/151/3/68

Koch, D. G., Borucki, W. J., Dunham, E. W., et al. 2000, in Proc. SPIE, Vol. 4013, UV, Optical, and IR Space Telescopes and Instruments, ed. J. B. Breckinridge & P. Jakobsen, 508–519

Koch, D. G., Borucki, W. J., Basri, G., et al. 2010, ApJ, 713, L79, doi: 10.1088/2041-8205/713/2/L79

Kokubo, E., & Ida, S. 1995, Icarus, 114, 247, doi: 10.1006/icar.1995.1059

Konacki, M., Torres, G., Jha, S., & Sasselov, D. D. 2003, Nature, 421, 507, doi: 10.1038/nature01379

Kopparapu, R. K., Ramirez, R., Kasting, J. F., et al. 2013, ApJ, 765, 131, doi: 10.1088/0004-637X/765/2/131

Kovács, G., Zucker, S., & Mazeh, T. 2002, A&A, 391, 369, doi: 10.1051/0004-6361:20020802

Kowalski, P. M., & Saumon, D. 2006, ApJ, 651, L137, doi: 10.1086/509723

Kruse, E., & Agol, E. 2014, Science, 344, 275, doi: 10.1126/science.1251999

Kürster, M., Endl, M., Rouesnel, F., et al. 2003, A&A, 403, 1077, doi: 10.1051/0004-6361:20030396

LaCourse, D. M., & Jacobs, T. L. 2018, Research Notes of the American Astronomical Society, 2, 28, doi: 10.3847/2515-5172/aaad61

Lagrange, A.-M. 2014, Philosophical Transactions of the Royal Society of London Series A, 372, 20130090, doi: 10.1098/rsta.2013.0090

Lagrange, A.-M., Gratadour, D., Chauvin, G., et al. 2009, A&A, 493, L21, doi: 10.1051/0004-6361:200811325

Lambrechts, M., & Johansen, A. 2012, A&A, 544, A32, doi: 10.1051/0004-6361/201219127

Lardner, D. 1853, Hand-books of Natural Philosphy and Astronomy, Vol. 3 (Walton and Maberly), 771

Lee, E. J., Chiang, E., & Ormel, C. W. 2014, ApJ, 797, 95, doi: 10.1088/0004-637X/797/2/95

Libralato, M., Nardiello, D., Bedin, L. R., et al. 2016, MNRAS, 463, 1780, doi: 10.1093/mnras/stw1932

Lissauer, J. J. 1987, Icarus, 69, 249, doi: 10.1016/0019-1035(87)90104-7

—. 1995, Icarus, 114, 217, doi: 10.1006/icar.1995.1057

Lissauer, J. J., Fabrycky, D. C., Ford, E. B., et al. 2011a, Nature, 470, 53, doi: 10.1038/nature09760

Lissauer, J. J., Ragozzine, D., Fabrycky, D. C., et al. 2011b, ApJS, 197, 8, doi: 10.1088/0067-0049/197/1/8

Lissauer, J. J., Marcy, G. W., Bryson, S. T., et al. 2014, ApJ, 784, 44, doi: 10.1088/0004-637X/784/1/44

Lodders, K. 2003, ApJ, 591, 1220, doi: 10.1086/375492

Loeb, A., & Gaudi, B. S. 2003, ApJ, 588, L117, doi: 10.1086/375551

Lopez, E. D., & Fortney, J. J. 2013, ApJ, 776, 2, doi: 10.1088/0004-637X/776/1/2

—. 2014, ApJ, 792, 1, doi: 10.1088/0004-637X/792/1/1

Lopez, E. D., Fortney, J. J., & Miller, N. 2012, ApJ, 761, 59, doi: 10.1088/0004-637X/761/1/59

Lopez, E. D., & Rice, K. 2016, ArXiv e-prints. https://arxiv.org/abs/1610.09390

Lovis, C., & Fischer, D. 2010, in Exoplanets, ed. S. Seager (University of Arizona Press), 27–53

Luger, R., Agol, E., Kruse, E., et al. 2016, AJ, 152, 100, doi: 10.3847/0004-6256/152/4/100

Luger, R., Barnes, R., Lopez, E., et al. 2015, Astrobiology, 15, 57, doi: 10.1089/ast.2014.1215

Luger, R., Kruse, E., Foreman-Mackey, D., Agol, E., & Saunders, N. 2017a, ArXiv e-prints. https://arxiv.org/abs/1702.05488

Luger, R., Sestovic, M., Kruse, E., et al. 2017b, Nature Astronomy, 1, 0129, doi: 10.1038/s41550-017-0129

Lund, M. N., Handberg, R., Davies, G. R., Chaplin, W. J., & Jones, C. D. 2015, ApJ, 806, 30, doi: 10.1088/0004-637X/806/1/30

Lurie, J. C., Vyhmeister, K., Hawley, S. L., et al. 2017, AJ, 154, 250, doi: 10.3847/1538-3881/aa974d

Maeder, A. 1973, A&A, 26, 215

Mamajek, E. E. 2009, in American Institute of Physics Conference Series, Vol. 1158, American Institute of Physics Conference Series, ed. T. Usuda, M. Tamura, & M. Ishii, 3–10

Mamajek, E. E., & Hillenbrand, L. A. 2008, ApJ, 687, 1264, doi: 10.1086/591785

Mandel, K., & Agol, E. 2002, ApJ, 580, L171, doi: 10.1086/345520

Mann, A. W., Gaidos, E., Mace, G. N., et al. 2016, ApJ, 818, 46, doi: 10.3847/0004-637X/818/1/46

Mann, A. W., Gaidos, E., Vanderburg, A., et al. 2017, AJ, 153, 64, doi: 10.1088/1361-6528/aa5276

Mao, S. 2012, Research in Astronomy and Astrophysics, 12, 947, doi: 10.1088/1674-4527/12/8/005

Marcy, G. W., & Benitz, K. J. 1989, ApJ, 344, 441, doi: 10.1086/167812

Marcy, G. W., & Butler, R. P. 1998, ARA&A, 36, 57, doi: 10.1146/annurev.astro.36.1.57

Marcy, G. W., Isaacson, H., Howard, A. W., et al. 2014, ApJS, 210, 20, doi: 10.1088/0067-0049/210/2/20

Marois, C., Macintosh, B., Barman, T., et al. 2008, Science, 322, 1348, doi: 10.1126/science.1166585

Marsh, T. R. 2001, MNRAS, 324, 547, doi: 10.1046/j.1365-8711.2001.04293.x

Mayo, A. W., Vanderburg, A., Latham, D. W., et al. 2018, AJ, 155, 136, doi: 10.3847/1538-3881/aaadff

Mayor, M., & Queloz, D. 1995, Nature, 378, 355, doi: 10.1038/378355a0

Mazeh, T. 2008, in EAS Publications Series, Vol. 29, EAS Publications Series, ed. M.-J. Goupil & J.-P. Zahn, 1–65

Mazeh, T., Naef, D., Torres, G., et al. 2000, ApJ, 532, L55, doi: 10.1086/312558

Mazeh, T., Nachmani, G., Holczer, T., et al. 2013, ApJS, 208, 16, doi: 10.1088/0067-0049/208/2/16

McArthur, B. E., Endl, M., Cochran, W. D., et al. 2004, ApJ, 614, L81, doi: 10.1086/425561

Meylan, G., Jetzer, P., North, P., et al., eds. 2006, Gravitational Lensing: Strong, Weak and Micro

Montet, B. T., Morton, T. D., Foreman-Mackey, D., et al. 2015, ApJ, 809, 25, doi: 10.1088/0004-637X/809/1/25

Morbidelli, A., & Nesvorny, D. 2012, A&A, 546, A18, doi: 10.1051/0004-6361/201219824

Morbidelli, A., & Raymond, S. N. 2016, Journal of Geophysical Research (Planets), 121, 1962, doi: 10.1002/2016JE005088

Morton, T. D. 2012, ApJ, 761, 6, doi: 10.1088/0004-637X/761/1/6

Moulton, F. R. 1899, AJ, 20, 33, doi: 10.1086/103096

Muirhead, P. S., Vanderburg, A., Shporer, A., et al. 2013, ApJ, 767, 111, doi: 10.1088/0004-637X/767/2/111

Mulders, G. D., Pascucci, I., & Apai, D. 2015, ApJ, 798, 112, doi: 10.1088/0004-637X/798/2/112

Mullally, F., Coughlin, J. L., Thompson, S. E., et al. 2015, ApJS, 217, 31, doi: 10.1088/0067-0049/217/2/31

Muterspaugh, M. W., Lane, B. F., Kulkarni, S. R., et al. 2010, AJ, 140, 1657, doi: 10.1088/0004-6256/140/6/1657

Naoz, S., Kocsis, B., Loeb, A., & Yunes, N. 2013, ApJ, 773, 187, doi: 10.1088/0004-637X/773/2/187

Nardiello, D., Libralato, M., Bedin, L. R., et al. 2016, MNRAS, 463, 1831, doi: 10.1093/mnras/stw2169

Obermeier, C., Henning, T., Schlieder, J. E., et al. 2016, AJ, 152, 223, doi: 10.3847/1538-3881/152/6/223

Oppenheimer, B. R., & Hinkley, S. 2009, ARA&A, 47, 253, doi: 10.1146/annurev-astro-082708-101717

Ormel, C. W., Dullemond, C. P., & Spaans, M. 2010, Icarus, 210, 507, doi: 10.1016/j.icarus.2010.06.011

Osborn, H. P., Armstrong, D. J., Brown, D. J. A., et al. 2016, MNRAS, 457, 2273, doi: 10.1093/mnras/stw137

Owen, J. E., & Wu, Y. 2013, ApJ, 775, 105, doi: 10.1088/0004-637X/775/2/105

Paczynski, B. 1976, in IAU Symposium, Vol. 73, Structure and Evolution of Close Binary Systems, ed. P. Eggleton, S. Mitton, & J. Whelan, 75

Paczynski, B. 1996, ARA&A, 34, 419, doi: 10.1146/annurev.astro.34.1.419

Parsons, S. G., Marsh, T. R., Gänsicke, B. T., et al. 2012, MNRAS, 420, 3281, doi: 10.1111/j.1365-2966.2011.20251.x

Paulson, D. B., Cochran, W. D., & Hatzes, A. P. 2004, AJ, 127, 3579, doi: 10.1086/420710

Perryman, M., Hartman, J., Bakos, G. Á., & Lindegren, L. 2014, ApJ, 797, 14, doi: 10.1088/0004-637X/797/1/14

Perryman, M. A. C., de Boer, K. S., Gilmore, G., et al. 2001, A&A, 369, 339, doi: 10.1051/0004-6361:20010085

Petigura, E. A., Howard, A. W., & Marcy, G. W. 2013a, Proceedings of the National Academy of Science, 110, 19273, doi: 10.1073/pnas.1319909110

Petigura, E. A., & Marcy, G. W. 2012, PASP, 124, 1073, doi: 10.1086/668291

Petigura, E. A., Marcy, G. W., & Howard, A. W. 2013b, ApJ, 770, 69, doi: 10.1088/0004-637X/770/1/69

Petigura, E. A., Schlieder, J. E., Crossfield, I. J. M., et al. 2015, ApJ, 811, 102, doi: 10.1088/0004-637X/811/2/102

Petigura, E. A., Howard, A. W., Marcy, G. W., et al. 2017, AJ, 154, 107, doi: 10.3847/1538-3881/aa80de

Petigura, E. A., Crossfield, I. J. M., Isaacson, H., et al. 2018, AJ, 155, 21, doi: 10.3847/1538-3881/aa9b83

Pickles, A. J. 1998, PASP, 110, 863, doi: 10.1086/316197

Pinsonneault, M. H., An, D., Molenda-Żakowicz, J., et al. 2012, ApJS, 199, 30, doi: 10.1088/0067-0049/199/2/30

Pollacco, D. L., Skillen, I., Collier Cameron, A., et al. 2006, PASP, 118, 1407, doi: 10.1086/508556

Pollack, J. B., Hubickyj, O., Bodenheimer, P., et al. 1996, Icarus, 124, 62, doi: 10.1006/icar.1996.0190

Pope, B. J. S., Parviainen, H., & Aigrain, S. 2016, MNRAS, 461, 3399, doi: 10.1093/mnras/stw1373

Provencal, J. L., Shipman, H. L., Høg, E., & Thejll, P. 1998, ApJ, 494, 759, doi: 10.1086/305238

Quinn, S. N., White, R. J., Latham, D. W., et al. 2012, ApJ, 756, L33, doi: 10.1088/2041-8205/756/2/L33

Quintana, E. V., Jenkins, J. M., Clarke, B. D., et al. 2010, in Proc. SPIE, Vol. 7740, Software and Cyberinfrastructure for Astronomy, 77401X

Rahvar, S., Mehrabi, A., & Dominik, M. 2011, MNRAS, 410, 912, doi: 10.1111/j.1365-2966.2010.17490.x

Rebassa-Mansergas, A., Zorotovic, M., Schreiber, M. R., et al. 2012, MNRAS, 423, 320, doi: 10.1111/j.1365-2966.2012.20880.x

Reinhold, T., Reiners, A., & Basri, G. 2013, A&A, 560, A4, doi: 10.1051/0004-6361/201321970

Ricker, G. R., Winn, J. N., Vanderspek, R., et al. 2014, in Proc. SPIE, Vol. 9143, Space Telescopes and Instrumentation 2014: Optical, Infrared, and Millimeter Wave, 914320

Rogers, L. A. 2015, ApJ, 801, 41, doi: 10.1088/0004-637X/801/1/41

Rosenblatt, F. 1971, Icarus, 14, 71, doi: 10.1016/0019-1035(71)90103-5

Rowe, J. F., Borucki, W. J., Koch, D., et al. 2010, ApJ, 713, L150, doi: 10.1088/2041-8205/713/2/L150

Rowe, J. F., Bryson, S. T., Marcy, G. W., et al. 2014, ApJ, 784, 45, doi: 10.1088/0004-637X/784/1/45

Rowe, J. F., Coughlin, J. L., Antoci, V., et al. 2015, ApJS, 217, 16, doi: 10.1088/0067-0049/217/1/16

Russell, H. N. 1912a, ApJ, 35, 315, doi: 10.1086/141942

—. 1912b, ApJ, 36, 54, doi: 10.1086/141952

Safronov, V. S. 1972, Evolution of the protoplanetary cloud and formation of the earth and planets. (Keter Publishing House)

Sahlmann, J., Lazorenko, P. F., Ségransan, D., et al. 2013, A&A, 556, A133, doi: 10.1051/0004-6361/201321871

Sahu, K. C., & Gilliland, R. L. 2003, ApJ, 584, 1042, doi: 10.1086/345776

Sanchis-Ojeda, R., Rappaport, S., Winn, J. N., et al. 2014, ApJ, 787, 47, doi: 10.1088/0004-637X/787/1/47

Santos, N. C., Bouchy, F., Mayor, M., et al. 2004, A&A, 426, L19, doi: 10.1051/0004-6361:200400076

Schäfer, U., Yang, C.-C., & Johansen, A. 2017, A&A, 597, A69, doi: 10.1051/0004-6361/201629561

Schlafly, E. F., & Finkbeiner, D. P. 2011, ApJ, 737, 103, doi: 10.1088/0004-637X/737/2/103

Schreiber, M. R., & Gänsicke, B. T. 2003, A&A, 406, 305, doi: 10.1051/0004-6361:20030801

Seabold, S., & Perktold, J. 2010, in 9th Python in Science Conference

Seager, S., Kuchner, M., Hier-Majumder, C. A., & Militzer, B. 2007, ApJ, 669, 1279, doi: 10.1086/521346

Seager, S., & Mallén-Ornelas, G. 2003, ApJ, 585, 1038, doi: 10.1086/346105

See, T. J. J. 1896, AJ, 16, 17, doi: 10.1086/102368

Sestovic, M., Demory, B.-O., & Queloz, D. 2018, ArXiv e-prints. https://arxiv.org/abs/1804.03075

Shu, F., Najita, J., Ostriker, E., et al. 1994, ApJ, 429, 781, doi: 10.1086/174363

Sing, D. K. 2010, A&A, 510, A21, doi: 10.1051/0004-6361/200913675

Smith, W. 1769, Transactions of the American Philosophical Society, 1, 54

Spada, F., Demarque, P., Kim, Y.-C., & Sills, A. 2013, ApJ, 776, 87, doi: 10.1088/0004-637X/776/2/87

Steffen, J. H., Batalha, N. M., Borucki, W. J., et al. 2010, ApJ, 725, 1226, doi: 10.1088/0004-637X/725/1/1226

Steinfadt, J. D. R., Kaplan, D. L., Shporer, A., Bildsten, L., & Howell, S. B. 2010, ApJ, 716, L146, doi: 10.1088/2041-8205/716/2/L146

Stevenson, D. J. 1982, Planet. Space Sci., 30, 755, doi: 10.1016/0032-0633(82)90108-8

Strand, K. A. 1943, PASP, 55, 29, doi: 10.1086/125484

Struve, O. 1952, The Observatory, 72, 199

Tenenbaum, P., Jenkins, J. M., Seader, S., et al. 2014, ApJS, 211, 6, doi: 10.1088/0067-0049/211/1/6

Testi, L., Birnstiel, T., Ricci, L., et al. 2014, Protostars and Planets VI, 339, doi: 10.2458/azu_uapress_9780816531240-ch015

Thompson, S. E., Everett, M., Mullally, F., et al. 2012, ApJ, 753, 86, doi: 10.1088/0004-637X/753/1/86

Thompson, S. E., Coughlin, J. L., Hoffman, K., et al. 2018, ApJS, 235, 38, doi: 10.3847/1538-4365/aab4f9

Toonen, S., & Nelemans, G. 2013, A&A, 557, A87, doi: 10.1051/0004-6361/201321753

Torres, G., Andersen, J., & Giménez, A. 2010, A&A Rev., 18, 67, doi: 10.1007/s00159-009-0025-1

Tout, C. A., Aarseth, S. J., Pols, O. R., & Eggleton, P. P. 1997, MNRAS, 291, 732, doi: 10.1093/mnras/291.4.732

Tremblay, P.-E., Bergeron, P., & Gianninas, A. 2011, ApJ, 730, 128, doi: 10.1088/0004-637X/730/2/128

Twicken, J. D., Chandrasekaran, H., Jenkins, J. M., et al. 2010a, in Proc. SPIE, Vol. 7740, Software and Cyberinfrastructure for Astronomy, 77401U

Twicken, J. D., Clarke, B. D., Bryson, S. T., et al. 2010b, in Proc. SPIE, Vol. 7740, Software and Cyberinfrastructure for Astronomy, 774023

Uehara, S., Kawahara, H., Masuda, K., Yamada, S., & Aizawa, M. 2016, ApJ, 822, 2, doi: 10.3847/0004-637X/822/1/2

van de Kamp, P. 1963, AJ, 68, 515, doi: 10.1086/109001

van de Kamp, P., & Lippincott, S. L. 1951, AJ, 56, 49, doi: 10.1086/106503

Van Eylen, V., Agentoft, C., Lundkvist, M. S., et al. 2017, ArXiv e-prints. https://arxiv.org/abs/1710.05398

Van Eylen, V., Winn, J. N., & Albrecht, S. 2016, ApJ, 824, 15, doi: 10.3847/0004-637X/824/1/15

Vanderburg, A. 2014, ArXiv e-prints. https://arxiv.org/abs/1412.1827

Vanderburg, A., & Johnson, J. A. 2014, PASP, 126, 948, doi: 10.1086/678764

Vanderburg, A., Becker, J. C., Kristiansen, M. H., et al. 2016a, ApJ, 827, L10, doi: 10.3847/2041-8205/827/1/L10

Vanderburg, A., Latham, D. W., Buchhave, L. A., et al. 2016b, ApJS, 222, 14, doi: 10.3847/0067-0049/222/1/14

Wada, K., Tanaka, H., Suyama, T., Kimura, H., & Yamamoto, T. 2009, ApJ, 702, 1490, doi: 10.1088/0004-637X/702/2/1490

Wambsganss, J. 1998, Living Reviews in Relativity, 1, 12, doi: 10.12942/lrr-1998-12

Wang, J., Fischer, D. A., Horch, E. P., & Huang, X. 2015a, ApJ, 799, 229, doi: 10.1088/0004-637X/799/2/229

Wang, J., Fischer, D. A., Barclay, T., et al. 2015b, ApJ, 815, 127, doi: 10.1088/0004-637X/815/2/127

Weidemann, V. 2000, A&A, 363, 647

Weidenschilling, S. J. 1977, MNRAS, 180, 57, doi: 10.1093/mnras/180.1.57

Weiss, L. M., & Marcy, G. W. 2014, ApJ, 783, L6, doi: 10.1088/2041-8205/783/1/L6

Welsh, W. F., Orosz, J. A., Aerts, C., et al. 2011, ApJS, 197, 4, doi: 10.1088/0067-0049/197/1/4

Wetherill, G. W., & Stewart, G. R. 1989, Icarus, 77, 330, doi: 10.1016/0019-1035(89)90093-6

Willems, B., & Kolb, U. 2004, A&A, 419, 1057, doi: 10.1051/0004-6361:20040085

Winn, J. N. 2010, in Exoplanets, ed. S. Seager (University of Arizona Press), 55–77

Wright, J. T. 2017, in Handbook of Exoplanets, ed. H. J. Deeg & J. A. Belmonte (Springer), 4

Wu, Y. 2018, ArXiv e-prints. https://arxiv.org/abs/1806.04693

Wuchterl, G. 1993, Icarus, 106, 323, doi: 10.1006/icar.1993.1174

Youdin, A. N., & Goodman, J. 2005, ApJ, 620, 459, doi: 10.1086/426895

Zhao, J. K., Oswalt, T. D., Willson, L. A., Wang, Q., & Zhao, G. 2012, ApJ, 746, 144, doi: 10.1088/0004-637X/746/2/144

Zhu, W., Petrovich, C., Wu, Y., Dong, S., & Xie, J. 2018, ArXiv e-prints. https://arxiv.org/abs/1802.09526

Ziegler, C., Law, N. M., Baranec, C., et al. 2016, in Proc. SPIE, Vol. 9909, Adaptive Optics Systems V, 99095U

Zorotovic, M., & Schreiber, M. R. 2013, A&A, 549, A95, doi: 10.1051/0004-6361/201220321

Zorotovic, M., Schreiber, M. R., Gänsicke, B. T., & Nebot Gómez-Morán, A. 2010, A&A, 520, A86, doi: 10.1051/0004-6361/200913658

Zucker, S., Mazeh, T., & Alexander, T. 2007, ApJ, 670, 1326, doi: 10.1086/521389

Appendix A

FULL TABLES OF PLANET CANDIDATES AND ECLIPSING BINARIES FOUND IN K2 C0-8

Table A.1: Our sample of planet candidates from C0-8.

Candidate	C#	Period (days)	t_0 (BJD - 2455000)	Duration (hours)	Depth (ppm)	R_p/R_*	R_p ($R_\oplus$)	R_* ($R_\odot$)	a/R_*	Inc. Flux ($S_\oplus$)
201147085.1	1	$1.17589^{+0.00010}_{-0.00010}$	$1810.7406^{+0.0042}_{-0.0040}$	$1.24^{+0.14}_{-0.20}$	686^{+80}_{-85}	$0.0254^{+0.0025}_{-0.0052}$	$0.86^{+0.18}_{-0.26}$	$0.309^{+0.057}_{-0.070}$	$6.3^{+2.6}_{-1.4}$	200^{+190}_{-150}
201152065.1	1	$10.6966^{+0.0020}_{-0.0021}$	$1817.3147^{+0.0072}_{-0.0069}$	$3.25^{+0.34}_{-0.43}$	557^{+56}_{-59}	$0.0226^{+0.0022}_{-0.0055}$	$1.45^{+0.18}_{-0.36}$	$0.588^{+0.041}_{-0.015}$	$21.9^{+9.6}_{-4.6}$	33^{+29}_{-14}
201155177.1	1	$6.68851^{+0.00074}_{-0.00075}$	$1814.6747^{+0.0047}_{-0.0044}$	$3.25^{+0.22}_{-0.31}$	1042^{+69}_{-72}	$0.0313^{+0.0023}_{-0.0047}$	$2.25^{+0.27}_{-0.47}$	$0.658^{+0.062}_{-0.098}$	$14.0^{+5.1}_{-2.5}$	108^{+82}_{-51}
201160662.1	1	$1.5374115^{+0.0000062}_{-0.0000061}$	$1810.49714^{+0.00019}_{-0.00019}$	$2.380^{+0.047}_{-0.046}$	14564^{+69}_{-69}	$0.259^{+0.071}_{-0.099}$	45^{+12}_{-17}	$1.599^{+0.047}_{-0.044}$	$3.41^{+0.12}_{-0.20}$	7970^{+810}_{-1110}
201176672.1	1		$1877.80380^{+0.00050}_{-0.00050}$	$14.47^{+0.19}_{-0.21}$	30600^{+110}_{-120}	$0.39^{+0.10}_{-0.14}$	$30.0^{+8.3}_{-10.6}$	$0.707^{+0.050}_{-0.050}$		
201197348.1	1	$14.9139^{+0.0018}_{-0.0020}$	$1825.1108^{+0.0045}_{-0.0042}$	$3.26^{+0.23}_{-0.32}$	2400^{+170}_{-180}	$0.0460^{+0.0038}_{-0.0078}$	$3.24^{+0.33}_{-0.56}$	$0.647^{+0.038}_{-0.024}$	$32.6^{+9.7}_{-4.8}$	$13.7^{+8.4}_{-4.2}$
201205469.1	1	$3.471136^{+0.000079}_{-0.000079}$	$1813.3563^{+0.0011}_{-0.0011}$	$2.045^{+0.072}_{-0.105}$	6650^{+160}_{-170}	$0.0775^{+0.0034}_{-0.0063}$	$5.16^{+0.49}_{-0.49}$	$0.610^{+0.051}_{-0.029}$	$12.8^{+2.8}_{-1.3}$	46^{+22}_{-11}
201205469.2	1	$2.19945^{+0.00015}_{-0.00014}$	$1810.3943^{+0.0030}_{-0.0032}$	$1.43^{+0.16}_{-0.23}$	1630^{+150}_{-160}	$0.0391^{+0.0039}_{-0.0113}$	$2.60^{+0.34}_{-0.76}$	$0.610^{+0.051}_{-0.029}$	$10.4^{+5.0}_{-2.5}$	71^{+69}_{-34}
201208431.1	1	$10.00510^{+0.00044}_{-0.00043}$	$1815.5157^{+0.0019}_{-0.0020}$	$2.923^{+0.093}_{-0.128}$	1482^{+53}_{-55}	$0.0368^{+0.0015}_{-0.0031}$	$2.29^{+0.36}_{-0.28}$	$0.572^{+0.085}_{-0.050}$	$24.6^{+5.8}_{-2.6}$	$24.0^{+13.5}_{-6.6}$
201238110.1	1	$7.90417^{+0.00091}_{-0.00148}$	$1813.6895^{+0.0106}_{-0.0049}$	$1.91^{+0.31}_{-0.53}$	2680^{+230}_{-240}	$0.0505^{+0.0050}_{-0.0129}$	$2.06^{+0.53}_{-0.56}$	$0.374^{+0.089}_{-0.035}$	$27.3^{+12.5}_{-9.5}$	$11.4^{+13.1}_{-8.5}$
201238110.2	1	$28.1696^{+0.0038}_{-0.0043}$	$1824.4836^{+0.0063}_{-0.0051}$	$3.35^{+0.19}_{-0.26}$	3160^{+230}_{-240}	$0.0540^{+0.0034}_{-0.0054}$	$2.20^{+0.54}_{-0.30}$	$0.374^{+0.089}_{-0.035}$	$61.5^{+15.2}_{-7.6}$	$2.25^{+1.92}_{-0.84}$
201239401.1	1	$0.905650^{+0.000050}_{-0.000050}$	$1810.9375^{+0.0024}_{-0.0024}$	$1.49^{+0.11}_{-0.14}$	680^{+42}_{-45}	$0.0251^{+0.0020}_{-0.0042}$	$1.57^{+0.17}_{-0.28}$	$0.576^{+0.040}_{-0.028}$	$4.13^{+1.53}_{-0.73}$	480^{+360}_{-170}
201247497.1	1	$2.75421^{+0.00012}_{-0.00012}$	$1810.8999^{+0.0020}_{-0.0019}$	$1.32^{+0.16}_{-0.25}$	7460^{+540}_{-560}	$0.087^{+0.011}_{-0.070}$	$8.4^{+1.2}_{-6.8}$	$0.890^{+0.063}_{-0.010}$	$13.7^{+5.7}_{-4.7}$	52^{+46}_{-38}
201258341.1	1	$10.50439^{+0.00059}_{-0.00061}$	$1818.9185^{+0.0026}_{-0.0026}$	$3.38^{+0.16}_{-0.21}$	402^{+16}_{-16}	$0.0183^{+0.0016}_{-0.0045}$	$1.75^{+0.15}_{-0.43}$	$0.878^{+0.018}_{-0.020}$	$21.4^{+7.7}_{-2.8}$	88^{+63}_{-23}
201259803.1	1	$1.684208^{+0.000024}_{-0.000024}$	$1810.89293^{+0.00069}_{-0.00067}$	$1.323^{+0.038}_{-0.042}$	14760^{+300}_{-320}	$0.1173^{+0.0034}_{-0.0035}$	$5.51^{+0.67}_{-0.90}$	$0.431^{+0.051}_{-0.069}$	$10.56^{+0.82}_{-0.50}$	94^{+36}_{-48}
201295312.1	1	$5.65621^{+0.00026}_{-0.00027}$	$1811.7221^{+0.0019}_{-0.0019}$	$4.296^{+0.089}_{-0.112}$	$334.2^{+9.4}_{-9.7}$	$0.01775^{+0.00066}_{-0.00165}$	$3.13^{+0.13}_{-0.30}$	$1.617^{+0.028}_{-0.030}$	$9.1^{+2.4}_{-1.1}$	580^{+310}_{-140}
201324549.1	1	$2.519386^{+0.000014}_{-0.000014}$	$1812.51211^{+0.00025}_{-0.00025}$	$1.584^{+0.037}_{-0.050}$	2036^{+21}_{-19}	$0.089^{+0.022}_{-0.039}$	$19.6^{+5.1}_{-8.7}$	$2.030^{+0.178}_{-0.068}$	$5.11^{+0.45}_{-0.56}$	2670^{+800}_{-760}
201338508.1	1	$5.73649^{+0.00033}_{-0.00034}$	$1814.5919^{+0.0025}_{-0.0025}$	$3.30^{+0.17}_{-0.18}$	1496^{+62}_{-60}	$0.073^{+0.021}_{-0.039}$	$4.2^{+1.3}_{-2.3}$	$0.532^{+0.041}_{-0.048}$	$5.32^{+0.58}_{-0.76}$	480^{+130}_{-160}
201338508.2	1	$10.93459^{+0.00088}_{-0.00105}$	$1814.5923^{+0.0039}_{-0.0034}$	$2.73^{+0.17}_{-0.29}$	1378^{+71}_{-75}	$0.0348^{+0.0031}_{-0.0079}$	$2.02^{+0.24}_{-0.49}$	$0.532^{+0.041}_{-0.048}$	$27.8^{+10.3}_{-4.3}$	$17.4^{+13.2}_{-6.3}$
201345483.1	1	$1.7292577^{+0.0000049}_{-0.0000050}$	$1811.25551^{+0.00013}_{-0.00013}$	$1.774^{+0.029}_{-0.027}$	24060^{+130}_{-130}	$0.1431^{+0.0050}_{-0.0044}$	$11.4^{+3.9}_{-1.2}$	$0.729^{+0.249}_{-0.076}$	$7.63^{+0.36}_{-0.50}$	272^{+188}_{-68}
201359834.1	1	$40.1401^{+0.0012}_{-0.0012}$	$1838.65281^{+0.00082}_{-0.00082}$	$3.023^{+0.099}_{-0.112}$	18960^{+370}_{-370}	$0.266^{+0.081}_{-0.128}$	$20.8^{+7.4}_{-10.0}$	$0.716^{+0.131}_{-0.025}$	$74.5^{+3.2}_{-4.7}$	$1.59^{+0.60}_{-0.24}$
201366540.1	1	$7.4433^{+0.0011}_{-0.0012}$	$1810.6468^{+0.0057}_{-0.0056}$	$1.63^{+0.33}_{-0.39}$	1160^{+140}_{-170}	$0.0346^{+0.0054}_{-0.0295}$	$2.73^{+0.47}_{-2.33}$	$0.724^{+0.053}_{-0.041}$	28^{+17}_{-12}	15^{+18}_{-12}
201367065.1	1	$10.05467^{+0.00011}_{-0.00011}$	$1813.41639^{+0.00043}_{-0.00043}$	$2.621^{+0.046}_{-0.067}$	1416^{+16}_{-16}	$0.0358^{+0.0012}_{-0.0031}$	$1.45^{+0.23}_{-0.21}$	$0.371^{+0.057}_{-0.043}$	$27.3^{+6.6}_{-2.9}$	$12.1^{+7.9}_{-4.8}$
201367065.2	1	$24.64671^{+0.00054}_{-0.00053}$	$1812.27612^{+0.00099}_{-0.00099}$	$3.59^{+0.12}_{-0.25}$	822^{+15}_{-16}	$0.0291^{+0.0027}_{-0.0027}$	$1.18^{+0.21}_{-0.18}$	$0.371^{+0.057}_{-0.043}$	38^{+15}_{-15}	$6.1^{+5.5}_{-5.3}$
201367065.3	1	$44.5574^{+0.0023}_{-0.0023}$	$1826.2286^{+0.0016}_{-0.0016}$	$4.50^{+0.18}_{-0.23}$	782^{+20}_{-20}	$0.0273^{+0.0029}_{-0.0048}$	$1.11^{+0.21}_{-0.23}$	$0.371^{+0.057}_{-0.043}$	61^{+21}_{-16}	$2.4^{+1.9}_{-1.5}$
201384232.1	1	$30.9403^{+0.0023}_{-0.0027}$	$1827.5014^{+0.0039}_{-0.0032}$	$5.29^{+0.19}_{-0.24}$	724^{+25}_{-27}	$0.0259^{+0.0013}_{-0.0030}$	$2.44^{+0.12}_{-0.28}$	$0.8649^{+0.0064}_{-0.0087}$	$40.6^{+13.3}_{-5.2}$	$28.4^{+18.7}_{-7.3}$
201384894.1	1	$13.1007^{+0.0035}_{-0.0037}$	$1816.049^{+0.012}_{-0.011}$	$4.82^{+0.61}_{-0.78}$	118^{+13}_{-14}	$0.0104^{+0.0014}_{-0.0075}$	$1.47^{+0.19}_{-1.07}$	$1.296^{+0.024}_{-0.049}$	$17.5^{+12.8}_{-4.4}$	91^{+134}_{-47}
201393098.1	1	$28.6911^{+0.0037}_{-0.0042}$	$1824.6074^{+0.0046}_{-0.0045}$	$7.88^{+0.26}_{-0.39}$	681^{+31}_{-33}	$0.0247^{+0.0015}_{-0.0036}$	$4.30^{+0.26}_{-0.62}$	$1.597^{+0.016}_{-0.015}$	$25.0^{+7.5}_{-3.4}$	74^{+44}_{-21}
201403446.1	1	$19.1530^{+0.0020}_{-0.0022}$	$1815.3395^{+0.0043}_{-0.0038}$	$7.01^{+0.20}_{-0.27}$	333^{+13}_{-13}	$0.01764^{+0.00086}_{-0.00210}$	$2.40^{+0.34}_{-0.53}$	$1.25^{+0.16}_{-0.23}$	$18.5^{+6.1}_{-2.6}$	200^{+160}_{-120}
201441872.1	1	$4.44044^{+0.00037}_{-0.00038}$	$1812.8841^{+0.0032}_{-0.0031}$	$2.71^{+0.18}_{-0.37}$	$141.4^{+8.8}_{-9.4}$	$0.01147^{+0.00096}_{-0.00273}$	$1.32^{+0.15}_{-0.33}$	$1.053^{+0.081}_{-0.088}$	$10.5^{+5.0}_{-2.2}$	450^{+440}_{-220}
201445392.1	1	$10.35160^{+0.00079}_{-0.00074}$	$1813.6125^{+0.0025}_{-0.0025}$	$2.46^{+0.18}_{-0.29}$	1470^{+81}_{-84}	$0.0368^{+0.0035}_{-0.0083}$	$2.86^{+0.37}_{-0.66}$	$0.712^{+0.064}_{-0.028}$	$28.3^{+12.1}_{-5.6}$	27^{+24}_{-11}
201445392.2	1	$5.06347^{+0.00026}_{-0.00023}$	$1813.0722^{+0.0019}_{-0.0021}$	$1.683^{+0.088}_{-0.108}$	993^{+50}_{-52}	$0.0299^{+0.0019}_{-0.0036}$	$2.32^{+0.26}_{-0.30}$	$0.712^{+0.064}_{-0.028}$	$21.1^{+5.8}_{-2.8}$	49^{+29}_{-14}
201445732.1	1	$11.20381^{+0.00055}_{-0.00055}$	$1817.4926^{+0.0021}_{-0.0023}$	$1.133^{+0.091}_{-0.111}$	354^{+27}_{-26}	$0.0182^{+0.0015}_{-0.0027}$	$2.18^{+0.33}_{-0.60}$	$1.10^{+0.14}_{-0.25}$	66^{+23}_{-12}	$11.3^{+9.0}_{-8.5}$
201460826.1	1	$17.3678^{+0.0047}_{-0.0053}$	$1816.7303^{+0.0090}_{-0.0090}$	$9.17^{+0.55}_{-0.82}$	211^{+12}_{-12}	$0.0139^{+0.0014}_{-0.0042}$	$1.93^{+0.39}_{-0.71}$	$1.27^{+0.22}_{-0.27}$	$12.2^{+6.6}_{-2.4}$	360^{+430}_{-260}
201465501.1	1	$18.44951^{+0.00057}_{-0.00059}$	$1822.66979^{+0.00100}_{-0.00104}$	$2.414^{+0.095}_{-0.110}$	3990^{+120}_{-130}	$0.0605^{+0.0026}_{-0.0044}$	$3.09^{+0.58}_{-0.47}$	$0.468^{+0.086}_{-0.063}$	$57.4^{+11.7}_{-5.3}$	$3.4^{+2.3}_{-1.5}$
201497682.1	1	$7.79983^{+0.00075}_{-0.00073}$	$1814.2678^{+0.0043}_{-0.0045}$	$2.99^{+0.23}_{-0.41}$	561^{+35}_{-37}	$0.0227^{+0.0023}_{-0.0072}$	$1.37^{+0.15}_{-0.44}$	$0.554^{+0.016}_{-0.023}$	$17.1^{+9.2}_{-3.6}$	88^{+95}_{-38}
201497682.2	1	$13.8394^{+0.0030}_{-0.0029}$	$1820.9555^{+0.0049}_{-0.0050}$	$2.53^{+0.34}_{-0.31}$	487^{+45}_{-46}	$0.0214^{+0.0017}_{-0.0027}$	$1.29^{+0.11}_{-0.17}$	$0.554^{+0.016}_{-0.023}$	$37.0^{+11.8}_{-8.2}$	$18.9^{+12.1}_{-8.5}$
201497682.3	1	$3.88539^{+0.00133}_{-0.00075}$	$1810.8322^{+0.0084}_{-0.0077}$	$0.16^{+0.11}_{-0.43}$	890^{+640}_{-1450}	$0.029^{+0.014}_{-0.017}$	$1.76^{+0.84}_{-1.05}$	$0.554^{+0.016}_{-0.023}$	150^{+120}_{-360}	$1.1^{+1.7}_{-5.2}$

Table A.1: Our sample of planet candidates from C0-8. (continued)

Candidate	C#	Period (days)	t_0 (BJD - 2455000)	Duration (hours)	Depth (ppm)	R_p/R_*	R_p ($R_\oplus$)	R_* ($R_\odot$)	a/R_*	Inc. Flux ($S_\oplus$)
201505350.1	1	$7.919454^{+0.000040}_{-0.000042}$	$1813.38374^{+0.00023}_{-0.00022}$	$3.261^{+0.035}_{-0.036}$	6673^{+51}_{-50}	$0.0743^{+0.0011}_{-0.0020}$	$6.67^{+0.37}_{-0.42}$	$0.823^{+0.044}_{-0.047}$	$19.53^{+1.04}_{-0.48}$	89^{+14}_{-11}
201505350.2	1	$23.81486^{+0.00050}_{-0.00055}$	$1817.27527^{+0.00090}_{-0.00087}$	$3.784^{+0.075}_{-0.097}$	2325^{+40}_{-42}	$0.0456^{+0.0012}_{-0.0030}$	$4.10^{+0.24}_{-0.36}$	$0.823^{+0.044}_{-0.047}$	$47.1^{+7.6}_{-3.3}$	$15.2^{+5.2}_{-2.8}$
201512465.1	1	$2.333123^{+0.000106}_{-0.000096}$	$1812.4806^{+0.0019}_{-0.0021}$	$1.13^{+0.15}_{-0.18}$	12700^{+1300}_{-1300}	$0.121^{+0.022}_{-0.123}$	$2.95^{+0.65}_{-3.02}$	$0.224^{+0.026}_{-0.025}$	$12.6^{+3.4}_{-6.1}$	40^{+25}_{-41}
201515470.1	1	$20.2073^{+0.0029}_{-0.0027}$	$1822.8668^{+0.0058}_{-0.0063}$	$3.71^{+0.28}_{-0.30}$	735^{+50}_{-52}	$0.0255^{+0.0021}_{-0.0044}$	$2.12^{+0.29}_{-0.37}$	$0.7624^{+0.0811}_{-0.0074}$	$37.3^{+11.8}_{-6.0}$	$17.2^{+11.5}_{-5.5}$
201528215.1	1	$6.39916^{+0.00074}_{-0.00073}$	$1816.1536^{+0.0053}_{-0.0056}$	$2.47^{+0.20}_{-0.26}$	401^{+34}_{-36}	$0.0194^{+0.0016}_{-0.0030}$	$1.48^{+0.12}_{-0.24}$	$0.7006^{+0.0045}_{-0.0300}$	$17.2^{+6.1}_{-3.2}$	114^{+80}_{-44}
201543531.1	1	$2.48038^{+0.00028}_{-0.00031}$	$1812.5024^{+0.0052}_{-0.0048}$	$1.84^{+0.32}_{-0.39}$	116^{+12}_{-13}	$0.0104^{+0.0015}_{-0.0091}$	$1.44^{+0.30}_{-1.27}$	$1.27^{+0.20}_{-0.12}$	$8.5^{+6.4}_{-2.7}$	850^{+1300}_{-580}
201546136.1	1	$1.96712^{+0.00017}_{-0.00017}$	$1810.5937^{+0.0037}_{-0.0036}$	$2.70^{+0.25}_{-0.41}$	361^{+24}_{-24}	$0.0192^{+0.0036}_{-0.0215}$	$1.73^{+0.36}_{-1.94}$	$0.826^{+0.074}_{-0.033}$	$4.4^{+3.0}_{-1.5}$	1460^{+2000}_{-980}
201546283.1	1	$6.771375^{+0.000053}_{-0.000053}$	$1812.84481^{+0.00034}_{-0.00034}$	$2.856^{+0.051}_{-0.063}$	2804^{+22}_{-23}	$0.0496^{+0.0015}_{-0.0024}$	$5.05^{+0.42}_{-0.31}$	$0.932^{+0.072}_{-0.034}$	$17.1^{+2.8}_{-1.8}$	96^{+35}_{-22}
201549860.1	1	$5.60871^{+0.00028}_{-0.00023}$	$1812.1166^{+0.0015}_{-0.0017}$	$1.798^{+0.085}_{-0.118}$	938^{+55}_{-54}	$0.0289^{+0.0020}_{-0.0040}$	$1.90^{+0.14}_{-0.30}$	$0.603^{+0.015}_{-0.042}$	$21.7^{+6.2}_{-2.9}$	42^{+24}_{-13}
201549860.2	1	$2.39901^{+0.00022}_{-0.00020}$	$1810.5969^{+0.0029}_{-0.0029}$	$1.99^{+0.13}_{-0.15}$	404^{+30}_{-32}	$0.0192^{+0.0015}_{-0.0028}$	$1.27^{+0.10}_{-0.21}$	$0.603^{+0.015}_{-0.042}$	$8.2^{+2.6}_{-1.3}$	300^{+190}_{-100}
201561956.1	1	$13.2359^{+0.0030}_{-0.0031}$	$1814.500^{+0.012}_{-0.011}$	$2.64^{+0.30}_{-0.38}$	469^{+52}_{-58}	$0.0208^{+0.0022}_{-0.0046}$	$2.09^{+0.23}_{-0.48}$	$0.924^{+0.033}_{-0.050}$	$33.4^{+12.9}_{-7.3}$	43^{+34}_{-20}
201565013.1	1	$8.63795^{+0.00013}_{-0.00013}$	$1811.42828^{+0.00066}_{-0.00066}$	$2.047^{+0.073}_{-0.081}$	27380^{+500}_{-500}	$0.317^{+0.094}_{-0.150}$	$15.1^{+4.7}_{-7.3}$	$0.438^{+0.044}_{-0.040}$	$26.14^{+0.95}_{-1.39}$	$14.9^{+4.4}_{-4.2}$
201577035.1	1	$19.30481^{+0.00056}_{-0.00055}$	$1819.5804^{+0.0011}_{-0.0012}$	$3.806^{+0.064}_{-0.090}$	1691^{+28}_{-28}	$0.0379^{+0.0013}_{-0.0032}$	$2.98^{+0.38}_{-0.84}$	$0.721^{+0.090}_{-0.194}$	$37.5^{+6.8}_{-2.7}$	45^{+20}_{-25}
201577112.1	1	$44.3940^{+0.0024}_{-0.0024}$	$1826.0074^{+0.0017}_{-0.0018}$	$2.79^{+0.14}_{-0.23}$	15170^{+640}_{-680}	$0.1174^{+0.0070}_{-0.0114}$	$4.07^{+1.02}_{-0.98}$	$0.318^{+0.077}_{-0.070}$	123^{+27}_{-16}	$0.52^{+0.44}_{-0.37}$
201588420.1	1	$3.29163^{+0.00015}_{-0.00015}$	$1813.4812^{+0.0020}_{-0.0020}$	$1.290^{+0.092}_{-0.128}$	394^{+26}_{-28}	$0.0189^{+0.0015}_{-0.0037}$	$1.17^{+0.10}_{-0.24}$	$0.567^{+0.019}_{-0.031}$	$17.1^{+6.6}_{-3.0}$	92^{+71}_{-33}
201596316.1	1	$39.8642^{+0.0055}_{-0.0057}$	$1829.8511^{+0.0039}_{-0.0037}$	$5.80^{+0.30}_{-0.43}$	916^{+41}_{-43}	$0.0298^{+0.0030}_{-0.0053}$	$2.92^{+0.30}_{-0.53}$	$0.896^{+0.020}_{-0.040}$	43^{+19}_{-11}	$15.3^{+13.6}_{-8.2}$
201596733.1	1	$2.896528^{+0.000061}_{-0.000060}$	$1812.10578^{+0.00095}_{-0.00105}$	$1.598^{+0.075}_{-0.132}$	3274^{+82}_{-87}	$0.0551^{+0.0037}_{-0.0072}$	$1.45^{+0.29}_{-0.29}$	$0.242^{+0.045}_{-0.036}$	$12.6^{+4.1}_{-2.2}$	39^{+33}_{-22}
201613023.1	1	$8.28192^{+0.00037}_{-0.00036}$	$1815.3732^{+0.0020}_{-0.0020}$	$4.14^{+0.12}_{-0.20}$	481^{+14}_{-15}	$0.0210^{+0.0011}_{-0.0032}$	$2.48^{+0.42}_{-0.41}$	$1.084^{+0.177}_{-0.070}$	$13.7^{+5.3}_{-1.9}$	249^{+210}_{-78}
201617985.1	1	$7.28076^{+0.00034}_{-0.00038}$	$1812.6405^{+0.0020}_{-0.0020}$	$1.87^{+0.35}_{-0.19}$	1293^{+74}_{-74}	$0.060^{+0.027}_{-0.042}$	$2.6^{+1.2}_{-1.8}$	$0.3990^{+0.0430}_{-0.0080}$	$12.0^{+1.9}_{-21.3}$	59^{+26}_{-209}
201619647.1	1	$4.58328^{+0.00034}_{-0.00033}$	$1813.6033^{+0.0039}_{-0.0041}$	$2.21^{+0.17}_{-0.21}$	1520^{+100}_{-120}	$0.0372^{+0.0027}_{-0.0050}$	$2.21^{+0.27}_{-0.38}$	$0.545^{+0.054}_{-0.056}$	$14.5^{+4.2}_{-2.3}$	52^{+32}_{-20}
201619647.2	1	$1.65336^{+0.00012}_{-0.00011}$	$1810.8473^{+0.0031}_{-0.0034}$	$1.61^{+0.14}_{-0.24}$	686^{+49}_{-52}	$0.0254^{+0.0022}_{-0.0054}$	$1.51^{+0.20}_{-0.36}$	$0.545^{+0.054}_{-0.056}$	$6.8^{+3.0}_{-1.5}$	240^{+220}_{-110}
201635132.1	1		$1826.98524^{+0.00037}_{-0.00037}$	$5.16^{+0.11}_{-0.12}$	31770^{+240}_{-240}	$0.38^{+0.11}_{-0.15}$	$24.9^{+7.5}_{-9.8}$	$0.6009^{+0.0627}_{-0.0072}$		
201635569.1	1	$8.36779^{+0.00011}_{-0.00011}$	$1811.45284^{+0.00053}_{-0.00054}$	$2.330^{+0.077}_{-0.064}$	12260^{+180}_{-190}	$0.1102^{+0.0057}_{-0.0071}$	$8.51^{+0.48}_{-0.57}$	$0.708^{+0.015}_{-0.012}$	$23.7^{+2.2}_{-4.0}$	$17.6^{+3.5}_{-6.1}$
201637175.1	1	$0.3810654^{+0.0000019}_{-0.0000018}$	$1810.35561^{+0.00018}_{-0.00018}$	$0.586^{+0.015}_{-0.023}$	6240^{+150}_{-170}	$0.0774^{+0.0044}_{-0.0059}$	$5.40^{+0.73}_{-0.46}$	$0.640^{+0.079}_{-0.024}$	$4.44^{+0.58}_{-0.71}$	480^{+170}_{-160}
201647718.1	1	$31.6551^{+0.0030}_{-0.0029}$	$1825.6892^{+0.0038}_{-0.0037}$	$4.64^{+0.23}_{-0.31}$	999^{+51}_{-52}	$0.0293^{+0.0025}_{-0.0062}$	$2.48^{+0.21}_{-0.52}$	$0.7740^{+0.0080}_{-0.0104}$	$46.8^{+17.1}_{-7.1}$	$11.6^{+8.5}_{-3.5}$
201650711.1	1	$5.54583^{+0.00067}_{-0.00069}$	$1814.8943^{+0.0047}_{-0.0044}$	$2.09^{+0.18}_{-0.26}$	152^{+15}_{-16}	$0.0119^{+0.0011}_{-0.0023}$	$0.441^{+0.068}_{-0.106}$	$0.340^{+0.041}_{-0.047}$	$17.4^{+6.8}_{-3.5}$	26^{+23}_{-15}
201654498.1	1	$18.4420^{+0.0064}_{-0.0062}$	$1816.9638^{+0.0079}_{-0.0083}$	$4.91^{+1.30}_{-0.95}$	902^{+84}_{-89}	$0.037^{+0.012}_{-0.039}$	$2.92^{+0.96}_{-3.05}$	$0.717^{+0.055}_{-0.029}$	$14.4^{+5.9}_{-19.4}$	74^{+61}_{-200}
201666578.1	1	$4.13339^{+0.00058}_{-0.00048}$	$1813.1309^{+0.0056}_{-0.0050}$	$1.70^{+0.40}_{-0.60}$	1030^{+160}_{-170}	$0.0327^{+0.0054}_{-0.0296}$	$1.11^{+0.28}_{-1.03}$	$0.312^{+0.058}_{-0.059}$	$13.5^{+7.5}_{-8.6}$	43^{+54}_{-60}
201677835.1	1	$20.5107^{+0.0020}_{-0.0020}$	$1817.4772^{+0.0039}_{-0.0036}$	$3.39^{+0.20}_{-0.29}$	1104^{+66}_{-69}	$0.0309^{+0.0027}_{-0.0071}$	$2.23^{+0.23}_{-0.54}$	$0.662^{+0.035}_{-0.051}$	$42.0^{+15.9}_{-6.2}$	$13.1^{+10.0}_{-4.4}$
201690311.1	1	$2.770522^{+0.000097}_{-0.000097}$	$1812.7938^{+0.0016}_{-0.0016}$	$2.348^{+0.096}_{-0.142}$	2090^{+83}_{-80}	$0.0420^{+0.0028}_{-0.0066}$	$3.19^{+0.31}_{-0.52}$	$0.696^{+0.049}_{-0.030}$	$8.50^{+2.29}_{-0.97}$	222^{+124}_{-55}
201713348.1	1	$1.422602^{+0.000019}_{-0.000019}$	$1810.89245^{+0.00082}_{-0.00060}$	$1.123^{+0.033}_{-0.031}$	345^{+10}_{-11}	$0.01770^{+0.00073}_{-0.00190}$	$1.407^{+0.073}_{-0.153}$	$0.729^{+0.023}_{-0.012}$	$9.03^{+2.28}_{-0.81}$	273^{+139}_{-50}
201717274.1	1	$3.52725^{+0.00030}_{-0.00030}$	$1813.4405^{+0.0033}_{-0.0033}$	$1.68^{+0.17}_{-0.29}$	1990^{+160}_{-170}	$0.0430^{+0.0043}_{-0.0140}$	$1.21^{+0.34}_{-0.52}$	$0.257^{+0.067}_{-0.073}$	$14.2^{+7.2}_{-3.3}$	36^{+46}_{-34}
201732557.1	1	$6.6620^{+0.0012}_{-0.0011}$	$1814.0819^{+0.0070}_{-0.0065}$	$3.08^{+0.37}_{-0.72}$	946^{+97}_{-102}	$0.0302^{+0.0037}_{-0.0161}$	$1.59^{+0.37}_{-0.93}$	$0.483^{+0.094}_{-0.116}$	$13.8^{+8.4}_{-4.1}$	64^{+87}_{-61}
201736247.1	1	$11.81004^{+0.00060}_{-0.00058}$	$1811.8513^{+0.0022}_{-0.0022}$	$2.403^{+0.095}_{-0.119}$	1329^{+53}_{-54}	$0.0354^{+0.0016}_{-0.0028}$	$3.08^{+0.44}_{-0.56}$	$0.80^{+0.11}_{-0.13}$	$35.4^{+9.3}_{-3.8}$	$20.5^{+12.2}_{-8.1}$
201754305.1	1	$7.62117^{+0.00056}_{-0.00053}$	$1811.6773^{+0.0035}_{-0.0039}$	$2.19^{+0.13}_{-0.16}$	1041^{+58}_{-61}	$0.0314^{+0.0020}_{-0.0033}$	$1.87^{+0.13}_{-0.21}$	$0.544^{+0.012}_{-0.021}$	$24.1^{+7.6}_{-3.7}$	47^{+29}_{-15}
201754305.2	1	$19.0702^{+0.0022}_{-0.0025}$	$1828.5663^{+0.0047}_{-0.0044}$	$3.37^{+0.26}_{-0.52}$	1065^{+79}_{-82}	$0.0310^{+0.0032}_{-0.0118}$	$1.84^{+0.20}_{-0.70}$	$0.544^{+0.012}_{-0.021}$	$37.8^{+20.9}_{-7.7}$	$19.0^{+21.0}_{-7.9}$
201775904.1	1		$1835.54205^{+0.00021}_{-0.00022}$	$4.808^{+0.056}_{-0.069}$	13972^{+53}_{-53}	$0.253^{+0.067}_{-0.094}$	35^{+11}_{-13}	$1.266^{+0.202}_{-0.016}$		
201779067.1	1	$27.242808^{+0.000071}_{-0.000074}$	$1820.25998^{+0.00011}_{-0.00010}$	$6.566^{+0.029}_{-0.032}$	37137^{+54}_{-113}	$0.336^{+0.068}_{-0.174}$	93^{+19}_{-48}	$2.54^{+0.12}_{-0.15}$	$26.74^{+0.37}_{-0.59}$	$67.4^{+7.0}_{-9.0}$

Table A.1: Our sample of planet candidates from C0-8. (continued)

Candidate	C#	Period (days)	t_0 (BJD - 2455000)	Duration (hours)	Depth (ppm)	R_p/R_*	R_p ($R_\oplus$)	R_* ($R_\odot$)	a/R_*	Inc. Flux ($S_\oplus$)
201785059.1	1	$1.395336^{+0.000052}_{-0.000056}$	$1811.5947^{+0.0018}_{-0.0017}$	$1.232^{+0.076}_{-0.097}$	665^{+35}_{-37}	$0.0248^{+0.0017}_{-0.0035}$	$0.76^{+0.15}_{-0.24}$	$0.280^{+0.053}_{-0.080}$	$7.8^{+2.5}_{-1.2}$	120^{+100}_{-100}
201793642.1	1	$15.3797^{+0.0019}_{-0.0018}$	$1817.0838^{+0.0042}_{-0.0043}$	$2.08^{+0.29}_{-0.38}$	2700^{+440}_{-440}	$0.054^{+0.010}_{-0.055}$	$1.98^{+0.59}_{-2.06}$	$0.336^{+0.077}_{-0.060}$	42^{+20}_{-21}	$4.6^{+5.3}_{-5.2}$
201828749.1	1	$33.5116^{+0.0015}_{-0.0016}$	$1813.1520^{+0.0019}_{-0.0018}$	$5.35^{+0.60}_{-0.22}$	732^{+19}_{-20}	$0.0302^{+0.0032}_{-0.0033}$	$2.89^{+0.41}_{-0.38}$	$0.875^{+0.083}_{-0.067}$	$21.3^{+2.3}_{-20.7}$	94^{+27}_{-184}
201833600.1	1	$8.75198^{+0.00060}_{-0.00063}$	$1819.0859^{+0.0033}_{-0.0029}$	$3.00^{+0.16}_{-0.27}$	1337^{+63}_{-67}	$0.0331^{+0.0028}_{-0.0090}$	$2.29^{+0.24}_{-0.64}$	$0.634^{+0.039}_{-0.045}$	$20.6^{+7.7}_{-2.7}$	36^{+27}_{-11}
201833600.2	1	$3.96165^{+0.00035}_{-0.00034}$	$1813.0387^{+0.0037}_{-0.0038}$	$2.16^{+0.14}_{-0.17}$	485^{+36}_{-38}	$0.0214^{+0.0014}_{-0.0026}$	$1.48^{+0.14}_{-0.21}$	$0.634^{+0.039}_{-0.045}$	$12.4^{+4.0}_{-2.0}$	100^{+66}_{-36}
201837434.1	1	$6.97251^{+0.00080}_{-0.00093}$	$1814.3554^{+0.0065}_{-0.0051}$	$2.81^{+0.25}_{-0.56}$	916^{+64}_{-69}	$0.0294^{+0.0031}_{-0.0114}$	$2.01^{+0.21}_{-0.78}$	$0.6252^{+0.0061}_{-0.0203}$	$16.0^{+9.5}_{-4.0}$	64^{+75}_{-32}
201841433.1	1	$12.3389^{+0.0016}_{-0.0017}$	$1819.8344^{+0.0054}_{-0.0045}$	$2.76^{+0.25}_{-0.44}$	1021^{+86}_{-90}	$0.0308^{+0.0031}_{-0.0087}$	$2.11^{+0.23}_{-0.61}$	$0.628^{+0.025}_{-0.043}$	$29.5^{+14.7}_{-6.7}$	31^{+31}_{-15}
201841433.2	1	$4.16888^{+0.00050}_{-0.00056}$	$1811.6338^{+0.0062}_{-0.0056}$	$2.40^{+0.27}_{-0.34}$	447^{+47}_{-50}	$0.0205^{+0.0020}_{-0.0047}$	$1.41^{+0.15}_{-0.34}$	$0.628^{+0.025}_{-0.043}$	$11.4^{+5.2}_{-2.6}$	207^{+190}_{-98}
201846824.1	1	$2.89465^{+0.00036}_{-0.00034}$	$1810.6167^{+0.0054}_{-0.0055}$	$1.43^{+0.19}_{-0.25}$	551^{+63}_{-69}	$0.0228^{+0.0024}_{-0.0057}$	$1.75^{+0.24}_{-0.46}$	$0.702^{+0.059}_{-0.049}$	$13.2^{+6.3}_{-3.4}$	67^{+64}_{-36}
201855371.1	1	$17.96832^{+0.00085}_{-0.00090}$	$1817.9472^{+0.0021}_{-0.0019}$	$2.59^{+0.13}_{-0.17}$	915^{+37}_{-39}	$0.0293^{+0.0016}_{-0.0034}$	$1.78^{+0.31}_{-0.29}$	$0.556^{+0.090}_{-0.063}$	$47.7^{+16.8}_{-7.2}$	$6.6^{+5.1}_{-2.5}$
201856786.1	1	$3.83794^{+0.00041}_{-0.00039}$	$1812.6581^{+0.0042}_{-0.0042}$	$2.12^{+0.18}_{-0.25}$	315^{+25}_{-26}	$0.0172^{+0.0015}_{-0.0030}$	$1.51^{+0.33}_{-0.27}$	$0.809^{+0.162}_{-0.042}$	$11.9^{+4.6}_{-2.4}$	66^{+57}_{-27}
201856786.2	1	$5.24086^{+0.00094}_{-0.00147}$	$1810.7424^{+0.0172}_{-0.0096}$	$2.57^{+0.28}_{-0.34}$	292^{+33}_{-34}	$0.0166^{+0.0015}_{-0.0027}$	$1.46^{+0.32}_{-0.25}$	$0.809^{+0.162}_{-0.042}$	$13.5^{+5.0}_{-2.8}$	51^{+43}_{-22}
201862715.1	1	$2.6556760^{+0.0000017}_{-0.0000017}$	$1812.949114^{+0.000027}_{-0.000027}$	$2.6171^{+0.0050}_{-0.0049}$	14877^{+16}_{-17}	$0.11512^{+0.00083}_{-0.00081}$	$11.1^{+1.0}_{-11.1}$	$0.884^{+0.083}_{-0.884}$	$7.798^{+0.091}_{-0.110}$	590^{+170}_{-1680}
201896171.1	1	$8.91058^{+0.00088}_{-0.00087}$	$1819.0428^{+0.0038}_{-0.0039}$	$2.87^{+0.35}_{-0.61}$	592^{+37}_{-38}	$0.0249^{+0.0041}_{-0.0201}$	$2.80^{+0.76}_{-2.26}$	$1.028^{+0.222}_{-0.033}$	$18.1^{+11.6}_{-7.2}$	116^{+157}_{-94}
201912552.1	1	$32.94171^{+0.00080}_{-0.00084}$	$1836.17194^{+0.00059}_{-0.00064}$	$2.629^{+0.056}_{-0.067}$	3098^{+62}_{-65}	$0.0517^{+0.0017}_{-0.0038}$	$1.40^{+0.29}_{-0.18}$	$0.249^{+0.050}_{-0.027}$	$94.3^{+14.6}_{-6.6}$	$0.70^{+0.46}_{-0.24}$
201920032.1	1	$28.2671^{+0.0020}_{-0.0021}$	$1833.2111^{+0.0026}_{-0.0026}$	$4.22^{+0.14}_{-0.17}$	757^{+32}_{-34}	$0.0263^{+0.0013}_{-0.0029}$	$2.94^{+0.78}_{-0.34}$	$1.028^{+0.266}_{-0.030}$	$47.3^{+12.8}_{-5.3}$	$16.9^{+12.6}_{-4.0}$
201920032.2	1	$4.73172^{+0.00035}_{-0.00037}$	$1811.3374^{+0.0032}_{-0.0034}$	$1.20^{+0.16}_{-0.17}$	245^{+31}_{-33}	$0.0152^{+0.0015}_{-0.0028}$	$1.70^{+0.47}_{-0.32}$	$1.028^{+0.266}_{-0.030}$	$26.0^{+10.0}_{-6.0}$	56^{+51}_{-26}
201923289.1	1	$0.782027^{+0.000045}_{-0.000052}$	$1810.3854^{+0.0028}_{-0.0025}$	$1.43^{+0.13}_{-0.19}$	268^{+20}_{-21}	$0.0156^{+0.0015}_{-0.0041}$	$1.60^{+0.25}_{-0.42}$	$0.940^{+0.113}_{-0.021}$	$3.61^{+1.64}_{-0.74}$	2200^{+2070}_{-910}
201925324.1	1	$15.4769^{+0.0015}_{-0.0015}$	$1819.2588^{+0.0037}_{-0.0038}$	$3.53^{+0.21}_{-0.27}$	1730^{+110}_{-120}	$0.0401^{+0.0026}_{-0.0046}$	$2.89^{+0.23}_{-0.38}$	$0.660^{+0.032}_{-0.043}$	$30.9^{+9.1}_{-4.4}$	$15.7^{+9.4}_{-5.0}$
201927336.1	1	$6.45027^{+0.00029}_{-0.00032}$	$1811.9392^{+0.0026}_{-0.0022}$	$1.62^{+0.10}_{-0.14}$	606^{+32}_{-33}	$0.0235^{+0.0018}_{-0.0039}$	$2.29^{+0.20}_{-0.38}$	$0.894^{+0.033}_{-0.012}$	$27.1^{+9.5}_{-4.4}$	48^{+34}_{-16}
202060800.1	0	$3.262038^{+0.000012}_{-0.000012}$	$1773.678726^{+0.000066}_{-0.000065}$	$2.253^{+0.027}_{-0.031}$	24289^{+50}_{-47}	$0.277^{+0.060}_{-0.141}$			$8.58^{+0.22}_{-0.57}$	
202065819.1	0	$5.74372^{+0.00017}_{-0.00017}$	$1776.25053^{+0.00045}_{-0.00045}$	$4.205^{+0.089}_{-0.093}$	7985^{+53}_{-53}	$0.205^{+0.054}_{-0.074}$			$6.42^{+0.32}_{-0.41}$	
202066537.1	0	$6.905053^{+0.000092}_{-0.000092}$	$1775.09723^{+0.00023}_{-0.00023}$	$3.873^{+0.063}_{-0.064}$	25067^{+97}_{-98}	$0.352^{+0.099}_{-0.128}$			$11.06^{+0.26}_{-0.47}$	
202066811.1	0	$1.696374^{+0.000012}_{-0.000012}$	$1773.58891^{+0.00014}_{-0.00014}$	$3.729^{+0.020}_{-0.022}$	37790^{+100}_{-100}	$0.1803^{+0.0037}_{-0.0044}$	$35.3^{+3.7}_{-1.0}$	$1.793^{+0.185}_{-0.029}$	$3.978^{+0.071}_{-0.074}$	6700^{+1900}_{-1300}
202071289.1	0	$3.046136^{+0.000021}_{-0.000022}$	$1774.35565^{+0.00014}_{-0.00013}$	$2.521^{+0.028}_{-0.036}$	37780^{+200}_{-210}	$0.41^{+0.11}_{-0.15}$	76^{+26}_{-28}	$1.698^{+0.350}_{-0.060}$	$7.93^{+0.15}_{-0.30}$	613^{+255}_{-68}
202071401.1	0	$3.23792^{+0.00025}_{-0.00026}$	$1772.2298^{+0.0015}_{-0.0014}$	$1.446^{+0.074}_{-0.105}$	431^{+19}_{-20}	$0.0200^{+0.0013}_{-0.0030}$			$15.1^{+5.2}_{-2.4}$	
202071725.1	0	$1.42637^{+0.00012}_{-0.00012}$	$1773.3447^{+0.0015}_{-0.0016}$	$2.329^{+0.102}_{-0.098}$	$304.9^{+8.5}_{-8.6}$	$0.01422^{+0.00099}_{-0.00278}$	$6.64^{+0.52}_{-1.33}$	$4.28^{+0.16}_{-0.20}$	$4.45^{+0.76}_{-0.34}$	8000^{+2800}_{-1500}
202073152.1	0	$0.720917^{+0.000938}_{-0.000080}$	$1772.6124^{+0.0059}_{-0.0037}$	$0.029^{+0.019}_{-0.019}$	19800^{+3700}_{-3700}	$0.140^{+0.016}_{-0.013}$			210^{+87}_{-444}	
202073154.1	0	$0.713918^{+0.000023}_{-0.000020}$	$1772.16656^{+0.00051}_{-0.00066}$	$6.7753^{+0.0101}_{-0.0098}$	33990^{+430}_{-490}	$0.1842^{+0.0010}_{-0.0013}$	$80.6^{+9.6}_{-4.8}$	$4.01^{+0.48}_{-0.24}$	$0.9531^{+0.0021}_{-0.0021}$	50700^{+13200}_{-8000}
202083828.1	0	$14.56594^{+0.00093}_{-0.00090}$	$1775.1661^{+0.0012}_{-0.0012}$	$4.71^{+0.11}_{-0.26}$	2589^{+49}_{-53}	$0.0490^{+0.0023}_{-0.0043}$			$22.4^{+8.4}_{-2.6}$	
202084970.1	0	$2.86136^{+0.00086}_{-0.00091}$	$1774.8909^{+0.0057}_{-0.0055}$	$2.16^{+0.21}_{-0.26}$	1169^{+91}_{-97}	$0.0330^{+0.0025}_{-0.0046}$			$9.1^{+2.8}_{-1.7}$	
202085553.1	0	$3.10622^{+0.00049}_{-0.00050}$	$1772.4445^{+0.0032}_{-0.0030}$	$2.71^{+0.26}_{-0.26}$	1950^{+110}_{-110}	$0.101^{+0.030}_{-0.039}$			$3.80^{+0.47}_{-0.58}$	
202085597.1	0	$1.814553^{+0.000052}_{-0.000052}$	$1773.01721^{+0.00054}_{-0.00056}$	$3.436^{+0.038}_{-0.044}$	12890^{+140}_{-130}	$0.181^{+0.036}_{-0.092}$			$2.54^{+0.13}_{-0.16}$	
202085698.1	0	$17.1541^{+0.0017}_{-0.0016}$	$1778.8849^{+0.0012}_{-0.0013}$	$8.48^{+0.20}_{-0.17}$	19480^{+190}_{-180}	$0.354^{+0.080}_{-0.109}$			$12.91^{+0.31}_{-0.87}$	
202085934.1	0	$12.1507^{+0.0023}_{-0.0022}$	$1779.5445^{+0.0029}_{-0.0031}$	$3.85^{+0.15}_{-0.20}$	290^{+13}_{-14}	$0.01639^{+0.00095}_{-0.00233}$	$1.48^{+0.14}_{-0.23}$	$0.830^{+0.059}_{-0.045}$	$21.2^{+7.3}_{-3.2}$	64^{+45}_{-20}
202088212.1	0	$2.620799^{+0.000030}_{-0.000032}$	$1772.29873^{+0.00018}_{-0.00017}$	$2.619^{+0.040}_{-0.042}$	9410^{+38}_{-36}	$0.195^{+0.048}_{-0.082}$	37^{+10}_{-15}	$1.725^{+0.208}_{-0.071}$	$4.69^{+0.20}_{-0.33}$	2430^{+620}_{-400}
202090723.1	0	$6.14818^{+0.00032}_{-0.00032}$	$1777.67006^{+0.00084}_{-0.00078}$	$3.885^{+0.047}_{-0.072}$	1513^{+19}_{-20}	$0.03756^{+0.00079}_{-0.00211}$			$11.80^{+2.28}_{-0.73}$	
202090737.1	0	$1.49761^{+0.00012}_{-0.00012}$	$1772.3826^{+0.0015}_{-0.0015}$	$2.711^{+0.076}_{-0.105}$	$222.8^{+6.1}_{-6.3}$	$0.01452^{+0.00067}_{-0.00183}$			$3.70^{+1.35}_{-0.55}$	

Table A.1: Our sample of planet candidates from C0-8. (continued)

Candidate	C#	Period (days)	t_0 (BJD - 2455000)	Duration (hours)	Depth (ppm)	R_p/R_*	R_p ($R_\oplus$)	R_* ($R_\odot$)	a/R_*	Inc. Flux ($S_\oplus$)
202091388.1	0	$6.48167^{+0.00069}_{-0.00068}$	$1773.3779^{+0.0016}_{-0.0016}$	$2.82^{+0.12}_{-0.16}$	1249^{+38}_{-39}	$0.0344^{+0.0021}_{-0.0041}$	$3.46^{+0.22}_{-0.43}$	$0.922^{+0.017}_{-0.031}$	$15.5^{+5.4}_{-2.7}$	152^{+107}_{-55}
202092559.1	0	$0.66870^{+0.00012}_{-0.00011}$	$1772.2339^{+0.0027}_{-0.0030}$	$2.17^{+0.14}_{-0.21}$	$119.6^{+7.5}_{-8.1}$	$0.01048^{+0.00082}_{-0.00190}$	$2.22^{+0.20}_{-0.41}$	$1.942^{+0.092}_{-0.085}$	$2.03^{+0.76}_{-0.36}$	13800^{+10500}_{-5100}
202092782.1	0	$13.34610^{+0.00043}_{-0.00044}$	$1779.48747^{+0.00038}_{-0.00037}$	$2.657^{+0.051}_{-0.063}$	5465^{+37}_{-37}	$0.151^{+0.037}_{-0.060}$	42^{+10}_{-17}	$2.575^{+0.110}_{-0.037}$	$20.3^{+1.3}_{-1.7}$	170^{+27}_{-31}
202093020.1	0	$4.137370^{+0.000092}_{-0.000095}$	$1774.31149^{+0.00039}_{-0.00038}$	$2.238^{+0.067}_{-0.069}$	10490^{+110}_{-110}	$0.217^{+0.061}_{-0.086}$	$24.5^{+8.6}_{-10.1}$	$1.03^{+0.22}_{-0.13}$	$8.98^{+0.43}_{-0.54}$	270^{+140}_{-110}
202093968.1	0	$2.469851^{+0.000080}_{-0.000083}$	$1774.54812^{+0.00062}_{-0.00058}$	$2.658^{+0.203}_{-0.075}$	1234^{+85}_{-39}	$0.0406^{+0.0117}_{-0.0063}$	$6.6^{+2.0}_{-1.1}$	$1.479^{+0.127}_{-0.086}$	$3.32^{+0.43}_{-4.10}$	9400^{+2900}_{-23200}
202094740.1	0	$0.690458^{+0.000020}_{-0.000020}$	$1772.40441^{+0.00076}_{-0.00074}$	$5.890^{+0.086}_{-0.075}$	6655^{+66}_{-65}	$0.256^{+0.059}_{-0.060}$			$0.5988^{+0.0065}_{-0.0360}$	
202126849.1	0	$3.799878^{+0.000014}_{-0.000014}$	$1774.286563^{+0.000060}_{-0.000061}$	$1.762^{+0.093}_{-0.045}$	25600^{+400}_{-290}	$0.1558^{+0.0205}_{-0.0067}$	$11.8^{+1.8}_{-1.0}$	$0.693^{+0.048}_{-0.054}$	$15.5^{+1.3}_{-3.6}$	56^{+13}_{-28}
202126852.1	0	$2.790862^{+0.000015}_{-0.000016}$	$1774.09164^{+0.00011}_{-0.00011}$	$2.314^{+0.027}_{-0.021}$	9773^{+42}_{-36}	$0.1065^{+0.0021}_{-0.0037}$	$16.72^{+1.98}_{-0.86}$	$1.439^{+0.168}_{-0.054}$	$6.81^{+0.26}_{-0.23}$	1720^{+420}_{-180}
202126853.1	0	$21.17051^{+0.00029}_{-0.00028}$	$1780.92731^{+0.00022}_{-0.00026}$	$5.003^{+0.051}_{-0.062}$	15771^{+39}_{-38}	$0.295^{+0.073}_{-0.088}$	81^{+20}_{-25}	$2.536^{+0.076}_{-0.189}$	$22.47^{+0.62}_{-0.98}$	130^{+12}_{-23}
202126884.1	0	$5.319075^{+0.000090}_{-0.000089}$	$1773.95146^{+0.00026}_{-0.00026}$	$6.755^{+0.035}_{-0.032}$	7124^{+25}_{-25}	$0.08027^{+0.00092}_{-0.00186}$	$20.0^{+1.6}_{-1.7}$	$2.28^{+0.19}_{-0.18}$	$5.94^{+0.18}_{-0.25}$	1800^{+340}_{-350}
202126887.1	0	$12.866412^{+0.000078}_{-0.000078}$	$1777.24074^{+0.00010}_{-0.00010}$	$3.120^{+0.034}_{-0.043}$	31311^{+76}_{-74}	$0.342^{+0.091}_{-0.156}$	61^{+16}_{-28}	$1.642^{+0.029}_{-0.025}$	$25.80^{+0.48}_{-0.82}$	$75.6^{+5.5}_{-6.6}$
202137637.1	0	$6.62230^{+0.00085}_{-0.00155}$	$1777.4417^{+0.0053}_{-0.0023}$	$1.23^{+0.13}_{-0.18}$	3480^{+210}_{-240}	$0.0573^{+0.0058}_{-0.0231}$			$36.6^{+17.3}_{-9.0}$	
202139294.1	0	$0.5217136^{+0.0000031}_{-0.0000031}$	$1772.253278^{+0.000097}_{-0.000097}$	$4.014^{+0.040}_{-0.050}$	14286^{+21}_{-21}	$0.367^{+0.059}_{-0.071}$	452^{+78}_{-96}	$11.27^{+0.69}_{-1.00}$	$0.820^{+0.060}_{-0.044}$	27100^{+5800}_{-6200}
202600948.1	2	$5.98950^{+0.00028}_{-0.00026}$	$1899.2199^{+0.0019}_{-0.0020}$	$1.84^{+0.17}_{-0.36}$	354^{+17}_{-17}	$0.0182^{+0.0023}_{-0.0106}$	$2.04^{+0.39}_{-1.21}$	$1.03^{+0.15}_{-0.11}$	$20.8^{+14.1}_{-5.1}$	119^{+165}_{-63}
202688980.1	2	$1.45556515^{+0.00000091}_{-0.00000088}$	$1895.183454^{+0.000027}_{-0.000028}$	$2.550^{+0.012}_{-0.014}$	27008^{+21}_{-19}	$0.318^{+0.067}_{-0.137}$	71^{+15}_{-34}	$2.043^{+0.051}_{-0.435}$	$3.380^{+0.051}_{-0.130}$	3130^{+200}_{-1360}
202710713.1	2	$3.32550^{+0.00017}_{-0.00017}$	$1895.3803^{+0.0018}_{-0.0018}$	$7.10^{+0.25}_{-0.22}$	1179^{+23}_{-23}	$0.116^{+0.029}_{-0.030}$	1080^{+320}_{-350}	85^{+14}_{-17}	$1.657^{+0.080}_{-0.093}$	3200^{+1500}_{-1800}
202774883.1	2	$13.1426^{+0.0028}_{-0.0025}$	$1906.5997^{+0.0064}_{-0.0078}$	$5.72^{+0.55}_{-0.58}$	5290^{+310}_{-310}	$0.130^{+0.044}_{-0.075}$	200^{+150}_{-180}	$13.9^{+9.5}_{-9.4}$	$9.6^{+1.2}_{-2.0}$	210^{+410}_{-420}
202821899.1	2	$4.47471^{+0.00011}_{-0.00011}$	$1895.68674^{+0.00100}_{-0.00099}$	$3.033^{+0.081}_{-0.102}$	1730^{+30}_{-29}	$0.081^{+0.020}_{-0.037}$	$22.0^{+5.7}_{-10.1}$	$2.486^{+0.154}_{-0.032}$	$4.58^{+0.43}_{-0.55}$	1160^{+270}_{-290}
202900527.1	2	$13.00819^{+0.00010}_{-0.00010}$	$1905.75787^{+0.00033}_{-0.00034}$	$5.395^{+0.040}_{-0.039}$	12279^{+70}_{-76}	$0.1047^{+0.0032}_{-0.0061}$	$20.1^{+2.1}_{-1.7}$	$1.76^{+0.17}_{-0.10}$	$19.1^{+1.1}_{-1.1}$	$46.1^{+10.6}_{-7.6}$
203042994.1	2	$12.99109^{+0.00073}_{-0.00077}$	$1898.9179^{+0.0026}_{-0.0024}$	$1.65^{+0.24}_{-0.24}$	6020^{+530}_{-520}	$0.088^{+0.020}_{-0.089}$	43^{+34}_{-85}	$4.5^{+3.4}_{-7.7}$	40^{+11}_{-30}	15^{+34}_{-78}
203099398.1	2	$1.839160^{+0.000060}_{-0.000063}$	$1896.0112^{+0.0014}_{-0.0014}$	$1.507^{+0.068}_{-0.072}$	$151.5^{+5.7}_{-6.0}$	$0.01194^{+0.00063}_{-0.00150}$	$0.62^{+0.17}_{-0.24}$	$0.48^{+0.13}_{-0.18}$	$8.3^{+2.7}_{-1.1}$	160^{+180}_{-190}
203139512.1	2	$2.032699^{+0.000095}_{-0.000093}$	$1895.4329^{+0.0021}_{-0.0022}$	$1.407^{+0.074}_{-0.092}$	1096^{+57}_{-59}	$0.0323^{+0.0017}_{-0.0031}$	$1.89^{+0.26}_{-0.22}$	$0.535^{+0.069}_{-0.037}$	$10.2^{+3.0}_{-1.3}$	61^{+39}_{-18}
203139512.2	2	$6.11706^{+0.00052}_{-0.00058}$	$1895.0074^{+0.0049}_{-0.0041}$	$2.06^{+0.15}_{-0.21}$	976^{+79}_{-83}	$0.0302^{+0.0023}_{-0.0044}$	$1.76^{+0.26}_{-0.29}$	$0.535^{+0.069}_{-0.037}$	$20.2^{+7.1}_{-3.6}$	$15.8^{+11.7}_{-6.0}$
203311200.1	2		$1954.01476^{+0.00066}_{-0.00066}$	$13.021^{+0.087}_{-0.087}$	3511^{+25}_{-26}	$0.0603^{+0.0011}_{-0.0029}$	$12.81^{+0.65}_{-0.65}$	$1.947^{+0.092}_{-0.029}$		
203616858.1	2	$1.68027^{+0.00011}_{-0.00011}$	$1894.9732^{+0.0027}_{-0.0027}$	$2.62^{+0.29}_{-0.31}$	262^{+12}_{-13}	$0.0207^{+0.0077}_{-0.0238}$	$2.9^{+1.1}_{-3.3}$	$1.275^{+0.103}_{-0.047}$	$2.3^{+1.1}_{-3.0}$	6900^{+7000}_{-18400}
203633064.1	2	$0.7099504^{+0.0000013}_{-0.0000013}$	$1894.832672^{+0.000081}_{-0.000080}$	$2.172^{+0.020}_{-0.016}$	16512^{+34}_{-34}	$0.357^{+0.057}_{-0.079}$	80^{+13}_{-21}	$2.065^{+0.024}_{-0.289}$	$2.201^{+0.170}_{-0.088}$	9500^{+1500}_{-2800}
203753577.1	2	$3.400858^{+0.000022}_{-0.000022}$	$1895.09284^{+0.00030}_{-0.00031}$	$2.281^{+0.055}_{-0.062}$	3404^{+23}_{-23}	$0.132^{+0.033}_{-0.046}$	$14.1^{+3.6}_{-5.0}$	$0.983^{+0.038}_{-0.027}$	$5.42^{+0.34}_{-0.45}$	1260^{+280}_{-300}
203771098.2	2	$20.88506^{+0.00027}_{-0.00028}$	$1905.79581^{+0.00062}_{-0.00058}$	$5.475^{+0.073}_{-0.090}$	2213^{+21}_{-21}	$0.0436^{+0.0011}_{-0.0024}$	$5.94^{+0.48}_{-0.50}$	$1.249^{+0.097}_{-0.081}$	$28.6^{+3.9}_{-1.8}$	$36.7^{+11.4}_{-6.7}$
203776696.1	2	$3.535155^{+0.000075}_{-0.000074}$	$1896.02500^{+0.00085}_{-0.00087}$	$5.431^{+0.062}_{-0.069}$	6314^{+77}_{-77}	$0.0732^{+0.0011}_{-0.0021}$	$16.6^{+3.8}_{-1.9}$	$2.07^{+0.47}_{-0.23}$	$5.24^{+0.27}_{-0.12}$	420^{+200}_{-110}
203784668.1	2		$1949.2030^{+0.0018}_{-0.0018}$	$14.67^{+0.39}_{-0.33}$	5701^{+79}_{-77}	$0.231^{+0.056}_{-0.058}$				
203826436.1	2	$6.42959^{+0.00014}_{-0.00014}$	$1898.85448^{+0.00092}_{-0.00096}$	$2.901^{+0.084}_{-0.109}$	1027^{+19}_{-19}	$0.0306^{+0.0018}_{-0.0037}$	$2.64^{+0.21}_{-0.34}$	$0.792^{+0.042}_{-0.029}$	$15.1^{+4.2}_{-2.3}$	110^{+62}_{-34}
203826436.2	2	$14.09292^{+0.00050}_{-0.00052}$	$1907.2322^{+0.0012}_{-0.0012}$	$2.80^{+0.13}_{-0.24}$	893^{+23}_{-24}	$0.0298^{+0.0028}_{-0.0044}$	$2.58^{+0.28}_{-0.39}$	$0.792^{+0.042}_{-0.029}$	$30.2^{+13.7}_{-9.4}$	28^{+25}_{-17}
203826436.3	2	$4.44360^{+0.00030}_{-0.00028}$	$1898.1167^{+0.0025}_{-0.0026}$	$2.84^{+0.15}_{-0.25}$	358^{+16}_{-17}	$0.0182^{+0.0015}_{-0.0041}$	$1.57^{+0.15}_{-0.36}$	$0.792^{+0.042}_{-0.029}$	$10.2^{+5.0}_{-2.0}$	241^{+237}_{-97}
203867512.1	2	$28.46762^{+0.00089}_{-0.00028}$	$1918.54638^{+0.00025}_{-0.00088}$	$7.621^{+0.023}_{-0.021}$	31445^{+51}_{-50}	$0.1704^{+0.0036}_{-0.0022}$	37^{+11}_{-17}	$1.97^{+0.61}_{-0.90}$	$29.85^{+0.60}_{-0.96}$	88^{+79}_{-113}
203925865.1	2	$8.79689^{+0.00058}_{-0.00059}$	$1898.2838^{+0.0028}_{-0.0028}$	$6.97^{+0.15}_{-0.22}$	527^{+14}_{-15}	$0.0217^{+0.0011}_{-0.0030}$	$4.85^{+0.52}_{-0.68}$	$2.047^{+0.193}_{-0.061}$	$8.7^{+2.6}_{-1.2}$	342^{+219}_{-94}
204057095.1	2	$23.21037^{+0.00018}_{-0.00017}$	$1913.62734^{+0.00022}_{-0.00023}$	$2.440^{+0.049}_{-0.060}$	4533^{+36}_{-32}	$0.116^{+0.023}_{-0.059}$	$15.3^{+3.0}_{-7.8}$	$1.207^{+0.024}_{-0.117}$	$37.6^{+3.1}_{-4.4}$	$23.7^{+4.1}_{-7.2}$
204128016.1	2	$50.73641^{+0.00088}_{-0.00087}$	$1895.16594^{+0.00062}_{-0.00062}$	$5.034^{+0.062}_{-0.070}$	3938^{+45}_{-45}	$0.0701^{+0.0027}_{-0.0048}$	$10.31^{+0.42}_{-0.77}$	$1.349^{+0.017}_{-0.042}$	$45.9^{+2.2}_{-2.9}$	$17.0^{+1.8}_{-2.4}$
204197636.1	2	$46.1373^{+0.0066}_{-0.0076}$	$1921.9703^{+0.0040}_{-0.0036}$	$6.94^{+0.21}_{-0.27}$	1137^{+47}_{-50}	$0.0330^{+0.0012}_{-0.0024}$	$2.60^{+0.16}_{-0.32}$	$0.723^{+0.035}_{-0.071}$	$47.6^{+11.3}_{-4.9}$	$10.8^{+5.3}_{-3.1}$

Table A.1: Our sample of planet candidates from C0-8. (continued)

Candidate	C#	Period (days)	t_0 (BJD - 2455000)	Duration (hours)	Depth (ppm)	R_p/R_*	R_p ($R_\oplus$)	R_* ($R_\odot$)	a/R_*	Inc. Flux ($S_\oplus$)
204221263.1	2	$10.56131^{+0.00053}_{-0.00053}$	$1900.4756^{+0.0021}_{-0.0021}$	$2.65^{+0.13}_{-0.27}$	484^{+23}_{-23}	$0.0209^{+0.0018}_{-0.0055}$	$2.83^{+0.26}_{-0.76}$	$1.241^{+0.038}_{-0.060}$	$26.4^{+11.7}_{-4.7}$	43^{+38}_{-16}
204221263.2	2	$4.01663^{+0.00023}_{-0.00023}$	$1896.8693^{+0.0024}_{-0.0024}$	$3.18^{+0.14}_{-0.23}$	$260.7^{+9.5}_{-9.4}$	$0.0145^{+0.0013}_{-0.0045}$	$1.96^{+0.19}_{-0.62}$	$1.241^{+0.038}_{-0.060}$	$8.7^{+3.5}_{-1.1}$	400^{+320}_{-110}
204308061.1	2	$22.6398^{+0.0012}_{-0.0012}$	$1900.4428^{+0.0022}_{-0.0022}$	$3.75^{+0.13}_{-0.16}$	$200.0^{+8.0}_{-8.3}$	$0.01350^{+0.00077}_{-0.00184}$	$1.27^{+0.10}_{-0.22}$	$0.862^{+0.049}_{-0.090}$	$40.8^{+12.7}_{-5.6}$	$24.3^{+15.4}_{-8.4}$
204322265.1	2	$2.784496^{+0.000053}_{-0.000060}$	$1894.83627^{+0.00090}_{-0.00088}$	$0.466^{+0.053}_{-0.097}$	5850^{+560}_{-690}	$0.0750^{+0.0082}_{-0.0482}$	$2.09^{+0.49}_{-1.42}$	$0.256^{+0.053}_{-0.055}$	41^{+18}_{-12}	$4.0^{+4.4}_{-3.4}$
204529573.1	2	$2.75180^{+0.00015}_{-0.00015}$	$1896.3915^{+0.0025}_{-0.0024}$	$1.25^{+0.12}_{-0.14}$	$99.2^{+7.4}_{-7.8}$	$0.00948^{+0.00087}_{-0.00160}$	$0.669^{+0.083}_{-0.124}$	$0.647^{+0.054}_{-0.050}$	$14.5^{+4.9}_{-2.8}$	96^{+67}_{-40}
204546592.1	2		$1899.9637^{+0.0013}_{-0.0013}$	$20.74^{+0.21}_{-0.25}$	9753^{+71}_{-68}	$0.150^{+0.022}_{-0.062}$	133^{+21}_{-55}	$8.12^{+0.46}_{-0.32}$		
204579445.1	2	$24.6842^{+0.0025}_{-0.0023}$	$1900.4870^{+0.0028}_{-0.0027}$	$4.96^{+0.12}_{-0.14}$	408^{+18}_{-19}	$0.01951^{+0.00078}_{-0.00168}$	$2.49^{+0.53}_{-0.23}$	$1.170^{+0.244}_{-0.032}$	$35.1^{+8.5}_{-3.5}$	$28.4^{+18.2}_{-6.0}$
204750116.1	2	$23.44701^{+0.00093}_{-0.00089}$	$1898.8365^{+0.0017}_{-0.0018}$	$5.71^{+0.11}_{-0.14}$	783^{+20}_{-20}	$0.02666^{+0.00098}_{-0.00236}$	$3.24^{+0.13}_{-0.29}$	$1.115^{+0.017}_{-0.016}$	$29.0^{+6.4}_{-3.1}$	$31.4^{+13.9}_{-6.7}$
204750116.2	2	$7.8392^{+0.0015}_{-0.0011}$	$1897.0670^{+0.0057}_{-0.0066}$	$3.50^{+0.20}_{-0.28}$	158^{+12}_{-12}	$0.01204^{+0.00091}_{-0.00197}$	$1.46^{+0.11}_{-0.24}$	$1.115^{+0.017}_{-0.016}$	$14.9^{+5.2}_{-2.5}$	119^{+83}_{-40}
204763194.1	2	$2.320937^{+0.000018}_{-0.000018}$	$1895.69697^{+0.00033}_{-0.00035}$	$2.735^{+0.046}_{-0.057}$	3298^{+35}_{-31}	$0.125^{+0.031}_{-0.045}$	$15.7^{+3.9}_{-5.6}$	$1.157^{+0.011}_{-0.027}$	$3.02^{+0.20}_{-0.26}$	5600^{+1200}_{-1300}
204884005.1	2	$46.38363^{+0.00094}_{-0.00094}$	$1924.04264^{+0.00070}_{-0.00071}$	$5.237^{+0.057}_{-0.069}$	1771^{+20}_{-20}	$0.03871^{+0.00091}_{-0.00238}$	$3.22^{+0.16}_{-0.22}$	$0.762^{+0.032}_{-0.022}$	$66.7^{+8.5}_{-3.5}$	$4.94^{+1.33}_{-0.60}$
204888276.1	2	$16.56127^{+0.00064}_{-0.00065}$	$1900.5356^{+0.0017}_{-0.0017}$	$4.36^{+0.22}_{-0.25}$	1090^{+26}_{-27}	$0.0340^{+0.0034}_{-0.0028}$	$0.957^{+0.098}_{-0.289}$	$0.2580^{+0.0050}_{-0.0750}$	$18.8^{+5.1}_{-11.2}$	19^{+11}_{-28}
204890128.1	2	$12.20773^{+0.00030}_{-0.00030}$	$1896.3850^{+0.0011}_{-0.0011}$	$3.626^{+0.080}_{-0.104}$	1001^{+19}_{-19}	$0.0301^{+0.0012}_{-0.0030}$	$2.34^{+0.27}_{-0.35}$	$0.713^{+0.076}_{-0.079}$	$23.7^{+5.7}_{-2.7}$	38^{+20}_{-12}
204914585.1	2	$18.3647^{+0.0021}_{-0.0021}$	$1895.1671^{+0.0055}_{-0.0047}$	$5.86^{+0.22}_{-0.27}$	421^{+19}_{-20}	$0.0196^{+0.0011}_{-0.0028}$	$2.61^{+0.79}_{-0.45}$	$1.22^{+0.36}_{-0.12}$	$21.3^{+6.9}_{-3.1}$	63^{+56}_{-22}
204990932.1	2	$21.9184^{+0.0021}_{-0.0022}$	$1900.2769^{+0.0035}_{-0.0035}$	$2.91^{+0.36}_{-0.45}$	1330^{+100}_{-100}	$0.0404^{+0.0096}_{-0.0435}$	$3.18^{+1.00}_{-3.52}$	$0.72^{+0.15}_{-0.18}$	38^{+18}_{-25}	10^{+11}_{-15}
204991696.1	2	$49.8558^{+0.0034}_{-0.0035}$	$1901.9230^{+0.0023}_{-0.0023}$	$7.03^{+0.14}_{-0.19}$	539^{+17}_{-18}	$0.02222^{+0.00093}_{-0.00237}$	$3.29^{+0.16}_{-0.36}$	$1.359^{+0.037}_{-0.024}$	$49.6^{+13.6}_{-5.6}$	$14.2^{+7.8}_{-3.2}$
205029914.1	2	$4.98150^{+0.00011}_{-0.00011}$	$1894.7341^{+0.0010}_{-0.0011}$	$3.828^{+0.075}_{-0.150}$	$590.2^{+9.3}_{-9.4}$	$0.02384^{+0.00093}_{-0.00230}$	$2.39^{+0.68}_{-0.68}$	$0.92^{+0.26}_{-0.24}$	$8.6^{+2.7}_{-1.5}$	510^{+430}_{-330}
205040048.1	2	$3.30524^{+0.00019}_{-0.00021}$	$1894.5466^{+0.0024}_{-0.0023}$	$1.07^{+0.11}_{-0.26}$	1210^{+100}_{-110}	$0.0341^{+0.0034}_{-0.0110}$	$6.6^{+3.4}_{-24.7}$	$1.79^{+0.90}_{-6.63}$	$20.3^{+11.2}_{-5.2}$	90^{+180}_{-970}
205064326.1	2	$8.02335^{+0.00018}_{-0.00017}$	$1896.67107^{+0.00096}_{-0.00097}$	$4.48^{+0.12}_{-0.13}$	5030^{+58}_{-58}	$0.153^{+0.041}_{-0.058}$	86^{+23}_{-33}	$5.13^{+0.14}_{-0.22}$	$7.20^{+0.45}_{-0.61}$	245^{+41}_{-52}
205071984.1	2	$8.992018^{+0.000081}_{-0.000084}$	$1900.92650^{+0.00033}_{-0.00032}$	$3.486^{+0.052}_{-0.057}$	3802^{+27}_{-27}	$0.0596^{+0.0028}_{-0.0025}$	$4.92^{+0.33}_{-0.39}$	$0.757^{+0.036}_{-0.050}$	$17.6^{+1.8}_{-2.7}$	84^{+19}_{-28}
205071984.2	2	$31.7236^{+0.0013}_{-0.0011}$	$1903.7795^{+0.0027}_{-0.0043}$	$5.06^{+0.30}_{-0.16}$	1562^{+31}_{-30}	$0.0380^{+0.0013}_{-0.0026}$	$3.14^{+0.18}_{-0.30}$	$0.757^{+0.036}_{-0.050}$	$46.0^{+9.7}_{-4.3}$	$12.4^{+5.4}_{-2.9}$
205071984.3	2	$20.66178^{+0.00070}_{-0.00068}$	$1899.4217^{+0.0015}_{-0.0015}$	$4.503^{+0.097}_{-0.148}$	1346^{+24}_{-24}	$0.0331^{+0.0013}_{-0.0034}$	$2.73^{+0.17}_{-0.34}$	$0.757^{+0.036}_{-0.050}$	$33.8^{+6.1}_{-2.5}$	$23.0^{+8.6}_{-4.6}$
205071984.4	2	$4.34910^{+0.00063}_{-0.00057}$	$1894.5261^{+0.0062}_{-0.0062}$	$3.56^{+0.66}_{-0.47}$	255^{+18}_{-19}	$0.027^{+0.014}_{-0.020}$	$2.2^{+1.1}_{-1.7}$	$0.757^{+0.036}_{-0.050}$	$2.67^{+0.58}_{-7.66}$	3700^{+1600}_{-21100}
205084841.1	2	$11.31028^{+0.00032}_{-0.00032}$	$1905.17019^{+0.00096}_{-0.00097}$	$4.439^{+0.079}_{-0.084}$	17730^{+280}_{-280}	$0.1203^{+0.0029}_{-0.0050}$	$18.9^{+4.6}_{-1.1}$	$1.440^{+0.352}_{-0.058}$	$21.35^{+1.33}_{-0.66}$	$22.0^{+11.3}_{-3.1}$
205111664.1	2	$15.93709^{+0.00084}_{-0.00081}$	$1906.4327^{+0.0022}_{-0.0025}$	$3.29^{+0.10}_{-0.13}$	590^{+20}_{-21}	$0.0235^{+0.0011}_{-0.0027}$	$1.87^{+0.13}_{-0.25}$	$0.731^{+0.038}_{-0.048}$	$33.3^{+11.5}_{-4.5}$	$25.0^{+17.8}_{-8.9}$
205117205.1	2	$5.42526^{+0.00026}_{-0.00024}$	$1898.6903^{+0.0020}_{-0.0021}$	$4.53^{+0.20}_{-0.24}$	3018^{+66}_{-66}	$0.0550^{+0.0047}_{-0.0041}$	$3.17^{+0.53}_{-0.39}$	$0.529^{+0.076}_{-0.051}$	$7.1^{+1.4}_{-2.5}$	190^{+95}_{-138}
205146011.1	2	$1.057171^{+0.000061}_{-0.000059}$	$1894.7388^{+0.0024}_{-0.0024}$	$1.472^{+0.095}_{-0.110}$	204^{+16}_{-17}	$0.0137^{+0.0010}_{-0.0020}$	$1.51^{+0.25}_{-0.23}$	$1.004^{+0.151}_{-0.050}$	$4.83^{+1.63}_{-0.77}$	700^{+520}_{-230}
205148699.1	2	$4.377339^{+0.000010}_{-0.000010}$	$1896.512322^{+0.000096}_{-0.000095}$	$4.589^{+0.014}_{-0.016}$	33397^{+85}_{-83}	$0.1727^{+0.0021}_{-0.0024}$	$31.9^{+1.3}_{-1.8}$	$1.691^{+0.063}_{-0.094}$	$8.054^{+0.071}_{-0.104}$	489^{+49}_{-64}
205152172.1	2	$0.980294^{+0.000026}_{-0.000024}$	$1894.6069^{+0.0011}_{-0.0012}$	$1.116^{+0.067}_{-0.124}$	655^{+27}_{-29}	$0.0242^{+0.0020}_{-0.0058}$	$1.81^{+0.34}_{-0.45}$	$0.685^{+0.115}_{-0.047}$	$6.0^{+2.6}_{-1.0}$	330^{+300}_{-120}
205170307.2	2	$67.50274^{+0.00027}_{-0.00027}$	$1898.81359^{+0.00019}_{-0.00020}$	$13.528^{+0.025}_{-0.025}$	28686^{+40}_{-40}	$0.23735^{+0.00151}_{-0.00079}$	$48.6^{+8.7}_{-3.9}$	$1.88^{+0.34}_{-0.15}$	$39.38^{+0.13}_{-0.10}$	$19.9^{+7.1}_{-3.3}$
205170731.1	2	$14.2005^{+0.0027}_{-0.0025}$	$1901.8980^{+0.0083}_{-0.0084}$	$3.72^{+0.19}_{-0.29}$	856^{+51}_{-51}	$0.0276^{+0.0023}_{-0.0053}$	$2.36^{+0.30}_{-1.97}$	$0.786^{+0.078}_{-0.639}$	$26.3^{+8.8}_{-3.9}$	44^{+33}_{-103}
205205452.1	2	$28.8077^{+0.0024}_{-0.0028}$	$1895.5605^{+0.0035}_{-0.0033}$	$2.19^{+0.21}_{-0.39}$	8530^{+630}_{-650}	$0.0886^{+0.0067}_{-0.0136}$	$2.08^{+0.88}_{-53.27}$	$0.215^{+0.090}_{-5.510}$	97^{+30}_{-18}	$0.66^{+0.91}_{-48.21}$
205224877.1	2	$3.75927^{+0.00031}_{-0.00032}$	$1894.6320^{+0.0037}_{-0.0037}$	$1.61^{+0.19}_{-0.26}$	3610^{+310}_{-340}	$0.0581^{+0.0057}_{-0.0147}$	68^{+64}_{-35}	$10.7^{+10.0}_{-4.8}$	$16.2^{+7.0}_{-3.7}$	69^{+193}_{-93}
205242733.1	2	$2.41628^{+0.00016}_{-0.00017}$	$1896.7150^{+0.0029}_{-0.0027}$	$2.49^{+0.13}_{-0.16}$	704^{+38}_{-39}	$0.0243^{+0.0019}_{-0.0046}$	$2.68^{+0.58}_{-0.74}$	$1.01^{+0.21}_{-0.21}$	$6.79^{+1.92}_{-0.85}$	260^{+180}_{-120}
205377483.1	2	$0.3938505^{+0.0000049}_{-0.0000049}$	$1894.38661^{+0.00055}_{-0.00056}$	$1.312^{+0.051}_{-0.056}$	488^{+11}_{-12}	$0.058^{+0.017}_{-0.019}$	$13.7^{+4.1}_{-4.9}$	$2.16^{+0.18}_{-0.27}$	$0.725^{+0.077}_{-0.096}$	$282000^{+82000}_{-106000}$
205470347.1	2	$1.86732^{+0.00016}_{-0.00014}$	$1895.4386^{+0.0038}_{-0.0042}$	$1.65^{+0.13}_{-0.18}$	$79.4^{+6.4}_{-6.7}$	$0.00857^{+0.00072}_{-0.00146}$	$0.648^{+0.063}_{-0.112}$	$0.693^{+0.033}_{-0.021}$	$7.4^{+2.7}_{-1.4}$	460^{+340}_{-180}
205483055.1	2	$22.9735^{+0.0019}_{-0.0019}$	$1896.8155^{+0.0037}_{-0.0036}$	$3.39^{+0.16}_{-0.19}$	541^{+34}_{-36}	$0.0224^{+0.0014}_{-0.0029}$	$2.61^{+0.32}_{-0.37}$	$1.067^{+0.113}_{-0.062}$	$46.7^{+14.4}_{-6.5}$	$9.2^{+6.0}_{-2.8}$
205489894.1	2	$14.65835^{+0.00043}_{-0.00043}$	$1907.0762^{+0.0010}_{-0.0011}$	$1.548^{+0.066}_{-0.089}$	1029^{+38}_{-40}	$0.0303^{+0.0018}_{-0.0037}$	$1.12^{+0.30}_{-0.17}$	$0.339^{+0.090}_{-0.031}$	$66.3^{+17.8}_{-8.5}$	$1.73^{+1.62}_{-0.64}$

Table A.1: Our sample of planet candidates from C0-8. (continued)

Candidate	C#	Period (days)	t_0 (BJD - 2455000)	Duration (hours)	Depth (ppm)	R_p/R_*	R_p ($R_\oplus$)	R_* ($R_\odot$)	a/R_*	Inc. Flux ($S_\oplus$)
205503762.1	2	$6.4349^{+0.0012}_{-0.0011}$	$1899.8097^{+0.0068}_{-0.0072}$	$4.35^{+0.29}_{-0.43}$	263^{+20}_{-21}	$0.0152^{+0.0015}_{-0.0052}$	$2.47^{+0.30}_{-0.86}$	$1.493^{+0.104}_{-0.056}$	$9.9^{+5.1}_{-1.7}$	260^{+272}_{-92}
205530323.1	2	$4.27065^{+0.00034}_{-0.00035}$	$1894.5860^{+0.0036}_{-0.0035}$	$1.39^{+0.13}_{-0.17}$	2200^{+180}_{-180}	$0.0453^{+0.0033}_{-0.0049}$	$7.6^{+6.7}_{-5.8}$	$1.5^{+1.4}_{-1.2}$	$21.6^{+5.9}_{-3.9}$	180^{+610}_{-420}
205530323.2	2	$7.64309^{+0.00052}_{-0.00051}$	$1900.5155^{+0.0028}_{-0.0029}$	$1.29^{+0.19}_{-0.28}$	2360^{+230}_{-250}	$0.0479^{+0.0053}_{-0.0187}$	$8.0^{+7.1}_{-6.9}$	$1.5^{+1.4}_{-1.2}$	39^{+21}_{-11}	60^{+190}_{-130}
205618538.1	2	$2.167697^{+0.000021}_{-0.000022}$	$1894.51767^{+0.00046}_{-0.00045}$	$4.875^{+0.035}_{-0.044}$	2228^{+15}_{-15}	$0.04472^{+0.00059}_{-0.00154}$	$12.14^{+0.20}_{-0.44}$	$2.489^{+0.023}_{-0.026}$	$3.39^{+0.29}_{-0.15}$	2950^{+530}_{-310}
205652650.1	2	$5.07152^{+0.00030}_{-0.00029}$	$1898.1420^{+0.0026}_{-0.0027}$	$2.05^{+0.37}_{-0.21}$	2160^{+120}_{-120}	$0.068^{+0.026}_{-0.054}$	$3.2^{+1.2}_{-3.2}$	$0.426^{+0.018}_{-0.257}$	$8.7^{+1.5}_{-12.6}$	131^{+48}_{-453}
205686202.1	2	$13.15727^{+0.00022}_{-0.00021}$	$1897.14385^{+0.00068}_{-0.00071}$	$3.873^{+0.046}_{-0.057}$	7619^{+88}_{-83}	$0.0801^{+0.0013}_{-0.0025}$	$10.83^{+1.99}_{-0.75}$	$1.240^{+0.227}_{-0.077}$	$27.44^{+1.64}_{-0.72}$	$12.5^{+4.8}_{-1.7}$
205924614.1	3	$2.849302^{+0.000019}_{-0.000019}$	$1977.72404^{+0.00026}_{-0.00026}$	$2.061^{+0.027}_{-0.037}$	3954^{+31}_{-32}	$0.0563^{+0.0018}_{-0.0044}$	$4.07^{+0.30}_{-0.41}$	$0.662^{+0.044}_{-0.042}$	$10.54^{+1.57}_{-0.60}$	143^{+47}_{-24}
205938820.1	3	$4.20773^{+0.00075}_{-0.00060}$	$1979.2539^{+0.0039}_{-0.0046}$	$2.22^{+0.17}_{-0.22}$	277^{+26}_{-28}	$0.0161^{+0.0013}_{-0.0023}$	$1.47^{+0.25}_{-0.26}$	$0.834^{+0.122}_{-0.081}$	$12.6^{+4.3}_{-2.3}$	280^{+210}_{-120}
205939498.1	3	$1.1761477^{+0.0000088}_{-0.0000088}$	$1977.44240^{+0.00030}_{-0.00029}$	$1.305^{+0.039}_{-0.050}$	1360^{+21}_{-19}	$0.074^{+0.021}_{-0.034}$	$19.3^{+5.6}_{-8.9}$	$2.38^{+0.17}_{-0.16}$	$2.68^{+0.27}_{-0.36}$	7400^{+1800}_{-2300}
205944181.1	3	$2.475573^{+0.000048}_{-0.000042}$	$1979.34116^{+0.00062}_{-0.00073}$	$0.882^{+0.089}_{-0.137}$	898^{+53}_{-53}	$0.0308^{+0.0057}_{-0.0393}$	$2.98^{+0.57}_{-3.81}$	$0.888^{+0.033}_{-0.033}$	$16.8^{+10.3}_{-6.4}$	105^{+129}_{-81}
205947161.1	3	$17.72590^{+0.00012}_{-0.00012}$	$1989.19345^{+0.00022}_{-0.00022}$	$1.752^{+0.046}_{-0.054}$	3338^{+37}_{-35}	$0.123^{+0.034}_{-0.051}$	$23.4^{+6.6}_{-9.7}$	$1.752^{+0.095}_{-0.096}$	$37.1^{+2.7}_{-3.4}$	$33.6^{+6.2}_{-7.2}$
205950854.1	3	$15.8523^{+0.0012}_{-0.0013}$	$1990.8928^{+0.0026}_{-0.0025}$	$3.80^{+0.12}_{-0.15}$	532^{+19}_{-20}	$0.0222^{+0.0010}_{-0.0022}$	$2.19^{+0.14}_{-0.22}$	$0.904^{+0.037}_{-0.013}$	$29.0^{+8.6}_{-3.5}$	45^{+27}_{-11}
205950854.2	3	$8.0516^{+0.0012}_{-0.0011}$	$1981.8136^{+0.0046}_{-0.0053}$	$3.71^{+0.29}_{-0.32}$	303^{+18}_{-18}	$0.0164^{+0.0015}_{-0.0038}$	$1.62^{+0.16}_{-0.38}$	$0.904^{+0.037}_{-0.013}$	$14.6^{+6.1}_{-2.5}$	178^{+149}_{-61}
205951125.1	3	$6.79143^{+0.00077}_{-0.00080}$	$1979.7964^{+0.0040}_{-0.0040}$	$2.50^{+0.21}_{-0.31}$	739^{+52}_{-54}	$0.0259^{+0.0024}_{-0.0064}$	$1.72^{+0.17}_{-0.43}$	$0.609^{+0.014}_{-0.017}$	$18.2^{+8.1}_{-3.5}$	79^{+71}_{-31}
205957328.1	3	$14.3533^{+0.0014}_{-0.0014}$	$1981.5858^{+0.0032}_{-0.0033}$	$3.26^{+0.23}_{-0.28}$	625^{+33}_{-33}	$0.0234^{+0.0022}_{-0.0053}$	$2.18^{+0.21}_{-0.50}$	$0.855^{+0.014}_{-0.030}$	$30.0^{+11.6}_{-4.8}$	$30.2^{+23.5}_{-10.0}$
205962305.1	3	$1.88282^{+0.00015}_{-0.00015}$	$1977.8386^{+0.0031}_{-0.0031}$	$4.00^{+0.44}_{-0.30}$	5950^{+270}_{-260}	$0.093^{+0.025}_{-0.071}$	$2.6^{+1.1}_{-2.5}$	$0.257^{+0.080}_{-0.144}$	$2.19^{+0.36}_{-1.73}$	1500^{+1500}_{-3400}
205969319.1	3	$6.4756^{+0.0011}_{-0.0014}$	$1978.2161^{+0.0083}_{-0.0069}$	$3.48^{+0.27}_{-0.32}$	174^{+16}_{-17}	$0.0127^{+0.0011}_{-0.0023}$	$1.85^{+0.17}_{-0.34}$	$1.339^{+0.016}_{-0.018}$	$12.4^{+4.5}_{-2.2}$	310^{+230}_{-110}
205976958.1	3	$2.31803^{+0.00017}_{-0.00018}$	$1978.3875^{+0.0029}_{-0.0029}$	$1.73^{+0.16}_{-0.28}$	1430^{+110}_{-110}	$0.0364^{+0.0035}_{-0.0112}$	$2.34^{+0.46}_{-0.74}$	$0.589^{+0.102}_{-0.045}$	$9.0^{+4.6}_{-1.9}$	94^{+101}_{-43}
205981465.1	3	$6.37733^{+0.00047}_{-0.00046}$	$1978.0934^{+0.0027}_{-0.0028}$	$1.58^{+0.14}_{-0.24}$	769^{+54}_{-60}	$0.0267^{+0.0025}_{-0.0080}$	$0.76^{+0.25}_{-0.49}$	$0.262^{+0.082}_{-0.150}$	$26.7^{+14.0}_{-5.7}$	10^{+14}_{-17}
205998649.1	3	$8.3958^{+0.0028}_{-0.0026}$	$1985.2790^{+0.0102}_{-0.0099}$	$6.69^{+0.62}_{-1.41}$	340^{+23}_{-24}	$0.0181^{+0.0021}_{-0.0070}$	$3.95^{+0.46}_{-1.53}$	$1.996^{+0.044}_{-0.018}$	$7.8^{+4.8}_{-2.2}$	590^{+740}_{-340}
205999468.1	3	$12.26422^{+0.00072}_{-0.00074}$	$1984.0926^{+0.0019}_{-0.0019}$	$1.67^{+0.19}_{-0.31}$	726^{+40}_{-41}	$0.0268^{+0.0038}_{-0.0168}$	$2.22^{+0.32}_{-1.39}$	$0.7596^{+0.0200}_{-0.0065}$	46^{+29}_{-14}	$12.4^{+15.7}_{-7.5}$
206007892.1	3	$6.38092^{+0.00055}_{-0.00056}$	$1982.0095^{+0.0029}_{-0.0029}$	$3.09^{+0.10}_{-0.12}$	$160.4^{+8.3}_{-8.6}$	$0.01254^{+0.00056}_{-0.00110}$	$1.341^{+0.069}_{-0.124}$	$0.981^{+0.025}_{-0.027}$	$13.9^{+5.0}_{-1.9}$	171^{+123}_{-49}
206008091.1	3	$12.3988^{+0.0017}_{-0.0018}$	$1985.6641^{+0.0049}_{-0.0042}$	$4.17^{+0.20}_{-0.27}$	311^{+17}_{-17}	$0.0170^{+0.0011}_{-0.0025}$	$2.01^{+0.14}_{-0.30}$	$1.0849^{+0.0244}_{-0.0076}$	$19.9^{+7.5}_{-3.2}$	117^{+88}_{-37}
206008091.2	3	$7.5734^{+0.0014}_{-0.0012}$	$1978.6141^{+0.0061}_{-0.0073}$	$3.44^{+0.22}_{-0.30}$	197^{+14}_{-15}	$0.01370^{+0.00097}_{-0.00191}$	$1.62^{+0.12}_{-0.23}$	$1.0849^{+0.0244}_{-0.0076}$	$14.5^{+5.6}_{-2.6}$	219^{+168}_{-78}
206011496.1	3	$2.369019^{+0.000058}_{-0.000060}$	$1979.27599^{+0.00100}_{-0.00095}$	$2.341^{+0.055}_{-0.094}$	$319.4^{+6.8}_{-6.8}$	$0.01675^{+0.00077}_{-0.00239}$	$1.67^{+0.14}_{-0.24}$	$0.914^{+0.063}_{-0.018}$	$7.01^{+2.03}_{-0.83}$	720^{+430}_{-170}
206011691.1	3	$15.50195^{+0.00056}_{-0.00056}$	$1988.4703^{+0.0011}_{-0.0010}$	$2.378^{+0.071}_{-0.102}$	1294^{+33}_{-35}	$0.0345^{+0.0016}_{-0.0036}$	$2.17^{+0.18}_{-0.26}$	$0.576^{+0.040}_{-0.033}$	$45.6^{+12.7}_{-6.0}$	$6.3^{+3.6}_{-1.8}$
206011691.2	3	$9.32448^{+0.00033}_{-0.00034}$	$1980.1007^{+0.0017}_{-0.0016}$	$2.525^{+0.079}_{-0.092}$	809^{+21}_{-21}	$0.0270^{+0.0013}_{-0.0031}$	$1.70^{+0.14}_{-0.22}$	$0.576^{+0.040}_{-0.033}$	$25.8^{+7.0}_{-3.2}$	$19.7^{+11.1}_{-5.3}$
206011849.1	3	$10.3631^{+0.0031}_{-0.0042}$	$1982.1617^{+0.0102}_{-0.0098}$	$2.60^{+0.66}_{-0.87}$	620^{+87}_{-96}	$0.0246^{+0.0033}_{-0.0098}$	$1.64^{+0.25}_{-0.67}$	$0.613^{+0.041}_{-0.053}$	25^{+14}_{-12}	30^{+35}_{-31}
206024342.1	3	$14.6435^{+0.0011}_{-0.0010}$	$1985.4830^{+0.0026}_{-0.0026}$	$4.02^{+0.14}_{-0.21}$	872^{+31}_{-31}	$0.0281^{+0.0017}_{-0.0040}$	$2.52^{+0.34}_{-0.38}$	$0.823^{+0.100}_{-0.042}$	$25.1^{+8.0}_{-3.5}$	73^{+50}_{-22}
206024342.2	3	$0.911618^{+0.000073}_{-0.000077}$	$1977.3380^{+0.0034}_{-0.0032}$	$1.42^{+0.13}_{-0.15}$	179^{+16}_{-17}	$0.0129^{+0.0011}_{-0.0022}$	$1.16^{+0.17}_{-0.20}$	$0.823^{+0.100}_{-0.042}$	$4.22^{+1.52}_{-0.81}$	2600^{+2000}_{-1000}
206024342.3	3	$4.50717^{+0.00042}_{-0.00041}$	$1979.6895^{+0.0037}_{-0.0034}$	$2.18^{+0.15}_{-0.16}$	267^{+18}_{-19}	$0.0160^{+0.0010}_{-0.0019}$	$1.44^{+0.20}_{-0.18}$	$0.823^{+0.100}_{-0.042}$	$13.9^{+4.9}_{-2.3}$	240^{+178}_{-83}
206026136.1	3	$9.0074^{+0.0011}_{-0.0010}$	$1984.3335^{+0.0032}_{-0.0037}$	$2.42^{+0.16}_{-0.25}$	1254^{+96}_{-101}	$0.0334^{+0.0028}_{-0.0074}$	$2.18^{+0.22}_{-0.51}$	$0.599^{+0.034}_{-0.043}$	$25.7^{+9.7}_{-4.2}$	29^{+22}_{-10}
206026904.1	3	$7.05235^{+0.00017}_{-0.00016}$	$1979.92418^{+0.00087}_{-0.00091}$	$2.047^{+0.069}_{-0.094}$	1030^{+24}_{-24}	$0.0298^{+0.0021}_{-0.0048}$	$2.72^{+0.22}_{-0.44}$	$0.837^{+0.033}_{-0.019}$	$23.9^{+7.0}_{-3.2}$	45^{+27}_{-12}
206026904.2	3	$2.53712^{+0.00011}_{-0.00011}$	$1979.5850^{+0.0016}_{-0.0016}$	$2.16^{+0.12}_{-0.18}$	375^{+12}_{-12}	$0.0188^{+0.0017}_{-0.0042}$	$1.71^{+0.17}_{-0.38}$	$0.837^{+0.033}_{-0.019}$	$7.5^{+4.0}_{-1.6}$	450^{+480}_{-200}
206026904.3	3	$22.8820^{+0.0018}_{-0.0018}$	$1998.0691^{+0.0022}_{-0.0023}$	$3.13^{+0.12}_{-0.18}$	425^{+18}_{-19}	$0.0201^{+0.0011}_{-0.0022}$	$1.84^{+0.12}_{-0.21}$	$0.837^{+0.033}_{-0.019}$	$49.8^{+17.6}_{-7.2}$	$10.3^{+7.3}_{-3.0}$
206027655.1	3	$11.29665^{+0.00074}_{-0.00074}$	$1986.7061^{+0.0026}_{-0.0025}$	$1.801^{+0.095}_{-0.117}$	940^{+51}_{-52}	$0.0298^{+0.0016}_{-0.0027}$	$2.08^{+0.17}_{-0.19}$	$0.640^{+0.042}_{-0.013}$	$44.0^{+12.2}_{-5.8}$	$12.8^{+7.3}_{-3.5}$
206028176.1	3	$9.38053^{+0.00076}_{-0.00077}$	$1978.7481^{+0.0032}_{-0.0031}$	$5.15^{+0.14}_{-0.20}$	385^{+15}_{-15}	$0.01879^{+0.00096}_{-0.00262}$	$2.89^{+0.17}_{-0.41}$	$1.412^{+0.040}_{-0.022}$	$12.5^{+4.2}_{-1.6}$	440^{+300}_{-120}
206029450.1	3	$4.23119^{+0.00043}_{-0.00042}$	$1980.9403^{+0.0035}_{-0.0035}$	$2.17^{+0.13}_{-0.16}$	1580^{+110}_{-110}	$0.0386^{+0.0022}_{-0.0032}$	$2.17^{+0.30}_{-0.30}$	$0.516^{+0.065}_{-0.058}$	$13.9^{+3.7}_{-1.8}$	65^{+38}_{-22}

Table A.1: Our sample of planet candidates from C0-8. (continued)

Candidate	C#	Period (days)	t_0 (BJD - 2455000)	Duration (hours)	Depth (ppm)	R_p/R_*	R_p ($R_\oplus$)	R_* ($R_\odot$)	a/R_*	Inc. Flux ($S_\oplus$)
206031623.1	3	$9.9487^{+0.0013}_{-0.0020}$	$1986.3592^{+0.0048}_{-0.0045}$	$3.64^{+0.20}_{-0.26}$	$152.5^{+9.7}_{-10.2}$	$0.01191^{+0.00083}_{-0.00184}$	$1.48^{+0.21}_{-0.23}$	$1.136^{+0.138}_{-0.041}$	$18.2^{+6.3}_{-3.0}$	176^{+130}_{-59}
206036749.1	3	$1.131305^{+0.000012}_{-0.000012}$	$1977.59433^{+0.00041}_{-0.00041}$	$1.237^{+0.053}_{-0.125}$	1366^{+23}_{-25}	$0.0321^{+0.0036}_{-0.0182}$	$3.93^{+0.77}_{-2.23}$	$1.122^{+0.179}_{-0.027}$	$6.52^{+3.44}_{-0.74}$	800^{+890}_{-190}
206038483.1	3	$3.002654^{+0.000013}_{-0.000013}$	$1979.05672^{+0.00017}_{-0.00017}$	$3.117^{+0.023}_{-0.026}$	4774^{+17}_{-17}	$0.06280^{+0.00066}_{-0.00100}$	$10.45^{+0.64}_{-0.39}$	$1.525^{+0.092}_{-0.051}$	$7.67^{+0.39}_{-0.16}$	587^{+94}_{-50}
206042996.1	3	$5.29853^{+0.00080}_{-0.00094}$	$1978.4877^{+0.0054}_{-0.0055}$	$3.14^{+0.45}_{-0.76}$	1970^{+180}_{-190}	$0.0455^{+0.0070}_{-0.0360}$	$3.32^{+0.62}_{-2.63}$	$0.668^{+0.070}_{-0.035}$	$10.0^{+5.5}_{-4.4}$	108^{+120}_{-96}
206044803.1	3	$2.57333^{+0.00016}_{-0.00015}$	$1978.0676^{+0.0023}_{-0.0023}$	$2.81^{+0.13}_{-0.19}$	364^{+14}_{-14}	$0.0178^{+0.0014}_{-0.0037}$	$2.03^{+0.21}_{-0.43}$	$1.046^{+0.071}_{-0.029}$	$6.20^{+2.12}_{-0.92}$	1010^{+700}_{-310}
206047055.1	3	$4.1029^{+0.0018}_{-0.0016}$	$1978.078^{+0.016}_{-0.017}$	$5.10^{+0.47}_{-0.56}$	124^{+12}_{-12}	$0.0106^{+0.0010}_{-0.0022}$	$2.28^{+0.46}_{-0.48}$	$1.980^{+0.348}_{-0.089}$	$5.3^{+2.0}_{-1.0}$	1060^{+870}_{-410}
206049764.1	3	$5.6228^{+0.0017}_{-0.0013}$	$1979.4938^{+0.0134}_{-0.0080}$	$8.20^{+0.63}_{-1.45}$	219^{+13}_{-13}	$0.0143^{+0.0012}_{-0.0035}$	$3.71^{+0.32}_{-0.91}$	$2.378^{+0.018}_{-0.038}$	$4.3^{+2.3}_{-1.1}$	1420^{+1490}_{-720}
206055981.1	3	$20.6460^{+0.0080}_{-0.0062}$	$1997.395^{+0.010}_{-0.016}$	$2.37^{+0.31}_{-0.44}$	1320^{+120}_{-140}	$0.0376^{+0.0065}_{-0.0396}$	$2.38^{+0.48}_{-2.51}$	$0.580^{+0.059}_{-0.039}$	50^{+28}_{-23}	$7.0^{+8.0}_{-6.4}$
206061524.1	3	$5.879829^{+0.000052}_{-0.000052}$	$1980.44412^{+0.00034}_{-0.00033}$	$2.530^{+0.054}_{-0.062}$	9542^{+91}_{-90}	$0.0912^{+0.0038}_{-0.0055}$	$6.97^{+0.57}_{-0.60}$	$0.701^{+0.049}_{-0.044}$	$17.6^{+2.2}_{-1.8}$	45^{+13}_{-11}
206082454.1	3	$29.6245^{+0.0016}_{-0.0015}$	$1993.5410^{+0.0011}_{-0.0013}$	$5.00^{+0.12}_{-0.12}$	1302^{+26}_{-27}	$0.0336^{+0.0013}_{-0.0025}$	$3.02^{+0.39}_{-0.30}$	$0.824^{+0.102}_{-0.056}$	$43.1^{+7.7}_{-3.6}$	$21.5^{+9.4}_{-4.7}$
206082454.2	3	$14.3181^{+0.0017}_{-0.0016}$	$1982.2891^{+0.0042}_{-0.0046}$	$3.83^{+0.19}_{-0.28}$	375^{+20}_{-21}	$0.0188^{+0.0012}_{-0.0028}$	$1.69^{+0.24}_{-0.28}$	$0.824^{+0.102}_{-0.056}$	$25.0^{+9.7}_{-4.2}$	64^{+52}_{-23}
206096602.1	3	$6.67196^{+0.00016}_{-0.00017}$	$1982.68502^{+0.00087}_{-0.00089}$	$1.560^{+0.048}_{-0.074}$	788^{+20}_{-22}	$0.0269^{+0.0012}_{-0.0029}$	$1.697^{+0.089}_{-0.204}$	$0.577^{+0.015}_{-0.032}$	$29.8^{+8.7}_{-3.7}$	$25.8^{+15.0}_{-7.0}$
206096602.2	3	$16.19803^{+0.00073}_{-0.00068}$	$1991.5447^{+0.0011}_{-0.0012}$	$1.60^{+0.14}_{-0.21}$	828^{+31}_{-33}	$0.0275^{+0.0029}_{-0.0081}$	$1.73^{+0.19}_{-0.52}$	$0.577^{+0.015}_{-0.032}$	68^{+35}_{-14}	$5.0^{+5.2}_{-2.1}$
206101302.1	3	$25.4569^{+0.0019}_{-0.0019}$	$1983.6453^{+0.0024}_{-0.0022}$	$4.80^{+0.15}_{-0.19}$	790^{+27}_{-28}	$0.0264^{+0.0015}_{-0.0037}$	$3.66^{+0.35}_{-0.52}$	$1.269^{+0.097}_{-0.013}$	$36.5^{+10.9}_{-4.9}$	$35.7^{+22.1}_{-9.9}$
206101302.2	3	$20.2653^{+0.0039}_{-0.0041}$	$1989.5813^{+0.0038}_{-0.0039}$	$5.25^{+0.21}_{-0.27}$	481^{+25}_{-26}	$0.0209^{+0.0012}_{-0.0029}$	$2.89^{+0.28}_{-0.40}$	$1.269^{+0.097}_{-0.013}$	$26.5^{+8.2}_{-3.6}$	68^{+43}_{-19}
206103150.1	3	$4.159170^{+0.000011}_{-0.000012}$	$1978.818020^{+0.000095}_{-0.000091}$	$3.578^{+0.011}_{-0.012}$	12712^{+24}_{-25}	$0.10173^{+0.00052}_{-0.00112}$	$13.18^{+0.34}_{-0.19}$	$1.188^{+0.030}_{-0.011}$	$9.725^{+0.152}_{-0.067}$	367^{+23}_{-12}
206114294.1	3	$3.292013^{+0.000058}_{-0.000058}$	$1980.04971^{+0.00068}_{-0.00069}$	$1.103^{+0.073}_{-0.100}$	6580^{+210}_{-260}	$0.0783^{+0.0059}_{-0.0099}$	$5.76^{+0.94}_{-0.75}$	$0.674^{+0.098}_{-0.018}$	$21.4^{+5.6}_{-3.7}$	$18.0^{+10.9}_{-6.5}$
206125618.1	3	$6.53142^{+0.00034}_{-0.00034}$	$1979.6593^{+0.0020}_{-0.0020}$	$3.26^{+0.11}_{-0.13}$	950^{+34}_{-35}	$0.0295^{+0.0015}_{-0.0030}$	$2.79^{+0.14}_{-0.29}$	$0.867^{+0.013}_{-0.023}$	$13.9^{+4.0}_{-1.8}$	173^{+100}_{-48}
206133795.1	3	$13.8543^{+0.0029}_{-0.0027}$	$1980.7839^{+0.0078}_{-0.0086}$	$5.05^{+0.29}_{-0.46}$	269^{+16}_{-16}	$0.0158^{+0.0011}_{-0.0025}$	$3.18^{+0.33}_{-0.51}$	$1.848^{+0.143}_{-0.058}$	$18.3^{+6.4}_{-3.1}$	100^{+72}_{-34}
206135170.1	3	$2.59824^{+0.00012}_{-0.00012}$	$1978.8059^{+0.0019}_{-0.0021}$	$1.044^{+0.096}_{-0.159}$	8700^{+500}_{-620}	$0.0895^{+0.0074}_{-0.0384}$	$7.70^{+0.93}_{-3.39}$	$0.788^{+0.069}_{-0.079}$	$18.1^{+7.4}_{-3.6}$	40^{+33}_{-18}
206135682.1	3	$20.2009^{+0.0032}_{-0.0019}$	$1988.5398^{+0.0025}_{-0.0031}$	$3.58^{+0.15}_{-0.18}$	982^{+37}_{-39}	$0.0300^{+0.0016}_{-0.0036}$	$1.89^{+0.13}_{-0.26}$	$0.577^{+0.025}_{-0.040}$	$39.2^{+11.6}_{-5.3}$	$16.6^{+9.9}_{-5.1}$
206135682.2	3	$5.02629^{+0.00027}_{-0.00027}$	$1978.7646^{+0.0020}_{-0.0020}$	$2.27^{+0.10}_{-0.12}$	485^{+22}_{-23}	$0.0210^{+0.0012}_{-0.0030}$	$1.322^{+0.096}_{-0.213}$	$0.577^{+0.025}_{-0.040}$	$15.1^{+4.8}_{-2.1}$	112^{+72}_{-35}
206135682.3	3	$9.65869^{+0.00070}_{-0.00071}$	$1977.8750^{+0.0029}_{-0.0029}$	$2.85^{+0.14}_{-0.20}$	522^{+25}_{-26}	$0.0220^{+0.0014}_{-0.0035}$	$1.38^{+0.11}_{-0.24}$	$0.577^{+0.025}_{-0.040}$	$22.8^{+8.0}_{-3.7}$	49^{+35}_{-17}
206135682.4	3	$37.8270^{+0.0049}_{-0.0044}$	$1995.0715^{+0.0033}_{-0.0038}$	$3.41^{+0.15}_{-0.18}$	556^{+34}_{-36}	$0.0226^{+0.0013}_{-0.0026}$	$1.42^{+0.10}_{-0.19}$	$0.577^{+0.025}_{-0.040}$	$77.0^{+21.6}_{-9.8}$	$4.3^{+2.4}_{-1.2}$
206144956.1	3	$12.64655^{+0.00050}_{-0.00050}$	$1986.3299^{+0.0012}_{-0.0012}$	$2.94^{+0.12}_{-0.16}$	391^{+10}_{-11}	$0.0187^{+0.0013}_{-0.0029}$	$1.47^{+0.13}_{-0.25}$	$0.722^{+0.039}_{-0.041}$	$29.2^{+8.9}_{-4.1}$	$26.9^{+17.0}_{-9.0}$
206146957.1	3	$5.76218^{+0.00055}_{-0.00054}$	$1979.8688^{+0.0032}_{-0.0033}$	$2.24^{+0.12}_{-0.14}$	174^{+10}_{-11}	$0.01285^{+0.00074}_{-0.00168}$	$1.217^{+0.073}_{-0.162}$	$0.868^{+0.016}_{-0.023}$	$17.2^{+6.5}_{-2.7}$	151^{+115}_{-47}
206151047.1	3	$0.3584061^{+0.0000087}_{-0.0000087}$	$1977.32944^{+0.00097}_{-0.00097}$	$0.98^{+0.16}_{-0.15}$	341^{+18}_{-19}	$0.0238^{+0.0078}_{-0.0256}$	$2.66^{+0.96}_{-2.87}$	$1.03^{+0.15}_{-0.11}$	$1.05^{+0.38}_{-2.01}$	$48000^{+37000}_{-185000}$
206154641.1	3	$2.4841981^{+0.0000032}_{-0.0000032}$	$1977.651370^{+0.000049}_{-0.000049}$	$2.013^{+0.021}_{-0.020}$	9384^{+24}_{-25}	$0.1077^{+0.0029}_{-0.0039}$	$15.54^{+0.68}_{-0.76}$	$1.322^{+0.046}_{-0.043}$	$6.59^{+0.15}_{-0.18}$	1158^{+100}_{-102}
206155547.1	3	$24.38752^{+0.00032}_{-0.00042}$	$1985.88403^{+0.00028}_{-0.00028}$	$6.029^{+0.035}_{-0.037}$	23710^{+100}_{-100}	$0.1438^{+0.0019}_{-0.0029}$	$22.4^{+3.6}_{-4.1}$	$1.43^{+0.23}_{-0.26}$	$34.68^{+1.03}_{-0.65}$	55^{+20}_{-22}
206155922.1	3	$4.00932^{+0.00047}_{-0.00047}$	$1978.8761^{+0.0040}_{-0.0037}$	$1.90^{+0.13}_{-0.15}$	227^{+18}_{-18}	$0.0146^{+0.0011}_{-0.0020}$	$1.08^{+0.13}_{-0.20}$	$0.680^{+0.062}_{-0.085}$	$14.1^{+4.9}_{-2.4}$	114^{+81}_{-48}
206159027.1	3	$8.05423^{+0.00045}_{-0.00048}$	$1982.3290^{+0.0019}_{-0.0019}$	$2.98^{+0.13}_{-0.18}$	668^{+25}_{-26}	$0.0242^{+0.0018}_{-0.0045}$	$1.73^{+0.15}_{-0.33}$	$0.655^{+0.030}_{-0.018}$	$18.4^{+6.3}_{-2.8}$	68^{+47}_{-21}
206159027.2	3	$20.6714^{+0.0025}_{-0.0024}$	$1994.7682^{+0.0028}_{-0.0031}$	$2.48^{+0.16}_{-0.21}$	455^{+26}_{-27}	$0.0205^{+0.0015}_{-0.0034}$	$1.47^{+0.13}_{-0.25}$	$0.655^{+0.030}_{-0.018}$	$56.0^{+20.7}_{-9.6}$	$7.3^{+5.4}_{-2.5}$
206162305.1	3	$7.06500^{+0.00040}_{-0.00040}$	$1982.7863^{+0.0020}_{-0.0020}$	$1.76^{+0.13}_{-0.21}$	2210^{+120}_{-130}	$0.0449^{+0.0043}_{-0.0107}$	$2.40^{+0.35}_{-0.68}$	$0.491^{+0.055}_{-0.076}$	$27.5^{+11.7}_{-5.2}$	$15.9^{+14.6}_{-9.8}$
206169157.1	3		$2005.43632^{+0.00088}_{-0.00070}$	$5.60^{+0.67}_{-0.52}$	2243^{+15}_{-15}	$0.0402^{+0.0033}_{-0.0056}$	$7.72^{+0.74}_{-1.14}$	$1.763^{+0.084}_{-0.081}$		
206169157.2	3		$2030.8137^{+0.0013}_{-0.0014}$	$10.71^{+0.27}_{-0.29}$	1821^{+120}_{-26}	$0.162^{+0.034}_{-0.027}$	$31.1^{+6.7}_{-5.4}$	$1.763^{+0.084}_{-0.081}$		
206169375.1	3	$0.3674645^{+0.0000043}_{-0.0000043}$	$1977.33220^{+0.00047}_{-0.00047}$	$0.838^{+0.079}_{-0.100}$	631^{+25}_{-26}	$0.030^{+0.010}_{-0.036}$	$3.9^{+1.4}_{-4.7}$	$1.18^{+0.13}_{-0.11}$	$1.92^{+0.96}_{-1.66}$	18000^{+18000}_{-31000}
206181769.1	3	$13.97820^{+0.00048}_{-0.00047}$	$1984.4452^{+0.0012}_{-0.0013}$	$3.445^{+0.081}_{-0.108}$	1076^{+25}_{-25}	$0.0315^{+0.0012}_{-0.0028}$	$2.69^{+0.23}_{-0.26}$	$0.783^{+0.060}_{-0.032}$	$28.7^{+7.5}_{-3.2}$	$31.9^{+17.5}_{-7.6}$
206192335.1	3	$3.59922^{+0.00014}_{-0.00015}$	$1979.9449^{+0.0016}_{-0.0016}$	$1.90^{+0.11}_{-0.18}$	360^{+13}_{-14}	$0.0185^{+0.0014}_{-0.0037}$	$1.63^{+0.15}_{-0.34}$	$0.809^{+0.042}_{-0.050}$	$12.3^{+6.0}_{-2.6}$	230^{+230}_{-100}

Table A.1: Our sample of planet candidates from C0-8. (continued)

Candidate	C#	Period (days)	t_0 (BJD - 2455000)	Duration (hours)	Depth (ppm)	R_p/R_*	R_p ($R_\oplus$)	R_* ($R_\odot$)	a/R_*	Inc. Flux ($S_\oplus$)
206208956.1	3	$5.01038^{+0.00019}_{-0.00017}$	$1979.4663^{+0.0015}_{-0.0016}$	$0.838^{+0.085}_{-0.094}$	718^{+55}_{-59}	$0.0257^{+0.0023}_{-0.0047}$	$4.28^{+0.76}_{-0.85}$	$1.53^{+0.23}_{-0.11}$	$40.7^{+15.1}_{-7.7}$	28^{+23}_{-12}
206215704.1	3	$2.25558^{+0.00016}_{-0.00015}$	$1978.4312^{+0.0027}_{-0.0026}$	$0.99^{+0.13}_{-0.15}$	2690^{+230}_{-270}	$0.0501^{+0.0043}_{-0.0095}$	$2.00^{+0.45}_{-0.54}$	$0.367^{+0.076}_{-0.070}$	$16.0^{+5.8}_{-3.6}$	36^{+34}_{-27}
206215704.2	3	$3.11551^{+0.00032}_{-0.00032}$	$1977.2914^{+0.0032}_{-0.0038}$	$0.79^{+0.20}_{-0.24}$	1880^{+360}_{-520}	$0.0434^{+0.0067}_{-0.0194}$	$1.74^{+0.45}_{-0.84}$	$0.367^{+0.076}_{-0.070}$	26^{+13}_{-12}	14^{+16}_{-15}
206226146.1	3	$11.63547^{+0.00082}_{-0.00101}$	$1984.1245^{+0.0032}_{-0.0026}$	$2.30^{+0.15}_{-0.22}$	767^{+39}_{-41}	$0.0268^{+0.0018}_{-0.0041}$	$2.60^{+0.20}_{-0.41}$	$0.892^{+0.037}_{-0.029}$	$34.2^{+12.3}_{-5.9}$	$24.7^{+17.9}_{-8.7}$
206245553.1	3	$7.49569^{+0.00025}_{-0.00025}$	$1980.1755^{+0.0012}_{-0.0012}$	$3.591^{+0.067}_{-0.088}$	589^{+12}_{-13}	$0.02300^{+0.00080}_{-0.00212}$	$2.71^{+0.11}_{-0.29}$	$1.079^{+0.026}_{-0.059}$	$14.8^{+3.3}_{-1.4}$	204^{+91}_{-45}
206260577.1	3	$1.982116^{+0.000012}_{-0.000012}$	$1977.27663^{+0.00024}_{-0.00024}$	$1.604^{+0.047}_{-0.052}$	3731^{+35}_{-35}	$0.157^{+0.042}_{-0.048}$	35^{+10}_{-13}	$2.05^{+0.26}_{-0.47}$	$4.92^{+0.35}_{-0.32}$	1700^{+510}_{-820}
206262341.1	3	$36.9321^{+0.0020}_{-0.0020}$	$1991.5570^{+0.0014}_{-0.0015}$	$6.103^{+0.074}_{-0.095}$	856^{+19}_{-20}	$0.02864^{+0.00054}_{-0.00121}$	$2.98^{+0.45}_{-0.28}$	$0.955^{+0.143}_{-0.080}$	$45.0^{+7.4}_{-2.5}$	$22.9^{+10.2}_{-4.7}$
206268084.1	3	$8.4532^{+0.0021}_{-0.0021}$	$1982.7546^{+0.0085}_{-0.0087}$	$3.48^{+0.32}_{-0.49}$	595^{+54}_{-58}	$0.0234^{+0.0021}_{-0.0044}$	$2.66^{+0.23}_{-0.50}$	$1.0419^{+0.0064}_{-0.0130}$	$16.2^{+6.2}_{-3.3}$	130^{+99}_{-54}
206268299.1	3	$19.5688^{+0.0014}_{-0.0014}$	$1978.4251^{+0.0029}_{-0.0030}$	$5.70^{+0.36}_{-0.29}$	818^{+24}_{-24}	$0.0321^{+0.0065}_{-0.0041}$	$3.66^{+0.81}_{-0.48}$	$1.047^{+0.094}_{-0.032}$	$13.8^{+2.7}_{-12.5}$	250^{+110}_{-460}
206298289.1	3	$0.434832^{+0.000012}_{-0.000011}$	$1977.16325^{+0.00098}_{-0.00102}$	$0.895^{+0.092}_{-0.091}$	762^{+35}_{-39}	$0.0265^{+0.0024}_{-0.0051}$	$0.96^{+0.16}_{-0.20}$	$0.333^{+0.048}_{-0.027}$	$3.30^{+1.34}_{-0.64}$	730^{+670}_{-330}
206315178.1	3	$0.3176828^{+0.0000017}_{-0.0000017}$	$1977.20771^{+0.00022}_{-0.00022}$	$0.818^{+0.050}_{-0.082}$	15930^{+480}_{-680}	$0.116^{+0.011}_{-0.043}$	$11.9^{+1.7}_{-4.5}$	$0.944^{+0.102}_{-0.070}$	$2.97^{+1.02}_{-0.43}$	1150^{+850}_{-420}
206317286.1	3	$17.5125^{+0.0029}_{-0.0025}$	$1977.8273^{+0.0048}_{-0.0061}$	$3.93^{+0.20}_{-0.29}$	948^{+57}_{-58}	$0.0294^{+0.0022}_{-0.0046}$	$2.15^{+0.20}_{-0.37}$	$0.669^{+0.037}_{-0.050}$	$30.5^{+10.1}_{-4.7}$	$28.3^{+19.0}_{-9.8}$
206317286.2	3	$1.58316^{+0.00013}_{-0.00013}$	$1978.0822^{+0.0035}_{-0.0034}$	$1.75^{+0.12}_{-0.15}$	300^{+26}_{-27}	$0.0168^{+0.0013}_{-0.0023}$	$1.22^{+0.12}_{-0.19}$	$0.669^{+0.037}_{-0.050}$	$6.1^{+2.0}_{-1.0}$	710^{+490}_{-260}
206329937.1	3	$10.49927^{+0.00088}_{-0.00086}$	$1984.0477^{+0.0026}_{-0.0027}$	$2.78^{+0.15}_{-0.23}$	575^{+28}_{-28}	$0.0219^{+0.0020}_{-0.0060}$	$1.43^{+0.16}_{-0.44}$	$0.599^{+0.037}_{-0.083}$	$26.1^{+9.7}_{-3.6}$	32^{+25}_{-13}
206344313.1	3	$5.23189^{+0.00047}_{-0.00046}$	$1978.9027^{+0.0034}_{-0.0035}$	$2.27^{+0.23}_{-0.37}$	2860^{+220}_{-250}	$0.0529^{+0.0074}_{-0.0322}$	$3.62^{+0.77}_{-2.21}$	$0.627^{+0.100}_{-0.036}$	$14.8^{+7.4}_{-4.5}$	42^{+44}_{-26}
206348688.1	3	$7.81751^{+0.00059}_{-0.00059}$	$1983.4321^{+0.0029}_{-0.0028}$	$5.19^{+0.14}_{-0.20}$	392^{+13}_{-14}	$0.01892^{+0.00093}_{-0.00253}$	$3.08^{+0.39}_{-0.41}$	$1.492^{+0.175}_{-0.025}$	$10.3^{+3.3}_{-1.4}$	440^{+300}_{-120}
206348688.2	3	$18.2890^{+0.0073}_{-0.0054}$	$1992.7346^{+0.0054}_{-0.0057}$	$6.73^{+0.37}_{-0.57}$	410^{+21}_{-22}	$0.0194^{+0.0012}_{-0.0034}$	$3.16^{+0.42}_{-0.56}$	$1.492^{+0.175}_{-0.025}$	$18.2^{+7.1}_{-3.1}$	140^{+114}_{-48}
206358352.1	3	$1.136660^{+0.000058}_{-0.000057}$	$1978.0229^{+0.0018}_{-0.0021}$	$1.24^{+0.12}_{-0.20}$	308^{+21}_{-22}	$0.0169^{+0.0018}_{-0.0066}$	$3.18^{+0.34}_{-1.25}$	$1.724^{+0.022}_{-0.104}$	$6.0^{+3.7}_{-1.3}$	1330^{+1650}_{-610}
206360885.1	3	$12.4404^{+0.0031}_{-0.0026}$	$1987.3510^{+0.0056}_{-0.0060}$	$3.98^{+0.60}_{-0.81}$	1690^{+120}_{-120}	$0.0426^{+0.0074}_{-0.0369}$	$2.72^{+0.53}_{-2.36}$	$0.586^{+0.051}_{-0.015}$	$18.5^{+10.1}_{-8.4}$	20^{+22}_{-18}
206360885.2	3	$1.49462^{+0.00014}_{-0.00014}$	$1978.4813^{+0.0035}_{-0.0035}$	$1.84^{+0.25}_{-0.39}$	779^{+71}_{-75}	$0.0281^{+0.0042}_{-0.0265}$	$1.80^{+0.31}_{-1.69}$	$0.586^{+0.051}_{-0.015}$	$4.9^{+3.1}_{-1.8}$	280^{+360}_{-200}
206369173.1	3	$2.018725^{+0.000066}_{-0.000064}$	$1979.0270^{+0.0011}_{-0.0011}$	$2.235^{+0.090}_{-0.099}$	435^{+10}_{-10}	$0.056^{+0.016}_{-0.018}$	91^{+26}_{-30}	$14.96^{+0.47}_{-1.21}$	$2.13^{+0.23}_{-0.29}$	5100^{+1500}_{-1900}
206414361.1	3	$3.47722^{+0.00037}_{-0.00038}$	$1977.4625^{+0.0042}_{-0.0043}$	$2.09^{+0.22}_{-0.36}$	684^{+55}_{-59}	$0.0253^{+0.0027}_{-0.0086}$	$1.53^{+0.23}_{-0.54}$	$0.556^{+0.061}_{-0.053}$	$10.9^{+6.1}_{-2.6}$	62^{+71}_{-32}
206417197.1	3	$0.442185^{+0.000013}_{-0.000013}$	$1977.4157^{+0.0012}_{-0.0012}$	$1.55^{+0.22}_{-0.14}$	291^{+12}_{-12}	$0.025^{+0.011}_{-0.022}$	$2.02^{+0.88}_{-1.83}$	$0.754^{+0.030}_{-0.017}$	$0.69^{+0.17}_{-0.11}$	$55000^{+27000}_{-270000}$
206432863.1	3	$11.98934^{+0.00013}_{-0.00014}$	$1983.82772^{+0.00041}_{-0.00041}$	$5.685^{+0.032}_{-0.036}$	7257^{+37}_{-37}	$0.07846^{+0.00070}_{-0.00134}$	$14.77^{+0.41}_{-0.40}$	$1.726^{+0.046}_{-0.036}$	$17.12^{+0.66}_{-0.27}$	$126.0^{+14.0}_{-10.0}$
206476150.1	3	$12.19649^{+0.00082}_{-0.00080}$	$1980.1794^{+0.0025}_{-0.0026}$	$1.928^{+0.100}_{-0.132}$	387^{+25}_{-26}	$0.0192^{+0.0011}_{-0.0019}$	$2.23^{+0.15}_{-0.24}$	$1.062^{+0.038}_{-0.034}$	$42.9^{+13.7}_{-6.5}$	$16.2^{+10.4}_{-5.0}$
206535016.1	3	$20.3997^{+0.0013}_{-0.0012}$	$1996.3695^{+0.0013}_{-0.0014}$	$1.649^{+0.096}_{-0.128}$	1066^{+42}_{-43}	$0.0312^{+0.0021}_{-0.0044}$	$2.65^{+0.29}_{-0.40}$	$0.778^{+0.066}_{-0.041}$	85^{+27}_{-14}	$4.0^{+2.7}_{-1.4}$
210363145.1	4	$8.20023^{+0.00023}_{-0.00023}$	$2062.60496^{+0.00099}_{-0.00102}$	$2.564^{+0.075}_{-0.096}$	1007^{+24}_{-25}	$0.0296^{+0.0017}_{-0.0040}$	$2.53^{+0.18}_{-0.35}$	$0.782^{+0.031}_{-0.024}$	$22.3^{+5.7}_{-2.8}$	45^{+23}_{-12}
210371175.1	4	$11.3256^{+0.0019}_{-0.0018}$	$2063.1621^{+0.0061}_{-0.0059}$	$4.81^{+0.28}_{-0.38}$	427^{+30}_{-31}	$0.0192^{+0.0017}_{-0.0047}$	$2.18^{+0.24}_{-0.57}$	$1.043^{+0.070}_{-0.082}$	$16.1^{+6.3}_{-2.4}$	106^{+84}_{-36}
210384192.1	4	$2.92370^{+0.00030}_{-0.00055}$	$2063.5270^{+0.0082}_{-0.0040}$	$1.48^{+0.19}_{-0.47}$	1790^{+220}_{-220}	$0.0411^{+0.0041}_{-0.0080}$	$2.57^{+0.95}_{-0.67}$	$0.573^{+0.204}_{-0.098}$	$13.0^{+5.2}_{-3.6}$	54^{+58}_{-36}
210394706.1	4	$15.0818^{+0.0025}_{-0.0024}$	$2065.5478^{+0.0075}_{-0.0063}$	$3.20^{+0.21}_{-0.36}$	1161^{+73}_{-78}	$0.0326^{+0.0023}_{-0.0045}$	$1.83^{+0.25}_{-0.29}$	$0.514^{+0.058}_{-0.039}$	$32.3^{+10.4}_{-5.4}$	$11.9^{+8.1}_{-4.4}$
210394706.2	4	$3.16363^{+0.00029}_{-0.00029}$	$2063.9343^{+0.0040}_{-0.0040}$	$1.76^{+0.14}_{-0.19}$	530^{+46}_{-49}	$0.0222^{+0.0019}_{-0.0038}$	$1.25^{+0.18}_{-0.23}$	$0.514^{+0.058}_{-0.039}$	$12.0^{+4.5}_{-2.2}$	85^{+67}_{-34}
210401157.1	4	$1.3155918^{+0.0000043}_{-0.0000084}$	$2062.020838^{+0.000089}_{-0.000071}$	$2.197^{+0.039}_{-0.041}$	37330^{+120}_{-120}	$0.2082^{+0.0048}_{-0.0085}$	$38.3^{+7.3}_{-7.8}$	$1.69^{+0.32}_{-0.34}$	$4.056^{+0.060}_{-0.090}$	3400^{+1300}_{-1400}
210402237.1	4	$10.99501^{+0.00034}_{-0.00034}$	$2070.2428^{+0.0010}_{-0.0010}$	$4.485^{+0.058}_{-0.085}$	1050^{+19}_{-19}	$0.03045^{+0.00073}_{-0.00203}$	$4.55^{+0.11}_{-0.31}$	$1.3704^{+0.0074}_{-0.0131}$	$18.1^{+2.8}_{-1.2}$	78^{+24}_{-10}
210403955.1	4	$28.8819^{+0.0028}_{-0.0030}$	$2082.9257^{+0.0020}_{-0.0019}$	$4.22^{+0.12}_{-0.16}$	864^{+32}_{-33}	$0.0279^{+0.0013}_{-0.0027}$	$2.39^{+0.20}_{-0.30}$	$0.785^{+0.055}_{-0.065}$	$48.5^{+12.1}_{-5.2}$	$11.8^{+6.1}_{-3.2}$
210403955.2	4	$19.0912^{+0.0045}_{-0.0041}$	$2077.6099^{+0.0062}_{-0.0068}$	$5.14^{+0.47}_{-0.58}$	562^{+29}_{-30}	$0.0237^{+0.0030}_{-0.0059}$	$2.03^{+0.30}_{-0.53}$	$0.785^{+0.055}_{-0.065}$	$22.6^{+12.0}_{-6.9}$	54^{+58}_{-35}
210403955.3	4	$5.60473^{+0.00058}_{-0.00062}$	$2066.4919^{+0.0043}_{-0.0040}$	$3.04^{+0.17}_{-0.23}$	301^{+17}_{-18}	$0.0164^{+0.0012}_{-0.0027}$	$1.41^{+0.14}_{-0.26}$	$0.785^{+0.055}_{-0.065}$	$12.4^{+4.1}_{-1.9}$	179^{+121}_{-63}
210423938.1	4	$19.8606^{+0.0015}_{-0.0015}$	$2072.0136^{+0.0029}_{-0.0031}$	$3.88^{+0.39}_{-0.40}$	903^{+37}_{-39}	$0.0312^{+0.0053}_{-0.0070}$	$2.21^{+0.45}_{-0.54}$	$0.648^{+0.071}_{-0.064}$	28^{+13}_{-13}	24^{+23}_{-22}
210448987.1	4	$6.10241^{+0.00028}_{-0.00027}$	$2064.3396^{+0.0019}_{-0.0020}$	$2.344^{+0.100}_{-0.147}$	1076^{+41}_{-42}	$0.0310^{+0.0034}_{-0.0043}$	$2.38^{+0.19}_{-0.34}$	$0.702^{+0.034}_{-0.023}$	$18.1^{+5.4}_{-2.5}$	50^{+30}_{-14}

Table A.1: Our sample of planet candidates from C0-8. (continued)

Candidate	C#	Period (days)	t_0 (BJD - 2455000)	Duration (hours)	Depth (ppm)	R_p/R_*	R_p ($R_\oplus$)	R_* ($R_\odot$)	a/R_*	Inc. Flux ($S_\oplus$)
210495066.1	4	$3.74234^{+0.00027}_{-0.00027}$	$2063.4744^{+0.0026}_{-0.0027}$	$1.87^{+0.12}_{-0.15}$	944^{+59}_{-63}	$0.0293^{+0.0021}_{-0.0039}$	$1.61^{+0.37}_{-0.22}$	$0.502^{+0.110}_{-0.020}$	$13.8^{+4.1}_{-2.2}$	39^{+29}_{-13}
210508766.1	4	$2.747128^{+0.000095}_{-0.000100}$	$2064.3154^{+0.0014}_{-0.0014}$	$1.662^{+0.072}_{-0.081}$	920^{+33}_{-35}	$0.0293^{+0.0015}_{-0.0030}$	$1.36^{+0.11}_{-0.14}$	$0.424^{+0.025}_{-0.010}$	$11.6^{+3.2}_{-1.5}$	72^{+42}_{-19}
210508766.2	4	$9.99791^{+0.00055}_{-0.00053}$	$2066.2688^{+0.0018}_{-0.0019}$	$2.72^{+0.15}_{-0.20}$	1462^{+53}_{-55}	$0.0368^{+0.0032}_{-0.0059}$	$1.70^{+0.18}_{-0.28}$	$0.424^{+0.025}_{-0.010}$	$24.7^{+9.2}_{-4.7}$	$16.0^{+12.2}_{-6.2}$
210508766.3	4	$24.2747^{+0.0014}_{-0.0014}$	$2074.4696^{+0.0017}_{-0.0018}$	$1.27^{+0.12}_{-0.16}$	1239^{+91}_{-93}	$0.0337^{+0.0032}_{-0.0053}$	$1.56^{+0.17}_{-0.25}$	$0.424^{+0.025}_{-0.010}$	130^{+43}_{-26}	$0.57^{+0.39}_{-0.23}$
210524811.1	4	$7.46967^{+0.00052}_{-0.00056}$	$2069.1588^{+0.0030}_{-0.0026}$	$1.66^{+0.33}_{-0.26}$	3800^{+310}_{-310}	$0.079^{+0.024}_{-0.073}$	$2.40^{+0.81}_{-2.25}$	$0.279^{+0.042}_{-0.036}$	$18.9^{+4.3}_{-21.3}$	21^{+13}_{-47}
210550063.1	4	$2.165976^{+0.000033}_{-0.000028}$	$2062.81932^{+0.00057}_{-0.00062}$	$1.526^{+0.029}_{-0.102}$	$502.5^{+9.3}_{-9.5}$	$0.0217^{+0.0012}_{-0.0033}$	$2.61^{+0.44}_{-0.53}$	$1.10^{+0.18}_{-0.15}$	$9.4^{+4.4}_{-1.6}$	520^{+520}_{-230}
210558622.1	4	$19.56236^{+0.00059}_{-0.00058}$	$2064.2158^{+0.0011}_{-0.0011}$	$6.22^{+0.16}_{-0.19}$	1500^{+22}_{-22}	$0.0381^{+0.0030}_{-0.0033}$	$2.78^{+0.30}_{-0.32}$	$0.669^{+0.049}_{-0.052}$	$18.9^{+3.4}_{-5.3}$	45^{+17}_{-26}
210559259.1	4	$14.26763^{+0.00090}_{-0.00091}$	$2063.4255^{+0.0021}_{-0.0022}$	$3.62^{+0.12}_{-0.18}$	1051^{+36}_{-38}	$0.0310^{+0.0016}_{-0.0036}$	$2.04^{+0.11}_{-0.25}$	$0.603^{+0.013}_{-0.020}$	$27.5^{+8.0}_{-3.6}$	$33.3^{+19.4}_{-9.0}$
210564155.1	4	$4.86496^{+0.00029}_{-0.00028}$	$2062.7025^{+0.0020}_{-0.0021}$	$1.27^{+0.13}_{-0.22}$	1561^{+97}_{-111}	$0.0382^{+0.0035}_{-0.0104}$	$1.09^{+0.18}_{-0.35}$	$0.261^{+0.037}_{-0.044}$	$25.7^{+12.3}_{-6.0}$	$10.3^{+10.8}_{-7.0}$
210577548.1	4	$6.42149^{+0.00027}_{-0.00027}$	$2065.0006^{+0.0016}_{-0.0017}$	$2.883^{+0.080}_{-0.096}$	814^{+23}_{-23}	$0.0275^{+0.0011}_{-0.0023}$	$2.51^{+0.20}_{-0.24}$	$0.836^{+0.056}_{-0.037}$	$15.7^{+4.0}_{-1.7}$	101^{+54}_{-24}
210577548.2	4	$27.8522^{+0.0031}_{-0.0041}$	$2068.6225^{+0.0065}_{-0.0042}$	$4.61^{+0.22}_{-0.31}$	704^{+39}_{-39}	$0.0237^{+0.0018}_{-0.0048}$	$2.16^{+0.22}_{-0.45}$	$0.836^{+0.056}_{-0.037}$	$42.8^{+11.0}_{-4.8}$	$13.6^{+7.3}_{-3.3}$
210598340.1	4	$3.7342439^{+0.0000090}_{-0.0000091}$	$2063.094022^{+0.000092}_{-0.000091}$	$5.736^{+0.010}_{-0.010}$	12859^{+17}_{-17}	$0.10655^{+0.00053}_{-0.00183}$	$30.71^{+0.54}_{-6.89}$	$2.642^{+0.044}_{-0.591}$	$5.257^{+0.064}_{-0.084}$	1286^{+87}_{-581}
210605073.1	4	$0.5670195^{+0.0000091}_{-0.0000091}$	$2062.22752^{+0.00071}_{-0.00070}$	$0.963^{+0.086}_{-0.122}$	12460^{+670}_{-790}	$0.110^{+0.014}_{-0.081}$			$4.1^{+1.4}_{-1.1}$	
210625740.1	4	$2.386772^{+0.000072}_{-0.000073}$	$2062.6930^{+0.0013}_{-0.0013}$	$1.09^{+0.16}_{-0.15}$	12960^{+920}_{-950}	$0.128^{+0.027}_{-0.126}$	$4.0^{+1.5}_{-6.5}$	$0.286^{+0.090}_{-0.370}$	$12.6^{+2.7}_{-7.6}$	48^{+49}_{-197}
210626797.1	4	$43.36143^{+0.00065}_{-0.00066}$	$2072.56623^{+0.00046}_{-0.00045}$	$6.83^{+0.11}_{-0.13}$	8280^{+64}_{-66}	$0.186^{+0.048}_{-0.076}$	$29.8^{+9.3}_{-12.3}$	$1.472^{+0.258}_{-0.075}$	$28.4^{+1.4}_{-2.1}$	65^{+24}_{-12}
210659688.1	4	$2.357651^{+0.000092}_{-0.000090}$	$2062.6638^{+0.0012}_{-0.0012}$	$0.835^{+0.100}_{-0.136}$	4690^{+410}_{-470}	$0.0670^{+0.0073}_{-0.0343}$	$1.95^{+0.38}_{-1.09}$	$0.267^{+0.043}_{-0.060}$	$19.2^{+8.8}_{-5.1}$	20^{+21}_{-17}
210659945.1	4	$27.9329^{+0.0083}_{-0.0040}$	$2073.1600^{+0.0045}_{-0.0126}$	$3.24^{+0.27}_{-0.34}$	1740^{+100}_{-110}	$0.0402^{+0.0030}_{-0.0066}$	$2.51^{+0.66}_{-0.42}$	$0.573^{+0.144}_{-0.019}$	60^{+22}_{-11}	$2.22^{+2.00}_{-0.92}$
210664763.1	4	$3.72007^{+0.00047}_{-0.00035}$	$2064.2512^{+0.0045}_{-0.0065}$	$1.22^{+0.17}_{-0.18}$	225^{+26}_{-29}	$0.0145^{+0.0015}_{-0.0030}$	$1.55^{+0.20}_{-0.33}$	$0.986^{+0.077}_{-0.033}$	$19.9^{+7.9}_{-4.8}$	104^{+84}_{-50}
210667381.1	4	$5.32944^{+0.00062}_{-0.00064}$	$2066.7830^{+0.0040}_{-0.0038}$	$2.76^{+0.16}_{-0.20}$	260^{+18}_{-18}	$0.0156^{+0.0011}_{-0.0021}$	$1.55^{+0.11}_{-0.22}$	$0.911^{+0.017}_{-0.027}$	$12.9^{+4.6}_{-2.1}$	150^{+106}_{-50}
210678858.1	4	$31.3537^{+0.0019}_{-0.0019}$	$2073.0196^{+0.0014}_{-0.0015}$	$5.01^{+0.11}_{-0.15}$	1970^{+39}_{-40}	$0.0432^{+0.0022}_{-0.0030}$	$3.85^{+0.25}_{-0.29}$	$0.816^{+0.033}_{-0.023}$	$43.2^{+11.4}_{-6.6}$	$12.8^{+6.9}_{-4.0}$
210678858.2	4	$14.8484^{+0.0011}_{-0.0010}$	$2070.2224^{+0.0021}_{-0.0020}$	$3.60^{+0.13}_{-0.16}$	1018^{+34}_{-35}	$0.0302^{+0.0016}_{-0.0038}$	$2.68^{+0.18}_{-0.35}$	$0.816^{+0.033}_{-0.023}$	$28.9^{+7.8}_{-3.6}$	$28.8^{+15.8}_{-7.3}$
210678858.3	4	$10.0696^{+0.0012}_{-0.0013}$	$2071.2654^{+0.0042}_{-0.0042}$	$3.09^{+0.20}_{-0.29}$	395^{+32}_{-35}	$0.0190^{+0.0015}_{-0.0033}$	$1.69^{+0.15}_{-0.29}$	$0.816^{+0.033}_{-0.023}$	$21.9^{+7.9}_{-3.7}$	50^{+36}_{-17}
210696763.1	4	$5.76808^{+0.00040}_{-0.00040}$	$2062.4419^{+0.0026}_{-0.0027}$	$1.81^{+0.14}_{-0.22}$	2090^{+200}_{-210}	$0.0438^{+0.0038}_{-0.0080}$	$1.19^{+0.26}_{-0.25}$	$0.249^{+0.050}_{-0.025}$	$22.2^{+8.1}_{-4.0}$	$12.6^{+11.7}_{-5.9}$
210696763.2	4	$7.98471^{+0.00104}_{-0.00090}$	$2067.9254^{+0.0039}_{-0.0039}$	$1.92^{+0.25}_{-0.39}$	2020^{+160}_{-170}	$0.0439^{+0.0047}_{-0.0187}$	$1.19^{+0.27}_{-0.52}$	$0.249^{+0.050}_{-0.025}$	$27.5^{+14.8}_{-7.7}$	$8.2^{+10.0}_{-5.2}$
210696763.3	4	$3.65017^{+0.00029}_{-0.00027}$	$2065.1470^{+0.0025}_{-0.0026}$	$1.28^{+0.14}_{-0.21}$	1920^{+170}_{-170}	$0.0423^{+0.0037}_{-0.0079}$	$1.15^{+0.25}_{-0.24}$	$0.249^{+0.050}_{-0.025}$	$19.6^{+7.5}_{-4.2}$	$16.0^{+15.3}_{-8.3}$
210707130.1	4	$0.6845410^{+0.0000084}_{-0.0000100}$	$2061.94482^{+0.00063}_{-0.00050}$	$0.819^{+0.026}_{-0.046}$	400^{+15}_{-16}	$0.0186^{+0.0010}_{-0.0027}$	$1.36^{+0.13}_{-0.23}$	$0.671^{+0.052}_{-0.064}$	$5.80^{+1.52}_{-0.69}$	440^{+240}_{-130}
210718708.1	4	$8.77709^{+0.00062}_{-0.00061}$	$2070.0194^{+0.0026}_{-0.0027}$	$4.23^{+0.23}_{-0.23}$	865^{+28}_{-27}	$0.058^{+0.017}_{-0.029}$	$5.1^{+1.9}_{-2.6}$	$0.800^{+0.186}_{-0.028}$	$5.67^{+0.67}_{-0.97}$	920^{+480}_{-320}
210731500.1	4	$9.72664^{+0.00031}_{-0.00032}$	$2062.5749^{+0.0014}_{-0.0013}$	$4.68^{+0.19}_{-0.23}$	2692^{+51}_{-51}	$0.0512^{+0.0035}_{-0.0035}$	$8.42^{+0.79}_{-0.72}$	$1.508^{+0.099}_{-0.074}$	$12.9^{+3.1}_{-3.7}$	97^{+49}_{-57}
210750726.1	4	$4.61244^{+0.00011}_{-0.00011}$	$2066.21770^{+0.00101}_{-0.00093}$	$1.146^{+0.072}_{-0.084}$	2194^{+74}_{-79}	$0.0454^{+0.0026}_{-0.0038}$	$1.27^{+0.16}_{-0.42}$	$0.256^{+0.029}_{-0.082}$	$28.8^{+7.7}_{-4.1}$	$7.8^{+4.9}_{-7.6}$
210769880.1	4	$1.436756^{+0.000033}_{-0.000034}$	$2062.60861^{+0.00089}_{-0.00088}$	$2.556^{+0.091}_{-0.093}$	1125^{+21}_{-21}	$0.093^{+0.024}_{-0.026}$	110^{+31}_{-31}	$10.91^{+1.15}_{-0.51}$	$1.68^{+0.15}_{-0.17}$	4060^{+1150}_{-960}
210775710.1	4	$59.84871^{+0.00016}_{-0.00016}$	$2064.69716^{+0.00012}_{-0.00011}$	$4.285^{+0.042}_{-0.033}$	11942^{+35}_{-34}	$0.1031^{+0.0027}_{-0.0024}$	$12.00^{+1.35}_{-0.34}$	$1.067^{+0.117}_{-0.017}$	$108.1^{+5.3}_{-7.8}$	$3.06^{+0.74}_{-0.45}$
210777017.1	4	$11.3760^{+0.0015}_{-0.0013}$	$2070.3329^{+0.0035}_{-0.0037}$	$3.44^{+0.17}_{-0.20}$	946^{+50}_{-56}	$0.0293^{+0.0017}_{-0.0036}$	$2.03^{+0.21}_{-0.33}$	$0.636^{+0.055}_{-0.067}$	$23.0^{+6.7}_{-3.2}$	30^{+18}_{-10}
210801536.1	4	$0.89250^{+0.00013}_{-0.00013}$	$2062.0816^{+0.0069}_{-0.0061}$	$2.00^{+0.19}_{-0.23}$	162^{+14}_{-14}	$0.0123^{+0.0010}_{-0.0019}$	$2.7^{+1.7}_{-2.3}$	$2.0^{+1.3}_{-1.7}$	$2.94^{+1.01}_{-0.58}$	3800^{+7200}_{-9000}
210813978.1	4	$14.7619^{+0.0014}_{-0.0014}$	$2067.6011^{+0.0037}_{-0.0038}$	$2.69^{+0.11}_{-0.14}$	714^{+43}_{-43}	$0.0263^{+0.0012}_{-0.0020}$	$2.11^{+0.16}_{-5.40}$	$0.735^{+0.045}_{-1.884}$	$38.5^{+10.8}_{-4.7}$	17^{+10}_{-121}
210838726.1	4	$1.095962^{+0.000044}_{-0.000045}$	$2062.7201^{+0.0017}_{-0.0016}$	$0.927^{+0.091}_{-0.093}$	346^{+24}_{-26}	$0.0178^{+0.0016}_{-0.0039}$	$0.617^{+0.081}_{-0.151}$	$0.318^{+0.031}_{-0.035}$	$8.0^{+3.3}_{-1.5}$	122^{+105}_{-59}
210852232.1	4	$1.93426^{+0.00016}_{-0.00015}$	$2063.2550^{+0.0031}_{-0.0031}$	$2.18^{+0.21}_{-0.46}$	278^{+16}_{-17}	$0.0162^{+0.0020}_{-0.0097}$	$1.64^{+0.24}_{-0.99}$	$0.928^{+0.073}_{-0.042}$	$5.6^{+3.9}_{-1.4}$	760^{+1080}_{-390}
210852232.2	4	$3.43827^{+0.00016}_{-0.00017}$	$2065.0442^{+0.0019}_{-0.0019}$	$0.802^{+0.086}_{-0.089}$	414^{+39}_{-43}	$0.0195^{+0.0017}_{-0.0029}$	$1.98^{+0.23}_{-0.31}$	$0.928^{+0.073}_{-0.042}$	$29.1^{+9.3}_{-5.4}$	29^{+19}_{-11}
210894022.1	4	$5.35185^{+0.00048}_{-0.00050}$	$2062.6117^{+0.0037}_{-0.0036}$	$3.61^{+0.21}_{-0.30}$	$118.4^{+6.4}_{-6.4}$	$0.01011^{+0.00093}_{-0.00276}$	$1.41^{+0.15}_{-0.39}$	$1.275^{+0.064}_{-0.019}$	$9.9^{+4.2}_{-1.5}$	380^{+330}_{-120}

Table A.1: Our sample of planet candidates from C0-8. (continued)

Candidate	C#	Period (days)	t_0 (BJD - 2455000)	Duration (hours)	Depth (ppm)	R_p/R_*	R_p ($R_\oplus$)	R_* ($R_\odot$)	a/R_*	Inc. Flux ($S_\oplus$)
210933299.1	4	$8.4044^{+0.0015}_{-0.0024}$	$2066.6995^{+0.0071}_{-0.0067}$	$2.25^{+0.40}_{-0.83}$	1440^{+140}_{-150}	$0.0370^{+0.0040}_{-0.0121}$	$1.24^{+0.27}_{-0.58}$	$0.307^{+0.057}_{-0.102}$	$23.4^{+12.4}_{-9.5}$	14^{+17}_{-18}
210935498.1	4	$1.1829266^{+0.0000013}_{-0.0000014}$	$2061.845390^{+0.000042}_{-0.000041}$	$2.116^{+0.012}_{-0.014}$	15889^{+36}_{-38}	$0.1760^{+0.0047}_{-0.0026}$	$29.0^{+7.5}_{-14.0}$	$1.51^{+0.39}_{-0.73}$	$3.793^{+0.050}_{-0.034}$	4500^{+3300}_{-6200}
210956385.1	4	$56.6205^{+0.0011}_{-0.0011}$	$2065.41887^{+0.00078}_{-0.00079}$	$5.74^{+0.11}_{-0.12}$	7187^{+86}_{-84}	$0.0779^{+0.0028}_{-0.0044}$	$7.68^{+0.68}_{-0.58}$	$0.904^{+0.073}_{-0.046}$	$76.0^{+7.7}_{-5.4}$	$4.23^{+1.11}_{-0.75}$
210957318.1	4	$4.0984897^{+0.0000093}_{-0.0000093}$	$2063.807130^{+0.000087}_{-0.000087}$	$2.397^{+0.016}_{-0.016}$	17119^{+48}_{-48}	$0.1309^{+0.0024}_{-0.0040}$	$13.14^{+0.35}_{-1.38}$	$0.921^{+0.018}_{-0.092}$	$11.21^{+0.19}_{-0.26}$	210^{+12}_{-44}
210961508.1	4	$0.3499146^{+0.0000024}_{-0.0000024}$	$2062.10959^{+0.00027}_{-0.00027}$	$1.902^{+0.028}_{-0.025}$	$1103.6^{+8.7}_{-8.8}$	$0.149^{+0.021}_{-0.014}$	$39.4^{+5.8}_{-6.1}$	$2.43^{+0.10}_{-0.30}$	$0.668^{+0.011}_{-0.037}$	51200^{+5200}_{-14000}
210965800.1	4	$8.74809^{+0.00021}_{-0.00018}$	$2070.33654^{+0.00081}_{-0.00091}$	$3.426^{+0.059}_{-0.100}$	1449^{+20}_{-20}	$0.03745^{+0.00078}_{-0.00214}$	$3.83^{+0.24}_{-0.28}$	$0.938^{+0.055}_{-0.044}$	$18.4^{+4.2}_{-1.9}$	81^{+38}_{-18}
210965800.2	4	$4.27681^{+0.00022}_{-0.00023}$	$2063.8492^{+0.0023}_{-0.0022}$	$2.81^{+0.12}_{-0.22}$	536^{+18}_{-19}	$0.0222^{+0.0016}_{-0.0045}$	$2.27^{+0.21}_{-0.47}$	$0.938^{+0.055}_{-0.044}$	$10.0^{+4.1}_{-1.8}$	270^{+220}_{-100}
210965800.3	4	$13.16121^{+0.00099}_{-0.00096}$	$2071.1456^{+0.0024}_{-0.0023}$	$4.06^{+0.15}_{-0.22}$	731^{+30}_{-30}	$0.0256^{+0.0017}_{-0.0040}$	$2.62^{+0.24}_{-0.43}$	$0.938^{+0.055}_{-0.044}$	$22.0^{+6.9}_{-3.4}$	57^{+36}_{-18}
210965800.4	4	$21.0858^{+0.0012}_{-0.0012}$	$2064.5448^{+0.0024}_{-0.0021}$	$4.72^{+0.15}_{-0.35}$	872^{+25}_{-27}	$0.0289^{+0.0017}_{-0.0039}$	$2.95^{+0.25}_{-0.42}$	$0.938^{+0.055}_{-0.044}$	$29.7^{+13.7}_{-5.6}$	31^{+29}_{-12}
210965800.6	4	$1.82876^{+0.00015}_{-0.00015}$	$2062.0985^{+0.0032}_{-0.0031}$	$2.35^{+0.19}_{-0.39}$	235^{+13}_{-13}	$0.0143^{+0.0018}_{-0.0120}$	$1.46^{+0.20}_{-1.23}$	$0.938^{+0.055}_{-0.044}$	$5.19^{+3.76}_{-0.98}$	1010^{+1480}_{-400}
210968143.1	4	$13.73288^{+0.00042}_{-0.00043}$	$2064.9290^{+0.0011}_{-0.0011}$	$2.860^{+0.066}_{-0.084}$	1582^{+37}_{-38}	$0.0374^{+0.0013}_{-0.0029}$	$2.64^{+0.34}_{-0.29}$	$0.646^{+0.081}_{-0.048}$	$35.4^{+6.1}_{-2.7}$	$9.5^{+4.1}_{-2.0}$
210968143.2	4	$2.90022^{+0.00015}_{-0.00015}$	$2063.8466^{+0.0020}_{-0.0021}$	$1.304^{+0.080}_{-0.118}$	389^{+22}_{-23}	$0.0192^{+0.0012}_{-0.0022}$	$1.36^{+0.19}_{-0.19}$	$0.646^{+0.081}_{-0.048}$	$14.9^{+5.0}_{-2.6}$	54^{+39}_{-20}
211002562.1	4	$3.347872^{+0.000010}_{-0.000010}$	$2062.10541^{+0.00012}_{-0.00012}$	$3.726^{+0.010}_{-0.010}$	13334^{+34}_{-35}	$0.1169^{+0.0010}_{-0.0030}$	$28.1^{+5.8}_{-2.4}$	$2.20^{+0.46}_{-0.18}$	$5.407^{+0.051}_{-0.084}$	1150^{+480}_{-200}
211048999.1	4	$5.17222^{+0.00014}_{-0.00013}$	$2066.58058^{+0.00092}_{-0.00107}$	$1.766^{+0.063}_{-0.073}$	964^{+22}_{-23}	$0.0304^{+0.0013}_{-0.0022}$	$2.12^{+0.10}_{-0.17}$	$0.639^{+0.012}_{-0.021}$	$20.6^{+5.5}_{-2.4}$	66^{+36}_{-16}
211058748.1	4	$3.32257^{+0.00016}_{-0.00016}$	$2061.9237^{+0.0020}_{-0.0021}$	$1.65^{+0.10}_{-0.13}$	476^{+26}_{-28}	$0.0209^{+0.0015}_{-0.0032}$	$2.53^{+0.25}_{-0.39}$	$1.108^{+0.076}_{-0.024}$	$13.6^{+4.6}_{-2.2}$	128^{+91}_{-46}
211064647.1	4		$2106.9788^{+0.0011}_{-0.0011}$	$7.18^{+0.22}_{-0.25}$	12650^{+190}_{-190}	$0.252^{+0.072}_{-0.096}$	44^{+13}_{-17}	$1.60^{+0.12}_{-0.12}$		
211077024.1	4	$1.419714^{+0.000040}_{-0.000042}$	$2062.5891^{+0.0011}_{-0.0011}$	$1.38^{+0.11}_{-0.22}$	1565^{+70}_{-72}	$0.0380^{+0.0044}_{-0.0152}$	$1.18^{+0.19}_{-0.52}$	$0.284^{+0.030}_{-0.055}$	$6.9^{+3.8}_{-1.5}$	150^{+180}_{-110}
211087003.1	4		$2084.10719^{+0.00028}_{-0.00033}$	$6.793^{+0.066}_{-0.064}$	7960^{+43}_{-43}	$0.0824^{+0.0023}_{-0.0029}$	$8.7^{+1.6}_{-1.3}$	$0.96^{+0.18}_{-0.14}$		
211087003.2	4	$28.29213^{+0.00126}_{-0.00100}$	$2064.1582^{+0.0014}_{-0.0027}$	$4.46^{+0.11}_{-0.15}$	1270^{+20}_{-20}	$0.0338^{+0.0011}_{-0.0023}$	$3.55^{+0.66}_{-0.56}$	$0.96^{+0.18}_{-0.14}$	$46.5^{+8.1}_{-3.7}$	$23.8^{+12.0}_{-7.9}$
211089792.1	4	$3.2588130^{+0.0000053}_{-0.0000058}$	$2064.431699^{+0.000065}_{-0.000060}$	$2.196^{+0.016}_{-0.014}$	19011^{+53}_{-55}	$0.1292^{+0.0054}_{-0.0038}$	$11.38^{+0.87}_{-0.63}$	$0.807^{+0.051}_{-0.038}$	$11.23^{+0.41}_{-0.68}$	198^{+29}_{-30}
211107835.1	4	$18.8652^{+0.0025}_{-0.0025}$	$2066.3613^{+0.0045}_{-0.0043}$	$3.93^{+0.25}_{-0.34}$	561^{+36}_{-37}	$0.0224^{+0.0018}_{-0.0043}$	$1.57^{+0.22}_{-0.31}$	$0.642^{+0.075}_{-0.030}$	$32.5^{+11.8}_{-5.4}$	$16.1^{+12.2}_{-5.5}$
211147528.1	4	$2.349545^{+0.000083}_{-0.000085}$	$2063.0589^{+0.0013}_{-0.0013}$	$2.70^{+0.14}_{-0.18}$	7570^{+200}_{-200}	$0.0828^{+0.0096}_{-0.0127}$	$15.3^{+2.7}_{-2.5}$	$1.695^{+0.228}_{-0.097}$	$6.2^{+1.8}_{-1.1}$	1790^{+1130}_{-690}
211201576.1	4	$5.88165^{+0.00074}_{-0.00075}$	$2063.4053^{+0.0050}_{-0.0049}$	$3.54^{+0.17}_{-0.24}$	323^{+20}_{-20}	$0.0173^{+0.0011}_{-0.0023}$	$2.58^{+0.48}_{-1.12}$	$1.37^{+0.24}_{-0.56}$	$11.2^{+3.5}_{-1.7}$	480^{+390}_{-580}
211315836.1	5	$1.385246^{+0.000013}_{-0.000011}$	$2139.73756^{+0.00036}_{-0.00040}$	$0.880^{+0.016}_{-0.088}$	1243^{+33}_{-38}	$0.0326^{+0.0012}_{-0.0045}$	$5.01^{+0.34}_{-0.71}$	$1.407^{+0.080}_{-0.058}$	$11.49^{+3.02}_{-0.94}$	511^{+275}_{-96}
211319617.1	5	$8.86638^{+0.00044}_{-0.00041}$	$2143.3922^{+0.0018}_{-0.0022}$	$2.96^{+0.11}_{-0.17}$	1189^{+32}_{-32}	$0.0335^{+0.0024}_{-0.0046}$	$2.51^{+0.18}_{-0.35}$	$0.6867^{+0.0069}_{-0.0055}$	$19.7^{+7.1}_{-4.0}$	90^{+65}_{-36}
211327855.1	5	$1.72397^{+0.00027}_{-0.00022}$	$2139.7005^{+0.0044}_{-0.0046}$	$1.48^{+0.24}_{-0.31}$	201^{+27}_{-31}	$0.0137^{+0.0017}_{-0.0038}$	$1.33^{+0.20}_{-0.37}$	$0.885^{+0.074}_{-0.027}$	$7.5^{+3.5}_{-2.2}$	490^{+470}_{-290}
211331236.1	5	$1.291605^{+0.000018}_{-0.000019}$	$2140.19095^{+0.00067}_{-0.00067}$	$1.151^{+0.069}_{-0.058}$	1817^{+64}_{-69}	$0.0399^{+0.0027}_{-0.0058}$	$1.74^{+0.33}_{-0.27}$	$0.400^{+0.070}_{-0.023}$	$8.16^{+2.65}_{-0.87}$	144^{+121}_{-39}
211331236.2	5	$5.44425^{+0.00014}_{-0.00014}$	$2143.5638^{+0.0012}_{-0.0012}$	$2.110^{+0.058}_{-0.078}$	1686^{+48}_{-53}	$0.0402^{+0.0012}_{-0.0021}$	$1.75^{+0.31}_{-0.14}$	$0.400^{+0.070}_{-0.023}$	$18.8^{+4.0}_{-1.7}$	$27.1^{+18.5}_{-6.8}$
211342524.1	5	$14.448987^{+0.000026}_{-0.000026}$	$2149.367541^{+0.000064}_{-0.000064}$	$3.762^{+0.014}_{-0.018}$	38361^{+43}_{-43}	$0.45^{+0.11}_{-0.13}$	86^{+20}_{-25}	$1.739^{+0.030}_{-0.023}$	$25.22^{+0.37}_{-0.91}$	$79.5^{+4.7}_{-6.8}$
211351816.1	5	$8.40685^{+0.00094}_{-0.00095}$	$2142.0487^{+0.0041}_{-0.0042}$	$6.07^{+0.20}_{-0.26}$	680^{+30}_{-31}	$0.0244^{+0.0015}_{-0.0037}$	$10.88^{+0.82}_{-1.84}$	$4.09^{+0.18}_{-0.30}$	$9.6^{+2.8}_{-1.2}$	250^{+146}_{-76}
211355342.1	5	$6.89442^{+0.00025}_{-0.00024}$	$2143.7935^{+0.0014}_{-0.0015}$	$2.670^{+0.087}_{-0.125}$	828^{+27}_{-26}	$0.0272^{+0.0017}_{-0.0041}$	$3.17^{+0.28}_{-0.51}$	$1.071^{+0.066}_{-0.054}$	$17.7^{+5.5}_{-2.5}$	123^{+78}_{-37}
211357309.1	5	$0.463954^{+0.000011}_{-0.000011}$	$2139.7522^{+0.0010}_{-0.0010}$	$0.988^{+0.092}_{-0.191}$	326^{+16}_{-17}	$0.0180^{+0.0028}_{-0.0153}$	$0.53^{+0.11}_{-0.46}$	$0.272^{+0.037}_{-0.028}$	$2.86^{+1.98}_{-0.87}$	820^{+1170}_{-550}
211359660.1	5	$4.736893^{+0.000048}_{-0.000050}$	$2141.20525^{+0.00045}_{-0.00045}$	$2.579^{+0.037}_{-0.040}$	1178^{+12}_{-13}	$0.03188^{+0.00072}_{-0.00192}$	$2.86^{+0.15}_{-0.22}$	$0.822^{+0.041}_{-0.040}$	$13.74^{+1.92}_{-0.73}$	146^{+43}_{-21}
211372788.1	5	$1.529084^{+0.000013}_{-0.000013}$	$2140.33284^{+0.00036}_{-0.00036}$	$2.193^{+0.071}_{-0.062}$	10527^{+95}_{-95}	$0.267^{+0.073}_{-0.089}$	48^{+13}_{-16}	$1.654^{+0.011}_{-0.012}$	$3.799^{+0.075}_{-0.104}$	2360^{+260}_{-270}
211383821.1	5	$1.56699^{+0.00011}_{-0.00011}$	$2140.1535^{+0.0033}_{-0.0033}$	$2.11^{+0.16}_{-0.27}$	460^{+30}_{-31}	$0.0203^{+0.0020}_{-0.0067}$	$1.34^{+0.16}_{-0.44}$	$0.603^{+0.039}_{-0.028}$	$4.94^{+2.60}_{-0.95}$	670^{+710}_{-260}
211391664.1	5	$10.13682^{+0.00039}_{-0.00036}$	$2145.9809^{+0.0012}_{-0.0012}$	$5.122^{+0.094}_{-0.123}$	1043^{+18}_{-18}	$0.0307^{+0.0011}_{-0.0027}$	$4.60^{+0.79}_{-0.55}$	$1.37^{+0.23}_{-0.11}$	$14.2^{+3.4}_{-1.3}$	373^{+220}_{-92}
211399359.1	5	$3.1149085^{+0.0000092}_{-0.0000092}$	$2141.41748^{+0.00012}_{-0.00012}$	$2.337^{+0.016}_{-0.021}$	28460^{+120}_{-120}	$0.1536^{+0.0016}_{-0.0019}$	$12.03^{+1.63}_{-0.30}$	$0.718^{+0.097}_{-0.015}$	$11.64^{+0.25}_{-0.15}$	192^{+53}_{-12}
211401787.1	5	$13.7730^{+0.0015}_{-0.0015}$	$2151.0724^{+0.0029}_{-0.0028}$	$4.68^{+0.23}_{-0.27}$	$209.2^{+8.1}_{-8.4}$	$0.01356^{+0.00099}_{-0.00260}$	$2.17^{+0.19}_{-0.44}$	$1.469^{+0.069}_{-0.102}$	$19.8^{+6.7}_{-3.0}$	162^{+112}_{-54}

Table A.1: Our sample of planet candidates from C0-8. (continued)

Candidate	C#	Period (days)	t_0 (BJD - 2455000)	Duration (hours)	Depth (ppm)	R_p/R_*	R_p ($R_\oplus$)	R_* ($R_\odot$)	a/R_*	Inc. Flux ($S_\oplus$)
211407755.1	5	$36.109^{+0.032}_{-0.050}$	$2160.2353^{+0.0013}_{-0.0013}$	$3.20^{+0.23}_{-0.18}$	4900^{+180}_{-180}	$0.145^{+0.047}_{-0.065}$	$8.0^{+2.7}_{-3.6}$	$0.504^{+0.050}_{-0.018}$	$46.0^{+4.0}_{-5.8}$	$11.9^{+3.2}_{-3.1}$
211413752.1	5	$9.32705^{+0.00061}_{-0.00061}$	$2140.8461^{+0.0027}_{-0.0027}$	$4.08^{+0.44}_{-0.39}$	1239^{+48}_{-50}	$0.043^{+0.010}_{-0.016}$	$3.63^{+0.89}_{-1.32}$	$0.773^{+0.035}_{-0.025}$	$8.3^{+2.0}_{-8.9}$	380^{+190}_{-820}
211413752.2	5	$4.52905^{+0.00051}_{-0.00058}$	$2143.9728^{+0.0049}_{-0.0043}$	$2.83^{+0.20}_{-0.23}$	531^{+30}_{-31}	$0.0220^{+0.0016}_{-0.0035}$	$1.85^{+0.16}_{-0.30}$	$0.773^{+0.035}_{-0.025}$	$10.9^{+3.7}_{-1.8}$	221^{+151}_{-74}
211413752.3	5	$26.2678^{+0.0060}_{-0.0031}$	$2142.1943^{+0.0043}_{-0.0039}$	$4.84^{+0.24}_{-0.47}$	1025^{+59}_{-59}	$0.0309^{+0.0022}_{-0.0052}$	$2.60^{+0.22}_{-0.44}$	$0.773^{+0.035}_{-0.025}$	$36.1^{+14.1}_{-6.9}$	$20.1^{+15.8}_{-7.7}$
211413752.4	5	$2.15228^{+0.00023}_{-0.00023}$	$2141.4957^{+0.0047}_{-0.0045}$	$2.42^{+0.22}_{-0.28}$	398^{+35}_{-38}	$0.0191^{+0.0019}_{-0.0045}$	$1.61^{+0.17}_{-0.39}$	$0.773^{+0.035}_{-0.025}$	$5.9^{+2.6}_{-1.2}$	750^{+670}_{-300}
211413752.5	5	$6.13174^{+0.00059}_{-0.00062}$	$2142.3404^{+0.0037}_{-0.0036}$	$2.45^{+0.12}_{-0.15}$	436^{+26}_{-27}	$0.0204^{+0.0011}_{-0.0024}$	$1.72^{+0.12}_{-0.21}$	$0.773^{+0.035}_{-0.025}$	$17.1^{+5.7}_{-2.4}$	89^{+60}_{-26}
211418290.1	5	$5.032134^{+0.000042}_{-0.000042}$	$2141.80767^{+0.00034}_{-0.00034}$	$8.600^{+0.023}_{-0.025}$	10480^{+55}_{-54}	$0.09410^{+0.00037}_{-0.00060}$	$25.83^{+3.94}_{-0.37}$	$2.516^{+0.384}_{-0.033}$	$4.873^{+0.047}_{-0.023}$	1437^{+441}_{-56}
211418729.1	5	$11.390955^{+0.000093}_{-0.000092}$	$2140.32404^{+0.00033}_{-0.00033}$	$3.863^{+0.035}_{-0.041}$	16232^{+98}_{-96}	$0.1150^{+0.0017}_{-0.0029}$	$10.71^{+0.58}_{-0.35}$	$0.854^{+0.044}_{-0.018}$	$24.67^{+0.96}_{-0.52}$	$39.7^{+5.4}_{-2.8}$
211419451.1	5	$6.45795^{+0.00042}_{-0.00040}$	$2140.1818^{+0.0023}_{-0.0024}$	$1.04^{+0.11}_{-0.15}$	788^{+75}_{-82}	$0.0271^{+0.0026}_{-0.0065}$	$2.78^{+0.27}_{-0.67}$	$0.9389^{+0.0127}_{-0.0060}$	$41.6^{+18.2}_{-9.0}$	$20.0^{+17.5}_{-8.7}$
211428897.1	5	$1.610888^{+0.000039}_{-0.000034}$	$2140.66515^{+0.00095}_{-0.00100}$	$1.205^{+0.071}_{-0.109}$	696^{+29}_{-31}	$0.0250^{+0.0020}_{-0.0052}$	$0.82^{+0.17}_{-0.19}$	$0.299^{+0.056}_{-0.033}$	$9.1^{+3.6}_{-1.5}$	86^{+83}_{-40}
211428897.2	5	$2.178008^{+0.000082}_{-0.000083}$	$2141.4709^{+0.0017}_{-0.0017}$	$1.276^{+0.058}_{-0.067}$	453^{+23}_{-24}	$0.0205^{+0.0011}_{-0.0021}$	$0.67^{+0.13}_{-0.10}$	$0.299^{+0.056}_{-0.033}$	$11.9^{+3.3}_{-1.4}$	50^{+39}_{-20}
211428897.3	5	$4.96792^{+0.00029}_{-0.00028}$	$2143.7150^{+0.0027}_{-0.0027}$	$1.30^{+0.10}_{-0.12}$	572^{+32}_{-33}	$0.0231^{+0.0015}_{-0.0027}$	$0.75^{+0.15}_{-0.12}$	$0.299^{+0.056}_{-0.033}$	$26.1^{+8.1}_{-4.4}$	$10.4^{+8.7}_{-4.9}$
211428897.4	5	$6.26561^{+0.00069}_{-0.00070}$	$2144.2594^{+0.0044}_{-0.0056}$	$1.51^{+0.21}_{-0.28}$	580^{+45}_{-50}	$0.0235^{+0.0027}_{-0.0146}$	$0.77^{+0.17}_{-0.48}$	$0.299^{+0.056}_{-0.033}$	$26.6^{+16.9}_{-7.8}$	$10.1^{+13.9}_{-6.7}$
211428897.5	5	$3.28963^{+0.00077}_{-0.00089}$	$2142.5903^{+0.0097}_{-0.0087}$	$2.04^{+0.36}_{-0.38}$	259^{+27}_{-29}	$0.0156^{+0.0018}_{-0.0062}$	$0.51^{+0.11}_{-0.21}$	$0.299^{+0.056}_{-0.033}$	$10.5^{+6.5}_{-3.0}$	65^{+88}_{-43}
211432922.1	5	$5.81861^{+0.00074}_{-0.00082}$	$2141.9226^{+0.0046}_{-0.0044}$	$3.88^{+0.30}_{-0.45}$	6890^{+460}_{-500}	$0.081^{+0.011}_{-0.066}$	$3.4^{+1.3}_{-3.0}$	$0.38^{+0.13}_{-0.14}$	$10.1^{+4.0}_{-2.6}$	100^{+140}_{-120}
211439059.1	5	$18.6393^{+0.0031}_{-0.0030}$	$2146.5107^{+0.0054}_{-0.0053}$	$5.64^{+0.28}_{-0.42}$	399^{+24}_{-25}	$0.0193^{+0.0013}_{-0.0030}$	$1.73^{+0.20}_{-0.31}$	$0.821^{+0.078}_{-0.066}$	$22.0^{+8.2}_{-3.8}$	63^{+50}_{-27}
211442297.1	5	$20.27285^{+0.00018}_{-0.00018}$	$2157.15720^{+0.00021}_{-0.00021}$	$3.858^{+0.033}_{-0.036}$	17257^{+78}_{-78}	$0.1274^{+0.0034}_{-0.0023}$	$11.55^{+0.95}_{-0.53}$	$0.831^{+0.065}_{-0.035}$	$37.28^{+0.87}_{-1.11}$	$33.0^{+5.4}_{-3.5}$
211442571.1	5	$5.19287^{+0.00060}_{-0.00056}$	$2143.0584^{+0.0045}_{-0.0049}$	$2.48^{+0.16}_{-0.20}$	211^{+17}_{-17}	$0.01434^{+0.00098}_{-0.00161}$	$1.29^{+0.13}_{-0.16}$	$0.826^{+0.061}_{-0.037}$	$13.8^{+5.1}_{-2.5}$	245^{+186}_{-92}
211442571.2	5	$3.39934^{+0.00054}_{-0.00051}$	$2140.1609^{+0.0059}_{-0.0050}$	$2.18^{+0.19}_{-0.22}$	150^{+17}_{-17}	$0.0120^{+0.0010}_{-0.0016}$	$1.08^{+0.12}_{-0.15}$	$0.826^{+0.061}_{-0.037}$	$10.3^{+3.6}_{-1.9}$	440^{+310}_{-170}
211469889.1	5	$7.07737^{+0.00092}_{-0.00088}$	$2144.3867^{+0.0043}_{-0.0049}$	$3.08^{+0.19}_{-0.28}$	907^{+60}_{-62}	$0.0291^{+0.0020}_{-0.0039}$	$2.10^{+0.26}_{-0.30}$	$0.662^{+0.067}_{-0.027}$	$15.7^{+5.4}_{-2.6}$	110^{+80}_{-38}
211490999.1	5	$9.84413^{+0.00039}_{-0.00039}$	$2146.3288^{+0.0014}_{-0.0014}$	$3.69^{+0.11}_{-0.16}$	1093^{+27}_{-27}	$0.0315^{+0.0017}_{-0.0036}$	$3.23^{+0.18}_{-0.38}$	$0.9395^{+0.0079}_{-0.0114}$	$18.2^{+5.3}_{-2.8}$	112^{+66}_{-35}
211505089.1	5	$24.4472^{+0.0028}_{-0.0028}$	$2146.9623^{+0.0036}_{-0.0033}$	$6.37^{+0.18}_{-0.23}$	718^{+28}_{-29}	$0.0257^{+0.0011}_{-0.0023}$	$1.82^{+0.18}_{-0.24}$	$0.647^{+0.059}_{-0.061}$	$27.1^{+6.9}_{-2.9}$	$28.0^{+15.1}_{-7.9}$
211509553.1	5	$20.35919^{+0.00046}_{-0.00046}$	$2151.41247^{+0.00093}_{-0.00093}$	$3.650^{+0.087}_{-0.090}$	39120^{+630}_{-660}	$0.1887^{+0.0072}_{-0.0146}$	$11.3^{+3.5}_{-1.2}$	$0.550^{+0.170}_{-0.041}$	$47.6^{+3.2}_{-3.3}$	$3.67^{+2.32}_{-0.75}$
211510580.1	5	$5.31471^{+0.00039}_{-0.00036}$	$2143.1306^{+0.0029}_{-0.0033}$	$1.90^{+0.17}_{-0.36}$	1511^{+96}_{-103}	$0.0374^{+0.0039}_{-0.0152}$	$1.45^{+0.15}_{-0.96}$	$0.3550^{+0.0070}_{-0.1870}$	$18.6^{+10.5}_{-4.2}$	26^{+30}_{-43}
211516501.1	5	$3.84981^{+0.00055}_{-0.00053}$	$2141.9314^{+0.0060}_{-0.0063}$	$3.37^{+0.21}_{-0.27}$	153^{+11}_{-12}	$0.01204^{+0.00086}_{-0.00190}$	$1.86^{+0.32}_{-0.34}$	$1.42^{+0.22}_{-0.13}$	$7.5^{+3.1}_{-1.3}$	1020^{+890}_{-420}
211525389.1	5	$8.26698^{+0.00013}_{-0.00013}$	$2139.72408^{+0.00071}_{-0.00074}$	$3.410^{+0.060}_{-0.075}$	1338^{+17}_{-17}	$0.03439^{+0.00095}_{-0.00287}$	$3.55^{+0.11}_{-0.31}$	$0.947^{+0.016}_{-0.027}$	$17.9^{+2.9}_{-1.3}$	103^{+34}_{-16}
211529065.1	5	$4.399739^{+0.000070}_{-0.000072}$	$2142.97910^{+0.00071}_{-0.00068}$	$1.691^{+0.071}_{-0.125}$	1682^{+41}_{-39}	$0.0375^{+0.0030}_{-0.0079}$	$3.01^{+0.34}_{-0.66}$	$0.735^{+0.059}_{-0.049}$	$18.4^{+5.9}_{-2.3}$	70^{+47}_{-20}
211529065.2	5	$1.543452^{+0.000091}_{-0.000089}$	$2140.8716^{+0.0026}_{-0.0027}$	$1.645^{+0.095}_{-0.133}$	286^{+15}_{-16}	$0.0163^{+0.0011}_{-0.0024}$	$1.30^{+0.14}_{-0.21}$	$0.735^{+0.059}_{-0.049}$	$6.3^{+2.2}_{-1.0}$	600^{+430}_{-210}
211535327.1	5	$20.2244^{+0.0021}_{-0.0020}$	$2144.9905^{+0.0038}_{-0.0040}$	$4.18^{+0.19}_{-0.29}$	1132^{+58}_{-60}	$0.0323^{+0.0020}_{-0.0043}$	$2.94^{+0.18}_{-0.39}$	$0.8325^{+0.0095}_{-0.0110}$	$33.2^{+11.2}_{-5.1}$	32^{+22}_{-10}
211539054.1	5	$11.0213^{+0.0011}_{-0.0012}$	$2150.2916^{+0.0031}_{-0.0032}$	$4.33^{+0.15}_{-0.20}$	202^{+10}_{-11}	$0.01371^{+0.00076}_{-0.00175}$	$2.25^{+0.27}_{-0.31}$	$1.507^{+0.162}_{-0.072}$	$17.0^{+5.5}_{-2.6}$	187^{+127}_{-59}
211551160.1	5	$37.4059^{+0.0045}_{-0.0046}$	$2165.7023^{+0.0033}_{-0.0032}$	$3.84^{+0.21}_{-0.26}$	1450^{+68}_{-72}	$0.0366^{+0.0025}_{-0.0048}$	$2.32^{+0.19}_{-0.45}$	$0.581^{+0.026}_{-0.083}$	67^{+22}_{-11}	$4.7^{+3.1}_{-2.0}$
211562654.1	5	$10.79274^{+0.00056}_{-0.00057}$	$2147.7772^{+0.0022}_{-0.0022}$	$4.18^{+0.33}_{-0.37}$	901^{+23}_{-24}	$0.0321^{+0.0045}_{-0.0042}$	$3.45^{+0.49}_{-0.45}$	$0.984^{+0.026}_{-0.015}$	$11.6^{+3.6}_{-9.0}$	260^{+160}_{-400}
211562654.2	5	$22.6302^{+0.0015}_{-0.0016}$	$2144.1526^{+0.0028}_{-0.0028}$	$4.93^{+0.28}_{-0.24}$	947^{+35}_{-33}	$0.049^{+0.012}_{-0.030}$	$5.2^{+1.3}_{-3.2}$	$0.984^{+0.026}_{-0.015}$	$12.9^{+1.7}_{-4.0}$	209^{+57}_{-130}
211562654.3	5	$0.469287^{+0.000015}_{-0.000016}$	$2139.6618^{+0.0014}_{-0.0014}$	$1.540^{+0.069}_{-0.093}$	$215.2^{+8.9}_{-9.2}$	$0.01359^{+0.00093}_{-0.00196}$	$1.46^{+0.11}_{-0.21}$	$0.984^{+0.026}_{-0.015}$	$2.08^{+0.59}_{-0.28}$	8100^{+4600}_{-2200}
211579112.1	5	$17.7037^{+0.0016}_{-0.0016}$	$2156.4255^{+0.0033}_{-0.0033}$	$2.01^{+0.13}_{-0.17}$	6770^{+530}_{-560}	$0.0786^{+0.0049}_{-0.0071}$	$1.76^{+0.51}_{-0.51}$	$0.205^{+0.058}_{-0.056}$	$66.9^{+13.7}_{-7.9}$	$1.3^{+1.3}_{-1.1}$
211579683.1	5	$9.0102^{+0.0010}_{-0.0010}$	$2144.6162^{+0.0045}_{-0.0045}$	$4.86^{+0.62}_{-0.43}$	982^{+51}_{-51}	$0.044^{+0.017}_{-0.034}$	$3.6^{+1.4}_{-2.7}$	$0.738^{+0.073}_{-0.044}$	$5.6^{+1.1}_{-9.5}$	770^{+330}_{-2600}
211586387.1	5	$35.3972^{+0.0058}_{-0.0057}$	$2142.8804^{+0.0067}_{-0.0065}$	$4.69^{+0.61}_{-0.67}$	1470^{+120}_{-120}	$0.045^{+0.012}_{-0.041}$	$2.60^{+0.72}_{-2.36}$	$0.531^{+0.018}_{-0.015}$	30^{+10}_{-33}	29^{+20}_{-64}
211594205.1	5	$16.9960^{+0.0011}_{-0.0010}$	$2148.4966^{+0.0021}_{-0.0024}$	$2.63^{+0.13}_{-0.22}$	265^{+11}_{-12}	$0.0158^{+0.0012}_{-0.0034}$	$1.40^{+0.13}_{-0.31}$	$0.816^{+0.038}_{-0.025}$	$41.7^{+21.4}_{-8.4}$	$16.3^{+16.8}_{-6.6}$

Table A.1: Our sample of planet candidates from C0-8. (continued)

Candidate	C#	Period (days)	t_0 (BJD - 2455000)	Duration (hours)	Depth (ppm)	R_p/R_*	R_p ($R_\oplus$)	R_* ($R_\odot$)	a/R_*	Inc. Flux ($S_\oplus$)
211606790.1	5	$37.24703^{+0.00054}_{-0.00054}$	$2150.08888^{+0.00038}_{-0.00038}$	$4.929^{+0.090}_{-0.107}$	7202^{+43}_{-43}	$0.189^{+0.048}_{-0.063}$	$35.0^{+9.0}_{-11.8}$	$1.696^{+0.079}_{-0.060}$	$32.4^{+1.5}_{-2.1}$	$33.8^{+4.5}_{-5.1}$
211611158.1	5	$52.7099^{+0.0027}_{-0.0027}$	$2159.1568^{+0.0019}_{-0.0019}$	$4.93^{+0.17}_{-0.28}$	757^{+24}_{-24}	$0.0255^{+0.0019}_{-0.0051}$	$2.48^{+0.19}_{-0.50}$	$0.8910^{+0.0072}_{-0.0057}$	74^{+25}_{-10}	$8.7^{+5.9}_{-2.4}$
211611158.2	5	$10.6161^{+0.0018}_{-0.0017}$	$2144.7353^{+0.0057}_{-0.0058}$	$2.54^{+0.22}_{-0.26}$	162^{+15}_{-16}	$0.0122^{+0.0011}_{-0.0020}$	$1.19^{+0.10}_{-0.19}$	$0.8910^{+0.0072}_{-0.0057}$	$27.7^{+9.7}_{-5.2}$	62^{+43}_{-23}
211613886.1	5	$0.9587591^{+0.0000092}_{-0.0000087}$	$2140.20130^{+0.00045}_{-0.00048}$	$1.776^{+0.063}_{-0.058}$	16260^{+220}_{-220}	$0.308^{+0.085}_{-0.105}$	39^{+11}_{-14}	$1.171^{+0.087}_{-0.046}$	$3.184^{+0.084}_{-0.145}$	2810^{+450}_{-350}
211619879.1	5	$15.7512^{+0.0012}_{-0.0012}$	$2150.5187^{+0.0029}_{-0.0029}$	$2.56^{+0.12}_{-0.16}$	500^{+27}_{-28}	$0.0218^{+0.0012}_{-0.0023}$	$1.38^{+0.22}_{-0.22}$	$0.582^{+0.087}_{-0.071}$	$42.2^{+14.2}_{-6.1}$	$8.8^{+7.4}_{-4.3}$
211642307.1	5	$20.9913^{+0.0026}_{-0.0025}$	$2148.3388^{+0.0049}_{-0.0050}$	$2.94^{+0.23}_{-0.40}$	1290^{+90}_{-97}	$0.0342^{+0.0031}_{-0.0088}$	$1.44^{+0.17}_{-0.39}$	$0.386^{+0.031}_{-0.034}$	$48.2^{+21.5}_{-9.3}$	$3.8^{+3.5}_{-1.8}$
211645912.1	5	$10.6741^{+0.0015}_{-0.0014}$	$2140.5504^{+0.0054}_{-0.0057}$	$3.76^{+0.26}_{-0.40}$	354^{+22}_{-23}	$0.0178^{+0.0017}_{-0.0051}$	$1.86^{+0.18}_{-0.53}$	$0.9538^{+0.0122}_{-0.0076}$	$18.8^{+9.2}_{-3.5}$	136^{+132}_{-50}
211680698.1	5	$50.9254^{+0.0041}_{-0.0040}$	$2160.4701^{+0.0027}_{-0.0028}$	$4.11^{+0.18}_{-0.24}$	1193^{+58}_{-61}	$0.0325^{+0.0021}_{-0.0047}$	$2.48^{+0.24}_{-0.38}$	$0.702^{+0.049}_{-0.034}$	87^{+24}_{-11}	$3.42^{+1.99}_{-0.97}$
211682544.1	5	$50.8213^{+0.0023}_{-0.0023}$	$2145.5660^{+0.0017}_{-0.0017}$	$3.42^{+0.10}_{-0.13}$	582^{+21}_{-21}	$0.0228^{+0.0012}_{-0.0029}$	$2.18^{+0.20}_{-0.28}$	$0.879^{+0.064}_{-0.024}$	103^{+27}_{-13}	$3.20^{+1.76}_{-0.81}$
211713099.1	5	$8.56222^{+0.00019}_{-0.00013}$	$2141.15021^{+0.00043}_{-0.00043}$	$3.256^{+0.039}_{-0.044}$	5513^{+43}_{-41}	$0.0681^{+0.0011}_{-0.0027}$	$6.89^{+0.55}_{-0.49}$	$0.928^{+0.072}_{-0.055}$	$20.79^{+1.73}_{-0.71}$	105^{+25}_{-16}
211718187.1	5	$5.51633^{+0.00041}_{-0.00041}$	$2141.7112^{+0.0033}_{-0.0035}$	$1.92^{+0.17}_{-0.22}$	1830^{+190}_{-220}	$0.0413^{+0.0036}_{-0.0068}$	$1.38^{+0.19}_{-0.25}$	$0.306^{+0.032}_{-0.024}$	$19.9^{+6.8}_{-3.6}$	$18.9^{+14.2}_{-8.2}$
211731298.1	5	$1.990422^{+0.000080}_{-0.000085}$	$2141.3418^{+0.0018}_{-0.0017}$	$2.074^{+0.089}_{-0.122}$	447^{+19}_{-20}	$0.0200^{+0.0013}_{-0.0032}$	$1.80^{+0.19}_{-0.29}$	$0.824^{+0.066}_{-0.026}$	$6.56^{+2.04}_{-0.91}$	650^{+420}_{-190}
211732801.1	5	$2.1372783^{+0.0000055}_{-0.0000087}$	$2141.284020^{+0.000092}_{-0.000058}$	$0.0314^{+0.0036}_{-0.0033}$	15950^{+750}_{-850}	$0.1222^{+0.0082}_{-0.0098}$	$27.6^{+2.9}_{-4.3}$	$2.07^{+0.17}_{-0.27}$	520^{+115}_{-99}	$0.29^{+0.14}_{-0.14}$
211733267.1	5	$8.658143^{+0.000027}_{-0.000026}$	$2144.93197^{+0.00012}_{-0.00013}$	$1.698^{+0.036}_{-0.035}$	7969^{+49}_{-47}	$0.195^{+0.052}_{-0.075}$	$19.1^{+5.4}_{-7.4}$	$0.900^{+0.085}_{-0.037}$	$23.3^{+1.1}_{-1.5}$	$51.9^{+11.0}_{-7.9}$
211736305.1	5	$14.5616^{+0.0026}_{-0.0026}$	$2152.1209^{+0.0065}_{-0.0066}$	$3.14^{+0.27}_{-0.44}$	1029^{+94}_{-105}	$0.0305^{+0.0033}_{-0.0149}$	$2.82^{+0.32}_{-1.38}$	$0.849^{+0.023}_{-0.030}$	$31.0^{+18.1}_{-6.5}$	27^{+31}_{-11}
211736671.1	5	$4.73363^{+0.00013}_{-0.00013}$	$2140.3649^{+0.0011}_{-0.0011}$	$3.629^{+0.083}_{-0.116}$	973^{+17}_{-18}	$0.0297^{+0.0016}_{-0.0035}$	$5.81^{+0.36}_{-0.71}$	$1.797^{+0.055}_{-0.068}$	$8.9^{+2.4}_{-1.3}$	440^{+240}_{-140}
211743874.1	5	$12.2812^{+0.0017}_{-0.0015}$	$2148.2148^{+0.0046}_{-0.0059}$	$4.31^{+0.16}_{-0.22}$	314^{+18}_{-19}	$0.01710^{+0.00098}_{-0.00210}$	$2.47^{+0.20}_{-0.40}$	$1.323^{+0.077}_{-0.142}$	$19.5^{+5.9}_{-2.6}$	168^{+103}_{-58}
211754962.1	5	$3.41065^{+0.00029}_{-0.00027}$	$2141.8515^{+0.0032}_{-0.0031}$	$1.95^{+0.22}_{-0.33}$	494^{+35}_{-37}	$0.0216^{+0.0023}_{-0.0068}$	$1.65^{+0.25}_{-0.53}$	$0.701^{+0.078}_{-0.046}$	$11.3^{+6.5}_{-2.8}$	87^{+102}_{-45}
211762841.1	5	$1.564940^{+0.000074}_{-0.000067}$	$2140.2672^{+0.0019}_{-0.0022}$	$0.666^{+0.097}_{-0.123}$	1220^{+130}_{-160}	$0.0340^{+0.0035}_{-0.0091}$	$2.06^{+0.40}_{-0.62}$	$0.556^{+0.091}_{-0.073}$	$15.7^{+7.3}_{-4.2}$	50^{+49}_{-29}
211763214.1	5	$21.1976^{+0.0048}_{-0.0058}$	$2146.579^{+0.014}_{-0.011}$	$5.03^{+0.47}_{-0.56}$	263^{+18}_{-19}	$0.0158^{+0.0015}_{-0.0035}$	$1.33^{+0.13}_{-0.29}$	$0.7747^{+0.0064}_{-0.0101}$	$27.2^{+13.9}_{-6.2}$	46^{+47}_{-21}
211770696.1	5	$16.2713^{+0.0012}_{-0.0012}$	$2145.9732^{+0.0029}_{-0.0029}$	$7.69^{+0.15}_{-0.22}$	418^{+12}_{-12}	$0.01997^{+0.00072}_{-0.00164}$	$2.77^{+0.16}_{-0.23}$	$1.270^{+0.060}_{-0.019}$	$14.7^{+5.0}_{-1.7}$	228^{+155}_{-53}
211770795.1	5	$7.72850^{+0.00053}_{-0.00053}$	$2141.0984^{+0.0027}_{-0.0026}$	$2.91^{+0.14}_{-0.19}$	1233^{+53}_{-56}	$0.0337^{+0.0021}_{-0.0044}$	$2.16^{+0.14}_{-0.31}$	$0.589^{+0.013}_{-0.032}$	$18.4^{+6.0}_{-2.7}$	71^{+46}_{-22}
211779390.1	5	$3.85064^{+0.00023}_{-0.00022}$	$2141.5282^{+0.0023}_{-0.0025}$	$1.601^{+0.089}_{-0.149}$	391^{+23}_{-24}	$0.0193^{+0.0013}_{-0.0029}$	$1.073^{+0.082}_{-0.196}$	$0.510^{+0.020}_{-0.054}$	$16.1^{+6.0}_{-2.8}$	89^{+67}_{-36}
211783206.1	5	$7.13142^{+0.00098}_{-0.00094}$	$2146.4727^{+0.0050}_{-0.0063}$	$1.92^{+0.30}_{-0.38}$	707^{+70}_{-77}	$0.0258^{+0.0029}_{-0.0086}$	$9.6^{+7.9}_{-11.6}$	$3.4^{+2.8}_{-4.0}$	$24.2^{+13.1}_{-7.0}$	39^{+100}_{-131}
211788221.1	5	$12.89398^{+0.00084}_{-0.00083}$	$2139.8876^{+0.0019}_{-0.0020}$	$1.19^{+0.10}_{-0.15}$	3140^{+240}_{-260}	$0.0539^{+0.0041}_{-0.0089}$	$1.12^{+0.39}_{-0.73}$	$0.191^{+0.064}_{-0.120}$	77^{+25}_{-14}	$1.1^{+1.4}_{-2.0}$
211791178.1	5	$9.56183^{+0.00065}_{-0.00064}$	$2146.9183^{+0.0027}_{-0.0027}$	$3.65^{+0.18}_{-0.34}$	1025^{+43}_{-44}	$0.0302^{+0.0030}_{-0.0079}$	$1.97^{+0.29}_{-0.53}$	$0.598^{+0.066}_{-0.046}$	$17.5^{+8.3}_{-3.2}$	56^{+56}_{-25}
211796070.1	5	$1.88993^{+0.00014}_{-0.00014}$	$2140.7331^{+0.0031}_{-0.0033}$	$1.66^{+0.19}_{-0.34}$	367^{+30}_{-31}	$0.0186^{+0.0021}_{-0.0084}$	$1.29^{+0.17}_{-0.60}$	$0.638^{+0.044}_{-0.066}$	$7.3^{+4.8}_{-1.9}$	390^{+510}_{-210}
211797637.1	5	$1.640707^{+0.000096}_{-0.000096}$	$2139.7875^{+0.0024}_{-0.0025}$	$2.20^{+0.38}_{-0.27}$	469^{+27}_{-28}	$0.034^{+0.015}_{-0.028}$	$2.09^{+0.95}_{-1.75}$	$0.572^{+0.037}_{-0.028}$	$1.90^{+0.41}_{-4.52}$	5700^{+2600}_{-27300}
211816003.1	5	$14.45107^{+0.00098}_{-0.00095}$	$2144.8610^{+0.0024}_{-0.0025}$	$3.63^{+0.12}_{-0.14}$	1225^{+39}_{-40}	$0.0339^{+0.0016}_{-0.0030}$	$2.96^{+0.15}_{-0.34}$	$0.802^{+0.020}_{-0.058}$	$28.1^{+8.1}_{-3.4}$	44^{+25}_{-12}
211817229.1	5	$2.176955^{+0.000040}_{-0.000037}$	$2140.69416^{+0.00070}_{-0.00067}$	$0.541^{+0.066}_{-0.103}$	4800^{+410}_{-490}	$0.0680^{+0.0072}_{-0.0325}$	$1.25^{+0.39}_{-0.87}$	$0.169^{+0.049}_{-0.086}$	$26.9^{+11.9}_{-8.0}$	8^{+11}_{-12}
211818569.1	5	$5.185758^{+0.000010}_{-0.000010}$	$2143.560482^{+0.000077}_{-0.000078}$	$2.126^{+0.023}_{-0.022}$	13112^{+47}_{-45}	$0.1070^{+0.0032}_{-0.0036}$	$7.44^{+0.62}_{-0.50}$	$0.637^{+0.049}_{-0.037}$	$17.67^{+0.82}_{-1.05}$	64^{+12}_{-11}
211822797.1	5	$21.1686^{+0.0021}_{-0.0021}$	$2144.4069^{+0.0036}_{-0.0034}$	$3.57^{+0.17}_{-0.20}$	1041^{+63}_{-67}	$0.0311^{+0.0018}_{-0.0032}$	$2.18^{+0.22}_{-0.23}$	$0.642^{+0.055}_{-0.020}$	$41.9^{+11.1}_{-5.3}$	$4.9^{+2.8}_{-1.3}$
211837343.1	5	$12.0808^{+0.0016}_{-0.0016}$	$2147.6313^{+0.0053}_{-0.0049}$	$2.29^{+0.25}_{-0.45}$	1218^{+100}_{-106}	$0.0341^{+0.0040}_{-0.0187}$	$2.53^{+0.33}_{-1.39}$	$0.682^{+0.040}_{-0.033}$	$34.3^{+20.2}_{-9.2}$	22^{+26}_{-12}
211843564.1	5	$0.4520313^{+0.0000041}_{-0.0000041}$	$2140.07707^{+0.00039}_{-0.00039}$	$0.727^{+0.066}_{-0.105}$	7560^{+320}_{-430}	$0.0848^{+0.0069}_{-0.0259}$	$5.3^{+1.0}_{-1.8}$	$0.569^{+0.102}_{-0.084}$	$4.3^{+1.6}_{-1.1}$	550^{+470}_{-320}
211886472.1	5	$19.640151^{+0.000070}_{-0.000069}$	$2152.37945^{+0.00013}_{-0.00013}$	$2.183^{+0.027}_{-0.035}$	6212^{+26}_{-26}	$0.179^{+0.044}_{-0.055}$	43^{+11}_{-13}	$2.188^{+0.153}_{-0.052}$	$36.3^{+1.8}_{-2.7}$	$52.0^{+9.6}_{-8.8}$
211897272.1	5	$11.23620^{+0.00065}_{-0.00064}$	$2143.5692^{+0.0019}_{-0.0018}$	$1.18^{+0.22}_{-0.16}$	491^{+44}_{-68}	$0.0216^{+0.0025}_{-0.0090}$	$2.25^{+0.28}_{-0.94}$	$0.955^{+0.042}_{-0.032}$	64^{+36}_{-17}	$7.2^{+8.2}_{-3.9}$
211897691.1	5	$5.75052^{+0.00032}_{-0.00037}$	$2142.4955^{+0.0018}_{-0.0018}$	$1.43^{+0.13}_{-0.18}$	1123^{+66}_{-71}	$0.0321^{+0.0033}_{-0.0084}$	$2.01^{+0.21}_{-0.55}$	$0.576^{+0.018}_{-0.043}$	$27.2^{+12.8}_{-5.4}$	37^{+35}_{-16}
211897691.2	5	$19.5080^{+0.0019}_{-0.0019}$	$2153.0076^{+0.0032}_{-0.0034}$	$3.79^{+0.19}_{-0.26}$	1237^{+69}_{-71}	$0.0336^{+0.0022}_{-0.0044}$	$2.11^{+0.15}_{-0.32}$	$0.576^{+0.018}_{-0.043}$	$35.6^{+11.2}_{-5.3}$	$21.6^{+13.7}_{-7.2}$

Table A.1: Our sample of planet candidates from C0-8. (continued)

Candidate	C#	Period (days)	t_0 (BJD - 2455000)	Duration (hours)	Depth (ppm)	R_p/R_*	R_p ($R_\oplus$)	R_* ($R_\odot$)	a/R_*	Inc. Flux ($S_\oplus$)
211906650.1	5	$41.4661^{+0.0025}_{-0.0026}$	$2154.8470^{+0.0018}_{-0.0017}$	$6.13^{+0.12}_{-0.18}$	980^{+24}_{-25}	$0.0299^{+0.0011}_{-0.0026}$	$3.45^{+0.13}_{-0.30}$	$1.0574^{+0.0145}_{-0.0098}$	$48.5^{+10.8}_{-4.7}$	$19.8^{+8.9}_{-3.9}$
211913395.1	5	$9.35739^{+0.00097}_{-0.00114}$	$2147.8769^{+0.0044}_{-0.0042}$	$1.69^{+0.24}_{-0.61}$	1710^{+190}_{-190}	$0.0414^{+0.0054}_{-0.0314}$	$2.69^{+0.47}_{-2.05}$	$0.595^{+0.069}_{-0.048}$	34^{+20}_{-14}	13^{+16}_{-11}
211913977.1	5	$14.67665^{+0.00058}_{-0.00060}$	$2152.6838^{+0.0015}_{-0.0015}$	$3.33^{+0.10}_{-0.13}$	749^{+21}_{-21}	$0.0261^{+0.0013}_{-0.0030}$	$1.94^{+0.13}_{-0.25}$	$0.682^{+0.032}_{-0.043}$	$30.6^{+8.6}_{-3.9}$	$27.1^{+15.4}_{-7.7}$
211916756.1	5	$10.13446^{+0.00039}_{-0.00039}$	$2140.7404^{+0.0016}_{-0.0016}$	$2.85^{+0.14}_{-0.21}$	7050^{+250}_{-250}	$0.0777^{+0.0056}_{-0.0113}$	$1.92^{+0.49}_{-0.58}$	$0.226^{+0.056}_{-0.060}$	$26.5^{+6.5}_{-3.3}$	$8.9^{+7.9}_{-7.2}$
211919004.1	5	$11.71885^{+0.00060}_{-0.00060}$	$2149.0999^{+0.0020}_{-0.0019}$	$4.86^{+0.15}_{-0.23}$	1434^{+34}_{-34}	$0.0351^{+0.0023}_{-0.0056}$	$3.34^{+0.23}_{-0.55}$	$0.872^{+0.014}_{-0.035}$	$16.9^{+4.7}_{-2.2}$	93^{+52}_{-25}
211923431.1	5	$29.7361^{+0.0036}_{-0.0035}$	$2143.8180^{+0.0038}_{-0.0038}$	$5.44^{+0.21}_{-0.27}$	888^{+45}_{-47}	$0.0282^{+0.0017}_{-0.0036}$	$3.52^{+0.22}_{-0.44}$	$1.144^{+0.020}_{-0.011}$	$38.2^{+10.7}_{-4.8}$	$23.7^{+13.4}_{-6.2}$
211924657.1	5	$2.643528^{+0.000058}_{-0.000061}$	$2142.00628^{+0.00085}_{-0.00077}$	$1.320^{+0.072}_{-0.109}$	3860^{+110}_{-120}	$0.0595^{+0.0043}_{-0.0079}$	$1.47^{+0.28}_{-0.37}$	$0.226^{+0.040}_{-0.049}$	$14.0^{+4.2}_{-2.4}$	30^{+24}_{-22}
211925181.1	5	$8.8410^{+0.0016}_{-0.0020}$	$2146.0044^{+0.0103}_{-0.0075}$	$1.76^{+0.23}_{-0.34}$	1550^{+190}_{-200}	$0.0381^{+0.0040}_{-0.0091}$	$2.43^{+0.38}_{-0.61}$	$0.584^{+0.067}_{-0.045}$	$33.7^{+14.5}_{-8.6}$	$13.3^{+11.9}_{-7.2}$
211929937.1	5	$3.4766506^{+0.0000082}_{-0.0000082}$	$2142.412110^{+0.000091}_{-0.000093}$	$2.584^{+0.020}_{-0.020}$	20961^{+74}_{-78}	$0.1314^{+0.0025}_{-0.0037}$	$12.60^{+0.41}_{-0.40}$	$0.879^{+0.023}_{-0.013}$	$11.31^{+0.41}_{-0.29}$	220^{+22}_{-16}
211941472.1	5	$5.7837^{+0.0012}_{-0.0011}$	$2143.6098^{+0.0077}_{-0.0083}$	$4.20^{+0.34}_{-0.55}$	$107.0^{+9.2}_{-9.6}$	$0.0096^{+0.0010}_{-0.0039}$	$1.38^{+0.37}_{-0.88}$	$1.31^{+0.33}_{-0.65}$	$9.1^{+5.2}_{-1.7}$	610^{+820}_{-880}
211945201.1	5	$19.49183^{+0.00038}_{-0.00038}$	$2158.82598^{+0.00049}_{-0.00050}$	$3.566^{+0.069}_{-0.121}$	1639^{+21}_{-25}	$0.0390^{+0.0012}_{-0.0031}$	$5.96^{+0.26}_{-0.49}$	$1.403^{+0.042}_{-0.030}$	$38.9^{+9.5}_{-4.5}$	$36.3^{+17.9}_{-8.5}$
211959012.1	5	$9.2363^{+0.0017}_{-0.0014}$	$2145.5430^{+0.0067}_{-0.0079}$	$2.07^{+0.27}_{-0.32}$	248^{+29}_{-30}	$0.0152^{+0.0017}_{-0.0036}$	$1.37^{+0.16}_{-0.33}$	$0.828^{+0.033}_{-0.031}$	$29.2^{+12.7}_{-7.0}$	44^{+38}_{-21}
211965883.1	5	$10.55532^{+0.00048}_{-0.00048}$	$2146.4947^{+0.0017}_{-0.0017}$	$1.68^{+0.16}_{-0.31}$	1580^{+87}_{-93}	$0.0389^{+0.0049}_{-0.0246}$	$2.64^{+0.38}_{-1.68}$	$0.623^{+0.042}_{-0.044}$	41^{+24}_{-11}	$8.0^{+9.4}_{-4.5}$
211969807.1	5	$1.974202^{+0.000089}_{-0.000091}$	$2140.3794^{+0.0022}_{-0.0021}$	$1.58^{+0.14}_{-0.23}$	1749^{+86}_{-95}	$0.0400^{+0.0036}_{-0.0099}$	$2.43^{+0.59}_{-0.60}$	$0.5573^{+0.1253}_{-0.0046}$	$8.5^{+3.8}_{-1.7}$	89^{+88}_{-37}
211978988.1	5	$36.5563^{+0.0053}_{-0.0041}$	$2152.7063^{+0.0027}_{-0.0041}$	$6.41^{+0.19}_{-0.29}$	802^{+27}_{-28}	$0.0265^{+0.0013}_{-0.0034}$	$3.18^{+0.17}_{-0.42}$	$1.100^{+0.017}_{-0.021}$	$39.9^{+10.8}_{-4.8}$	$30.7^{+16.7}_{-7.5}$
211987231.1	5	$17.035203^{+0.000035}_{-0.000034}$	$2141.813552^{+0.000077}_{-0.000078}$	$2.508^{+0.040}_{-0.045}$	22080^{+130}_{-170}	$0.321^{+0.098}_{-0.134}$	53^{+24}_{-30}	$1.51^{+0.52}_{-0.56}$	$42.47^{+0.79}_{-1.66}$	26^{+26}_{-28}
211988320.1	5	$63.8432^{+0.0056}_{-0.0056}$	$2142.7160^{+0.0034}_{-0.0036}$	$4.95^{+0.30}_{-0.48}$	1930^{+100}_{-110}	$0.0430^{+0.0029}_{-0.0054}$	$2.78^{+0.51}_{-0.38}$	$0.594^{+0.100}_{-0.030}$	85^{+33}_{-19}	$1.82^{+1.53}_{-0.84}$
211990866.1	5	$1.675451^{+0.000032}_{-0.000020}$	$2140.68942^{+0.00044}_{-0.00090}$	$0.050^{+0.033}_{-0.015}$	1563^{+73}_{-76}	$0.0311^{+0.0013}_{-0.0022}$	$4.31^{+0.34}_{-0.36}$	$1.273^{+0.085}_{-0.054}$	253^{+60}_{-470}	$0.82^{+0.40}_{-3.03}$
211991987.1	5	$5.19220^{+0.00093}_{-0.00088}$	$2142.5175^{+0.0069}_{-0.0073}$	$4.69^{+0.91}_{-0.72}$	5970^{+440}_{-460}	$0.098^{+0.028}_{-0.089}$	$4.0^{+1.7}_{-3.9}$	$0.37^{+0.12}_{-0.14}$	$5.04^{+1.00}_{-5.03}$	390^{+410}_{-910}
211995398.1	5	$32.5795^{+0.0023}_{-0.0022}$	$2169.8535^{+0.0015}_{-0.0015}$	$5.09^{+0.17}_{-0.16}$	24210^{+540}_{-560}	$0.1513^{+0.0077}_{-0.0078}$	$10.44^{+0.90}_{-1.14}$	$0.633^{+0.044}_{-0.061}$	$49.6^{+4.8}_{-6.3}$	$5.8^{+1.6}_{-2.0}$
212006318.1	5	$14.4584^{+0.0032}_{-0.0030}$	$2147.3335^{+0.0083}_{-0.0085}$	$6.79^{+0.29}_{-0.35}$	298^{+17}_{-18}	$0.01676^{+0.00098}_{-0.00219}$	$2.84^{+0.17}_{-0.37}$	$1.551^{+0.022}_{-0.022}$	$14.3^{+5.6}_{-2.2}$	232^{+182}_{-74}
212006344.1	5	$2.219368^{+0.000051}_{-0.000052}$	$2141.82963^{+0.00109}_{-0.00098}$	$1.236^{+0.058}_{-0.119}$	432^{+16}_{-17}	$0.0202^{+0.0012}_{-0.0024}$	$1.17^{+0.14}_{-0.19}$	$0.532^{+0.054}_{-0.059}$	$12.0^{+4.1}_{-2.0}$	79^{+57}_{-32}
212008766.1	5	$14.13168^{+0.00066}_{-0.00067}$	$2145.1175^{+0.0016}_{-0.0016}$	$3.64^{+0.12}_{-0.17}$	974^{+25}_{-24}	$0.0278^{+0.0020}_{-0.0058}$	$2.18^{+0.15}_{-0.46}$	$0.7209^{+0.0066}_{-0.0230}$	$27.8^{+6.8}_{-2.8}$	$34.7^{+17.1}_{-7.3}$
212009150.1	5	$6.83292^{+0.00069}_{-0.00060}$	$2145.1674^{+0.0034}_{-0.0038}$	$2.20^{+0.31}_{-0.44}$	3890^{+260}_{-270}	$0.066^{+0.011}_{-0.060}$	$1.30^{+0.26}_{-1.19}$	$0.180^{+0.018}_{-0.012}$	$17.8^{+7.8}_{-9.4}$	19^{+18}_{-21}
212012119.1	5	$3.280948^{+0.000045}_{-0.000045}$	$2142.13378^{+0.00057}_{-0.00057}$	$1.908^{+0.032}_{-0.066}$	968^{+16}_{-16}	$0.0294^{+0.0011}_{-0.0027}$	$2.26^{+0.13}_{-0.23}$	$0.704^{+0.032}_{-0.028}$	$12.3^{+2.8}_{-1.2}$	153^{+72}_{-32}
212012119.2	5	$8.43903^{+0.00016}_{-0.00016}$	$2142.48576^{+0.00080}_{-0.00082}$	$2.44^{+0.12}_{-0.19}$	1095^{+26}_{-26}	$0.0327^{+0.0033}_{-0.0047}$	$2.51^{+0.28}_{-0.37}$	$0.704^{+0.032}_{-0.028}$	$20.5^{+7.6}_{-6.7}$	55^{+41}_{-36}
212066407.1	5	$0.8218241^{+0.0000093}_{-0.0000089}$	$2140.36496^{+0.00047}_{-0.00048}$	$1.126^{+0.072}_{-0.060}$	615^{+13}_{-12}	$0.0209^{+0.0017}_{-0.0047}$	$6.1^{+1.2}_{-1.4}$	$2.66^{+0.46}_{-0.10}$	$5.30^{+1.16}_{-0.53}$	1840^{+1060}_{-470}
212069861.1	5	$30.9540^{+0.0018}_{-0.0018}$	$2147.4926^{+0.0023}_{-0.0024}$	$3.77^{+0.17}_{-0.27}$	2117^{+87}_{-90}	$0.0442^{+0.0028}_{-0.0057}$	$3.07^{+0.80}_{-0.45}$	$0.637^{+0.162}_{-0.043}$	$57.2^{+16.6}_{-8.9}$	$2.87^{+2.21}_{-0.97}$
212072539.1	5	$7.67689^{+0.00060}_{-0.00050}$	$2144.6262^{+0.0027}_{-0.0031}$	$2.22^{+0.13}_{-0.18}$	2074^{+96}_{-100}	$0.0441^{+0.0025}_{-0.0049}$	$2.44^{+0.43}_{-0.30}$	$0.507^{+0.085}_{-0.025}$	$24.3^{+7.3}_{-3.7}$	$12.1^{+8.4}_{-3.9}$
212072539.2	5	$2.78711^{+0.00015}_{-0.00015}$	$2141.3237^{+0.0021}_{-0.0021}$	$1.72^{+0.14}_{-0.23}$	1470^{+97}_{-104}	$0.0362^{+0.0037}_{-0.0123}$	$2.00^{+0.39}_{-0.69}$	$0.507^{+0.085}_{-0.025}$	$11.0^{+5.6}_{-2.1}$	59^{+63}_{-23}
212088059.1	5	$10.36627^{+0.00052}_{-0.00054}$	$2141.7142^{+0.0021}_{-0.0020}$	$2.31^{+0.14}_{-0.20}$	1946^{+82}_{-85}	$0.0418^{+0.0035}_{-0.0078}$	$1.82^{+0.39}_{-0.40}$	$0.400^{+0.079}_{-0.047}$	$31.0^{+11.8}_{-5.3}$	$9.5^{+9.1}_{-4.6}$
212088895.1	5	$10.3427^{+0.0023}_{-0.0020}$	$2141.9727^{+0.0082}_{-0.0090}$	$3.49^{+0.23}_{-0.27}$	322^{+31}_{-33}	$0.0174^{+0.0014}_{-0.0023}$	$1.41^{+0.12}_{-0.19}$	$0.746^{+0.026}_{-0.012}$	$20.1^{+6.6}_{-3.2}$	62^{+41}_{-20}
212088968.1	5	$21.2666^{+0.0053}_{-0.0061}$	$2142.4981^{+0.0119}_{-0.0094}$	$4.32^{+0.56}_{-0.88}$	6340^{+700}_{-750}	$0.0781^{+0.0091}_{-0.0416}$	$3.0^{+1.3}_{-3.0}$	$0.36^{+0.14}_{-0.30}$	$33.6^{+14.8}_{-9.9}$	9^{+13}_{-24}
212110888.1	5	$2.9956372^{+0.0000046}_{-0.0000046}$	$2141.351251^{+0.000063}_{-0.000061}$	$2.4768^{+0.0091}_{-0.0089}$	7493^{+16}_{-15}	$0.0901^{+0.0014}_{-0.0019}$	$13.7^{+1.1}_{-1.1}$	$1.40^{+0.11}_{-0.11}$	$6.449^{+0.082}_{-0.083}$	1380^{+230}_{-220}
212120773.1	5	$5.17518^{+0.00062}_{-0.00065}$	$2140.5606^{+0.0053}_{-0.0052}$	$3.29^{+0.27}_{-0.54}$	317^{+24}_{-25}	$0.0170^{+0.0022}_{-0.0141}$	$1.53^{+0.30}_{-1.28}$	$0.826^{+0.119}_{-0.054}$	$10.2^{+7.1}_{-2.3}$	300^{+430}_{-140}
212130773.1	5	$18.7132^{+0.0017}_{-0.0017}$	$2151.8846^{+0.0032}_{-0.0034}$	$6.89^{+0.19}_{-0.29}$	1816^{+60}_{-62}	$0.0408^{+0.0019}_{-0.0038}$	$3.63^{+0.34}_{-0.38}$	$0.816^{+0.066}_{-0.039}$	$19.4^{+6.1}_{-2.3}$	67^{+43}_{-17}
212132195.1	5	$26.1956^{+0.0026}_{-0.0026}$	$2164.3913^{+0.0019}_{-0.0018}$	$3.43^{+0.13}_{-0.16}$	965^{+40}_{-41}	$0.0291^{+0.0018}_{-0.0036}$	$2.08^{+0.19}_{-0.30}$	$0.656^{+0.044}_{-0.048}$	$53.8^{+13.4}_{-6.3}$	$7.7^{+4.0}_{-2.1}$
212136123.1	5	$2.22645^{+0.00014}_{-0.00014}$	$2140.2532^{+0.0031}_{-0.0029}$	$1.73^{+0.12}_{-0.15}$	997^{+62}_{-65}	$0.0305^{+0.0022}_{-0.0038}$	$2.60^{+0.19}_{-0.33}$	$0.782^{+0.012}_{-0.018}$	$8.9^{+2.7}_{-1.4}$	320^{+200}_{-100}

Table A.1: Our sample of planet candidates from C0-8. (continued)

Candidate	C#	Period (days)	t_0 (BJD - 2455000)	Duration (hours)	Depth (ppm)	R_p/R_*	R_p ($R_\oplus$)	R_* ($R_\odot$)	a/R_*	Inc. Flux ($S_\oplus$)
212141021.1	5	$2.91825^{+0.00020}_{-0.00020}$	$2140.1008^{+0.0029}_{-0.0028}$	$2.21^{+0.12}_{-0.15}$	402^{+20}_{-21}	$0.0196^{+0.0011}_{-0.0023}$	$1.65^{+0.13}_{-0.20}$	$0.776^{+0.045}_{-0.013}$	$8.9^{+3.1}_{-1.4}$	306^{+219}_{-100}
212150006.1	5	$0.898344^{+0.000014}_{-0.000013}$	$2139.98140^{+0.00064}_{-0.00064}$	$1.402^{+0.056}_{-0.065}$	2531^{+64}_{-60}	$0.101^{+0.032}_{-0.048}$	$9.8^{+3.3}_{-15.0}$	$0.90^{+0.10}_{-1.30}$	$2.21^{+0.20}_{-0.26}$	8000^{+3200}_{-32700}
212152114.1	5	$2.90491^{+0.00047}_{-0.00043}$	$2140.0595^{+0.0073}_{-0.0078}$	$2.58^{+0.56}_{-0.56}$	134^{+14}_{-14}	$0.0143^{+0.0046}_{-0.0180}$	$1.47^{+0.51}_{-1.86}$	$0.944^{+0.136}_{-0.031}$	$4.3^{+2.7}_{-5.5}$	2800^{+3600}_{-7100}
212154564.1	5	$6.41362^{+0.00016}_{-0.00016}$	$2142.18149^{+0.00096}_{-0.00094}$	$1.649^{+0.063}_{-0.079}$	5530^{+160}_{-160}	$0.0723^{+0.0029}_{-0.0039}$	$2.36^{+0.61}_{-0.49}$	$0.299^{+0.076}_{-0.060}$	$29.8^{+5.7}_{-2.6}$	$8.2^{+6.8}_{-5.0}$
212157262.1	5	$7.14998^{+0.00032}_{-0.00031}$	$2146.3213^{+0.0017}_{-0.0018}$	$3.28^{+0.16}_{-0.25}$	1224^{+31}_{-32}	$0.0350^{+0.0039}_{-0.0052}$	$3.51^{+0.41}_{-0.59}$	$0.919^{+0.035}_{-0.074}$	$12.8^{+4.8}_{-4.4}$	210^{+150}_{-140}
212157262.2	5	$13.60496^{+0.00091}_{-0.00085}$	$2141.4772^{+0.0025}_{-0.0027}$	$4.22^{+0.18}_{-0.41}$	748^{+25}_{-25}	$0.0268^{+0.0021}_{-0.0049}$	$2.69^{+0.23}_{-0.54}$	$0.919^{+0.035}_{-0.074}$	$20.5^{+9.0}_{-4.9}$	81^{+71}_{-40}
212157262.3	5	$0.773987^{+0.000035}_{-0.000035}$	$2140.3180^{+0.0019}_{-0.0020}$	$1.578^{+0.085}_{-0.121}$	237^{+11}_{-12}	$0.01499^{+0.00085}_{-0.00174}$	$1.50^{+0.10}_{-0.21}$	$0.919^{+0.035}_{-0.074}$	$3.31^{+1.17}_{-0.52}$	3100^{+2200}_{-1100}
212157262.4	5	$2.87162^{+0.00021}_{-0.00019}$	$2141.7708^{+0.0027}_{-0.0029}$	$2.37^{+0.15}_{-0.20}$	390^{+20}_{-21}	$0.0189^{+0.0014}_{-0.0037}$	$1.90^{+0.16}_{-0.40}$	$0.919^{+0.035}_{-0.074}$	$8.1^{+3.2}_{-1.4}$	520^{+420}_{-200}
212159623.1	5	$4.70751^{+0.00065}_{-0.00062}$	$2143.1423^{+0.0063}_{-0.0070}$	$2.94^{+0.18}_{-0.22}$	209^{+16}_{-17}	$0.0139^{+0.0010}_{-0.0020}$	$1.52^{+0.13}_{-0.23}$	$0.998^{+0.041}_{-0.053}$	$10.7^{+3.6}_{-1.8}$	370^{+250}_{-130}
212161956.1	5	$7.18662^{+0.00042}_{-0.00044}$	$2140.7018^{+0.0025}_{-0.0024}$	$2.81^{+0.13}_{-0.18}$	1829^{+76}_{-78}	$0.0405^{+0.0025}_{-0.0053}$	$2.58^{+0.29}_{-0.35}$	$0.584^{+0.055}_{-0.017}$	$18.1^{+5.0}_{-2.4}$	50^{+30}_{-14}
212164470.1	5	$7.80905^{+0.00054}_{-0.00054}$	$2144.8589^{+0.0027}_{-0.0026}$	$3.70^{+0.14}_{-0.18}$	520^{+21}_{-22}	$0.0217^{+0.0013}_{-0.0032}$	$2.79^{+0.27}_{-0.41}$	$1.181^{+0.088}_{-0.019}$	$14.5^{+4.5}_{-2.0}$	242^{+156}_{-68}
212270970.1	6	$0.7165461^{+0.0000086}_{-0.0000087}$	$2218.13876^{+0.00056}_{-0.00056}$	$1.750^{+0.075}_{-0.084}$	2089^{+40}_{-43}	$0.133^{+0.035}_{-0.038}$	$25.5^{+6.8}_{-7.4}$	$1.754^{+0.032}_{-0.075}$	$1.523^{+0.136}_{-0.096}$	20600^{+3900}_{-3400}
212297394.1	6	$5.21378^{+0.00035}_{-0.00033}$	$2222.4789^{+0.0028}_{-0.0028}$	$2.47^{+0.10}_{-0.12}$	828^{+45}_{-47}	$0.0280^{+0.0013}_{-0.0023}$	$2.29^{+0.13}_{-0.19}$	$0.749^{+0.025}_{-0.010}$	$15.0^{+4.0}_{-1.7}$	115^{+62}_{-26}
212297394.2	6	$2.28896^{+0.00025}_{-0.00024}$	$2217.9789^{+0.0050}_{-0.0051}$	$1.61^{+0.20}_{-0.29}$	535^{+41}_{-43}	$0.0224^{+0.0021}_{-0.0054}$	$1.83^{+0.18}_{-0.44}$	$0.749^{+0.025}_{-0.010}$	$9.3^{+4.4}_{-2.3}$	300^{+280}_{-150}
212300977.1	6	$4.4656243^{+0.0000060}_{-0.0000064}$	$2220.529448^{+0.000063}_{-0.000058}$	$3.5333^{+0.0080}_{-0.0079}$	18355^{+22}_{-22}	$0.12595^{+0.00094}_{-0.00130}$	$14.73^{+0.96}_{-0.70}$	$1.072^{+0.069}_{-0.050}$	$10.49^{+0.16}_{-0.17}$	474^{+64}_{-48}
212315941.1	6	$12.93562^{+0.00011}_{-0.00011}$	$2226.55444^{+0.00033}_{-0.00033}$	$2.230^{+0.044}_{-0.059}$	15730^{+150}_{-150}	$0.204^{+0.047}_{-0.115}$	$33.6^{+8.3}_{-19.0}$	$1.511^{+0.127}_{-0.078}$	$30.2^{+1.4}_{-2.0}$	$24.9^{+7.0}_{-6.7}$
212315941.2	6	$51.7350^{+0.0027}_{-0.0057}$	$2230.1901^{+0.0024}_{-0.0016}$	$2.67^{+0.42}_{-0.27}$	5910^{+220}_{-220}	$0.093^{+0.026}_{-0.084}$	$15.3^{+4.5}_{-13.9}$	$1.511^{+0.127}_{-0.078}$	90^{+18}_{-84}	$2.8^{+1.3}_{-5.3}$
212321305.1	6	$34.1365^{+0.0030}_{-0.0028}$	$2228.9374^{+0.0020}_{-0.0022}$	$9.19^{+0.18}_{-0.21}$	3371^{+68}_{-69}	$0.0539^{+0.0020}_{-0.0038}$	$10.54^{+0.42}_{-0.76}$	$1.791^{+0.030}_{-0.030}$	$27.5^{+4.1}_{-2.4}$	$46.7^{+15.0}_{-9.6}$
212328538.1	6	$3.56467^{+0.00041}_{-0.00037}$	$2218.0187^{+0.0046}_{-0.0053}$	$1.86^{+0.17}_{-0.23}$	750^{+60}_{-64}	$0.0263^{+0.0022}_{-0.0045}$	$1.62^{+0.16}_{-0.30}$	$0.564^{+0.033}_{-0.035}$	$12.9^{+4.6}_{-2.5}$	85^{+62}_{-35}
212329106.1	6	$21.0791^{+0.0029}_{-0.0027}$	$2231.7039^{+0.0045}_{-0.0050}$	$3.52^{+0.21}_{-0.28}$	353^{+26}_{-27}	$0.0182^{+0.0013}_{-0.0024}$	$2.71^{+0.33}_{-0.37}$	$1.362^{+0.137}_{-0.039}$	$40.1^{+13.7}_{-6.7}$	$29.2^{+20.8}_{-9.9}$
212330265.1	6	$4.17458^{+0.00030}_{-0.00029}$	$2220.4236^{+0.0035}_{-0.0037}$	$1.96^{+0.11}_{-0.14}$	1339^{+89}_{-92}	$0.0354^{+0.0020}_{-0.0033}$	$1.08^{+0.20}_{-0.22}$	$0.280^{+0.050}_{-0.050}$	$15.1^{+4.0}_{-2.0}$	31^{+23}_{-18}
212343520.2	6		$2296.08787^{+0.00064}_{-0.00064}$	$10.38^{+0.21}_{-0.23}$	16430^{+120}_{-120}	$0.278^{+0.081}_{-0.110}$	84^{+25}_{-33}	$2.77^{+0.10}_{-0.11}$		
212346723.1	6	$15.9489^{+0.0024}_{-0.0025}$	$2230.0850^{+0.0058}_{-0.0069}$	$5.65^{+0.24}_{-0.28}$	331^{+21}_{-21}	$0.0177^{+0.0010}_{-0.0020}$	$2.48^{+0.46}_{-0.90}$	$1.29^{+0.23}_{-0.44}$	$19.4^{+6.3}_{-2.6}$	140^{+100}_{-100}
212357477.1	6	$6.32669^{+0.00012}_{-0.00012}$	$2221.23116^{+0.00076}_{-0.00072}$	$1.945^{+0.048}_{-0.059}$	$450.0^{+9.5}_{-9.4}$	$0.02028^{+0.00097}_{-0.00251}$	$2.16^{+0.14}_{-0.27}$	$0.974^{+0.043}_{-0.024}$	$22.3^{+6.9}_{-2.9}$	85^{+53}_{-22}
212362217.1	6	$0.6962935^{+0.0000079}_{-0.0000087}$	$2217.84757^{+0.00045}_{-0.00050}$	$0.794^{+0.097}_{-0.172}$	1033^{+53}_{-57}	$0.0319^{+0.0035}_{-0.0369}$	$3.85^{+0.48}_{-4.45}$	$1.107^{+0.065}_{-0.027}$	$5.7^{+3.6}_{-1.9}$	770^{+990}_{-510}
212380207.1	6	$26.1430^{+0.0029}_{-0.0029}$	$2241.8803^{+0.0043}_{-0.0043}$	$4.48^{+0.24}_{-0.37}$	848^{+42}_{-44}	$0.0285^{+0.0020}_{-0.0043}$	$2.52^{+0.18}_{-0.38}$	$0.8091^{+0.0066}_{-0.0079}$	$38.1^{+16.7}_{-8.0}$	$23.6^{+20.6}_{-9.9}$
212394689.1	6	$6.67913^{+0.00017}_{-0.00017}$	$2223.4198^{+0.0011}_{-0.0011}$	$2.699^{+0.074}_{-0.151}$	784^{+18}_{-18}	$0.0268^{+0.0015}_{-0.0041}$	$2.58^{+0.14}_{-0.41}$	$0.882^{+0.010}_{-0.036}$	$17.0^{+7.4}_{-2.5}$	119^{+103}_{-36}
212394689.2	6	$2.58819^{+0.00014}_{-0.00013}$	$2219.5578^{+0.0020}_{-0.0021}$	$2.221^{+0.093}_{-0.114}$	300^{+14}_{-15}	$0.01650^{+0.00100}_{-0.00239}$	$1.587^{+0.098}_{-0.238}$	$0.882^{+0.010}_{-0.036}$	$8.0^{+2.6}_{-1.1}$	540^{+360}_{-160}
212398508.1	6	$46.4221^{+0.0052}_{-0.0050}$	$2237.2772^{+0.0036}_{-0.0040}$	$6.75^{+0.18}_{-0.23}$	793^{+35}_{-36}	$0.0273^{+0.0011}_{-0.0022}$	$2.66^{+0.12}_{-0.23}$	$0.893^{+0.017}_{-0.035}$	$49.2^{+12.3}_{-4.8}$	$14.8^{+7.4}_{-3.2}$
212406474.1	6	$1.852487^{+0.000050}_{-0.000051}$	$2217.7697^{+0.0012}_{-0.0011}$	$2.53^{+0.11}_{-0.12}$	1299^{+33}_{-33}	$0.136^{+0.030}_{-0.026}$	$36.8^{+8.4}_{-7.1}$	$2.479^{+0.180}_{-0.057}$	$2.69^{+0.13}_{-0.16}$	7700^{+1400}_{-1000}
212409658.1	6	$4.12741^{+0.00012}_{-0.00013}$	$2219.3063^{+0.0018}_{-0.0019}$	$0.78^{+0.22}_{-0.17}$	1460^{+180}_{-550}	$0.0391^{+0.0059}_{-0.0187}$	$2.70^{+0.46}_{-1.32}$	$0.634^{+0.052}_{-0.064}$	35^{+17}_{-15}	16^{+16}_{-14}
212418133.1	6	$3.33253^{+0.00024}_{-0.00024}$	$2219.8529^{+0.0032}_{-0.0032}$	$3.94^{+0.19}_{-0.32}$	374^{+16}_{-17}	$0.0189^{+0.0014}_{-0.0036}$	$3.63^{+0.34}_{-0.70}$	$1.766^{+0.100}_{-0.027}$	$5.4^{+2.7}_{-1.2}$	1250^{+1250}_{-540}
212420823.1	6	$9.0333^{+0.0016}_{-0.0012}$	$2219.1182^{+0.0057}_{-0.0063}$	$3.43^{+0.29}_{-0.42}$	1028^{+49}_{-51}	$0.0305^{+0.0029}_{-0.0080}$	$2.75^{+0.29}_{-0.72}$	$0.825^{+0.035}_{-0.028}$	$17.7^{+8.7}_{-3.6}$	80^{+79}_{-33}
212421673.1	6	$28.24765^{+0.00047}_{-0.00047}$	$2227.59337^{+0.00061}_{-0.00062}$	$13.976^{+0.048}_{-0.048}$	9811^{+42}_{-43}	$0.09873^{+0.00032}_{-0.00489}$	$38.5^{+1.8}_{-2.9}$	$3.57^{+0.17}_{-0.20}$	$14.09^{+0.22}_{-0.37}$	136^{+21}_{-23}
212421749.1	6	$25.3606^{+0.0043}_{-0.0045}$	$2240.4076^{+0.0050}_{-0.0050}$	$4.65^{+0.34}_{-0.51}$	1341^{+85}_{-87}	$0.0350^{+0.0044}_{-0.0120}$	$3.11^{+0.41}_{-1.07}$	$0.815^{+0.035}_{-0.039}$	$36.1^{+18.6}_{-7.7}$	$19.1^{+19.8}_{-8.4}$
212422536.1	6	$15.7086^{+0.0014}_{-0.0014}$	$2230.4647^{+0.0035}_{-0.0033}$	$3.64^{+0.21}_{-0.30}$	1002^{+56}_{-58}	$0.0303^{+0.0022}_{-0.0048}$	$1.96^{+0.16}_{-0.35}$	$0.595^{+0.021}_{-0.046}$	$29.4^{+9.9}_{-4.9}$	$26.4^{+18.0}_{-9.7}$
212422536.2	6	$9.88600^{+0.00096}_{-0.00092}$	$2225.5976^{+0.0044}_{-0.0047}$	$3.17^{+0.20}_{-0.29}$	652^{+37}_{-38}	$0.0245^{+0.0018}_{-0.0043}$	$1.59^{+0.13}_{-0.30}$	$0.595^{+0.021}_{-0.046}$	$21.1^{+7.9}_{-3.6}$	51^{+39}_{-19}
212424622.1	6	$12.0156^{+0.0012}_{-0.0012}$	$2219.4850^{+0.0044}_{-0.0045}$	$5.39^{+0.28}_{-0.39}$	489^{+24}_{-24}	$0.0211^{+0.0043}_{-0.0043}$	$2.81^{+0.24}_{-0.59}$	$1.2247^{+0.0049}_{-0.0469}$	$14.7^{+6.0}_{-2.7}$	216^{+175}_{-82}

Table A.1: Our sample of planet candidates from C0-8. (continued)

Candidate	C#	Period (days)	t_0 (BJD - 2455000)	Duration (hours)	Depth (ppm)	R_p/R_*	R_p ($R_\oplus$)	R_* ($R_\odot$)	a/R_*	Inc. Flux ($S_\oplus$)
212424622.2	6	$18.0971^{+0.0044}_{-0.0044}$	$2227.0642^{+0.0074}_{-0.0078}$	$4.33^{+0.28}_{-0.41}$	298^{+27}_{-28}	$0.0165^{+0.0014}_{-0.0031}$	$2.21^{+0.19}_{-0.43}$	$1.2247^{+0.0049}_{-0.0469}$	$27.9^{+10.7}_{-4.8}$	60^{+46}_{-21}
212425103.1	6	$0.946033^{+0.000069}_{-0.000061}$	$2218.1754^{+0.0024}_{-0.0024}$	$1.64^{+0.12}_{-0.17}$	425^{+29}_{-30}	$0.0200^{+0.0014}_{-0.0026}$	$1.81^{+0.18}_{-0.26}$	$0.827^{+0.060}_{-0.055}$	$3.88^{+1.34}_{-0.68}$	1990^{+1410}_{-750}
212432685.1	6	$0.531678^{+0.000015}_{-0.000017}$	$2217.99512^{+0.00125}_{-0.00073}$	$2.03^{+0.26}_{-0.28}$	249^{+11}_{-11}	$0.0191^{+0.0062}_{-0.0201}$	$2.68^{+0.94}_{-2.86}$	$1.29^{+0.17}_{-0.24}$	$1.01^{+0.56}_{-1.15}$	$61000^{+72000}_{-143000}$
212435047.1	6	$1.115563^{+0.000047}_{-0.000048}$	$2218.4419^{+0.0019}_{-0.0019}$	$2.03^{+0.11}_{-0.16}$	$196.9^{+7.8}_{-8.0}$	$0.0120^{+0.0011}_{-0.0053}$	$1.29^{+0.28}_{-0.61}$	$0.98^{+0.20}_{-0.17}$	$3.88^{+1.50}_{-0.42}$	3600^{+3100}_{-1400}
212440430.1	6	$19.9901^{+0.0022}_{-0.0020}$	$2228.1623^{+0.0040}_{-0.0044}$	$4.56^{+0.20}_{-0.26}$	748^{+35}_{-36}	$0.0256^{+0.0016}_{-0.0037}$	$2.81^{+0.66}_{-0.41}$	$1.006^{+0.227}_{-0.029}$	$30.6^{+8.1}_{-3.9}$	43^{+30}_{-11}
212443457.1	6	$24.4820^{+0.0011}_{-0.0011}$	$2233.6552^{+0.0015}_{-0.0015}$	$8.01^{+0.12}_{-0.13}$	8040^{+190}_{-230}	$0.0937^{+0.0026}_{-0.0061}$	$28.2^{+1.2}_{-3.0}$	$2.763^{+0.087}_{-0.232}$	$16.17^{+0.66}_{-0.96}$	97^{+12}_{-21}
212454422.1	6	$3.26945^{+0.00015}_{-0.00014}$	$2220.2279^{+0.0018}_{-0.0017}$	$0.95^{+0.27}_{-0.21}$	15500^{+2100}_{-6300}	$0.130^{+0.022}_{-0.101}$	$3.9^{+1.3}_{-3.3}$	$0.276^{+0.079}_{-0.090}$	$25.7^{+9.5}_{-11.1}$	11^{+13}_{-15}
212460519.1	6	$7.38711^{+0.00020}_{-0.00020}$	$2223.7942^{+0.0011}_{-0.0011}$	$2.587^{+0.068}_{-0.090}$	882^{+21}_{-21}	$0.0281^{+0.0011}_{-0.0029}$	$1.92^{+0.15}_{-0.23}$	$0.625^{+0.043}_{-0.037}$	$20.3^{+4.9}_{-2.2}$	$35.0^{+17.6}_{-8.6}$
212464382.1	6	$4.07337^{+0.00051}_{-0.00047}$	$2219.7133^{+0.0048}_{-0.0056}$	$2.76^{+0.21}_{-0.29}$	125^{+10}_{-11}	$0.01071^{+0.00091}_{-0.00184}$	$0.928^{+0.085}_{-0.162}$	$0.794^{+0.026}_{-0.028}$	$9.7^{+3.4}_{-1.8}$	259^{+180}_{-98}
212480208.1	6	$10.1016^{+0.0018}_{-0.0015}$	$2224.7587^{+0.0075}_{-0.0094}$	$4.22^{+0.19}_{-0.23}$	$73.1^{+4.5}_{-4.7}$	$0.00836^{+0.00049}_{-0.00110}$	$0.91^{+0.21}_{-0.13}$	$1.000^{+0.227}_{-0.039}$	$15.8^{+6.0}_{-2.5}$	152^{+135}_{-49}
212495601.1	6	$21.6768^{+0.0021}_{-0.0022}$	$2229.6446^{+0.0043}_{-0.0043}$	$4.87^{+0.20}_{-0.23}$	726^{+38}_{-39}	$0.0262^{+0.0013}_{-0.0024}$	$2.87^{+0.18}_{-0.28}$	$1.003^{+0.037}_{-0.028}$	$31.1^{+9.3}_{-3.9}$	42^{+25}_{-11}
212496592.1	6	$2.85847^{+0.00016}_{-0.00016}$	$2219.5594^{+0.0026}_{-0.0026}$	$2.23^{+0.14}_{-0.16}$	308^{+15}_{-16}	$0.0167^{+0.0014}_{-0.0036}$	$1.63^{+0.14}_{-0.36}$	$0.8988^{+0.0108}_{-0.0092}$	$8.6^{+3.5}_{-1.4}$	340^{+280}_{-110}
212497862.1	6	$6.80213^{+0.00038}_{-0.00037}$	$2223.3540^{+0.0021}_{-0.0023}$	$1.27^{+0.10}_{-0.15}$	2080^{+150}_{-160}	$0.0440^{+0.0033}_{-0.0065}$	$1.82^{+0.34}_{-0.32}$	$0.379^{+0.065}_{-0.037}$	$37.5^{+12.3}_{-6.6}$	$6.4^{+5.4}_{-3.0}$
212499835.1	6	$6.88385^{+0.00037}_{-0.00037}$	$2221.0138^{+0.0021}_{-0.0022}$	$7.58^{+0.20}_{-0.23}$	12070^{+240}_{-240}	$0.1023^{+0.0074}_{-0.0079}$	$8.3^{+1.2}_{-29.7}$	$0.743^{+0.094}_{-2.659}$	$6.73^{+0.71}_{-0.83}$	580^{+260}_{-5840}
212499991.1	6	$15.3866^{+0.0011}_{-0.0012}$	$2225.4491^{+0.0030}_{-0.0028}$	$2.41^{+0.28}_{-0.46}$	796^{+52}_{-54}	$0.0292^{+0.0052}_{-0.0297}$	$2.41^{+0.43}_{-2.46}$	$0.758^{+0.013}_{-0.013}$	37^{+23}_{-15}	19^{+23}_{-16}
212521166.1	6	$13.86360^{+0.00018}_{-0.00018}$	$2219.87496^{+0.00055}_{-0.00056}$	$3.218^{+0.052}_{-0.071}$	1361^{+16}_{-15}	$0.03406^{+0.00096}_{-0.00226}$	$2.55^{+0.18}_{-0.18}$	$0.686^{+0.043}_{-0.019}$	$31.6^{+5.4}_{-2.4}$	$24.3^{+8.9}_{-3.9}$
212524671.1	6	$11.52898^{+0.00051}_{-0.00053}$	$2223.3662^{+0.0017}_{-0.0016}$	$1.49^{+0.10}_{-0.13}$	4940^{+250}_{-270}	$0.0675^{+0.0041}_{-0.0070}$	$3.93^{+0.92}_{-0.43}$	$0.533^{+0.120}_{-0.019}$	$56.9^{+14.9}_{-8.1}$	$1.91^{+1.32}_{-0.56}$
212525174.1	6	$3.44791^{+0.00020}_{-0.00020}$	$2218.3841^{+0.0025}_{-0.0025}$	$1.63^{+0.11}_{-0.14}$	480^{+31}_{-33}	$0.0211^{+0.0016}_{-0.0032}$	$1.46^{+0.14}_{-0.23}$	$0.637^{+0.041}_{-0.028}$	$14.3^{+4.9}_{-2.4}$	74^{+51}_{-25}
212525618.1	6	$14.4307^{+0.0020}_{-0.0021}$	$2231.8631^{+0.0044}_{-0.0046}$	$3.00^{+0.26}_{-0.40}$	487^{+33}_{-35}	$0.0212^{+0.0023}_{-0.0070}$	$2.28^{+0.35}_{-0.76}$	$0.986^{+0.108}_{-0.031}$	$31.5^{+18.0}_{-6.8}$	50^{+58}_{-22}
212529560.1	6	$8.12088^{+0.00090}_{-0.00092}$	$2219.0861^{+0.0051}_{-0.0050}$	$3.49^{+0.23}_{-0.31}$	534^{+37}_{-38}	$0.0224^{+0.0016}_{-0.0032}$	$2.69^{+0.27}_{-0.40}$	$1.101^{+0.077}_{-0.039}$	$15.6^{+5.6}_{-2.7}$	159^{+116}_{-57}
212530118.1	6	$12.83306^{+0.00097}_{-0.00099}$	$2230.1421^{+0.0033}_{-0.0032}$	$3.41^{+0.20}_{-0.25}$	754^{+39}_{-40}	$0.0256^{+0.0022}_{-0.0052}$	$1.82^{+0.17}_{-0.38}$	$0.649^{+0.022}_{-0.040}$	$25.9^{+8.9}_{-3.9}$	$23.2^{+16.1}_{-7.5}$
212534729.1	6	$13.4850^{+0.0014}_{-0.0016}$	$2223.5257^{+0.0050}_{-0.0042}$	$2.89^{+0.20}_{-0.31}$	337^{+27}_{-28}	$0.0174^{+0.0015}_{-0.0033}$	$1.67^{+0.23}_{-0.49}$	$0.879^{+0.094}_{-0.198}$	$31.3^{+10.8}_{-5.3}$	37^{+28}_{-27}
212540985.1	6	$1.096473^{+0.000024}_{-0.000024}$	$2218.2510^{+0.0011}_{-0.0011}$	$3.76^{+0.14}_{-0.12}$	29770^{+410}_{-410}	$0.373^{+0.099}_{-0.151}$	78^{+21}_{-32}	$1.913^{+0.094}_{-0.099}$	$1.998^{+0.059}_{-0.107}$	35900^{+6200}_{-7100}
212543933.1	6	$7.80692^{+0.00062}_{-0.00065}$	$2223.4913^{+0.0032}_{-0.0029}$	$2.80^{+0.12}_{-0.17}$	681^{+34}_{-35}	$0.0252^{+0.0013}_{-0.0026}$	$3.03^{+0.17}_{-0.35}$	$1.103^{+0.019}_{-0.059}$	$19.3^{+5.5}_{-2.6}$	100^{+58}_{-29}
212554013.1	6	$3.588162^{+0.000012}_{-0.000012}$	$2220.33788^{+0.00016}_{-0.00016}$	$2.321^{+0.029}_{-0.027}$	15120^{+68}_{-70}	$0.1187^{+0.0030}_{-0.0040}$	$12.72^{+1.11}_{-0.46}$	$0.982^{+0.082}_{-0.013}$	$10.68^{+0.42}_{-0.56}$	222^{+44}_{-28}
212555594.1	6	$4.16328^{+0.00016}_{-0.00016}$	$2220.4418^{+0.0017}_{-0.0016}$	$1.618^{+0.084}_{-0.106}$	318^{+16}_{-16}	$0.0170^{+0.0012}_{-0.0026}$	$1.47^{+0.23}_{-0.25}$	$0.791^{+0.112}_{-0.056}$	$17.4^{+5.7}_{-2.7}$	101^{+72}_{-34}
212560683.1	6	$13.7043^{+0.0037}_{-0.0028}$	$2227.4182^{+0.0084}_{-0.0124}$	$4.27^{+0.29}_{-0.46}$	158^{+13}_{-14}	$0.0118^{+0.0011}_{-0.0033}$	$1.30^{+0.14}_{-0.37}$	$1.014^{+0.047}_{-0.032}$	$21.3^{+9.2}_{-3.7}$	101^{+88}_{-36}
212562715.1	6	$13.52583^{+0.00099}_{-0.00099}$	$2220.4675^{+0.0028}_{-0.0028}$	$2.75^{+0.17}_{-0.20}$	704^{+36}_{-36}	$0.0246^{+0.0022}_{-0.0054}$	$2.49^{+0.30}_{-0.55}$	$0.927^{+0.074}_{-0.021}$	$33.8^{+11.8}_{-5.0}$	$32.4^{+23.2}_{-9.7}$
212575828.1	6	$2.060368^{+0.000076}_{-0.000068}$	$2217.8500^{+0.0015}_{-0.0016}$	$1.490^{+0.072}_{-0.096}$	1697^{+77}_{-81}	$0.0398^{+0.0021}_{-0.0035}$	$3.16^{+0.21}_{-0.33}$	$0.727^{+0.031}_{-0.041}$	$9.9^{+2.5}_{-1.2}$	234^{+120}_{-65}
212577658.1	6	$14.06928^{+0.00063}_{-0.00062}$	$2221.3218^{+0.0019}_{-0.0018}$	$3.005^{+0.094}_{-0.107}$	402^{+13}_{-14}	$0.01915^{+0.00095}_{-0.00231}$	$1.83^{+0.14}_{-0.25}$	$0.876^{+0.051}_{-0.054}$	$32.4^{+9.6}_{-3.9}$	34^{+21}_{-11}
212580872.1	6	$14.78708^{+0.00051}_{-0.00051}$	$2224.2595^{+0.0013}_{-0.0013}$	$4.387^{+0.075}_{-0.101}$	1692^{+32}_{-32}	$0.0380^{+0.0011}_{-0.0028}$	$4.18^{+0.13}_{-0.32}$	$1.0085^{+0.0073}_{-0.0156}$	$25.1^{+4.0}_{-1.7}$	$56.1^{+17.8}_{-7.9}$
212585579.1	6	$3.021944^{+0.000054}_{-0.000058}$	$2218.53908^{+0.00090}_{-0.00086}$	$2.031^{+0.079}_{-0.082}$	1186^{+45}_{-44}	$0.092^{+0.026}_{-0.029}$	$10.8^{+3.1}_{-3.5}$	$1.082^{+0.035}_{-0.028}$	$4.50^{+0.43}_{-0.49}$	2390^{+490}_{-540}
212586030.1	6	$7.78608^{+0.00070}_{-0.00067}$	$2220.8799^{+0.0039}_{-0.0039}$	$2.48^{+0.34}_{-0.37}$	622^{+40}_{-40}	$0.0298^{+0.0090}_{-0.0312}$	$10.9^{+3.3}_{-11.4}$	$3.34^{+0.16}_{-0.28}$	$12.5^{+5.8}_{-13.7}$	160^{+150}_{-360}
212587672.1	6	$23.2259^{+0.0029}_{-0.0027}$	$2237.0457^{+0.0040}_{-0.0034}$	$3.34^{+0.21}_{-0.30}$	506^{+27}_{-28}	$0.0217^{+0.0015}_{-0.0032}$	$2.31^{+0.16}_{-0.35}$	$0.9757^{+0.0133}_{-0.0098}$	$46.8^{+17.0}_{-8.1}$	$22.5^{+16.4}_{-7.9}$
212587672.2	6	$15.2841^{+0.0020}_{-0.0020}$	$2227.6405^{+0.0048}_{-0.0049}$	$3.56^{+0.20}_{-0.22}$	187^{+15}_{-16}	$0.0130^{+0.0010}_{-0.0020}$	$1.39^{+0.11}_{-0.21}$	$0.9757^{+0.0133}_{-0.0098}$	$28.9^{+9.2}_{-4.3}$	59^{+37}_{-18}
212590677.1	6		$2271.08485^{+0.00064}_{-0.00064}$	$3.58^{+0.11}_{-0.13}$	11010^{+210}_{-200}	$0.175^{+0.047}_{-0.101}$	$15.2^{+4.1}_{-8.8}$	$0.797^{+0.012}_{-0.020}$		
212592101.1	6	$4.54462^{+0.00025}_{-0.00025}$	$2217.5553^{+0.0024}_{-0.0023}$	$1.52^{+0.27}_{-0.21}$	9290^{+690}_{-710}	$0.125^{+0.037}_{-0.112}$	$6.6^{+2.3}_{-6.1}$	$0.487^{+0.087}_{-0.087}$	$14.9^{+2.6}_{-12.1}$	54^{+35}_{-93}
212621075.1	6	$31.4782^{+0.0030}_{-0.0030}$	$2227.7215^{+0.0036}_{-0.0039}$	$4.49^{+0.24}_{-0.32}$	1052^{+51}_{-54}	$0.0316^{+0.0023}_{-0.0044}$	$2.60^{+0.19}_{-0.37}$	$0.7556^{+0.0060}_{-0.0204}$	$46.6^{+18.9}_{-9.1}$	$11.8^{+9.6}_{-4.7}$

Table A.1: Our sample of planet candidates from C0-8. (continued)

Candidate	C#	Period (days)	t_0 (BJD - 2455000)	Duration (hours)	Depth (ppm)	R_p/R_*	R_p ($R_\oplus$)	R_* ($R_\odot$)	a/R_*	Inc. Flux ($S_\oplus$)
212622766.1	6	$6.02226^{+0.00055}_{-0.00054}$	$2218.8618^{+0.0045}_{-0.0042}$	$2.08^{+0.23}_{-0.45}$	384^{+27}_{-28}	$0.0190^{+0.0022}_{-0.0100}$	$2.02^{+0.25}_{-1.06}$	$0.9738^{+0.0329}_{-0.0087}$	$18.5^{+12.5}_{-4.8}$	102^{+138}_{-53}
212624936.1	6	$11.81387^{+0.00085}_{-0.00093}$	$2221.9709^{+0.0038}_{-0.0034}$	$2.07^{+0.12}_{-0.20}$	722^{+42}_{-44}	$0.0258^{+0.0018}_{-0.0036}$	$2.67^{+0.43}_{-0.39}$	$0.948^{+0.137}_{-0.044}$	$39.0^{+12.4}_{-6.4}$	$24.7^{+17.2}_{-8.4}$
212634172.1	6	$2.851702^{+0.000037}_{-0.000036}$	$2217.59720^{+0.00058}_{-0.00059}$	$0.864^{+0.051}_{-0.142}$	4880^{+230}_{-280}	$0.0655^{+0.0064}_{-0.0477}$	$2.16^{+0.52}_{-1.69}$	$0.303^{+0.067}_{-0.085}$	$23.5^{+11.6}_{-4.0}$	15^{+18}_{-14}
212639319.1	6	$13.83851^{+0.00053}_{-0.00062}$	$2222.4571^{+0.0017}_{-0.0018}$	$1.496^{+0.069}_{-0.094}$	882^{+42}_{-45}	$0.0286^{+0.0015}_{-0.0027}$	$8.26^{+0.46}_{-0.91}$	$2.650^{+0.061}_{-0.147}$	$65.2^{+17.2}_{-8.0}$	$7.8^{+4.1}_{-2.2}$
212646483.1	6	$8.25178^{+0.00037}_{-0.00038}$	$2219.8752^{+0.0018}_{-0.0018}$	$1.143^{+0.077}_{-0.103}$	954^{+87}_{-96}	$0.0296^{+0.0022}_{-0.0040}$	$6.99^{+0.59}_{-0.98}$	$2.161^{+0.083}_{-0.077}$	$50.1^{+15.0}_{-7.7}$	$12.6^{+7.7}_{-4.1}$
212648083.1	6	$20.5827^{+0.0022}_{-0.0018}$	$2229.7807^{+0.0041}_{-0.0051}$	$3.72^{+0.14}_{-0.16}$	664^{+34}_{-35}	$0.0249^{+0.0012}_{-0.0021}$	$2.98^{+0.16}_{-0.27}$	$1.099^{+0.032}_{-0.042}$	$39.2^{+10.0}_{-4.3}$	$27.9^{+14.3}_{-6.5}$
212652418.1	6	$19.1324^{+0.0031}_{-0.0023}$	$2234.9751^{+0.0035}_{-0.0067}$	$3.33^{+0.23}_{-0.20}$	366^{+20}_{-20}	$0.0186^{+0.0011}_{-0.0022}$	$2.73^{+0.18}_{-0.33}$	$1.347^{+0.038}_{-0.036}$	$39.3^{+13.1}_{-5.9}$	$30.0^{+20.1}_{-9.1}$
212661144.1	6	$2.458783^{+0.000058}_{-0.000063}$	$2218.9082^{+0.0013}_{-0.0012}$	$1.257^{+0.098}_{-0.164}$	943^{+36}_{-39}	$0.0295^{+0.0026}_{-0.0069}$	$3.11^{+0.44}_{-0.72}$	$0.964^{+0.109}_{-0.013}$	$13.0^{+6.3}_{-2.7}$	207^{+205}_{-87}
212672300.1	6	$39.7268^{+0.0052}_{-0.0055}$	$2242.9988^{+0.0037}_{-0.0037}$	$8.52^{+0.21}_{-0.29}$	741^{+28}_{-28}	$0.0254^{+0.0013}_{-0.0034}$	$3.63^{+0.54}_{-0.50}$	$1.312^{+0.184}_{-0.049}$	$32.8^{+8.4}_{-3.6}$	55^{+32}_{-13}
212679181.1	6	$1.0546040^{+0.0000073}_{-0.0000089}$	$2217.54967^{+0.00029}_{-0.00030}$	$0.462^{+0.018}_{-0.052}$	658^{+26}_{-28}	$0.0252^{+0.0015}_{-0.0032}$	$0.824^{+0.052}_{-0.126}$	$0.3000^{+0.0060}_{-0.0250}$	$14.5^{+5.4}_{-3.3}$	34^{+26}_{-18}
212685467.1	6		$2242.66141^{+0.00041}_{-0.00041}$	$7.31^{+0.13}_{-0.14}$	9679^{+57}_{-57}	$0.231^{+0.060}_{-0.072}$	$24.0^{+6.2}_{-7.5}$	$0.951^{+0.021}_{-0.024}$		
212686205.1	6	$5.67556^{+0.00029}_{-0.00026}$	$2221.4503^{+0.0021}_{-0.0023}$	$1.805^{+0.092}_{-0.109}$	332^{+17}_{-17}	$0.0177^{+0.0010}_{-0.0023}$	$1.117^{+0.088}_{-0.161}$	$0.578^{+0.032}_{-0.038}$	$21.2^{+7.2}_{-3.2}$	47^{+32}_{-16}
212689874.1	6	$15.85388^{+0.00066}_{-0.00067}$	$2225.0446^{+0.0016}_{-0.0016}$	$4.80^{+0.12}_{-0.15}$	1118^{+21}_{-21}	$0.0318^{+0.0014}_{-0.0031}$	$3.29^{+0.16}_{-0.40}$	$0.948^{+0.023}_{-0.069}$	$23.0^{+6.4}_{-3.0}$	86^{+48}_{-26}
212689874.2	6	$28.4707^{+0.0055}_{-0.0047}$	$2243.0235^{+0.0036}_{-0.0043}$	$5.97^{+0.21}_{-0.29}$	747^{+28}_{-29}	$0.0260^{+0.0014}_{-0.0034}$	$2.68^{+0.16}_{-0.40}$	$0.948^{+0.023}_{-0.069}$	$33.0^{+9.4}_{-4.4}$	42^{+24}_{-13}
212690867.1	6	$25.8614^{+0.0023}_{-0.0022}$	$2229.6014^{+0.0033}_{-0.0029}$	$2.97^{+0.17}_{-0.31}$	2650^{+150}_{-160}	$0.0491^{+0.0032}_{-0.0065}$	$1.58^{+0.55}_{-0.32}$	$0.295^{+0.100}_{-0.044}$	$61.3^{+17.5}_{-9.6}$	$1.85^{+2.10}_{-1.00}$
212697709.1	6	$3.9516283^{+0.0000084}_{-0.0000086}$	$2218.28700^{+0.00010}_{-0.00010}$	$1.938^{+0.024}_{-0.027}$	7628^{+37}_{-38}	$0.0959^{+0.0028}_{-0.0052}$	$11.81^{+0.91}_{-0.93}$	$1.130^{+0.080}_{-0.064}$	$10.27^{+0.35}_{-0.51}$	394^{+63}_{-60}
212703473.1	6	$6.78882^{+0.00027}_{-0.00027}$	$2222.7288^{+0.0018}_{-0.0017}$	$2.933^{+0.082}_{-0.103}$	$234.8^{+6.9}_{-7.0}$	$0.01436^{+0.00087}_{-0.00224}$	$2.8^{+1.1}_{-1.2}$	$1.76^{+0.68}_{-0.74}$	$15.7^{+4.9}_{-2.1}$	210^{+270}_{-260}
212703473.2	6	$18.51590^{+0.00064}_{-0.00067}$	$2221.1692^{+0.0021}_{-0.0019}$	$2.807^{+0.089}_{-0.118}$	$306.7^{+9.9}_{-10.3}$	$0.01712^{+0.00078}_{-0.00183}$	$3.3^{+1.3}_{-1.4}$	$1.76^{+0.68}_{-0.74}$	$44.9^{+17.7}_{-6.2}$	26^{+35}_{-32}
212730483.1	6	$3.49140^{+0.00040}_{-0.00033}$	$2219.7264^{+0.0028}_{-0.0030}$	$1.83^{+0.22}_{-0.35}$	376^{+32}_{-34}	$0.0190^{+0.0027}_{-0.0167}$	$1.18^{+0.18}_{-1.04}$	$0.572^{+0.024}_{-0.024}$	$12.1^{+8.3}_{-3.4}$	167^{+232}_{-95}
212732378.2	6		$2277.6661^{+0.0010}_{-0.0010}$	$3.88^{+0.16}_{-0.17}$	8280^{+260}_{-240}	$0.126^{+0.024}_{-0.086}$	$11.8^{+2.5}_{-8.1}$	$0.861^{+0.080}_{-0.068}$		
212743333.1	6	$14.78545^{+0.00067}_{-0.00069}$	$2228.1816^{+0.0017}_{-0.0017}$	$1.86^{+0.13}_{-0.29}$	1633^{+81}_{-87}	$0.0385^{+0.0036}_{-0.0116}$	$2.62^{+0.25}_{-0.79}$	$0.623^{+0.016}_{-0.017}$	54^{+27}_{-10}	$8.6^{+8.5}_{-3.3}$
212756297.1	6	$1.33711569^{+0.00000063}_{-0.00000063}$	$2218.110041^{+0.000023}_{-0.000023}$	$1.8317^{+0.0059}_{-0.0065}$	33335^{+41}_{-40}	$0.1638^{+0.0019}_{-0.0018}$	$11.85^{+0.56}_{-0.20}$	$0.6629^{+0.0304}_{-0.0086}$	$6.394^{+0.079}_{-0.069}$	476^{+46}_{-17}
212757601.1	6	$1.017977^{+0.000015}_{-0.000015}$	$2218.01357^{+0.00068}_{-0.00068}$	$2.080^{+0.079}_{-0.089}$	13960^{+260}_{-260}	$0.259^{+0.076}_{-0.099}$	$18.1^{+5.6}_{-54.5}$	$0.638^{+0.065}_{-1.911}$	$2.62^{+0.12}_{-0.14}$	4300^{+1400}_{-36700}
212768333.1	6	$17.04354^{+0.00026}_{-0.00025}$	$2221.61111^{+0.00054}_{-0.00055}$	$2.958^{+0.054}_{-0.072}$	2737^{+40}_{-40}	$0.0490^{+0.0015}_{-0.0034}$	$4.28^{+0.23}_{-0.36}$	$0.801^{+0.035}_{-0.037}$	$43.0^{+6.9}_{-3.3}$	$15.4^{+5.1}_{-2.7}$
212768333.2	6	$7.44976^{+0.00015}_{-0.00016}$	$2221.02659^{+0.00084}_{-0.00083}$	$3.003^{+0.087}_{-0.133}$	1082^{+19}_{-20}	$0.0323^{+0.0020}_{-0.0034}$	$2.82^{+0.22}_{-0.32}$	$0.801^{+0.035}_{-0.037}$	$15.8^{+4.8}_{-3.6}$	114^{+71}_{-53}
212772113.1	6	$8.95366^{+0.00022}_{-0.00021}$	$2223.8033^{+0.0010}_{-0.0011}$	$0.895^{+0.077}_{-0.122}$	1420^{+74}_{-86}	$0.0361^{+0.0031}_{-0.0093}$	$3.32^{+0.34}_{-0.86}$	$0.841^{+0.046}_{-0.024}$	68^{+31}_{-13}	$5.4^{+4.9}_{-2.1}$
212779596.1	6	$7.37426^{+0.00012}_{-0.00012}$	$2222.93279^{+0.00057}_{-0.00057}$	$2.572^{+0.056}_{-0.064}$	1739^{+19}_{-19}	$0.0387^{+0.0015}_{-0.0024}$	$2.45^{+0.15}_{-0.23}$	$0.582^{+0.027}_{-0.040}$	$20.3^{+3.9}_{-2.4}$	57^{+22}_{-15}
212779596.2	6	$3.225369^{+0.000045}_{-0.000044}$	$2218.73785^{+0.00057}_{-0.00058}$	$2.066^{+0.035}_{-0.056}$	726^{+12}_{-12}	$0.02511^{+0.00091}_{-0.00258}$	$1.593^{+0.095}_{-0.197}$	$0.582^{+0.027}_{-0.040}$	$11.2^{+2.6}_{-1.0}$	187^{+88}_{-43}
212782836.1	6	$7.12471^{+0.00058}_{-0.00056}$	$2222.1244^{+0.0029}_{-0.0029}$	$3.06^{+0.14}_{-0.18}$	207^{+11}_{-11}	$0.0133^{+0.0010}_{-0.0026}$	$1.244^{+0.099}_{-0.243}$	$0.857^{+0.018}_{-0.011}$	$15.8^{+5.0}_{-2.1}$	150^{+95}_{-41}
212803289.1	6	$18.24841^{+0.00053}_{-0.00055}$	$2233.82582^{+0.00098}_{-0.00096}$	$11.49^{+0.13}_{-0.15}$	1930^{+17}_{-17}	$0.0422^{+0.0012}_{-0.0021}$	$12.48^{+1.95}_{-0.87}$	$2.71^{+0.42}_{-0.13}$	$11.1^{+1.4}_{-1.4}$	440^{+170}_{-120}
212805678.2	6		$2225.07634^{+0.00033}_{-0.00032}$	$22.707^{+0.038}_{-0.039}$	31770^{+49}_{-50}	$0.17820^{+0.00024}_{-0.00382}$	$59.10^{+0.88}_{-2.34}$	$3.040^{+0.045}_{-0.101}$		
212813907.1	6	$6.72511^{+0.00013}_{-0.00014}$	$2221.83500^{+0.00080}_{-0.00081}$	$1.082^{+0.099}_{-0.172}$	2800^{+110}_{-130}	$0.0509^{+0.0042}_{-0.0128}$	$4.37^{+0.39}_{-1.11}$	$0.787^{+0.024}_{-0.024}$	$42.8^{+19.2}_{-9.2}$	$12.8^{+11.5}_{-5.6}$
212821706.1	6	$13.8883^{+0.0017}_{-0.0017}$	$2222.1936^{+0.0050}_{-0.0053}$	$3.33^{+0.21}_{-0.29}$	558^{+40}_{-42}	$0.0226^{+0.0017}_{-0.0037}$	$1.46^{+0.13}_{-0.26}$	$0.592^{+0.024}_{-0.044}$	$28.3^{+10.5}_{-4.7}$	29^{+22}_{-11}
212828909.1	6	$2.85009^{+0.00012}_{-0.00012}$	$2218.5553^{+0.0019}_{-0.0019}$	$1.342^{+0.099}_{-0.124}$	273^{+15}_{-16}	$0.0158^{+0.0012}_{-0.0026}$	$1.38^{+0.16}_{-0.24}$	$0.800^{+0.071}_{-0.042}$	$14.2^{+5.1}_{-2.5}$	129^{+95}_{-47}
212833814.1	6	$27.7985^{+0.0086}_{-0.0053}$	$2236.1256^{+0.0061}_{-0.0062}$	$11.63^{+0.33}_{-0.41}$	255^{+10}_{-11}	$0.01524^{+0.00078}_{-0.00197}$	$2.47^{+0.15}_{-0.36}$	$1.484^{+0.044}_{-0.097}$	$16.3^{+5.0}_{-2.2}$	180^{+111}_{-53}
213123443.1	7	$0.546127^{+0.000013}_{-0.000013}$	$2301.9503^{+0.0011}_{-0.0011}$	$3.17^{+0.16}_{-0.16}$	$392.3^{+8.6}_{-10.3}$	$0.072^{+0.017}_{-0.019}$	$11.3^{+2.9}_{-3.1}$	$1.447^{+0.110}_{-0.059}$	$0.473^{+0.053}_{-0.035}$	328000^{+90000}_{-57000}
213408445.1	7	$2.49686^{+0.00022}_{-0.00022}$	$2302.0093^{+0.0042}_{-0.0041}$	$6.82^{+0.29}_{-0.32}$	692^{+21}_{-21}	$0.072^{+0.019}_{-0.022}$	90^{+89}_{-137}	11^{+11}_{-17}	$0.972^{+0.100}_{-0.116}$	17000^{+47000}_{-73000}
213462890.1	7	$5.84643^{+0.00014}_{-0.00011}$	$2306.73271^{+0.00091}_{-0.00120}$	$1.97^{+0.12}_{-0.13}$	15210^{+510}_{-510}	$0.136^{+0.012}_{-0.089}$	$10.4^{+4.4}_{-6.9}$	$0.698^{+0.287}_{-0.091}$	$17.4^{+2.4}_{-2.3}$	26^{+23}_{-10}

Table A.1: Our sample of planet candidates from C0-8. (continued)

Candidate	C#	Period (days)	t_0 (BJD - 2455000)	Duration (hours)	Depth (ppm)	R_p/R_*	R_p ($R_\oplus$)	R_* ($R_\odot$)	a/R_*	Inc. Flux ($S_\oplus$)
213546283.1	7	$9.77060^{+0.00024}_{-0.00024}$	$2302.3542^{+0.0012}_{-0.0012}$	$3.227^{+0.096}_{-0.128}$	988^{+21}_{-21}	$0.0292^{+0.0019}_{-0.0043}$	$3.80^{+0.25}_{-0.56}$	$1.195^{+0.018}_{-0.012}$	$21.1^{+6.0}_{-2.7}$	79^{+45}_{-20}
213715787.1	7	$0.961916^{+0.000019}_{-0.000019}$	$2301.94672^{+0.00098}_{-0.00093}$	$1.029^{+0.070}_{-0.077}$	654^{+27}_{-30}	$0.0243^{+0.0018}_{-0.0036}$	$0.82^{+0.18}_{-0.25}$	$0.311^{+0.063}_{-0.080}$	$6.45^{+1.95}_{-0.98}$	200^{+170}_{-160}
213722591.1	7	$6.7826^{+0.0035}_{-0.0018}$	$2302.877^{+0.013}_{-0.017}$	$2.72^{+0.63}_{-0.60}$	633^{+42}_{-45}	$0.0245^{+0.0021}_{-0.0056}$	$1.88^{+0.17}_{-0.43}$	$0.705^{+0.016}_{-0.015}$	$16.6^{+7.8}_{-6.2}$	95^{+89}_{-71}
213748480.1	7	$3.12951^{+0.00011}_{-0.00011}$	$2304.1846^{+0.0016}_{-0.0017}$	$3.96^{+0.16}_{-0.17}$	898^{+20}_{-20}	$0.086^{+0.022}_{-0.024}$	$18.6^{+5.9}_{-9.6}$	$1.99^{+0.36}_{-0.85}$	$2.30^{+0.23}_{-0.24}$	30000^{+17000}_{-37000}
213817056.1	7	$13.61242^{+0.00043}_{-0.00043}$	$2311.9444^{+0.0013}_{-0.0013}$	$3.024^{+0.089}_{-0.118}$	1453^{+37}_{-38}	$0.0351^{+0.0020}_{-0.0046}$	$3.03^{+0.28}_{-0.51}$	$0.793^{+0.060}_{-0.084}$	$32.3^{+7.7}_{-3.4}$	$20.4^{+10.2}_{-6.1}$
213832800.2	7		$2376.08281^{+0.00051}_{-0.00051}$	$8.723^{+0.053}_{-0.058}$	4390^{+28}_{-29}	$0.0703^{+0.0020}_{-0.0042}$	$8.54^{+0.58}_{-0.54}$	$1.113^{+0.068}_{-0.023}$		
213919434.1	7	$6.79867^{+0.00037}_{-0.00037}$	$2307.7525^{+0.0025}_{-0.0025}$	$2.77^{+0.33}_{-0.34}$	436^{+18}_{-18}	$0.0254^{+0.0086}_{-0.0284}$	$4.4^{+1.5}_{-5.0}$	$1.601^{+0.086}_{-0.065}$	$10.8^{+5.9}_{-9.5}$	830^{+920}_{-1480}
213919915.1	7	$1.489154^{+0.000090}_{-0.000083}$	$2302.4440^{+0.0020}_{-0.0019}$	$1.51^{+0.10}_{-0.12}$	$56.2^{+3.1}_{-3.2}$	$0.00724^{+0.00052}_{-0.00118}$	$1.9^{+1.1}_{-1.6}$	$2.4^{+1.4}_{-1.9}$	$6.5^{+2.5}_{-1.1}$	1200^{+2100}_{-2600}
214173069.1	7	$8.77830^{+0.00042}_{-0.00047}$	$2303.9054^{+0.0019}_{-0.0018}$	$2.91^{+0.20}_{-0.32}$	934^{+34}_{-33}	$0.0301^{+0.0040}_{-0.0078}$	$2.27^{+0.31}_{-0.61}$	$0.690^{+0.028}_{-0.045}$	$18.7^{+9.2}_{-5.2}$	57^{+56}_{-33}
214173069.2	7	$14.1297^{+0.0018}_{-0.0022}$	$2304.8032^{+0.0074}_{-0.0059}$	$3.54^{+0.24}_{-0.28}$	383^{+28}_{-29}	$0.0186^{+0.0015}_{-0.0029}$	$1.40^{+0.12}_{-0.24}$	$0.690^{+0.028}_{-0.045}$	$27.2^{+8.9}_{-4.2}$	$27.2^{+17.9}_{-9.2}$
214234110.1	7	$4.63789^{+0.00012}_{-0.00011}$	$2303.8788^{+0.0011}_{-0.0012}$	$1.065^{+0.085}_{-0.126}$	362^{+15}_{-16}	$0.0183^{+0.0017}_{-0.0040}$	$2.04^{+0.45}_{-0.46}$	$1.021^{+0.202}_{-0.050}$	$28.8^{+11.8}_{-5.6}$	40^{+37}_{-16}
214419545.1	7	$9.40172^{+0.00048}_{-0.00046}$	$2302.9343^{+0.0022}_{-0.0023}$	$2.11^{+0.11}_{-0.14}$	275^{+14}_{-15}	$0.0160^{+0.0010}_{-0.0021}$	$1.96^{+0.29}_{-0.41}$	$1.13^{+0.15}_{-0.19}$	$30.2^{+9.6}_{-4.5}$	50^{+34}_{-22}
214512594.1	7	$1.876899^{+0.000020}_{-0.000020}$	$2303.18414^{+0.00050}_{-0.00049}$	$4.047^{+0.028}_{-0.031}$	24090^{+300}_{-340}	$0.1564^{+0.0018}_{-0.0150}$	$13.2^{+1.5}_{-1.7}$	$0.774^{+0.089}_{-0.068}$	$3.112^{+0.061}_{-0.145}$	2440^{+620}_{-550}
214630761.1	7	$1.236438^{+0.000022}_{-0.000022}$	$2301.93490^{+0.00081}_{-0.00080}$	$2.490^{+0.095}_{-0.106}$	2554^{+47}_{-48}	$0.143^{+0.038}_{-0.040}$	50^{+15}_{-15}	$3.20^{+0.43}_{-0.28}$	$1.90^{+0.16}_{-0.13}$	5000^{+1800}_{-1300}
214741009.1	7	$7.269213^{+0.000091}_{-0.000090}$	$2301.58585^{+0.00058}_{-0.00057}$	$2.644^{+0.079}_{-0.084}$	9220^{+110}_{-110}	$0.215^{+0.061}_{-0.081}$	163^{+48}_{-62}	$6.93^{+0.60}_{-0.48}$	$13.27^{+0.73}_{-0.84}$	103^{+32}_{-31}
214787262.1	7	$8.23981^{+0.00030}_{-0.00035}$	$2302.0501^{+0.0012}_{-0.0011}$	$1.513^{+0.077}_{-0.080}$	858^{+28}_{-30}	$0.0282^{+0.0015}_{-0.0029}$	$0.661^{+0.090}_{-0.249}$	$0.215^{+0.027}_{-0.078}$	$38.3^{+10.9}_{-4.8}$	$3.9^{+2.7}_{-4.2}$
214888033.1	7	$7.457597^{+0.000096}_{-0.000091}$	$2306.88507^{+0.00058}_{-0.00061}$	$1.87^{+0.16}_{-0.14}$	5730^{+170}_{-200}	$0.077^{+0.014}_{-0.015}$	$8.7^{+1.7}_{-1.9}$	$1.037^{+0.066}_{-0.105}$	$24.8^{+8.1}_{-9.1}$	42^{+28}_{-32}
214912104.1	7	$43.1029^{+0.0066}_{-0.0067}$	$2303.7453^{+0.0047}_{-0.0049}$	$22.90^{+0.50}_{-0.55}$	3263^{+57}_{-58}	$0.0580^{+0.0056}_{-0.0038}$	$12.2^{+1.2}_{-1.3}$	$1.923^{+0.042}_{-0.162}$	$11.34^{+0.97}_{-2.26}$	262^{+57}_{-118}
215101303.1	7	$15.20726^{+0.00011}_{-0.00013}$	$2305.63198^{+0.00059}_{-0.00035}$	$3.667^{+0.030}_{-0.031}$	24110^{+120}_{-120}	$0.1514^{+0.0039}_{-0.0103}$	$26.2^{+7.8}_{-2.6}$	$1.59^{+0.47}_{-0.11}$	$31.6^{+1.2}_{-1.9}$	$33.7^{+21.0}_{-8.5}$
215125108.1	7	$0.738067^{+0.000026}_{-0.000026}$	$2301.7963^{+0.0016}_{-0.0016}$	$2.92^{+0.15}_{-0.16}$	902^{+24}_{-24}	$0.095^{+0.024}_{-0.027}$	260^{+200}_{-140}	25^{+18}_{-11}	$0.791^{+0.086}_{-0.067}$	24000^{+50000}_{-32000}
215171927.1	7	$4.13556^{+0.00029}_{-0.00028}$	$2301.8764^{+0.0032}_{-0.0031}$	$2.21^{+0.13}_{-0.17}$	320^{+19}_{-20}	$0.0173^{+0.0012}_{-0.0025}$	$1.44^{+0.10}_{-0.21}$	$0.761^{+0.021}_{-0.022}$	$12.6^{+4.4}_{-2.1}$	150^{+107}_{-50}
215171927.2	7	$6.63107^{+0.00054}_{-0.00056}$	$2306.8960^{+0.0038}_{-0.0038}$	$2.27^{+0.15}_{-0.20}$	360^{+24}_{-24}	$0.0184^{+0.0014}_{-0.0027}$	$1.52^{+0.12}_{-0.23}$	$0.761^{+0.021}_{-0.022}$	$19.5^{+7.3}_{-3.4}$	62^{+46}_{-22}
215175768.1	7	$1.726115^{+0.000098}_{-0.000097}$	$2302.2917^{+0.0026}_{-0.0026}$	$3.10^{+0.17}_{-0.19}$	589^{+24}_{-25}	$0.061^{+0.018}_{-0.021}$	$5.6^{+2.2}_{-2.0}$	$0.839^{+0.225}_{-0.096}$	$1.38^{+0.15}_{-0.18}$	14400^{+8400}_{-5000}
215234145.1	7	$1.2539936^{+0.0000026}_{-0.0000026}$	$2302.587456^{+0.000094}_{-0.000095}$	$2.127^{+0.037}_{-0.041}$	13183^{+38}_{-38}	$0.306^{+0.074}_{-0.091}$	$31.7^{+7.9}_{-11.7}$	$0.948^{+0.054}_{-0.209}$	$3.393^{+0.041}_{-0.150}$	2190^{+260}_{-990}
215353525.1	7	$0.9085915^{+0.0000051}_{-0.0000051}$	$2301.66785^{+0.00027}_{-0.00027}$	$1.918^{+0.055}_{-0.067}$	8450^{+74}_{-74}	$0.223^{+0.062}_{-0.077}$	$23.1^{+6.6}_{-8.0}$	$0.950^{+0.065}_{-0.034}$	$2.34^{+0.13}_{-0.12}$	4420^{+810}_{-600}
215364084.1	7	$2.74324^{+0.00017}_{-0.00017}$	$2302.9668^{+0.0025}_{-0.0025}$	$5.92^{+0.23}_{-0.23}$	1350^{+45}_{-42}	$0.0526^{+0.0089}_{-0.0265}$	$28.0^{+5.3}_{-14.2}$	$4.88^{+0.39}_{-0.27}$	$1.45^{+0.19}_{-0.25}$	7800^{+2700}_{-3000}
215381481.1	7	$0.533393^{+0.000025}_{-0.000027}$	$2301.9033^{+0.0022}_{-0.0022}$	$1.98^{+0.13}_{-0.12}$	$206.3^{+8.6}_{-8.6}$	$0.01206^{+0.00098}_{-0.00232}$	$19.5^{+4.8}_{-12.6}$	$14.8^{+3.5}_{-9.2}$	$1.92^{+0.36}_{-0.19}$	4100^{+3200}_{-7300}
215525178.1	7	$5.33988^{+0.00057}_{-0.00054}$	$2304.9212^{+0.0052}_{-0.0055}$	$1.79^{+0.17}_{-0.23}$	390^{+36}_{-38}	$0.0190^{+0.0017}_{-0.0033}$	$1.27^{+0.18}_{-0.26}$	$0.611^{+0.069}_{-0.067}$	$19.8^{+7.2}_{-4.0}$	32^{+24}_{-15}
215714765.1	7	$6.689131^{+0.000051}_{-0.000055}$	$2307.52381^{+0.00037}_{-0.00033}$	$2.459^{+0.053}_{-0.053}$	17280^{+130}_{-130}	$0.271^{+0.077}_{-0.114}$	$29.9^{+9.0}_{-13.4}$	$1.011^{+0.099}_{-0.159}$	$15.06^{+0.55}_{-0.86}$	112^{+25}_{-39}
215717520.1	7		$2357.95486^{+0.00032}_{-0.00039}$	$12.334^{+0.042}_{-0.040}$	38470^{+420}_{-320}	$0.16958^{+0.00097}_{-0.00727}$	$13.66^{+1.09}_{-0.77}$	$0.738^{+0.059}_{-0.027}$		
215739094.1	7	$3.6322288^{+0.0000097}_{-0.0000098}$	$2303.98183^{+0.00012}_{-0.00012}$	$7.209^{+0.011}_{-0.011}$	13613^{+22}_{-22}	$0.11044^{+0.00050}_{-0.00416}$	$32.2^{+3.1}_{-2.0}$	$2.67^{+0.26}_{-0.13}$	$4.062^{+0.041}_{-0.076}$	2720^{+540}_{-320}
215816368.1	7	$10.14588^{+0.00020}_{-0.00021}$	$2304.55391^{+0.00085}_{-0.00084}$	$5.359^{+0.077}_{-0.084}$	25580^{+300}_{-290}	$0.1488^{+0.0035}_{-0.0053}$	$19.43^{+1.31}_{-0.90}$	$1.198^{+0.075}_{-0.035}$	$16.17^{+0.80}_{-0.55}$	111^{+25}_{-20}
215854715.1	7	$11.12366^{+0.00086}_{-0.00089}$	$2310.0772^{+0.0033}_{-0.0031}$	$3.57^{+0.15}_{-0.20}$	427^{+21}_{-22}	$0.0198^{+0.0012}_{-0.0027}$	$1.80^{+0.11}_{-0.25}$	$0.8327^{+0.0088}_{-0.0129}$	$21.3^{+7.0}_{-3.0}$	57^{+37}_{-16}
215894766.1	7		$2334.37475^{+0.00014}_{-0.00014}$	$4.680^{+0.059}_{-0.071}$	24814^{+84}_{-83}	$0.338^{+0.090}_{-0.122}$	57^{+15}_{-21}	$1.532^{+0.082}_{-0.079}$		
215969174.1	7	$4.175235^{+0.000013}_{-0.000013}$	$2301.93694^{+0.00014}_{-0.00014}$	$3.433^{+0.023}_{-0.024}$	13791^{+47}_{-47}	$0.1076^{+0.0015}_{-0.0028}$	$12.77^{+0.88}_{-0.33}$	$1.0878^{+0.0732}_{-0.0027}$	$10.08^{+0.44}_{-0.21}$	448^{+77}_{-34}
216008129.1	7	$22.77680^{+0.00081}_{-0.00079}$	$2319.7875^{+0.0010}_{-0.0010}$	$3.648^{+0.094}_{-0.136}$	1252^{+24}_{-24}	$0.0338^{+0.0017}_{-0.0038}$	$3.39^{+0.22}_{-0.40}$	$0.920^{+0.039}_{-0.030}$	$43.7^{+11.4}_{-5.6}$	$15.2^{+8.0}_{-4.0}$
216008129.2	7	$1.059806^{+0.000029}_{-0.000031}$	$2301.9847^{+0.0013}_{-0.0013}$	$1.749^{+0.091}_{-0.110}$	$251.4^{+8.8}_{-8.9}$	$0.0147^{+0.0012}_{-0.0032}$	$1.47^{+0.14}_{-0.33}$	$0.920^{+0.039}_{-0.030}$	$4.13^{+1.43}_{-0.57}$	1700^{+1190}_{-490}
216050437.1	7	$14.94889^{+0.00022}_{-0.00022}$	$2308.24039^{+0.00053}_{-0.00053}$	$3.242^{+0.066}_{-0.087}$	3574^{+35}_{-35}	$0.119^{+0.029}_{-0.050}$	$21.9^{+7.6}_{-15.7}$	$1.69^{+0.42}_{-0.99}$	$16.7^{+1.3}_{-1.7}$	270^{+200}_{-450}

Table A.1: Our sample of planet candidates from C0-8. (continued)

Candidate	C#	Period (days)	t_0 (BJD - 2455000)	Duration (hours)	Depth (ppm)	R_p/R_*	R_p ($R_\oplus$)	R_* ($R_\odot$)	a/R_*	Inc. Flux ($S_\oplus$)
216111905.1	7	$3.02030^{+0.00032}_{-0.00032}$	$2304.4740^{+0.0046}_{-0.0046}$	$5.17^{+0.36}_{-0.36}$	375^{+18}_{-18}	$0.041^{+0.013}_{-0.020}$	$5.6^{+1.8}_{-2.7}$	$1.265^{+0.091}_{-0.081}$	$1.32^{+0.18}_{-0.24}$	13100^{+4000}_{-5100}
216114172.1	7	$13.12227^{+0.00082}_{-0.00082}$	$2303.2154^{+0.0030}_{-0.0028}$	$3.93^{+0.13}_{-0.17}$	367^{+17}_{-18}	$0.01849^{+0.00094}_{-0.00212}$	$2.02^{+0.13}_{-0.23}$	$1.004^{+0.037}_{-0.015}$	$22.8^{+7.0}_{-3.0}$	71^{+44}_{-19}
216166748.1	7	$19.68075^{+0.00091}_{-0.00081}$	$2303.3631^{+0.0017}_{-0.0018}$	$4.32^{+0.12}_{-0.15}$	497^{+13}_{-14}	$0.02165^{+0.00090}_{-0.00199}$	$2.55^{+0.22}_{-0.24}$	$1.079^{+0.082}_{-0.023}$	$31.6^{+9.4}_{-3.8}$	$35.7^{+21.9}_{-8.7}$
216212516.1	7	$3.38492^{+0.00017}_{-0.00013}$	$2301.6833^{+0.0015}_{-0.0017}$	$0.856^{+0.085}_{-0.123}$	722^{+61}_{-71}	$0.0258^{+0.0022}_{-0.0063}$	$1.48^{+0.21}_{-0.45}$	$0.528^{+0.058}_{-0.096}$	$26.5^{+11.4}_{-5.6}$	24^{+21}_{-13}
216231580.1	7	$3.905180^{+0.000064}_{-0.000066}$	$2302.52322^{+0.00085}_{-0.00081}$	$3.444^{+0.079}_{-0.089}$	15730^{+220}_{-220}	$0.1168^{+0.0046}_{-0.0075}$	$16.3^{+1.9}_{-1.3}$	$1.282^{+0.137}_{-0.060}$	$9.06^{+0.99}_{-0.67}$	347^{+110}_{-66}
216357880.1	7	$11.86386^{+0.00082}_{-0.00083}$	$2313.1296^{+0.0025}_{-0.0025}$	$3.76^{+0.18}_{-0.23}$	605^{+21}_{-22}	$0.0239^{+0.0016}_{-0.0037}$	$2.21^{+0.16}_{-0.35}$	$0.848^{+0.016}_{-0.019}$	$20.7^{+8.3}_{-4.0}$	58^{+46}_{-23}
216363472.1	7	$8.69290^{+0.00085}_{-0.00082}$	$2301.8853^{+0.0043}_{-0.0042}$	$3.77^{+0.29}_{-0.85}$	248^{+14}_{-15}	$0.0154^{+0.0023}_{-0.0170}$	$1.81^{+0.28}_{-2.01}$	$1.079^{+0.042}_{-0.031}$	$14.3^{+10.4}_{-3.9}$	138^{+202}_{-76}
216405287.1	7	$3.405087^{+0.000076}_{-0.000076}$	$2304.2522^{+0.0011}_{-0.0011}$	$2.034^{+0.044}_{-0.071}$	579^{+17}_{-18}	$0.02293^{+0.00083}_{-0.00200}$	$2.31^{+0.24}_{-0.22}$	$0.923^{+0.088}_{-0.031}$	$11.9^{+2.8}_{-1.1}$	176^{+90}_{-35}
216414930.1	7	$3.619167^{+0.000011}_{-0.000010}$	$2302.41660^{+0.00013}_{-0.00013}$	$4.390^{+0.013}_{-0.014}$	13734^{+31}_{-31}	$0.10747^{+0.00050}_{-0.00096}$	$17.7^{+2.2}_{-1.7}$	$1.51^{+0.19}_{-0.14}$	$6.937^{+0.103}_{-0.045}$	870^{+230}_{-180}
216468514.1	7	$3.3139095^{+0.0000090}_{-0.0000090}$	$2304.52451^{+0.00012}_{-0.00012}$	$3.224^{+0.012}_{-0.012}$	6658^{+20}_{-20}	$0.0835^{+0.0012}_{-0.0015}$	$17.38^{+3.77}_{-0.46}$	$1.908^{+0.413}_{-0.037}$	$5.659^{+0.079}_{-0.087}$	1156^{+504}_{-77}
216494238.1	7	$19.89531^{+0.00028}_{-0.00027}$	$2307.58121^{+0.00052}_{-0.00054}$	$8.277^{+0.053}_{-0.061}$	3463^{+20}_{-20}	$0.05374^{+0.00070}_{-0.00168}$	$8.01^{+0.39}_{-0.37}$	$1.367^{+0.065}_{-0.046}$	$18.87^{+1.11}_{-0.48}$	$95.9^{+14.7}_{-8.4}$
216876207.1	7	$32.3204^{+0.0090}_{-0.0103}$	$2307.609^{+0.012}_{-0.012}$	$8.8^{+1.4}_{-1.2}$	6090^{+440}_{-460}	$0.122^{+0.044}_{-0.086}$	$3.3^{+1.6}_{-120.3}$	$0.245^{+0.077}_{-9.002}$	$16.2^{+2.5}_{-10.0}$	25^{+24}_{-2572}
217084873.1	7	$8.60133^{+0.00030}_{-0.00031}$	$2306.6403^{+0.0014}_{-0.0014}$	$4.053^{+0.088}_{-0.121}$	2804^{+64}_{-64}	$0.0479^{+0.0019}_{-0.0043}$	$5.31^{+0.28}_{-0.49}$	$1.016^{+0.036}_{-0.022}$	$16.0^{+2.6}_{-1.1}$	102^{+34}_{-16}
217084873.2	7	$29.8411^{+0.0034}_{-0.0035}$	$2328.2028^{+0.0026}_{-0.0025}$	$5.29^{+0.19}_{-0.27}$	2388^{+80}_{-83}	$0.0472^{+0.0026}_{-0.0043}$	$5.23^{+0.35}_{-0.49}$	$1.016^{+0.036}_{-0.022}$	$38.6^{+10.3}_{-6.6}$	$17.4^{+9.4}_{-6.2}$
217192839.1	7	$16.03430^{+0.00070}_{-0.00071}$	$2304.2922^{+0.0016}_{-0.0016}$	$3.15^{+0.18}_{-0.26}$	947^{+28}_{-29}	$0.0306^{+0.0042}_{-0.0069}$	$2.05^{+0.33}_{-0.48}$	$0.616^{+0.049}_{-0.038}$	$31.0^{+13.4}_{-9.0}$	21^{+19}_{-13}
217192839.2	7	$26.8054^{+0.0017}_{-0.0017}$	$2307.9132^{+0.0022}_{-0.0022}$	$2.92^{+0.15}_{-0.17}$	522^{+26}_{-26}	$0.0221^{+0.0014}_{-0.0025}$	$1.48^{+0.15}_{-0.19}$	$0.616^{+0.049}_{-0.038}$	$63.2^{+20.0}_{-8.9}$	$5.1^{+3.3}_{-1.6}$
217192839.3	7	$7.9388^{+0.0011}_{-0.0011}$	$2304.8454^{+0.0048}_{-0.0044}$	$1.47^{+0.21}_{-0.28}$	209^{+28}_{-29}	$0.0139^{+0.0016}_{-0.0035}$	$0.94^{+0.13}_{-0.24}$	$0.616^{+0.049}_{-0.038}$	$34.7^{+15.7}_{-9.3}$	$17.0^{+15.6}_{-9.4}$
217231249.1	7	$4.833191^{+0.000014}_{-0.000014}$	$2304.96905^{+0.00013}_{-0.00013}$	$4.800^{+0.015}_{-0.015}$	18419^{+40}_{-40}	$0.1257^{+0.0012}_{-0.0016}$	$25.31^{+0.27}_{-0.40}$	$1.8456^{+0.0093}_{-0.0167}$	$8.52^{+0.18}_{-0.13}$	471^{+47}_{-45}
217393088.1	7	$1.3194719^{+0.0000073}_{-0.0000074}$	$2302.43259^{+0.00026}_{-0.00026}$	$3.187^{+0.034}_{-0.035}$	12036^{+67}_{-69}	$0.1004^{+0.0017}_{-0.0035}$	$14.3^{+2.8}_{-4.3}$	$1.31^{+0.26}_{-0.39}$	$3.425^{+0.164}_{-0.072}$	4500^{+2600}_{-3800}
217671466.1	7	$1.9153196^{+0.0000038}_{-0.0000038}$	$2302.174558^{+0.000094}_{-0.000095}$	$3.549^{+0.011}_{-0.013}$	8470^{+15}_{-15}	$0.08305^{+0.00043}_{-0.00096}$	$14.42^{+2.77}_{-0.31}$	$1.592^{+0.305}_{-0.029}$	$4.435^{+0.090}_{-0.034}$	1750^{+680}_{-110}
217941732.1	7	$2.494206^{+0.000099}_{-0.000101}$	$2303.2000^{+0.0016}_{-0.0016}$	$1.70^{+0.13}_{-0.16}$	304^{+13}_{-13}	$0.0169^{+0.0013}_{-0.0031}$	$1.22^{+0.13}_{-0.23}$	$0.663^{+0.046}_{-0.022}$	$9.7^{+4.2}_{-1.8}$	177^{+155}_{-67}
217977895.1	7	$21.7000^{+0.0016}_{-0.0014}$	$2314.3647^{+0.0028}_{-0.0031}$	$4.10^{+0.21}_{-0.28}$	789^{+31}_{-32}	$0.0268^{+0.0020}_{-0.0045}$	$2.38^{+0.25}_{-0.45}$	$0.811^{+0.062}_{-0.073}$	$35.7^{+13.0}_{-5.9}$	$26.3^{+19.6}_{-10.0}$
218131080.1	7	$3.142811^{+0.000013}_{-0.000013}$	$2301.80888^{+0.00018}_{-0.00018}$	$4.572^{+0.031}_{-0.026}$	4291^{+13}_{-13}	$0.0634^{+0.0010}_{-0.0011}$	$5.69^{+1.23}_{-0.61}$	$0.822^{+0.178}_{-0.087}$	$4.69^{+0.18}_{-0.27}$	2710^{+1240}_{-740}
218170789.1	7	$3.04108^{+0.00022}_{-0.00021}$	$2303.4095^{+0.0032}_{-0.0033}$	$3.84^{+0.21}_{-0.21}$	563^{+22}_{-22}	$0.057^{+0.017}_{-0.022}$	$11.9^{+3.5}_{-4.5}$	$1.91^{+0.10}_{-0.11}$	$1.95^{+0.22}_{-0.27}$	6500^{+1700}_{-2000}
218195416.1	7	$0.4951253^{+0.0000031}_{-0.0000031}$	$2301.94383^{+0.00029}_{-0.00029}$	$2.560^{+0.027}_{-0.025}$	$827.6^{+5.2}_{-5.2}$	$0.141^{+0.013}_{-0.010}$	$28.8^{+3.4}_{-2.8}$	$1.87^{+0.14}_{-0.12}$	$0.6685^{+0.0091}_{-0.0496}$	274000^{+45000}_{-58000}
218212249.1	7	$1.9902718^{+0.0000040}_{-0.0000039}$	$2303.08842^{+0.00012}_{-0.00012}$	$0.0295^{+0.0040}_{-0.0053}$	10370^{+850}_{-830}	$0.100^{+0.011}_{-0.024}$	130^{+24}_{-71}	$11.9^{+1.8}_{-5.8}$	430^{+120}_{-160}	$0.094^{+0.068}_{-0.147}$
218300572.1	7	$1.589843^{+0.000013}_{-0.000013}$	$2301.59453^{+0.00040}_{-0.00040}$	$2.388^{+0.073}_{-0.083}$	1741^{+15}_{-15}	$0.114^{+0.029}_{-0.033}$	49^{+13}_{-14}	$3.93^{+0.40}_{-0.17}$	$2.28^{+0.20}_{-0.20}$	8200^{+2300}_{-1800}
218304292.1	7	$8.42177^{+0.00017}_{-0.00024}$	$2306.8159^{+0.0012}_{-0.0011}$	$0.698^{+0.049}_{-0.077}$	837^{+52}_{-62}	$0.0273^{+0.0019}_{-0.0039}$	$3.13^{+0.22}_{-0.47}$	$1.0511^{+0.0066}_{-0.0502}$	84^{+23}_{-13}	$6.6^{+3.6}_{-2.2}$
218668602.1	7	$1.866025^{+0.000068}_{-0.000066}$	$2302.0911^{+0.0016}_{-0.0016}$	$1.962^{+0.088}_{-0.110}$	383^{+16}_{-17}	$0.0183^{+0.0013}_{-0.0031}$	$1.75^{+0.16}_{-0.32}$	$0.878^{+0.049}_{-0.060}$	$6.54^{+1.98}_{-0.86}$	530^{+330}_{-160}
218695436.1	7	$1.5493180^{+0.0000043}_{-0.0000043}$	$2301.64689^{+0.00013}_{-0.00013}$	$4.018^{+0.045}_{-0.036}$	37890^{+110}_{-110}	$0.235^{+0.014}_{-0.029}$	$42.6^{+5.9}_{-8.4}$	$1.67^{+0.21}_{-0.26}$	$2.875^{+0.084}_{-0.209}$	7200^{+2100}_{-2700}
218709665.1	7	$1.9363475^{+0.0000022}_{-0.0000022}$	$2303.303686^{+0.000050}_{-0.000050}$	$2.271^{+0.015}_{-0.026}$	24595^{+47}_{-42}	$0.250^{+0.048}_{-0.134}$	46^{+12}_{-25}	$1.687^{+0.274}_{-0.037}$	$4.90^{+0.13}_{-0.20}$	1130^{+380}_{-110}
218874453.1	7	$2.17469^{+0.00013}_{-0.00012}$	$2302.1007^{+0.0027}_{-0.0026}$	$1.08^{+0.11}_{-0.12}$	251^{+23}_{-24}	$0.0152^{+0.0013}_{-0.0024}$	$1.80^{+0.17}_{-0.29}$	$1.083^{+0.043}_{-0.033}$	$13.5^{+4.7}_{-2.6}$	131^{+91}_{-51}
218901589.1	7	$1.658223^{+0.000096}_{-0.000097}$	$2303.1303^{+0.0026}_{-0.0026}$	$2.91^{+0.14}_{-0.15}$	$109.3^{+4.1}_{-4.2}$	$0.00867^{+0.00065}_{-0.00186}$	$0.867^{+0.068}_{-0.186}$	$0.917^{+0.021}_{-0.014}$	$4.07^{+0.77}_{-0.35}$	1570^{+600}_{-280}
218916923.1	7	$28.38246^{+0.00020}_{-0.00020}$	$2325.81726^{+0.00031}_{-0.00029}$	$4.987^{+0.036}_{-0.034}$	11093^{+64}_{-73}	$0.0966^{+0.0022}_{-0.0040}$	$9.62^{+0.48}_{-0.69}$	$0.913^{+0.040}_{-0.054}$	$46.0^{+2.7}_{-1.5}$	$13.2^{+2.0}_{-1.8}$
218952024.1	7	$0.560070^{+0.000029}_{-0.000028}$	$2301.8512^{+0.0024}_{-0.0025}$	$2.46^{+0.15}_{-0.15}$	$166.3^{+7.2}_{-7.4}$	$0.0348^{+0.0100}_{-0.0120}$	$1.67^{+0.51}_{-0.58}$	$0.4410^{+0.0480}_{-0.0090}$	$0.428^{+0.056}_{-0.066}$	50000^{+20000}_{-16000}
218973982.1	7	$4.88451^{+0.00032}_{-0.00028}$	$2303.5531^{+0.0025}_{-0.0024}$	$3.00^{+0.23}_{-0.18}$	16470^{+740}_{-690}	$0.202^{+0.074}_{-0.138}$	$16.1^{+8.3}_{-76.4}$	$0.73^{+0.27}_{-3.43}$	$8.99^{+0.71}_{-2.70}$	240^{+290}_{-3260}
219111248.1	7	$4.35967^{+0.00017}_{-0.00022}$	$2301.7010^{+0.0020}_{-0.0017}$	$1.857^{+0.079}_{-0.116}$	1568^{+66}_{-72}	$0.0379^{+0.0019}_{-0.0036}$	$2.31^{+0.73}_{-0.36}$	$0.559^{+0.174}_{-0.069}$	$16.8^{+4.1}_{-1.9}$	38^{+30}_{-13}
219114906.1	7	$1.81053^{+0.00012}_{-0.00011}$	$2302.6107^{+0.0028}_{-0.0026}$	$1.67^{+0.15}_{-0.21}$	326^{+22}_{-24}	$0.0173^{+0.0016}_{-0.0044}$	$1.024^{+0.099}_{-0.268}$	$0.543^{+0.013}_{-0.038}$	$7.2^{+3.3}_{-1.4}$	450^{+420}_{-190}

Table A.1: Our sample of planet candidates from C0-8. (continued)

Candidate	C#	Period (days)	t_0 (BJD - 2455000)	Duration (hours)	Depth (ppm)	R_p/R_*	R_p ($R_\oplus$)	R_* ($R_\odot$)	a/R_*	Inc. Flux ($S_\oplus$)
219256848.1	7	$20.94388^{+0.00046}_{-0.00044}$	$2304.84599^{+0.00084}_{-0.00083}$	$3.67^{+0.10}_{-0.12}$	4736^{+126}_{-87}	$0.125^{+0.034}_{-0.065}$	170^{+46}_{-89}	$12.43^{+0.58}_{-0.63}$	$22.7^{+1.7}_{-2.2}$	$26.0^{+8.9}_{-9.6}$
219266595.1	7	$0.944284^{+0.000100}_{-0.000099}$	$2301.8455^{+0.0040}_{-0.0040}$	$4.03^{+0.44}_{-0.53}$	271^{+15}_{-15}	$0.0199^{+0.0062}_{-0.0132}$	$1.48^{+0.46}_{-0.99}$	$0.684^{+0.028}_{-0.055}$	$0.70^{+0.27}_{-1.18}$	$55000^{+43000}_{-187000}$
219388192.1	7	$5.292627^{+0.000019}_{-0.000019}$	$2303.98852^{+0.00017}_{-0.00018}$	$3.294^{+0.016}_{-0.018}$	10517^{+59}_{-53}	$0.09517^{+0.00089}_{-0.00164}$	$10.98^{+0.65}_{-0.22}$	$1.058^{+0.062}_{-0.010}$	$13.19^{+0.54}_{-0.25}$	$198.4^{+28.5}_{-9.5}$
219420915.1	7	$0.5150196^{+0.0000020}_{-0.0000021}$	$2301.54475^{+0.00014}_{-0.00014}$	$1.974^{+0.025}_{-0.020}$	6020^{+30}_{-28}	$0.270^{+0.050}_{-0.045}$	$36.2^{+6.7}_{-6.4}$	$1.230^{+0.013}_{-0.073}$	$1.314^{+0.012}_{-0.087}$	19500^{+1300}_{-3700}
219480273.1	7	$26.4837^{+0.0050}_{-0.0051}$	$2306.9592^{+0.0068}_{-0.0063}$	$6.05^{+0.35}_{-0.52}$	201^{+13}_{-14}	$0.0132^{+0.0012}_{-0.0033}$	$1.98^{+0.34}_{-0.50}$	$1.378^{+0.199}_{-0.053}$	$29.4^{+11.6}_{-4.6}$	59^{+49}_{-19}
219610716.1	7	$2.08807^{+0.00019}_{-0.00019}$	$2301.6891^{+0.0043}_{-0.0043}$	$3.07^{+0.22}_{-0.46}$	717^{+40}_{-41}	$0.0255^{+0.0031}_{-0.0118}$	$12.4^{+1.7}_{-5.8}$	$4.44^{+0.28}_{-0.44}$	$4.45^{+2.70}_{-0.97}$	1080^{+1340}_{-570}
219747794.1	7	$34.3797^{+0.0010}_{-0.0011}$	$2307.1715^{+0.0013}_{-0.0012}$	$3.92^{+0.14}_{-0.16}$	19430^{+410}_{-390}	$0.268^{+0.080}_{-0.129}$	118^{+99}_{-72}	$4.0^{+3.2}_{-1.5}$	$50.0^{+2.2}_{-3.1}$	11^{+25}_{-12}
219747794.2	7	$15.6594^{+0.0043}_{-0.0043}$	$2304.914^{+0.010}_{-0.011}$	$6.87^{+0.96}_{-0.76}$	2530^{+210}_{-210}	$0.084^{+0.037}_{-0.056}$	37^{+33}_{-28}	$4.0^{+3.2}_{-1.5}$	$8.1^{+1.2}_{-9.8}$	410^{+940}_{-1090}
219760360.1	7	$1.4095126^{+0.0000098}_{-0.0000098}$	$2302.16392^{+0.00033}_{-0.00033}$	$3.290^{+0.064}_{-0.052}$	19080^{+100}_{-100}	$0.353^{+0.081}_{-0.108}$	70^{+16}_{-22}	$1.820^{+0.058}_{-0.038}$	$2.724^{+0.053}_{-0.187}$	3310^{+290}_{-500}
219800881.1	7	$13.84457^{+0.00100}_{-0.00154}$	$2306.1493^{+0.0036}_{-0.0029}$	$2.95^{+0.16}_{-0.19}$	635^{+27}_{-28}	$0.0248^{+0.0011}_{-0.0018}$	$2.79^{+0.12}_{-0.21}$	$1.0306^{+0.0087}_{-0.0213}$	$32.4^{+9.9}_{-4.6}$	$32.0^{+19.6}_{-9.1}$
220168663.1	8	$3.22513^{+0.00034}_{-0.00037}$	$2394.5096^{+0.0044}_{-0.0044}$	$1.67^{+0.26}_{-0.34}$	2400^{+300}_{-340}	$0.0489^{+0.0067}_{-0.0381}$	$2.33^{+0.55}_{-1.86}$	$0.437^{+0.084}_{-0.072}$	$12.3^{+6.5}_{-4.4}$	68^{+81}_{-60}
220170303.1	8	$9.6897^{+0.0017}_{-0.0014}$	$2396.6577^{+0.0048}_{-0.0056}$	$3.55^{+0.22}_{-0.33}$	284^{+17}_{-17}	$0.0162^{+0.0012}_{-0.0030}$	$1.37^{+0.13}_{-0.26}$	$0.776^{+0.046}_{-0.027}$	$18.0^{+7.2}_{-3.3}$	77^{+62}_{-29}
220170303.2	8	$4.9234^{+0.0011}_{-0.0012}$	$2396.4093^{+0.0077}_{-0.0080}$	$2.02^{+0.29}_{-0.42}$	210^{+21}_{-22}	$0.0140^{+0.0017}_{-0.0072}$	$1.18^{+0.16}_{-0.61}$	$0.776^{+0.046}_{-0.027}$	$15.6^{+10.6}_{-4.3}$	103^{+140}_{-57}
220173278.1	8	$8.03216^{+0.00103}_{-0.00097}$	$2396.5500^{+0.0047}_{-0.0052}$	$5.81^{+0.21}_{-0.27}$	$148.4^{+7.7}_{-8.0}$	$0.01198^{+0.00063}_{-0.00134}$	$2.42^{+0.25}_{-0.33}$	$1.85^{+0.16}_{-0.14}$	$9.1^{+3.5}_{-1.5}$	580^{+450}_{-210}
220186645.1	8	$7.05647^{+0.00045}_{-0.00048}$	$2396.5064^{+0.0028}_{-0.0027}$	$4.46^{+0.10}_{-0.14}$	554^{+20}_{-21}	$0.02313^{+0.00073}_{-0.00147}$	$2.76^{+0.34}_{-0.57}$	$1.09^{+0.13}_{-0.22}$	$11.1^{+2.9}_{-1.2}$	430^{+270}_{-260}
220187552.1	8	$17.093319^{+0.000036}_{-0.000036}$	$2399.314816^{+0.000089}_{-0.000087}$	$2.268^{+0.027}_{-0.032}$	28067^{+75}_{-75}	$0.380^{+0.096}_{-0.118}$	$17.7^{+4.6}_{-5.6}$	$0.426^{+0.026}_{-0.033}$	$46.7^{+1.0}_{-1.9}$	$4.32^{+0.83}_{-1.14}$
220192485.1	8	$50.69369^{+0.00024}_{-0.00024}$	$2409.22337^{+0.00017}_{-0.00017}$	$4.434^{+0.025}_{-0.027}$	11041^{+49}_{-47}	$0.1039^{+0.0017}_{-0.0013}$	$8.85^{+0.50}_{-0.62}$	$0.781^{+0.042}_{-0.054}$	$75.8^{+1.3}_{-1.6}$	$5.1^{+1.0}_{-1.2}$
220194974.1	8	$6.92251^{+0.00047}_{-0.00041}$	$2394.6522^{+0.0019}_{-0.0020}$	$2.030^{+0.097}_{-0.139}$	537^{+25}_{-26}	$0.0222^{+0.0014}_{-0.0032}$	$0.90^{+0.10}_{-0.24}$	$0.371^{+0.036}_{-0.083}$	$23.2^{+7.8}_{-3.5}$	18^{+14}_{-13}
220194974.2	8	$9.75833^{+0.00084}_{-0.00091}$	$2396.0988^{+0.0042}_{-0.0038}$	$1.79^{+0.15}_{-0.24}$	504^{+35}_{-37}	$0.0217^{+0.0019}_{-0.0048}$	$0.88^{+0.11}_{-0.27}$	$0.371^{+0.036}_{-0.083}$	$35.9^{+15.6}_{-7.5}$	$7.7^{+7.0}_{-5.9}$
220194974.3	8	$4.38393^{+0.00028}_{-0.00028}$	$2394.4473^{+0.0028}_{-0.0029}$	$1.78^{+0.12}_{-0.17}$	324^{+21}_{-22}	$0.0173^{+0.0014}_{-0.0032}$	$0.701^{+0.088}_{-0.205}$	$0.371^{+0.036}_{-0.083}$	$16.3^{+6.3}_{-2.9}$	37^{+31}_{-27}
220198551.1	8	$0.7988453^{+0.0000083}_{-0.0000082}$	$2392.64066^{+0.00044}_{-0.00045}$	$1.097^{+0.041}_{-0.048}$	1357^{+33}_{-32}	$0.079^{+0.024}_{-0.035}$	$6.2^{+2.0}_{-2.8}$	$0.728^{+0.076}_{-0.025}$	$2.18^{+0.21}_{-0.27}$	4700^{+1700}_{-1300}
220201207.1	8	$0.4378443^{+0.0000024}_{-0.0000024}$	$2392.44980^{+0.00026}_{-0.00026}$	$2.224^{+0.024}_{-0.023}$	5530^{+37}_{-37}	$0.293^{+0.041}_{-0.036}$	41^{+13}_{-26}	$1.30^{+0.35}_{-0.79}$	$1.053^{+0.074}_{-0.053}$	42000^{+33000}_{-73000}
220204960.1	8	$13.26931^{+0.00024}_{-0.00025}$	$2401.86280^{+0.00074}_{-0.00072}$	$3.714^{+0.106}_{-0.094}$	3648^{+53}_{-48}	$0.194^{+0.045}_{-0.045}$	$23.8^{+6.4}_{-5.6}$	$1.127^{+0.146}_{-0.019}$	$15.82^{+0.41}_{-0.62}$	268^{+72}_{-25}
220207765.1	8	$7.12113^{+0.00043}_{-0.00046}$	$2396.4196^{+0.0040}_{-0.0025}$	$1.95^{+0.15}_{-0.15}$	482^{+29}_{-31}	$0.0214^{+0.0012}_{-0.0022}$	$1.99^{+0.14}_{-0.23}$	$0.853^{+0.033}_{-0.048}$	$25.3^{+8.3}_{-3.9}$	41^{+27}_{-14}
220209578.1	8	$8.904672^{+0.000084}_{-0.000081}$	$2394.76562^{+0.00038}_{-0.00039}$	$3.086^{+0.066}_{-0.065}$	12320^{+110}_{-100}	$0.236^{+0.067}_{-0.094}$	$26.1^{+9.8}_{-10.6}$	$1.014^{+0.252}_{-0.068}$	$14.72^{+0.61}_{-0.90}$	211^{+107}_{-41}
220211923.1	8	$26.6820^{+0.0036}_{-0.0042}$	$2413.4025^{+0.0039}_{-0.0044}$	$6.04^{+0.19}_{-0.24}$	291^{+14}_{-15}	$0.01692^{+0.00068}_{-0.00139}$	$2.209^{+0.095}_{-0.186}$	$1.197^{+0.018}_{-0.023}$	$29.5^{+9.8}_{-4.6}$	58^{+39}_{-18}
220218012.1	8	$12.4904^{+0.0014}_{-0.0012}$	$2403.6429^{+0.0032}_{-0.0033}$	$4.29^{+0.47}_{-0.55}$	904^{+39}_{-40}	$0.0354^{+0.0098}_{-0.0181}$	$3.59^{+1.00}_{-1.83}$	$0.929^{+0.027}_{-0.017}$	$10.7^{+3.5}_{-13.1}$	310^{+210}_{-760}
220221272.1	8	$13.62757^{+0.00092}_{-0.00069}$	$2392.5987^{+0.0023}_{-0.0033}$	$2.15^{+0.11}_{-0.18}$	4370^{+200}_{-230}	$0.0636^{+0.0038}_{-0.0070}$	$1.78^{+0.36}_{-0.30}$	$0.257^{+0.049}_{-0.032}$	$45.9^{+13.3}_{-6.5}$	$3.1^{+2.5}_{-1.5}$
220221272.2	8	$6.67910^{+0.00049}_{-0.00049}$	$2392.4290^{+0.0035}_{-0.0034}$	$1.52^{+0.13}_{-0.18}$	1690^{+130}_{-140}	$0.0393^{+0.0032}_{-0.0062}$	$1.10^{+0.23}_{-0.22}$	$0.257^{+0.049}_{-0.032}$	$30.4^{+10.1}_{-5.6}$	$7.1^{+6.1}_{-3.7}$
220221272.3	8	$4.19525^{+0.00034}_{-0.00033}$	$2394.4110^{+0.0035}_{-0.0035}$	$1.27^{+0.16}_{-0.23}$	1460^{+150}_{-170}	$0.0373^{+0.0040}_{-0.0116}$	$1.05^{+0.23}_{-0.35}$	$0.257^{+0.049}_{-0.032}$	$21.9^{+11.3}_{-5.7}$	$13.8^{+16.0}_{-8.8}$
220221272.4	8	$9.71601^{+0.00083}_{-0.00080}$	$2398.9604^{+0.0034}_{-0.0038}$	$1.98^{+0.14}_{-0.19}$	1750^{+130}_{-130}	$0.0406^{+0.0026}_{-0.0046}$	$1.14^{+0.23}_{-0.19}$	$0.257^{+0.049}_{-0.032}$	$34.5^{+10.4}_{-5.4}$	$5.5^{+4.5}_{-2.7}$
220225178.1	8	$4.19121^{+0.00027}_{-0.00027}$	$2392.3184^{+0.0033}_{-0.0032}$	$2.19^{+0.16}_{-0.24}$	365^{+21}_{-22}	$0.0180^{+0.0017}_{-0.0050}$	$1.75^{+0.40}_{-0.49}$	$0.889^{+0.187}_{-0.050}$	$12.8^{+5.9}_{-2.3}$	219^{+221}_{-82}
220228500.1	8	$2.504853^{+0.000033}_{-0.000033}$	$2392.95973^{+0.00061}_{-0.00059}$	$2.240^{+0.056}_{-0.071}$	1806^{+28}_{-28}	$0.0401^{+0.0013}_{-0.0026}$	$3.95^{+0.87}_{-0.26}$	$0.905^{+0.197}_{-0.014}$	$8.01^{+1.74}_{-0.88}$	520^{+320}_{-120}
220245303.1	8	$3.68047^{+0.00036}_{-0.00035}$	$2392.7933^{+0.0035}_{-0.0034}$	$2.10^{+0.20}_{-0.36}$	191^{+14}_{-14}	$0.0131^{+0.0016}_{-0.0084}$	$1.11^{+0.15}_{-0.71}$	$0.777^{+0.054}_{-0.026}$	$11.4^{+8.2}_{-2.5}$	199^{+288}_{-88}
220256496.1	8	$0.669573^{+0.000028}_{-0.000030}$	$2392.4742^{+0.0020}_{-0.0018}$	$1.325^{+0.093}_{-0.113}$	278^{+16}_{-17}	$0.0157^{+0.0013}_{-0.0032}$	$1.44^{+0.18}_{-0.30}$	$0.839^{+0.078}_{-0.032}$	$3.43^{+1.26}_{-0.54}$	2300^{+1740}_{-740}
220256496.2	8	$2.60170^{+0.00024}_{-0.00025}$	$2392.7147^{+0.0038}_{-0.0031}$	$1.69^{+0.13}_{-0.16}$	285^{+20}_{-21}	$0.0161^{+0.0013}_{-0.0025}$	$1.47^{+0.18}_{-0.23}$	$0.839^{+0.078}_{-0.032}$	$10.3^{+3.4}_{-1.8}$	254^{+174}_{-91}
220260084.1	8	$16.9616^{+0.0029}_{-0.0030}$	$2408.9901^{+0.0058}_{-0.0058}$	$5.42^{+0.24}_{-0.31}$	413^{+27}_{-29}	$0.0194^{+0.0013}_{-0.0026}$	$2.70^{+0.19}_{-0.37}$	$1.277^{+0.030}_{-0.025}$	$21.5^{+6.3}_{-2.9}$	104^{+62}_{-29}
220263105.1	8	$0.7175747^{+0.0000014}_{-0.0000014}$	$2392.400760^{+0.000088}_{-0.000089}$	$1.524^{+0.030}_{-0.030}$	25140^{+110}_{-110}	$0.315^{+0.094}_{-0.140}$	$28.1^{+8.5}_{-13.1}$	$0.818^{+0.043}_{-0.108}$	$2.876^{+0.075}_{-0.121}$	3120^{+380}_{-870}

Table A.1: Our sample of planet candidates from C0-8. (continued)

Candidate	C#	Period (days)	t_0 (BJD - 2455000)	Duration (hours)	Depth (ppm)	R_p/R_*	R_p ($R_\oplus$)	R_* ($R_\odot$)	a/R_*	Inc. Flux ($S_\oplus$)
220267210.1	8	$5.16450^{+0.00069}_{-0.00080}$	$2393.4221^{+0.0064}_{-0.0058}$	$2.10^{+0.20}_{-0.21}$	867^{+79}_{-85}	$0.0282^{+0.0023}_{-0.0043}$	$0.784^{+0.076}_{-0.133}$	$0.255^{+0.013}_{-0.019}$	$16.9^{+5.4}_{-3.0}$	27^{+18}_{-11}
220275625.1	8	$3.44795^{+0.00036}_{-0.00038}$	$2394.8983^{+0.0052}_{-0.0046}$	$1.75^{+0.26}_{-0.42}$	715^{+81}_{-82}	$0.0268^{+0.0040}_{-0.0264}$	$0.97^{+0.21}_{-0.96}$	$0.332^{+0.054}_{-0.047}$	$12.1^{+7.8}_{-4.4}$	55^{+76}_{-46}
220280237.1	8		$2454.14443^{+0.00036}_{-0.00035}$	$4.36^{+0.12}_{-0.14}$	14080^{+130}_{-120}	$0.274^{+0.078}_{-0.099}$	36^{+11}_{-14}	$1.208^{+0.085}_{-0.192}$		
220287611.1	8	$6.26242^{+0.00072}_{-0.00078}$	$2397.8835^{+0.0071}_{-0.0049}$	$2.24^{+0.24}_{-0.22}$	628^{+75}_{-82}	$0.0244^{+0.0022}_{-0.0034}$	$2.03^{+0.21}_{-0.33}$	$0.762^{+0.036}_{-0.066}$	$19.3^{+6.3}_{-3.5}$	33^{+22}_{-13}
220288191.1	8	$24.41473^{+0.00107}_{-0.00071}$	$2416.3267^{+0.0013}_{-0.0032}$	$1.57^{+0.27}_{-0.28}$	17700^{+6200}_{-1500}	$0.159^{+0.055}_{-0.158}$	$11.1^{+4.3}_{-11.3}$	$0.64^{+0.11}_{-0.15}$	93^{+17}_{-46}	$1.40^{+0.72}_{-1.54}$
220288594.1	8	$4.02748^{+0.00026}_{-0.00027}$	$2394.9119^{+0.0031}_{-0.0030}$	$1.24^{+0.11}_{-0.14}$	399^{+33}_{-34}	$0.0193^{+0.0016}_{-0.0031}$	$1.24^{+0.10}_{-0.20}$	$0.5901^{+0.0025}_{-0.0138}$	$21.8^{+7.9}_{-4.2}$	55^{+40}_{-21}
220290988.1	8	$10.55369^{+0.00081}_{-0.00080}$	$2395.0434^{+0.0034}_{-0.0033}$	$3.76^{+0.24}_{-0.38}$	906^{+49}_{-50}	$0.0283^{+0.0032}_{-0.0085}$	$2.72^{+0.46}_{-0.81}$	$0.880^{+0.111}_{-0.014}$	$18.9^{+9.1}_{-3.4}$	80^{+79}_{-29}
220292715.1	8	$41.55209^{+0.00065}_{-0.00063}$	$2407.48594^{+0.00039}_{-0.00040}$	$2.96^{+0.11}_{-0.14}$	3044^{+36}_{-37}	$0.0540^{+0.0039}_{-0.0046}$	$4.30^{+0.33}_{-0.38}$	$0.730^{+0.017}_{-0.013}$	89^{+19}_{-23}	$3.0^{+1.3}_{-1.5}$
220294712.1	8	$23.6088^{+0.0019}_{-0.0019}$	$2413.7218^{+0.0023}_{-0.0024}$	$6.01^{+0.14}_{-0.21}$	783^{+24}_{-24}	$0.0261^{+0.0012}_{-0.0030}$	$3.43^{+0.28}_{-0.45}$	$1.203^{+0.082}_{-0.075}$	$27.8^{+6.4}_{-3.0}$	70^{+34}_{-17}
220309058.1	8	$9.64954^{+0.00027}_{-0.00026}$	$2392.9595^{+0.0012}_{-0.0014}$	$1.006^{+0.077}_{-0.122}$	1900^{+100}_{-110}	$0.0423^{+0.0027}_{-0.0057}$	$2.74^{+0.80}_{-0.38}$	$0.593^{+0.170}_{-0.020}$	68^{+23}_{-11}	$1.51^{+1.33}_{-0.51}$
220315508.1	8	$6.55340^{+0.00037}_{-0.00038}$	$2395.0771^{+0.0026}_{-0.0024}$	$2.51^{+0.11}_{-0.14}$	$192.4^{+9.6}_{-10.2}$	$0.01331^{+0.00079}_{-0.00176}$	$1.11^{+0.12}_{-0.15}$	$0.766^{+0.067}_{-0.031}$	$17.6^{+6.0}_{-2.5}$	102^{+72}_{-30}
220316844.1	8	$0.6719977^{+0.0000021}_{-0.0000021}$	$2392.35532^{+0.00014}_{-0.00014}$	$1.715^{+0.036}_{-0.040}$	2257^{+12}_{-12}	$0.129^{+0.031}_{-0.037}$	$25.2^{+6.3}_{-7.6}$	$1.79^{+0.13}_{-0.18}$	$1.43^{+0.11}_{-0.12}$	45100^{+9900}_{-12300}
220317172.1	8	$4.43580^{+0.00025}_{-0.00025}$	$2396.1533^{+0.0023}_{-0.0024}$	$0.935^{+0.098}_{-0.113}$	197^{+18}_{-20}	$0.0135^{+0.0012}_{-0.0023}$	$1.30^{+0.14}_{-0.23}$	$0.879^{+0.048}_{-0.047}$	$31.1^{+11.4}_{-6.6}$	32^{+24}_{-14}
220321605.1	8	$9.79546^{+0.00020}_{-0.00020}$	$2399.64096^{+0.00080}_{-0.00082}$	$2.622^{+0.068}_{-0.100}$	1603^{+29}_{-28}	$0.0364^{+0.0017}_{-0.0044}$	$2.57^{+0.34}_{-0.38}$	$0.648^{+0.080}_{-0.054}$	$27.3^{+5.8}_{-2.4}$	$18.2^{+9.0}_{-4.5}$
220322327.1	8	$3.31347^{+0.00024}_{-0.00024}$	$2393.9488^{+0.0032}_{-0.0032}$	$2.97^{+0.43}_{-0.30}$	775^{+47}_{-47}	$0.042^{+0.019}_{-0.033}$	$3.8^{+1.7}_{-3.0}$	$0.824^{+0.055}_{-0.014}$	$3.17^{+0.61}_{-6.22}$	2500^{+1000}_{-10000}
220342163.1	8	$4.69942^{+0.00052}_{-0.00046}$	$2394.7423^{+0.0041}_{-0.0046}$	$3.80^{+0.68}_{-0.46}$	601^{+36}_{-35}	$0.038^{+0.017}_{-0.031}$	$2.5^{+1.1}_{-2.1}$	$0.605^{+0.025}_{-0.084}$	$3.31^{+0.67}_{-7.47}$	2370^{+980}_{-10710}
220376054.1	8	$8.59627^{+0.00051}_{-0.00062}$	$2396.6007^{+0.0030}_{-0.0024}$	$3.78^{+0.14}_{-0.24}$	400^{+16}_{-16}	$0.0191^{+0.0013}_{-0.0035}$	$2.60^{+0.18}_{-0.48}$	$1.251^{+0.020}_{-0.030}$	$15.1^{+6.0}_{-2.6}$	203^{+162}_{-70}
220393791.1	8	$12.7256^{+0.0019}_{-0.0018}$	$2397.7779^{+0.0057}_{-0.0059}$	$3.44^{+0.23}_{-0.28}$	425^{+31}_{-33}	$0.0198^{+0.0015}_{-0.0032}$	$2.16^{+0.25}_{-0.44}$	$1.001^{+0.087}_{-0.121}$	$25.0^{+8.6}_{-4.1}$	95^{+68}_{-39}
220395416.1	8	$45.4939^{+0.0072}_{-0.0077}$	$2407.8853^{+0.0047}_{-0.0036}$	$8.28^{+0.43}_{-0.43}$	1221^{+40}_{-47}	$0.0404^{+0.0033}_{-0.0055}$	$7.17^{+0.59}_{-0.97}$	$1.626^{+0.013}_{-0.017}$	$19.3^{+1.6}_{-1.9}$	126^{+22}_{-26}
220397060.1	8	$12.09259^{+0.00033}_{-0.00033}$	$2403.23130^{+0.00097}_{-0.00099}$	$8.712^{+0.098}_{-0.110}$	3608^{+33}_{-33}	$0.0548^{+0.0015}_{-0.0030}$	$14.7^{+3.2}_{-1.2}$	$2.46^{+0.53}_{-0.15}$	$10.59^{+1.07}_{-0.58}$	270^{+130}_{-48}
220400100.1	8	$10.79460^{+0.00074}_{-0.00091}$	$2402.4235^{+0.0020}_{-0.0019}$	$3.33^{+0.12}_{-0.15}$	1344^{+45}_{-46}	$0.0347^{+0.0018}_{-0.0037}$	$2.34^{+0.14}_{-0.30}$	$0.618^{+0.019}_{-0.045}$	$23.0^{+5.6}_{-2.7}$	51^{+25}_{-14}
220400100.2	8	$4.06643^{+0.00041}_{-0.00039}$	$2394.5845^{+0.0043}_{-0.0045}$	$1.57^{+0.16}_{-0.20}$	350^{+41}_{-42}	$0.0181^{+0.0018}_{-0.0037}$	$1.22^{+0.13}_{-0.26}$	$0.618^{+0.019}_{-0.045}$	$17.2^{+6.9}_{-3.6}$	92^{+74}_{-41}
220400525.1	8	$57.8396^{+0.0025}_{-0.0025}$	$2401.6557^{+0.0021}_{-0.0029}$	$6.56^{+0.26}_{-0.20}$	8990^{+160}_{-150}	$0.123^{+0.022}_{-0.068}$	$9.8^{+1.8}_{-5.5}$	$0.729^{+0.048}_{-0.065}$	$41.5^{+3.9}_{-13.1}$	$13.7^{+3.2}_{-9.0}$
220401029.1	8	$4.49161^{+0.00052}_{-0.00056}$	$2394.2081^{+0.0045}_{-0.0046}$	$2.65^{+0.24}_{-0.42}$	538^{+39}_{-42}	$0.0224^{+0.0023}_{-0.0072}$	$2.01^{+0.34}_{-0.65}$	$0.823^{+0.111}_{-0.022}$	$11.0^{+6.1}_{-2.5}$	230^{+260}_{-110}
220410754.1	8	$19.4989^{+0.0033}_{-0.0027}$	$2403.2529^{+0.0051}_{-0.0055}$	$4.60^{+0.26}_{-0.51}$	402^{+23}_{-24}	$0.0196^{+0.0014}_{-0.0035}$	$2.32^{+0.17}_{-0.41}$	$1.085^{+0.012}_{-0.010}$	$27.3^{+13.8}_{-5.9}$	63^{+64}_{-27}
220416518.1	8	$3.78177^{+0.00048}_{-0.00047}$	$2393.3863^{+0.0049}_{-0.0055}$	$2.45^{+0.21}_{-0.29}$	249^{+27}_{-29}	$0.0151^{+0.0015}_{-0.0035}$	$1.81^{+0.33}_{-0.42}$	$1.095^{+0.170}_{-0.028}$	$10.2^{+4.4}_{-2.0}$	360^{+330}_{-140}
220431824.1	8	$9.073266^{+0.000037}_{-0.000037}$	$2394.22405^{+0.00018}_{-0.00018}$	$6.946^{+0.026}_{-0.031}$	17165^{+74}_{-77}	$0.1213^{+0.0020}_{-0.0026}$	$23.32^{+2.90}_{-0.97}$	$1.763^{+0.217}_{-0.063}$	$10.97^{+0.22}_{-0.17}$	278^{+70}_{-25}
220436189.1	8	$13.6094^{+0.0033}_{-0.0028}$	$2393.324^{+0.011}_{-0.012}$	$2.79^{+0.28}_{-0.49}$	1680^{+140}_{-150}	$0.0396^{+0.0028}_{-0.0045}$	$2.44^{+0.33}_{-0.35}$	$0.564^{+0.066}_{-0.049}$	$33.3^{+9.8}_{-7.1}$	$8.7^{+5.5}_{-4.0}$
220436208.1	8	$5.23587^{+0.00019}_{-0.00020}$	$2396.5057^{+0.0017}_{-0.0016}$	$3.68^{+0.13}_{-0.30}$	1336^{+30}_{-31}	$0.0357^{+0.0033}_{-0.0055}$	$4.86^{+0.46}_{-0.77}$	$1.248^{+0.030}_{-0.050}$	$8.9^{+3.5}_{-2.4}$	460^{+360}_{-250}
220436943.1	8	$2.43807^{+0.00014}_{-0.00013}$	$2393.8593^{+0.0024}_{-0.0027}$	$1.42^{+0.12}_{-0.16}$	1079^{+80}_{-86}	$0.0315^{+0.0026}_{-0.0058}$	$2.15^{+0.22}_{-0.50}$	$0.625^{+0.038}_{-0.090}$	$11.7^{+4.3}_{-2.1}$	154^{+116}_{-71}
220443340.1	8	$6.80111^{+0.00036}_{-0.00037}$	$2396.1081^{+0.0021}_{-0.0020}$	$1.17^{+0.11}_{-0.14}$	4150^{+310}_{-350}	$0.0617^{+0.0047}_{-0.0099}$	$1.96^{+0.39}_{-0.48}$	$0.291^{+0.054}_{-0.054}$	$41.6^{+13.0}_{-7.3}$	$4.3^{+3.6}_{-2.8}$
220459477.1	8	$2.38098^{+0.00017}_{-0.00018}$	$2393.4515^{+0.0035}_{-0.0034}$	$1.91^{+0.15}_{-0.19}$	506^{+34}_{-35}	$0.0215^{+0.0017}_{-0.0038}$	$1.72^{+0.17}_{-0.31}$	$0.734^{+0.039}_{-0.016}$	$8.4^{+3.1}_{-1.5}$	340^{+260}_{-120}
220466136.1	8	$17.10570^{+0.00088}_{-0.00080}$	$2409.2893^{+0.0014}_{-0.0016}$	$3.43^{+0.12}_{-0.16}$	10060^{+250}_{-240}	$0.0915^{+0.0049}_{-0.0093}$	$5.91^{+0.58}_{-0.65}$	$0.592^{+0.049}_{-0.026}$	$38.9^{+6.0}_{-3.2}$	$10.3^{+3.7}_{-2.1}$
220470563.1	8	$7.30383^{+0.00039}_{-0.00043}$	$2398.1010^{+0.0021}_{-0.0021}$	$1.370^{+0.089}_{-0.117}$	849^{+56}_{-58}	$0.0279^{+0.0019}_{-0.0036}$	$2.18^{+0.20}_{-0.28}$	$0.715^{+0.040}_{-0.015}$	$36.7^{+11.2}_{-5.7}$	$18.5^{+11.5}_{-5.9}$
220471666.1	8	$8.26947^{+0.00033}_{-0.00032}$	$2394.3300^{+0.0017}_{-0.0017}$	$2.24^{+0.15}_{-0.19}$	543^{+23}_{-23}	$0.0223^{+0.0017}_{-0.0043}$	$2.63^{+0.23}_{-0.50}$	$1.0807^{+0.0403}_{-0.0093}$	$24.5^{+9.8}_{-4.5}$	62^{+50}_{-23}
220481411.1	8	$2.174829^{+0.000047}_{-0.000049}$	$2394.04121^{+0.00081}_{-0.00078}$	$1.856^{+0.054}_{-0.083}$	620^{+14}_{-15}	$0.0235^{+0.0013}_{-0.0032}$	$1.63^{+0.11}_{-0.24}$	$0.638^{+0.022}_{-0.033}$	$8.1^{+2.3}_{-1.1}$	312^{+179}_{-87}
220482322.1	8	$57.8415^{+0.0024}_{-0.0024}$	$2393.0699^{+0.0017}_{-0.0017}$	$8.17^{+0.14}_{-0.22}$	1602^{+32}_{-32}	$0.0376^{+0.0015}_{-0.0031}$	$6.13^{+1.47}_{-0.57}$	$1.495^{+0.354}_{-0.066}$	$50.3^{+10.1}_{-5.7}$	$18.7^{+11.6}_{-4.6}$
220487418.1	8	$14.0721^{+0.0017}_{-0.0011}$	$2395.0102^{+0.0035}_{-0.0048}$	$5.68^{+0.17}_{-0.23}$	636^{+23}_{-24}	$0.0241^{+0.0012}_{-0.0030}$	$3.36^{+0.68}_{-0.43}$	$1.278^{+0.168}_{-0.023}$	$17.0^{+5.2}_{-2.3}$	167^{+113}_{-46}

Table A.1: Our sample of planet candidates from C0-8. (continued)

Candidate	C#	Period (days)	t_0 (BJD - 2455000)	Duration (hours)	Depth (ppm)	R_p/R_*	R_p ($R_\oplus$)	R_* ($R_\odot$)	a/R_*	Inc. Flux ($S_\oplus$)
220492492.1	8	$9.4538^{+0.0022}_{-0.0020}$	$2397.9708^{+0.0067}_{-0.0073}$	$4.91^{+0.39}_{-0.64}$	375^{+26}_{-27}	$0.0188^{+0.0018}_{-0.0048}$	$1.91^{+0.25}_{-0.59}$	$0.932^{+0.086}_{-0.156}$	$12.4^{+6.5}_{-2.8}$	270^{+300}_{-180}
220501947.1	8	$4.0248883^{+0.0000060}_{-0.0000060}$	$2395.413923^{+0.000061}_{-0.000062}$	$2.510^{+0.012}_{-0.014}$	21878^{+45}_{-50}	$0.1318^{+0.0028}_{-0.0033}$	$9.56^{+0.71}_{-1.27}$	$0.665^{+0.048}_{-0.087}$	$13.47^{+0.36}_{-0.28}$	111^{+17}_{-29}
220503236.1	8	$8.68055^{+0.00042}_{-0.00043}$	$2396.4588^{+0.0019}_{-0.0019}$	$3.83^{+0.10}_{-0.13}$	598^{+20}_{-21}	$0.0232^{+0.0011}_{-0.0024}$	$2.79^{+0.34}_{-0.29}$	$1.102^{+0.125}_{-0.012}$	$15.9^{+3.9}_{-1.8}$	151^{+81}_{-35}
220504338.1	8	$5.817649^{+0.000025}_{-0.000025}$	$2392.88665^{+0.00019}_{-0.00019}$	$3.074^{+0.033}_{-0.030}$	8378^{+36}_{-37}	$0.0894^{+0.0021}_{-0.0034}$	$12.55^{+0.48}_{-0.51}$	$1.288^{+0.039}_{-0.017}$	$12.02^{+0.49}_{-0.64}$	247^{+28}_{-30}
220510874.1	8	$7.47331^{+0.00031}_{-0.00031}$	$2395.9060^{+0.0018}_{-0.0018}$	$3.556^{+0.091}_{-0.126}$	661^{+21}_{-21}	$0.02479^{+0.00100}_{-0.00228}$	$2.74^{+0.14}_{-0.27}$	$1.012^{+0.032}_{-0.031}$	$14.7^{+3.7}_{-1.7}$	187^{+94}_{-44}
220522262.1	8	$8.687812^{+0.000063}_{-0.000062}$	$2393.88141^{+0.00030}_{-0.00030}$	$2.710^{+0.036}_{-0.046}$	12388^{+95}_{-95}	$0.1016^{+0.0021}_{-0.0036}$	$7.36^{+0.42}_{-0.83}$	$0.664^{+0.036}_{-0.071}$	$26.23^{+1.76}_{-0.88}$	$34.4^{+6.1}_{-7.9}$
220526079.1	8	$7.51114^{+0.00095}_{-0.00107}$	$2398.0604^{+0.0071}_{-0.0053}$	$2.41^{+0.29}_{-0.40}$	1930^{+140}_{-150}	$0.0425^{+0.0046}_{-0.0152}$	$2.98^{+0.38}_{-1.07}$	$0.643^{+0.042}_{-0.031}$	$20.8^{+10.8}_{-5.3}$	33^{+35}_{-17}
220527374.1	8	$10.4347^{+0.0018}_{-0.0018}$	$2393.7531^{+0.0082}_{-0.0075}$	$3.45^{+0.39}_{-0.61}$	390^{+34}_{-36}	$0.0190^{+0.0021}_{-0.0069}$	$1.69^{+0.19}_{-0.61}$	$0.816^{+0.011}_{-0.012}$	$19.7^{+11.6}_{-4.8}$	91^{+107}_{-44}
220554210.1	8	$4.17032^{+0.00017}_{-0.00018}$	$2394.9946^{+0.0017}_{-0.0017}$	$2.89^{+0.10}_{-0.14}$	935^{+30}_{-31}	$0.0289^{+0.0016}_{-0.0039}$	$3.19^{+0.23}_{-0.45}$	$1.013^{+0.045}_{-0.045}$	$10.0^{+2.8}_{-1.3}$	274^{+158}_{-77}
220554210.2	8	$0.705386^{+0.000052}_{-0.000049}$	$2392.7569^{+0.0033}_{-0.0036}$	$1.70^{+0.11}_{-0.16}$	262^{+16}_{-17}	$0.0156^{+0.0011}_{-0.0026}$	$1.73^{+0.15}_{-0.30}$	$1.013^{+0.045}_{-0.045}$	$2.75^{+1.02}_{-0.49}$	3600^{+2700}_{-1300}
220555384.1	8	$4.28446^{+0.00011}_{-0.00011}$	$2393.4878^{+0.0011}_{-0.0011}$	$1.196^{+0.060}_{-0.069}$	424^{+19}_{-20}	$0.0194^{+0.0013}_{-0.0024}$	$1.98^{+0.17}_{-0.25}$	$0.934^{+0.053}_{-0.021}$	$24.7^{+6.9}_{-3.2}$	$22.3^{+12.8}_{-6.2}$
220556827.1	8	$6.53046^{+0.00064}_{-0.00122}$	$2394.9957^{+0.0056}_{-0.0033}$	$2.40^{+0.19}_{-0.27}$	2200^{+120}_{-130}	$0.0445^{+0.0030}_{-0.0056}$	$3.36^{+0.46}_{-0.44}$	$0.692^{+0.083}_{-0.024}$	$19.2^{+5.1}_{-3.2}$	$19.6^{+11.4}_{-6.6}$
220562610.1	8		$2396.68650^{+0.00096}_{-0.00104}$	$11.65^{+0.17}_{-0.23}$	2809^{+30}_{-31}	$0.0490^{+0.0021}_{-0.0030}$	$6.71^{+0.32}_{-0.46}$	$1.256^{+0.030}_{-0.036}$		
220565337.1	8	$14.7530^{+0.0012}_{-0.0013}$	$2393.2431^{+0.0040}_{-0.0041}$	$2.34^{+0.18}_{-0.22}$	2510^{+200}_{-220}	$0.0486^{+0.0034}_{-0.0056}$	$3.00^{+0.59}_{-0.35}$	$0.5666^{+0.1044}_{-0.0091}$	$44.7^{+13.1}_{-7.3}$	$3.8^{+2.6}_{-1.2}$
220565349.1	8	$21.77635^{+0.00014}_{-0.00014}$	$2407.47340^{+0.00019}_{-0.00019}$	$2.169^{+0.038}_{-0.051}$	28430^{+180}_{-170}	$0.306^{+0.085}_{-0.155}$	37^{+10}_{-21}	$1.122^{+0.011}_{-0.269}$	$60.8^{+1.4}_{-2.4}$	$6.78^{+0.50}_{-3.31}$
220571481.1	8	$8.78627^{+0.00042}_{-0.00042}$	$2392.6068^{+0.0019}_{-0.0020}$	$1.40^{+0.11}_{-0.22}$	645^{+43}_{-49}	$0.0244^{+0.0024}_{-0.0102}$	$3.16^{+0.31}_{-1.32}$	$1.184^{+0.014}_{-0.048}$	$41.1^{+24.6}_{-8.9}$	27^{+32}_{-12}
220573228.1	8	$57.10412^{+0.00054}_{-0.00053}$	$2409.84280^{+0.00038}_{-0.00038}$	$5.170^{+0.065}_{-0.085}$	3222^{+26}_{-26}	$0.0529^{+0.0013}_{-0.0028}$	$5.61^{+0.17}_{-0.31}$	$0.971^{+0.016}_{-0.016}$	$82.6^{+11.8}_{-6.2}$	$6.44^{+1.85}_{-0.99}$
220573228.2	8	$20.21535^{+0.00102}_{-0.00089}$	$2392.5241^{+0.0015}_{-0.0017}$	$3.408^{+0.097}_{-0.132}$	661^{+19}_{-19}	$0.0246^{+0.0013}_{-0.0026}$	$2.61^{+0.14}_{-0.28}$	$0.971^{+0.016}_{-0.016}$	$41.2^{+10.8}_{-5.1}$	$26.0^{+13.7}_{-6.5}$
220579319.1	8	$39.3266^{+0.0131}_{-0.0078}$	$2416.7410^{+0.0060}_{-0.0072}$	$8.29^{+0.27}_{-0.43}$	630^{+33}_{-31}	$0.0243^{+0.0011}_{-0.0023}$	$3.57^{+0.28}_{-0.35}$	$1.346^{+0.088}_{-0.038}$	$33.3^{+8.8}_{-3.8}$	$33.7^{+18.4}_{-8.1}$
220592745.1	8	$11.13878^{+0.00071}_{-0.00070}$	$2393.4499^{+0.0025}_{-0.0026}$	$4.90^{+0.11}_{-0.16}$	419^{+14}_{-14}	$0.01969^{+0.00081}_{-0.00194}$	$2.84^{+0.15}_{-0.29}$	$1.321^{+0.042}_{-0.027}$	$15.7^{+4.0}_{-1.9}$	152^{+79}_{-38}
220592745.2	8	$6.6674^{+0.0015}_{-0.0014}$	$2398.4167^{+0.0071}_{-0.0077}$	$4.82^{+0.39}_{-0.41}$	140^{+10}_{-11}	$0.01154^{+0.00089}_{-0.00206}$	$1.66^{+0.14}_{-0.30}$	$1.321^{+0.042}_{-0.027}$	$9.0^{+4.2}_{-1.8}$	460^{+430}_{-180}
220592745.3	8	$3.90090^{+0.00057}_{-0.00059}$	$2392.8408^{+0.0059}_{-0.0060}$	$3.40^{+0.27}_{-0.32}$	$117.3^{+8.7}_{-9.0}$	$0.01020^{+0.00089}_{-0.00205}$	$1.47^{+0.14}_{-0.30}$	$1.321^{+0.042}_{-0.027}$	$7.6^{+2.8}_{-1.3}$	640^{+470}_{-220}
220598331.1	8	$10.59366^{+0.00069}_{-0.00070}$	$2402.5547^{+0.0027}_{-0.0027}$	$2.40^{+0.14}_{-0.20}$	2100^{+120}_{-120}	$0.0437^{+0.0030}_{-0.0058}$	$1.71^{+0.38}_{-0.31}$	$0.360^{+0.075}_{-0.045}$	$31.2^{+9.3}_{-4.7}$	$8.9^{+7.6}_{-4.2}$
220598367.2	8	$7.64514^{+0.00022}_{-0.00022}$	$2396.6846^{+0.0011}_{-0.0011}$	$2.60^{+0.27}_{-0.18}$	2285^{+58}_{-61}	$0.056^{+0.017}_{-0.024}$	$6.5^{+2.5}_{-2.9}$	$1.06^{+0.24}_{-0.12}$	$12.2^{+3.1}_{-12.4}$	190^{+130}_{-390}
220605820.1	8	$46.47688^{+0.00092}_{-0.00091}$	$2423.88017^{+0.00066}_{-0.00065}$	$6.51^{+0.15}_{-0.15}$	15000^{+120}_{-110}	$0.238^{+0.065}_{-0.108}$	62^{+17}_{-28}	$2.394^{+0.053}_{-0.035}$	$38.1^{+1.4}_{-2.3}$	$17.9^{+2.2}_{-2.7}$
220606084.1	8		$2451.25079^{+0.00064}_{-0.00067}$	$8.17^{+0.15}_{-0.15}$	4902^{+57}_{-57}	$0.0665^{+0.0020}_{-0.0034}$	$12.32^{+1.37}_{-0.78}$	$1.698^{+0.182}_{-0.062}$		
220616148.1	8	$6.73511^{+0.00078}_{-0.00078}$	$2398.5020^{+0.0051}_{-0.0050}$	$5.00^{+0.55}_{-0.65}$	661^{+31}_{-32}	$0.0304^{+0.0086}_{-0.0135}$	$3.9^{+1.1}_{-1.8}$	$1.167^{+0.098}_{-0.098}$	$4.6^{+1.5}_{-6.3}$	2200^{+1400}_{-6000}
220616148.2	8	$15.1563^{+0.0020}_{-0.0021}$	$2392.6491^{+0.0065}_{-0.0058}$	$4.91^{+0.37}_{-0.58}$	622^{+39}_{-40}	$0.0237^{+0.0029}_{-0.0088}$	$3.01^{+0.44}_{-1.15}$	$1.167^{+0.098}_{-0.098}$	$20.3^{+11.7}_{-4.2}$	110^{+127}_{-49}
220621087.1	8	$3.83553^{+0.00011}_{-0.00011}$	$2395.2382^{+0.0012}_{-0.0012}$	$1.640^{+0.095}_{-0.160}$	983^{+31}_{-33}	$0.0301^{+0.0023}_{-0.0058}$	$1.054^{+0.091}_{-0.232}$	$0.321^{+0.013}_{-0.034}$	$15.6^{+6.4}_{-3.0}$	31^{+26}_{-15}
220621788.1	8	$13.68275^{+0.00066}_{-0.00058}$	$2401.2699^{+0.0017}_{-0.0016}$	$3.36^{+0.19}_{-0.25}$	537^{+15}_{-15}	$0.0228^{+0.0013}_{-0.0031}$	$2.62^{+0.21}_{-0.36}$	$1.056^{+0.058}_{-0.021}$	$27.0^{+11.8}_{-5.1}$	50^{+44}_{-19}
220629489.1	8	$1.921111^{+0.000038}_{-0.000039}$	$2392.98603^{+0.00092}_{-0.00089}$	$1.828^{+0.078}_{-0.135}$	1967^{+40}_{-40}	$0.0418^{+0.0024}_{-0.0065}$	$3.23^{+0.22}_{-0.62}$	$0.709^{+0.025}_{-0.078}$	$7.4^{+2.5}_{-1.1}$	500^{+340}_{-190}
220639177.1	8	$7.14238^{+0.00043}_{-0.00069}$	$2396.8612^{+0.0030}_{-0.0021}$	$1.15^{+0.13}_{-0.18}$	589^{+69}_{-65}	$0.0236^{+0.0027}_{-0.0057}$	$1.75^{+0.22}_{-0.43}$	$0.679^{+0.039}_{-0.031}$	$41.2^{+19.3}_{-9.5}$	$15.1^{+14.3}_{-7.1}$
220643470.1	8	$2.653275^{+0.000025}_{-0.000024}$	$2393.81052^{+0.00045}_{-0.00046}$	$3.917^{+0.030}_{-0.031}$	$1438.4^{+9.9}_{-9.9}$	$0.0434^{+0.0020}_{-0.0035}$	118^{+10}_{-14}	$24.8^{+1.9}_{-2.2}$	$2.374^{+0.089}_{-0.115}$	3330^{+770}_{-850}
220644522.1	8	$40.9380^{+0.0047}_{-0.0047}$	$2418.8252^{+0.0033}_{-0.0034}$	$6.54^{+0.17}_{-0.22}$	1009^{+44}_{-46}	$0.0302^{+0.0013}_{-0.0028}$	$3.57^{+0.16}_{-0.33}$	$1.083^{+0.011}_{-0.015}$	$44.9^{+9.9}_{-4.4}$	$17.1^{+7.6}_{-3.5}$
220650439.1	8	$2.398982^{+0.000091}_{-0.000092}$	$2392.9598^{+0.0017}_{-0.0017}$	$2.504^{+0.086}_{-0.097}$	312^{+11}_{-11}	$0.01695^{+0.00088}_{-0.00216}$	$1.98^{+0.11}_{-0.25}$	$1.0711^{+0.0249}_{-0.0069}$	$6.49^{+2.05}_{-0.91}$	830^{+520}_{-230}
220650843.1	8	$10.22657^{+0.00063}_{-0.00066}$	$2394.7155^{+0.0026}_{-0.0027}$	$3.33^{+0.20}_{-0.51}$	1552^{+72}_{-75}	$0.0365^{+0.0043}_{-0.0235}$	$2.71^{+0.36}_{-1.75}$	$0.681^{+0.041}_{-0.046}$	$21.0^{+12.5}_{-3.8}$	31^{+36}_{-12}
220657558.1	8	$3.91764^{+0.00056}_{-0.00053}$	$2395.0915^{+0.0051}_{-0.0052}$	$2.50^{+0.29}_{-0.50}$	419^{+33}_{-34}	$0.0200^{+0.0023}_{-0.0089}$	$2.94^{+0.50}_{-1.33}$	$1.35^{+0.17}_{-0.12}$	$10.0^{+6.5}_{-2.7}$	420^{+550}_{-240}
220663602.1	8	$6.40630^{+0.00034}_{-0.00036}$	$2396.1719^{+0.0024}_{-0.0023}$	$1.74^{+0.13}_{-0.21}$	1900^{+110}_{-130}	$0.0418^{+0.0034}_{-0.0088}$	$0.888^{+0.075}_{-0.187}$	$0.1950^{+0.0040}_{-0.0040}$	$25.3^{+9.9}_{-4.6}$	$7.9^{+6.2}_{-2.9}$

Table A.1: Our sample of planet candidates from C0-8. (continued)

Candidate	C#	Period (days)	t_0 (BJD - 2455000)	Duration (hours)	Depth (ppm)	R_p/R_*	R_p ($R_\oplus$)	R_* ($R_\odot$)	a/R_*	Inc. Flux ($S_\oplus$)
220666631.1	8	$31.9761^{+0.0046}_{-0.0046}$	$2405.7252^{+0.0050}_{-0.0048}$	$5.92^{+0.33}_{-0.49}$	653^{+36}_{-37}	$0.0246^{+0.0019}_{-0.0044}$	$3.92^{+0.34}_{-0.70}$	$1.461^{+0.062}_{-0.034}$	$35.7^{+14.2}_{-6.8}$	40^{+32}_{-15}
220674823.1	8	$0.5712893^{+0.0000097}_{-0.0000101}$	$2392.29678^{+0.00080}_{-0.00077}$	$1.487^{+0.037}_{-0.059}$	$280.0^{+7.7}_{-8.9}$	$0.01630^{+0.00061}_{-0.00176}$	$1.813^{+0.084}_{-0.200}$	$1.020^{+0.028}_{-0.024}$	$2.67^{+0.75}_{-0.31}$	4800^{+2700}_{-1200}
220674823.2	8	$13.33877^{+0.00098}_{-0.00107}$	$2392.3976^{+0.0032}_{-0.0031}$	$4.45^{+0.60}_{-0.38}$	903^{+24}_{-25}	$0.0341^{+0.0057}_{-0.0049}$	$3.79^{+0.65}_{-0.55}$	$1.020^{+0.028}_{-0.024}$	$11.1^{+2.1}_{-12.7}$	280^{+110}_{-640}
220679255.1	8	$8.13440^{+0.00045}_{-0.00042}$	$2392.8508^{+0.0023}_{-0.0024}$	$1.921^{+0.097}_{-0.117}$	389^{+21}_{-22}	$0.0188^{+0.0013}_{-0.0028}$	$2.36^{+0.17}_{-0.38}$	$1.153^{+0.031}_{-0.067}$	$28.8^{+9.2}_{-4.2}$	53^{+34}_{-17}
220679255.2	8	$17.78804^{+0.00077}_{-0.00080}$	$2399.1266^{+0.0021}_{-0.0020}$	$1.68^{+0.14}_{-0.34}$	527^{+30}_{-32}	$0.0221^{+0.0024}_{-0.0113}$	$2.78^{+0.32}_{-1.43}$	$1.153^{+0.031}_{-0.067}$	69^{+45}_{-16}	$9.4^{+12.4}_{-4.6}$
220696233.1	8	$28.7342^{+0.0011}_{-0.0011}$	$2401.9793^{+0.0011}_{-0.0011}$	$3.29^{+0.14}_{-0.16}$	13980^{+320}_{-330}	$0.1134^{+0.0067}_{-0.0076}$	$8.22^{+1.31}_{-0.60}$	$0.664^{+0.098}_{-0.020}$	$64.7^{+9.9}_{-10.3}$	$1.79^{+0.76}_{-0.58}$
220708327.1	8	$2.52894^{+0.00028}_{-0.00028}$	$2393.0020^{+0.0049}_{-0.0047}$	$1.81^{+0.17}_{-0.23}$	204^{+20}_{-21}	$0.0137^{+0.0013}_{-0.0027}$	$1.44^{+0.26}_{-0.29}$	$0.962^{+0.151}_{-0.053}$	$9.2^{+3.6}_{-1.9}$	510^{+420}_{-210}
229228348.1	7	$3.137611^{+0.000048}_{-0.000049}$	$2301.92110^{+0.00073}_{-0.00072}$	$1.720^{+0.071}_{-0.091}$	36710^{+970}_{-950}	$0.1713^{+0.0097}_{-0.0169}$			$15.6^{+1.9}_{-1.1}$	

Table A.2: Our sample of eclipsing binaries from C0-8.

Binary	C#	Period (days)	t_0 (BJD - 2455000)	Duration (hours)	Depth (ppm)
201160323.1	1	$22.27219^{+0.00020}_{-0.00021}$	$1811.49231^{+0.00036}_{-0.00039}$	$4.270^{+0.051}_{-0.061}$	404200^{+4100}_{-4300}
201160323.2	1	$22.30081^{+0.00028}_{-0.00029}$	$1820.00209^{+0.00055}_{-0.00055}$	$4.95^{+0.13}_{-0.13}$	229800^{+1800}_{-1700}
201173390.1	1	$16.99563^{+0.00011}_{-0.00011}$	$1816.43055^{+0.00026}_{-0.00026}$	$12.630^{+0.082}_{-0.103}$	42230^{+150}_{-150}
201173390.2	1	$16.99471^{+0.00041}_{-0.00041}$	$1824.81490^{+0.00079}_{-0.00080}$	$9.039^{+0.057}_{-0.058}$	6199^{+36}_{-37}
201174640.1	1		$1812.70325^{+0.00020}_{-0.00018}$	$5.696^{+0.077}_{-0.084}$	180830^{+600}_{-610}
201182911.1	1	$1.9931320^{+0.0000018}_{-0.0000015}$	$1811.089992^{+0.000041}_{-0.000048}$	$2.298^{+0.015}_{-0.021}$	381690^{+1420}_{-970}
201182911.2	1	$1.9931318^{+0.0000021}_{-0.0000019}$	$1812.086692^{+0.000050}_{-0.000057}$	$2.343^{+0.021}_{-0.021}$	366470^{+780}_{-690}
201184068.1	1	$1.58854625^{+0.00000043}_{-0.00000044}$	$1810.576497^{+0.000014}_{-0.000013}$	$2.6675^{+0.0090}_{-0.0103}$	598060^{+1050}_{-640}
201184068.2	1	$1.58854245^{+0.00000088}_{-0.00000088}$	$1811.370975^{+0.000028}_{-0.000028}$	$2.750^{+0.010}_{-0.011}$	276680^{+280}_{-270}
201207683.1	1		$1835.316456^{+0.000022}_{-0.000022}$	$7.579^{+0.019}_{-0.021}$	258310^{+3330}_{-430}
201246763.1	1		$1814.893165^{+0.000014}_{-0.000013}$	$14.945^{+0.021}_{-0.022}$	315999^{+46}_{-45}
201246763.2	1		$1858.576051^{+0.000026}_{-0.000028}$	$14.951^{+0.035}_{-0.038}$	311990^{+140}_{-140}
201253025.1	1	$6.7863912^{+0.0000045}_{-0.0000045}$	$1810.404622^{+0.000029}_{-0.000028}$	$6.6821^{+0.0100}_{-0.0138}$	262860^{+180}_{-170}
201253025.2	1	$6.7863944^{+0.0000047}_{-0.0000047}$	$1813.762803^{+0.000026}_{-0.000027}$	$7.2049^{+0.0087}_{-0.0118}$	244810^{+260}_{-230}
201306196.1	1	$7.25671^{+0.00011}_{-0.00011}$	$1812.47262^{+0.00069}_{-0.00069}$	$3.080^{+0.089}_{-0.094}$	5193^{+64}_{-64}
201306196.2	1	$7.25743^{+0.00017}_{-0.00018}$	$1816.0941^{+0.0011}_{-0.0011}$	$3.30^{+0.11}_{-0.13}$	3553^{+60}_{-59}
201333466.1	1	$10.998756^{+0.000039}_{-0.000039}$	$1814.85368^{+0.00014}_{-0.00014}$	$3.153^{+0.041}_{-0.044}$	67320^{+200}_{-200}
201333466.2	1	$10.99867^{+0.00010}_{-0.00010}$	$1810.50953^{+0.00042}_{-0.00043}$	$2.535^{+0.076}_{-0.090}$	15680^{+160}_{-160}
201353434.1	1	$1.0835056^{+0.0000018}_{-0.0000018}$	$1811.165644^{+0.000069}_{-0.000069}$	$1.753^{+0.011}_{-0.011}$	58090^{+260}_{-280}
201368515.1	1	$14.92942^{+0.00011}_{-0.00011}$	$1816.27640^{+0.00027}_{-0.00027}$	$3.884^{+0.066}_{-0.068}$	119150^{+550}_{-550}
201368515.2	1	$14.92905^{+0.00010}_{-0.00010}$	$1820.59914^{+0.00026}_{-0.00026}$	$3.912^{+0.067}_{-0.073}$	156200^{+1400}_{-1200}
201379113.1	1	$21.214513^{+0.000017}_{-0.000017}$	$1822.235101^{+0.000032}_{-0.000033}$	$3.992^{+0.032}_{-0.029}$	333710^{+260}_{-260}
201379113.2	1	$21.21372^{+0.00039}_{-0.00039}$	$1830.07237^{+0.00051}_{-0.00051}$	$5.06^{+0.10}_{-0.12}$	15510^{+110}_{-110}
201382417.1	1	$5.1977379^{+0.0000040}_{-0.0000040}$	$1811.073637^{+0.000036}_{-0.000037}$	$5.3853^{+0.0087}_{-0.0092}$	75269^{+91}_{-91}
201382417.2	1	$5.197728^{+0.000023}_{-0.000022}$	$1813.67210^{+0.00017}_{-0.00018}$	$5.166^{+0.026}_{-0.032}$	14154^{+40}_{-38}
201382958.1	1	$3.2040992^{+0.0000033}_{-0.0000035}$	$1811.856200^{+0.000060}_{-0.000054}$	$6.9581^{+0.0034}_{-0.0041}$	224760^{+110}_{-110}
201382958.2	1	$3.2040884^{+0.0000030}_{-0.0000030}$	$1813.458589^{+0.000033}_{-0.000035}$	$7.028^{+0.021}_{-0.023}$	215970^{+140}_{-140}
201390608.1	1	$9.8135053^{+0.0000050}_{-0.0000050}$	$1812.567337^{+0.000022}_{-0.000022}$	$4.069^{+0.011}_{-0.011}$	151190^{+92}_{-92}
201390608.2	1	$9.813625^{+0.000076}_{-0.000075}$	$1817.38939^{+0.00033}_{-0.00033}$	$3.833^{+0.022}_{-0.022}$	7096^{+35}_{-36}
201407812.1	1	$5.6536215^{+0.0000062}_{-0.0000054}$	$1812.488280^{+0.000035}_{-0.000042}$	$6.7642^{+0.0084}_{-0.0110}$	143696^{+40}_{-40}
201407812.2	1	$5.6536163^{+0.0000031}_{-0.0000031}$	$1815.315385^{+0.000025}_{-0.000025}$	$6.753^{+0.010}_{-0.011}$	140731^{+42}_{-42}
201408204.1	1	$8.4821731^{+0.0000045}_{-0.0000050}$	$1818.494360^{+0.000021}_{-0.000017}$	$6.217^{+0.014}_{-0.016}$	410881^{+83}_{-78}
201408204.2	1	$8.4818371^{+0.0000024}_{-0.0000025}$	$1815.195520^{+0.000011}_{-0.000012}$	$7.4200^{+0.0080}_{-0.0080}$	386520^{+2490}_{-880}
201464977.1	1	$15.89502^{+0.00018}_{-0.00018}$	$1825.40831^{+0.00044}_{-0.00045}$	$2.876^{+0.061}_{-0.080}$	12860^{+130}_{-130}
201464977.2	1	$15.89562^{+0.00100}_{-0.00100}$	$1818.1316^{+0.0023}_{-0.0023}$	$3.49^{+0.23}_{-0.20}$	3290^{+140}_{-140}
201523873.1	1	$1.24041805^{+0.00000078}_{-0.00000081}$	$1811.249102^{+0.000025}_{-0.000025}$	$2.568^{+0.025}_{-0.020}$	206560^{+400}_{-370}
201523873.2	1	$1.2404435^{+0.0000011}_{-0.0000011}$	$1810.628136^{+0.000042}_{-0.000043}$	$2.572^{+0.026}_{-0.028}$	101700^{+110}_{-110}
201530296.1	1	$10.3434301^{+0.0000035}_{-0.0000035}$	$1814.295137^{+0.000015}_{-0.000015}$	$3.513^{+0.023}_{-0.016}$	437100^{+7800}_{-2100}

Table A.2: Our sample of eclipsing binaries from C0-8. (continued)

Binary	C#	Period (days)	t_0 (BJD - 2455000)	Duration (hours)	Depth (ppm)
201530296.2	1	$10.3433657^{+0.0000085}_{-0.0000086}$	$1817.341858^{+0.000039}_{-0.000040}$	$5.363^{+0.014}_{-0.019}$	279780^{+140}_{-130}
201567796.1	1	$5.0086607^{+0.0000037}_{-0.0000038}$	$1812.566298^{+0.000033}_{-0.000033}$	$4.9637^{+0.0044}_{-0.0044}$	46463^{+34}_{-34}
201567796.2	1	$5.008598^{+0.000076}_{-0.000076}$	$1815.07178^{+0.00069}_{-0.00067}$	$4.799^{+0.059}_{-0.058}$	1416^{+13}_{-13}
201569483.1	1	$11.5935968^{+0.0000098}_{-0.0000128}$	$1819.111009^{+0.000035}_{-0.000033}$	$2.498^{+0.013}_{-0.018}$	98620^{+150}_{-140}
201569483.2	1	$11.5938598^{+0.0000066}_{-0.0000071}$	$1813.312695^{+0.000027}_{-0.000024}$	$2.584^{+0.019}_{-0.023}$	95450^{+130}_{-170}
201576812.1	1	$11.466^{+0.014}_{-0.012}$	$1814.554^{+0.056}_{-0.070}$	$0.036^{+0.027}_{-0.193}$	894000^{+29000}_{-27000}
201576812.2	1	$11.4565576^{+0.0000060}_{-0.0000065}$	$1820.328538^{+0.000034}_{-0.000031}$	$3.244^{+0.011}_{-0.011}$	125840^{+92}_{-87}
201584594.1	1	$3.1800956^{+0.0000099}_{-0.0000098}$	$1812.37917^{+0.00011}_{-0.00011}$	$2.189^{+0.036}_{-0.049}$	67240^{+410}_{-270}
201584594.2	1	$3.1800630^{+0.0000055}_{-0.0000058}$	$1810.790520^{+0.000084}_{-0.000081}$	$2.155^{+0.027}_{-0.024}$	53490^{+120}_{-120}
201594823.1	1	$1.30061863^{+0.00000066}_{-0.00000067}$	$1810.967699^{+0.000030}_{-0.000029}$	$3.003^{+0.011}_{-0.014}$	316910^{+370}_{-330}
201594823.2	1	$1.3006245^{+0.0000025}_{-0.0000025}$	$1810.317532^{+0.000089}_{-0.000089}$	$2.939^{+0.024}_{-0.033}$	44340^{+110}_{-110}
201607088.1	1	$0.5308968^{+0.0000012}_{-0.0000012}$	$1810.34524^{+0.00011}_{-0.00011}$	$2.343^{+0.034}_{-0.027}$	179630^{+660}_{-700}
201607088.2	1	$0.5308993^{+0.0000032}_{-0.0000032}$	$1810.61092^{+0.00028}_{-0.00028}$	$2.319^{+0.042}_{-0.036}$	65550^{+440}_{-440}
201638314.1	1	$5.429724^{+0.000014}_{-0.000015}$	$1812.30922^{+0.00012}_{-0.00011}$	$2.208^{+0.036}_{-0.036}$	80900^{+390}_{-300}
201638314.2	1	$5.429785^{+0.000056}_{-0.000049}$	$1814.99876^{+0.00023}_{-0.00023}$	$2.335^{+0.069}_{-0.077}$	32930^{+230}_{-230}
201649426.1	1	$55.540893^{+0.000054}_{-0.000053}$	$1821.347712^{+0.000037}_{-0.000038}$	$3.184^{+0.028}_{-0.031}$	113620^{+310}_{-980}
201663371.1	1		$1812.72914^{+0.00022}_{-0.00021}$	$5.626^{+0.041}_{-0.051}$	47980^{+240}_{-240}
201665500.1	1	$3.0535414^{+0.0000013}_{-0.0000013}$	$1810.538033^{+0.000018}_{-0.000019}$	$4.1220^{+0.0085}_{-0.0084}$	69808^{+75}_{-69}
201665500.2	1	$3.053548^{+0.000015}_{-0.000015}$	$1812.06494^{+0.00022}_{-0.00022}$	$4.027^{+0.016}_{-0.016}$	3160^{+11}_{-11}
201680569.1	1	$0.78482015^{+0.00000024}_{-0.00000024}$	$1810.885588^{+0.000014}_{-0.000014}$	$2.416^{+0.014}_{-0.014}$	361720^{+240}_{-250}
201680569.2	1	$0.78481444^{+0.00000050}_{-0.00000051}$	$1810.493359^{+0.000034}_{-0.000033}$	$2.459^{+0.032}_{-0.031}$	252900^{+820}_{-380}
201683540.1	1	$3.922283^{+0.000037}_{-0.000037}$	$1812.17589^{+0.00044}_{-0.00043}$	$1.677^{+0.046}_{-0.057}$	9680^{+160}_{-160}
201683540.2	1	$3.922243^{+0.000067}_{-0.000062}$	$1814.13771^{+0.00062}_{-0.00065}$	$1.536^{+0.162}_{-0.086}$	6670^{+270}_{-200}
201691826.1	1	$0.89939646^{+0.00000043}_{-0.00000042}$	$1810.946360^{+0.000023}_{-0.000023}$	$2.427^{+0.015}_{-0.020}$	475700^{+1200}_{-1200}
201691826.2	1	$0.89939388^{+0.00000069}_{-0.00000066}$	$1810.496291^{+0.000042}_{-0.000044}$	$2.416^{+0.015}_{-0.020}$	403930^{+890}_{-960}
201715262.1	1	$2.1082069^{+0.0000016}_{-0.0000016}$	$1811.507646^{+0.000037}_{-0.000037}$	$6.653^{+0.021}_{-0.025}$	223626^{+93}_{-94}
201715262.2	1	$2.1081663^{+0.0000027}_{-0.0000030}$	$1810.453801^{+0.000034}_{-0.000031}$	$6.598^{+0.012}_{-0.013}$	209760^{+120}_{-110}
201720463.1	1	$3.5577272^{+0.0000031}_{-0.0000031}$	$1812.328714^{+0.000039}_{-0.000039}$	$4.9954^{+0.0040}_{-0.0050}$	95210^{+80}_{-76}
201720463.2	1	$3.557788^{+0.000032}_{-0.000032}$	$1810.54907^{+0.00041}_{-0.00041}$	$4.934^{+0.028}_{-0.028}$	6108^{+30}_{-32}
201723461.1	1	$22.731968^{+0.000027}_{-0.000028}$	$1830.145343^{+0.000036}_{-0.000037}$	$4.485^{+0.037}_{-0.039}$	344760^{+350}_{-340}
201723461.2	1	$22.731894^{+0.000094}_{-0.000092}$	$1815.26084^{+0.00017}_{-0.00017}$	$5.234^{+0.060}_{-0.062}$	62680^{+150}_{-150}
201740472.1	1	$0.958726^{+0.000023}_{-0.000023}$	$1811.18133^{+0.00098}_{-0.00098}$	$1.370^{+0.121}_{-0.090}$	4980^{+230}_{-220}
201740472.2	1	$0.958767^{+0.000025}_{-0.000023}$	$1810.91353^{+0.00108}_{-0.00079}$	$0.385^{+0.093}_{-0.051}$	5460^{+690}_{-950}
201763507.1	1	$11.23258^{+0.00025}_{-0.00024}$	$1814.5791^{+0.0011}_{-0.0011}$	$2.211^{+0.081}_{-0.089}$	2301^{+47}_{-51}
201763507.2	1	$11.23282^{+0.00032}_{-0.00032}$	$1819.5584^{+0.0012}_{-0.0012}$	$2.91^{+0.11}_{-0.12}$	1525^{+36}_{-35}
201790675.1	1	$33.827476^{+0.000074}_{-0.000074}$	$1837.109184^{+0.000052}_{-0.000052}$	$4.575^{+0.038}_{-0.051}$	499100^{+2200}_{-3600}
201790675.2	1	$33.827774^{+0.000067}_{-0.000071}$	$1813.816142^{+0.000066}_{-0.000067}$	$3.202^{+0.033}_{-0.040}$	381200^{+2100}_{-1600}
201810513.1	1	$1.6466397^{+0.0000026}_{-0.0000026}$	$1811.930504^{+0.000070}_{-0.000070}$	$1.892^{+0.024}_{-0.019}$	50530^{+120}_{-120}

Table A.2: Our sample of eclipsing binaries from C0-8. (continued)

Binary	C#	Period (days)	t_0 (BJD - 2455000)	Duration (hours)	Depth (ppm)
201810513.2	1	$1.6466334^{+0.0000030}_{-0.0000030}$	$1811.107312^{+0.000083}_{-0.000083}$	$1.908^{+0.023}_{-0.018}$	43910^{+120}_{-120}
201818963.1	1	$1.0345213^{+0.0000062}_{-0.0000064}$	$1810.54360^{+0.00028}_{-0.00028}$	$0.936^{+0.030}_{-0.036}$	14130^{+290}_{-280}
201818963.2	1	$1.034479^{+0.000018}_{-0.000018}$	$1811.06179^{+0.00079}_{-0.00078}$	$1.055^{+0.156}_{-0.092}$	4780^{+260}_{-240}
201843069.1	1	$1.0967675^{+0.0000014}_{-0.0000015}$	$1811.155848^{+0.000060}_{-0.000061}$	$1.750^{+0.032}_{-0.032}$	130590^{+340}_{-330}
201843069.2	1	$1.0967717^{+0.0000036}_{-0.0000036}$	$1810.60772^{+0.00015}_{-0.00014}$	$1.742^{+0.049}_{-0.049}$	60350^{+330}_{-320}
201848566.1	1	$0.9568451^{+0.0000023}_{-0.0000023}$	$1811.15863^{+0.00011}_{-0.00011}$	$1.748^{+0.041}_{-0.041}$	21271^{+90}_{-85}
201848566.2	1	$0.9568401^{+0.0000029}_{-0.0000028}$	$1810.68046^{+0.00014}_{-0.00014}$	$1.799^{+0.045}_{-0.041}$	18341^{+87}_{-83}
201890494.1	1	$2.5366028^{+0.0000014}_{-0.0000014}$	$1810.446160^{+0.000024}_{-0.000025}$	$3.188^{+0.016}_{-0.025}$	117660^{+130}_{-130}
201890494.2	1	$2.5365985^{+0.0000025}_{-0.0000025}$	$1811.714699^{+0.000044}_{-0.000045}$	$3.309^{+0.025}_{-0.018}$	31002^{+23}_{-22}
201893576.1	1	$0.92981512^{+0.00000054}_{-0.00000055}$	$1811.122015^{+0.000027}_{-0.000027}$	$1.8596^{+0.0072}_{-0.0049}$	71652^{+54}_{-53}
201893576.2	1	$0.92981567^{+0.00000064}_{-0.00000064}$	$1810.656983^{+0.000032}_{-0.000033}$	$1.809^{+0.024}_{-0.024}$	38277^{+44}_{-44}
202060506.1	0	$1.9597350^{+0.0000063}_{-0.0000063}$	$1773.823428^{+0.000055}_{-0.000055}$	$5.452^{+0.017}_{-0.019}$	161790^{+150}_{-150}
202060506.2	0	$1.959686^{+0.000012}_{-0.000012}$	$1772.87276^{+0.00012}_{-0.00012}$	$5.491^{+0.015}_{-0.015}$	71000^{+120}_{-120}
202060551.1	0	$16.49590^{+0.00034}_{-0.00041}$	$1779.27390^{+0.00039}_{-0.00032}$	$10.746^{+0.033}_{-0.041}$	90180^{+140}_{-180}
202060551.2	0	$16.49644^{+0.00055}_{-0.00055}$	$1787.77070^{+0.00038}_{-0.00038}$	$10.406^{+0.090}_{-0.112}$	23902^{+79}_{-79}
202060911.1	0	$7.02512^{+0.00016}_{-0.00016}$	$1778.83656^{+0.00030}_{-0.00029}$	$5.316^{+0.058}_{-0.074}$	56870^{+210}_{-210}
202060911.2	0	$7.02571^{+0.00033}_{-0.00033}$	$1775.32689^{+0.00080}_{-0.00080}$	$5.58^{+0.14}_{-0.14}$	21350^{+190}_{-190}
202060921.1	0		$1804.327600^{+0.000028}_{-0.000029}$	$7.349^{+0.013}_{-0.012}$	105465^{+54}_{-56}
202061000.1	0	$5.868844^{+0.000032}_{-0.000032}$	$1776.021305^{+0.000078}_{-0.000078}$	$7.098^{+0.029}_{-0.029}$	61229^{+55}_{-55}
202062450.1	0	$8.8345^{+0.0059}_{-0.0159}$	$1776.3893^{+0.0079}_{-0.0126}$	$5.47^{+0.52}_{-1.10}$	27350^{+6550}_{-950}
202062450.2	0	$8.996^{+0.016}_{-0.016}$	$1780.705^{+0.012}_{-0.010}$	$14.85^{+0.74}_{-1.06}$	943^{+81}_{-85}
202064253.1	0	$21.14070^{+0.00013}_{-0.00014}$	$1777.993683^{+0.000098}_{-0.000096}$	$4.650^{+0.031}_{-0.039}$	51350^{+101}_{-97}
202064549.1	0	$9.763645^{+0.000020}_{-0.000017}$	$1777.798540^{+0.000023}_{-0.000030}$	$5.2203^{+0.0087}_{-0.0127}$	363730^{+180}_{-170}
202064549.2	0	$9.763718^{+0.000044}_{-0.000071}$	$1772.92396^{+0.00019}_{-0.00010}$	$5.702^{+0.031}_{-0.034}$	83920^{+120}_{-1280}
202066192.1	0	$3.292620^{+0.000088}_{-0.000088}$	$1774.82474^{+0.00050}_{-0.00052}$	$1.879^{+0.057}_{-0.067}$	9640^{+140}_{-130}
202066192.2	0	$3.29371^{+0.00100}_{-0.00108}$	$1773.0382^{+0.0052}_{-0.0044}$	$1.32^{+0.16}_{-0.20}$	764^{+97}_{-104}
202066212.1	0	$6.16019^{+0.00060}_{-0.00059}$	$1775.4865^{+0.0015}_{-0.0014}$	$5.595^{+0.056}_{-0.076}$	2118^{+40}_{-41}
202066212.2	0	$6.1659^{+0.0021}_{-0.0024}$	$1772.3890^{+0.0079}_{-0.0079}$	$5.52^{+0.30}_{-0.34}$	993^{+60}_{-65}
202066394.1	0	$3.186386^{+0.000014}_{-0.000014}$	$1774.790987^{+0.000075}_{-0.000074}$	$4.108^{+0.031}_{-0.039}$	53343^{+77}_{-75}
202066394.2	0	$3.18645^{+0.00015}_{-0.00015}$	$1773.16520^{+0.00089}_{-0.00091}$	$3.698^{+0.083}_{-0.092}$	3773^{+60}_{-62}
202066699.1	0	$2.2157283^{+0.0000028}_{-0.0000028}$	$1772.821989^{+0.000023}_{-0.000022}$	$5.239^{+0.010}_{-0.015}$	325830^{+190}_{-190}
202066699.2	0	$2.2157403^{+0.0000046}_{-0.0000047}$	$1773.930055^{+0.000038}_{-0.000038}$	$5.233^{+0.018}_{-0.019}$	176100^{+320}_{-250}
202067245.1	0	$6.17241^{+0.00042}_{-0.00038}$	$1778.05262^{+0.00193}_{-0.00071}$	$3.30^{+0.11}_{-0.10}$	28990^{+980}_{-410}
202067245.2	0	$6.17227^{+0.00031}_{-0.00031}$	$1774.97112^{+0.00076}_{-0.00077}$	$3.290^{+0.096}_{-0.115}$	14290^{+220}_{-210}
202068807.1	0	$4.2447232^{+0.0000045}_{-0.0000045}$	$1775.143676^{+0.000019}_{-0.000018}$	$5.842^{+0.015}_{-0.012}$	129490^{+31}_{-30}
202068807.2	0	$4.244735^{+0.000013}_{-0.000013}$	$1773.619583^{+0.000054}_{-0.000055}$	$5.487^{+0.022}_{-0.028}$	40477^{+34}_{-33}
202071505.1	0	$3.555334^{+0.000015}_{-0.000015}$	$1772.216798^{+0.000093}_{-0.000096}$	$3.976^{+0.021}_{-0.028}$	59047^{+55}_{-47}
202071505.2	0	$3.5553782^{+0.0000094}_{-0.0000095}$	$1773.341461^{+0.000045}_{-0.000046}$	$3.778^{+0.010}_{-0.012}$	37986^{+28}_{-28}

Table A.2: Our sample of eclipsing binaries from C0-8. (continued)

Binary	C#	Period (days)	t_0 (BJD - 2455000)	Duration (hours)	Depth (ppm)
202071579.1	0	$3.1271724^{+0.0000024}_{-0.0000024}$	$1774.409949^{+0.000013}_{-0.000013}$	$4.3411^{+0.0091}_{-0.0088}$	90887^{+20}_{-20}
202071579.2	0	$3.1271792^{+0.0000021}_{-0.0000021}$	$1772.846320^{+0.000012}_{-0.000013}$	$4.3392^{+0.0086}_{-0.0082}$	71488^{+16}_{-16}
202071635.1	0	$6.271214^{+0.000038}_{-0.000038}$	$1775.43225^{+0.00010}_{-0.00010}$	$5.348^{+0.046}_{-0.049}$	88700^{+120}_{-110}
202071945.1	0		$1782.324378^{+0.000035}_{-0.000034}$	$10.793^{+0.022}_{-0.024}$	287530^{+130}_{-130}
202072430.1	0	$20.01082^{+0.00015}_{-0.00014}$	$1776.98043^{+0.00010}_{-0.00010}$	$7.474^{+0.043}_{-0.050}$	460120^{+890}_{-900}
202072485.1	0	$14.615622^{+0.000041}_{-0.000042}$	$1776.255704^{+0.000032}_{-0.000031}$	$6.679^{+0.032}_{-0.035}$	228055^{+101}_{-98}
202072485.2	0	$14.61624^{+0.00023}_{-0.00023}$	$1781.15749^{+0.00016}_{-0.00016}$	$10.274^{+0.073}_{-0.082}$	44499^{+56}_{-55}
202072486.1	0	$2.9219671^{+0.0000066}_{-0.0000064}$	$1773.374295^{+0.000039}_{-0.000040}$	$5.207^{+0.014}_{-0.012}$	48175^{+24}_{-23}
202072486.2	0	$2.921983^{+0.000020}_{-0.000020}$	$1774.83560^{+0.00012}_{-0.00012}$	$5.159^{+0.024}_{-0.029}$	14123^{+19}_{-19}
202072502.1	0	$1.9237286^{+0.0000048}_{-0.0000048}$	$1772.548782^{+0.000046}_{-0.000045}$	$6.402^{+0.017}_{-0.018}$	179670^{+120}_{-120}
202072502.2	0	$1.9237324^{+0.0000064}_{-0.0000064}$	$1773.510709^{+0.000062}_{-0.000062}$	$6.3102^{+0.0063}_{-0.0070}$	118155^{+84}_{-86}
202072563.1	0	$2.123834^{+0.000013}_{-0.000013}$	$1773.36386^{+0.00012}_{-0.00012}$	$4.480^{+0.039}_{-0.053}$	216970^{+380}_{-380}
202072563.2	0	$2.123881^{+0.000016}_{-0.000017}$	$1772.30163^{+0.00016}_{-0.00016}$	$4.504^{+0.049}_{-0.056}$	201650^{+410}_{-420}
202072596.1	0	$3.9785526^{+0.0000088}_{-0.0000090}$	$1772.897244^{+0.000043}_{-0.000042}$	$4.620^{+0.020}_{-0.020}$	36454^{+23}_{-22}
202072596.2	0	$3.978646^{+0.000095}_{-0.000094}$	$1775.24147^{+0.00038}_{-0.00039}$	$3.805^{+0.080}_{-0.079}$	3358^{+21}_{-21}
202072704.1	0	$2.666196^{+0.000015}_{-0.000015}$	$1774.30030^{+0.00010}_{-0.00010}$	$3.686^{+0.013}_{-0.013}$	6816^{+15}_{-14}
202072704.2	0	$2.66642^{+0.00064}_{-0.00058}$	$1773.0151^{+0.0040}_{-0.0047}$	$3.85^{+0.17}_{-0.25}$	$129.3^{+6.8}_{-7.1}$
202072932.1	0	$3.1330805^{+0.0000068}_{-0.0000068}$	$1774.529807^{+0.000037}_{-0.000035}$	$3.730^{+0.021}_{-0.033}$	43644^{+31}_{-30}
202072932.2	0	$3.1330413^{+0.0000098}_{-0.0000097}$	$1772.963987^{+0.000065}_{-0.000065}$	$3.730^{+0.021}_{-0.032}$	33777^{+42}_{-42}
202072947.1	0	$3.685796^{+0.000032}_{-0.000032}$	$1773.47577^{+0.00016}_{-0.00016}$	$5.632^{+0.023}_{-0.027}$	96990^{+200}_{-190}
202072947.2	0	$3.685488^{+0.000029}_{-0.000029}$	$1775.32128^{+0.00015}_{-0.00015}$	$5.686^{+0.037}_{-0.053}$	95890^{+360}_{-400}
202072963.1	0	$4.2102164^{+0.0000024}_{-0.0000024}$	$1774.505072^{+0.000011}_{-0.000011}$	$7.4326^{+0.0092}_{-0.0098}$	295674^{+45}_{-41}
202072963.2	0	$4.2102033^{+0.0000025}_{-0.0000025}$	$1772.215735^{+0.000011}_{-0.000011}$	$7.259^{+0.012}_{-0.013}$	195842^{+41}_{-39}
202072972.1	0	$5.038289^{+0.000077}_{-0.000077}$	$1773.62995^{+0.00029}_{-0.00029}$	$7.231^{+0.068}_{-0.090}$	83450^{+250}_{-250}
202072972.2	0	$5.038092^{+0.000099}_{-0.000103}$	$1776.15129^{+0.00034}_{-0.00032}$	$7.184^{+0.067}_{-0.088}$	75730^{+220}_{-210}
202072982.1	0	$15.601064^{+0.000026}_{-0.000026}$	$1782.052015^{+0.000019}_{-0.000019}$	$7.145^{+0.016}_{-0.016}$	383410^{+180}_{-180}
202072982.2	0	$15.600856^{+0.000029}_{-0.000029}$	$1774.251703^{+0.000029}_{-0.000031}$	$7.107^{+0.020}_{-0.024}$	356000^{+1200}_{-1500}
202073063.1	0	$2.4122930^{+0.0000027}_{-0.0000025}$	$1773.430293^{+0.000017}_{-0.000018}$	$4.6167^{+0.0081}_{-0.0089}$	108174^{+35}_{-34}
202073063.2	0	$2.4123339^{+0.0000092}_{-0.0000088}$	$1774.441575^{+0.000064}_{-0.000064}$	$4.354^{+0.039}_{-0.044}$	41526^{+39}_{-39}
202073074.1	0	$1.1215679^{+0.0000011}_{-0.0000011}$	$1772.311746^{+0.000017}_{-0.000017}$	$6.102^{+0.013}_{-0.014}$	267437^{+81}_{-90}
202073088.1	0	$0.8241783^{+0.0000070}_{-0.0000072}$	$1772.69483^{+0.00019}_{-0.00018}$	$2.985^{+0.051}_{-0.054}$	337600^{+1600}_{-1500}
202073088.2	0	$0.8242207^{+0.0000067}_{-0.0000068}$	$1772.28120^{+0.00017}_{-0.00017}$	$2.978^{+0.059}_{-0.070}$	242530^{+1060}_{-990}
202073124.1	0	$1.679210^{+0.000016}_{-0.000021}$	$1773.60716^{+0.00017}_{-0.00014}$	$1.226^{+0.021}_{-0.021}$	999953^{+2140}_{-42}
202073125.1	0	$1.677980^{+0.000015}_{-0.000015}$	$1773.7988^{+0.0051}_{-0.0089}$	$7.25^{+0.26}_{-0.46}$	$999990.2^{+50.3}_{-7.8}$
202073135.1	0	$3.231594^{+0.000039}_{-0.000037}$	$1774.26307^{+0.00026}_{-0.00030}$	$1.403^{+0.056}_{-0.100}$	690800^{+23100}_{-9000}
202073135.2	0	$3.233883^{+0.000054}_{-0.000053}$	$1772.63861^{+0.00031}_{-0.00030}$	$5.231^{+0.014}_{-0.015}$	336000^{+1200}_{-1300}
202073144.1	0	$1.550522^{+0.000025}_{-0.000016}$	$1772.46398^{+0.00018}_{-0.00033}$	$4.016^{+0.047}_{-0.054}$	43550^{+150}_{-140}
202073144.2	0	$1.549849^{+0.000050}_{-0.000051}$	$1773.24964^{+0.00062}_{-0.00061}$	$17.688^{+0.012}_{-0.011}$	15889^{+61}_{-62}

Table A.2: Our sample of eclipsing binaries from C0-8. (continued)

Binary	C#	Period (days)	t_0 (BJD - 2455000)	Duration (hours)	Depth (ppm)
202073160.1	0	$2.836697^{+0.001082}_{-0.000071}$	$1773.97294^{+0.00054}_{-0.00507}$	$1.069^{+0.089}_{-0.340}$	758000^{+86000}_{-38000}
202073160.2	0	$2.825740^{+0.000038}_{-0.000042}$	$1772.64659^{+0.00026}_{-0.00024}$	$6.316^{+0.086}_{-0.082}$	675600^{+5600}_{-6700}
202073161.1	0	$1.4035184^{+0.0000022}_{-0.0000023}$	$1772.524493^{+0.000029}_{-0.000030}$	$4.585^{+0.035}_{-0.034}$	521920^{+820}_{-740}
202073161.2	0	$1.4035648^{+0.0000074}_{-0.0000071}$	$1773.225823^{+0.000089}_{-0.000090}$	$4.558^{+0.041}_{-0.047}$	286230^{+630}_{-490}
202073174.1	0	$0.644097^{+0.000022}_{-0.000023}$	$1772.17245^{+0.00075}_{-0.00074}$	$6.80^{+0.13}_{-0.15}$	54180^{+540}_{-560}
202073175.1	0	$1.2811854^{+0.0000026}_{-0.0000027}$	$1772.257598^{+0.000046}_{-0.000044}$	$3.837^{+0.028}_{-0.019}$	340280^{+340}_{-350}
202073175.2	0	$1.2811844^{+0.0000048}_{-0.0000049}$	$1772.901465^{+0.000074}_{-0.000076}$	$3.999^{+0.026}_{-0.035}$	111180^{+140}_{-130}
202073186.1	0	$2.451036^{+0.000058}_{-0.000063}$	$1773.59971^{+0.00045}_{-0.00043}$	$3.354^{+0.070}_{-0.107}$	102610^{+560}_{-470}
202073186.2	0	$2.450428^{+0.000070}_{-0.000058}$	$1772.36732^{+0.00049}_{-0.00050}$	$3.391^{+0.065}_{-0.070}$	99700^{+440}_{-450}
202073210.1	0	$1.0250484^{+0.0000027}_{-0.0000033}$	$1773.003517^{+0.000048}_{-0.000044}$	$2.858^{+0.024}_{-0.026}$	496300^{+1300}_{-1200}
202073210.2	0	$1.0250530^{+0.0000044}_{-0.0000044}$	$1772.490506^{+0.000088}_{-0.000087}$	$2.938^{+0.050}_{-0.054}$	164390^{+530}_{-490}
202073217.1	0	$0.941123^{+0.000015}_{-0.000014}$	$1772.44609^{+0.00030}_{-0.00032}$	$4.660^{+0.073}_{-0.082}$	339600^{+1200}_{-1200}
202073438.1	0	$2.4059906^{+0.0000047}_{-0.0000046}$	$1773.614025^{+0.000037}_{-0.000038}$	$6.726^{+0.032}_{-0.040}$	437420^{+210}_{-200}
202083510.1	0	$3.3076086^{+0.0000073}_{-0.0000079}$	$1772.915784^{+0.000042}_{-0.000038}$	$1.848^{+0.024}_{-0.025}$	368200^{+2300}_{-1500}
202083510.2	0	$3.3075991^{+0.0000063}_{-0.0000079}$	$1774.569591^{+0.000029}_{-0.000027}$	$1.835^{+0.022}_{-0.022}$	330800^{+1200}_{-1100}
202085432.1	0	$8.69397^{+0.00040}_{-0.00040}$	$1773.88571^{+0.00077}_{-0.00078}$	$4.14^{+0.10}_{-0.13}$	13410^{+180}_{-160}
202085432.2	0	$8.69498^{+0.00061}_{-0.00063}$	$1778.2670^{+0.0012}_{-0.0012}$	$4.11^{+0.12}_{-0.15}$	7760^{+140}_{-130}
202086223.1	0	$11.53901^{+0.00011}_{-0.00011}$	$1782.754222^{+0.000084}_{-0.000083}$	$3.634^{+0.049}_{-0.051}$	23499^{+43}_{-42}
202086223.2	0	$11.53930^{+0.00049}_{-0.00049}$	$1778.42883^{+0.00065}_{-0.00065}$	$3.90^{+0.10}_{-0.12}$	2891^{+31}_{-31}
202086225.1	0	$25.647817^{+0.000014}_{-0.000014}$	$1778.938662^{+0.000013}_{-0.000013}$	$8.8146^{+0.0080}_{-0.0085}$	475000^{+6100}_{-2400}
202086291.1	0	$4.8688439^{+0.0000023}_{-0.0000023}$	$1774.1308488^{+0.0000086}_{-0.0000086}$	$7.7340^{+0.0096}_{-0.0098}$	404221^{+58}_{-56}
202086291.2	0	$4.8688409^{+0.0000028}_{-0.0000028}$	$1776.5651264^{+0.0000081}_{-0.0000081}$	$7.737^{+0.010}_{-0.010}$	402448^{+56}_{-56}
202086627.1	0	$7.1497742^{+0.0000046}_{-0.0000044}$	$1777.6826373^{+0.0000071}_{-0.0000076}$	$5.0736^{+0.0074}_{-0.0066}$	470490^{+160}_{-150}
202086627.2	0	$7.1498240^{+0.0000092}_{-0.0000114}$	$1774.129598^{+0.000020}_{-0.000019}$	$4.9990^{+0.0098}_{-0.0113}$	247116^{+99}_{-104}
202086968.1	0	$3.698152^{+0.000022}_{-0.000022}$	$1774.03603^{+0.00012}_{-0.00012}$	$3.539^{+0.029}_{-0.021}$	31192^{+52}_{-51}
202086968.2	0	$3.697906^{+0.000015}_{-0.000016}$	$1772.180375^{+0.000074}_{-0.000074}$	$3.468^{+0.040}_{-0.044}$	26440^{+180}_{-150}
202087156.1	0	$1.895086^{+0.000030}_{-0.000030}$	$1773.53099^{+0.00028}_{-0.00028}$	$2.952^{+0.056}_{-0.047}$	4665^{+24}_{-24}
202087156.2	0	$1.895108^{+0.000032}_{-0.000032}$	$1772.58375^{+0.00031}_{-0.00031}$	$2.911^{+0.060}_{-0.052}$	3644^{+21}_{-21}
202087553.1	0	$9.002686^{+0.000030}_{-0.000030}$	$1776.822423^{+0.000055}_{-0.000058}$	$6.050^{+0.026}_{-0.037}$	109090^{+360}_{-310}
202087553.2	0	$9.002458^{+0.000103}_{-0.000074}$	$1772.33313^{+0.00015}_{-0.00018}$	$6.394^{+0.075}_{-0.097}$	91710^{+110}_{-120}
202087711.1	0	$4.595046^{+0.000023}_{-0.000024}$	$1775.465131^{+0.000047}_{-0.000049}$	$2.095^{+0.033}_{-0.033}$	999890^{+2180}_{-110}
202087711.2	0	$4.590786^{+0.000099}_{-0.000110}$	$1773.18005^{+0.00031}_{-0.00027}$	$2.041^{+0.034}_{-0.039}$	529500^{+3700}_{-1200}
202088178.1	0	$2.371351^{+0.000034}_{-0.000034}$	$1773.02171^{+0.00027}_{-0.00028}$	$6.151^{+0.068}_{-0.077}$	148920^{+480}_{-480}
202088178.2	0	$2.371175^{+0.000044}_{-0.000043}$	$1774.20791^{+0.00034}_{-0.00033}$	$6.150^{+0.088}_{-0.095}$	133410^{+410}_{-410}
202088387.1	0	$3.551216^{+0.000012}_{-0.000012}$	$1774.150183^{+0.000062}_{-0.000065}$	$5.479^{+0.019}_{-0.030}$	148120^{+180}_{-190}
202088387.2	0	$3.551401^{+0.000019}_{-0.000019}$	$1772.42034^{+0.00010}_{-0.00010}$	$5.260^{+0.014}_{-0.015}$	40882^{+63}_{-63}
202091197.1	0		$1799.016217^{+0.000083}_{-0.000081}$	$11.847^{+0.092}_{-0.110}$	76220^{+770}_{-2230}
202091197.2	0		$1782.987852^{+0.000044}_{-0.000044}$	$5.161^{+0.053}_{-0.054}$	60013^{+98}_{-106}

Table A.2: Our sample of eclipsing binaries from C0-8. (continued)

Binary	C#	Period (days)	t_0 (BJD - 2455000)	Duration (hours)	Depth (ppm)
202091203.1	0	$5.214179^{+0.000025}_{-0.000024}$	$1775.755086^{+0.000071}_{-0.000073}$	$5.815^{+0.024}_{-0.030}$	100020^{+81}_{-81}
202091203.2	0	$5.214257^{+0.000040}_{-0.000039}$	$1773.14115^{+0.00014}_{-0.00014}$	$5.813^{+0.034}_{-0.046}$	57558^{+89}_{-89}
202091514.1	0	$8.3219906^{+0.0000081}_{-0.0000079}$	$1774.386634^{+0.000022}_{-0.000021}$	$5.504^{+0.012}_{-0.018}$	447360^{+220}_{-230}
202091514.2	0	$8.3213148^{+0.0000058}_{-0.0000058}$	$1778.564330^{+0.000011}_{-0.000011}$	$5.5222^{+0.0085}_{-0.0130}$	297240^{+81}_{-81}
202092480.1	0	$5.6891553^{+0.0000042}_{-0.0000042}$	$1772.339106^{+0.000013}_{-0.000013}$	$5.765^{+0.013}_{-0.014}$	264281^{+105}_{-97}
202092480.2	0	$5.689089^{+0.000012}_{-0.000010}$	$1775.183401^{+0.000033}_{-0.000029}$	$5.7389^{+0.0072}_{-0.0106}$	259776^{+87}_{-130}
202092530.1	0	$15.602375^{+0.000035}_{-0.000051}$	$1774.251738^{+0.000074}_{-0.000033}$	$7.244^{+0.017}_{-0.029}$	419170^{+1490}_{-740}
202092530.2	0	$15.601098^{+0.000039}_{-0.000038}$	$1782.052091^{+0.000029}_{-0.000033}$	$7.141^{+0.012}_{-0.012}$	363304^{+81}_{-75}
202092613.1	0	$3.18680^{+0.00018}_{-0.00018}$	$1773.2633^{+0.0010}_{-0.0010}$	$4.45^{+0.13}_{-0.15}$	46490^{+600}_{-600}
202092613.2	0	$3.18658^{+0.00028}_{-0.00028}$	$1774.8578^{+0.0015}_{-0.0015}$	$4.42^{+0.15}_{-0.16}$	32050^{+590}_{-590}
202094117.1	0	$1.6344577^{+0.0000022}_{-0.0000022}$	$1772.169550^{+0.000026}_{-0.000026}$	$2.488^{+0.010}_{-0.012}$	28118^{+25}_{-25}
202094117.2	0	$1.634455^{+0.000098}_{-0.000098}$	$1772.9870^{+0.0012}_{-0.0012}$	$2.22^{+0.10}_{-0.27}$	761^{+20}_{-21}
202095298.1	0	$11.25124^{+0.00016}_{-0.00017}$	$1772.43825^{+0.00016}_{-0.00018}$	$1.666^{+0.040}_{-0.058}$	11270^{+100}_{-100}
202095298.2	0	$11.2536^{+0.0012}_{-0.0012}$	$1778.0614^{+0.0016}_{-0.0016}$	$3.83^{+0.13}_{-0.17}$	1567^{+125}_{-82}
202122545.1	0	$19.266843^{+0.000038}_{-0.000026}$	$1783.881854^{+0.000013}_{-0.000020}$	$4.7691^{+0.0063}_{-0.0080}$	343130^{+170}_{-180}
202126825.1	0	$9.20348^{+0.00058}_{-0.00059}$	$1780.80379^{+0.00075}_{-0.00073}$	$7.64^{+0.10}_{-0.11}$	14910^{+120}_{-120}
202126825.2	0	$9.20808^{+0.00080}_{-0.00080}$	$1776.4174^{+0.0014}_{-0.0014}$	$7.36^{+0.13}_{-0.15}$	5963^{+97}_{-100}
202126851.1	0	$4.480050^{+0.000042}_{-0.000041}$	$1774.42465^{+0.00015}_{-0.00016}$	$5.209^{+0.027}_{-0.031}$	42677^{+98}_{-102}
202126851.2	0	$4.480003^{+0.000097}_{-0.000097}$	$1772.18493^{+0.00041}_{-0.00041}$	$5.028^{+0.049}_{-0.057}$	10989^{+63}_{-63}
202126864.1	0	$6.1874507^{+0.0000074}_{-0.0000074}$	$1772.902528^{+0.000023}_{-0.000023}$	$6.249^{+0.016}_{-0.017}$	220480^{+110}_{-100}
202126864.2	0	$6.187445^{+0.000054}_{-0.000053}$	$1775.36204^{+0.00013}_{-0.00013}$	$3.607^{+0.029}_{-0.043}$	29405^{+97}_{-95}
202126866.1	0	$2.3372718^{+0.0000061}_{-0.0000059}$	$1772.798204^{+0.000044}_{-0.000044}$	$2.786^{+0.018}_{-0.022}$	51251^{+61}_{-58}
202126866.2	0	$2.337260^{+0.000066}_{-0.000066}$	$1773.96677^{+0.00048}_{-0.00048}$	$2.887^{+0.083}_{-0.090}$	3773^{+36}_{-36}
202126867.1	0	$4.826729^{+0.000081}_{-0.000107}$	$1775.28960^{+0.00089}_{-0.00038}$	$3.429^{+0.063}_{-0.076}$	141970^{+600}_{-740}
202126867.2	0	$4.827358^{+0.000071}_{-0.000066}$	$1772.87819^{+0.00025}_{-0.00027}$	$3.388^{+0.021}_{-0.030}$	104970^{+480}_{-470}
202126876.1	0	$10.358673^{+0.000070}_{-0.000066}$	$1774.124955^{+0.000089}_{-0.000094}$	$5.664^{+0.042}_{-0.051}$	73500^{+450}_{-300}
202126878.1	0	$5.559988^{+0.000067}_{-0.000069}$	$1773.65411^{+0.00022}_{-0.00022}$	$6.387^{+0.055}_{-0.075}$	226730^{+500}_{-500}
202126878.2	0	$5.5479^{+0.0015}_{-0.0016}$	$1776.4828^{+0.0067}_{-0.0055}$	$8.41^{+0.49}_{-0.45}$	22090^{+470}_{-470}
202126880.1	0	$3.4607339^{+0.0000031}_{-0.0000031}$	$1774.511343^{+0.000015}_{-0.000015}$	$3.917^{+0.014}_{-0.013}$	126618^{+43}_{-42}
202126880.2	0	$3.460725^{+0.000046}_{-0.000046}$	$1772.78126^{+0.00024}_{-0.00024}$	$3.833^{+0.053}_{-0.064}$	10999^{+41}_{-41}
202137190.1	0		$1804.129559^{+0.000098}_{-0.000093}$	$6.689^{+0.056}_{-0.076}$	78530^{+160}_{-150}
202137209.1	0	$2.382492^{+0.000077}_{-0.000076}$	$1774.01903^{+0.00059}_{-0.00059}$	$4.250^{+0.059}_{-0.068}$	29920^{+280}_{-280}
202137209.2	0	$2.38221^{+0.00034}_{-0.00035}$	$1772.8324^{+0.0028}_{-0.0027}$	$3.87^{+0.30}_{-0.31}$	5100^{+200}_{-200}
202137558.1	0	$3.12690^{+0.00013}_{-0.00013}$	$1773.78585^{+0.00078}_{-0.00078}$	$3.26^{+0.10}_{-0.11}$	4288^{+58}_{-59}
202137558.2	0	$3.12659^{+0.00043}_{-0.00045}$	$1772.2287^{+0.0026}_{-0.0025}$	$2.19^{+0.15}_{-0.29}$	835^{+46}_{-50}
202139332.1	0		$1793.383936^{+0.000098}_{-0.000100}$	$4.510^{+0.048}_{-0.064}$	293070^{+940}_{-900}
202565282.1	2	$11.97681^{+0.00025}_{-0.00023}$	$1900.74193^{+0.00086}_{-0.00099}$	$6.727^{+0.062}_{-0.084}$	77380^{+520}_{-550}
202634963.1	2		$1948.817877^{+0.000079}_{-0.000081}$	$3.692^{+0.034}_{-0.048}$	41594^{+83}_{-83}

Table A.2: Our sample of eclipsing binaries from C0-8. (continued)

Binary	C#	Period (days)	t_0 (BJD - 2455000)	Duration (hours)	Depth (ppm)
202634963.2	2		$1920.109635^{+0.000092}_{-0.000092}$	$3.710^{+0.052}_{-0.067}$	40046^{+97}_{-96}
202834934.1	2	$2.956939^{+0.000025}_{-0.000025}$	$1895.48633^{+0.00038}_{-0.00038}$	$1.965^{+0.049}_{-0.062}$	28990^{+350}_{-320}
202834934.2	2	$2.956871^{+0.000037}_{-0.000038}$	$1896.96428^{+0.00056}_{-0.00057}$	$1.864^{+0.075}_{-0.070}$	14530^{+320}_{-260}
202843107.1	2	$2.1988969^{+0.0000017}_{-0.0000017}$	$1896.495032^{+0.000033}_{-0.000034}$	$7.216^{+0.014}_{-0.018}$	318200^{+1500}_{-1600}
203060993.1	2	$5.955188^{+0.000042}_{-0.000037}$	$1897.93550^{+0.00015}_{-0.00016}$	$6.371^{+0.053}_{-0.060}$	230140^{+770}_{-720}
203060993.2	2	$5.954696^{+0.000031}_{-0.000036}$	$1894.96079^{+0.00017}_{-0.00013}$	$6.262^{+0.020}_{-0.025}$	208360^{+520}_{-860}
203294831.1	2	$1.8590183^{+0.0000014}_{-0.0000014}$	$1895.524827^{+0.000033}_{-0.000033}$	$3.448^{+0.012}_{-0.016}$	45787^{+33}_{-32}
203361171.1	2	$7.3217752^{+0.0000059}_{-0.0000058}$	$1894.492499^{+0.000040}_{-0.000039}$	$6.6264^{+0.0088}_{-0.0111}$	107082^{+44}_{-42}
203361171.2	2	$7.3217711^{+0.0000063}_{-0.0000062}$	$1898.071128^{+0.000043}_{-0.000044}$	$6.5603^{+0.0083}_{-0.0099}$	106801^{+51}_{-46}
203466879.1	2	$5.8369609^{+0.0000091}_{-0.0000091}$	$1897.189748^{+0.000066}_{-0.000066}$	$9.3290^{+0.0097}_{-0.0095}$	61748^{+38}_{-38}
203466879.2	2	$5.836971^{+0.000021}_{-0.000021}$	$1900.10858^{+0.00015}_{-0.00015}$	$9.234^{+0.010}_{-0.010}$	18433^{+21}_{-21}
203488803.1	2	$31.92484^{+0.00021}_{-0.00020}$	$1916.26316^{+0.00015}_{-0.00015}$	$12.715^{+0.020}_{-0.021}$	38609^{+72}_{-69}
203488803.2	2	$31.9239^{+0.0019}_{-0.0018}$	$1907.5604^{+0.0024}_{-0.0024}$	$7.59^{+0.21}_{-0.18}$	1220^{+23}_{-24}
203543668.1	2	$36.761830^{+0.000027}_{-0.000025}$	$1895.639113^{+0.000026}_{-0.000025}$	$4.335^{+0.022}_{-0.031}$	219100^{+1410}_{-330}
203543668.2	2	$36.76300^{+0.00022}_{-0.00022}$	$1902.91204^{+0.00015}_{-0.00016}$	$9.757^{+0.057}_{-0.066}$	56501^{+73}_{-69}
203610780.1	2	$29.594571^{+0.000074}_{-0.000072}$	$1915.590558^{+0.000060}_{-0.000064}$	$8.393^{+0.024}_{-0.022}$	134140^{+190}_{-300}
203610780.2	2	$29.59364^{+0.00032}_{-0.00032}$	$1900.25390^{+0.00040}_{-0.00040}$	$12.74^{+0.14}_{-0.15}$	18565^{+58}_{-55}
203636784.1	2	$6.7645728^{+0.0000075}_{-0.0000062}$	$1899.546022^{+0.000054}_{-0.000078}$	$5.877^{+0.016}_{-0.018}$	230140^{+130}_{-160}
203636784.2	2	$6.764589^{+0.000020}_{-0.000021}$	$1896.16373^{+0.00011}_{-0.00012}$	$5.687^{+0.025}_{-0.064}$	37330^{+120}_{-110}
203637922.1	2	$4.307268^{+0.000018}_{-0.000019}$	$1896.21544^{+0.00017}_{-0.00018}$	$6.238^{+0.045}_{-0.067}$	218500^{+490}_{-480}
203637922.2	2	$4.307158^{+0.000020}_{-0.000020}$	$1898.36918^{+0.00020}_{-0.00020}$	$6.274^{+0.062}_{-0.076}$	186590^{+360}_{-360}
203692974.1	2	$1.005915^{+0.000023}_{-0.000023}$	$1895.3099^{+0.0011}_{-0.0011}$	$3.007^{+0.150}_{-0.084}$	1259^{+22}_{-24}
203692974.2	2	$1.006054^{+0.000051}_{-0.000051}$	$1894.8014^{+0.0024}_{-0.0025}$	$3.53^{+0.16}_{-0.17}$	718^{+23}_{-22}
203710387.1	2	$2.808819^{+0.000020}_{-0.000020}$	$1894.71442^{+0.00033}_{-0.00032}$	$2.396^{+0.048}_{-0.059}$	78010^{+690}_{-610}
203710387.2	2	$2.808878^{+0.000019}_{-0.000019}$	$1896.11238^{+0.00029}_{-0.00029}$	$2.363^{+0.053}_{-0.060}$	72170^{+700}_{-620}
203764177.1	2	$7.949525^{+0.000030}_{-0.000032}$	$1895.75466^{+0.00016}_{-0.00015}$	$5.549^{+0.055}_{-0.044}$	163570^{+540}_{-550}
203764177.2	2	$7.94958^{+0.00013}_{-0.00013}$	$1899.73025^{+0.00067}_{-0.00067}$	$5.517^{+0.085}_{-0.095}$	21550^{+180}_{-180}
203771098.1	2		$1957.98832^{+0.00021}_{-0.00021}$	$6.408^{+0.045}_{-0.065}$	4372^{+26}_{-26}
203771098.2	2		$1915.62427^{+0.00035}_{-0.00033}$	$6.546^{+0.059}_{-0.053}$	3145^{+22}_{-21}
203849738.1	2	$0.6198339^{+0.0000076}_{-0.0000076}$	$1894.60663^{+0.00058}_{-0.00058}$	$3.924^{+0.073}_{-0.063}$	44250^{+340}_{-350}
203868608.1	2	$4.541725^{+0.000016}_{-0.000017}$	$1896.19676^{+0.00016}_{-0.00016}$	$3.191^{+0.039}_{-0.032}$	132170^{+400}_{-370}
203868608.2	2	$4.541620^{+0.000025}_{-0.000025}$	$1898.30430^{+0.00024}_{-0.00024}$	$5.879^{+0.099}_{-0.109}$	109620^{+280}_{-280}
203878683.1	2	$13.755986^{+0.000222}_{-0.000047}$	$1905.29513^{+0.00013}_{-0.00077}$	$6.8867^{+0.0118}_{-0.0082}$	111840^{+34}_{-36}
203878683.2	2	$13.752651^{+0.000087}_{-0.000087}$	$1899.63801^{+0.00026}_{-0.00027}$	$6.019^{+0.026}_{-0.027}$	9508^{+27}_{-27}
203919499.1	2	$30.28772^{+0.00015}_{-0.00015}$	$1919.323994^{+0.000077}_{-0.000077}$	$6.439^{+0.031}_{-0.039}$	48952^{+63}_{-62}
203919499.2	2	$30.28769^{+0.00016}_{-0.00012}$	$1895.23881^{+0.00013}_{-0.00015}$	$6.270^{+0.018}_{-0.022}$	43161^{+59}_{-74}
203929178.1	2	$2.307889^{+0.000010}_{-0.000011}$	$1895.88682^{+0.00013}_{-0.00012}$	$3.601^{+0.025}_{-0.036}$	63140^{+160}_{-160}
203929178.2	2	$2.307850^{+0.000012}_{-0.000012}$	$1894.73327^{+0.00014}_{-0.00014}$	$3.609^{+0.030}_{-0.041}$	55320^{+140}_{-140}

Table A.2: Our sample of eclipsing binaries from C0-8. (continued)

Binary	C#	Period (days)	t_0 (BJD - 2455000)	Duration (hours)	Depth (ppm)
203936580.1	2	$1.2075867^{+0.0000059}_{-0.0000059}$	$1894.36181^{+0.00023}_{-0.00024}$	$1.974^{+0.050}_{-0.050}$	3448^{+24}_{-24}
203936580.2	2	$1.207543^{+0.000018}_{-0.000018}$	$1894.96844^{+0.00070}_{-0.00069}$	$2.023^{+0.077}_{-0.083}$	1250^{+20}_{-20}
203942067.1	2	$3.2797645^{+0.0000024}_{-0.0000026}$	$1897.186949^{+0.000043}_{-0.000037}$	$4.0084^{+0.0096}_{-0.0106}$	151340^{+86}_{-89}
203942067.2	2	$3.2797943^{+0.0000011}_{-0.0000011}$	$1895.546698^{+0.000014}_{-0.000014}$	$4.0127^{+0.0080}_{-0.0094}$	145916^{+43}_{-43}
204043888.1	2	$2.972527^{+0.000013}_{-0.000013}$	$1897.16965^{+0.00020}_{-0.00021}$	$3.462^{+0.045}_{-0.060}$	74930^{+310}_{-270}
204043888.2	2	$2.972599^{+0.000020}_{-0.000020}$	$1895.68195^{+0.00029}_{-0.00028}$	$3.526^{+0.061}_{-0.059}$	58590^{+330}_{-330}
204073447.1	2	$3.2504135^{+0.0000015}_{-0.0000015}$	$1896.523203^{+0.000020}_{-0.000021}$	$2.896^{+0.011}_{-0.011}$	48072^{+35}_{-37}
204073447.2	2	$3.250425^{+0.000038}_{-0.000038}$	$1894.89821^{+0.00052}_{-0.00051}$	$2.837^{+0.058}_{-0.067}$	1522^{+19}_{-20}
204124270.1	2	$2.660090^{+0.000054}_{-0.000053}$	$1896.91434^{+0.00092}_{-0.00092}$	$1.553^{+0.086}_{-0.097}$	2876^{+86}_{-88}
204124270.2	2	$2.66003^{+0.00027}_{-0.00027}$	$1895.5921^{+0.0050}_{-0.0049}$	$10.72^{+0.41}_{-0.45}$	1461^{+35}_{-35}
204193529.1	2	$5.5019972^{+0.0000033}_{-0.0000033}$	$1894.424487^{+0.000029}_{-0.000028}$	$4.590^{+0.012}_{-0.010}$	167920^{+120}_{-130}
204193529.2	2	$5.501973^{+0.000037}_{-0.000037}$	$1897.17617^{+0.00028}_{-0.00028}$	$4.419^{+0.026}_{-0.028}$	8111^{+35}_{-35}
204275121.1	2	$2.1948429^{+0.0000017}_{-0.0000017}$	$1895.780882^{+0.000025}_{-0.000025}$	$5.774^{+0.015}_{-0.016}$	195070^{+150}_{-150}
204275121.2	2	$2.1948405^{+0.0000023}_{-0.0000019}$	$1894.683512^{+0.000048}_{-0.000059}$	$5.798^{+0.021}_{-0.022}$	166140^{+150}_{-140}
204312847.1	2	$24.193677^{+0.000017}_{-0.000017}$	$1906.329629^{+0.000021}_{-0.000022}$	$7.514^{+0.014}_{-0.014}$	107632^{+36}_{-35}
204321014.1	2	$3.7921333^{+0.0000015}_{-0.0000012}$	$1897.854084^{+0.000013}_{-0.000015}$	$4.635^{+0.010}_{-0.011}$	431170^{+210}_{-180}
204321014.2	2	$3.7921455^{+0.0000011}_{-0.0000011}$	$1895.957876^{+0.000014}_{-0.000014}$	$4.676^{+0.012}_{-0.011}$	363970^{+120}_{-120}
204407880.1	2	$34.367865^{+0.000061}_{-0.000062}$	$1917.712527^{+0.000044}_{-0.000043}$	$7.494^{+0.018}_{-0.019}$	103540^{+110}_{-110}
204407880.2	2	$34.36634^{+0.00034}_{-0.00034}$	$1908.00126^{+0.00023}_{-0.00023}$	$17.927^{+0.097}_{-0.105}$	33499^{+41}_{-41}
204470067.1	2	$1.8468865^{+0.0000025}_{-0.0000022}$	$1895.914005^{+0.000056}_{-0.000064}$	$2.420^{+0.022}_{-0.021}$	150340^{+380}_{-360}
204470067.2	2	$1.8468718^{+0.0000033}_{-0.0000033}$	$1894.990829^{+0.000078}_{-0.000079}$	$2.400^{+0.029}_{-0.032}$	48291^{+98}_{-97}
204531124.1	2	$3.4301763^{+0.0000042}_{-0.0000041}$	$1897.465037^{+0.000051}_{-0.000053}$	$2.269^{+0.013}_{-0.016}$	15783^{+21}_{-21}
204531124.2	2	$3.430163^{+0.000026}_{-0.000024}$	$1895.75173^{+0.00031}_{-0.00035}$	$2.295^{+0.054}_{-0.056}$	3632^{+27}_{-26}
204576757.1	2	$23.277594^{+0.000026}_{-0.000033}$	$1898.089720^{+0.000080}_{-0.000061}$	$4.720^{+0.032}_{-0.028}$	202080^{+140}_{-140}
204576757.2	2	$23.2778^{+0.0029}_{-0.0027}$	$1906.6176^{+0.0038}_{-0.0040}$	$2.77^{+0.33}_{-0.24}$	1262^{+81}_{-82}
204596569.1	2	$2.290608^{+0.000017}_{-0.000017}$	$1894.85106^{+0.00034}_{-0.00033}$	$2.195^{+0.069}_{-0.062}$	1795^{+15}_{-15}
204596569.2	2	$2.290609^{+0.000044}_{-0.000044}$	$1895.99515^{+0.00084}_{-0.00086}$	$2.114^{+0.080}_{-0.091}$	713^{+14}_{-14}
204643057.1	2	$3.381026^{+0.000089}_{-0.000090}$	$1895.7154^{+0.0011}_{-0.0011}$	$4.18^{+0.13}_{-0.16}$	3083^{+48}_{-49}
204643057.2	2	$3.38108^{+0.00019}_{-0.00019}$	$1897.4041^{+0.0025}_{-0.0025}$	$4.03^{+0.18}_{-0.19}$	1299^{+41}_{-39}
204649811.1	2	$5.2906412^{+0.0000069}_{-0.0000069}$	$1894.857298^{+0.000057}_{-0.000057}$	$2.765^{+0.029}_{-0.037}$	12890^{+22}_{-20}
204649811.2	2	$5.2906466^{+0.0000093}_{-0.0000093}$	$1897.512674^{+0.000081}_{-0.000078}$	$2.762^{+0.020}_{-0.029}$	12099^{+22}_{-20}
204748201.1	2	$7.3656839^{+0.0000087}_{-0.0000088}$	$1896.154520^{+0.000049}_{-0.000048}$	$4.747^{+0.028}_{-0.028}$	178640^{+240}_{-250}
204748201.2	2	$7.36565^{+0.00013}_{-0.00013}$	$1899.83753^{+0.00065}_{-0.00064}$	$4.459^{+0.042}_{-0.044}$	10479^{+90}_{-94}
204822463.1	2	$1.20857548^{+0.00000085}_{-0.00000082}$	$1894.648124^{+0.000034}_{-0.000036}$	$2.724^{+0.019}_{-0.023}$	467140^{+700}_{-670}
204822463.2	2	$1.2085761^{+0.0000018}_{-0.0000018}$	$1895.252800^{+0.000045}_{-0.000045}$	$2.805^{+0.027}_{-0.032}$	274770^{+590}_{-510}
204870619.1	2	$34.06856^{+0.00012}_{-0.00013}$	$1906.703852^{+0.000080}_{-0.000080}$	$10.722^{+0.017}_{-0.018}$	85161^{+73}_{-76}
204870619.2	2	$34.06895^{+0.00023}_{-0.00022}$	$1921.35892^{+0.00016}_{-0.00016}$	$16.441^{+0.027}_{-0.024}$	38935^{+36}_{-36}
204882444.1	2	$0.3829048^{+0.0000029}_{-0.0000029}$	$1894.60082^{+0.00035}_{-0.00035}$	$2.300^{+0.061}_{-0.054}$	69710^{+660}_{-660}

Table A.2: Our sample of eclipsing binaries from C0-8. (continued)

Binary	C#	Period (days)	t_0 (BJD - 2455000)	Duration (hours)	Depth (ppm)
204918110.1	2		$1944.862891^{+0.000081}_{-0.000080}$	$22.109^{+0.071}_{-0.072}$	120170^{+640}_{-740}
204942752.1	2	$4.960028^{+0.000035}_{-0.000036}$	$1896.56846^{+0.00031}_{-0.00032}$	$5.290^{+0.074}_{-0.081}$	8836^{+31}_{-31}
204942752.2	2	$4.960083^{+0.000051}_{-0.000050}$	$1899.04879^{+0.00041}_{-0.00041}$	$5.307^{+0.085}_{-0.084}$	7443^{+35}_{-34}
204971139.1	2	$34.5490^{+0.0028}_{-0.0030}$	$1917.6814^{+0.0026}_{-0.0024}$	$1.37^{+0.17}_{-0.39}$	2380^{+160}_{-160}
204971139.2	2	$34.5766^{+0.0011}_{-0.0011}$	$1900.3661^{+0.0014}_{-0.0014}$	$1.43^{+0.15}_{-0.27}$	1918^{+99}_{-106}
205000535.1	2		$1907.76926^{+0.00069}_{-0.00068}$	$20.157^{+0.049}_{-0.051}$	95910^{+190}_{-200}
205020466.1	2	$8.7589249^{+0.0000040}_{-0.0000040}$	$1900.968724^{+0.000024}_{-0.000021}$	$4.2115^{+0.0083}_{-0.0123}$	430700^{+1100}_{-1200}
205020466.2	2	$8.7589186^{+0.0000058}_{-0.0000056}$	$1895.054158^{+0.000030}_{-0.000030}$	$6.196^{+0.029}_{-0.035}$	387200^{+4000}_{-1300}
205030103.1	2	$34.00130^{+0.00053}_{-0.00053}$	$1909.25457^{+0.00037}_{-0.00038}$	$7.26^{+0.11}_{-0.12}$	64610^{+260}_{-260}
205050711.1	2	$8.598551^{+0.000027}_{-0.000026}$	$1894.95993^{+0.00012}_{-0.00012}$	$7.586^{+0.032}_{-0.046}$	30470^{+32}_{-32}
205050711.2	2	$8.598503^{+0.000033}_{-0.000030}$	$1899.28903^{+0.00013}_{-0.00014}$	$7.295^{+0.025}_{-0.030}$	28472^{+98}_{-157}
205068000.1	2	$0.6861368^{+0.0000039}_{-0.0000039}$	$1894.68296^{+0.00025}_{-0.00026}$	$1.625^{+0.046}_{-0.038}$	2021^{+17}_{-17}
205068000.2	2	$0.6861427^{+0.0000073}_{-0.0000073}$	$1894.33831^{+0.00049}_{-0.00049}$	$1.268^{+0.052}_{-0.057}$	815^{+19}_{-18}
205074878.1	2	$9.504802^{+0.000019}_{-0.000020}$	$1901.358887^{+0.000078}_{-0.000080}$	$2.562^{+0.034}_{-0.034}$	312900^{+1000}_{-1000}
205074878.2	2	$9.504766^{+0.000025}_{-0.000025}$	$1896.50710^{+0.00011}_{-0.00010}$	$2.633^{+0.040}_{-0.044}$	213880^{+620}_{-620}
205129673.1	2	$0.95524113^{+0.00000091}_{-0.00000091}$	$1894.591179^{+0.000044}_{-0.000044}$	$5.066^{+0.038}_{-0.028}$	554350^{+710}_{-730}
205129673.2	2	$0.9552335^{+0.0000053}_{-0.0000053}$	$1895.06987^{+0.00028}_{-0.00027}$	$5.764^{+0.031}_{-0.026}$	97030^{+270}_{-270}
205131464.1	2	$1.5547181^{+0.0000069}_{-0.0000070}$	$1895.85112^{+0.00020}_{-0.00020}$	$6.165^{+0.084}_{-0.092}$	152000^{+310}_{-300}
205145448.1	2	$16.632665^{+0.000032}_{-0.000033}$	$1902.267353^{+0.000096}_{-0.000092}$	$2.311^{+0.012}_{-0.017}$	42000^{+140}_{-130}
205170307.1	2		$1945.824144^{+0.000044}_{-0.000043}$	$11.496^{+0.028}_{-0.029}$	143077^{+91}_{-91}
205195789.1	2	$3.250001^{+0.000025}_{-0.000026}$	$1896.10144^{+0.00034}_{-0.00034}$	$4.501^{+0.019}_{-0.030}$	7885^{+36}_{-37}
205195789.2	2	$3.24992^{+0.00010}_{-0.00010}$	$1894.4773^{+0.0013}_{-0.0013}$	$4.48^{+0.11}_{-0.15}$	2875^{+50}_{-52}
205463986.1	2	$4.64809354^{+0.00000097}_{-0.00000095}$	$1895.9139650^{+0.0000097}_{-0.0000096}$	$4.0274^{+0.0066}_{-0.0064}$	156652^{+43}_{-41}
205463986.2	2	$4.6481000^{+0.0000015}_{-0.0000015}$	$1898.237841^{+0.000016}_{-0.000017}$	$4.0192^{+0.0077}_{-0.0073}$	155328^{+44}_{-41}
205483258.1	2	$11.33868^{+0.00039}_{-0.00048}$	$1901.7578^{+0.0013}_{-0.0012}$	$10.28^{+0.24}_{-0.22}$	124100^{+1300}_{-1200}
205483258.2	2	$11.30732^{+0.00052}_{-0.00049}$	$1896.1632^{+0.0016}_{-0.0016}$	$7.07^{+0.19}_{-0.20}$	61100^{+1500}_{-1700}
205485891.1	2	$15.5854527^{+0.0000046}_{-0.0000047}$	$1904.370518^{+0.000013}_{-0.000012}$	$7.326^{+0.010}_{-0.011}$	323717^{+46}_{-44}
205485891.2	2	$15.585456^{+0.000010}_{-0.000013}$	$1898.883224^{+0.000020}_{-0.000021}$	$6.526^{+0.017}_{-0.016}$	247580^{+83}_{-75}
205546169.1	2	$24.4358607^{+0.0000093}_{-0.0000094}$	$1909.7187906^{+0.0000096}_{-0.0000095}$	$4.7300^{+0.0046}_{-0.0057}$	236293^{+60}_{-62}
205546169.2	2	$24.43587^{+0.00019}_{-0.00019}$	$1916.19352^{+0.00024}_{-0.00024}$	$8.136^{+0.096}_{-0.081}$	12866^{+27}_{-27}
205554809.1	2	$4.0949247^{+0.0000028}_{-0.0000028}$	$1896.501872^{+0.000032}_{-0.000031}$	$3.967^{+0.012}_{-0.013}$	32139^{+26}_{-26}
205554809.2	2	$4.094910^{+0.000017}_{-0.000016}$	$1894.45480^{+0.00018}_{-0.00018}$	$4.056^{+0.058}_{-0.068}$	4034^{+11}_{-11}
205632508.1	2	$40.626^{+0.015}_{-0.465}$	$1931.4826^{+0.0043}_{-0.0046}$	$3.06^{+0.31}_{-0.40}$	1020^{+140}_{-160}
205632508.2	2	$38.327^{+0.028}_{-0.136}$	$1912.356^{+0.124}_{-0.027}$	$3.8^{+1.1}_{-1.5}$	920^{+120}_{-110}
205684800.1	2	$3.1141100^{+0.0000033}_{-0.0000033}$	$1897.403566^{+0.000047}_{-0.000048}$	$2.967^{+0.013}_{-0.017}$	20688^{+20}_{-19}
205684800.2	2	$3.1141213^{+0.0000039}_{-0.0000039}$	$1895.846553^{+0.000052}_{-0.000051}$	$2.983^{+0.018}_{-0.022}$	17859^{+21}_{-20}
205703649.1	2	$8.116823^{+0.000035}_{-0.000035}$	$1899.88939^{+0.00016}_{-0.00014}$	$7.459^{+0.022}_{-0.030}$	148730^{+150}_{-150}
205703649.2	2	$8.116803^{+0.000020}_{-0.000021}$	$1895.842595^{+0.000093}_{-0.000090}$	$7.496^{+0.023}_{-0.030}$	145140^{+150}_{-150}

Table A.2: Our sample of eclipsing binaries from C0-8. (continued)

Binary	C#	Period (days)	t_0 (BJD - 2455000)	Duration (hours)	Depth (ppm)
205934874.1	3	$1.2361310^{+0.0000023}_{-0.0000022}$	$1978.011830^{+0.000071}_{-0.000072}$	$2.029^{+0.033}_{-0.036}$	97250^{+250}_{-250}
205934874.2	3	$1.2361301^{+0.0000027}_{-0.0000026}$	$1977.394665^{+0.000079}_{-0.000075}$	$1.989^{+0.037}_{-0.056}$	76670^{+490}_{-290}
205936222.1	3		$1985.768653^{+0.000011}_{-0.000011}$	$5.8063^{+0.0075}_{-0.0091}$	313200^{+15700}_{-2900}
205947214.1	3	$54.16974^{+0.00030}_{-0.00030}$	$1983.71059^{+0.00019}_{-0.00019}$	$4.281^{+0.065}_{-0.067}$	138650^{+560}_{-610}
205962262.1	3	$0.8497635^{+0.0000016}_{-0.0000016}$	$1977.525586^{+0.000072}_{-0.000074}$	$2.805^{+0.020}_{-0.014}$	146360^{+330}_{-340}
205966706.1	3		$2017.785623^{+0.000094}_{-0.000150}$	$8.157^{+0.040}_{-0.053}$	49487^{+36}_{-31}
205968100.1	3	$0.5136389^{+0.0000052}_{-0.0000046}$	$1977.63585^{+0.00036}_{-0.00041}$	$3.141^{+0.077}_{-0.086}$	120800^{+1100}_{-1100}
205982900.1	3	$6.71607^{+0.00076}_{-0.00503}$	$1983.6359^{+0.0105}_{-0.0070}$	$0.58^{+0.23}_{-0.33}$	$143000^{+34000}_{-139000}$
205985357.1	3	$4.128299^{+0.000015}_{-0.000017}$	$1977.59925^{+0.00020}_{-0.00016}$	$7.382^{+0.019}_{-0.020}$	69060^{+110}_{-110}
205985357.2	3	$4.128392^{+0.000067}_{-0.000067}$	$1979.66261^{+0.00062}_{-0.00062}$	$7.150^{+0.042}_{-0.043}$	7298^{+42}_{-44}
205990339.1	3	$19.44217^{+0.00025}_{-0.00025}$	$1992.13620^{+0.00033}_{-0.00033}$	$2.356^{+0.062}_{-0.076}$	125300^{+1200}_{-1200}
205996447.1	3	$1.6006726^{+0.0000022}_{-0.0000022}$	$1977.690789^{+0.000055}_{-0.000054}$	$2.124^{+0.026}_{-0.029}$	114190^{+240}_{-230}
205996447.2	3	$1.6006503^{+0.0000030}_{-0.0000029}$	$1978.491970^{+0.000073}_{-0.000074}$	$2.049^{+0.023}_{-0.028}$	105200^{+400}_{-450}
206019504.1	3	$4.854893^{+0.000013}_{-0.000011}$	$1981.742931^{+0.000073}_{-0.000071}$	$2.337^{+0.029}_{-0.034}$	147390^{+940}_{-530}
206019504.2	3	$4.854924^{+0.000015}_{-0.000014}$	$1979.31558^{+0.00011}_{-0.00011}$	$2.270^{+0.034}_{-0.032}$	79330^{+290}_{-280}
206027655.2	3		$2007.7403^{+0.0027}_{-0.0026}$	$2.33^{+0.20}_{-0.23}$	1260^{+97}_{-102}
206027655.3	3	$41.1429^{+0.0053}_{-0.0094}$	$1987.3038^{+0.0083}_{-0.0036}$	$2.60^{+0.24}_{-0.28}$	778^{+93}_{-111}
206029242.1	3	$11.278478^{+0.000011}_{-0.000012}$	$1980.466380^{+0.000025}_{-0.000023}$	$0.0620^{+0.0011}_{-0.0016}$	121000^{+29000}_{-15000}
206029242.2	3	$11.2984^{+0.0021}_{-0.0021}$	$1986.0240^{+0.0054}_{-0.0053}$	$2.94^{+0.25}_{-0.31}$	191^{+18}_{-19}
206029314.1	3	$7.025987^{+0.000049}_{-0.000046}$	$1981.06818^{+0.00025}_{-0.00026}$	$5.962^{+0.038}_{-0.048}$	32610^{+1050}_{-950}
206029314.2	3	$7.02539^{+0.00049}_{-0.00048}$	$1977.5580^{+0.0027}_{-0.0027}$	$5.70^{+0.40}_{-0.25}$	1604^{+48}_{-50}
206038470.1	3	$1.8908167^{+0.0000052}_{-0.0000051}$	$1978.51551^{+0.00010}_{-0.00011}$	$1.464^{+0.032}_{-0.035}$	58560^{+480}_{-490}
206038470.2	3	$1.890785^{+0.000012}_{-0.000012}$	$1977.57077^{+0.00024}_{-0.00024}$	$1.513^{+0.046}_{-0.053}$	25490^{+260}_{-250}
206047297.1	3	$27.31459^{+0.00016}_{-0.00016}$	$1999.45575^{+0.00012}_{-0.00012}$	$5.641^{+0.042}_{-0.062}$	32201^{+48}_{-48}
206047297.2	3	$27.31469^{+0.00017}_{-0.00017}$	$1989.91660^{+0.00022}_{-0.00022}$	$5.635^{+0.069}_{-0.067}$	19847^{+54}_{-54}
206049222.1	3	$0.7032609^{+0.0000010}_{-0.0000120}$	$1977.548957^{+0.000064}_{-0.000044}$	$0.0143^{+0.0042}_{-0.0013}$	7590^{+570}_{-580}
206049222.2	3	$0.703999^{+0.000027}_{-0.000027}$	$1977.1681^{+0.0016}_{-0.0016}$	$4.25^{+0.16}_{-0.16}$	$435.3^{+7.8}_{-7.7}$
206060972.1	3	$29.76323^{+0.00036}_{-0.00039}$	$1990.19914^{+0.00031}_{-0.00027}$	$4.449^{+0.070}_{-0.069}$	30260^{+170}_{-170}
206060972.2	3	$29.76140^{+0.00025}_{-0.00026}$	$1982.62819^{+0.00028}_{-0.00026}$	$4.918^{+0.088}_{-0.096}$	22090^{+120}_{-150}
206066442.1	3	$1.0542998^{+0.0000022}_{-0.0000021}$	$1977.197030^{+0.000077}_{-0.000080}$	$2.198^{+0.033}_{-0.033}$	55200^{+140}_{-140}
206066909.1	3	$12.9371715^{+0.0000055}_{-0.0000056}$	$1982.070013^{+0.000016}_{-0.000015}$	$4.724^{+0.011}_{-0.012}$	251300^{+180}_{-100}
206066909.2	3	$12.937049^{+0.000038}_{-0.000046}$	$1978.016638^{+0.000079}_{-0.000079}$	$7.951^{+0.021}_{-0.023}$	39349^{+49}_{-75}
206075677.1	3	$31.027305^{+0.000052}_{-0.000051}$	$1987.229777^{+0.000044}_{-0.000044}$	$6.605^{+0.027}_{-0.029}$	281620^{+230}_{-230}
206075677.2	3	$31.02577^{+0.00081}_{-0.00079}$	$2004.87215^{+0.00055}_{-0.00057}$	$9.72^{+0.12}_{-0.15}$	7645^{+48}_{-45}
206094715.1	3	$0.5876242^{+0.0000015}_{-0.0000015}$	$1977.658359^{+0.000093}_{-0.000093}$	$2.137^{+0.036}_{-0.045}$	368600^{+3100}_{-3200}
206094715.2	3	$0.5876192^{+0.0000018}_{-0.0000018}$	$1977.36461^{+0.00012}_{-0.00012}$	$2.255^{+0.036}_{-0.028}$	307500^{+1500}_{-1400}
206109113.1	3	$1.323825^{+0.000022}_{-0.000021}$	$1978.15400^{+0.00056}_{-0.00055}$	$1.492^{+0.059}_{-0.072}$	4100^{+110}_{-120}
206109113.2	3	$1.323669^{+0.000052}_{-0.000052}$	$1977.4955^{+0.0014}_{-0.0014}$	$1.83^{+0.17}_{-0.11}$	1839^{+88}_{-85}

Table A.2: Our sample of eclipsing binaries from C0-8. (continued)

Binary	C#	Period (days)	t_0 (BJD - 2455000)	Duration (hours)	Depth (ppm)
206109641.1	3		$2011.1749999^{+0.0000071}_{-0.0000071}$	$10.340^{+0.018}_{-0.020}$	463000^{+180}_{-180}
206109641.2	3		$2018.872929^{+0.000016}_{-0.000016}$	$11.098^{+0.021}_{-0.024}$	367300^{+41200}_{-7700}
206134477.1	3	$4.2366202^{+0.0000016}_{-0.0000016}$	$1979.302368^{+0.000016}_{-0.000016}$	$7.336^{+0.012}_{-0.011}$	366390^{+490}_{-510}
206134477.2	3	$4.2365887^{+0.0000018}_{-0.0000019}$	$1977.184422^{+0.000020}_{-0.000020}$	$7.2581^{+0.0050}_{-0.0057}$	325740^{+270}_{-290}
206135075.1	3		$2037.843814^{+0.000038}_{-0.000038}$	$6.117^{+0.045}_{-0.039}$	69120^{+370}_{-360}
206135075.2	3		$1982.868137^{+0.000073}_{-0.000117}$	$5.574^{+0.012}_{-0.020}$	63450^{+51}_{-56}
206139574.1	3	$0.67304705^{+0.00000078}_{-0.00000078}$	$1977.711456^{+0.000045}_{-0.000046}$	$2.229^{+0.030}_{-0.025}$	211240^{+460}_{-420}
206139574.2	3	$0.6730552^{+0.0000051}_{-0.0000052}$	$1977.37384^{+0.00032}_{-0.00032}$	$2.081^{+0.059}_{-0.069}$	32090^{+480}_{-530}
206143957.1	3	$4.2475214^{+0.0000013}_{-0.0000013}$	$1979.210393^{+0.000015}_{-0.000016}$	$5.7738^{+0.0055}_{-0.0060}$	272780^{+160}_{-110}
206143957.2	3	$4.2475222^{+0.0000015}_{-0.0000015}$	$1981.334291^{+0.000013}_{-0.000013}$	$5.7795^{+0.0093}_{-0.0104}$	266330^{+140}_{-150}
206159239.1	3	$1.848838^{+0.000013}_{-0.000013}$	$1977.88864^{+0.00027}_{-0.00027}$	$2.159^{+0.042}_{-0.034}$	26590^{+160}_{-160}
206159239.2	3	$1.848770^{+0.000024}_{-0.000023}$	$1978.81355^{+0.00037}_{-0.00039}$	$2.348^{+0.054}_{-0.045}$	22260^{+200}_{-190}
206173295.1	3	$2.1757810^{+0.0000040}_{-0.0000041}$	$1978.607178^{+0.000096}_{-0.000088}$	$2.584^{+0.030}_{-0.029}$	30533^{+110}_{-99}
206173295.2	3	$2.175806^{+0.000020}_{-0.000021}$	$1977.51861^{+0.00036}_{-0.00036}$	$2.588^{+0.068}_{-0.063}$	3868^{+30}_{-30}
206187484.1	3	$3.6510341^{+0.0000020}_{-0.0000020}$	$1979.481460^{+0.000020}_{-0.000020}$	$3.5700^{+0.0052}_{-0.0076}$	139160^{+50}_{-45}
206187484.2	3	$3.651032^{+0.000010}_{-0.000010}$	$1977.65644^{+0.00011}_{-0.00011}$	$3.601^{+0.045}_{-0.041}$	9515^{+29}_{-26}
206212261.1	3	$30.985158^{+0.000087}_{-0.000087}$	$1995.031657^{+0.000061}_{-0.000061}$	$12.424^{+0.017}_{-0.017}$	98470^{+53}_{-53}
206212261.2	3	$30.98804^{+0.00023}_{-0.00023}$	$1980.30583^{+0.00031}_{-0.00031}$	$10.362^{+0.021}_{-0.021}$	15511^{+29}_{-30}
206226010.1	3	$6.914995^{+0.000010}_{-0.000010}$	$1983.409141^{+0.000057}_{-0.000055}$	$3.567^{+0.018}_{-0.024}$	57851^{+93}_{-92}
206226010.2	3	$6.914973^{+0.000040}_{-0.000040}$	$1978.74448^{+0.00022}_{-0.00022}$	$3.557^{+0.050}_{-0.055}$	8746^{+34}_{-34}
206241558.1	3		$1993.262272^{+0.000016}_{-0.000016}$	$7.256^{+0.031}_{-0.037}$	280380^{+100}_{-100}
206241558.2	3		$2005.59227^{+0.00014}_{-0.00014}$	$10.274^{+0.067}_{-0.103}$	53690^{+82}_{-81}
206253908.1	3		$1983.658486^{+0.000033}_{-0.000032}$	$6.720^{+0.036}_{-0.036}$	92860^{+130}_{-120}
206260730.1	3	$4.121531^{+0.000038}_{-0.000059}$	$1979.62253^{+0.00023}_{-0.00019}$	$5.894^{+0.070}_{-0.070}$	786200^{+2300}_{-2100}
206260730.2	3	$4.117108^{+0.000046}_{-0.000044}$	$1977.5473^{+0.0016}_{-0.0013}$	$5.279^{+0.081}_{-0.072}$	545000^{+16000}_{-15000}
206268154.1	3	$1.081042^{+0.000015}_{-0.000014}$	$1977.80272^{+0.00015}_{-0.00016}$	$4.928^{+0.032}_{-0.024}$	355700^{+1000}_{-1000}
206288770.1	3	$24.756458^{+0.000011}_{-0.000011}$	$1993.039680^{+0.000014}_{-0.000014}$	$5.9151^{+0.0091}_{-0.0095}$	188298^{+53}_{-53}
206288770.2	3	$24.75624^{+0.00020}_{-0.00020}$	$1985.10660^{+0.00026}_{-0.00026}$	$8.360^{+0.035}_{-0.037}$	13567^{+35}_{-35}
206311743.1	3	$8.624578^{+0.000060}_{-0.000057}$	$1979.41978^{+0.00022}_{-0.00020}$	$7.746^{+0.044}_{-0.069}$	43760^{+130}_{-140}
206311743.2	3	$8.625539^{+0.000073}_{-0.000094}$	$1983.72657^{+0.00046}_{-0.00034}$	$7.577^{+0.053}_{-0.069}$	39270^{+100}_{-110}
206314138.1	3	$2.0750990^{+0.0000028}_{-0.0000028}$	$1978.923002^{+0.000054}_{-0.000054}$	$3.167^{+0.029}_{-0.032}$	33126^{+47}_{-46}
206314138.2	3	$2.0750918^{+0.0000067}_{-0.0000066}$	$1977.88579^{+0.00012}_{-0.00012}$	$3.169^{+0.043}_{-0.051}$	13160^{+36}_{-35}
206357270.1	3		$2044.37^{+0.12}_{-0.12}$	$3.6^{+2.6}_{-3.8}$	$968000^{+564000}_{-32000}$
206380678.1	3	$4.540479^{+0.000064}_{-0.000070}$	$1978.01069^{+0.00057}_{-0.00057}$	$2.204^{+0.068}_{-0.075}$	6280^{+170}_{-100}
206380678.2	3	$4.540298^{+0.000083}_{-0.000085}$	$1980.28218^{+0.00068}_{-0.00067}$	$2.418^{+0.083}_{-0.085}$	3491^{+58}_{-59}
206412289.1	3	$3.3068317^{+0.0000050}_{-0.0000046}$	$1978.482064^{+0.000056}_{-0.000061}$	$2.710^{+0.018}_{-0.025}$	187720^{+400}_{-400}
206412289.2	3	$3.3068232^{+0.0000059}_{-0.0000059}$	$1980.135756^{+0.000058}_{-0.000060}$	$2.765^{+0.031}_{-0.034}$	125860^{+210}_{-200}
206433263.1	3	$21.1938344^{+0.0000103}_{-0.0000097}$	$1981.377819^{+0.000014}_{-0.000014}$	$10.503^{+0.011}_{-0.011}$	253482^{+48}_{-48}

Table A.2: Our sample of eclipsing binaries from C0-8. (continued)

Binary	C#	Period (days)	t_0 (BJD - 2455000)	Duration (hours)	Depth (ppm)
206433263.2	3	$21.193835^{+0.000020}_{-0.000023}$	$1991.584198^{+0.000019}_{-0.000019}$	$8.765^{+0.016}_{-0.018}$	165370^{+190}_{-160}
206474395.1	3	$2.1979393^{+0.0000057}_{-0.0000067}$	$1977.48190^{+0.00015}_{-0.00012}$	$2.1458^{+0.0099}_{-0.0141}$	156660^{+860}_{-770}
206474395.2	3	$2.197942^{+0.000022}_{-0.000022}$	$1978.58147^{+0.00038}_{-0.00038}$	$2.366^{+0.069}_{-0.079}$	25010^{+310}_{-310}
206477939.1	3	$2.6856625^{+0.0000055}_{-0.0000037}$	$1977.852929^{+0.000061}_{-0.000113}$	$2.108^{+0.021}_{-0.029}$	63010^{+160}_{-130}
206477939.2	3	$2.6856363^{+0.0000056}_{-0.0000060}$	$1979.196086^{+0.000056}_{-0.000051}$	$2.117^{+0.032}_{-0.043}$	43520^{+140}_{-180}
206489474.1	3	$1.5171994^{+0.0000033}_{-0.0000034}$	$1977.878414^{+0.000100}_{-0.000096}$	$2.055^{+0.031}_{-0.034}$	74160^{+250}_{-230}
206489474.2	3	$1.5172062^{+0.0000050}_{-0.0000051}$	$1978.63667^{+0.00014}_{-0.00014}$	$2.099^{+0.048}_{-0.044}$	31660^{+200}_{-190}
206500801.1	3	$8.155253^{+0.000021}_{-0.000021}$	$1977.20742^{+0.00011}_{-0.00010}$	$4.730^{+0.018}_{-0.019}$	25129^{+37}_{-39}
206500801.2	3	$8.15515^{+0.00063}_{-0.00062}$	$1981.4536^{+0.0024}_{-0.0025}$	$4.85^{+0.30}_{-0.21}$	721^{+22}_{-23}
206532093.1	3	$4.4043451^{+0.0000031}_{-0.0000026}$	$1977.386402^{+0.000024}_{-0.000026}$	$6.3502^{+0.0055}_{-0.0075}$	296030^{+140}_{-140}
206532093.2	3	$4.4043865^{+0.0000017}_{-0.0000016}$	$1979.588185^{+0.000016}_{-0.000017}$	$6.353^{+0.011}_{-0.011}$	290050^{+160}_{-160}
206543223.1	3	$17.812982^{+0.000022}_{-0.000022}$	$1988.772099^{+0.000042}_{-0.000042}$	$3.204^{+0.022}_{-0.027}$	51550^{+47}_{-47}
210375290.1	4	$2.41773063^{+0.00000072}_{-0.00000072}$	$2063.884185^{+0.000012}_{-0.000011}$	$4.3790^{+0.0058}_{-0.0060}$	134718^{+47}_{-51}
210375290.2	4	$2.4177650^{+0.0000088}_{-0.0000089}$	$2062.67510^{+0.00016}_{-0.00016}$	$4.2147^{+0.0074}_{-0.0073}$	11475^{+18}_{-19}
210386880.1	4	$7.2143392^{+0.0000022}_{-0.0000019}$	$2068.9575591^{+0.0000078}_{-0.0000075}$	$3.566^{+0.011}_{-0.011}$	327798^{+99}_{-81}
210386883.1	4	$7.2143591^{+0.0000013}_{-0.0000013}$	$2068.9575922^{+0.0000070}_{-0.0000068}$	$3.5432^{+0.0063}_{-0.0086}$	324630^{+260}_{-240}
210389383.1	4	$14.087122^{+0.000037}_{-0.000037}$	$2069.772722^{+0.000092}_{-0.000090}$	$6.3166^{+0.0096}_{-0.0098}$	29768^{+39}_{-39}
210389383.2	4	$14.08684^{+0.00085}_{-0.00084}$	$2065.6810^{+0.0021}_{-0.0021}$	$7.54^{+0.20}_{-0.19}$	1100^{+21}_{-21}
210391114.1	4	$29.205627^{+0.000025}_{-0.000024}$	$2072.978538^{+0.000029}_{-0.000031}$	$5.251^{+0.016}_{-0.019}$	177827^{+102}_{-94}
210391114.2	4	$29.20534^{+0.00020}_{-0.00020}$	$2081.00839^{+0.00014}_{-0.00014}$	$5.523^{+0.050}_{-0.066}$	23207^{+47}_{-47}
210404228.1	4	$1.1200568^{+0.0000015}_{-0.0000015}$	$2062.912116^{+0.000041}_{-0.000042}$	$3.532^{+0.023}_{-0.017}$	66928^{+86}_{-85}
210404228.2	4	$1.1200401^{+0.0000016}_{-0.0000016}$	$2062.352859^{+0.000056}_{-0.000056}$	$3.510^{+0.021}_{-0.014}$	54208^{+93}_{-94}
210414957.1	4	$1.9398901^{+0.0000082}_{-0.0000082}$	$2063.16225^{+0.00016}_{-0.00016}$	$2.541^{+0.036}_{-0.028}$	5995^{+22}_{-22}
210414957.2	4	$1.9398986^{+0.0000094}_{-0.0000095}$	$2062.19177^{+0.00019}_{-0.00019}$	$2.542^{+0.046}_{-0.038}$	5381^{+24}_{-24}
210434247.1	4	$0.45383039^{+0.00000098}_{-0.00000099}$	$2061.830713^{+0.000078}_{-0.000078}$	$1.261^{+0.019}_{-0.019}$	6785^{+61}_{-58}
210434247.2	4	$0.4538395^{+0.0000024}_{-0.0000024}$	$2062.05775^{+0.00022}_{-0.00022}$	$1.936^{+0.026}_{-0.022}$	2491^{+14}_{-14}
210467408.1	4	$2.80865070^{+0.00000054}_{-0.00000055}$	$2062.8051302^{+0.0000056}_{-0.0000057}$	$5.0724^{+0.0054}_{-0.0048}$	326540^{+110}_{-120}
210467408.2	4	$2.80865096^{+0.00000042}_{-0.00000043}$	$2064.2094612^{+0.0000050}_{-0.0000048}$	$5.0153^{+0.0039}_{-0.0042}$	287751^{+90}_{-90}
210470747.1	4	$4.4296761^{+0.0000021}_{-0.0000025}$	$2065.043611^{+0.000012}_{-0.000011}$	$6.002^{+0.011}_{-0.012}$	396220^{+160}_{-160}
210470747.2	4	$4.4296696^{+0.0000014}_{-0.0000014}$	$2062.849737^{+0.000010}_{-0.000010}$	$5.8779^{+0.0043}_{-0.0058}$	293070^{+790}_{-1290}
210472483.1	4	$2.2856899^{+0.0000054}_{-0.0000055}$	$2063.453029^{+0.000098}_{-0.000096}$	$5.098^{+0.025}_{-0.028}$	53160^{+63}_{-63}
210472483.2	4	$2.2856831^{+0.0000063}_{-0.0000063}$	$2062.310918^{+0.000096}_{-0.000098}$	$5.212^{+0.043}_{-0.046}$	45499^{+56}_{-56}
210475773.1	4	$2.7357538^{+0.0000014}_{-0.0000014}$	$2063.631616^{+0.000018}_{-0.000019}$	$6.757^{+0.014}_{-0.012}$	197975^{+80}_{-76}
210475773.2	4	$2.7357455^{+0.0000016}_{-0.0000016}$	$2062.264016^{+0.000026}_{-0.000027}$	$6.6677^{+0.0056}_{-0.0051}$	150468^{+60}_{-60}
210476794.1	4	$2.6000989^{+0.0000047}_{-0.0000046}$	$2064.265435^{+0.000071}_{-0.000071}$	$5.610^{+0.015}_{-0.014}$	53578^{+53}_{-53}
210476794.2	4	$2.600120^{+0.000020}_{-0.000020}$	$2062.96542^{+0.00031}_{-0.00031}$	$5.505^{+0.022}_{-0.023}$	9000^{+32}_{-33}
210512162.1	4	$4.1103601^{+0.0000072}_{-0.0000071}$	$2064.402990^{+0.000059}_{-0.000058}$	$5.095^{+0.024}_{-0.027}$	100274^{+98}_{-104}
210512162.2	4	$4.110407^{+0.000031}_{-0.000010}$	$2062.305072^{+0.000091}_{-0.000259}$	$5.0419^{+0.0089}_{-0.0117}$	90644^{+2553}_{-94}

Table A.2: Our sample of eclipsing binaries from C0-8. (continued)

Binary	C#	Period (days)	t_0 (BJD - 2455000)	Duration (hours)	Depth (ppm)
210513446.1	4	$2.2979877^{+0.0000037}_{-0.0000037}$	$2062.420767^{+0.000061}_{-0.000061}$	$2.241^{+0.017}_{-0.012}$	27693^{+48}_{-48}
210513446.2	4	$2.2979817^{+0.0000034}_{-0.0000033}$	$2063.569553^{+0.000057}_{-0.000058}$	$2.243^{+0.019}_{-0.014}$	26254^{+39}_{-38}
210522228.1	4	$10.8114200^{+0.0000099}_{-0.0000098}$	$2063.894125^{+0.000036}_{-0.000036}$	$6.5766^{+0.0035}_{-0.0034}$	121788^{+50}_{-50}
210530173.1	4		$2099.303870^{+0.000016}_{-0.000016}$	$4.2492^{+0.0097}_{-0.0130}$	147643^{+66}_{-65}
210530173.2	4	$37.687066^{+0.000043}_{-0.000044}$	$2080.460090^{+0.000018}_{-0.000018}$	$4.2413^{+0.0082}_{-0.0117}$	145359^{+78}_{-81}
210562330.1	4	$42.7629802^{+0.0000085}_{-0.0000084}$	$2071.044896^{+0.000013}_{-0.000012}$	$3.019^{+0.014}_{-0.018}$	327356^{+220}_{-94}
210562330.2	4		$2092.426320^{+0.000023}_{-0.000020}$	$3.107^{+0.024}_{-0.038}$	324340^{+140}_{-160}
210574135.1	4	$1.858241^{+0.000018}_{-0.000017}$	$2061.86247^{+0.00014}_{-0.00014}$	$4.672^{+0.064}_{-0.052}$	301000^{+1100}_{-1000}
210574135.2	4	$1.859404^{+0.000023}_{-0.000025}$	$2062.78488^{+0.00023}_{-0.00019}$	$4.631^{+0.075}_{-0.062}$	295100^{+1900}_{-1700}
210576234.1	4	$15.973411^{+0.000035}_{-0.000033}$	$2071.681846^{+0.000065}_{-0.000070}$	$5.390^{+0.023}_{-0.029}$	30581^{+24}_{-24}
210576234.2	4	$15.973380^{+0.000034}_{-0.000033}$	$2062.151045^{+0.000079}_{-0.000080}$	$4.044^{+0.045}_{-0.036}$	16965^{+22}_{-22}
210609071.1	4	$2.4171583^{+0.0000067}_{-0.0000068}$	$2062.40149^{+0.00011}_{-0.00011}$	$1.208^{+0.029}_{-0.033}$	51750^{+550}_{-420}
210622523.1	4	$3.614059^{+0.000012}_{-0.000012}$	$2062.42217^{+0.00014}_{-0.00014}$	$2.574^{+0.050}_{-0.070}$	332900^{+2000}_{-2000}
210622523.2	4	$3.614026^{+0.000047}_{-0.000047}$	$2064.22975^{+0.00047}_{-0.00047}$	$2.568^{+0.061}_{-0.067}$	84700^{+1200}_{-1200}
210642322.1	4	$4.339154^{+0.000032}_{-0.000037}$	$2064.54315^{+0.00023}_{-0.00022}$	$1.495^{+0.050}_{-0.055}$	334400^{+6100}_{-9100}
210642322.2	4	$4.339146^{+0.000068}_{-0.000063}$	$2062.37455^{+0.00066}_{-0.00071}$	$1.162^{+0.073}_{-0.102}$	101400^{+5300}_{-6700}
210654881.1	4	$12.1619238^{+0.0000099}_{-0.0000097}$	$2064.015191^{+0.000029}_{-0.000029}$	$5.812^{+0.022}_{-0.024}$	132593^{+61}_{-62}
210654881.2	4	$12.161902^{+0.000017}_{-0.000017}$	$2068.360570^{+0.000051}_{-0.000049}$	$6.344^{+0.026}_{-0.031}$	72345^{+52}_{-51}
210668314.1	4	$15.5762840^{+0.0000071}_{-0.0000072}$	$2068.016051^{+0.000017}_{-0.000017}$	$3.481^{+0.017}_{-0.027}$	196240^{+190}_{-180}
210668314.2	4	$15.57624^{+0.00014}_{-0.00014}$	$2074.67933^{+0.00026}_{-0.00026}$	$5.180^{+0.048}_{-0.062}$	12366^{+42}_{-41}
210673168.1	4		$2123.06804^{+0.00039}_{-0.00036}$	$5.28^{+0.15}_{-0.23}$	352800^{+2600}_{-2100}
210734262.1	4	$9.637313^{+0.000053}_{-0.000053}$	$2062.49055^{+0.00023}_{-0.00023}$	$3.454^{+0.088}_{-0.091}$	277300^{+2100}_{-1800}
210734262.2	4	$9.637604^{+0.000080}_{-0.000080}$	$2067.05305^{+0.00028}_{-0.00028}$	$3.450^{+0.082}_{-0.089}$	184500^{+1000}_{-1000}
210740200.1	4	$6.7889906^{+0.0000034}_{-0.0000037}$	$2064.748083^{+0.000015}_{-0.000015}$	$4.944^{+0.011}_{-0.014}$	256119^{+80}_{-70}
210740200.2	4	$6.7889737^{+0.0000091}_{-0.0000089}$	$2068.142911^{+0.000053}_{-0.000052}$	$4.943^{+0.013}_{-0.014}$	84544^{+50}_{-51}
210742688.1	4	$11.407663^{+0.000082}_{-0.000082}$	$2072.20850^{+0.00025}_{-0.00024}$	$4.321^{+0.068}_{-0.057}$	13231^{+79}_{-82}
210742688.2	4	$11.40754^{+0.00013}_{-0.00013}$	$2067.10980^{+0.00041}_{-0.00040}$	$4.938^{+0.070}_{-0.056}$	9752^{+47}_{-47}
210750052.1	4	$4.621256^{+0.000014}_{-0.000014}$	$2062.02559^{+0.00012}_{-0.00012}$	$4.531^{+0.057}_{-0.047}$	22748^{+38}_{-38}
210750052.2	4	$4.621172^{+0.000036}_{-0.000035}$	$2064.57183^{+0.00027}_{-0.00027}$	$4.166^{+0.081}_{-0.077}$	10214^{+40}_{-40}
210754505.1	4	$1.741355^{+0.000021}_{-0.000021}$	$2063.15049^{+0.00042}_{-0.00042}$	$1.696^{+0.048}_{-0.059}$	2293^{+32}_{-31}
210754505.2	4	$1.741365^{+0.000023}_{-0.000023}$	$2062.27957^{+0.00052}_{-0.00053}$	$1.682^{+0.052}_{-0.065}$	1693^{+30}_{-29}
210754756.1	4	$0.7394927^{+0.0000015}_{-0.0000015}$	$2062.466879^{+0.000080}_{-0.000080}$	$1.840^{+0.017}_{-0.013}$	11610^{+28}_{-28}
210754756.2	4	$0.7394943^{+0.0000028}_{-0.0000029}$	$2062.09641^{+0.00016}_{-0.00015}$	$1.999^{+0.021}_{-0.017}$	6076^{+27}_{-26}
210760314.1	4		$2081.15421^{+0.00033}_{-0.00033}$	$8.95^{+0.14}_{-0.16}$	283000^{+1300}_{-1300}
210766835.1	4	$24.78153^{+0.00018}_{-0.00016}$	$2082.15357^{+0.00026}_{-0.00032}$	$13.033^{+0.066}_{-0.087}$	108830^{+120}_{-110}
210766835.2	4	$24.77952^{+0.00031}_{-0.00029}$	$2070.77059^{+0.00023}_{-0.00023}$	$11.899^{+0.054}_{-0.063}$	35389^{+77}_{-76}
210779706.1	4	$31.478810^{+0.000039}_{-0.000038}$	$2082.265674^{+0.000024}_{-0.000024}$	$5.987^{+0.013}_{-0.018}$	219000^{+14000}_{-10000}
210780851.1	4	$15.779873^{+0.000033}_{-0.000033}$	$2065.381151^{+0.000086}_{-0.000086}$	$6.1284^{+0.0086}_{-0.0086}$	17445^{+24}_{-24}

Table A.2: Our sample of eclipsing binaries from C0-8. (continued)

Binary	C#	Period (days)	t_0 (BJD - 2455000)	Duration (hours)	Depth (ppm)
210780851.2	4	$15.7829^{+0.0020}_{-0.0020}$	$2073.5438^{+0.0038}_{-0.0037}$	$6.01^{+0.19}_{-0.31}$	326^{+13}_{-14}
210784039.1	4	$3.5129702^{+0.0000027}_{-0.0000026}$	$2061.844936^{+0.000031}_{-0.000033}$	$4.824^{+0.013}_{-0.015}$	54266^{+26}_{-26}
210784039.2	4	$3.512983^{+0.000021}_{-0.000020}$	$2063.69965^{+0.00024}_{-0.00024}$	$4.793^{+0.054}_{-0.054}$	7431^{+25}_{-25}
210786891.1	4	$1.717181^{+0.000011}_{-0.000011}$	$2061.90003^{+0.00017}_{-0.00016}$	$5.563^{+0.045}_{-0.060}$	309490^{+930}_{-1090}
210789323.1	4	$29.126677^{+0.000028}_{-0.000027}$	$2073.719754^{+0.000037}_{-0.000037}$	$2.463^{+0.016}_{-0.022}$	74911^{+89}_{-87}
210793743.1	4	$2.2719069^{+0.0000021}_{-0.0000020}$	$2064.088833^{+0.000027}_{-0.000028}$	$2.412^{+0.011}_{-0.013}$	224130^{+210}_{-200}
210793743.2	4	$2.2718895^{+0.0000018}_{-0.0000019}$	$2062.952857^{+0.000034}_{-0.000033}$	$2.467^{+0.018}_{-0.024}$	207470^{+180}_{-180}
210821360.1	4	$0.73365566^{+0.00000040}_{-0.00000041}$	$2061.861460^{+0.000024}_{-0.000024}$	$1.612^{+0.032}_{-0.036}$	445300^{+2600}_{-2600}
210822691.1	4	$8.0746441^{+0.0000023}_{-0.0000024}$	$2064.1602087^{+0.0000098}_{-0.0000089}$	$6.0264^{+0.0073}_{-0.0076}$	294769^{+96}_{-89}
210822691.2	4	$8.0746092^{+0.0000033}_{-0.0000036}$	$2068.234898^{+0.000012}_{-0.000011}$	$5.6859^{+0.0032}_{-0.0033}$	246072^{+53}_{-54}
210823406.1	4		$2090.35510^{+0.00016}_{-0.00016}$	$6.05^{+0.10}_{-0.12}$	168750^{+540}_{-530}
210837460.1	4	$5.404212^{+0.000049}_{-0.000021}$	$2063.85563^{+0.00016}_{-0.00046}$	$3.416^{+0.039}_{-0.041}$	22803^{+73}_{-73}
210837460.2	4	$5.404106^{+0.000014}_{-0.000014}$	$2066.613081^{+0.000096}_{-0.000096}$	$3.390^{+0.044}_{-0.045}$	14433^{+28}_{-28}
210857749.1	4		$2084.981939^{+0.000031}_{-0.000031}$	$13.925^{+0.022}_{-0.023}$	179804^{+62}_{-62}
210865148.1	4	$6.481618^{+0.000077}_{-0.000078}$	$2064.83348^{+0.00045}_{-0.00046}$	$7.98^{+0.10}_{-0.11}$	127550^{+440}_{-440}
210865148.2	4	$6.481683^{+0.000098}_{-0.000100}$	$2068.06520^{+0.00054}_{-0.00053}$	$8.13^{+0.13}_{-0.14}$	116180^{+540}_{-510}
210879084.1	4	$31.50585^{+0.00013}_{-0.00013}$	$2074.345111^{+0.000091}_{-0.000092}$	$10.737^{+0.045}_{-0.050}$	121690^{+430}_{-340}
210879084.2	4	$31.50602^{+0.00012}_{-0.00012}$	$2070.114384^{+0.000079}_{-0.000080}$	$9.362^{+0.037}_{-0.042}$	122770^{+130}_{-140}
210903662.1	4	$4.820539^{+0.000018}_{-0.000018}$	$2065.83899^{+0.00014}_{-0.00014}$	$2.031^{+0.033}_{-0.039}$	6256^{+27}_{-26}
210903662.2	4	$4.820516^{+0.000015}_{-0.000015}$	$2063.42883^{+0.00012}_{-0.00012}$	$2.082^{+0.037}_{-0.038}$	5874^{+23}_{-22}
210941737.1	4	$1.1543198^{+0.0000022}_{-0.0000022}$	$2062.861122^{+0.000075}_{-0.000076}$	$1.402^{+0.030}_{-0.031}$	119800^{+580}_{-600}
210958990.1	4	$1.7023428^{+0.0000015}_{-0.0000015}$	$2062.377370^{+0.000036}_{-0.000036}$	$2.6139^{+0.0056}_{-0.0064}$	22715^{+31}_{-30}
210958990.2	4	$1.702129^{+0.000041}_{-0.000041}$	$2063.23295^{+0.00093}_{-0.00093}$	$2.414^{+0.066}_{-0.090}$	662^{+14}_{-14}
210960936.1	4	$1.4311072^{+0.0000018}_{-0.0000019}$	$2062.247641^{+0.000047}_{-0.000047}$	$4.052^{+0.025}_{-0.018}$	191290^{+280}_{-260}
210960936.2	4	$1.4311160^{+0.0000041}_{-0.0000040}$	$2062.96328^{+0.00011}_{-0.00012}$	$3.862^{+0.018}_{-0.022}$	44560^{+100}_{-100}
210961385.1	4	$2.8171889^{+0.0000077}_{-0.0000081}$	$2062.973603^{+0.000080}_{-0.000081}$	$2.432^{+0.030}_{-0.024}$	244180^{+710}_{-670}
210961385.2	4	$2.817134^{+0.000010}_{-0.000011}$	$2064.38537^{+0.00017}_{-0.00015}$	$2.458^{+0.044}_{-0.038}$	164090^{+1840}_{-990}
210965800.5	4		$2096.901^{+0.016}_{-0.017}$	$37.8^{+2.1}_{-3.0}$	903^{+40}_{-41}
210965800.6	4	$60.5771^{+0.0047}_{-0.0054}$	$2066.1451^{+0.0030}_{-0.0031}$	$4.95^{+0.26}_{-0.37}$	584^{+31}_{-33}
211000135.1	4	$1.8175230^{+0.0000043}_{-0.0000042}$	$2062.436162^{+0.000095}_{-0.000096}$	$4.111^{+0.046}_{-0.042}$	58868^{+104}_{-100}
211000135.2	4	$1.817530^{+0.000010}_{-0.000010}$	$2063.34524^{+0.00023}_{-0.00023}$	$4.107^{+0.063}_{-0.060}$	23859^{+78}_{-76}
211009047.1	4	$2.639890^{+0.000017}_{-0.000017}$	$2062.29961^{+0.00026}_{-0.00026}$	$2.013^{+0.056}_{-0.053}$	2595^{+20}_{-20}
211009047.2	4	$2.639892^{+0.000021}_{-0.000021}$	$2063.61911^{+0.00032}_{-0.00032}$	$2.082^{+0.064}_{-0.069}$	2152^{+20}_{-20}
211012889.1	4	$1.739225^{+0.000012}_{-0.000013}$	$2062.81874^{+0.00030}_{-0.00029}$	$1.528^{+0.046}_{-0.051}$	12460^{+320}_{-230}
211012889.2	4	$1.739196^{+0.000029}_{-0.000028}$	$2061.94932^{+0.00072}_{-0.00073}$	$1.30^{+0.12}_{-0.19}$	5030^{+180}_{-200}
211015722.1	4	$2.18384898^{+0.00000102}_{-0.00000091}$	$2063.290982^{+0.000016}_{-0.000017}$	$3.4271^{+0.0072}_{-0.0088}$	157120^{+130}_{-120}
211015722.2	4	$2.1838539^{+0.0000058}_{-0.0000057}$	$2062.19935^{+0.00010}_{-0.00010}$	$3.297^{+0.010}_{-0.011}$	12754^{+31}_{-32}
211041532.1	4	$17.383700^{+0.000025}_{-0.000027}$	$2075.388769^{+0.000056}_{-0.000051}$	$5.783^{+0.036}_{-0.045}$	48059^{+38}_{-32}

Table A.2: Our sample of eclipsing binaries from C0-8. (continued)

Binary	C#	Period (days)	t_0 (BJD - 2455000)	Duration (hours)	Depth (ppm)
211041532.2	4	$17.38359^{+0.00017}_{-0.00018}$	$2070.66832^{+0.00033}_{-0.00032}$	$5.400^{+0.100}_{-0.092}$	5254^{+24}_{-22}
211093684.1	4	$7.050515^{+0.000014}_{-0.000013}$	$2064.717930^{+0.000069}_{-0.000068}$	$2.412^{+0.030}_{-0.030}$	52240^{+230}_{-590}
211093684.2	4	$7.050272^{+0.000075}_{-0.000073}$	$2068.24397^{+0.00030}_{-0.00031}$	$2.281^{+0.052}_{-0.067}$	3960^{+35}_{-33}
211099781.1	4	$7.563996^{+0.000016}_{-0.000016}$	$2064.473396^{+0.000084}_{-0.000084}$	$6.6744^{+0.0081}_{-0.0082}$	18989^{+21}_{-21}
211099781.2	4	$7.56366^{+0.00041}_{-0.00041}$	$2068.2631^{+0.0019}_{-0.0019}$	$6.32^{+0.26}_{-0.19}$	647^{+12}_{-12}
211147178.1	4	$5.7316081^{+0.0000034}_{-0.0000034}$	$2063.851178^{+0.000025}_{-0.000025}$	$7.7045^{+0.0076}_{-0.0077}$	105561^{+28}_{-28}
211147178.2	4	$5.7316286^{+0.0000061}_{-0.0000063}$	$2066.716485^{+0.000039}_{-0.000040}$	$7.5417^{+0.0030}_{-0.0031}$	59270^{+20}_{-21}
211154046.1	4	$50.238212^{+0.000052}_{-0.000053}$	$2065.512311^{+0.000038}_{-0.000037}$	$5.468^{+0.018}_{-0.024}$	137111^{+81}_{-79}
211309989.1	5	$7.538107^{+0.000020}_{-0.000020}$	$2145.66503^{+0.00012}_{-0.00012}$	$3.638^{+0.034}_{-0.045}$	354500^{+11600}_{-2500}
211309989.2	5	$7.538475^{+0.000028}_{-0.000028}$	$2142.09534^{+0.00019}_{-0.00020}$	$3.273^{+0.017}_{-0.023}$	357930^{+870}_{-830}
211324599.1	5	$8.770178^{+0.000027}_{-0.000027}$	$2147.43918^{+0.00012}_{-0.00011}$	$2.250^{+0.040}_{-0.045}$	113200^{+470}_{-440}
211324599.2	5	$8.770242^{+0.000072}_{-0.000066}$	$2143.15385^{+0.00033}_{-0.00033}$	$2.245^{+0.056}_{-0.061}$	55290^{+490}_{-470}
211371463.1	5	$5.662866^{+0.000018}_{-0.000019}$	$2141.74007^{+0.00011}_{-0.00010}$	$7.0887^{+0.0083}_{-0.0100}$	112380^{+190}_{-180}
211371463.2	5	$5.662638^{+0.000012}_{-0.000013}$	$2144.572321^{+0.000101}_{-0.000098}$	$7.057^{+0.011}_{-0.011}$	77569^{+72}_{-77}
211380136.1	5	$1.7537269^{+0.0000030}_{-0.0000029}$	$2140.447909^{+0.000080}_{-0.000082}$	$3.860^{+0.031}_{-0.031}$	168720^{+320}_{-350}
211380136.2	5	$1.7536932^{+0.0000039}_{-0.0000039}$	$2141.325096^{+0.000061}_{-0.000061}$	$3.802^{+0.021}_{-0.024}$	129770^{+160}_{-170}
211391083.1	5	$39.239042^{+0.000031}_{-0.000031}$	$2150.425833^{+0.000022}_{-0.000022}$	$6.074^{+0.018}_{-0.013}$	432580^{+830}_{-650}
211394147.1	5	$19.507181^{+0.000070}_{-0.000071}$	$2147.12408^{+0.00011}_{-0.00011}$	$6.031^{+0.049}_{-0.059}$	196300^{+250}_{-240}
211394147.2	5	$19.50766^{+0.00013}_{-0.00013}$	$2140.92416^{+0.00024}_{-0.00024}$	$4.391^{+0.071}_{-0.077}$	46020^{+180}_{-180}
211396167.1	5	$4.4496374^{+0.0000045}_{-0.0000045}$	$2141.309593^{+0.000059}_{-0.000062}$	$3.316^{+0.010}_{-0.013}$	235910^{+280}_{-260}
211396167.2	5	$4.4496670^{+0.0000052}_{-0.0000050}$	$2143.468802^{+0.000046}_{-0.000047}$	$3.469^{+0.022}_{-0.030}$	187500^{+210}_{-200}
211409299.1	5	$13.919006^{+0.000011}_{-0.000011}$	$2149.647585^{+0.000026}_{-0.000026}$	$5.6630^{+0.0074}_{-0.0078}$	122584^{+42}_{-39}
211409299.2	5	$13.9196782^{+0.0000077}_{-0.0000079}$	$2143.943478^{+0.000026}_{-0.000022}$	$4.8017^{+0.0093}_{-0.0085}$	107540^{+290}_{-100}
211409713.1	5	$3.0996278^{+0.0000013}_{-0.0000013}$	$2141.095142^{+0.000018}_{-0.000018}$	$4.054^{+0.012}_{-0.013}$	115647^{+52}_{-54}
211409713.2	5	$3.099665^{+0.000013}_{-0.000013}$	$2142.64477^{+0.00017}_{-0.00017}$	$3.862^{+0.013}_{-0.013}$	6695^{+20}_{-21}
211417727.1	5	$4.91171^{+0.00011}_{-0.00011}$	$2140.1247^{+0.0011}_{-0.0012}$	$3.056^{+0.085}_{-0.098}$	7430^{+120}_{-110}
211417727.2	5	$4.91190^{+0.00022}_{-0.00022}$	$2142.5769^{+0.0016}_{-0.0016}$	$3.24^{+0.12}_{-0.14}$	2765^{+78}_{-78}
211421547.1	5	$3.1507781^{+0.0000020}_{-0.0000019}$	$2141.718331^{+0.000027}_{-0.000027}$	$5.390^{+0.015}_{-0.016}$	152614^{+45}_{-44}
211421547.2	5	$3.1507837^{+0.0000022}_{-0.0000022}$	$2140.142905^{+0.000030}_{-0.000031}$	$5.385^{+0.015}_{-0.014}$	116240^{+47}_{-47}
211430148.1	5	$15.090674^{+0.000021}_{-0.000019}$	$2145.277879^{+0.000054}_{-0.000060}$	$4.478^{+0.035}_{-0.044}$	389570^{+2370}_{-640}
211430148.2	5	$15.090639^{+0.000050}_{-0.000051}$	$2150.46056^{+0.00012}_{-0.00012}$	$9.957^{+0.060}_{-0.092}$	139110^{+160}_{-160}
211431013.1	5	$6.204558^{+0.000022}_{-0.000022}$	$2145.79526^{+0.00015}_{-0.00015}$	$6.987^{+0.038}_{-0.035}$	169060^{+290}_{-310}
211431013.2	5	$6.204184^{+0.000020}_{-0.000019}$	$2142.69652^{+0.00012}_{-0.00012}$	$6.890^{+0.015}_{-0.016}$	111070^{+150}_{-150}
211432946.1	5	$3.3439624^{+0.0000031}_{-0.0000032}$	$2141.374652^{+0.000046}_{-0.000044}$	$2.231^{+0.024}_{-0.027}$	382100^{+1300}_{-1600}
211432946.2	5	$3.3439576^{+0.0000031}_{-0.0000031}$	$2139.702673^{+0.000041}_{-0.000041}$	$2.181^{+0.011}_{-0.013}$	242920^{+970}_{-1040}
211462458.1	5	$3.601969^{+0.000022}_{-0.000022}$	$2141.38319^{+0.00027}_{-0.00026}$	$4.848^{+0.067}_{-0.066}$	111120^{+360}_{-350}
211462458.2	5	$3.601923^{+0.000071}_{-0.000071}$	$2143.17780^{+0.00080}_{-0.00079}$	$4.90^{+0.12}_{-0.12}$	34070^{+300}_{-300}
211479262.1	5	$1.482459^{+0.000038}_{-0.000039}$	$2140.5347^{+0.0011}_{-0.0010}$	$18.748^{+0.025}_{-0.025}$	347750^{+850}_{-860}

Table A.2: Our sample of eclipsing binaries from C0-8. (continued)

Binary	C#	Period (days)	t_0 (BJD - 2455000)	Duration (hours)	Depth (ppm)
211479262.2	5	$1.4835426^{+0.0000069}_{-0.0000071}$	$2139.76260^{+0.00015}_{-0.00015}$	$6.130^{+0.080}_{-0.100}$	292320^{+750}_{-650}
211480475.1	5	$0.5822420^{+0.0000068}_{-0.0000069}$	$2140.06264^{+0.00048}_{-0.00048}$	$3.017^{+0.048}_{-0.045}$	84790^{+760}_{-770}
211480475.2	5	$0.5822508^{+0.0000077}_{-0.0000077}$	$2139.76935^{+0.00057}_{-0.00057}$	$2.652^{+0.060}_{-0.055}$	62920^{+760}_{-770}
211489484.1	5		$2192.61935^{+0.00019}_{-0.00019}$	$4.578^{+0.083}_{-0.095}$	106720^{+500}_{-500}
211489484.2	5		$2208.60573^{+0.00037}_{-0.00038}$	$5.05^{+0.11}_{-0.12}$	55140^{+430}_{-430}
211490542.1	5		$2183.813365^{+0.000059}_{-0.000060}$	$9.280^{+0.024}_{-0.032}$	81139^{+59}_{-59}
211498244.1	5		$2154.545722^{+0.000026}_{-0.000026}$	$6.868^{+0.024}_{-0.029}$	98796^{+62}_{-59}
211509975.1	5	$36.224090^{+0.000073}_{-0.000077}$	$2161.206207^{+0.000049}_{-0.000048}$	$3.514^{+0.034}_{-0.040}$	359270^{+480}_{-490}
211518347.1	5	$1.87127402^{+0.00000087}_{-0.00000084}$	$2140.886271^{+0.000016}_{-0.000016}$	$3.2874^{+0.0066}_{-0.0085}$	270590^{+350}_{-300}
211518347.2	5	$1.8712470^{+0.0000038}_{-0.0000039}$	$2139.951144^{+0.000080}_{-0.000080}$	$3.256^{+0.020}_{-0.026}$	46364^{+89}_{-90}
211519965.1	5		$2144.652501^{+0.000059}_{-0.000058}$	$14.657^{+0.039}_{-0.054}$	74601^{+59}_{-60}
211526186.1	5	$0.4550904^{+0.0000094}_{-0.0000094}$	$2140.12768^{+0.00088}_{-0.00088}$	$4.605^{+0.080}_{-0.074}$	15130^{+170}_{-170}
211526186.2	5	$0.455105^{+0.000042}_{-0.000042}$	$2139.9020^{+0.0038}_{-0.0038}$	$1.40^{+0.22}_{-0.29}$	16300^{+2000}_{-2200}
211563123.1	5	$17.325546^{+0.000016}_{-0.000030}$	$2145.393640^{+0.000075}_{-0.000038}$	$9.147^{+0.016}_{-0.016}$	359400^{+150}_{-160}
211569350.1	5	$1.6557576^{+0.0000029}_{-0.0000029}$	$2140.702702^{+0.000075}_{-0.000078}$	$3.912^{+0.037}_{-0.031}$	37587^{+45}_{-44}
211569350.2	5	$1.655726^{+0.000014}_{-0.000014}$	$2139.87615^{+0.00037}_{-0.00037}$	$4.325^{+0.102}_{-0.095}$	8269^{+41}_{-40}
211569573.1	5	$1.433506^{+0.000010}_{-0.000010}$	$2139.73723^{+0.00032}_{-0.00032}$	$1.405^{+0.044}_{-0.053}$	56330^{+740}_{-730}
211569573.2	5	$1.433487^{+0.000027}_{-0.000027}$	$2140.45431^{+0.00080}_{-0.00079}$	$1.512^{+0.071}_{-0.078}$	22010^{+610}_{-620}
211573482.1	5	$7.0703214^{+0.0000056}_{-0.0000045}$	$2143.652799^{+0.000024}_{-0.000027}$	$3.6256^{+0.0091}_{-0.0164}$	169240^{+190}_{-210}
211581700.1	5	$2.582392^{+0.000015}_{-0.000013}$	$2140.830967^{+0.000100}_{-0.000098}$	$4.563^{+0.048}_{-0.050}$	218880^{+770}_{-630}
211581700.2	5	$2.581726^{+0.000018}_{-0.000018}$	$2142.12601^{+0.00015}_{-0.00015}$	$4.608^{+0.054}_{-0.048}$	216100^{+760}_{-680}
211604668.1	5	$0.5159775^{+0.0000029}_{-0.0000029}$	$2139.69983^{+0.00023}_{-0.00023}$	$2.173^{+0.041}_{-0.034}$	161300^{+1100}_{-1000}
211604668.2	5	$1.0319728^{+0.0000088}_{-0.0000089}$	$2139.69943^{+0.00035}_{-0.00035}$	$2.189^{+0.056}_{-0.050}$	159600^{+1600}_{-1600}
211617231.1	5		$2165.8546^{+0.0024}_{-0.0012}$	$14.88^{+0.19}_{-0.15}$	151630^{+160}_{-170}
211617231.2	5		$2196.92362^{+0.00045}_{-0.00044}$	$14.626^{+0.025}_{-0.026}$	141660^{+110}_{-120}
211623903.1	5	$1.6155992^{+0.0000034}_{-0.0000034}$	$2139.864101^{+0.000096}_{-0.000095}$	$1.736^{+0.026}_{-0.020}$	32063^{+100}_{-100}
211623903.2	5	$1.6156049^{+0.0000039}_{-0.0000038}$	$2140.671765^{+0.000095}_{-0.000096}$	$1.740^{+0.023}_{-0.018}$	28104^{+91}_{-92}
211703878.1	5		$2146.34017^{+0.00012}_{-0.00012}$	$5.247^{+0.062}_{-0.075}$	122590^{+300}_{-300}
211705654.1	5	$5.066515^{+0.000048}_{-0.000047}$	$2140.96362^{+0.00037}_{-0.00038}$	$1.094^{+0.085}_{-0.155}$	2729^{+63}_{-70}
211705654.2	5	$5.06632^{+0.00012}_{-0.00012}$	$2143.49738^{+0.00085}_{-0.00085}$	$1.507^{+0.036}_{-0.040}$	1032^{+35}_{-42}
211719484.1	5	$0.7217970^{+0.0000018}_{-0.0000018}$	$2140.354341^{+0.000099}_{-0.000100}$	$1.873^{+0.027}_{-0.022}$	6655^{+26}_{-26}
211719484.2	5	$0.7217931^{+0.0000018}_{-0.0000018}$	$2139.99318^{+0.00011}_{-0.00010}$	$1.897^{+0.026}_{-0.021}$	6047^{+27}_{-27}
211726283.1	5	$2.785543^{+0.000012}_{-0.000013}$	$2141.58688^{+0.00014}_{-0.00014}$	$5.402^{+0.026}_{-0.038}$	153750^{+350}_{-340}
211726283.2	5	$2.785501^{+0.000023}_{-0.000021}$	$2140.19572^{+0.00025}_{-0.00025}$	$5.388^{+0.044}_{-0.057}$	75600^{+300}_{-300}
211728689.1	5	$8.952611^{+0.000020}_{-0.000020}$	$2146.561911^{+0.000087}_{-0.000087}$	$4.533^{+0.041}_{-0.037}$	101060^{+240}_{-240}
211728689.2	5	$8.95276^{+0.00010}_{-0.00010}$	$2140.98790^{+0.00048}_{-0.00048}$	$2.470^{+0.044}_{-0.040}$	8283^{+98}_{-104}
211744153.1	5	$4.612088^{+0.000061}_{-0.000060}$	$2144.24486^{+0.00051}_{-0.00051}$	$2.717^{+0.090}_{-0.094}$	7241^{+80}_{-79}
211744153.2	5	$4.61233^{+0.00025}_{-0.00023}$	$2141.9378^{+0.0020}_{-0.0020}$	$2.38^{+0.21}_{-0.23}$	2351^{+83}_{-87}

Table A.2: Our sample of eclipsing binaries from C0-8. (continued)

Binary	C#	Period (days)	t_0 (BJD - 2455000)	Duration (hours)	Depth (ppm)
211770390.1	5	$7.5801902^{+0.0000089}_{-0.0000091}$	$2140.581269^{+0.000038}_{-0.000038}$	$8.039^{+0.018}_{-0.019}$	84100^{+35}_{-36}
211770390.2	5	$7.580295^{+0.000010}_{-0.000010}$	$2144.371164^{+0.000054}_{-0.000054}$	$8.047^{+0.023}_{-0.025}$	54830^{+25}_{-25}
211770578.1	5	$40.428862^{+0.000089}_{-0.000339}$	$2148.290418^{+0.000147}_{-0.000036}$	$6.646^{+0.055}_{-0.051}$	244054^{+73}_{-72}
211770578.2	5	$40.43286^{+0.00014}_{-0.00014}$	$2170.66131^{+0.00010}_{-0.00010}$	$8.124^{+0.094}_{-0.096}$	61683^{+62}_{-61}
211770867.1	5	$27.693591^{+0.000091}_{-0.000092}$	$2147.87127^{+0.00012}_{-0.00012}$	$7.636^{+0.014}_{-0.015}$	21632^{+34}_{-34}
211770867.2	5	$27.6938^{+0.0054}_{-0.0054}$	$2158.9404^{+0.0037}_{-0.0045}$	$8.41^{+0.37}_{-0.54}$	628^{+21}_{-22}
211772227.1	5	$34.95670^{+0.00056}_{-0.00057}$	$2147.59177^{+0.00040}_{-0.00040}$	$2.148^{+0.081}_{-0.090}$	9510^{+190}_{-140}
211772227.2	5	$34.8853^{+0.0014}_{-0.0014}$	$2157.30887^{+0.00096}_{-0.00096}$	$4.19^{+0.12}_{-0.14}$	6175^{+101}_{-100}
211797674.1	5	$2.6458428^{+0.0000038}_{-0.0000131}$	$2141.079478^{+0.000118}_{-0.000050}$	$1.756^{+0.031}_{-0.040}$	164250^{+430}_{-610}
211797674.2	5	$2.6460326^{+0.0000021}_{-0.0000021}$	$2139.755865^{+0.000040}_{-0.000040}$	$1.793^{+0.038}_{-0.054}$	140180^{+420}_{-2010}
211799258.1	5	$19.53404^{+0.00011}_{-0.00012}$	$2153.14622^{+0.00021}_{-0.00020}$	$1.424^{+0.040}_{-0.045}$	85000^{+2000}_{-1300}
211800191.1	5	$2.212378^{+0.000017}_{-0.000017}$	$2140.74911^{+0.00031}_{-0.00031}$	$1.321^{+0.045}_{-0.051}$	1574^{+36}_{-36}
211800191.2	5	$2.212346^{+0.000031}_{-0.000035}$	$2141.84460^{+0.00044}_{-0.00043}$	$0.496^{+0.027}_{-0.019}$	1069^{+60}_{-82}
211805860.1	5	$4.1420364^{+0.0000055}_{-0.0000194}$	$2142.723094^{+0.000054}_{-0.000037}$	$3.524^{+0.020}_{-0.017}$	265870^{+160}_{-190}
211805860.2	5	$4.1420506^{+0.0000024}_{-0.0000023}$	$2140.650968^{+0.000020}_{-0.000020}$	$3.502^{+0.016}_{-0.024}$	220450^{+150}_{-140}
211807843.1	5	$6.7642037^{+0.0000029}_{-0.0000026}$	$2145.9936614^{+0.0000076}_{-0.0000075}$	$6.6532^{+0.0059}_{-0.0066}$	398800^{+6300}_{-7400}
211807843.2	5	$6.7641440^{+0.0000015}_{-0.0000017}$	$2142.6141667^{+0.0000077}_{-0.0000073}$	$6.6418^{+0.0057}_{-0.0060}$	382234^{+40}_{-38}
211812160.1	5	$2.1702158^{+0.0000043}_{-0.0000043}$	$2141.030013^{+0.000082}_{-0.000081}$	$2.682^{+0.024}_{-0.018}$	15190^{+27}_{-27}
211812160.2	5	$2.1702060^{+0.0000079}_{-0.0000080}$	$2139.94528^{+0.00015}_{-0.00015}$	$2.678^{+0.039}_{-0.031}$	8202^{+26}_{-26}
211814733.1	5	$14.70905^{+0.00014}_{-0.00014}$	$2145.89166^{+0.00033}_{-0.00034}$	$3.292^{+0.077}_{-0.078}$	5918^{+39}_{-39}
211814733.2	5	$14.70834^{+0.00058}_{-0.00055}$	$2153.2452^{+0.0013}_{-0.0013}$	$3.29^{+0.12}_{-0.13}$	1868^{+56}_{-60}
211817572.1	5	$2.2597933^{+0.0000042}_{-0.0000042}$	$2140.015020^{+0.000077}_{-0.000078}$	$1.414^{+0.029}_{-0.028}$	5645^{+29}_{-29}
211817572.2	5	$2.259799^{+0.000053}_{-0.000052}$	$2141.14588^{+0.00098}_{-0.00100}$	$1.29^{+0.13}_{-0.20}$	473^{+22}_{-22}
211820126.1	5	$4.7551857^{+0.0000027}_{-0.0000027}$	$2141.023193^{+0.000021}_{-0.000021}$	$7.5157^{+0.0045}_{-0.0046}$	143462^{+66}_{-56}
211820126.2	5	$4.7551790^{+0.0000023}_{-0.0000024}$	$2143.448772^{+0.000019}_{-0.000019}$	$8.1385^{+0.0046}_{-0.0049}$	130873^{+58}_{-65}
211822953.1	5	$1.5493824^{+0.0000037}_{-0.0000036}$	$2139.875751^{+0.000095}_{-0.000095}$	$1.610^{+0.025}_{-0.025}$	81730^{+800}_{-860}
211822953.2	5	$1.549399^{+0.000024}_{-0.000024}$	$2140.64982^{+0.00066}_{-0.00067}$	$1.60^{+0.12}_{-0.15}$	15360^{+410}_{-470}
211834405.1	5	$10.5422971^{+0.0000033}_{-0.0000033}$	$2142.431230^{+0.000012}_{-0.000012}$	$5.8585^{+0.0060}_{-0.0070}$	413100^{+14300}_{-8800}
211834405.2	5	$10.5423180^{+0.0000040}_{-0.0000040}$	$2147.549368^{+0.000014}_{-0.000014}$	$6.596^{+0.016}_{-0.016}$	281010^{+600}_{-630}
211885185.1	5	$8.7946776^{+0.0000049}_{-0.0000057}$	$2141.691369^{+0.000013}_{-0.000013}$	$7.223^{+0.013}_{-0.014}$	319450^{+100}_{-160}
211885185.2	5	$8.7946678^{+0.0000055}_{-0.0000046}$	$2146.121096^{+0.000020}_{-0.000022}$	$7.2689^{+0.0102}_{-0.0095}$	233780^{+210}_{-130}
211894612.1	5		$2182.922862^{+0.000083}_{-0.000080}$	$8.488^{+0.036}_{-0.041}$	44285^{+47}_{-47}
211902535.1	5	$9.8115929^{+0.0000059}_{-0.0000058}$	$2142.847020^{+0.000026}_{-0.000029}$	$8.480^{+0.011}_{-0.011}$	162271^{+56}_{-56}
211902535.2	5	$9.811664^{+0.000019}_{-0.000019}$	$2146.597534^{+0.000078}_{-0.000076}$	$8.931^{+0.017}_{-0.021}$	60183^{+30}_{-30}
211910237.1	5	$2.2179996^{+0.0000063}_{-0.0000064}$	$2140.41023^{+0.00010}_{-0.00010}$	$2.241^{+0.031}_{-0.031}$	44570^{+130}_{-130}
211910237.2	5	$2.2179543^{+0.0000067}_{-0.0000067}$	$2141.52198^{+0.00011}_{-0.00011}$	$2.252^{+0.033}_{-0.035}$	35230^{+160}_{-140}
211936444.1	5	$4.9291168^{+0.0000038}_{-0.0000039}$	$2143.571457^{+0.000035}_{-0.000034}$	$3.871^{+0.020}_{-0.022}$	69814^{+52}_{-51}
211936444.2	5	$4.9291150^{+0.0000041}_{-0.0000040}$	$2141.106870^{+0.000033}_{-0.000036}$	$3.8285^{+0.0096}_{-0.0129}$	61674^{+39}_{-39}

Table A.2: Our sample of eclipsing binaries from C0-8. (continued)

Binary	C#	Period (days)	t_0 (BJD - 2455000)	Duration (hours)	Depth (ppm)
211942779.1	5	$1.749914^{+0.000035}_{-0.000036}$	$2141.02822^{+0.00083}_{-0.00083}$	$1.475^{+0.069}_{-0.078}$	10050^{+320}_{-320}
211942779.2	5	$1.750028^{+0.000071}_{-0.000074}$	$2140.1526^{+0.0020}_{-0.0018}$	$1.24^{+0.17}_{-0.16}$	4730^{+640}_{-550}
211946007.1	5	$1.9828032^{+0.0000051}_{-0.0000052}$	$2141.14457^{+0.00011}_{-0.00011}$	$1.231^{+0.029}_{-0.031}$	145600^{+2000}_{-1800}
211953866.1	5	$1.7889290^{+0.0000012}_{-0.0000012}$	$2141.008149^{+0.000028}_{-0.000029}$	$2.045^{+0.023}_{-0.023}$	365390^{+740}_{-680}
211953866.2	5	$1.7889388^{+0.0000014}_{-0.0000014}$	$2140.113404^{+0.000033}_{-0.000033}$	$2.014^{+0.019}_{-0.025}$	276760^{+630}_{-600}
211972086.1	5	$6.015744^{+0.000011}_{-0.000011}$	$2142.888366^{+0.000069}_{-0.000068}$	$2.272^{+0.032}_{-0.036}$	298630^{+880}_{-840}
211972086.2	5	$6.015732^{+0.000012}_{-0.000012}$	$2139.875881^{+0.000088}_{-0.000087}$	$2.238^{+0.031}_{-0.032}$	206530^{+570}_{-540}
211995462.1	5		$2203.280236^{+0.000049}_{-0.000045}$	$12.012^{+0.050}_{-0.063}$	249620^{+680}_{-220}
211997641.1	5	$3.4890875^{+0.0000023}_{-0.0000021}$	$2140.506871^{+0.000034}_{-0.000035}$	$5.734^{+0.022}_{-0.022}$	296151^{+81}_{-75}
211997641.2	5	$3.4890752^{+0.0000016}_{-0.0000016}$	$2142.251595^{+0.000020}_{-0.000020}$	$5.693^{+0.015}_{-0.016}$	278780^{+190}_{-190}
211999656.1	5	$1.94835297^{+0.00000043}_{-0.00000047}$	$2140.5237102^{+0.0000077}_{-0.0000075}$	$3.2078^{+0.0069}_{-0.0066}$	130622^{+29}_{-27}
211999656.2	5	$1.94834775^{+0.00000059}_{-0.00000061}$	$2141.497923^{+0.000011}_{-0.000012}$	$3.2005^{+0.0035}_{-0.0050}$	125066^{+68}_{-65}
212002525.1	5	$11.615509^{+0.000092}_{-0.000101}$	$2141.79306^{+0.00045}_{-0.00038}$	$2.218^{+0.050}_{-0.061}$	151200^{+1800}_{-1800}
212002525.2	5	$11.615267^{+0.000085}_{-0.000084}$	$2147.61527^{+0.00025}_{-0.00025}$	$2.131^{+0.052}_{-0.061}$	133200^{+1600}_{-1400}
212009702.1	5	$0.9238667^{+0.0000011}_{-0.0000011}$	$2140.173474^{+0.000053}_{-0.000052}$	$4.157^{+0.044}_{-0.037}$	396840^{+640}_{-580}
212009702.2	5	$0.9238641^{+0.0000016}_{-0.0000016}$	$2139.711666^{+0.000075}_{-0.000076}$	$4.065^{+0.055}_{-0.064}$	278640^{+440}_{-430}
212010289.1	5	$7.9502394^{+0.0000063}_{-0.0000067}$	$2144.437518^{+0.000038}_{-0.000029}$	$4.033^{+0.012}_{-0.018}$	562700^{+6500}_{-9700}
212010289.2	5	$7.9502919^{+0.0000083}_{-0.0000084}$	$2140.304388^{+0.000050}_{-0.000047}$	$4.251^{+0.011}_{-0.012}$	265600^{+1290}_{-770}
212012387.1	5	$6.4884955^{+0.0000038}_{-0.0000033}$	$2143.523004^{+0.000015}_{-0.000018}$	$3.858^{+0.013}_{-0.025}$	474110^{+940}_{-1000}
212012387.2	5	$6.4885440^{+0.0000031}_{-0.0000028}$	$2140.251168^{+0.000018}_{-0.000020}$	$3.9772^{+0.0069}_{-0.0089}$	356040^{+890}_{-1070}
212018340.1	5	$2.9564079^{+0.0000048}_{-0.0000028}$	$2141.042514^{+0.000047}_{-0.000080}$	$3.466^{+0.018}_{-0.032}$	241360^{+190}_{-170}
212018340.2	5	$2.9563808^{+0.0000025}_{-0.0000024}$	$2142.520915^{+0.000026}_{-0.000029}$	$3.4402^{+0.0097}_{-0.0104}$	202060^{+110}_{-110}
212019055.1	5	$0.8214380^{+0.0000035}_{-0.0000036}$	$2139.99551^{+0.00023}_{-0.00023}$	$2.642^{+0.032}_{-0.037}$	169220^{+690}_{-710}
212019055.2	5	$0.8214222^{+0.0000036}_{-0.0000037}$	$2140.40722^{+0.00024}_{-0.00023}$	$2.641^{+0.033}_{-0.037}$	148350^{+540}_{-550}
212020442.1	5	$7.778618^{+0.000217}_{-0.000053}$	$2143.81852^{+0.00028}_{-0.00134}$	$2.603^{+0.041}_{-0.038}$	61750^{+520}_{-420}
212020442.2	5	$7.778130^{+0.000050}_{-0.000065}$	$2139.88194^{+0.00046}_{-0.00033}$	$2.586^{+0.051}_{-0.051}$	46730^{+220}_{-200}
212029934.1	5	$1.2495047^{+0.0000032}_{-0.0000031}$	$2140.61335^{+0.00011}_{-0.00011}$	$1.727^{+0.043}_{-0.048}$	31900^{+150}_{-140}
212029934.2	5	$1.2495228^{+0.0000039}_{-0.0000039}$	$2139.98818^{+0.00014}_{-0.00014}$	$1.742^{+0.049}_{-0.047}$	24710^{+130}_{-120}
212037403.1	5	$3.4082073^{+0.0000030}_{-0.0000031}$	$2140.735239^{+0.000036}_{-0.000043}$	$3.227^{+0.016}_{-0.021}$	208640^{+3800}_{-310}
212037403.2	5	$3.408174^{+0.000014}_{-0.000014}$	$2142.43996^{+0.00016}_{-0.00016}$	$3.133^{+0.055}_{-0.055}$	18816^{+100}_{-90}
212082682.1	5	$3.7974804^{+0.0000076}_{-0.0000073}$	$2142.649312^{+0.000079}_{-0.000079}$	$2.820^{+0.032}_{-0.035}$	121180^{+380}_{-370}
212082682.2	5	$3.797546^{+0.000032}_{-0.000032}$	$2140.75081^{+0.00037}_{-0.00036}$	$2.740^{+0.059}_{-0.064}$	11670^{+130}_{-140}
212083250.1	5	$1.037601^{+0.000027}_{-0.000027}$	$2140.3862^{+0.0010}_{-0.0011}$	$4.849^{+0.092}_{-0.084}$	52000^{+1200}_{-1200}
212083250.2	5	$1.037332^{+0.000075}_{-0.000074}$	$2139.8833^{+0.0037}_{-0.0038}$	$6.29^{+0.20}_{-0.19}$	20370^{+660}_{-670}
212085740.1	5	$4.8455156^{+0.0000036}_{-0.0000037}$	$2141.587440^{+0.000030}_{-0.000031}$	$3.293^{+0.015}_{-0.015}$	96005^{+65}_{-64}
212085740.2	5	$4.845573^{+0.000050}_{-0.000050}$	$2144.03796^{+0.00041}_{-0.00041}$	$3.268^{+0.069}_{-0.079}$	5813^{+63}_{-55}
212096658.1	5	$2.9328177^{+0.0000200}_{-0.0000029}$	$2140.539695^{+0.000040}_{-0.000304}$	$2.447^{+0.015}_{-0.022}$	185920^{+310}_{-220}
212096658.2	5	$2.9329795^{+0.0000020}_{-0.0000014}$	$2142.027541^{+0.000087}_{-0.000023}$	$2.760^{+0.016}_{-0.024}$	185112^{+841}_{-82}

Table A.2: Our sample of eclipsing binaries from C0-8. (continued)

Binary	C#	Period (days)	t_0 (BJD - 2455000)	Duration (hours)	Depth (ppm)
212109135.1	5		$2198.1281159^{+0.0000093}_{-0.0000091}$	$8.492^{+0.017}_{-0.018}$	347276^{+71}_{-70}
212110007.1	5	$16.709436^{+0.000056}_{-0.000055}$	$2144.68458^{+0.00014}_{-0.00013}$	$3.298^{+0.043}_{-0.042}$	44580^{+140}_{-130}
212110007.2	5	$16.7080^{+0.0013}_{-0.0013}$	$2152.0045^{+0.0025}_{-0.0025}$	$2.96^{+0.37}_{-0.27}$	2860^{+140}_{-140}
212122623.1	5	$1.3132580^{+0.0000012}_{-0.0000012}$	$2139.919085^{+0.000040}_{-0.000041}$	$2.010^{+0.016}_{-0.017}$	65300^{+170}_{-180}
212122623.2	5	$1.313231^{+0.000018}_{-0.000018}$	$2140.57709^{+0.00059}_{-0.00058}$	$2.074^{+0.079}_{-0.063}$	4257^{+71}_{-75}
212137767.1	5	$15.178605^{+0.000040}_{-0.000041}$	$2148.248367^{+0.000101}_{-0.000097}$	$11.5813^{+0.0071}_{-0.0076}$	69691^{+45}_{-46}
212137767.2	5	$15.178245^{+0.000060}_{-0.000073}$	$2141.60318^{+0.00023}_{-0.00017}$	$12.072^{+0.015}_{-0.021}$	75060^{+100}_{-100}
212152922.1	5	$4.878370^{+0.000013}_{-0.000013}$	$2144.189481^{+0.000098}_{-0.000101}$	$2.486^{+0.033}_{-0.037}$	9166^{+27}_{-26}
212152922.2	5	$4.878379^{+0.000056}_{-0.000056}$	$2141.78938^{+0.00047}_{-0.00047}$	$2.169^{+0.068}_{-0.072}$	1867^{+27}_{-26}
212155299.1	5	$0.90171395^{+0.00000073}_{-0.00000072}$	$2139.710443^{+0.000035}_{-0.000035}$	$2.574^{+0.022}_{-0.016}$	300540^{+620}_{-610}
212155299.2	5	$0.9017286^{+0.0000072}_{-0.0000072}$	$2140.16108^{+0.00035}_{-0.00034}$	$3.015^{+0.078}_{-0.071}$	32350^{+240}_{-230}
212157058.1	5	$40.7897^{+0.0052}_{-0.0109}$	$2143.5495^{+0.0015}_{-0.0015}$	$3.66^{+0.19}_{-0.22}$	2731^{+105}_{-97}
212157058.2	5	$40.8038^{+0.0042}_{-0.0040}$	$2163.9256^{+0.0034}_{-0.0037}$	$4.88^{+0.25}_{-0.27}$	1249^{+62}_{-61}
212280209.1	6	$4.164046^{+0.000016}_{-0.000015}$	$2218.11949^{+0.00017}_{-0.00018}$	$2.148^{+0.053}_{-0.057}$	82810^{+460}_{-450}
212280209.2	6	$4.164085^{+0.000017}_{-0.000018}$	$2220.20102^{+0.00018}_{-0.00018}$	$2.116^{+0.046}_{-0.052}$	63030^{+340}_{-340}
212290847.1	6	$8.3949320^{+0.0000071}_{-0.0000065}$	$2222.298239^{+0.000032}_{-0.000033}$	$6.4920^{+0.0086}_{-0.0117}$	168200^{+74}_{-79}
212290847.2	6	$8.3949256^{+0.0000065}_{-0.0000072}$	$2218.156031^{+0.000033}_{-0.000031}$	$6.5484^{+0.0080}_{-0.0101}$	162243^{+53}_{-51}
212295183.1	6	$5.534617^{+0.000013}_{-0.000012}$	$2217.91804^{+0.00011}_{-0.00013}$	$2.389^{+0.030}_{-0.031}$	444300^{+4800}_{-4100}
212295183.2	6	$5.534644^{+0.000016}_{-0.000016}$	$2220.89218^{+0.00013}_{-0.00013}$	$2.916^{+0.025}_{-0.039}$	248900^{+1200}_{-1400}
212302722.1	6	$0.7837802^{+0.0000030}_{-0.0000030}$	$2218.12391^{+0.00019}_{-0.00019}$	$4.423^{+0.034}_{-0.026}$	225840^{+500}_{-500}
212310740.1	6	$3.5998164^{+0.0000027}_{-0.0000031}$	$2218.582053^{+0.000037}_{-0.000034}$	$2.7992^{+0.0070}_{-0.0087}$	59245^{+77}_{-72}
212310740.2	6	$3.599684^{+0.000037}_{-0.000039}$	$2220.39676^{+0.00044}_{-0.00043}$	$2.842^{+0.054}_{-0.069}$	1808^{+22}_{-24}
212311834.1	6	$17.788546^{+0.000063}_{-0.000068}$	$2233.41021^{+0.00019}_{-0.00013}$	$2.905^{+0.039}_{-0.043}$	114160^{+290}_{-290}
212327309.1	6	$6.7171911^{+0.0000052}_{-0.0000057}$	$2224.180659^{+0.000033}_{-0.000031}$	$3.989^{+0.022}_{-0.033}$	358170^{+350}_{-360}
212327309.2	6	$6.717197^{+0.000015}_{-0.000015}$	$2220.55740^{+0.00011}_{-0.00011}$	$3.895^{+0.026}_{-0.037}$	100950^{+140}_{-140}
212332380.1	6		$2282.8799^{+0.0071}_{-0.0097}$	$11.88^{+0.49}_{-0.36}$	220740^{+340}_{-280}
212334671.1	6	$15.459253^{+0.000067}_{-0.000069}$	$2230.29718^{+0.00017}_{-0.00017}$	$6.355^{+0.051}_{-0.067}$	77230^{+220}_{-180}
212334671.2	6	$15.45921^{+0.00014}_{-0.00014}$	$2225.72772^{+0.00036}_{-0.00036}$	$6.210^{+0.040}_{-0.056}$	51190^{+380}_{-500}
212339438.1	6	$2.7044449^{+0.0000030}_{-0.0000030}$	$2219.552515^{+0.000049}_{-0.000049}$	$4.687^{+0.019}_{-0.029}$	74037^{+100}_{-97}
212339438.2	6	$2.7044555^{+0.0000083}_{-0.0000082}$	$2218.20024^{+0.00014}_{-0.00014}$	$4.446^{+0.012}_{-0.012}$	13822^{+31}_{-31}
212343520.1	6		$2284.019643^{+0.000091}_{-0.000090}$	$6.106^{+0.067}_{-0.066}$	72430^{+740}_{-540}
212349750.1	6	$1.4343478^{+0.0000014}_{-0.0000013}$	$2218.337162^{+0.000043}_{-0.000044}$	$5.958^{+0.011}_{-0.010}$	171690^{+180}_{-170}
212358105.1	6	$1.5247051^{+0.0000057}_{-0.0000058}$	$2218.57268^{+0.00017}_{-0.00017}$	$4.095^{+0.055}_{-0.052}$	181360^{+530}_{-500}
212358105.2	6	$1.524716^{+0.000019}_{-0.000019}$	$2217.81021^{+0.00053}_{-0.00054}$	$4.991^{+0.078}_{-0.067}$	63540^{+400}_{-390}
212362957.1	6	$12.517087^{+0.000019}_{-0.000019}$	$2217.902888^{+0.000092}_{-0.000085}$	$5.044^{+0.036}_{-0.045}$	145540^{+160}_{-160}
212362957.2	6	$12.516861^{+0.000082}_{-0.000082}$	$2222.45360^{+0.00026}_{-0.00026}$	$5.921^{+0.046}_{-0.057}$	39540^{+140}_{-160}
212364002.1	6	$5.696293^{+0.000058}_{-0.000055}$	$2218.85476^{+0.00045}_{-0.00049}$	$4.735^{+0.048}_{-0.068}$	38150^{+310}_{-270}
212364002.2	6	$5.69624^{+0.00030}_{-0.00029}$	$2221.7084^{+0.0022}_{-0.0022}$	$4.66^{+0.18}_{-0.21}$	4630^{+110}_{-110}

Table A.2: Our sample of eclipsing binaries from C0-8. (continued)

Binary	C#	Period (days)	t_0 (BJD - 2455000)	Duration (hours)	Depth (ppm)
212370052.1	6	$7.7741581^{+0.0000057}_{-0.0000053}$	$2223.096261^{+0.000037}_{-0.000040}$	$7.028^{+0.026}_{-0.027}$	363250^{+130}_{-130}
212370052.2	6	$7.7741915^{+0.0000063}_{-0.0000064}$	$2219.203170^{+0.000038}_{-0.000040}$	$6.995^{+0.017}_{-0.014}$	275000^{+150}_{-190}
212397056.1	6	$38.74904^{+0.00015}_{-0.00016}$	$2223.37359^{+0.00011}_{-0.00011}$	$10.197^{+0.042}_{-0.050}$	87670^{+100}_{-110}
212421319.1	6	$11.04157^{+0.00058}_{-0.00058}$	$2227.1980^{+0.0022}_{-0.0021}$	$8.59^{+0.18}_{-0.21}$	26770^{+740}_{-830}
212421319.2	6	$11.04024^{+0.00056}_{-0.00056}$	$2221.6174^{+0.0020}_{-0.0020}$	$8.47^{+0.21}_{-0.25}$	22510^{+370}_{-360}
212426112.1	6	$1.5302161^{+0.0000022}_{-0.0000023}$	$2218.912184^{+0.000062}_{-0.000062}$	$2.009^{+0.023}_{-0.022}$	35886^{+84}_{-82}
212426112.2	6	$1.5302034^{+0.0000049}_{-0.0000048}$	$2218.14908^{+0.00013}_{-0.00013}$	$1.970^{+0.038}_{-0.043}$	13423^{+66}_{-68}
212428509.1	6	$5.335931^{+0.000013}_{-0.000013}$	$2219.83266^{+0.00010}_{-0.00011}$	$3.218^{+0.044}_{-0.037}$	11713^{+24}_{-24}
212428509.2	6	$5.335923^{+0.000017}_{-0.000017}$	$2222.50667^{+0.00013}_{-0.00013}$	$3.184^{+0.046}_{-0.038}$	10356^{+24}_{-24}
212432524.1	6	$4.944480^{+0.000022}_{-0.000021}$	$2219.49988^{+0.00020}_{-0.00021}$	$8.7838^{+0.0068}_{-0.0070}$	224100^{+210}_{-220}
212432524.2	6	$4.944590^{+0.000044}_{-0.000043}$	$2221.97344^{+0.00040}_{-0.00041}$	$8.671^{+0.027}_{-0.032}$	99350^{+540}_{-490}
212453473.1	6	$5.5122699^{+0.0000046}_{-0.0000047}$	$2222.841520^{+0.000032}_{-0.000032}$	$3.9110^{+0.0091}_{-0.0128}$	406730^{+260}_{-250}
212453473.2	6	$5.5121708^{+0.0000036}_{-0.0000035}$	$2220.086876^{+0.000027}_{-0.000026}$	$3.948^{+0.017}_{-0.026}$	335530^{+220}_{-210}
212456583.1	6	$5.7549083^{+0.0000032}_{-0.0000029}$	$2218.232124^{+0.000022}_{-0.000025}$	$4.428^{+0.016}_{-0.016}$	277260^{+110}_{-110}
212456583.2	6	$5.7548643^{+0.0000033}_{-0.0000033}$	$2221.117905^{+0.000028}_{-0.000029}$	$4.511^{+0.011}_{-0.017}$	154020^{+130}_{-170}
212469831.1	6	$5.075374^{+0.000035}_{-0.000035}$	$2221.19029^{+0.00028}_{-0.00028}$	$2.395^{+0.051}_{-0.042}$	6903^{+47}_{-45}
212469831.2	6	$5.075390^{+0.000036}_{-0.000036}$	$2218.29731^{+0.00032}_{-0.00032}$	$2.626^{+0.064}_{-0.059}$	6543^{+47}_{-45}
212481328.1	6	$3.4172309^{+0.0000033}_{-0.0000033}$	$2219.316557^{+0.000044}_{-0.000043}$	$2.813^{+0.012}_{-0.015}$	44532^{+43}_{-41}
212481328.2	6	$3.417257^{+0.000017}_{-0.000017}$	$2217.60763^{+0.00021}_{-0.00021}$	$2.853^{+0.049}_{-0.050}$	7586^{+35}_{-35}
212497267.2	6	$3.7451064^{+0.0000033}_{-0.0000034}$	$2217.626094^{+0.000038}_{-0.000037}$	$4.499^{+0.026}_{-0.019}$	74164^{+107}_{-78}
212499716.1	6	$0.4373843^{+0.0000023}_{-0.0000023}$	$2217.81357^{+0.00023}_{-0.00024}$	$1.268^{+0.044}_{-0.045}$	2707^{+32}_{-32}
212499716.2	6	$0.4374402^{+0.0000093}_{-0.0000092}$	$2217.60018^{+0.00096}_{-0.00096}$	$5.351^{+0.086}_{-0.079}$	1171^{+12}_{-12}
212504385.1	6	$0.8268852^{+0.0000024}_{-0.0000024}$	$2218.24611^{+0.00014}_{-0.00014}$	$3.440^{+0.041}_{-0.033}$	161620^{+520}_{-470}
212504385.2	6	$0.8268845^{+0.0000089}_{-0.0000089}$	$2217.83269^{+0.00050}_{-0.00050}$	$5.488^{+0.051}_{-0.048}$	81510^{+460}_{-450}
212504617.1	6	$39.26137^{+0.00018}_{-0.00018}$	$2240.62678^{+0.00013}_{-0.00013}$	$7.071^{+0.016}_{-0.017}$	34617^{+68}_{-69}
212504617.2	6	$39.2585^{+0.0042}_{-0.0044}$	$2249.4013^{+0.0030}_{-0.0031}$	$10.85^{+0.27}_{-0.32}$	1222^{+30}_{-31}
212508560.1	6	$1.4608827^{+0.0000040}_{-0.0000046}$	$2218.734397^{+0.000103}_{-0.000094}$	$1.525^{+0.038}_{-0.042}$	115180^{+840}_{-750}
212508560.2	6	$1.4608861^{+0.0000043}_{-0.0000042}$	$2218.00377^{+0.00013}_{-0.00013}$	$1.410^{+0.034}_{-0.039}$	60920^{+390}_{-390}
212535959.1	6	$17.733176^{+0.000030}_{-0.000031}$	$2232.777362^{+0.000052}_{-0.000052}$	$7.479^{+0.025}_{-0.027}$	129145^{+84}_{-84}
212535959.2	6	$17.73320^{+0.00013}_{-0.00013}$	$2224.84264^{+0.00032}_{-0.00032}$	$8.695^{+0.025}_{-0.026}$	15357^{+42}_{-44}
212536771.1	6	$2.7840819^{+0.0000032}_{-0.0000034}$	$2217.798470^{+0.000050}_{-0.000047}$	$3.9094^{+0.0058}_{-0.0076}$	213180^{+120}_{-110}
212536771.2	6	$2.7840613^{+0.0000045}_{-0.0000044}$	$2219.190983^{+0.000086}_{-0.000089}$	$3.910^{+0.011}_{-0.014}$	96951^{+84}_{-83}
212537106.1	6	$9.2621429^{+0.0000130}_{-0.0000089}$	$2218.113542^{+0.000038}_{-0.000067}$	$7.199^{+0.015}_{-0.020}$	188120^{+870}_{-120}
212537106.2	6	$9.262061^{+0.000011}_{-0.000012}$	$2222.745133^{+0.000046}_{-0.000046}$	$7.0881^{+0.0073}_{-0.0074}$	74244^{+41}_{-41}
212541386.1	6	$3.6303584^{+0.0000104}_{-0.0000062}$	$2219.700777^{+0.000079}_{-0.000084}$	$2.468^{+0.023}_{-0.032}$	88080^{+260}_{-300}
212541386.2	6	$3.630336^{+0.000022}_{-0.000022}$	$2217.88533^{+0.00027}_{-0.00028}$	$2.430^{+0.025}_{-0.030}$	9328^{+86}_{-90}
212545602.1	6	$1.7567349^{+0.0000019}_{-0.0000018}$	$2217.920431^{+0.000028}_{-0.000029}$	$5.940^{+0.014}_{-0.021}$	651100^{+810}_{-1090}
212545602.2	6	$1.7567275^{+0.0000066}_{-0.0000067}$	$2218.80003^{+0.00017}_{-0.00017}$	$6.287^{+0.032}_{-0.023}$	99750^{+210}_{-210}

Table A.2: Our sample of eclipsing binaries from C0-8. (continued)

Binary	C#	Period (days)	t_0 (BJD - 2455000)	Duration (hours)	Depth (ppm)
212549089.1	6		$2245.030394^{+0.000085}_{-0.000085}$	$14.262^{+0.082}_{-0.085}$	53439^{+40}_{-40}
212554009.1	6		$2295.25273^{+0.00014}_{-0.00014}$	$25.956^{+0.062}_{-0.068}$	140630^{+120}_{-120}
212559866.1	6	$19.701925^{+0.000015}_{-0.000015}$	$2229.197476^{+0.000028}_{-0.000028}$	$9.748^{+0.018}_{-0.018}$	120036^{+28}_{-26}
212559866.2	6	$19.701941^{+0.000013}_{-0.000013}$	$2218.603752^{+0.000024}_{-0.000024}$	$9.474^{+0.016}_{-0.020}$	127154^{+28}_{-29}
212570977.1	6	$8.853067^{+0.000032}_{-0.000032}$	$2223.89356^{+0.00014}_{-0.00014}$	$4.179^{+0.010}_{-0.013}$	27191^{+110}_{-99}
212570977.2	6	$8.8561^{+0.0018}_{-0.0039}$	$2220.1825^{+0.0091}_{-0.0065}$	$4.32^{+0.41}_{-1.40}$	401^{+33}_{-34}
212579164.1	6	$36.311620^{+0.000035}_{-0.000031}$	$2220.397445^{+0.000048}_{-0.000074}$	$3.563^{+0.051}_{-0.031}$	210430^{+400}_{-370}
212579164.2	6	$36.311159^{+0.000055}_{-0.000055}$	$2238.553486^{+0.000026}_{-0.000026}$	$3.462^{+0.024}_{-0.031}$	203310^{+410}_{-460}
212580081.1	6	$1.4918809^{+0.0000031}_{-0.0000032}$	$2218.157876^{+0.000090}_{-0.000090}$	$2.233^{+0.031}_{-0.036}$	406100^{+5600}_{-4700}
212586717.1	6	$8.591669^{+0.000024}_{-0.000024}$	$2223.76439^{+0.00011}_{-0.00012}$	$2.748^{+0.038}_{-0.043}$	22317^{+70}_{-64}
212586717.2	6	$8.591618^{+0.000037}_{-0.000038}$	$2219.43521^{+0.00018}_{-0.00018}$	$2.589^{+0.029}_{-0.040}$	17035^{+93}_{-84}
212588757.1	6	$6.751863^{+0.000024}_{-0.000025}$	$2218.90208^{+0.00016}_{-0.00016}$	$3.061^{+0.039}_{-0.042}$	37500^{+120}_{-120}
212588757.2	6	$6.751875^{+0.000092}_{-0.000093}$	$2222.27859^{+0.00054}_{-0.00054}$	$3.104^{+0.088}_{-0.102}$	8651^{+89}_{-88}
212606118.1	6	$12.24381^{+0.00018}_{-0.00018}$	$2224.56435^{+0.00056}_{-0.00055}$	$2.871^{+0.091}_{-0.100}$	275500^{+3900}_{-4000}
212606118.2	6	$12.24410^{+0.00010}_{-0.00011}$	$2218.20529^{+0.00036}_{-0.00033}$	$2.602^{+0.050}_{-0.076}$	631000^{+20000}_{-18000}
212613128.1	6	$0.7592040^{+0.0000031}_{-0.0000028}$	$2218.27273^{+0.00011}_{-0.00012}$	$1.861^{+0.031}_{-0.036}$	302800^{+1800}_{-1700}
212613128.2	6	$0.7591819^{+0.0000026}_{-0.0000027}$	$2217.89408^{+0.00014}_{-0.00014}$	$1.991^{+0.040}_{-0.036}$	192400^{+1300}_{-1100}
212615080.1	6	$7.3757273^{+0.0000090}_{-0.0000098}$	$2223.393351^{+0.000060}_{-0.000054}$	$3.570^{+0.015}_{-0.027}$	197190^{+260}_{-250}
212615080.2	6	$7.375657^{+0.000033}_{-0.000035}$	$2219.57322^{+0.00019}_{-0.00019}$	$3.503^{+0.020}_{-0.022}$	21230^{+110}_{-110}
212617879.1	6	$4.4216068^{+0.0000016}_{-0.0000016}$	$2218.143844^{+0.000017}_{-0.000015}$	$4.589^{+0.013}_{-0.013}$	246810^{+120}_{-110}
212617879.2	6	$4.4215824^{+0.0000020}_{-0.0000020}$	$2220.354614^{+0.000019}_{-0.000019}$	$4.5641^{+0.0048}_{-0.0067}$	187336^{+76}_{-72}
212627712.1	6	$19.913145^{+0.000023}_{-0.000022}$	$2230.387436^{+0.000043}_{-0.000042}$	$3.477^{+0.022}_{-0.035}$	66466^{+59}_{-58}
212627712.2	6	$19.9094^{+0.0022}_{-0.0024}$	$2225.1111^{+0.0050}_{-0.0045}$	$1.86^{+0.23}_{-0.39}$	557^{+56}_{-58}
212628098.1	6	$8.704849^{+0.000030}_{-0.000024}$	$2218.995763^{+0.000091}_{-0.000085}$	$1.850^{+0.029}_{-0.030}$	59840^{+230}_{-230}
212628098.2	6	$8.704748^{+0.000019}_{-0.000020}$	$2223.348503^{+0.000094}_{-0.000073}$	$1.765^{+0.013}_{-0.017}$	55560^{+280}_{-330}
212633681.1	6	$8.8383835^{+0.0000079}_{-0.0000077}$	$2223.375032^{+0.000036}_{-0.000033}$	$5.632^{+0.026}_{-0.034}$	447660^{+220}_{-220}
212633681.2	6	$8.8383144^{+0.0000092}_{-0.0000095}$	$2218.930776^{+0.000044}_{-0.000041}$	$6.040^{+0.018}_{-0.025}$	252850^{+250}_{-240}
212645173.1	6	$6.9789620^{+0.0000060}_{-0.0000050}$	$2222.448755^{+0.000028}_{-0.000031}$	$4.004^{+0.029}_{-0.033}$	369770^{+180}_{-170}
212645173.2	6	$6.978882^{+0.000011}_{-0.000011}$	$2218.970090^{+0.000059}_{-0.000057}$	$3.869^{+0.015}_{-0.018}$	217150^{+170}_{-170}
212652663.1	6	$3.3394988^{+0.0000026}_{-0.0000026}$	$2220.668137^{+0.000036}_{-0.000036}$	$2.669^{+0.025}_{-0.021}$	273320^{+330}_{-310}
212652663.2	6	$3.3394873^{+0.0000030}_{-0.0000032}$	$2218.998999^{+0.000040}_{-0.000040}$	$2.616^{+0.016}_{-0.023}$	244870^{+390}_{-340}
212656205.1	6	$72.79560^{+0.00055}_{-0.00051}$	$2222.48536^{+0.00022}_{-0.00023}$	$6.217^{+0.069}_{-0.068}$	61490^{+250}_{-430}
212656205.2	6		$2244.51865^{+0.00025}_{-0.00025}$	$6.190^{+0.102}_{-0.094}$	43380^{+200}_{-200}
212664590.1	6	$14.6963081^{+0.0000043}_{-0.0000046}$	$2224.559732^{+0.000011}_{-0.000011}$	$4.8305^{+0.0083}_{-0.0116}$	546670^{+130}_{-130}
212664590.2	6	$14.696278^{+0.000018}_{-0.000018}$	$2217.894114^{+0.000047}_{-0.000047}$	$5.382^{+0.016}_{-0.019}$	111760^{+170}_{-150}
212666524.1	6	$0.6705454^{+0.0000031}_{-0.0000031}$	$2217.67225^{+0.00022}_{-0.00022}$	$4.546^{+0.031}_{-0.025}$	200670^{+580}_{-570}
212666524.2	6	$0.670550^{+0.000010}_{-0.000010}$	$2218.00728^{+0.00072}_{-0.00072}$	$5.595^{+0.073}_{-0.064}$	63710^{+450}_{-450}
212676084.1	6	$3.9020030^{+0.0000061}_{-0.0000052}$	$2217.608035^{+0.000065}_{-0.000082}$	$2.670^{+0.032}_{-0.036}$	370460^{+680}_{-610}

Table A.2: Our sample of eclipsing binaries from C0-8. (continued)

Binary	C#	Period (days)	t_0 (BJD - 2455000)	Duration (hours)	Depth (ppm)
212676084.2	6	$3.9020163^{+0.0000071}_{-0.0000071}$	$2219.559223^{+0.000075}_{-0.000075}$	$2.625^{+0.034}_{-0.038}$	168660^{+630}_{-680}
212678026.1	6	$10.353494^{+0.000022}_{-0.000022}$	$2225.289071^{+0.000087}_{-0.000086}$	$8.293^{+0.012}_{-0.014}$	145180^{+110}_{-120}
212678026.2	6	$10.35371^{+0.00011}_{-0.00012}$	$2220.16890^{+0.00043}_{-0.00048}$	$8.412^{+0.086}_{-0.112}$	40370^{+170}_{-170}
212687040.1	6	$1.85301316^{+0.00000093}_{-0.00000103}$	$2218.564321^{+0.000021}_{-0.000020}$	$2.6179^{+0.0020}_{-0.0029}$	271670^{+190}_{-180}
212687040.2	6	$1.8530049^{+0.0000040}_{-0.0000039}$	$2217.638109^{+0.000095}_{-0.000096}$	$2.592^{+0.027}_{-0.028}$	20616^{+57}_{-58}
212691727.1	6	$12.862049^{+0.000016}_{-0.000016}$	$2219.522953^{+0.000048}_{-0.000048}$	$5.065^{+0.014}_{-0.015}$	62179^{+72}_{-86}
212691727.2	6	$12.86137^{+0.00062}_{-0.00085}$	$2225.9965^{+0.0035}_{-0.0018}$	$4.77^{+0.17}_{-0.24}$	1541^{+31}_{-32}
212694259.1	6		$2248.810892^{+0.000060}_{-0.000054}$	$7.688^{+0.029}_{-0.036}$	141110^{+640}_{-6420}
212694259.2	6	$66.58380^{+0.00025}_{-0.00025}$	$2227.99253^{+0.00018}_{-0.00017}$	$14.209^{+0.088}_{-0.122}$	43403^{+45}_{-45}
212701118.1	6	$2.43395589^{+0.00000101}_{-0.00000089}$	$2218.305400^{+0.000016}_{-0.000018}$	$3.5535^{+0.0039}_{-0.0045}$	553390^{+690}_{-580}
212701118.2	6	$2.4339566^{+0.0000024}_{-0.0000023}$	$2219.522350^{+0.000029}_{-0.000030}$	$3.596^{+0.015}_{-0.023}$	215810^{+340}_{-420}
212705192.1	6	$4.536764^{+0.000014}_{-0.000015}$	$2219.62067^{+0.00014}_{-0.00014}$	$2.612^{+0.038}_{-0.046}$	7623^{+25}_{-25}
212705192.2	6	$4.536725^{+0.000021}_{-0.000021}$	$2221.88916^{+0.00020}_{-0.00020}$	$2.664^{+0.048}_{-0.043}$	6780^{+33}_{-31}
212707624.1	6	$7.2107209^{+0.0000038}_{-0.0000038}$	$2219.350460^{+0.000023}_{-0.000024}$	$5.484^{+0.016}_{-0.017}$	192887^{+99}_{-84}
212707624.2	6	$7.2107310^{+0.0000056}_{-0.0000055}$	$2223.018475^{+0.000034}_{-0.000035}$	$6.074^{+0.016}_{-0.019}$	125671^{+58}_{-58}
212708296.1	6	$0.8032358^{+0.0000075}_{-0.0000070}$	$2217.97698^{+0.00042}_{-0.00048}$	$2.740^{+0.079}_{-0.088}$	361500^{+5100}_{-4600}
212708296.2	6	$0.8032285^{+0.0000056}_{-0.0000056}$	$2217.57520^{+0.00032}_{-0.00032}$	$2.739^{+0.077}_{-0.090}$	284900^{+4300}_{-4000}
212708783.1	6	$4.506738^{+0.000042}_{-0.000048}$	$2219.85510^{+0.00042}_{-0.00039}$	$0.614^{+0.031}_{-0.038}$	13730^{+510}_{-550}
212708783.2	6	$4.512406^{+0.000054}_{-0.000049}$	$2217.5465^{+0.0012}_{-0.0059}$	$1.70^{+0.12}_{-0.24}$	12550^{+150}_{-250}
212725385.1	6	$1.8879299^{+0.0000029}_{-0.0000028}$	$2218.126512^{+0.000059}_{-0.000058}$	$6.970^{+0.026}_{-0.029}$	784560^{+910}_{-890}
212732378.1	6		$2229.78893^{+0.00028}_{-0.00027}$	$5.885^{+0.095}_{-0.106}$	58710^{+210}_{-200}
212747879.1	6	$0.7057940^{+0.0000032}_{-0.0000033}$	$2217.97585^{+0.00026}_{-0.00023}$	$4.091^{+0.018}_{-0.028}$	129300^{+1800}_{-4100}
212770429.1	6	$40.455053^{+0.000070}_{-0.000065}$	$2228.443478^{+0.000036}_{-0.000035}$	$9.048^{+0.031}_{-0.032}$	241390^{+130}_{-130}
212770429.2	6	$40.453490^{+0.000038}_{-0.000038}$	$2248.671633^{+0.000025}_{-0.000025}$	$9.078^{+0.021}_{-0.023}$	240392^{+58}_{-58}
212773309.1	6	$4.6819531^{+0.0000065}_{-0.0000068}$	$2217.983043^{+0.000075}_{-0.000069}$	$2.504^{+0.024}_{-0.026}$	63240^{+230}_{-200}
212773309.2	6	$4.681911^{+0.000030}_{-0.000030}$	$2220.39758^{+0.00026}_{-0.00026}$	$2.465^{+0.055}_{-0.055}$	5568^{+42}_{-48}
212775692.1	6	$0.6411874^{+0.0000031}_{-0.0000031}$	$2217.62688^{+0.00021}_{-0.00021}$	$2.893^{+0.034}_{-0.028}$	58620^{+270}_{-270}
212776371.1	6		$2268.32732^{+0.00037}_{-0.00037}$	$4.843^{+0.090}_{-0.103}$	104300^{+1100}_{-1000}
212786474.1	6	$9.2713312^{+0.0000079}_{-0.0000078}$	$2224.635042^{+0.000038}_{-0.000038}$	$3.874^{+0.028}_{-0.023}$	377420^{+340}_{-320}
212786474.2	6	$9.271258^{+0.000017}_{-0.000018}$	$2219.999190^{+0.000072}_{-0.000076}$	$3.844^{+0.022}_{-0.030}$	100470^{+340}_{-240}
212788116.1	6	$9.252448^{+0.000012}_{-0.000012}$	$2224.830667^{+0.000043}_{-0.000045}$	$4.020^{+0.024}_{-0.032}$	120770^{+140}_{-140}
212788116.2	6	$9.252432^{+0.000022}_{-0.000023}$	$2220.22579^{+0.00010}_{-0.00010}$	$4.052^{+0.039}_{-0.046}$	35236^{+59}_{-59}
212797028.1	6	$29.98250^{+0.00023}_{-0.00023}$	$2230.46644^{+0.00031}_{-0.00031}$	$6.333^{+0.078}_{-0.085}$	18616^{+73}_{-76}
212797028.2	6	$29.9848^{+0.0055}_{-0.0056}$	$2224.0032^{+0.0067}_{-0.0069}$	$7.86^{+0.83}_{-0.60}$	780^{+42}_{-42}
212801667.1	6	$23.274535^{+0.000031}_{-0.000032}$	$2232.150975^{+0.000050}_{-0.000050}$	$5.2988^{+0.0080}_{-0.0077}$	85353^{+60}_{-62}
212801667.2	6	$23.27435^{+0.00031}_{-0.00031}$	$2222.67625^{+0.00059}_{-0.00060}$	$8.176^{+0.040}_{-0.041}$	2910^{+16}_{-17}
212805678.1	6		$2293.53886^{+0.00023}_{-0.00023}$	$22.427^{+0.066}_{-0.070}$	59703^{+90}_{-90}
212812349.1	6	$8.167509^{+0.000016}_{-0.000016}$	$2221.86324^{+0.00011}_{-0.00010}$	$4.833^{+0.024}_{-0.028}$	82120^{+110}_{-110}

Table A.2: Our sample of eclipsing binaries from C0-8. (continued)

Binary	C#	Period (days)	t_0 (BJD - 2455000)	Duration (hours)	Depth (ppm)
212812349.2	6	$8.16743^{+0.00014}_{-0.00014}$	$2217.78134^{+0.00076}_{-0.00076}$	$4.771^{+0.071}_{-0.080}$	4770^{+50}_{-49}
212822491.1	6	$14.3206444^{+0.0000074}_{-0.0000071}$	$2226.599362^{+0.000021}_{-0.000021}$	$6.741^{+0.012}_{-0.013}$	168106^{+58}_{-74}
212822491.2	6	$14.320543^{+0.000045}_{-0.000042}$	$2219.43998^{+0.00012}_{-0.00013}$	$6.693^{+0.040}_{-0.056}$	18976^{+31}_{-30}
212839127.1	6	$20.641563^{+0.000066}_{-0.000066}$	$2217.69770^{+0.00012}_{-0.00012}$	$4.069^{+0.034}_{-0.044}$	47300^{+130}_{-120}
213273052.1	7	$33.691288^{+0.000019}_{-0.000019}$	$2314.205333^{+0.000022}_{-0.000023}$	$20.210^{+0.016}_{-0.016}$	410000^{+1300}_{-2400}
213273052.2	7	$33.690370^{+0.000037}_{-0.000047}$	$2332.934345^{+0.000013}_{-0.000013}$	$14.037^{+0.028}_{-0.034}$	395340^{+110}_{-100}
213354839.1	7	$2.3431433^{+0.0000023}_{-0.0000022}$	$2302.351235^{+0.000044}_{-0.000044}$	$4.883^{+0.016}_{-0.019}$	174150^{+110}_{-110}
213354839.2	7	$2.343200^{+0.000023}_{-0.000023}$	$2303.52383^{+0.00044}_{-0.00044}$	$4.725^{+0.074}_{-0.088}$	14454^{+79}_{-77}
213455199.1	7		$2381.93549^{+0.00024}_{-0.00024}$	$32.007^{+0.077}_{-0.101}$	477860^{+380}_{-4870}
213455199.2	7		$2373.05801^{+0.00025}_{-0.00015}$	$31.87^{+0.34}_{-0.13}$	353000^{+10000}_{-20000}
213563657.1	7	$3.413240^{+0.000010}_{-0.000010}$	$2304.30543^{+0.00014}_{-0.00014}$	$3.864^{+0.036}_{-0.042}$	48410^{+130}_{-120}
213563657.2	7	$3.41295^{+0.00016}_{-0.00016}$	$2302.6022^{+0.0021}_{-0.0020}$	$3.30^{+0.16}_{-0.24}$	1850^{+57}_{-59}
213599585.1	7	$6.290272^{+0.000027}_{-0.000029}$	$2304.05701^{+0.00014}_{-0.00013}$	$5.916^{+0.042}_{-0.046}$	125070^{+240}_{-240}
213599585.2	7	$6.29177^{+0.00014}_{-0.00017}$	$2307.1980^{+0.0014}_{-0.0012}$	$6.144^{+0.054}_{-0.072}$	28700^{+690}_{-360}
213601365.1	7		$2335.95935^{+0.00014}_{-0.00014}$	$15.207^{+0.025}_{-0.030}$	337870^{+500}_{-500}
213631028.1	7	$7.871062^{+0.000019}_{-0.000019}$	$2306.484869^{+0.000100}_{-0.000100}$	$2.239^{+0.018}_{-0.022}$	25413^{+75}_{-74}
213631028.2	7	$7.871007^{+0.000032}_{-0.000031}$	$2302.52038^{+0.00018}_{-0.00019}$	$2.397^{+0.043}_{-0.043}$	12013^{+57}_{-57}
213689594.1	7	$45.96544^{+0.00015}_{-0.00015}$	$2322.49347^{+0.00010}_{-0.00010}$	$12.981^{+0.036}_{-0.039}$	47757^{+41}_{-41}
213832800.1	7		$2321.468034^{+0.000027}_{-0.000024}$	$8.106^{+0.023}_{-0.024}$	105773^{+55}_{-56}
213840781.1	7	$12.364786^{+0.000027}_{-0.000027}$	$2310.662309^{+0.000080}_{-0.000081}$	$2.942^{+0.036}_{-0.037}$	66730^{+1530}_{-550}
213843283.1	7	$11.2216911^{+0.0000111}_{-0.0000067}$	$2302.301680^{+0.000028}_{-0.000031}$	$6.3551^{+0.0090}_{-0.0101}$	178343^{+73}_{-73}
213843283.2	7	$11.221699^{+0.000060}_{-0.000059}$	$2307.92168^{+0.00022}_{-0.00022}$	$6.111^{+0.019}_{-0.020}$	13628^{+38}_{-38}
213951550.1	7	$1.1170268^{+0.0000012}_{-0.0000012}$	$2301.735845^{+0.000049}_{-0.000050}$	$1.529^{+0.023}_{-0.025}$	77580^{+230}_{-220}
213951550.2	7	$1.117123^{+0.000012}_{-0.000013}$	$2302.29117^{+0.00049}_{-0.00042}$	$0.482^{+0.026}_{-0.038}$	32600^{+1600}_{-1900}
214229494.1	7	$3.8691718^{+0.0000079}_{-0.0000116}$	$2303.140349^{+0.000084}_{-0.000093}$	$4.342^{+0.057}_{-0.060}$	266690^{+530}_{-490}
214229494.2	7	$3.870317^{+0.000013}_{-0.000012}$	$2305.06657^{+0.00017}_{-0.00017}$	$5.986^{+0.052}_{-0.041}$	151950^{+850}_{-880}
214576668.1	7	$0.7917042^{+0.0000072}_{-0.0000074}$	$2301.78042^{+0.00043}_{-0.00043}$	$1.744^{+0.066}_{-0.058}$	3151^{+40}_{-41}
214576668.2	7	$0.791713^{+0.000011}_{-0.000011}$	$2302.17587^{+0.00062}_{-0.00062}$	$1.717^{+0.070}_{-0.077}$	2072^{+37}_{-37}
214600459.1	7	$1.806835^{+0.000010}_{-0.000011}$	$2302.07394^{+0.00027}_{-0.00028}$	$2.730^{+0.022}_{-0.031}$	33010^{+220}_{-220}
214600459.2	7	$1.806839^{+0.000023}_{-0.000023}$	$2302.97738^{+0.00055}_{-0.00054}$	$2.90^{+0.11}_{-0.11}$	7572^{+96}_{-95}
214611894.1	7	$21.568456^{+0.000033}_{-0.000033}$	$2304.286542^{+0.000061}_{-0.000061}$	$4.1573^{+0.0087}_{-0.0093}$	30005^{+37}_{-37}
214611894.2	7	$21.5682^{+0.0016}_{-0.0016}$	$2309.2595^{+0.0029}_{-0.0029}$	$5.00^{+0.24}_{-0.53}$	657^{+23}_{-23}
214652580.1	7	$8.911956^{+0.000051}_{-0.000052}$	$2302.87589^{+0.00025}_{-0.00024}$	$4.198^{+0.061}_{-0.058}$	20280^{+75}_{-75}
214652580.2	7	$8.91134^{+0.00057}_{-0.00058}$	$2307.2605^{+0.0027}_{-0.0027}$	$4.02^{+0.19}_{-0.21}$	1377^{+48}_{-48}
214669044.1	7	$11.7908^{+0.0015}_{-0.0015}$	$2308.4973^{+0.0056}_{-0.0057}$	$9.10^{+0.42}_{-0.48}$	381^{+12}_{-12}
214669044.2	7	$11.7909^{+0.0022}_{-0.0022}$	$2301.8451^{+0.0084}_{-0.0079}$	$5.29^{+0.28}_{-0.38}$	235^{+15}_{-15}
214729274.1	7	$25.379689^{+0.000015}_{-0.000015}$	$2320.389025^{+0.000021}_{-0.000022}$	$3.125^{+0.013}_{-0.019}$	186790^{+220}_{-240}
214729274.2	7	$25.38098^{+0.00081}_{-0.00067}$	$2304.4112^{+0.0013}_{-0.0015}$	$3.92^{+0.20}_{-0.18}$	4393^{+68}_{-66}

Table A.2: Our sample of eclipsing binaries from C0-8. (continued)

Binary	C#	Period (days)	t_0 (BJD - 2455000)	Duration (hours)	Depth (ppm)
214860030.1	7	$27.05405^{+0.00062}_{-0.00061}$	$2305.50218^{+0.00077}_{-0.00079}$	$9.22^{+0.16}_{-0.14}$	75500^{+530}_{-510}
214860030.2	7	$27.05416^{+0.00020}_{-0.00020}$	$2321.63637^{+0.00025}_{-0.00025}$	$5.978^{+0.083}_{-0.080}$	237000^{+4500}_{-3600}
214984368.1	7	$0.526779^{+0.000014}_{-0.000014}$	$2301.5877^{+0.0013}_{-0.0013}$	$1.52^{+0.24}_{-0.16}$	433^{+18}_{-18}
214984368.2	7	$0.526805^{+0.000016}_{-0.000016}$	$2301.8508^{+0.0014}_{-0.0014}$	$1.95^{+0.11}_{-0.12}$	304^{+11}_{-12}
215037076.1	7	$38.92447^{+0.00024}_{-0.00029}$	$2305.94521^{+0.00012}_{-0.00012}$	$5.153^{+0.063}_{-0.063}$	409900^{+2900}_{-2700}
215037076.2	7	$38.92328^{+0.00012}_{-0.00012}$	$2317.000245^{+0.000094}_{-0.000095}$	$2.909^{+0.048}_{-0.053}$	427700^{+5300}_{-3400}
215279174.1	7	$14.966503^{+0.000011}_{-0.000010}$	$2310.779800^{+0.000030}_{-0.000029}$	$3.314^{+0.025}_{-0.023}$	82929^{+143}_{-90}
215279174.2	7	$14.9666096^{+0.0000096}_{-0.0000094}$	$2303.296309^{+0.000029}_{-0.000030}$	$3.286^{+0.019}_{-0.019}$	79436^{+95}_{-95}
215307988.1	7		$2322.405713^{+0.000032}_{-0.000025}$	$16.675^{+0.024}_{-0.025}$	377979^{+84}_{-83}
215358983.1	7	$6.421860^{+0.000024}_{-0.000024}$	$2303.43119^{+0.00017}_{-0.00017}$	$6.191^{+0.016}_{-0.017}$	22708^{+57}_{-57}
215358983.2	7	$6.42216^{+0.00049}_{-0.00052}$	$2306.6386^{+0.0035}_{-0.0030}$	$6.34^{+0.30}_{-0.46}$	803^{+23}_{-24}
215389654.1	7	$23.514041^{+0.000067}_{-0.000067}$	$2309.92954^{+0.00012}_{-0.00012}$	$8.846^{+0.017}_{-0.018}$	39844^{+49}_{-49}
215389654.2	7	$23.5168^{+0.0020}_{-0.0020}$	$2318.2739^{+0.0026}_{-0.0026}$	$3.14^{+0.15}_{-0.17}$	785^{+40}_{-43}
215474548.1	7	$1.2085418^{+0.0000062}_{-0.0000063}$	$2302.03032^{+0.00024}_{-0.00024}$	$2.486^{+0.067}_{-0.069}$	16650^{+120}_{-120}
215474548.2	7	$1.208555^{+0.000012}_{-0.000012}$	$2302.63432^{+0.00048}_{-0.00048}$	$2.419^{+0.073}_{-0.086}$	8144^{+81}_{-81}
215645072.1	7	$8.181033^{+0.000012}_{-0.000012}$	$2308.352597^{+0.000047}_{-0.000045}$	$5.215^{+0.012}_{-0.015}$	90572^{+51}_{-51}
215645072.2	7	$8.1811125^{+0.0000079}_{-0.0000081}$	$2305.083734^{+0.000046}_{-0.000046}$	$4.775^{+0.018}_{-0.025}$	100210^{+110}_{-110}
215716837.1	7	$8.683172^{+0.000065}_{-0.000065}$	$2302.68891^{+0.00035}_{-0.00034}$	$6.555^{+0.070}_{-0.068}$	20678^{+78}_{-78}
215716837.2	7	$8.68281^{+0.00085}_{-0.00079}$	$2307.3507^{+0.0036}_{-0.0040}$	$3.13^{+0.22}_{-0.42}$	1586^{+88}_{-93}
215786841.1	7	$2.801053^{+0.000041}_{-0.000043}$	$2302.46490^{+0.00049}_{-0.00049}$	$3.75^{+0.11}_{-0.11}$	9600^{+170}_{-190}
215786841.2	7	$2.801703^{+0.000082}_{-0.000084}$	$2303.8575^{+0.0012}_{-0.0012}$	$4.61^{+0.14}_{-0.12}$	6280^{+140}_{-140}
215845163.1	7	$3.4879813^{+0.0000018}_{-0.0000018}$	$2304.585648^{+0.000025}_{-0.000025}$	$4.6535^{+0.0095}_{-0.0096}$	151163^{+61}_{-64}
215845163.2	7	$3.4879901^{+0.0000044}_{-0.0000043}$	$2302.841641^{+0.000039}_{-0.000040}$	$4.677^{+0.031}_{-0.035}$	49924^{+43}_{-41}
216116973.1	7	$4.139468^{+0.000035}_{-0.000035}$	$2301.79791^{+0.00038}_{-0.00038}$	$3.716^{+0.072}_{-0.079}$	2632^{+16}_{-16}
216116973.2	7	$4.13918^{+0.00032}_{-0.00032}$	$2303.8703^{+0.0034}_{-0.0033}$	$3.27^{+0.26}_{-0.57}$	268^{+13}_{-13}
216442060.1	7	$5.202717^{+0.000012}_{-0.000011}$	$2301.883467^{+0.000080}_{-0.000081}$	$3.078^{+0.015}_{-0.017}$	19562^{+47}_{-53}
216442060.2	7	$5.20256^{+0.00017}_{-0.00016}$	$2304.4873^{+0.0014}_{-0.0015}$	$3.26^{+0.13}_{-0.14}$	819^{+19}_{-19}
216465617.1	7	$15.21259^{+0.00031}_{-0.00031}$	$2312.67741^{+0.00073}_{-0.00073}$	$5.34^{+0.15}_{-0.16}$	9466^{+97}_{-95}
216465617.2	7	$15.21341^{+0.00039}_{-0.00039}$	$2301.9273^{+0.0011}_{-0.0011}$	$6.18^{+0.13}_{-0.17}$	5517^{+60}_{-59}
216552798.1	7	$0.6203188^{+0.0000035}_{-0.0000035}$	$2301.95519^{+0.00023}_{-0.00023}$	$3.154^{+0.030}_{-0.025}$	9452^{+39}_{-39}
216552798.2	7	$0.6202901^{+0.0000090}_{-0.0000090}$	$2301.64740^{+0.00067}_{-0.00067}$	$5.316^{+0.057}_{-0.055}$	4655^{+32}_{-32}
216814711.1	7	$8.992748^{+0.000037}_{-0.000030}$	$2303.71143^{+0.00015}_{-0.00017}$	$2.668^{+0.053}_{-0.046}$	22380^{+130}_{-220}
216814711.2	7	$8.992772^{+0.000062}_{-0.000063}$	$2308.20693^{+0.00029}_{-0.00027}$	$2.502^{+0.026}_{-0.032}$	16220^{+130}_{-120}
217149884.1	7	$16.692301^{+0.000060}_{-0.000060}$	$2315.06320^{+0.00015}_{-0.00015}$	$5.662^{+0.039}_{-0.037}$	33699^{+69}_{-72}
217149884.2	7	$16.6912^{+0.0036}_{-0.0035}$	$2307.5165^{+0.0093}_{-0.0093}$	$5.39^{+0.61}_{-1.02}$	706^{+58}_{-60}
217284183.1	7	$4.9307851^{+0.0000185}_{-0.0000094}$	$2305.013551^{+0.000076}_{-0.000104}$	$3.574^{+0.047}_{-0.054}$	450100^{+1600}_{-1400}
217284183.2	7	$4.9302812^{+0.0000097}_{-0.0000450}$	$2302.551171^{+0.000471}_{-0.000069}$	$3.760^{+0.035}_{-0.028}$	359200^{+4400}_{-17500}
217402696.1	7	$1.9757484^{+0.0000013}_{-0.0000020}$	$2301.615489^{+0.000053}_{-0.000030}$	$1.883^{+0.016}_{-0.020}$	985300^{+12200}_{-6200}

Table A.2: Our sample of eclipsing binaries from C0-8. (continued)

Binary	C#	Period (days)	t_0 (BJD - 2455000)	Duration (hours)	Depth (ppm)
217402696.2	7	$1.9758765^{+0.0000017}_{-0.0000017}$	$2302.625091^{+0.000048}_{-0.000047}$	$0.1622^{+0.0042}_{-0.0048}$	915000^{+23000}_{-22000}
217783102.1	7	$6.9936538^{+0.0000022}_{-0.0000023}$	$2306.322109^{+0.000014}_{-0.000013}$	$3.5684^{+0.0078}_{-0.0081}$	132361^{+49}_{-47}
217783102.2	7	$6.9936424^{+0.0000024}_{-0.0000023}$	$2302.967328^{+0.000016}_{-0.000017}$	$3.6006^{+0.0036}_{-0.0049}$	101508^{+32}_{-32}
218128870.1	7	$2.016878^{+0.000041}_{-0.000041}$	$2303.34416^{+0.00086}_{-0.00089}$	$3.94^{+0.12}_{-0.13}$	11670^{+270}_{-270}
218128870.2	7	$2.017017^{+0.000077}_{-0.000080}$	$2302.3340^{+0.0012}_{-0.0012}$	$3.93^{+0.13}_{-0.14}$	6820^{+200}_{-200}
218210199.1	7	$1.9858010^{+0.0000047}_{-0.0000048}$	$2301.58132^{+0.00011}_{-0.00011}$	$2.524^{+0.035}_{-0.037}$	13280^{+35}_{-35}
218210199.2	7	$1.985835^{+0.000026}_{-0.000026}$	$2302.57360^{+0.00058}_{-0.00059}$	$2.456^{+0.081}_{-0.082}$	2175^{+31}_{-31}
218429184.1	7	$4.1117770^{+0.0000061}_{-0.0000060}$	$2302.619714^{+0.000065}_{-0.000066}$	$5.838^{+0.023}_{-0.026}$	42494^{+40}_{-39}
218429184.2	7	$4.1117834^{+0.0000076}_{-0.0000078}$	$2304.675809^{+0.000083}_{-0.000086}$	$5.840^{+0.028}_{-0.034}$	30502^{+35}_{-35}
218589724.1	7	$45.44031^{+0.00011}_{-0.00011}$	$2306.684124^{+0.000077}_{-0.000076}$	$9.908^{+0.021}_{-0.023}$	47047^{+35}_{-35}
218589724.2	7	$45.4415^{+0.0100}_{-0.0099}$	$2332.1085^{+0.0064}_{-0.0066}$	$10.84^{+0.66}_{-0.69}$	568^{+24}_{-24}
218712024.1	7	$1.2376763^{+0.0000093}_{-0.0000093}$	$2301.88916^{+0.00022}_{-0.00022}$	$2.224^{+0.042}_{-0.034}$	5730^{+27}_{-27}
218712024.2	7	$1.237621^{+0.000013}_{-0.000014}$	$2302.50820^{+0.00040}_{-0.00037}$	$2.161^{+0.068}_{-0.071}$	3709^{+42}_{-43}
218864897.1	7	$8.866879^{+0.000040}_{-0.000040}$	$2307.88551^{+0.00019}_{-0.00019}$	$7.716^{+0.027}_{-0.024}$	17659^{+31}_{-32}
218864897.2	7	$8.86721^{+0.00100}_{-0.00101}$	$2303.6561^{+0.0051}_{-0.0051}$	$7.05^{+0.23}_{-0.39}$	589^{+23}_{-24}
219340893.1	7	$11.1180632^{+0.0000084}_{-0.0000084}$	$2305.877758^{+0.000028}_{-0.000028}$	$3.301^{+0.025}_{-0.025}$	76852^{+69}_{-73}
219340893.2	7	$11.11792^{+0.00020}_{-0.00020}$	$2311.89185^{+0.00074}_{-0.00075}$	$3.975^{+0.084}_{-0.099}$	2458^{+31}_{-30}
219610822.1	7	$29.581^{+0.015}_{-0.013}$	$2303.852^{+0.012}_{-0.013}$	$8.89^{+0.90}_{-0.90}$	2097^{+79}_{-80}
219610822.2	7	$29.5364^{+0.0116}_{-0.0097}$	$2315.055^{+0.012}_{-0.014}$	$9.0^{+1.1}_{-2.0}$	915^{+64}_{-66}
220173169.1	8	$5.4502801^{+0.0000047}_{-0.0000050}$	$2395.791456^{+0.000043}_{-0.000040}$	$4.423^{+0.020}_{-0.021}$	349770^{+230}_{-220}
220173169.2	8	$5.450321^{+0.000032}_{-0.000030}$	$2392.98496^{+0.00028}_{-0.00029}$	$4.479^{+0.036}_{-0.048}$	31870^{+140}_{-140}
220179606.1	8	$23.353441^{+0.000041}_{-0.000043}$	$2402.494955^{+0.000063}_{-0.000059}$	$4.121^{+0.018}_{-0.026}$	75180^{+130}_{-120}
220179606.2	8	$23.35359^{+0.00011}_{-0.00012}$	$2396.32368^{+0.00024}_{-0.00021}$	$3.191^{+0.041}_{-0.054}$	14547^{+58}_{-57}
220196587.1	8	$11.391825^{+0.000021}_{-0.000020}$	$2396.348721^{+0.000074}_{-0.000074}$	$4.713^{+0.023}_{-0.026}$	23763^{+51}_{-40}
220196587.2	8	$11.39199^{+0.00055}_{-0.00055}$	$2402.4502^{+0.0016}_{-0.0016}$	$4.59^{+0.37}_{-0.38}$	793^{+20}_{-24}
220219177.1	8	$8.3612219^{+0.0000042}_{-0.0000088}$	$2392.482593^{+0.000149}_{-0.000024}$	$6.1608^{+0.0095}_{-0.0125}$	262260^{+190}_{-130}
220219177.2	8	$8.3612204^{+0.0000052}_{-0.0000063}$	$2397.165095^{+0.000038}_{-0.000026}$	$7.226^{+0.013}_{-0.014}$	219625^{+71}_{-74}
220222060.2	8	$6.365398^{+0.000035}_{-0.000035}$	$2397.92585^{+0.00023}_{-0.00023}$	$4.819^{+0.016}_{-0.016}$	7220^{+23}_{-24}
220230146.1	8	$5.455392^{+0.000019}_{-0.000019}$	$2397.02165^{+0.00017}_{-0.00016}$	$3.225^{+0.062}_{-0.067}$	316400^{+1600}_{-1300}
220230146.2	8	$5.455248^{+0.000023}_{-0.000022}$	$2394.46786^{+0.00015}_{-0.00015}$	$2.980^{+0.039}_{-0.047}$	304900^{+1500}_{-1500}
220231331.1	8	$23.6487^{+0.0013}_{-0.0013}$	$2411.1180^{+0.0017}_{-0.0017}$	$3.51^{+0.15}_{-0.16}$	75300^{+2600}_{-2400}
220243443.1	8	$11.859155^{+0.000015}_{-0.000016}$	$2398.320317^{+0.000063}_{-0.000057}$	$3.707^{+0.032}_{-0.032}$	455200^{+1700}_{-1300}
220243443.2	8	$11.859212^{+0.000024}_{-0.000024}$	$2403.459837^{+0.000064}_{-0.000064}$	$5.088^{+0.044}_{-0.039}$	432330^{+670}_{-630}
220257938.1	8	$6.402912^{+0.000034}_{-0.000035}$	$2395.51412^{+0.00022}_{-0.00025}$	$2.625^{+0.030}_{-0.037}$	319400^{+1400}_{-1500}
220257938.2	8	$6.4028393^{+0.0000096}_{-0.0000098}$	$2392.733165^{+0.000077}_{-0.000075}$	$1.995^{+0.013}_{-0.020}$	224500^{+1600}_{-1400}
220258394.1	8	$15.960497^{+0.000060}_{-0.000059}$	$2401.74756^{+0.00015}_{-0.00015}$	$4.886^{+0.033}_{-0.041}$	42880^{+120}_{-120}
220258394.2	8	$15.96248^{+0.00096}_{-0.00094}$	$2405.5053^{+0.0025}_{-0.0026}$	$3.59^{+0.16}_{-0.29}$	1543^{+60}_{-61}
220271452.1	8	$0.8739372^{+0.0000072}_{-0.0000073}$	$2392.85735^{+0.00036}_{-0.00037}$	$1.259^{+0.044}_{-0.053}$	58000^{+1200}_{-1100}

Table A.2: Our sample of eclipsing binaries from C0-8. (continued)

Binary	C#	Period (days)	t_0 (BJD - 2455000)	Duration (hours)	Depth (ppm)
220271452.2	8	$0.873934^{+0.000015}_{-0.000015}$	$2392.42153^{+0.00077}_{-0.00079}$	$1.226^{+0.075}_{-0.073}$	25400^{+1000}_{-1000}
220302728.1	8	$3.8524450^{+0.0000026}_{-0.0000023}$	$2392.335463^{+0.000022}_{-0.000023}$	$4.4255^{+0.0053}_{-0.0064}$	270270^{+170}_{-170}
220302728.2	8	$3.8524068^{+0.0000095}_{-0.0000096}$	$2394.26212^{+0.00010}_{-0.00010}$	$4.391^{+0.017}_{-0.021}$	44978^{+76}_{-77}
220303276.1	8	$8.092197^{+0.000024}_{-0.000024}$	$2394.72200^{+0.00015}_{-0.00015}$	$4.959^{+0.013}_{-0.013}$	6491^{+22}_{-20}
220303276.2	8	$8.092231^{+0.000091}_{-0.000060}$	$2398.76885^{+0.00031}_{-0.00056}$	$4.934^{+0.026}_{-0.034}$	5471^{+20}_{-21}
220305504.1	8	$2.9868499^{+0.0000026}_{-0.0000026}$	$2393.816726^{+0.000038}_{-0.000039}$	$3.7795^{+0.0084}_{-0.0124}$	82486^{+109}_{-92}
220305504.2	8	$2.986883^{+0.000012}_{-0.000012}$	$2392.32273^{+0.00019}_{-0.00019}$	$3.816^{+0.058}_{-0.054}$	7797^{+29}_{-32}
220314321.1	8	$2.4869748^{+0.0000013}_{-0.0000012}$	$2394.347251^{+0.000012}_{-0.000012}$	$2.801^{+0.018}_{-0.013}$	369910^{+470}_{-290}
220314321.2	8	$2.4869592^{+0.0000014}_{-0.0000014}$	$2393.104005^{+0.000019}_{-0.000021}$	$2.797^{+0.021}_{-0.027}$	294950^{+180}_{-170}
220336320.1	8	$1.7276524^{+0.0000031}_{-0.0000031}$	$2392.154138^{+0.000082}_{-0.000081}$	$1.564^{+0.031}_{-0.027}$	59020^{+210}_{-210}
220339564.1	8	$8.9813007^{+0.0000110}_{-0.0000099}$	$2396.665901^{+0.000058}_{-0.000064}$	$4.400^{+0.024}_{-0.016}$	379700^{+1690}_{-970}
220339564.2	8	$8.981252^{+0.000011}_{-0.000011}$	$2392.240288^{+0.000050}_{-0.000048}$	$4.224^{+0.011}_{-0.014}$	189900^{+150}_{-140}
220351987.1	8	$1.4779226^{+0.0000021}_{-0.0000021}$	$2392.292498^{+0.000071}_{-0.000069}$	$1.931^{+0.025}_{-0.028}$	28028^{+78}_{-76}
220351987.2	8	$1.477910^{+0.000018}_{-0.000018}$	$2393.03368^{+0.00053}_{-0.00053}$	$1.809^{+0.056}_{-0.066}$	2526^{+43}_{-42}
220352059.1	8	$43.51194^{+0.00019}_{-0.00012}$	$2407.31297^{+0.00012}_{-0.00027}$	$6.048^{+0.039}_{-0.045}$	90820^{+550}_{-1830}
220352059.2	8	$43.51199^{+0.00025}_{-0.00024}$	$2397.41324^{+0.00017}_{-0.00018}$	$8.116^{+0.072}_{-0.095}$	36400^{+71}_{-63}
220364369.1	8	$46.49793^{+0.00039}_{-0.00039}$	$2409.20576^{+0.00028}_{-0.00028}$	$4.060^{+0.087}_{-0.100}$	56780^{+330}_{-320}
220374480.1	8		$2464.754687^{+0.000095}_{-0.000099}$	$6.03^{+0.11}_{-0.11}$	662600^{+3800}_{-2400}
220398184.1	8	$1.34806124^{+0.00000049}_{-0.00000046}$	$2392.298660^{+0.000014}_{-0.000015}$	$2.5473^{+0.0051}_{-0.0060}$	367670^{+340}_{-360}
220402063.1	8	$2.083347^{+0.000051}_{-0.000052}$	$2393.92404^{+0.00094}_{-0.00093}$	$3.20^{+0.13}_{-0.15}$	14990^{+230}_{-230}
220402063.2	8	$2.083369^{+0.000059}_{-0.000057}$	$2392.8778^{+0.0014}_{-0.0015}$	$2.76^{+0.10}_{-0.11}$	10290^{+290}_{-250}
220429913.1	8	$6.0889492^{+0.0000074}_{-0.0000073}$	$2397.852181^{+0.000040}_{-0.000040}$	$3.675^{+0.025}_{-0.030}$	403620^{+490}_{-500}
220429913.2	8	$6.0889339^{+0.0000094}_{-0.0000091}$	$2394.924480^{+0.000065}_{-0.000065}$	$3.540^{+0.030}_{-0.038}$	221660^{+500}_{-390}
220440299.1	8	$4.4440531^{+0.0000029}_{-0.0000027}$	$2396.547969^{+0.000028}_{-0.000030}$	$2.792^{+0.010}_{-0.014}$	375950^{+930}_{-1180}
220440299.2	8	$4.4440122^{+0.0000064}_{-0.0000064}$	$2394.223241^{+0.000064}_{-0.000060}$	$3.566^{+0.017}_{-0.026}$	150720^{+160}_{-160}
220443255.1	8	$0.9097484^{+0.0000017}_{-0.0000017}$	$2393.019379^{+0.000085}_{-0.000084}$	$1.619^{+0.032}_{-0.034}$	3489^{+13}_{-12}
220443255.2	8	$0.9097451^{+0.0000024}_{-0.0000024}$	$2392.56466^{+0.00012}_{-0.00012}$	$1.620^{+0.041}_{-0.040}$	2376^{+12}_{-11}
220453029.1	8	$30.26900^{+0.00030}_{-0.00053}$	$2397.99553^{+0.00052}_{-0.00026}$	$6.067^{+0.031}_{-0.053}$	92430^{+960}_{-300}
220453029.2	8	$30.2722^{+0.0024}_{-0.0024}$	$2412.3154^{+0.0017}_{-0.0017}$	$12.16^{+0.14}_{-0.14}$	6506^{+75}_{-81}
220460233.1	8	$2.865556^{+0.000026}_{-0.000026}$	$2392.34974^{+0.00041}_{-0.00041}$	$6.424^{+0.062}_{-0.072}$	54710^{+250}_{-250}
220460233.2	8	$2.865568^{+0.000049}_{-0.000049}$	$2393.78173^{+0.00075}_{-0.00075}$	$6.309^{+0.049}_{-0.052}$	27440^{+210}_{-220}
220471927.1	8	$19.882917^{+0.000022}_{-0.000022}$	$2408.211694^{+0.000038}_{-0.000039}$	$8.5376^{+0.0087}_{-0.0086}$	282850^{+130}_{-130}
220471927.2	8	$19.882843^{+0.000020}_{-0.000020}$	$2401.604464^{+0.000038}_{-0.000038}$	$12.447^{+0.011}_{-0.011}$	324120^{+120}_{-100}
220476633.1	8	$3.040540^{+0.000014}_{-0.000013}$	$2393.69264^{+0.00020}_{-0.00021}$	$6.582^{+0.023}_{-0.025}$	54871^{+91}_{-92}
220477223.1	8	$9.3697587^{+0.0000059}_{-0.0000057}$	$2398.675649^{+0.000025}_{-0.000027}$	$3.947^{+0.013}_{-0.012}$	54043^{+27}_{-27}
220477223.2	8	$9.36982^{+0.00013}_{-0.00013}$	$2394.01094^{+0.00060}_{-0.00060}$	$3.679^{+0.095}_{-0.260}$	1714^{+14}_{-14}
220479880.1	8	$6.7896025^{+0.0000098}_{-0.0000100}$	$2393.401003^{+0.000060}_{-0.000060}$	$2.670^{+0.026}_{-0.030}$	176260^{+640}_{-660}
220479880.2	8	$6.789544^{+0.000024}_{-0.000024}$	$2396.80337^{+0.00016}_{-0.00015}$	$2.675^{+0.037}_{-0.038}$	78550^{+290}_{-270}

Table A.2: Our sample of eclipsing binaries from C0-8. (continued)

Binary	C#	Period (days)	t_0 (BJD - 2455000)	Duration (hours)	Depth (ppm)
220485301.1	8	$0.9396662^{+0.0000021}_{-0.0000021}$	$2392.791177^{+0.000098}_{-0.000098}$	$2.204^{+0.034}_{-0.029}$	84700^{+250}_{-240}
220490873.1	8	$12.044105^{+0.000016}_{-0.000016}$	$2402.037891^{+0.000054}_{-0.000052}$	$4.092^{+0.023}_{-0.021}$	65791^{+55}_{-55}
220490873.2	8	$12.04397^{+0.00030}_{-0.00030}$	$2392.8221^{+0.0010}_{-0.0010}$	$2.494^{+0.097}_{-0.107}$	1250^{+28}_{-28}
220496837.1	8	$8.897140^{+0.000049}_{-0.000052}$	$2397.31694^{+0.00032}_{-0.00027}$	$8.178^{+0.023}_{-0.034}$	83720^{+330}_{-290}
220496837.2	8	$8.89679^{+0.00029}_{-0.00028}$	$2392.4485^{+0.0013}_{-0.0013}$	$5.932^{+0.088}_{-0.088}$	7040^{+100}_{-100}
220502355.1	8	$11.039804^{+0.000015}_{-0.000014}$	$2396.746484^{+0.000060}_{-0.000063}$	$4.579^{+0.015}_{-0.019}$	96950^{+110}_{-110}
220502355.2	8	$11.03995^{+0.00022}_{-0.00022}$	$2393.62761^{+0.00079}_{-0.00084}$	$5.934^{+0.065}_{-0.080}$	6279^{+54}_{-57}
220514093.1	8	$3.5141539^{+0.0000011}_{-0.0000011}$	$2393.808507^{+0.000014}_{-0.000014}$	$5.545^{+0.011}_{-0.011}$	181370^{+48}_{-47}
220514093.2	8	$3.5141594^{+0.0000043}_{-0.0000044}$	$2395.565590^{+0.000057}_{-0.000057}$	$5.4491^{+0.0071}_{-0.0083}$	59390^{+64}_{-64}
220519942.1	8	$1.04116506^{+0.00000059}_{-0.00000060}$	$2392.124440^{+0.000024}_{-0.000023}$	$3.010^{+0.014}_{-0.010}$	535710^{+600}_{-600}
220519942.2	8	$1.04114862^{+0.00000096}_{-0.00000096}$	$2392.646685^{+0.000041}_{-0.000041}$	$3.078^{+0.028}_{-0.027}$	292090^{+780}_{-770}
220541275.1	8	$16.71926^{+0.00020}_{-0.00020}$	$2394.42754^{+0.00048}_{-0.00048}$	$2.807^{+0.074}_{-0.080}$	51140^{+550}_{-550}
220541275.2	8	$16.71991^{+0.00096}_{-0.00095}$	$2403.7088^{+0.0026}_{-0.0026}$	$3.02^{+0.16}_{-0.18}$	11130^{+470}_{-470}
220544503.1	8	$28.922213^{+0.000015}_{-0.000016}$	$2408.655764^{+0.000022}_{-0.000021}$	$6.180^{+0.016}_{-0.016}$	230454^{+99}_{-97}
220544503.2	8	$57.84408^{+0.00015}_{-0.00015}$	$2392.26517^{+0.00011}_{-0.00010}$	$7.387^{+0.037}_{-0.046}$	50719^{+57}_{-57}
220550457.1	8	$27.234313^{+0.000017}_{-0.000017}$	$2400.917978^{+0.000022}_{-0.000022}$	$6.917^{+0.019}_{-0.020}$	218618^{+56}_{-55}
220550457.2	8	$27.23450^{+0.00013}_{-0.00012}$	$2415.69311^{+0.00017}_{-0.00017}$	$5.425^{+0.069}_{-0.073}$	27891^{+96}_{-104}
220551856.1	8	$11.751408^{+0.000015}_{-0.000017}$	$2395.181440^{+0.000026}_{-0.000026}$	$5.529^{+0.014}_{-0.019}$	318520^{+170}_{-180}
220551856.2	8	$11.7514413^{+0.0000099}_{-0.0000098}$	$2392.466887^{+0.000031}_{-0.000031}$	$4.896^{+0.017}_{-0.027}$	275480^{+190}_{-170}
220559378.1	8		$2401.516062^{+0.000051}_{-0.000066}$	$6.765^{+0.037}_{-0.046}$	137920^{+110}_{-110}
220571578.1	8	$10.619180^{+0.000011}_{-0.000011}$	$2400.205751^{+0.000040}_{-0.000040}$	$5.221^{+0.018}_{-0.017}$	51343^{+33}_{-33}
220571578.2	8	$10.61941^{+0.00016}_{-0.00016}$	$2394.91953^{+0.00068}_{-0.00068}$	$5.187^{+0.092}_{-0.116}$	3144^{+29}_{-30}
220588021.1	8	$2.0980554^{+0.0000053}_{-0.0000053}$	$2393.93937^{+0.00012}_{-0.00011}$	$3.032^{+0.036}_{-0.043}$	21477^{+65}_{-63}
220588021.2	8	$2.098097^{+0.000078}_{-0.000078}$	$2392.8905^{+0.0017}_{-0.0017}$	$2.85^{+0.24}_{-0.41}$	1292^{+42}_{-43}
220592163.1	8	$9.982840^{+0.000011}_{-0.000011}$	$2394.957559^{+0.000048}_{-0.000048}$	$6.733^{+0.017}_{-0.018}$	147300^{+120}_{-120}
220592163.2	8	$9.98300^{+0.00016}_{-0.00015}$	$2400.07144^{+0.00057}_{-0.00057}$	$4.678^{+0.045}_{-0.046}$	7183^{+65}_{-67}
220598367.1	8	$5.27262^{+0.00012}_{-0.00012}$	$2395.40648^{+0.00090}_{-0.00086}$	$2.138^{+0.077}_{-0.087}$	2047^{+44}_{-44}
220598367.3	8	$5.27248^{+0.00025}_{-0.00027}$	$2393.0310^{+0.0021}_{-0.0021}$	$2.05^{+0.40}_{-0.17}$	1385^{+64}_{-59}
220610601.1	8	$0.9453051^{+0.0000034}_{-0.0000034}$	$2392.96400^{+0.00016}_{-0.00016}$	$5.857^{+0.038}_{-0.028}$	198820^{+490}_{-440}
220610601.2	8	$0.9453182^{+0.0000101}_{-0.0000100}$	$2392.49030^{+0.00048}_{-0.00049}$	$4.237^{+0.037}_{-0.051}$	41780^{+300}_{-330}
220619415.1	8	$16.045934^{+0.000043}_{-0.000047}$	$2397.47569^{+0.00013}_{-0.00011}$	$4.486^{+0.010}_{-0.012}$	40050^{+160}_{-120}
220620962.1	8	$6.857264^{+0.000020}_{-0.000020}$	$2393.83126^{+0.00012}_{-0.00012}$	$4.111^{+0.047}_{-0.054}$	254390^{+620}_{-600}
220620962.2	8	$6.857324^{+0.000094}_{-0.000095}$	$2397.25971^{+0.00052}_{-0.00053}$	$4.23^{+0.12}_{-0.14}$	59040^{+430}_{-430}
220628834.1	8	$0.812694^{+0.000015}_{-0.000015}$	$2392.19116^{+0.00070}_{-0.00068}$	$4.270^{+0.094}_{-0.079}$	62940^{+660}_{-650}
220629445.1	8	$7.361268^{+0.000011}_{-0.000011}$	$2399.221024^{+0.000044}_{-0.000044}$	$6.156^{+0.023}_{-0.031}$	150710^{+130}_{-130}
220629445.2	8	$7.361198^{+0.000019}_{-0.000018}$	$2395.28747^{+0.00011}_{-0.00011}$	$5.692^{+0.043}_{-0.052}$	44440^{+120}_{-100}
220655823.1	8	$7.241912^{+0.000025}_{-0.000024}$	$2396.46759^{+0.00014}_{-0.00014}$	$2.437^{+0.041}_{-0.043}$	38960^{+160}_{-160}
220655823.2	8	$7.241901^{+0.000082}_{-0.000083}$	$2392.56673^{+0.00056}_{-0.00056}$	$2.301^{+0.053}_{-0.068}$	16000^{+200}_{-170}

Table A.2: Our sample of eclipsing binaries from C0-8. (continued)

Binary	C#	Period (days)	t_0 (BJD - 2455000)	Duration (hours)	Depth (ppm)
220656006.1	8	$22.9343^{+0.0014}_{-0.0014}$	$2407.8832^{+0.0018}_{-0.0018}$	$10.71^{+0.27}_{-0.25}$	151200^{+1800}_{-1800}
220656006.2	8	$22.93534^{+0.00099}_{-0.00079}$	$2393.5880^{+0.0015}_{-0.0018}$	$4.03^{+0.15}_{-0.14}$	182400^{+3500}_{-3100}
220674623.1	8	$6.150068^{+0.000023}_{-0.000022}$	$2396.59509^{+0.00013}_{-0.00012}$	$4.839^{+0.044}_{-0.054}$	461800^{+5800}_{-4500}
220674623.2	8	$6.150025^{+0.000023}_{-0.000025}$	$2393.52361^{+0.00023}_{-0.00021}$	$4.849^{+0.045}_{-0.052}$	445500^{+1900}_{-2100}
220678893.1	8	$4.2510393^{+0.0000065}_{-0.0000065}$	$2395.072619^{+0.000066}_{-0.000065}$	$2.952^{+0.014}_{-0.017}$	40372^{+58}_{-56}
220678893.2	8	$4.250993^{+0.000052}_{-0.000050}$	$2392.94807^{+0.00053}_{-0.00053}$	$2.944^{+0.068}_{-0.091}$	4304^{+53}_{-51}
220688589.1	8	$3.8831652^{+0.0000020}_{-0.0000019}$	$2392.382536^{+0.000026}_{-0.000027}$	$5.3505^{+0.0044}_{-0.0058}$	147628^{+58}_{-58}
220688589.2	8	$3.8831809^{+0.0000076}_{-0.0000075}$	$2394.323402^{+0.000083}_{-0.000082}$	$5.212^{+0.015}_{-0.016}$	32278^{+48}_{-50}
220691721.1	8	$1.493836^{+0.000018}_{-0.000018}$	$2393.19248^{+0.00054}_{-0.00055}$	$11.422^{+0.091}_{-0.070}$	200620^{+570}_{-570}
220691721.2	8	$1.493707^{+0.000016}_{-0.000015}$	$2392.44899^{+0.00048}_{-0.00049}$	$12.774^{+0.115}_{-0.089}$	154580^{+710}_{-650}
220725183.1	8	$4.6223207^{+0.0000049}_{-0.0000050}$	$2396.697499^{+0.000047}_{-0.000046}$	$4.146^{+0.022}_{-0.023}$	63450^{+53}_{-50}
220725183.2	8	$4.6223528^{+0.0000038}_{-0.0000037}$	$2394.386148^{+0.000036}_{-0.000035}$	$4.117^{+0.018}_{-0.018}$	62452^{+41}_{-40}
220732672.1	8	$8.506741^{+0.000061}_{-0.000061}$	$2393.34539^{+0.00034}_{-0.00033}$	$4.031^{+0.075}_{-0.075}$	86650^{+470}_{-460}
220732672.2	8	$8.50578^{+0.00068}_{-0.00068}$	$2397.5981^{+0.0034}_{-0.0033}$	$3.91^{+0.24}_{-0.23}$	8600^{+480}_{-450}

VITA

Ethan Kruse was born to parents Gary and Rhonda in 1990 in Princeton, New Jersey. He spent most of his childhood in Indiana, graduating from Valparaiso High School in 2008. Ethan went on to Harvard University, receiving his AB cum laude in 2012 while concentrating in Astrophysics with a secondary focus of Computer Science. He joined the University of Washington Astronomy Department as a graduate student in the fall of 2012 and completed his PhD and this thesis in the summer of 2018. Ethan is looking forward to joining Goddard Space Flight Center in the fall of 2018 as a NASA Postdoctoral Program Fellow.